JOURNAL
OF
THE PHYSICAL SOCIETY
OF JAPAN

Being a continuation of "Proceedings of the
Physico-Mathematical Society of Japan"

Volume 2.
1947

Office of the Society
Faculty of Science; Tokyo Imperial University

On the Fine Structure of the Visibility Curves of the Stationary Ultrasonic Waves.

Bv Otohiko NOMOTO.

Kobayashi Institute of Physical Research, Kokubunji, Kokubunjimachi, Tokyo.

(Read April 29. 1946, Received September 20, 1946.)

§1. INTRODUCTION.

Some years ago I reported on a simple method for the visualization of the stationary ultrasonic waves(1). In this method, we send a beam of monochromatic light, which is emerged from a pin-hole or a slit, and made parallel through a collimator lense, through the ultrasonic waves, and along a direction, parallel to the sound wave fronts. By receiving the transmitted light on a screen, we obtain stripes of bright and dark bands with the periodicity of half wavelength of the ultrasonic wave, or the image of the stationary ultrasonic wave. (Cf. Fig. 2). As remarked there, a peculiar point accompanying this method of visualization is that the image of the sound wave does not appear equally well in every place, but the image appears most clearly at regular periodical distances behind the sound field. The distances D of these planes in which the images appear most clearly, measured from the plane of the emergence of light from the sound waves, are given by

$$D=(2n+1)\frac{\Lambda^2}{4\lambda},\quad (n=0,\ 1,\ 2,\ \cdots\cdots) \qquad (1)$$

where Λ means the ultrasonic wavelength in the medium, and λ the light wavelength in air. Immediately after the plane of emergence the image of the sound waves is usually not yet visible; and in the middle of each pair of successive positions of maximum visibility there are found the positions of evanescence of the image, the distance of which from the plane of emergence, including the latter being given by:

$$D=2n\frac{\Lambda^2}{4\lambda},\quad (n=0,\ 1,\ 2,\ \cdots\cdots) \qquad (2)$$

I(1)(2)(3) have explained this phenomenon as the Fresnel diffraction of light by the ultrasonic wave grating, assuming the existence of a phase-lattice——corrugated wave front of light——and the non-existence of the amplitude-lattice in the plane of the emergence of light from the sound waves; this is an assumption first introduced by Raman and Nagendra Nath(4) in their elementary theory on the diffraction of light by ultrasonic waves. This assumption corresponds to the fact that the sound wave is not visible in the plane of emergence of light from it, as was first found to be true by Baer(5). The relations (1) and (2) or rather the periodicity $\Delta D=\Lambda^2/\lambda$ were found independently of me also by Parthasarathy(6) in the Hiedemann's method of visualization of stationary ultrasonic waves, and a theoretical calculation was made also by Nagendra Nath(7).

The calculations of Nagendra Nath and of myself gave the periodic distances of maximum visibility and that of the evanescence of the image, also for the progressive ultrasonic waves, when they are illuminated by intermittent light of the same frequency as the ultrasonic waves (high frequency stroboscope). The periodicity in this latter case was also verified by experiments of Hiedemann and Schreuer(8).

I have also calculated the visibility curves of the images of the progressive and stationary ultrasonic waves in their positions of maximum visibility. According to the above calculation, the image shows more and more complicated structures with secondary maxima and minima, as the intensity of the sound wave increases. These fine structures of the image were also obtained experimentally at that time, but it was not possible to compare them with theoretical calculations, on account of the bad experimental conditions. Meanwhile, a paper by Mahler(9) appeared, in which he reported on the measurements of the visibility curves of progressive ultrasonic waves. His results are satisfactory, but his measurements are rather restricted to the cases of comparatively weak ultrasonic waves. He explained his results using Mascart's method of calculating the diffracted intensities; but his results are readily explicable with the use of our formula (reference (2), second table on p. 343) as well, simply by putting $v_0=1.5$, 1.2 and 0.3 respectively. (Cf. Nomoto and Oka[(10)]). For the stationary ultrasonic waves, there is, as I know, no experiments concerning visibility curves as yet. The present paper deals with some experiments carried out on this subject.

§2. VISIBILITY CURVES.

According to my previous results[(2)], the intensity distribution of the light in the image of the stationary ultrasonic wave in the plane of maximum visibility is given by

$$I=1+\frac{1}{2}\left\{J_0\left(2v_0\cos 2\pi\frac{x}{\Lambda}\right)-J_0\left(2v_0\sin 2\pi\frac{x}{\Lambda}\right)\right\} \qquad (3)$$

This can also be expressed in the following form, by suitable applications of Gegenbauer's addition theorem.

$$I=1-2\sum_{n=0}^{\infty}J_{2n+1}^2(v)\cdot\cos\left[\frac{4\pi(2n+1)x}{\Lambda}\right] \qquad (3a)$$

In this latter form it coincides with the result of Nagendra Nath. In these equations, x means the coordinate in a direction perpendicular to the fringe, or, parallel to the direction of propagation of the ultrasonic wave, and

$$v_0=2\pi p_0=\frac{2\pi\delta n_0\cdot L}{\lambda} \qquad (4)$$

is a quantity, proportional to the amplitude of the phase change p_0, produced in the light beam by crossing the stationary ultrasonic wave. In this equation δn_0 means the amplitude of periodic variation of the refractive index of the medium produced by the ultrasonic wave, L, the length of the path of the light in the ultrasonic wave, and λ, the light wave length in air.

As the result of the former numerical calculation proved to be too restricted as com

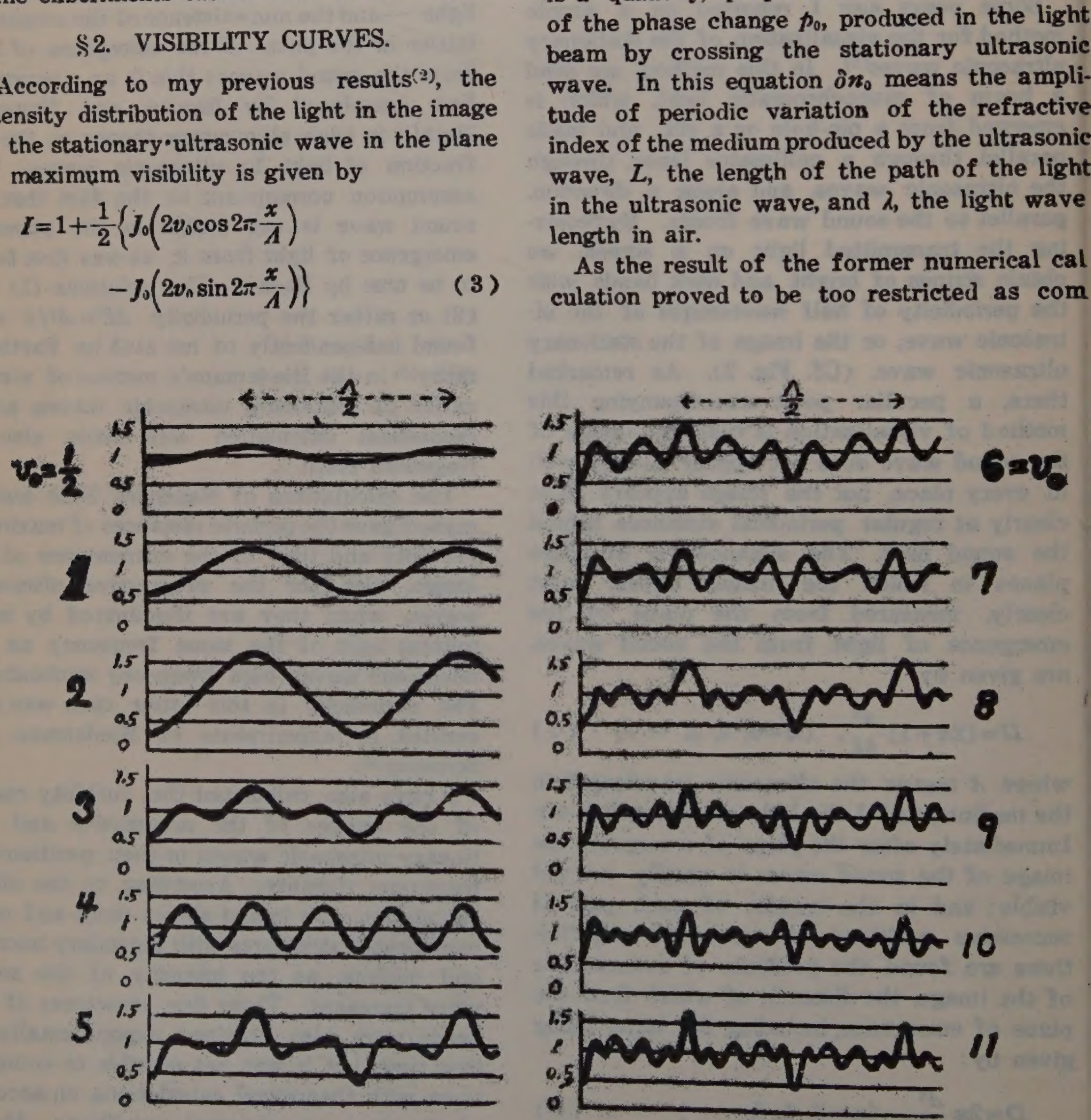

Fig. 1. Visibility curves of the stationary ultrasonic waves in the plane of maximum visibility.

pared with the results of the present experiment, it is extended now to include the values of $v_0>8$. For this purpose we used (3a) instead of (3), which is, though naturally more simple, but inconvenient in this case, on account of the lack of the calculated numerical tables of $J_0(x)$ for detailed values of the argument $x>16$. Fig. 1 gives the calculated visibility curves, of which the curves for $v_0=7$, 9, 10 and 11 are the newly calculated ones.

§3. METHOD AND RESULTS OF THE EXPERIMENT AND DISCUSSIONS.

The experimental apparatus is shown schematically in Fig. 2. An ultrasonic interferometer (I) with two parallel glass windows are filled with liquid and a stationary ultrasonic wave is produced between the oscillating quartz plate (Q) and the finely movable reflector (R). The establishment of the stationary wave was announced by the maximum complexity of the fringes at the first distance of maximum visibility; the observation being performed for this distance throughout the experiment. Different states of the fringe were obtained by varying the voltage applied to the quartz crystal. The ultrasonic wavelength is selected between about 1 and 1.5 mm. The results here reproduced are obtained with the wavelength $\Lambda=0.98$mm. For longer waves the unfavourable occurrence of the striae made it impossible to produce good images for higher ultrasonic intensities. Thus for $\Lambda=1.5$ mm we obtained good photographs only for $v_0\leqq 8$, while we can reproduce photographs for $v_0=10$ for $\Lambda=0.98$ mm.

In our arrangement the fringes were magnified to several times by the use of an auxiliary lense (F) of focal length 30.8 cm, $\lambda=5460$ A of a mercury lamp was used as the monochromatic light source.

The photographs reproduced in Fig. 3 are some of the typical ones obtained in this manner. They are once more enlarged from the original ones about five times. The photographs a, b, c, …… correspond respectively to increasing orders of sound intensity. Fig. 4 shows the microphotometer curves of these photographs. By comparing these photographs and their microphotometer curves with the theoretical curves of Fig. 2, we can recognize a very close analogy among them. Thus we can ascribe an roughly estimated value of v_0 for each of the photographs of Fig. 3. These experimental results show thus on the whole a very close agreement with theory in the whole range of ultrasonic intensities corresponding to $0\leqq v\leqq 10$.

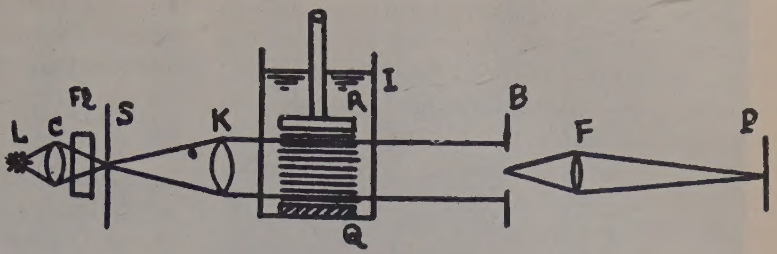

Fig. 2. Experimental apparatus.

But the quantitative agreement is not so good as the microphotmeter curves do suggest. There are three points to be noticed. The first discrepancy is caused by the superposition of diffused light; in order to explain the observed result quantitatively, we have to take into account an amount of diffused light as a general background, the quantity of which increasing from 0 to 20% with increasing intensity of the ultrasonic wave. We find, besides, in cases of higher ultrasonic intensities ($v_0\geqq 6$), that the peaks are somewhat steepened and the valleys shallowed, i. e., that the symmetry of the heights of the peaks and the depths of the valleys are lost to some extent. These diffused light may be due to some causes or the other; one source of it being undoubtedly the employment of a magnifying lense (lense F in Fig. 2) in this experiment. The other reason is, perhaps, the employment of a slit in this experiment, for, using a pin-hole as a light-source, we obtained results with increased symmetry. Finally, any slight deviation from the position of maximum visibility in either direction can result in a steepening of the peaks and a shallowing of the valleys.

But, the following, third discrepancy is the more essential. It concerns about the limit of applicability of the theory. While the numbers of subordinate maxima and minima are in complete agreement with theory, their shapes and positions are not necessarily in

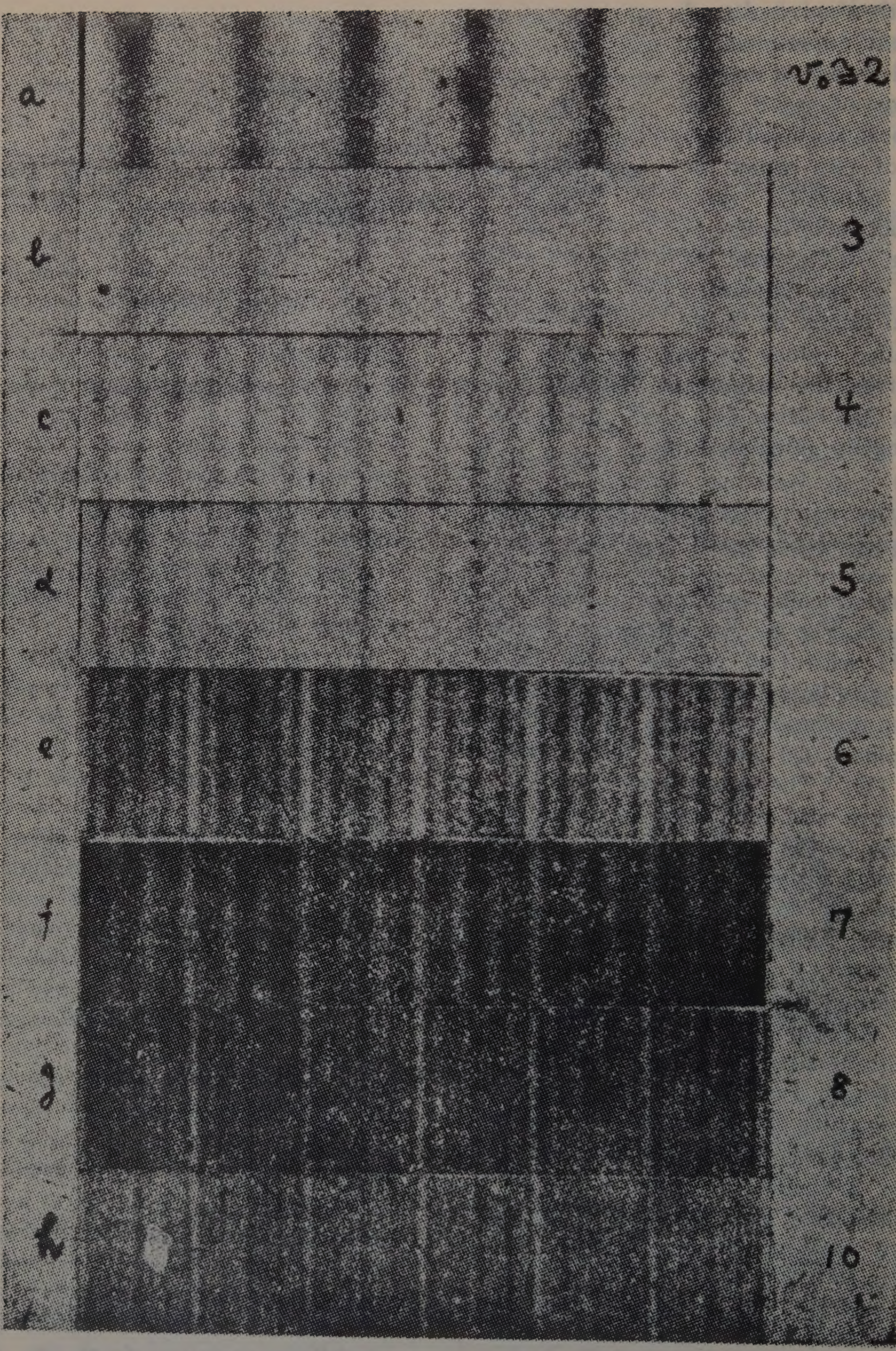

Fig. 3. Images of the stationary ultrasonic waves in the plane of maximum visibility.

accordance with theoretical curves for greater values of v_0($v_0 \geqq 7$)*. This, however, is, just the fact to be expected when we consider the limit of applicability of the basic assumption on the existence of pure phase lattice of our theory. According to Rytov(11), the pure phase-lattice assumption of the Raman-Nath's theory on the diffraction of light by ultrasonic waves fails to hold unless the following three conditions are satisfied:

$$u \equiv \frac{\pi \lambda L}{n_0 \Lambda^2} < 1, \quad \frac{vu}{2} < \frac{1}{4}, \quad \frac{v^2 u}{3} < \frac{1}{4} \qquad (5)$$

---

* Moreover, it was observed that the (first) plane of maximum visibility came somewhat nearer to the sound wave for greater values of v_0($v_0 \geqq 7$). This may be due to the formation of the amplitude lattice in the plane of emergence of light from the sound wave.

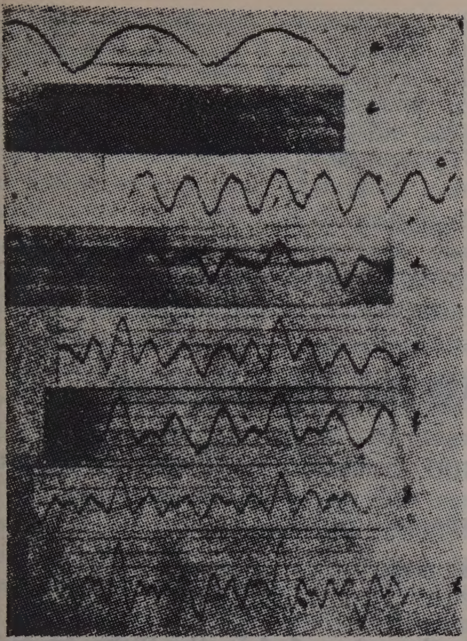

Fig. 4. Microphotometer curves of the Photographs of Fig. 3.

of which the third condition concerns on the linearity of the phase-lattice on v. Here the quantity n_0 means the refractive index of the medium. In the conditions of our experiments, where $L=2$ cm, $\Lambda=0.098$ cm, $\lambda=5.46\times10^{-5}$cm. $n_0\fallingdotseq1.54$, the third condition begins to fail for $v=5.68$. It may be rather by a chance that this somewhat arbitrary condition (5), where the inequality $>>1$ is replaced by $>1/4$, seems to give nearly a correct value for the limit of applicability of our theory in this case. At any rate we may conclude that the visibility curves of the stationary ultrasonic waves are given quantitatively well by our theory for the values of ultrasonic amplitudes corresponding to $0\leqq v_0<6$, and qualitatively well for $6\leqq v_0\leqq10$, under the above mentioned experimental conditions. Finally, Fig. 5 gives an example of a stationary ultrasonic wave of gradually varying intensities along the wave fronts. In this photograph, which was taken with the employment of a pin-hole as the light-source, we can perceive the gradual change of the fine structure with the increasing sound amplitude very well. Thus, these fine-structures of ultrasonic waves may be used for the purposes of intensity measurement or the test for uniformity of the ultrasonic wave field under appropriate conditions.

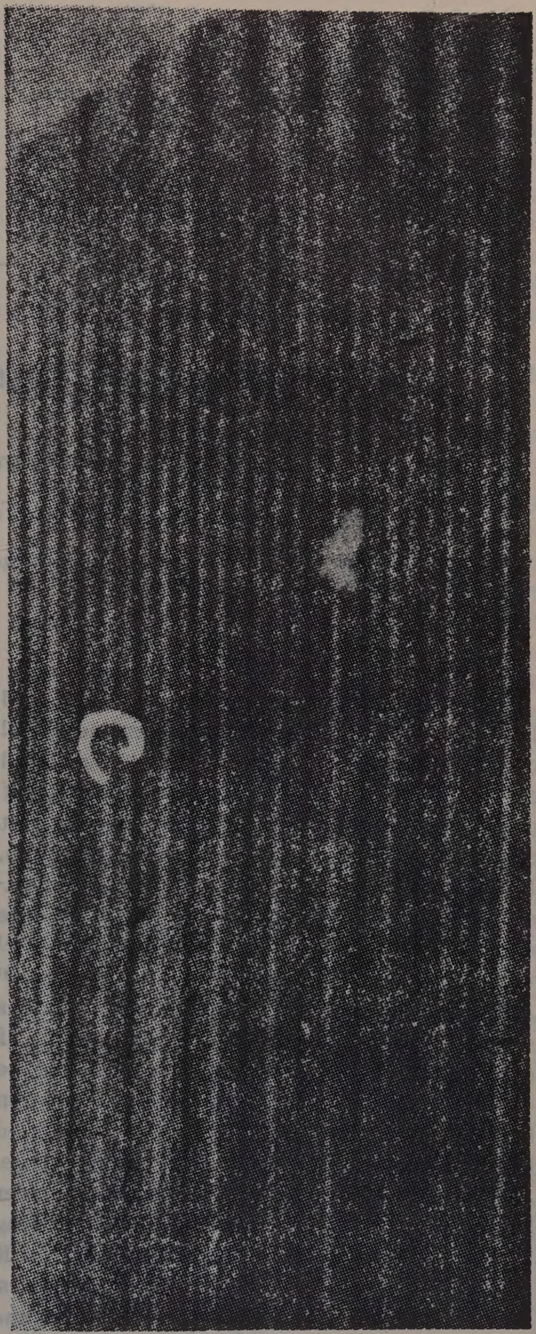

Fig. 5. Stationary ultrasonic wave with gradually varying intensity along the wave fronts.

References.

(1) O. Nomoto, Proc. Phys.-Math. Soc. Japan, **18** (1936), 402.

(2) O. Nomoto. ibid, **19** (1937), 337.

(3) O. Nomoto, ibid, **21** (1939), 493.

(4) C. V. Raman and N. S. Nagenda Nath, Proc. Indian Acad. Sci. (A), **2** (1936), 406, 413; **3** (1936), 75.

(5) R. Baer, Helv. Phys. Acta, **9** (1936), 265

(6) S. Parthasarathy, Current Science, **5** (1936), 136; Proc. Indian Acad. Sci. (A), **4** (1936), 555.

(7) N. S. Nagendra Nath, Proc. Indian Acad. Sci. (A), **4** (1936), 262.

(8) E. Hiedemann und E. Schreuer, Zeits. Phys. **107** (1937), 463.

(9) F. Mahler, Ann. Phys. **34** (1939), 689.

(10) O. Nomoto and S. Oka, Journ. Phys.-Math. Soc. Japan. (in Japanese), **14** (1940), 1.

(11) S. Rytov, Diffraction de la lumiere par les ultrasons. Actualites scientifiques et industrielles. No. 613. (Paris, 1938), p. 32–44.

Thermionic Constants of Platinum.

By Kenji KONDO.

Faculty of Science, Tokyo Imperial University.

(Received September 26, 1946.)

1. INTRODUCTION.

Since Richardson's famous work in 1901 and 1903, thermionic constants have been measured by numerous investigators for metals and semiconductors. Especially the problems of pure metals were believed to be solved. But the remarkably high value of A for platinum, 107.10 Amp/cm^2 deg^2, which Langmuir reported, drew attention again. In spite of the rigorus heat treatment, DuBridge's value(1) were high, i. e. $\varphi=6.27$ volts and $A=1.7\cdot10^4$ Amp/cm^2 deg^2. These abnormally high values were considered to be due to the effect of adsorbed layer of oxygen molecules, but he could not remove the monolayer of oxygen by heat treatment. Van Velzer(2) measured the constants in various outgassing stage. According to his results, in the pressure lower than 10 mmHg, in the stage of the outgassing of the filament at the temperature of 1755°K for 12 hours and of 1917°K for 15 minutes, $A=1.3\cdot10^8$ Amp/cm^2 deg^2 and $\varphi=7.4$ volts, and after the flashing at 1996°K for 15 minutes, for the first time $A=170$ Amp/cm^2 deg^2 and $\varphi=5.4$ volts. Thereafter Whitney(3) obtained the low values: $A=35$ Amp/cm^2 deg^2 and $\varphi=5.32$ volts by the enormously long heat treatment at comparatively low temperature.

The author obtained the slight low values of A and φ by the outgassing of comparatively high temperature for long hours. Especially the low value of φ is more important than that of A, because it is difficult to determine the value of A by the Richardson's line with high accuracy.

2. EXPERIMENTAL APPARATUS.

The sample is the purest one and its diameter is 0.03036 cm determined by a micrometer and weighing. One electron collector and two guard rings are made from nickel plate, and their diameters and lengths are 2 cms. The tubes of five types were made, but the final results were obtained by one of them. The pumping system consists of the two parts set in parallel. The one is constructed from the two oil diffusion pumps set in series and the pump in good vacuum side is of a Hickman's fractionating type and includes Octoil S oil. The other consists of a charcoal bulb and a mercury diffusion pump which was used in the outgassing of charcoal. During the outgassing, the parts were used in turn and during the measurement both parts were operated simultaneously. Pressure was measured by a Pirani gauge and an ionization gauge, of which sensitivity was 10^{-9} mmHg. Thermionic current was measured by the Northrup's galvanometer set at the sensitivity of $4\cdot10^{-9}$ Amp/mm. Collector potential was first taken from storage batteries, but afterwards using the circuit of a transformer, a rectifier and a voltage stabilizer, we were able to avoid large space and danger.

3. PROCEDURES.

The precise determination of temperature of filament was based on the temperature heating current relation given by van Velzer(2). Heating current was obtained from storage batteries of large power and measured by the standard resistance and the potentiometer.

The cleaning up of a tube is as follows: at first it was cleaned with dilute acid and alkali solutions. And then the baking of glass parts including a liquid air trap was continued for 140 hours at the temperature of 450°C in the electric furnace, and stopped when the vacuum of 10^{-5}~10^{-6} mmHg was attained. The metallic part of the tube except filament was outgassed by the induction furnace for 10 minutes repeatedly before the outgassing of a filament and the measurement.

The first stage of outgassing. The measurement of the filament which was not outgassed, revealed that the curve of $\log_{10} i$ *vs* $\sqrt{F}$ was concaved downwards, where i is current and F is the applied electric field on the surface (Fig. 1). The deviation from Schottky's law was remarkable and did not saturated up to $F=10^4$ volt/cm in the same manner like a composite surface. The effective surface force which attracts an electron toward the surface, deviates from the image force and its functional form is as follows: $F=5.71\cdot10^{-2}/s$, where s is the distance from the surface in cms. This force is enormously large compared to the image force in the range of $s>10^{-5}$ cms. It is impossible to consider this field as the potential of a single type. It may be considered that the patch field attracts the emitted electrons and makes the large space charge in front of surface. This new field is possibly of long range. That is, this current is the space charge current, and probably $i \propto F^{3/5}$.

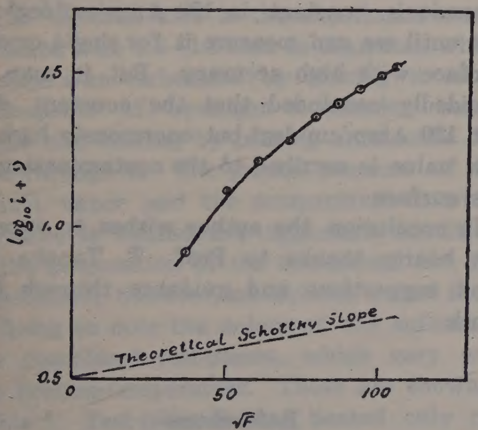

Fig.

The second stage of outgassing. After the outgassing at 1800°K for 15 minutes, the Schottky's curve was straightened but its slope was higher twice or three halves times than the theoretical value. The thermionic constants in this stage are: $A=1.18\cdot10^{-9}$ Amp/cm² deg² and $\varphi=1.6$ volts. From the low value of the work function, a monolayer of electropositive molecules, probably hydrogen, is presumed to exist.

The third stage of outgassing (Fig. 2a). After the baking of metallic part for 90 minutes and that of the filament at 1860°K for 120 hours, the vacuum of $8\cdot10^{-8}$ mmHg was gained. But in this stage the thermionic current was not completely reproducible yet, and the Richardson's line were discontinuous at the temperature of 1700°K. From the measurement of the lower region than 1700°K, the thermionic constants are as follows: $A=4.10\cdot10^3$ Amp/cm² deg² and $\varphi=5.59$ volts. In the higher region, the measured points were insufficient to determine the constants, but the presumed value of work function was 4.02 volts. Accordingly, at the temperature higher than 1700°K, the adsorbed layer, presumably a monolayer of oxygen is considered to evaporate remarkably. Owing to Roberts' measurement of the accommodation coefficient of tungsten, oxygen film was removed at 1900°K, and especially, as Whitney(3) could obtain the comparatively clean surface by the outgassing at 1730°K, the author considers that it is possible to clean the surface of

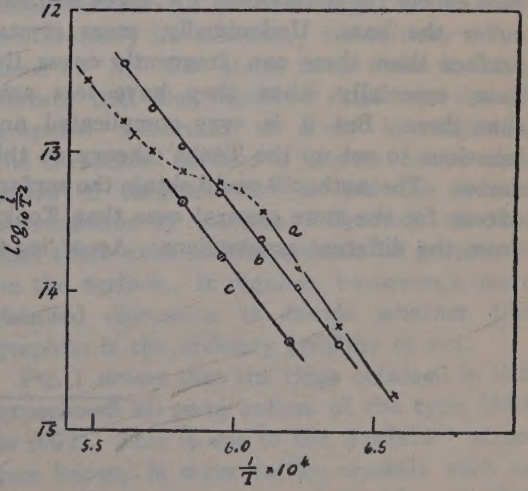

Fig. 2

platinum by the outgassing at the temperature from 1700 to 1800°K for long, long hours, if good vacuum can be sustained.

The fourth stage of outgassing (*Fig. 2b*). After the baking, i. e. at 1860°K for 140 hours, the discontinuity was disappeared. And the attained vacuum was better than $4\cdot10^{-8}$ mmHg. The value of constants were $A=432.5$ Amp/cm² deg² and $\varphi=5.08$ volts. These values are reasonable compared to DuBridge's results. But the higher value of work function compared to the other metals is the evidence that the oxygen layer is not completely removed.

The fifth stage of outgassing (*Fig. 2c*). The raising of the outgassing temperature to 1925°K changed the current again. After the final outgassing at 1860°K for 144 hours and at 1925°K for 12 hours, the current was stable and reproducible. Further baking did not change the current. The measured values are as follows: $A=92.8$ Amp/cm² deg² and $\varphi=4.72$ volts.

4. DISCUSSIONS.

As the thermionic current is the phenomenon on the surface, it is very important to know the true area of the surface. Especially A depends directly upon the true area. To this time Roberts concluded that the surface excess defined by him as the ratio of the difference between the true area and the apparent area to the apparent area was about 10% from the measurement of the accommodation coefficient of tungsten and Langmuir inferred that it was 40%. Theoretically Tonks(4) computed the surface excess for some cases, i. e., three surfaces cover the base. Undoubtedly, more crystal surface than three can frequently cover the base, especially when they have less area than three. But it is very complicated and laborious to set up the Tonks' theory on this factor. The author(7) could obtain the surface excess for the more general case than Tonks' from the different assumptions. According to it, when four surface cover the base and any sharp edges do not exist, the surface excess is about 0.11, and when more surfaces, i. e., thirteen surfaces cover the base, it is about 0.47. These values are in fair agreement with the observed values of Roberts and of Langmuir. If the lower limit of 6s-bands of platinum is about 13.4 eV, the transmission coefficient of an electron through the potential barrier is 0.938.(5) Adopting 4.72 eV as the value of work function and 9.50 eV as the Fermi energy at the absolute zero temperature, the correction of the temperature coefficient of work function is 1/0.576 times according to Seely's simple theory.(6) If we assume the surface excess to be 0.10, 0.25 or 0.40, from the author's observed value of $A=92.8$ Amp/cm² deg², we get respectively 156.0, 137.3 or 122.6 Amp/cm²deg² for thermionic constant A. Although these values are in good agreement with theoretical value of 120 Amp/cm²deg², we must postpone to decide whether the thermionic constant is 120 Amp/cm²deg² or not until we can measure it for single crystal surface with high accuracy. But it may be decidedly concluded that the constant A is not 120 Amp/cm²deg² but enormously high or low value is ascribed to the contamination of the surface.

In conclusion the author wishes to express his hearty thanks to Prof. T. Tanaka for kind suggestions and guidance through this work.

References.

(1) L. DuBridge: Phys. Rev. **31** (1928), 736, **3**

(1928), 961.

(2) Van Velzer: Phys. Rev. **44** (1933), 831.

(3) L. V. Whitney: Phys. Rev. **50** (1936), 1154.

(4) Tonks: Phys. Rev. **38** (1931), 1030.

(5) H. A. Bethe: Handbuch der Physik 24/II.

(6) Seely: Phys. Rev. **59** (1941), 75.

(7) The detail of this computation will be reported with another problem of thermionics in the later paper.

Investigation of Carbonised Tungsten Surfaces by the Method of Electron-diffraction.

By Ryozi UYEDA, Sinkiti ITO and Kazuo KIMOTO.

Cathode-ray Laboratory, Physical Institite, Faculty of Science, Nagoya Imperial University.

(Received October 3, 1946.)

The investigation of carbonised tungsten, i. e. tungsten carbide, by means of X-rays has long been undertaken(1), but the analysis by electron-diffraction of the same has not yet been made. The authors have made such an investigation, though a very rough one, and wish to report a summary of it in the following.

The material used in the experiment was a tungsten wire 0.8—1.0 mm. in diameter, whose surface was carbonised by placing it in an atmosphere of hydrogen containing benzol vapor and heating by passing an electric current through it. The partial pressure of the benzol vapor and the temperature to which the wire is heated are important conditions in the preparation of the test-pieces. In this experiment, however, we did not record them, sufficing to note the colors of the sufaces in the completed test-pieces, which vary with the heating-temperature. These are shown in Table I. Test-piece X was heated only red-hot, while the others were all heated to a white glow; the temperature of carbonising being higher in the sequence Y, Z, A, B, C. These test-pieces were cut into lengths of 2—3 mm., and fixed on the specimen holder of the electron-diffraction apparatus with a small amount of *aqua-dug*. The apparatus used was a small-scale one designed by the author(2).

Table I.

Test-piece	Color of Surface
X	Black (velvety)
Y	Grayish-black
Z	Grayish-black
A	Blackish-gray
B	Whitish-gray
C	White (lustrous)

The diffraction patterns of these test-pieces were all uniform Debye-Scherrer rings, whose diffuseness and intensities varied greatly with each test-piece, though their radii were approximately the same. This is illustrated in Fig. 1, where the reciprocal $1/d$ of the spacing, which is proportional to the radius of the rings, is taken as abscissa, and the intensity as estimated by inspection is plotted against it. Further the values(3) of $1/d$ are given in the right-hand side of Table II.

As the surface of test-piece X seems to be covered by soot on inspection with the naked eye, the results obtained above are compared with X-ray data for graphite(4)(5). The latter is shown in the first line of Fig. 1 and the left-hand side of Table II. The comparison shows that the rings 'b', 'd' and 'f' coincide well with *(100)*, *(110)* and *(200)* respectively for graphite, while ring 'a' approximately coincides with *(002)*. The rings 'c' and 'e' are probably the secondary and tertiary reflections of 'a'. The above facts make it fairly certain that the observed rings are due to graphite. According to X-ray investigation, the carbonised surface is known to be composed of tungsten carbide; but the present investigation by electron diffraction clarified that there exist minute crystals of graphite(6) on the surface. It requires, however, a more detailed discussion to decide whether this graphite is the ordinary graphite or not.

Fig. 1 shows that the rings obtained in this experiment all gave indices of the type *(hk0)* or *(001)*. This is due to the Arnfeld(7) structure known in layer lattice crystals such as graphite. In this structure, it is known that the *(hk0)* ring is assymetric in intensity and

Table II.

Graphite (X-ray data)				1/d (result of this experiment)					
Index	Int.	d	1/d	Testpiece	X	Y	Z	A	C
002	v.s.	3.379	0.294	a	0.279	0.278	0.290	0.275	0.277
100	m.s.	2.13	0.469	b	0.469	0.469	0.469	0.469	0.469
101	s.	2.03	0.492						
102	f.	1.80	0.555						
104	s.	1.70	0.588	c		0.561	0.564	0.564	
103	m.s.	1.55	0.645						
104	f.	1.33	0.751						
110	m.s.	1.23	0.813	d	0.915	0.814	0.820	0.815	0.818
112	m.s.	1.16	0.862						
105	f.	1.15	0.869						
106	m.s.	1.13	0.885	e				0.858	
200	f.	1.07	0.943	f		0.937	0.939	0.939	
201	f.	1.05	0.952						
202	f.	1.02	0.980						

diffuses outwards. We see from Fig. 1 that this assymetry is cleary present in the rings 'b' and 'd'

It is also observed, as shown in Fig. 1, that the positions of the rings 'a', 'c' and 'e' are displaced slightly inwards from where they would be expected. This implies that the spacing of the netplane (*002*) has expanded, and the percentage of expansion is about 4.5 %. A phenomenon similar to this is known

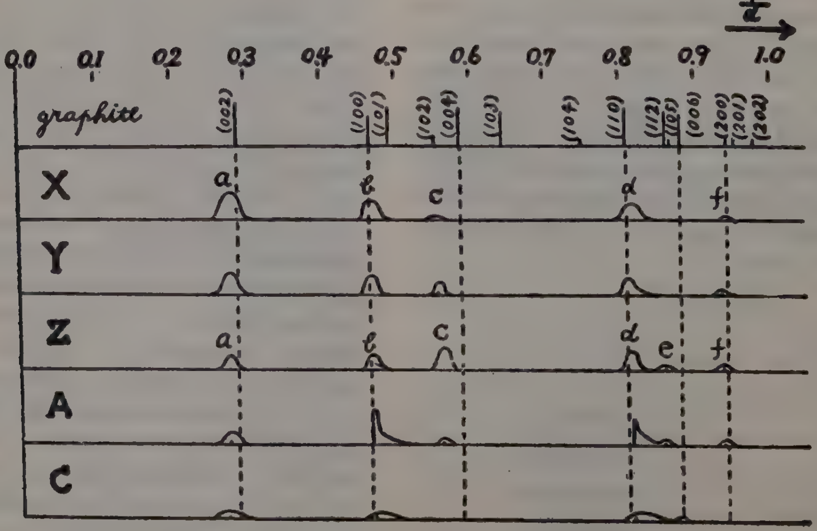

Fig. I.

in the study of carbon black(8)(9).

In test-piece X, the breadths of both *(001)* and *(hk0)* rings are nearly equal; and it is estimated that the minute crystals possess a magnitude of 10—20 A in either direction. As the carbonising temperature rises, the breadths of the *(001)* rings slightly decrease, while in the *(hk0)* rings the inner sides become sharper. This shows that, as the carbonising temperature rises, the graphite crystals grow in a plate-like form perpendicular to the c-axis. This tendency is most remarkable in test-piece A, where the area of the plate is estimated to be more than 100 A × 100 A, while its thickness is about 20 A. On a further rise in temperature, the rings become diffuse again, showing that the crystals become smaller. It is commonly known that the crystals are small when the temperature is low, and grows the more, the higher the temperature rises. That they become smaller again when the temperature rises further is presumably due to the fact that the crystals fuse into the basic metal at such a rate that they have no time to grow amply. In test-piece C, the surface possesses a metallic lustre and the diffraction rings are very faint, which leads us to conclude that here the surface is naked for the most part with minute crystals of graphite adhering here and there.

The intensity of ring 'c' increases with the temperature, attains a maximum in test-piece Z, and then falls off again. In Fig. 1 the intensity of 'c' in test-piece Z is shown greater than that of 'a', but as the latter lies very near the center, the comparison is difficult. Such a change of the intensity of *(004)* could not occur in pure graphite. The cause of this is not clear, but it is presumably due to the presence of impurities in the graphite crystals, and it is conceivable that there is also some correlation with the above mentioned expansion of the *(002)*-spacing.

In conclusion we express our scincere thanks to Professor R. Sagane for his encouragement throughout this work, and to Mr. T. Kuno and the members of the Research Laboratory of the Communication Apparatus Division of the Tokyo Shibaura Electric Co., Ltd. for providing the test pieces. We are also indebted to the members of the Electron-diffraction Society for many discussions and criticisms.

References.

(1) Becker: Z. f. Metaklunde, **51** (1928), 437.

(2) Uyeda: The X-ray (printed in Japanese) **4** (1944), 28.

(3) These figures are not the values of 1/d as determined directly from the observed values; for compensations have been made for the error in determining the centers of the rings. The compensation is such as to make the 1/d of ring 'b' coincide with the 1/d of *(100)* in graphite

(4) Hassel and Mark: Z. P. **25** (1924), 317.

(5) Finch and Wilman: Proc. Roy. Soc. **115** (1936), 345.

(6) Aquadug shows sharp rings of graphite. The contamination of aquadug is perfectly excluded in this experiment.

(7) Warren: Phys. Rev. **59** (1941), 693.

(8) Miwa: Sci. Rep. Tohoku Imp. Univ. Jap. **23** (1934).

(9) Hofmann and Wilm: Z. Elektrochem. **42** (1936), 504.

Ueber die Abnormale Rotation des OH Molekuels (III).

Von Hiromu WAKESIMA.

(Eingegangen am 18 Oktober, 1946.)

EINLEITUNG

Im vorigen Berichte(1) hat der Verfasser aus der Beziehung zwischen der Intensitaetverteilung des OH Bandes bei 3064 A und der Stromdichte einer Geisslerentladung durch Wasserdampf den Schluss gezogen, dass der Ursprung jeder Linien des Bandes das vom H_2O Molekuel dissoziert angeregte Radikal sei. Da man deshalb aus der Intensitaet des Bandes ersehen kann, wie haeufig das Radikal in einzelnen Rotationszustaenden bei der Dissoziation auskommt, waere es die naechste Frage vom Bedeutung, zu sehen wie weit die Experimentalbedingung den Einfluss auf dieser relativen Hauefigkeit hat. Wird die Temperatur der Entladungsroehre z. B. erhoeht, so vermehren sich die H_2O molekuele in hoeheren Schwingungs-und Rotationszustaenden und die angeregte Radikale aus der Dissoziation solcher Molekuele, verstaerkt sich dementsprechend irgend einer Teil des Bandes; aus der Analyse dieser Aenderung waere etwas naeheres von der abnormale Rotation des Molekuels zu erblicken. Im Hinblick darauf hat der Verfasser die Temperatur der Entladungsroehre im weiten Bereiche geaendert und die Intensitaet des Bandes photometrisch untersucht.

Fig I

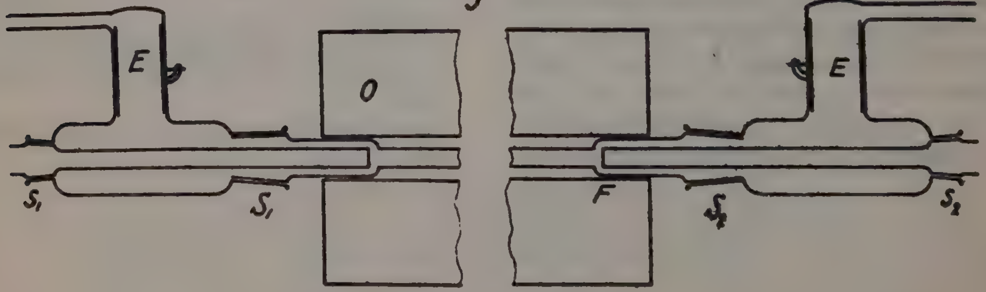

EXPERIMENTELLS UND RESULTATE.

In Fig. 1 ist die Entladungsroehre schematisch gezeigt. Eine Quarzroehre wird an den Schliffen S_1 S_2 den Telexglasroehren gekittet, die die Elektrode aus Aluminium E enthalten. Vom Schliff S_1 erstreckt sich ein zweiter Quarzzylinder mit einem Fenster F durch die Glasroehre bis zum Ofen O. Das Licht aus dem Fenster kam also von der positiven Saeule mit einer gleichmaessigen Temperatur und mit einem einheitlichen Emissionszustand, ohne von der Absorption des kuehleren Teiles verstoert zu werden. Um die Temperatur zu messen wurde ein Pt.—Pt.Rh. Thermoelement gebraucht. Waehrend der Entladung, floss der Dampf aus dem destillierten Wasser dauernd durch eine Kapillare in die Roehre ein und daraus abgepumpt. Durch den Waehlen von Kapillare mit passender Weite und dem Widerstandes angemessener Groesse zwischen der Entladungsroehre und dem Pumpe, wurde der Druck in der Roehre stets 0.7~0.8 mmHg, der Dampffluss moeglichst gering gehalten, soweites die Verunreinigung gestattete, um der Unterschied der Temperatu zwischen dem Thermoelemente und dem Dampfe klein zu halten. Der Entladungsstro war etwa 20mA. Zum Photometrieren wurd

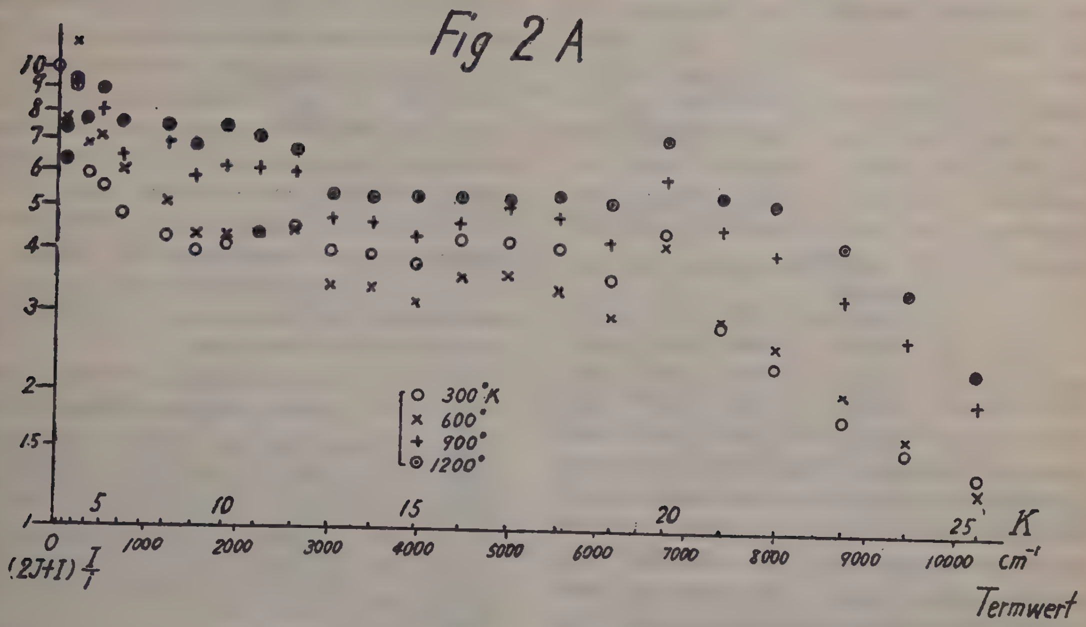
Fig 2 A

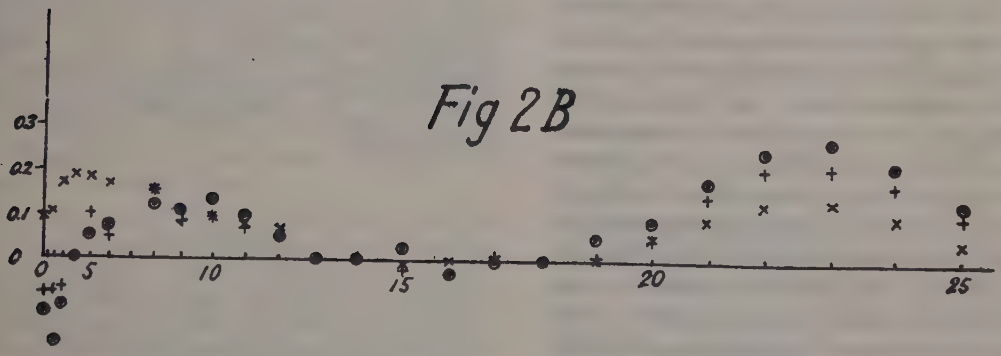
Fig 2B

ein Stufenkeil aus Quarz mit Pt. Ueberzug vor dem Spalte des Spektrographen gesetzt.

Die Messung wurde wie frueher fuer Q_1—Zweig ausgefuehrt. In Fig. 2A gibt die Ordinate die abgemessene relative Intensitaet I jeder Linien bei 300°K, 600°K, 900°K und 1200°K, mal statistisches Gewicht $(2J+1)$, durch Intensitaetfaktor i; also die relative Anzahl der angeregten Radikale, in logarithmischer Skala. Die Abzissa gibt den Termwert einzelner Rotationszustaende.

Die relative Zahl aendert sich mit der Temperatur auf nicht so einfacher Weise. Aber wohl gemerkt, die Aenderung des Teiles von den Laufzahlen $K=13$ bis 18 ist ziemlich einfach: Die relative Anzahl in diesem Gebiet verschiebt zwar in Bezug auf dem ersten Terme, aber die Aenderung untereinander mit der Temperatur ist recht klein. Wenn man also den vier Verteilungen passende relative Verschiebungen in der Richtung der Ordinate gibt, so kann man diesen Teil in grober Uebereinstimmung zu bringen. Das Verhaeltnis der relativen Zahlen von 600°K, 900°K und 1200°K zu 300°K wird dann in diesem Bereich fast 1, geht aber in kleineren und groesseren Rotationszustaenden auseinander. (Siehe die Fig. 2B).

Wie man ersieht, aendert sich die relative Anzahl fuer $K=1\sim12$ und $K=19\sim25$ (der letzte gemessene Terme) mit der Temperatur regelmaessig, besonders fuer $K=19\sim25$ vielmehr auf einfacher Weise. Besprechung der Ergebnisse. Die Thermodissoziation $H_2O \rightleftarrows H+OH$ kommt in unserem Temperaturbereich nicht in Frage. Der Dissoziationsgrad erreicht bei 1200°K nur die Ordnung 10^{-5}(2). H_2O Molekuel hat drei Grundfrequenz der Schwingung; a) $\nu_{//}=3600$ cm^{-1}, b) $\nu_{\perp}=3756$ cm^{-1}, c) $\delta=1595$ cm^{-1}. Die entsprechende Energie fuer Quantenzahl $v_n=0$ und 1 ε_0, ε_{a1}, ε_{b1}, ε_{c1} nach dem Formel $\varepsilon=hc\omega_n\Sigma(W_n+1/2)$ sind 8.78, 19.37, 19.85, 13.47×10^{-13} erg. Bolzmannsche Verteilung in den Schwingungszustaenden des H_2O Molekuels gibt die folgende relative Anzahl.

	Energie Temperatur	ε_{a1}	ε_{b1}	ε_{c1}
$\log_{10} e^{-\frac{\varepsilon}{KT}} \Big/ e^{-\frac{\varepsilon_0}{KT}}$	300°K	9.50	10.54	3.30
	600°K	4.75	5.27	1.65
	900°K	3.17	3.51	1.10
	1200°K	2.38	2.64	0.83

Fast alle molekuele H_2O dissozieren also bei 300°K vom Niveau ε_0 und meiste sogar bei 1200°K. Wenn man die Funktion, die die Wahrscheinlichkeit gibt, mit welcher eine beliebig ausgenommene Dissoziation des H_2O in einem bestimmten Schwingungszustand ohne Rotation durch Elektronenstoss das angeregte OH Radikal in einem bestimmten Rotationszustand erzeugt, kurz Dissoziationsfunktion nennt, koennte die Verteilung des Wertes $(2J+1)I\ i$ ungefaehr als die Rotation des Wassermolekuels fuer jede Temperatur gestoerte D. F. vom Niveau ε_0 angesehen werden. Diese Temperatureinfiuss vermehrt oder vermindert die Rotationsenergie des OH nach der Drehungsrichtung des H_2O um den Betrag, was mit der Rotationsenergie des H_2O und die des OH ohne Stoerung waechst. Die Stoerung uebt deshalb abflattenden Einfluss auf der D. F. aus und stark temperaturabhaengig.

Die D. F. haenge im Allgemeinen vom Potentialfeld der Molekuele bei der Anregung und die Lage des zu scheidenden Atom, aber nicht von der Geschwindigkeitverteilung der Elektronen in der Entladungsroehre ab(3). Waere also die Veraenderung der Verteilungskurve nur diesem Temperatureinfluss zuzuschreiben, so wuerde sie hinweisen, dass die D.F. vom ε_0 aus zwei Maxima habe, naemlich ein schmales an $K=1\sim4$ und ein breites an $K=12-18$. Wieweit die D.F. vom ε_{c1} aus drin beeinfliesse, steht noch offen. Naeheres wird an anderer Stelle diskutiert.

Es ist mir eine angenehme Pflicht, Herrn Prof. Dr. T. Tanaka der Kaiserlichen Universitaet zu Tokyo fuer das Interesse an dieser Arbeit und manche wertvolle Ratschlaege meinen besten Dank auszusprechen. Ich bin auch Herrn Hayakawa an der Kaiserlichen Universitaet zu Nagoya fuer seine wertvollen Diskussionen zum herzlichsten Dank verpflichtet.

Es soll hier noch hinzugefuegt werden, dass diese Arbeit teilweise mit Hilfe der von dem Unterrichtsministerium und dem Nippon Gakujutsu Shinkokai gestifteten Praemie zur Foerderung der Naturwissenschaften, ausgefuehrt wurde

Literaturen.

(1) Proc. Phys.-Math. Soc. Japan **24** (1942), 367.

(2) Dissoziationskonstante K_p betrug $-l_nK_p=33.4$.

(3) Die Geschwindigkeitkonstante der Elektronen sei konstant: Siehe A. v. Engel und Stehenbeck: Elektrische Gasentladungen, S 85.

Electron-Diffraction Study on Behaviors of Metals deposited on Crystal Surfaces. Part I. Metals deposited on Galena.

By Shizuo MIYAKE and Mieko KUBO.

Kobayashi Institute of Physical Research, Kokubunji, Tokyo.

(Read April 29, 1946; Received November 26, 1946.)

§1. INTRODUCTION.

There are already many investigations on the preferred crystalline orientation of metal films, deposited on fresh surfaces of cleaved crystals by the vaporization method in vacuo(1). The present authors have developped a systematic study of this phenomenon by the electron diffraction method, for many kinds of base crystals and metals at varied base temperatures, in order to accumulate the experimental facts ample to conclude some determining laws, namely some regular relationships in this phenomenon between the lattice of the base crystal and of the metal, which are in contact with each other.

The author previously investigated six differnt metals deposited on the cleaved surface of zincblende (ZnS)(2). Extending this study, a case of the galena crystal as the base is tried. Unexpectedly, however, it is found that the orientation of metal crystals is not the main process in this case. Instead, a more complicated phenomena, including the chemical reaction and the solid diffusion of metal atoms, is more predominant one, especially at high temperatures. In the present experiment an observation on these processes is performed in some detail by the electron diffraction method.

§2. EXPERIMENTAL PROCEDURE.

The heating of the sample (from room temperature to 500℃) and the vaporization of metals are carried out in the diffraction camera(3). The change of the diffraction pattern after the vaporization is continuously observed on a fluorescent screen, or by photographs.

Vaporized metals now examined are copper, iron, and nickel. Vaporized quantities are varied from about 20 A to 200 A in the mean thickness of the deposited metal films.

Fresh and smooth surfaces of galena here used are made by cleaving the crystal having a good nature.

§3. EXPERIMENTAL RESULT.

The phenomena which take place on the galena surface after vaporizing metal on it, are in general of exceedingly complicated nature. The diffraction pattern sometimes shows a very rapid change, especially at higher temperature, even in a period of only few seconds, and moreover, the surface products are not always simple. For the convenience of description, therefore, the entire process after the vaporization will be divided into the three stages as follows: *1. The initial stage.* This corresponds to a state of the surface during a period of few seconds after the vaporization. (Although, as a matter of fact, changes in pattern take place even during this interval and are sometimes too rapid to be caught by photograph.) *2. The second stage.* The pattern corresponding to the initial stage then generally changes its type within few seconds to few minutes. The second stage corresponds to the result of this change, whereby the base temperature is the same as in the preceding stage. *3. The third stage.* The state on the surface always receives a further change, when the base temperature is gradually raised after the vaporization. The third stage indicates the result of this afterward heating.

In the Tables I—III the surface products and the types of the orientations of these products are summarized. In fact, however, exceptional cases sometimes take place. Accordingly, it was necessary to simplify the fact to some extent in order to make these Tables.

Table I. Cu.

1. *The initial stage.*

Temperature of base.	State and substance.
Room temperature	Amorphous-like Cu.
100°–250°C	Cu (Spot)*
200°–300°C	Pb (Spot)** and Cu (Ring)
300°–400°C	PbS (Original surface) and Cu_2O (Spot)***

* Orientation: (110)Cu‖(001)PbS, 〔111〕Cu‖〔110〕PbS. Four possible orientations are superposing.

** Orientation: (001)Pb‖(001)Pbs, 〔010〕Pb‖〔010〕PbS.

*** Orientation: (001)Cu_2O‖(001)PbS, 〔010〕Cu_2O‖〔010〕PbS or
(111)Cu_2O‖(001)PbS, 〔110〕Cu_2O‖〔010〕PbS.

2. *The second stage.*

Temperature of base.	State and substance.
Room Temp. –200°C	No noticeable change
230°–300°C	Pb–spots disappear while 1–5 minutes. Then Cu–rings also disappear, leaving behind only PbS (Original surface).
300°–400°C	PbS (Original surface), Unknown substance I*, and faint Cu (Ring).

* Tetragonal a=10.92, c=12.40A, (001)I‖(001)PbS, 〔100〕I‖〔100〕PbS

3. *The third stage.*

At the highest temperature (450°–500°C), there remains in general only the original smooth surface of PbS, or the roughened surface of it due to surface attacking, and sometimes the unknown substance I. In the intermediate temperatures the formation of Cu_2O (Spot) and Cu_2O (Spot) can be detected.

Table II. Fe.

1. *The initial stage.*

Temperature of base.	State and substance.
230°–280°C	Amorphous pattern or diffuse rings of Fe.
300°–420°C	FeS I (Spot* and ring)
440°–480°C	FeS (Ring), FeS II (Spot)**

* Orientation: Fibrous structure (101)FeS‖(001)PbS

** Orientation: (001)FeS‖(001)PbS, 〔110〕FeS‖〔010〕PbS

2. *The second stage.*

Temperature of base.	State and substance.
230°–280°C	γ–Fe_2O_3*(Ring) is superposed.
300°–420°C	γ–Fe_2O_3(Sometimes FeS remains).
440°–460°C	γ–Fe_2O_3 (Ring or spot)**, rough surface of PbS. (In seldom cases FeO).

* No distinction between γ-Fe_2O_3 and Fe_3O_4 on account of the similar lattice of these two substances. $(111)\gamma\text{-}Fe_2O_3 \parallel (001)PbS$. $[110]\gamma\text{-}Fe_2O_3$ $[010]PbS$.

3. *The third stage.*

At the highest temperature (450°–500°C) only γ-Fe_2O_3 rings remain.

Table III. Ni.

1. *The initial stage.*

Temperature of base.	State and substance.
Room temperature.	Ni (Diffuse ring)
150°–200°C	Ni (Ring)*
300°–450°C	Ni (Ring), Unknown substance II (Spot)**, NiS_2 (Ring), and NiO (Ring).

* Generally a fibrous structure $(110)Ni \parallel (001)PbS$

** Cubic structure $a=7.74$A being $(001)II \parallel (001)PbS$, $[110]II \parallel [010]PbS$.

2. *The second stage.*

Temperature of base.	State and substance.
Room temp. to 300°C	No noticeable change.
300°–350°C	Pattern becomes obscure.
350°–450°C	NiO (Ring), Unknown substance II and PbS (Rough surface).

3. *The third stage.*

At 450°C ring-patterns of NiO or NiS_2 remain.

§ 4. DISSCUSSION.

Now, some remarkable phenomena in the observed process will be described below.

1. The chemical reaction. At lower temperatures, the diffraction patterns are in general corresponding to that of the vaporized metals, with or without some preferred orientations. But at higher temperatures, there are many cases where the patterns due to metals do not appear, even in the initial stage. In these cases, various chemical reactions readily take place between metals and the galena surface, and very frequently the formation of sulphides, oxides and other unknown substances are resulted in.

One of the most conspicuous process among them are the separation of pure lead from galena. Namely, when the copper is vaporized on the surface, a spot pattern of lead makes its appearance in the initial stage, in a temperature range 180°—300°C. In it, rings due to copper or cuprous oxide are generally overlapping on the Pb-spot pattern, but sometimes exclusively Pb-spot appears, in the case where the vaporized quantity of copper is comparatively scanty. This type of reaction seems to take place instantaneously when copper vapor reachs the surface. The preferred orientation of the separated lead is fairly perfect at first, but degenerates into rings soon. (Figs. 1a—1b).

Other chemical processes to be noted here are the formation of sulphides such as Cu_2S, NiS_2 and FeS, and of oxides such as Cu_2O, NiO, γ-Fe_2O_3 and FeO. The formation of oxides is not due to residual air in the diffraction camera, since the similar reaction could be ascertained only in fewer cases when zincblende is used as the base crystal. The oxidation process on galena as observed seems to be due to the peculiar property of this crystal, presumably because it contains much oxygen, although whether the oxigen in it exists in a form of some oxides, or in an occluded state in lattice, is not sure.

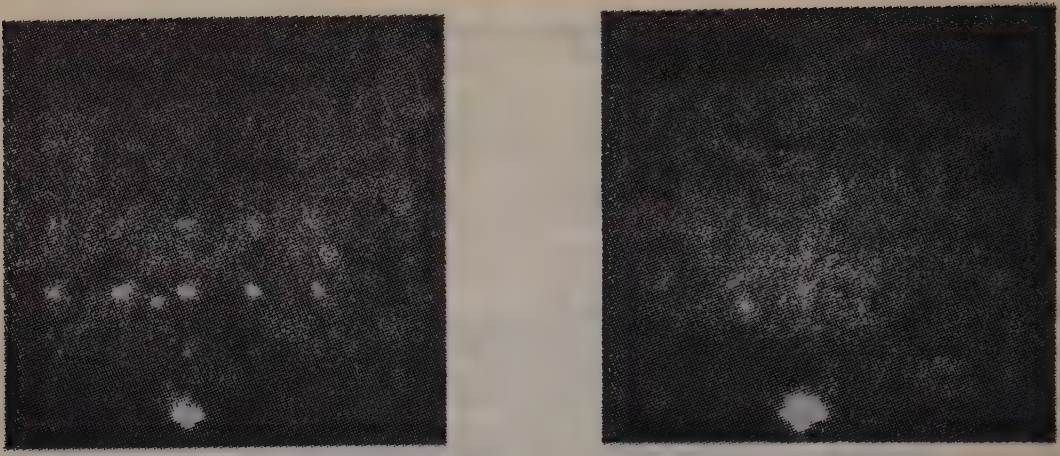

a. Just after the vaporization of Cu at 310°C. The spots are corresponding to Pb.

b. Shortly after of Fig. 1–a. The ring pattern corresponds to Cu_2O and Pb, degenerated from Pb spot pattern of Fig. 1–a. The pattern from PbS surface also begins to appear as the result of the diffusion of metals on it.

Fig. 1. Vaporization of Cu on to Galena.

2. The diffusion process. The spot pattern due to lead, which is made visible on vaporizing the copper, remaines itself for some half a minute, but the spots soon begin to degenerate into rings, and then these rings gradually fade away. Finally they disappear in about one or two minutes, leaving behind only copper rings. This phenomenon seems to be corresponding to the diffusion, in which lead separated on the surface is absorbed into the crystal. (Figs. 1a—1b).

Another more amazing example of the diffusion phenomenon is shown in Figs. 2a—2c, which is corresponding to the case where copper is vaporized on galena at 220°C. At first the pattern of copper appears with a certain orientation. When the temperature is raised to 275°C, spots become somewhat sharper, and then this copper pattern rapidly disappears. The last change completes in only few seconds, leaving behind the pattern of the galena surface only. This galena pattern shows sharp layer-lines and fair Kikuchi lines, indicating that thus recovered surface is maintained unchanged, kept almost the same as before the vaporization. To explain such an observation, there seems to be no other way than to consider it that, the copper atoms are absorbed under the surface during this short period by the diffusion. The similar effects are more frequently observed at higher temperatures, but accompanying other complicated chemical processes.

Disappearance of the metal from the surface could be also observed in the case of nickel.

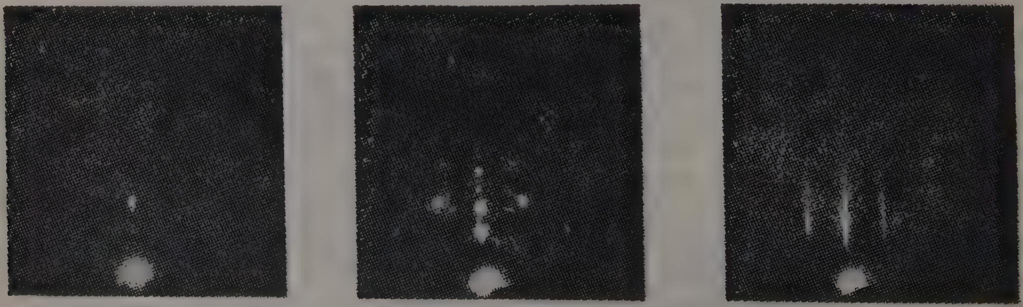

a. Just after the vaporization of Cu at 220°C. Rings and spots are due to Cu.

b. Temperature of base crystal is raised to 275°C.

c. 30 second after of photo. b. Pattern is corresponding to PbS surface.

Fig. 2. Diffusion of Cu inwards Galena.

3. Unknown substances. In the present experiment, two unidentifiable substances can be detected, whose lattices do not correspond to any substances ever studied by X-ray analysis. The one of these is formed in the case of copper at high temperatures, which is body-centered tetragonal, the lattice constants being a=5.46 A, c=12.40 A, showing a good orientation. Judging from the distribution of spot intensities, this lattice seems to be as if a super structure of face-centered tetragonal lattice with a=5.46 A, c=6.20 A.

The other unkown substance occured in the case of nickel in a temperature range 300°—450°C, whose lattice being face-centered cubic with a=7.74 A. It is reported in X-ray analysis that $Pb(NO_3)_2$ is a cubic crystal with the lattice constant a=7.84 A, but the formation of such a substance in the present case is not plausible, although it can not be utterly rejected from its possibility.

These substances are stable even if the temperature is lowered to room temperatures from the temperature of the formation.

5. Two forms of FeS. In the case of iron, a formation of two forms of ferric sulphide can be detected, the one (FeS II, hexagonal, a=5.95, c=11.7 A, being a super structure of FeS I.) is formed at higher temperatures, and the other (FeS I, hexagonal, a=3.43, c=5.79A.) at lower temperatures. According to Haegg and Sucksdorff(4), FeS II corresponds to a ferric sulphide with its iron and sulpher contents near 50—50%, but when sulpher content exceeds it by about 2%, the ferric sulphide takes the form of FeS I. Since, in the present experiment, the specimen to be examined is placed in a high vacuum of the diffraction camera, the sulpher content may decrease to its lower limit at higher temperatures, tending to near the value corresponding to the stoichiometric ratio of FeS.

References.

(1) See G. P. Thomson and Cochrane: Theory and Practice of Electron Difiraction.

(2) S. Miyake: Unpublished yet. Shortly will be reported on this Journal.

(3) R. Uyeda: Proc. Phys.-Math. Soc. Jap. **24** (1942), 809.

(4) G. Haegg u. I. Sucksdorff: Z. Phys. Chem. **22** (1933), 444.

Electron-Diffraction Study on Behaviors of Metals Deposited on Crystal Surfaces. Part II. Diffusion Phenomena of Metal Atoms on Galena.

By Shizuo MIYAKE and Mieko KUBO.

Kobayashi Institute of Physical Research, Kokubunji, Tokyo.

(Read October 22, 1946; Received November 26, 1946.)

§1. INTRODUCTION.

In the previous paper(1) the present authors described an observation by the electron diffraction method on a strange behavior of copper atoms, evaporated on to galena (PbS) surface in vacuum at higher temperatures. The pattern due to copper, appearing at first on the evaporation, gradually fades away, and then it finally disappears from the sight at all after a short period, leaving behind only the pattern due to the galena surface. This phenomenon was interpreted as a diffusion process of copper atoms inward the galena crystal.

More recently, another example of the similar effect was found in the case of silver on galena. Fig. 1a shows a diffraction photograph taken just after the evaporation at 400°C. Fig. 1b shows the state ten minutes after the former photograph, corresponding to the pattern of galena surface, which looks as if being in the same state as before the evaporation. The formation of chemical products was not observed in this case.

The phenomenon on silver seems to be explained too, only when the diffusion process of Ag atoms into galena is assumed. If such an interpretation is correct, then we have here a new method of measuring the diffusion coefficient of metal atoms in the solid, led by a simple consideration mentioned in the following paragraphs.

a. Ag pattern.
Just after the vaporization of Ag at 400°C.

b. Pattern of galena surface.
Ten minuites after.

Fig. 1. Diffusion of Ag inwards PbS crystal.

§2. THEORY.

We take first the case in which a metal layer of a uniform thickness is deposited on a crystal sur-

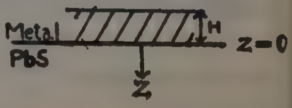

Fig. 2.

face (Fig. 2). The metal atoms are assumed to migrate within the crystal by diffusion, following the familiar equation

$$\frac{\partial c}{\partial t}=D\frac{\partial^2 c}{\partial z^2} \qquad (1)$$

where c is the concentration of the metal atoms (gr/cm³), and D the diffusion coefficient, t the time. The boundary condition for the present problem may be put as follows:

$$\left.\begin{array}{ll} c=\rho_0, & z=0. \\ c=0, & t=0. \end{array}\right\} \qquad (2)$$

in which ρ_0 corresponds to the saturated concentration of metal solute in the crystal. Under these conditions the solution of the above equation is given by the well known formula

$$c=\rho_0-\frac{2\rho_0}{\sqrt{\pi}}\int_0^{\frac{z}{2\sqrt{Dt}}} e^{-\beta^2}d\beta. \qquad (3)$$

The flow of the metal atoms within the crystal, i.e. the quantity of metal across a unit area perpendicular to the z-axis in a unit time is given by $q=-D\frac{\partial c}{\partial z}$. The flow at the surface, therefore, is given by

$$q_{z=0}=\rho_0\sqrt{\frac{D}{\pi t}}. \qquad (4)$$

If the thickness of the metal layer at $t=0$ is H, and the density of the metal ρ, then the superficial metal layer will be wholly absorbed in the crystal within a period t determined by the next relation.

$$H\rho=\int_0^t \rho_0\sqrt{\frac{D}{\pi t}}\,dt=2\rho_0\sqrt{\frac{Dt}{\pi}} \qquad (5)$$

From it we can obtain the diffusion constant D by

$$\gamma D=\frac{1}{4\pi}\cdot\frac{H^2}{t}; \qquad \gamma=\left(\frac{\rho_0}{\rho}\right)^2 \qquad (6)$$

Thus, the determination of D is now possible when we measure the period t, during which the superficial layer is completely absorbed in the base, provided values of H and γ. t can be directly mesured using the electron diffraction method by observing the diffraction pattern on the fluorescent screen.

In the above theory is assumed a metal layer of a uniform thickness, but this may be not true in general for the deposits prepared by the evaporation method, especially when the evaporated quantity of metal is scanty⁽²⁾. In the latter case, it is believed that the metal is apt to make scattered colonies or islands, rather than a uniform layer. The relation above obtained, therefore, must be suitably modified in the practical problem. We can however suppose that, a relation similar to Eq. (6) is probably hold even for the colonial distribution. In that case, the formula may be written in a form

$$\gamma D=\frac{1}{4\pi}\cdot\frac{H^2}{t}\cdot\frac{1}{C}, \qquad (7)$$

where C is a new factor which correlates to the state of the distribution of metal deposite, and H is now understood as the height of a single island. C may be unity when the vaporized quantity is sufficient so that a uniform layer is formed. But it will take a higher values, when the deposit distributes in many small islands scattered on the surface. For instance, if we treat a mathematically simple case of a spherical island, far isolated from the others, whose contact with the base being a hemispherical cavity of the base surface (Fig. 3), then, following a similar argument as above, it is found $C=9$ in (7), wherein H being understood as the diameter of the sphere. Taking this example in mind, it seems safe to assume that in general $C=1\sim5$.

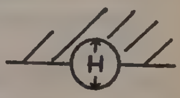

Fig. 3.

§3. EXPERIMENTAL PROCEDURE.

Following the method indicated in the former section, a determination of the diffusion coefficent D of silver and copper atoms in the galena crystal, as a function of temperature, was performed. The evaporation was performed on fresh cleavage surfaces (100) of galena. The evaporation of metals and the heating of crystals were carried out in the diffraction camera. The periods t between the instant of evaporation and the instant in which the pattern due to metal disappears from the sight on the fluorescent screen, were from about 0.5 minutes to 6 hours, during which the temperature of the crystal is kept constant.

The mean thickness H of the metal deposit was estimated from the quantity of the evaporated metal and the distance between the galena surface and the tungsten filament from which the metals are evaporated off. It must be noted that the mean thickness H' thus estimated is not in general equal to the above mentioned H used in Eq. (7), unless the vaporized quantity is sufficent to form uniform metallic layer.

§4. RESULT.

A. ***The case of Ag.*** The three kinds of the mean thickness, 20 A, 40 A and 80 A were studied. Fig. 4 indicates the result obtained, in which the ordinate is taken to be $\log(\gamma CD)$ calculated according to Eq. (7), and the abscissa the $1/T$, T being the absolute temperature. In these calculation, the mean thicknesses H were temporarily adopted as the values of H. This of course being not correct, the argument on this point will be discussed in the next section.

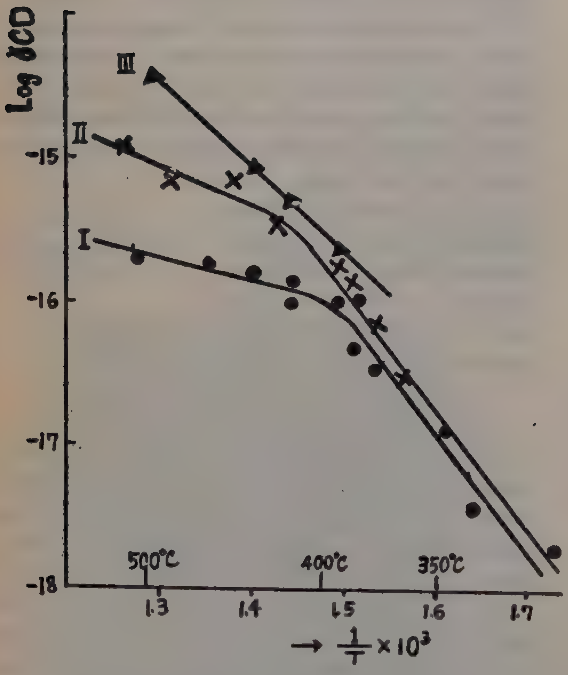

The mean thicknesses of Ag are 20A (curve I), 40A (curve II) and 80A (curve III).

Fig. 4. Ag

B. ***The case of Cu.*** The result obtained on copper is given in Fig. 5, which corresponds to the mean thickness 70A. This value is adopted as the value of H as before. The temperature range covered in the case of copper is much narrower than the case of silver, because complicated chemical reactions took place for copper in the outer tempertaure region, as formerly reported(1), which is not the case for silver at all.

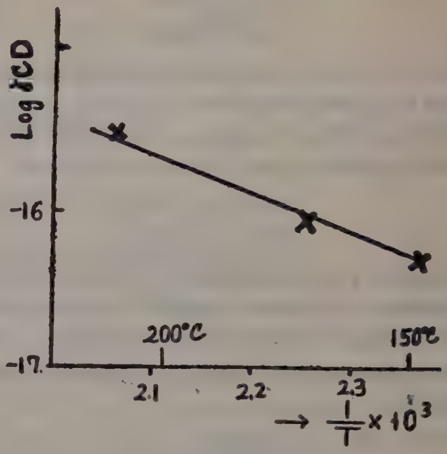

The mean thickness of Cu is 70A.

Fig. 5. Cu.

§5. DISCUSSION.

It is a well known relation in many cases that the diffusion coefficient of atoms in solid is expressed in a form

$$D=D_0 e^{-\varepsilon/kT}, \tag{8}$$

where T is the temperature, k, the Boltzmann's constant(3). According to it, $\log D$-$1/T$ curve must be a straight line. In fact Fig. 4 and Fig. 5 show a relationship of this kind.

But there are two difficulties to be explained. The one is the appearance of knicks in curves I and II in Fig. 4. The other is that, if the theory given in §2 is correct and is suitably applied, the three curves I, II, and III in Fig. 4 should coincide with each other. These problems, however, can be explained by a following consideration.

1) ***The existence of knicks.*** In the theory of §2, H was understood as the thickness of the layer, or the height of the island. The $\log.D$-$1/T$ curve may be represented by a single straight line, if H is a constant independent of the temperature, being determined only by the quantity of the vaporized metal. But it may not be the case when the evaporated metal is of small quantity. For, in the first place, it is a known fact in such a case that the metal deposit makes a colonial distribution as mentioned before, and higher the temperature, the size of a single island may become the larger. Secondly, when islands

are highly scattered on the surface and far isolated from each other, then the growth of the metal crystal may occur freely, so that some directional development will take place, if the temperature is high enough. This may result in a much elongated shape of the island in some direction. In face-centered cubic metals the development of (111)-plane is supposed to be the most pronounced one, as suggested by the appearance of the irrational spot and the twin formation⁽⁴⁾. On account of this free growth of the crystal, the island may take a form, as say, shown schematically in Fig. 6, at higher temperatures.

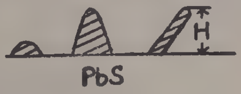

Islands of metals on PbS.
Fig. 6

As a result of these two factors the height H of the island may increase to larger values at higher temperatures, and consequently D, calculated on assuming a value of H constant throughout all temperature range, may apparently become smaller at higher temperatures. The existence of knicks in the curves I and II seems to be explained as due to these reasons. For instance, the discrepancy at 500°C between the curve I and the straight line, extrapolated from the lower temperature portion of the same curve, will be understood if we assume, for this temperature, a formation of a metal island of a height about three times taller than that for the lower temperature. This result seems not to be an absurd conclusion.

When the evaporated quantity is more ample, so that islands are distributed dense to each other, then the formation of especially large island or the free crystal growth will be suppressed, unless the temperature is sufficiently high. This tendency seems to correspond to the fact that the temperature at which the curves show the knick displaces into a higher temperature for the curve II (H' : 40 A), than for the curve I (H' : 20A). In the curve III, the knick does not appear, and in this case the height H of the metal deposit is supposed to be given correctly by the mean thickness H' to some extent.

· 2) *The discrepancy of curves.* We will now discuss the physical meaning of the vertical displacement of curves in Fig. 4. Concerning the curves I and III, only the portions corresponding to the temperature below the knick are considered in mind. Then the difference of I and III is about 4 by the multiplication factor. This difference is explained on assuming the state of the metal deposit, as follows.

Curve I corresponds to the smallest quantity of the vaporized metal (H' : 20A), so that the metal may be distributed in islands considerably scattered. In such a case C in Eq. (7) may exceedingly deviate from unity. Now we assume $C=4$ as its possible value. When this value of C is taken in account, then the differece of γD corresponding to the curves I and III must be about $4C(\fallingdotseq 16)$ by the multiplication factor, since C for the curve III can be supposed to be nearly unity. This discrepancy will be eliminated if the height H is taken $\sqrt{4C}$-times of the mean thickness 20 A for the curve I.

That means that the metal deposit in this case is not a uniform layer of the thickness 20 A, but it forms scattered islands, whose height being about 80 A. This result agrees fairly well with the hitherto known knowledge about the state of the metal deposit evaporated on the smooth crystal surface.

The diffusion coefficient. From the consideration given above, we can now presume that the theory can be applied in the case of the curve III without too large errors, because it is supposed that this case is roughly approximating the uniform layer, and probably being $C=1$.

The value of γD_0 and ε in Eq. (8) were obtained from this curve. The result is

$$\gamma D_0=4.5\times10^{-7}\ \mathrm{cm^2/sec},$$

$$\varepsilon=1.3 \text{ electron volts.}$$

ε is determind from the inclination of the curve. Similar value of ε were also obtained from the low temperature portion of the curves I and II.

In the same manner we obtained these quantities for copper from Fig. 5, assuming $C=1$. Namely,

$$\gamma D_0=2.7\times10^{-11}\ \mathrm{cm^2/sec};$$

$$\varepsilon=0.5 \text{ e.V.}$$

§6. CONCLUSION.

As described above, if we are provided the value of γ from some other sources, the diffusion constant D can be deduced by a comparatively simple procedure using the electron diffraction. Though this method can not be applied very widely, it may be utilized with success in suitable case as the present one.

Moreover, by the observation on the diffusion phenomenon, we can obtain several informations on the submicroscopic nature of the metallic deposit vaporized on the surface, as given in the present paper.

The authors wish to express their sincere thanks to Prof. Ryozi Uyeda for his valuable discussions.

References.

(1) S. Miyake and M. Kubo: J. Phys. Soc. Jap. 2 (1947), 15.

(2) R. Uyeda: Proc. Phys.-Math. Soc. Jap. 24 (1942), 809.

(3) e. g. N. F. Mott and R. W. Gurney: Electronic Processes in Ionic Crystals. (1940).

(4) F. Kirchner u. H. Lassen: Ann. Phys. 24 (1935), 113. W. Cochrane: Proc. Phys. Soc. 48 (1936), 723, etc.

Dissociation and Ionization of n-Hexane, Cyclohexane and Benzene by Electron Impacts, I.

By Toyozo KAMBARA.

Hitachi Central Research Laboratory, Hitachi Ltd.

(Received December 26, 1946.)

(1) INTRODUCTION

Since the experiments of methane by L. G. Smith(1) the investigations on the dissociation nd ionization of various gases or vapors vith massspectrometers were made by many nvestigators.

Experiments with massspectrographs on the ons formed by electron impacts in vapors re capable of giving valuable informations bout the molecular structures of these vapors nd the dissociation processes occuring in aseous molecules.

Namely, it is possible to determine the nature f ions produced under various conditions by he approximate determination of M/e of the bserved ion. The relative probability of ormation of ions and the minimum energy equired to produce the ion may also be etermined. This energy, usually called appearance potential, is the sum of dissociation nergy, ionization potential and the excess nergy, i.e. minimum excitational and kinetic energy f the dissociation products. n usual experience, this xcess energy is rather mall, and so the sum of issociation energy and nization potential is quite lose to its true value.

In this paper, the results btained by the investigaons on the dissociation of hexane, cyclohexane and enzene vapors by electron npacts are described. he investigation of cycloexane and benzene by ectron impacts has already been made by Hustrulid, Kusch and Tate(2). But the main purpose of this paper is to describe the difference between a straight chain type hydrocarbon as n-hexane and a ring type hydrocarbon as cyclohexane or benzene. Paucity of thermochemical and spectroscopic data on the dissociations of these vapors prohibits the satisfactory analysis of the processes by which the ion is formed, but simple considerations about the particular processes will be made in the explanation of the experimental results.

The other purpose is to describe the consideration about the relationship between the hardness of decomposition and the antiknocking tendency of these vapors.

The experiment described in this paper was made by the author in 1944 at the Hitachi Central Research Laboratory, Hitachi Ltd.

(2) APPARATUS AND PROCEDURE.

The massspectrograph(3) used in the present

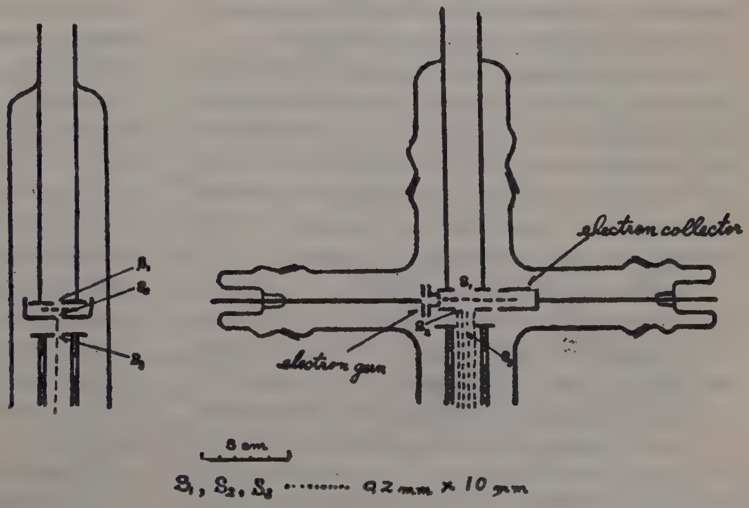

Fig. 1. Ion Source

investigation is Nier type, and the magnetic field adopted for this apparatus is V-shaped. Its angle is 60° and radius 22 cm.

A cross sectional view of the ion source is shown in Fig. 1.

The hydrocarbon vapors to be examined are admitted to the ion source through the slit S_1. The differential pumping method is used to protect the thermal dissociation of these vapors at the hot cathode. For these reasons the region between S_1 and the electrode S_2 has the maximum gas density in the ion source. In Fig. 1, the thick dotted line shows a electron beam and the thin one shows a ion beam.

The D. C. high voltage for the acceleration of the ions is supplied by a 1200 volt stabilized rectifier set of the Gingrich type in the 1st step and Street-Johnson type in the 2nd step. The stabilization constant of this circuit only using radio tubes UY-47B and UZ-57 is 10^{-4} against 10 % variation of the input voltage.

The analysed ion currents are measured with an electrometer tube UX-54 and a galvonometer (2.6×10^{-10} Amp/mm). The measuring circuit is a modified Barth circuit and has voltage sensitivity of 60,000~100,000 mm per volt at a scale distance of 1 meter. The high resistance of $1.3\times10^{10}\Omega$ is used as a grid leak. The analyzed ion currents are automatically recorded as shown in the following photographs.

Small quantity of the purified sample is placed in a bulb connected to the ionization region of the massspectragraph, and after cooled under pumping evaporated into the gas reservoir. The samples studied in this research are purified by the following methods.

The gas leakage and pumping speed are controlled such as to give a pressure of about 10^{-5} mmHg in the main part. The observations are carried out at very low pressure so that all the ions in the ion source are produced as the result of single electron impact on the normal molecule of the gas in question.

The relative probability of the ion formation by electron impacts is measured by changing the magnetic field strength, but the photographs of the massspectrum are taken by changing the accelerating voltage of the ions.

The ion peaks which are supposed to be due to impurities are always of very low intensity. The corrections to the abundance for the presence of the carbon isotope of mass 13 have not been made in the present pape According to the abberation of the apparatu and the kinetic energy of the produced ions the ion peaks are overlapping in the highe mass regions, and in C_6 group this effect i particularly great. The correction for thi effect has not also been made to the relativ probability.

(*A*) ***Purification of normal hexane*** (n–C_6H_{14}

Kahlbaum's petroleum hexane is shake several times with concentrated sulphuric acid washed twice with distilled water and decante then shaken with 10% sodium hydroxide, an finally shaken with N/10 solution of perma ganate in 10% sodium hydroxide; subsequentl it is washed with water, dried with acid pho phoric anhydride and then distilled.

(*B*) ***Purification of cyclohexane*** (C_6H_{12}).

Cyclohexane is cooled at about 0°C. an crystallized, and then benzene is removed b decantation of the benzene containing cycl hexane, Such procedures are repeated ten more times until cyclohexane is not colour with picric acid. Subsequently cyclohexane dried and distilled.

(*C*) ***Purification of benzene*** (C_6H_6).

Benzene is shaken with frequently renew quantities of concentrated sulphuric acid un the thiophene reaction is negative, then fra tionally crystallized three times, heated for day under a reflux with calcium chloride a distilled.

(3) INVESTIGATIONS ON THE n–HEXANE (n–C_6H_{14}).

Chemical evidence indicates that the carbons in normal hexane are connected in straight line, and C–C bond energy is 3.17 (73 Kcal/Mol) and C–H bond energy is 3.97 (92 Kcal/Mol).

It is a very interesting problem to kn that how C–C bonds in n-hexane will be brok by the electron with far greater energy th the value above-mentioned. At least, it expected that the two end C–C bonds are c ferent from the others.

The relative probabilities of the formati of ions and the appearance potentials of formed ions in n-hexane are described follows.

(A) Relative probabilities of the formati of ions in n-hexane by electron impact

The ions observed as the dissociation p

ducts of n-hexane under single electron impact and the relative abundance of the ions produced at the electron energy of 30, 50, and 100 eV are tabulated in Table I, II, and III respectively.

Table I. Nature and relative abundance of ions formed in n-hexane by electrons with 30 volts energy.

Ion	$n=1$	$n=2$	$n=3$	$n=4$	$n=5$	$n=6$
C_n^+						
C_nH^+		0.11	0.11			
$C_nH_2^+$		0.24	0.49			
$C_nH_3^+$	0.21	3.21	1.69			
$C_nH_4^+$	0.09	2.99	1.00	0.16		
$C_nH_5^+$		8.77	15.46	0.40		
$C_nH_6^+$		0.78	8.57	0.48		
$C_nH_7^+$			13.70	2.70	0.22	
$C_nH_8^+$			0.71	13.29	0.23	0.33
$C_nH_9^+$				15.32	1.31	0.18
$C_nH_{10}^+$				0.80	0.37	0.33
$C_nH_{11}^+$					1.09	0.41
$C_nH_{12}^+$						0.72
$C_nH_{13}^+$						0.48
$C_nH_{14}^+$						3.16
	0.30	16.10	41.73	33.15	3.15	5.61

Table II. Nature and relative abundance of ions formed in n-hexane by electrons with 50 volts energy.

Ion	$n=1$	$n=2$	$n=3$	$n=4$	$n=5$	$n=6$
C_n^+			0.05			
C_nH^+	0.01	0.11	0.27			
$C_nH_2^+$	0.11	0.54	0.38	0.09		
$C_nH_3^+$	0.53	7.49	4.68	0.26		
$C_nH_4^+$	0.06	3.11	1.11	0.13		
$C_nH_5^+$		8.99	15.46	0.67	0.06	0.06
$C_nH_6^+$		0.38	6.76	0.38	0.03	0.03
$C_nH_7^+$			11.20	2.44	0.34	0.11
$C_nH_8^+$			0.47	11.02	0.20	0.03
$C_nH_9^+$				13.14	1.34	0.18
$C_nH_{10}^+$				0.80	0.34	0.10
$C_nH_{11}^+$					1.04	0.20
$C_nH_{12}^+$					0.06	0.78
$C_nH_{13}^+$						0.38
$C_nH_{14}^+$						4.10
	0.72	20.62	40.38	29.93	3.41	5.97

Table III. Nature and ralative abundance of ions formed in n-hexane by electrons with 100 volts energy.

Ion	$n=1$	$n=2$	$n=3$	$n=4$	$n=5$	$n=6$
C_n^+	0.03	0.08	0.15	0.08		
C_nH^+	0.13	0.31	0.84	0.21		
$C_nH_2^+$	0.54	2.09	1.37	0.76	0.06	
$C_nH_3^+$	2.38	13.65	8.67	0.80	0.13	
$C_nH_4^+$	0.17	4.78	1.69	0.36	0.06	
$C_nH_5^+$		9.65	14.08	0.93	0.16	
$C_nH_6^+$		0.38	4.86	0.53	0.10	
$C_nH_7^+$			7.24	2.13	0.30	0.08
$C_nH_8^+$			0.53	6.89	0.18	0.09
$C_nH_9^+$				8.01	0.73	0.13
$C_nH_{10}^+$				0.64	0.23	0.06
$C_nH_{11}^+$					0.50	0.11
$C_nH_{12}^+$					0.04	0.35
$C_nH_{13}^+$						0.21
$C_nH_{14}^+$						1.43
	3.25	30.94	39.57	21.34	2.49	2.46

In these tables the suffix of C_n and H_n show respectively the number of carbon and hydrogen atoms of the ion, and the numerical value shows the percentage of each ion.

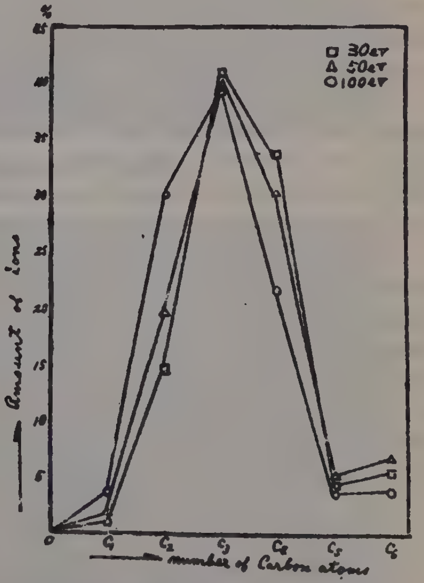

Fig. 2. The progress of dissociation of n-hexane by electrons with 30, 50 and 100 volts energy.

Fig. 2 shows the progress of dissociation of n-hexane as the energy of the bombarding

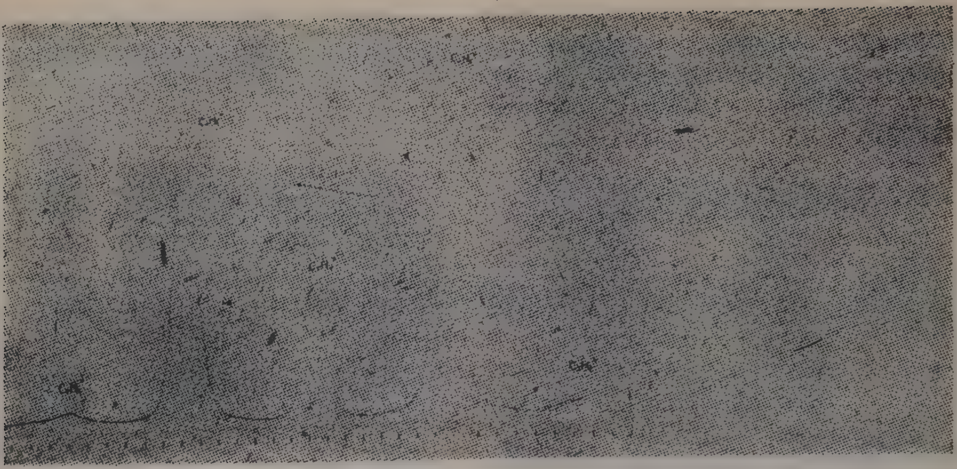

Fig. 3. Mass spectrum of ions of C_2-group in n-hexane.

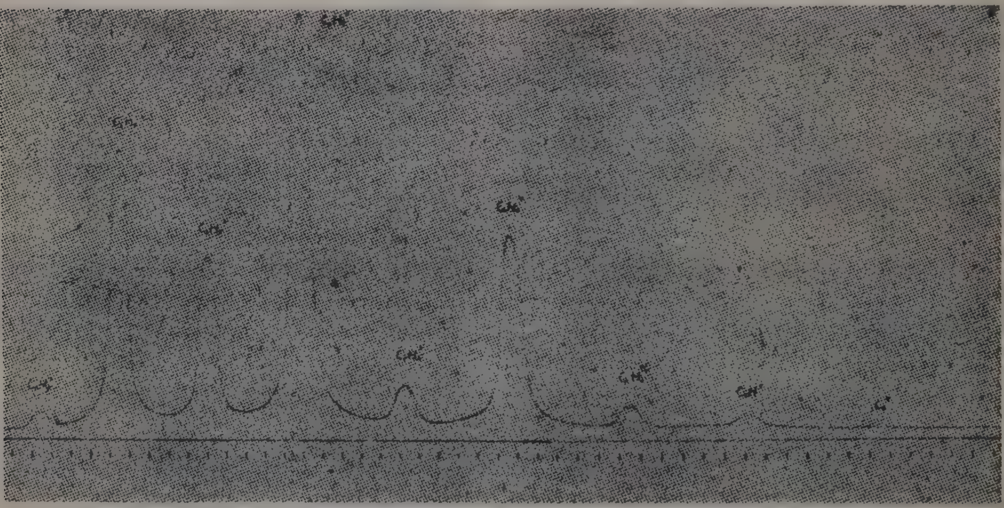

Fig. 4. Mass spectrum of ions of C_3 group in n-hexane.

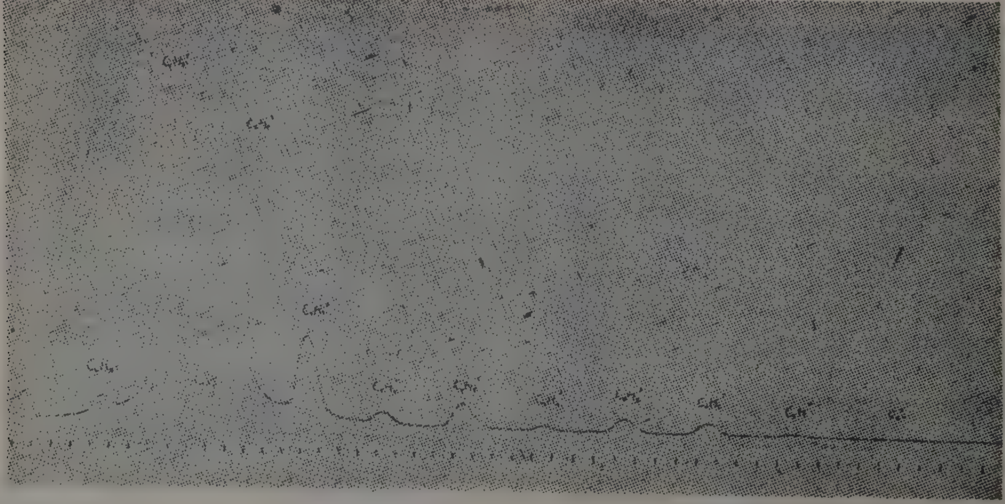

Fig. 5. Mass spectrum of ions of C_4 group in n-hexane.

electron increases.

The typical massspectrums of ions containing 2~4 carbons are shown in Fig. 3~Fig. 5.

As above mentioned, these photographs are taken by changing the accelerating voltage of the ions.

According to the Table I~III, it is noteworthy that the non-dissociated ions $C_6H_{14}^+$ are less abundant than the dissociated ions containing 4, 3 or 2 carbon atoms. This appearance of the massspectrum of the ions produced from n-hexane differs markedly from those of the ions produced from cyclohexane and benzene. It is also estimated that the two end C–C bonds are stronger than the others in n-hexane under the impacts of electrons with the far greater energy than the C–C bond energy (3. 17 eV).

Fig. 2 shows that the more the energy of impacted electrons increases the less abundant the ions containing the many carbon atoms. Moreover, the ions containing the hydrogen atoms of odd number are more abundant than the ions containing the even number. For example, the ions $C_3H_7^+$ and $C_3H_5^+$ are more abundant than the ions $C_3H_6^+$. Perhaps the ions

$C_3H_7^+$ 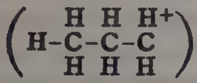
$\left(\begin{matrix} & H & H & H^+ \\ H- & C- & C- & C \\ & H & H & H \end{matrix}\right)$ and $C_3H_5^+$
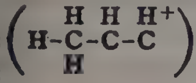
$\left(\begin{matrix} & H & H & H^+ \\ H- & C- & C- & C \\ & H & & \end{matrix}\right)$ may be more stable than ion
$C_3H_6^+$ 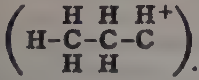
$\left(\begin{matrix} & H & H & H^+ \\ H- & C- & C- & C \\ & H & H & \end{matrix}\right)$.

(B) Appearance potentials of the formed ions in n-hexane.

The determination of appearance potentials was made by admitting a mixture of n-hexane vapor and argon gas into the mass spectrograph and observing the ion current as a function of electron energy near the threshold value. The accelerating voltage of electrons was corrected by the ionization potential of argon. Appearance potentials of the formed ions in n-hexane measured by above method are shown in Table IV.

In Table IV the appearance potentials of ions $C_6H_{14}^+$, $C_5H_{11}^+$, $C_4H_9^+$, $C_4H_8^+$, $C_3H_7^+$ and $C_3H_6^+$ are nearly equal to each other, viz. those values are 10.2~10.9 eV, and the appearance potentials of the other ions are apparently higher than those.

Table IV. Appearance potentials of formed ions in n-hexane.

Ion	Appearance Potential (eV)
$C_6H_{14}^+$	10.2
$C_5H_{11}^+$	10.9
$C_5H_9^+$	13.0
$C_4H_9^+$	10.2±0.4
$C_4H_8^+$	10.3±0.1
$C_3H_7^+$	10.5±0.1
$C_3H_6^+$	10.5±0.1
$C_3H_5^+$	12.5±0.1
$C_3H_3^+$	13.0±0.3
$C_2H_5^+$	13.4±0.2
$C_2H_4^+$	14.6±0.4
$C_2H_3^+$	14.1±0.4
CH_3	14.3±0.3

The following notations will be used in the discussion of the results.

$A(X^+)\equiv$Appearance potential of the ion X^+.
$I(X^+)\equiv$Ionization potential of X.
$D(X)\equiv$Dissociation energy of X.
$W(X^+)\equiv$Excess energy (kinetic or excitational) appearing in the production of the ion X^+ from the parent molecule.
$Q(X^+)\equiv$Energy evolved in the formation of X from its elements in the states in which they exist at room temperature and atomospheric pressure.
$L(C)\equiv$Heat of sublimation of carbon.

Appearance potential of the formed ions is the sum of three quantities; a dissociation energy, an ionization potential and a total minimum excitational and mutual kinetic energy, namely

$$A(X^+)=D(X)+I(X^+)+W(X^+).$$

The minimum kinetic and excitational energy with which the products can dissociate is usually small, so one may define a new quantity I′ by A−D=I′, which is nearly equal to I.

The ionization potentials of the several straight chain type hydrocarbons have already been measured by many investigators.

For examples:

$I(CH_4^+)=13.1$ eV Smith(1)
$I(C_2H_6^+)=11.6$ eV Hipple(4)
$I(C_2H_4^+)=10.8$ eV Bleakney(3)
$I(C_2H_2^+)=11.2$ eV Tate(7)
$I(C_3H_8^+)=11.3$ eV
$I(C_3H_6^+)=10.0$ eV Bleakney(6)
$I(C_3H_4^+)=9.9$ eV
$I(n\text{-}C_6H_{14}^+)=10.2$ eV Present work

Table V. Energies of dissociation of n-hexane into its various constituents and interpretation of the appearance potential.

	Configuration energy		Appearance potential	Ionization potential
a	n-C_6H_{14}	0 eV		$I(C_6H_{14}^+) = 10.2$ eV
b	$C_5H_{11}+CH_3$	2.4	$A(C_5H_{11}^+) = 10.9$ eV	$I(C_5H_{11}^+) \leq 8.5$
c	$C_5H_9+CH_3+H_2$	4.1	$A(C_5H_9^+) = 13.0$	$I(C_5H_9^+) \leq 8.9$
d	$C_4H_9+C_2H_5$	0.8	$A(C_4H_9^+) = 10.2$	$I(C_4H_9^+) \leq 9.4$
e	$C_4H_8+C_2H_6$	0.6	$A(C_4H_8^+) = 10.3$	$I(C_4H_8^+) \leq 9.7$
f	$C_3H_8+C_3H_6$	0.7	$A(C_3H_6^+) = 10.5$	$I(C_3H_6^+) \leq 9.8$
g	$C_3H_7+C_3H_7$	0.7	$A(C_3H_7^+) = 10.5$	$I(C_3H_7^+) \leq 9.8$
h	$C_3H_5+C_2H_8+H$	3.8	$A(C_3H_5^+) = 12.5$	$I(C_3H_5^+) \leq 8.7$
i	$C_3H_5+C_3H_7+H_2$	2.2		$I(C_3H_5^+) \leq 10.3$
j	$C_3H_3+C_3H_7+2H_2$	4.6	$A(C_3H_3^+) = 13.0$	$I(C_3H_3^+) \leq 8.4$
k	$C_2H_5+C_4H_8+H$	3.5	$A(C_2H_5^+) = 13.4$	$I(C_2H_5^+) \leq 9.9$
l	$C_2H_5+C_2H_4+C_2H_5$	2.0		$I(C_2H_5^+) \leq 11.4$
m	$C_2H_4+C_4H_9+H$	3.9	$A(C_2H_4^+) = 14.6$	$I(C_2H_4^+) \leq 10.7$
n	$CH_3+C_3H_6+C_2H_5$	3.2	$A(CH_3^+) = 14.3$	$I(CH_3^+) \leq 11.1$
o	$CH_3+C_2H_4+C_3H_7$	3.3		$I(CH_3^+) \leq 11.0$
p	6C+14H	65.4		

From above results it is assumed that the values of the ionization potentials of straight chain type hydrocarbons become smaller as the number of contained carbon atoms increase, and also that those values become slightly smaller for molecules having the double bond.

Before one can make analysis of the processes by which the ions are formed, it is necessary to estimate the various value of the heat of dissociation involved. The energy of possible states in which six carbon and fourteen hydrogen atoms can exist are shown in Table V.

The energy in Table V are calculated in each cases from the normal state of the complete molecule.

Now the heat of formation of n-hexane $Q(n\text{-}C_6H_{14})=2.0$ eV may be calculated from the heat of combustion. Dissociation energy of hydrogen molecule $D(H_2)=4.46$ eV is given by Sponer⁽⁷⁾; sublimation heat of carbon $L(C)=5.36\pm0.02$ eV is given by Goldfinger and Jeunehomme⁽⁸⁾.

For the determination of $D(n\text{-}C_6H_{14})$ the following cycle may be assumed.

$$7H_2+6C_{dia}=n\text{-}C_6H_{14}+Q(n\text{-}C_6H_{14})$$
$$6C_{dia}+6L(C)=6C_{gas}$$
$$7H_2+7D(H_2)=14H$$
$$14H+6C_{gas}=n\text{-}C_6H_{14}+D(n\text{-}C_6H_{14}).$$

This shows that

$$D(n\text{-}C_6H_{14})=7D(H_2)+6L(C)+Q(n\text{-}C_6H_{14}),$$

which yields

$$D(n\text{-}C_6H_{12})=65.4 \text{ eV}.$$

The dissociation energies of n-pentane, amylene, n-butane and α-butylene are determined by the similar calculations as n-hexane; those values are $D(n\text{-}C_5H_{12})=55.5$ eV, $D(C_5H_{10})=49.3$ eV, $D(n\text{-}C_4H_{10})=45.1$ eV and $D(C_4H_8)=39.8$ eV respectively.

The dissociation energies in the case of methane were given by Smith⁽¹⁾ as $D(CH_4)=15.1$ eV, $D(CH_3)=10.6$ eV and $D(CH_2)=7.0$ eV.

The dissociation energies in the case of ethylene and ethane were given by Kusch, Hustrulid and Tate⁽⁹⁾, for example $D(C_2H_4)=19.2$ eV, $D(C_2H_3)=16.1$ eV, $D(C_2H_6)=25.0$ eV and $D(C_2H_5)=22.1$ eV.

The dissociation energies in the case of propane, propylene and allene were given by Delfosse and Bleakney, for example $D(C_3H_7)=32.3$ eV, $D(C_3H_6)=29.5$ eV, $D(C_3H_5)=26.4$ and $D(C_3H_3)=19.5$ eV.

The dissociation energies of C_5H_{11}, C_5H_9 and C_4H_9 are estimated by the interpolation or extrapolation from the values of $D(n\text{-}C_5H_{12})$, $D(C_5H_{10})$, $D(n\text{-}C_4H_{10})$ and $D(C_4H_8)$.

The observation on the appearance potentials and the conclusions which may be drawn from them are also summarized in Table V.

The disscusions of some particular cases vill now be given.

. $C_5H_{11}+$, C_5H_9+.

As the dissociation processes b and c (Table 7) are unreliable, the upper limits of the onization potentials of $C_5H_{11}+$ and C_5H_9+, iz. 8.5 eV and 8.9 eV are also uncertain.

. C_4H_9+, C_4H_8+.

In n-hexane the simplest way to produce hese ions are the dissociation according to e nd f. Energetically those must be a unique olution.

$$n\text{-}C_6H_{14} \longrightarrow C_4H_9{+} + C_2H_5 + e \quad I(C_4H_9{+}) \leq 9.4\,\text{eV}$$

$$n\text{-}C_6H_{14} \longrightarrow C_4H_8{+} + C_2H_6 + e \quad I(C_4H_8{+}) \leq 9.7\,\text{eV}$$

. C_3H_7+.

In the investigation on propane Delfosse nd Bleakney(3) found a value of $I(C_3H_7+)$ $\leq$9.0 eV. In n-hexane the dissociation process lead to $I(C_3H_7+) \leq 9.8$ eV, but the dissociation nergy in both cases are not reliable.

. C_3H_6+.

In the investigation on propylene Delfosse nd Bleakney(6) found a value of 10.0±0.2 eV or the ionization potential of this molecule. hen there is only one possible explanation f the appearance potential of this ion in -hexane, namely the process -$C_6H_{14} \rightarrow C_3H_6{+} + C_3H_8 + e$. In this case the otal excess energy is equal to zero. All other onceivable processes require too much energy.

. C_3H_5+.

In the investigation on propylene Delfosse nd Bleakney found a value of $I(C_3H_5) \leq 8.7$eV In the process *h* the upper limit of ionization potential of this ion is the same value, ut in the process *i* the ionization products ave the excess energy of above one and half ectron volts. It seems rather surprising that e process *e*, *f* or *h* can happen as the result f single electron impact.

C_3H_3+.

In the investigation on allene Delfosse and leakney(6) found a value of $I(C_3H_3+) \leq 8.8$ eV. he most probable process seems to be the ormation of $C_3H_3{+} + C_3H_7 + 2H_2$ and in this case the upper limit of $I(C_3H_3+)$ is 8.4 eV.

7. C_2H_5+.

In the investigation on ethane Hipple(4) found a value of $I(C_2H_5+) \leq 9.8$ eV. In n-hexane the simplest way to produce this ion is the formation of $C_2H_5{+} + C_4H_9 + e$, but in this case the total excess energy of the products is abnormally high. Energetically the most probable process is *k* and in this case the upper limit of $I(C_2H_5+)$ is 9.9 eV.

8. C_2H_4+

In the investigation on ethylene Kusch, Hustrulid and Tate(8) found a value of 10.8 eV for the ionization potential of this molecule. The most probable and simplest process is the formation of $C_2H_4{+} + C_4H_9 + H + e$ and in this case the upper limit of $I(C_2H_4+)$ is 10.7 eV.

9. CH_3+.

The upper limit of ionization potential of CH_3 is measured as 9.9 eV by Smith, 10.4 eV by Hipple. The simplest way to produce CH_3+ is the manner of knocking a CH_3 off one end and ionizing it. Such a process may be *b* or *c* and in the process *c* the upper limit of $I(CH_3+)$ is 10.2 eV, but the processes *o* and *p* in which two C–C bonds will be broken are also probable, and in these cases the excess energy of the products are about one electron volt.

References.

(1) L. G. Smith: Phys. Rev. **51** (1937), 263.

(2) Hustrulid, Kusch and Tate: Phys. Rev. **54** (1938), 1037.

(3) T. Kambara, H. Yoshimoto and S. Shima: Hitachi Hyoron **26** (1943), 691.

(4) J. A. Hipple: Phys. Rev. **53** (1938), 530.

(5) Tate, Smith & Vaughan: Phys. Rev. **48** (1935), 525.

(6) J. Delfosse & W. Bleakney: Phys. Rev. **56** (1939), 256.

(7) Sponer: Molekulspektren (J. Springer (1935)).

(8) Goldfinger and Jeunehomme: Trans. Faraday Soc. **32** (1936), 1591.

On the Relation between Thermionic Constant and Work Function.

By Kenji KONDO.

Faculty of Science, Tokyo Imperial University.

(Received October 5, 1946.)

1. THE CHANGE IN THE VALUE OF A IN RICHARDSON'S FORMULA AND ITS PREVIOUS EXPLANATION.

Empirically it has been recognized that there is a linear relation between the logarithm of observed thermionic constant, i. e. log A and work function φ in various stages of outgassing. This fact was first recorded by O. W. Richardson and afterwards reformulated by Du Bridge(1). Van Velzer computed the work function of a clean surface of tungsten by this rule upon the assumption that the true value of thermionic constant A was 60 Amp/cm^2 deg^2 and found the value of 5.29 volts for work function. Recently R. H. Fowler(2) attempted to explain this relation by the transmission coefficient of an electron through the potential barrier existed between an adsorbed atom and a base metal (Fig. 1a).

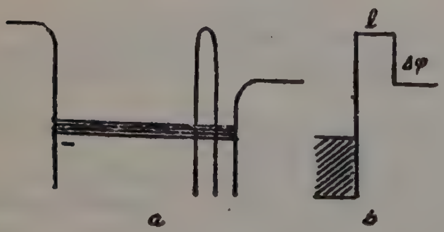

Fig. 1.

His result for the rectangular potential barrier (Fig. 1b) is as follows:

$$\log A = \text{const.} - 2\kappa(\Delta\varphi)^{\frac{1}{2}} l,$$

where $\kappa = \frac{2\pi}{h}\sqrt{2m}$, h is the Planck's constant, m the electronic mass, $\Delta\varphi$ the lowering of work function and l the thickness of barrier. Comparing this formula with the observed values by Du Bridge, he had the value of $l \geqq 10^{-7}$ cm. This layer is rather thick. And furthermore it is doubtful that there is a potential peak higher than that on the outsid of metal, when electronegative atom lik oxygen are adsorbed (Fig. 2). In the cases of tungsten, platinum and other metals abou which some investigators reported this fact,

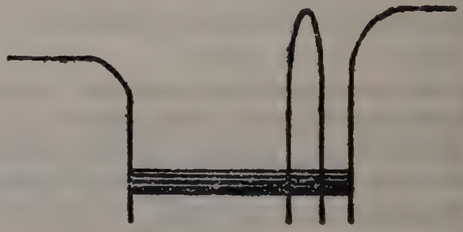

Fig. 2.

the work function in the stage of poo outgassing are usually large and decreas little by little to small values during sever heat treatment. Therefore these monolayers consist of electronegative atoms, presumably oxygen atoms which have the large heat of adsorption, and Fowler's theory can not be applied to these cases. Secondly Zwikker(3 assumed that the atoms adsorbed on the surface represent the rigid dipoles, upon which the thermal movement has a disorienting action, and the dependence of their effective moment on temperature is given by the relation:

$$p = c/T,$$

where c is a constant, which is a function of the concentration of the adsorbed atoms. His model is similar to Langevin's one of electric or magnetic dipole in homogeneous field. But the second assumption is not reasonable in this case. The author improved it and obtained the more proper result as we shall se later.

The theoretical relation deduced from th conception of Zwikker is as follows:

$$\log A_{\text{obs}} = \text{const.} + \frac{e}{2kT_0}\varphi_{\text{obs}},$$

where e is the electronic charge, k the Boltzmann's constant and T_0 the average temperature at which the measurement is performed. As we shall see later, the inclination of the straight line of log A vs. φ is different for various metals, but independent on the temperature. But according to Zwikker's theory, the inclination is common for different kinds of metal and dependent on the average temperature, of which the physical meaning is not necessarily clear.

2. EXPERIMENTAL RESULTS.

In order to confirm this relation experimentally, it is necessary to measure the thermionic current in some stages of outgassing. Therefore the monolayer must not evaporate easily, but has much heat of adsorption. For this purpose the layer of oxygen on tungsten or platinum is as suitable as possible.

The author measured the thermionic constant A and the work function φ for purest platinum in the various stage of outgassing. The observed log A are plotted against the observed φ in (Fig. 3). The inclination of this straight line is in agreement with that of Du Bridge, but its position deviates slightly from that, and its cause is unknown. The empirical expression from the data is as follows:

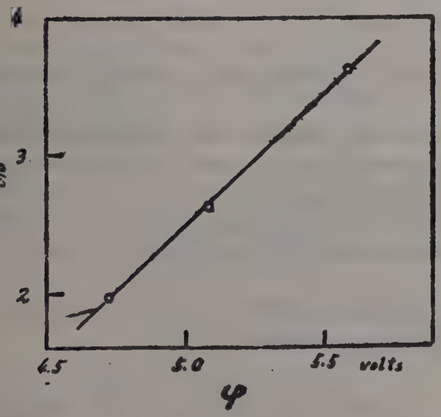

Fig. 3.

$$\log_{10} A = -6.85 + 1.87\varphi.$$

3. THEORETICAL EXPLANATION AND DISCUSSION.

Usualy it is comparatively difficult to remove the monolayer of oxygen on metallic surface. In tungsten it is necessary to heat to about 3000°K, and according to Langmuir evaporating molecules are not oxygen molecules but tungsten oxide. In platinum it is impossible to remove it at the temperature lower than 1700°K. Apparently this tight-bound chemisorbed atom is localized and can not emigrate at the temperature of thermionic measurement, but vibrate about the equilibrium point and making hinderedrotation about the ad-site (Fig. 4). These vibration and rotation change the dipole moment of monolayer and accordingly the work function. This variation depends upon the temperature and the value of moment at the absolute zero temperature. In this case the work function is

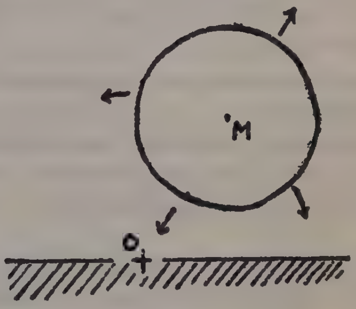

Fig. 4.

$$\varphi = \varphi_0 + \Delta\varphi(\theta)(1 - akT),$$

where φ_0 is the true work function of metal, $\Delta\varphi(\theta)$ the change of work function due to the double moment at the absolute zero temperature, θ the concentration of adsorbed atoms, α the temperature coefficient of the double moment, k the Boltzmann's constant and T the temperature in absolute scale. Therefore the thermionic current is:

$$i = AT^2 \exp\left\{-\frac{e}{kT}[\varphi_0 + \Delta\varphi(\theta)(1 - akT)]\right\},$$

where A is the theoretical or true thermionic constant, e the electronic charge. We have the following expression for observed thermionic constant and work function:

$$A_{\mathrm{obs}}=A\exp[ea\Delta\varphi(\theta)]$$

and

$$\varphi_{\mathrm{obs}}=\varphi_0+\Delta\varphi(\theta).$$

Consequently we get the relation between observed constant and work function as follows:

$$\log A_{\mathrm{obs}}=(\log A-ea\varphi_0)+ea\varphi_{\mathrm{obs}}.$$

Classically we can calculate the temperature coefficient a. In Fig. 4, O is the ad-site, M is the adsorbed atom and we determine the position of M by the polar coordinates q, θ and φ. In poor gas absorbers like platinum and tungsten, absorption and diffusion increase accordingly as temperature increase, that is, the activation energy is necessary for adsorbed atoms to penetrate into the lattice space. Therefore there is a large potential peak in $\theta=\pi/2$ and the adsorbed atom can not rotate over it at the lower temperature. Here we assume the potential as in the following,

$$V_{\mathrm{rot}}=2eD_{\mathrm{rot}}\theta\ ,$$

where e is the electronic charge, and D_{rot} is a constant.

We get as the rotational partition function,

$$r(T)=\frac{1}{h^2}\int_0^{2\pi}d\varphi\int_0^{\pi/2}d\varphi\int_{-\infty}^{\infty}dp_\varphi\int_{-\infty}^{\infty}dp_\theta\ \times$$

$$\exp\left\{-\frac{1}{2mq^2kT}\left(p_\theta^2+\frac{p_\varphi^2}{\sin^2\theta}\right)+\frac{2eD_{\mathrm{rot}}\theta^2}{kT}\right\},$$

where h is the Planck's constant, m the mass of the adsorbed atom and p_θ and p_φ are respectively the momentums for θ and φ. After the simple integration over p_θ, p_φ and φ we have:

$$r(T)\cong\frac{2\pi(2mq^2kT\pi)}{h^2}\int_0^{\pi/2}\sin\theta\exp\left(-\frac{2eD_{\mathrm{rot}}\theta^2}{kT}\right)d\theta.$$

As usual the averaged value of θ is small, we can expand $\sin\theta$ and keep only the first two terms. The approximate value of $r(T)$ is

$$r(T)\sim\frac{2\pi(2mq^2kT\pi)}{h^2}\ \frac{kT}{4eD_{\mathrm{rot}}}\left(1-\frac{kT}{12eD_{\mathrm{rot}}}\right)$$

The averaged value of double moment is

$$<p>_{AV}=p_0\frac{1}{r(T)h^2}\int_0^{2\pi}d\varphi\int_0^{\pi/2}d\theta\int_{-\infty}^{\infty}dp_\varphi\int_{-\infty}^{\infty}dp_\theta$$

$$\times\cos\theta\exp\left\{-\frac{1}{2mq^2kT}\left(p_\theta^2+\frac{p_\varphi^2}{\sin^2\theta}\right)\right.$$

$$\left.+\frac{2eD_{\mathrm{rot}}\theta^2}{kT}\right\},$$

where p_0 is the moment at the absolute zero temperaure. By the same approximation as the above we get the following formula,

$$<p>_{AV}\sim p_0\left(1-\frac{kT}{4eD_{\mathrm{rot}}}\right).$$

In the case of vibration we assume the Morse potential as in the following,

$$V_{\mathrm{vib}}=\mathrm{const}+eD_{\mathrm{vib}}[\exp\{-2a(q-q_0)\}$$

$$-2\exp\{-a(q-q_0)\}],$$

where q_0 is the distance of minimum potential, and D_{vib} and a are constants. As usual a is some A^{-1} and $q-q_0$ is less than 0.1A. Therefore we can expand it in power series of $q-q_0$ as follows:

$$V_{\mathrm{vib}}=\mathrm{const}+eD_{\mathrm{vib}}\{1-2a(q-q_0)+2a^2(q-q_0)$$

$$-\frac{8}{6}a^3(q-q_0)^3+\cdots\cdots$$

$$-2+2a(q-q_0)-a^2(q-q_0)^2$$

$$+\frac{2}{6}a^3(q-q_0)^3-\cdots\cdots\},$$

$$\sim\mathrm{const}+eD_{\mathrm{vib}}\{a^2(q-q_0)-a^3(q-q_0)^3\}.$$

The partition function of vibration is

$$v(T)=\frac{1}{h}\int^{\infty}e^{-\frac{p^2}{2mkT}}dp\int_0^{\infty}\exp\left[-\frac{eD_{\mathrm{vib}}a^2(q-q_0)^2}{kT}\right.$$

$$\left.+\frac{eD_{\mathrm{vib}}a^3(q-q_0)^3}{kT}\right]dq,$$

where p is the momentum for q.

In adsorption usually $\frac{eD_{\mathrm{vib}}}{kT}>10^2$, and $a^3(q-q_0)^3<10^{-3}$, we obtain

$$\exp\left\{\frac{eD_{\mathrm{vib}}}{kT}a^3(q-q_0)^3\right\}\sim1+\frac{eD_{\mathrm{vib}}}{kT}a^3(q-q_0)^3.$$

And in the integral over dq, we may replace the lower limit 0 with $-\infty$, the partition function obtained is

$$v(T)\simeq\frac{\pi kT}{ha}\sqrt{\frac{2m}{eD_{\mathrm{vib}}}}.$$

The averaged value of $q-q_0$ is given by the following expression,

$$<q-q_0>_{AV}=\frac{1}{v(T)h}\int_{-\infty}^{\infty}e^{-\frac{p^2}{2mkT}}dp\int_0^{\infty}(q-q_0)\times$$

$$\exp\left[-\frac{eD_{\mathrm{vib}}a^2(q-q_0)^2}{kT}+\frac{eD_{\mathrm{vib}}a^3(q-q_0)^3}{kT}\right]dq.$$

By the above-mentioned approximation, we get

$$<q-q_0>_{AV}=\frac{3}{4}\frac{kT}{aeD_{\mathrm{vib}}}.$$

The averaged value of double moment in rotation and vibration is

$$<p>_{AS}=p_0\left[1+\left(\frac{3}{4q\,aeD_{\rm vib}}-\frac{1}{4eD_{\rm rot}}\right)kT\right]$$

Unfortunately we have not the data of q_0, a, $D_{\rm vib}$ and $D_{\rm rot}$ for chemisorption. But it is probable that q_0 is slightly longer and a is slightly less than that of chemical binding, ecause the binding in adsorption may be mall compared to the chemical binding, and $D_{\rm vib}\sim D_{\rm rot}\frac{\pi^2}{2}$. This third assumption is reasonble in view of experimantal data, as we shall ee later. Here from the spectroscopic data f diatomic molecule we assume that $q_0\sim 2.5$A, ~ 2.5 A^{-1}, therefore $q_0a\sim 6.3$. Thus we can eglect the vibrational term against the roational term and obtain the final expression s follows:

$$<p>_{AT}=p_0\left(1-\frac{kT}{4eD_{\rm rot}}\right),$$

hat is, the temperature coefficient of the work unction due to chemisorbed layer is

$$a=\frac{1}{4eD_{\rm rot}}.$$

his formula has only one unknown constant $D_{\rm rot}$, and we can obtain the value of it from xperimental data.

omparing the above obtained formula with he author's observed results, we have the ollowing values as the height of potential arrier for $\theta=\frac{\pi}{2}$, i.e. $\frac{\pi^2}{2}D_{\rm rot}$,

oxygen on platinum	1.2 volts.

nd comparing with the data of Du Bridge(1), we get

oxygen on potassium	0.16 volts(4),
oxygen on molten metal	0.62 volts,
oxygen on tungsten	0.82 volts,
oxygen on platinum	1.3 volts,
oxygen on thoriated tungsten	2.5 volts.

rom 1.2 eV for oxygen on platinum, we have 5000 cal/gmol for one gram mol. This value is comparable with the heat of activated adsorption and is considered rather small. And theoretically it must be equal to the heat of diffusion, but usually the diffusion of gas atom progresses along the crystal surface rather than into crystal lattice, and we must not compare with it. The solution of a gas atom into metal begins to be striking at the temperature where the activated adsorption is maximum, that is, the adsorbed atom begins to evaporate from the surface or to penetrate into inside of metal at this temperature. Accordingly the assumption that $D_{\rm vib}\sim D_{\rm rot}\frac{\pi^2}{2}$ is consistent with the experimental facts. And furthermore the order of height of potential peak, i.e. potassium < tungsten < platinum is inverse to the order of lattice constant, i.e. potassium > tungsten > platinum. Therefore the above obtained values are reasonable.

In the electropositive atoms, the Fowler's theory can be applied and the two effects may arise simultaneously. But in the case of electropositive atom like hydrogen and others they easily evaporate and the current is too unstable to measure in every stage of outgassing.

In conclusion the author wishes to express his hearty thanks to Prof. T. Tanaka for his kind guidance throughout this work.

References.

(1) Du Bridge: Proc. Nat. Acad. Sci. **14** (1928); Phys. Rev. **31** (1928), 236, 912.

(2) R. H. Fowler: Proc. Roy. Soc. London A **122** (1928), 36.

(3) Zwikker: Phys. Zeits. **30** (1929), 578.

(4) This value is too small. The author considers it to be due to the incorrect data.

Thermionic Constant of Platinum, II. —On Face Excess Developed by Etching—

By Kenji KONDO.

Institute of Science and Technology, Tokyo Imperial University.

(Received December 3, 1946.)

§1. INTRODUCTION: PREVIOUS EXPERIMENTAL RESULTS.

In various problems which concern the surface of solid, for instance thermionics, adsorptions and etc., it is often necessary to know the true area of surface. When a polycrystal has been heated in order to outgass to such a high temperature that appreciable evaporation occurs, the surface consists of many crystal faces, which are inclined, in general, to the original or, strictly speaking, base surface and therefore increase the exposed area. As the true area is not equal to the apparent area, which we can usually measure, it is convenient to define the following quantity as Tonks did. The excess of true area of surface over underlying plane per unit area of the latter is

$$E=\frac{\text{true area}-\text{apparent area}}{\text{apparent area}}, \qquad (1)$$

and we shall call it the face excess. By this time the true area has been measured by numerous investigators by various methods, but their results are very different according to the treatment of surface and to the measuring method. Owing to Langmuir(1), a tungsten filament which has been etched during outgassing by heating it to 2900 K develops only dodecahedral crystal faces, i. e. (110 type, on which there are $1.425\cdot10^{15}$ tungsten atoms per cm². As it appears from the crystal structure of caesium and tungsten, that both metals have the same type of lattice structure, i. e. body-centred cubic lattice, and as the radius of a caesium atom is almost double that of a tungsten atom, it may be assumed that in a monolayer there will be one caesium atom per four tungsten atoms, such that $3.56\cdot10^{14}$ atoms per cm² can be adsorbed. But owing to his measurement it was found that $4.80\cdot10^{14}$ atoms of an apparent surface per unit area were covered by a monoatomic layer of caesium. Therefore a true surface must be 1.35 times an apparent area. From Becker's(2) similar measurement, it was concluded that the true area of a tungsten filament was 1.5 times the apparent.

Thereafter, in the measurement of accommodation coefficient of tungsten for inert gas, Roberts(3) compared the number of adsorbed hydrogen molecules with the number of tungsten atoms in the surface of filament. If filaments are smooth and one atom of hydrogen are adsorbed per one atom of tungsten in the surface, the number of molecules which can be adsorbed, will be $3.9\cdot10^{14}$. According to his observation, the numbers adsorbed were 4.2, 4.4 and $4.3\cdot10^{14}$. Therefore we must suppose that the roughness of the filament increases its true area in the ratio of 4.4/3.9 or 1.1 times.

§2. THEORETICAL CONSIDERATIONS.

In a thermionic filament the underlying base may be considered to be covered by pyramidal crystal faces and not needle-like or sheet-like structure as a blackened surface. The sum of the area of bases is the apparent area, and the sum of the area of covering crystal faces is the true area.

In general, we can express every crystal planes and base by the vectors which have the lengths equal to their areas and the directions parallel to their normals. Let the vectors, $\overrightarrow{OP}$; $\overrightarrow{OA}$, $\overrightarrow{OB}$, $\overrightarrow{OC}$ and etc. mean the base and every crystal plane, then there must be the following relations,

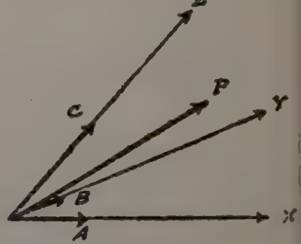

Fig. 1.

$$\overrightarrow{OP}=\overrightarrow{OA}+\overrightarrow{OB}+\overrightarrow{OC}+\cdots\cdots, \qquad (2)$$

In the most simple case where only three planes cover the base, if we make the coordinate axes parallel to three vectors $\overrightarrow{OA}$, $\overrightarrow{OB}$ and $\overrightarrow{OC}$, the absolute values of three vectors; $|OA|$, $|OB|$ and $|OC|$ are equal to the component of the vector $\overrightarrow{OP}$, and $\overrightarrow{OP}$ must lie in the region of solid angle XYZ of Fig. 1. And when $\overrightarrow{OP}$ has the constant length, $|OA|$, $|OB|$ and $|OC|$ are determined by the directions of $\overrightarrow{OP}$. If the frequency distribution of $\overrightarrow{OP}$ in the region of XYZ is independent of $|OP|$, we get as the face excess, the following expression:

$$E=\frac{\int(|OA|+|OB|+|OC|)g(w)dw}{|OP|\int g(w)dw}-1, \quad (3)$$

where $g(w)$ is the frequency distribution function of direction of $\overrightarrow{OP}$. Some years ago, Tonks(4) calculated the face excess from the following assumptions: (i) Only three crystal faces cover the base. (ii) The crystal orientation with respect to the underlying plane distributes in the whole directions with equal probabilities, that is, $g(w)$ is independent on w. (iii) As for the relative abundance of face types, given the type present, these occur in such a way as to give a minimum surface area or a minimum surface energy. Introducing his first assumption, he could avoid the complicated calculations, theory became very simple, but it has not been assured experimentally. On the contrary it is better to consider that there exist less frequently the configrations which have large area, because they have large surface energy, and more than three crystal faces can abundantly cover the base, when they have less area than that of three. Apparently his second assumption may be reasonable, but the author considers it to be not so; especially, in the case where more than three faces cover the base, this assumption is not moderate undoubtedly.

The form of crystal is principally determined by the velocity of growth of crystal plane. If we designate the area and the perpendicalar from the centre of cystal to crystal plane by S_1, S_2, …… and h_1, h_2, ……, and assume that S_i is the function of only h_i, we get the following relation:

$$S_i=a_ih_i^2,$$

where a_i is the constant of integration and the function of growth-velocity, $v_i=dh_i/dt$ and the angle between the face and the neighbouring faces. When the ratio of v_1/v_2 is in the neighbourhood of one or extreme values, by simple geometrical consideration we get the following relation:

$$\frac{a_1}{a_2}=\left(\frac{v_2}{v_1}\right)^2 f, \quad (4)$$

where f is the function of directions of crystal faces. Usually f is the degree of one or ten, but v_2/v_1 is infinitely large or very small (~0). Therefore we may assume that

$$a_1v_1^2\sim a_2v_2^2\sim\cdots\cdots . \quad (5)$$

The ratio of velocities of growth of two crystal faces is given by the following expression(5):

$$\frac{v_1}{v_2}=c_1\exp c_2\left(\frac{F_1}{kT}-\frac{F_2}{kT}\right), \quad (6)$$

where c_1 and c_2 are constants and F_1 and F_2 are surface energies of the crystal faces per unit area respectively. Surface energies F_1 and F_2 have not been accurately determined by observation, but may be order of some hundreds or some thousands ergs per cm². Outgassing of a filament are usually carried out at the temperature of between one and two thousand degrees. For instance, in the case where $T\sim2000$ K, $F_1/F_2\sim1.1$, $F_2\sim100$ ergs per cm², $v_1/v_2\sim\exp(3.5\cdot10^{13})$. That is, v_1 is enormously large compared to v_2, and a_1 is very small compared to a_2. As we shall see later, the mean values of area developed are in proportion to $a_i^{1/3}$ and only the net planes which have the minimum surface energy, i. e. the maximum a_i, can be developped. In body-centred cubic lattice, dodecahedral faces have the minimum surface energy. In considering the interaction with the first and second nearest neighbouring atoms, we get the following relations, $F_{(100)}/F_{(110)}\sim1.08$ and $F_{(111)}/F_{(110)}\sim1.11$. In face-centred cubic lattice, octahedral surface have the minimum energy. When we consider the interactions with the nearest neighbouring atoms, the ratio of surface energies are as follows: $F_{(100)}/F_{(111)}\sim1.15$ and $F_{(110)}/F_{(111)}\sim1.02$. That is, it is sufficient that we considered only dodecahedral faces in body-centred cubic lattice and only octahedral faces in face-centred cubic lattice. This conclusion coincides with Langmuir's opinion, for tungsten is of body-centred cubic structure. Let $f(S)$ means the probability that a crystal face has a larger area than S, and $\varphi\cdot ds$ the probability that a crystal face has the area between S and $S+dS$.

the following relation exists,

$$-\frac{df}{dS}=\varphi. \tag{7}$$

According to the increment dS of a surface area, the perpendicular to the surface increases by dh, where

$$dh=\frac{1}{2\sqrt{a}}\cdot\frac{dS}{\sqrt{S}}. \tag{8}$$

Every crystal grain grows from its nucleus, of which the orientation and the position distribute at random, and stops its growth, when its crystal face collides with crystal faces of other crystals. The probability that a crystal face stops its growth between S and $S+dS$ is as follows:

$$S\cdot n\cdot dh=n\cdot\frac{\sqrt{S}}{2\sqrt{a}}dS. \tag{9}$$

where n is the number of nuclei per unit volume.

Therefore the probability that a crystal face grows from S to $S+dS$ is equal to

$$(1-S\cdot n\cdot dh)=\left(1-n\frac{\sqrt{S}}{2\sqrt{a}}dS\right) \tag{10}$$

Accordingly the number of crystal faces which have an area larger than $S+dS$, i. e. $f(S+dS)$, is given by the following equation,

$$f(S+dS)=f(S)\left(1-\frac{n\sqrt{S}}{2\sqrt{a}}dS\right). \tag{11}$$

Expanding the left hand side of the above equation into Taylor's series and retaining its first and second terms, we get the following differential equation,

$$\frac{df}{dS}=-\frac{n\sqrt{S}}{2\sqrt{a}}f. \tag{12}$$

Integrating it, we have

$$f=\text{const.}\exp\left(-\frac{n}{3\sqrt{a}}S^{3/2}\right).$$

Differentiating by S, and normalizing it such that $\int_0^\infty\varphi dS=1$, we have the final distribution function as follows:

$$\varphi=\frac{n}{2\sqrt{a}}\sqrt{S}\cdot\exp\left(-\frac{n}{3\sqrt{a}}S^{3/2}\right). \tag{13}$$

This distribution means that of the interior and is not equal to that of a surface, because only one part of every crystal face can be exposed abundantly in a surface. In the cases, where crystal faces cover the base, the distributions does not obey (13), and in more than three crystal faces, some faces obey (13) and the other faces show the different distribution as we shall see later. Therefore, using (13) instead of exact distribution function we shall get the over face excess. When we assume that the probability that crystal faces, of which the area is S, expose the area between s and $s+ds$ in outside, is equal to ds/S, we get the corrected distribution function as follows:

$$\Psi(s)ds=ds\int_s^\infty\frac{1}{S}\varphi(S)dS. \tag{14}$$

As before, we use vectors for faces and base and designate the direction cosines and the area of i-th crystal face with l_i, m_i, n_i and s and the components of the base, X, Y and Z Then we get from the vector equation of (2 the following relations:

$$X=\sum_i s_i l_i,\ Y=\sum_i s_i m_i \text{ and } Z=\sum_i s_i n_i. \tag{15}$$

And the area of the base is

$$\sqrt{X^2+Y^2+Z^2}$$
$$=\{\sum_{ik}s_i s_k(l_i l_k+m_i m_k+n_i n_k)\}^{1/2}. \tag{16}$$

Therefore the obtained formula of face excess is as follows:

$$E_1=\frac{\int_0^\infty\cdots\int\sum_i s_i p(s_1)p(s_2)\cdots ds_1 ds_2\cdots}{\int_0^\infty\cdots\int\sqrt{H}p(s_1)p(s_2)\cdots ds_1 ds_2\cdots}-1, \tag{17}$$

where $H=\sum_{ik}s_i s_k(l_i l_k+m_i m_k+n_i n_k)$ and p i equal to Ψ or φ according to the positions o surfaces. But these formula are too complicated and laborious to estimate in practic and moreover, as mentioned in the first paragraph, the observed results do not coincide i each other within the probable error o measurement. Therefore, sacrificing the accuracy we may adopt the following approximate formula as the face excess in the plac of the above exact expressions,

$$E_2=\left\{\frac{\int_0^\infty\cdots\int\sum_{ik}s_i s_k p(s_1)\cdots ds_1\cdots}{\int_0^\infty\cdots\int H p(s_1)\cdots ds_1\cdots}\right\}^{1/2}-1. \tag{18}$$

This rough approximate formula does no deviate more than one tenth, and are sufficien for the purpose of this paper.

Integrating them, when all p are equal t Ψ or φ, we have

$$E_2=\left\{\frac{N<S^2>+N(N-1)<S>^2}{N<S^2>2\sum_{ik}n_{ik}<S>^2}\right\}^{1/2}-1, \tag{19}$$

where the terms in bracket < > means the averaged values; n_{ik} is $l_i l_k + m_i m_k + n_i n_k$, and N is the total number of exposed crystal faces. Using the φ distribution we get the following averaged values:

$$<S>=\int_0^\infty S\varphi(S)dS$$

$$=\frac{n}{2\sqrt{a}}\int_0^\infty S^{3/2}\exp\left(-\frac{n}{3\sqrt{a}}\sqrt{S^3}\right)dS$$

$$=\left(\frac{3\sqrt{a}}{n}\right)^{2/3}\Gamma\left(\frac{5}{3}\right)=0.9026\left(\frac{3\sqrt{a}}{n}\right)^{2/3}, \qquad (20)$$

where Γ is the gamma function. And the square mean value of area is as follows:

$$<S^2>=\int_0^\infty S^2\varphi(S)dS$$

$$=\frac{n}{2\sqrt{a}}\int_0^\infty S^{5/2}\exp\left(-\frac{n}{3\sqrt{a}}\sqrt{S^3}\right)dS$$

$$=\left(\frac{3\sqrt{a}}{n}\right)^{4/3}\Gamma\left(\frac{7}{3}\right)=1.1907\left(\frac{3\sqrt{a}}{n}\right)^{4/3} \qquad (21)$$

When we use the latter formula of the distribution function, the averaged area is as follows:

$$<S>=\int_0^\infty s\Psi(s)ds$$

$$=0.9026\left(\frac{3\sqrt{a}}{n}\right)^{2/3}\int_1^\infty\frac{dt}{t^3}=0.4513\left(\frac{3\sqrt{a}}{n}\right)^{2/3}. \quad (22)$$

And the square mean values of area is as follows:

$$<S^2>=\frac{n}{2\sqrt{a}}\int_0^\infty s^{5/2}ds$$

$$\times\int_1^\infty\frac{1}{\sqrt{t}}\exp\left(-\frac{n}{3\sqrt{a}}s^{3/2}t^{3/2}\right)dt$$

$$=0.3969\left(\frac{3\sqrt{a}}{n}\right)^{4/3}. \qquad (23)$$

Therefore, for the cases where the frequency distribution of all crystal faces are Ψ, we get from (19), (22) and (23) the final formula as follows:

$$E_2=\left[\frac{1.9481N+N(N-1)}{1.9481N+2\sum_{i>k}n_{ik}}\right]^{1/2}-1. \qquad (24)$$

§3. COMPARISON WITH TONKS' RESULTS, AND THE CORRECTION OF THERMIONIC CONSTANT OF PLATINUM.

First, in order to compare with the results of Tonks' theory, we calculate face excesses for the various cases as follows, though these are not considered to be realized.

(i) Three cubic faces (X, Y and Z in Fig. 2): E_1(Tonks)$=0.50$ and $E_2=0.42$. (ii) One cubic and two dodecahedral faces (C, B and Z in Fig. 2): $E_1=0.11$ and $E_2=0.10$. (iii) Three dodecahedral faces (A, B and C in Fig. 2): $E_1=0.16$ and $E_2=0.15$. (iv) One cubic, one dodecahedral and one octahedral faces (C, D and Z in Fig. 2): $E_1=0.09$ and $E_2=0.08$. That is, these two sorts of face excesses, which base on the complete different assumptions, are in fair agreement.

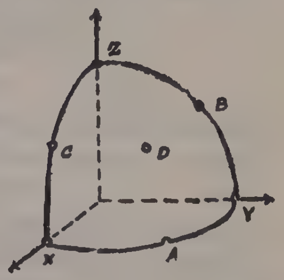

Fig. 2.

It is necessary to estimate the face excess of face-centred cubic lattice for the correction of thermionic constant A of platinum. As mentioned above, in this case only octahedral crystal faces are developped. Probably, three faces like A, B and C in Fig. 3 or four faces like A, B, C and D cover the base. Of course, the distribution function in this case is Ψ in four faces as well as in three faces. The calculated value of each excess by (24) is 0.34 or 0.28 respectively. The ratio of numbers of both configurations is 4 to 1, and the weighted mean of face excess is 0.33. In previous paper, the author assumed the excesses of 0.10, 0.25 and 0.40 for platinum filament and obtained the most reasonable value for 0.40.

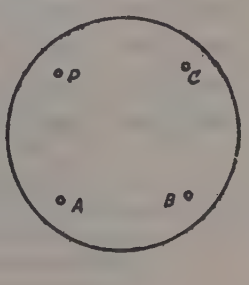

Fig. 3.

§ 4. COMPARISON WITH THE OBSERVED VALUES.

In order to compare the above theory with observed results, it is necessary to compute excess for the case of body-centred cubic structure like tungsten. As before mentioned, in this case only dodecahedral faces are developped. The results obtained by this theory are shown in the following table.

surface area. The weighted mean value of excess is 0.49. This value is in good agreement with Langmuir's and Becker's measured values, but different from Roberts'. Six faces are sufficient to cover hemisphere, and we omit the last two configurations in the table, then we get the excess of 0.41.

As mentioned above, the formula of (18) and the like are the rough approximation, and the exact theoretical values may be from 0.3 to 0.5 for face-centred cubic lattice and from 0.4 to 0.6 for body-centred cubic lattice. The experimental values of Langmuir and Tonks, which are too large compared with their theoretical values, are proved to be theoretically reasonable.

Table I.

No. of Crys. Faces	Crys. Faces (Fig. 4)	Excess +1	No. of Config.
3	a, b, c	1.15	9
3	a, b, d	1.21	24
4	a, c, e, f	1.29	6
4	a, b, c, d	1.35	48
5	a, b*, c, d, e	1.42	20
5	a, b, c, e, f	1.47	24
6	a, b*, c, d, e, f	1.47	24
6	a, b, c, e, f, g	1.74	24
7	a, b*, c, d, e*, f, g	1.71	48
8	a, b*, c*, d, e*, f*, g, h	1.89	6

Crystal faces which show the distribution of (13) are marked with asteriks. The directions of crystal faces designated by a, b and etc. are shown in Fig. 4. The above tabulated faces are selected in order to minimize the

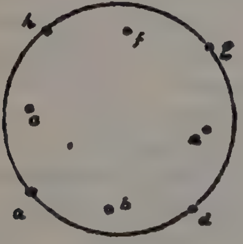

Fig. 4.

References.

(1) I. Langmuir: Phys. Rev. **22** (1923), 374.
(2) de Boer: Electron Emission and Adsorption Phaenomena.
(3) Roberts: Proc. Roy. Soc. London **152** (1935), 445.
(4) L. Tonks: Phys. Rev. **38** (1931), 1030.
(5) M. Volmer: Zeits. f. Phys-chem. **102** (1922), 267.

On the Phenomenon of the Periodical Exchange between the Phase-lattice and the Amplitude-lattice in the Fresnel's Diffraction Phenomenon by Gratings.—Theoretical Considerations and an Experiment by the Ultrasonic Wave.*

By Otohiko NOMOTO.

Kobayashi Institute of Physical Research, Kokubunji, Kokubunjimachi, Tokyo.

(Read May 27. 1944; Received October 21, 1946.)

§1. INTRODUCTION.

It was observed by Talbot(2), Lord Rayleigh(3) nd Winkelmann(4) that a beam of monochroatic light, when transmitted through an opcal grating perpendicularly, produces an nage of the grating, consisting of bright and ark stripes of the same periodicity as the rating. This image, however, is "not merely shadow of the grating", according to Rayigh; and shows the following peculiarities. he image vanishes periodically along the disnce behind the grating, and the positions of e bright and the dark stripes exchange one nother on crossing over the distances of anishing. These circumstances are illustrated hematically in Fig. 1, where GG′ means the rating, V_1, V_2, …… mean the planes of the nishing of the image, and A_1, A_2, …… those the maximum visibility of the image. The periodic distance of the recurrence of the same state of the image is given by

$$d=2a^2/\lambda, \qquad (1\cdot1)$$

where a is the lattice constant and λ the wave-length of the light (Cf. Fig. 1).

Observations similar to the above mentioned case of the optical grating were made some years ago by the present author(6) and by Parthasarathy(7) for the stationary ultrasonic wave, and then by Hiedemann and Schreuer

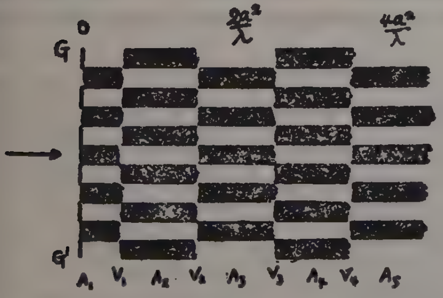

Fig. 1. Fresnel's diffraction phenomenon by an optical grating (Talbot's phenomenon).

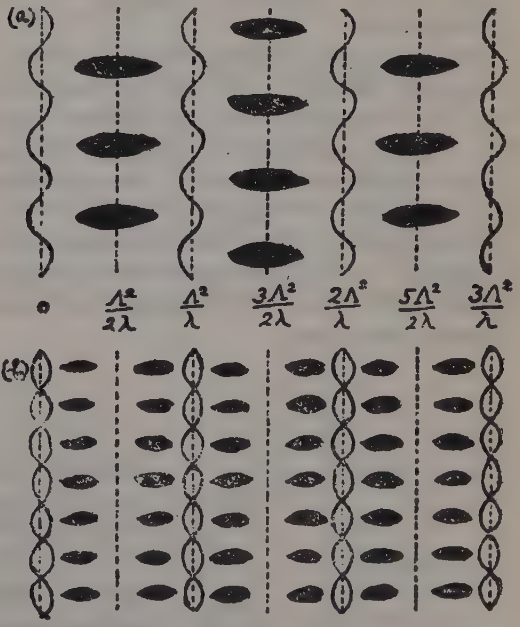
(a)
0
$\frac{\Lambda^2}{2\lambda}$
$\frac{\Lambda^2}{\lambda}$
$\frac{3\Lambda^2}{2\lambda}$
$\frac{2\Lambda^2}{\lambda}$
$\frac{5\Lambda^2}{2\lambda}$
$\frac{3\Lambda^2}{\lambda}$
(b)

Fig. 2. Periodical exchange between the phase-lattice and the amplitude-lattice by the Fresnel's diffraction of light by an ultrasonic grating.

(a) progressive ultrasonic wave.

(b) stationary ultrasonic wave.

A short account of this paper was published formerly n Japanese language(1).

for the progressive ultrasonic wave. The theoretical explanations for the periodicity of the image are given by the present author(6)(8) and by Nagendra Nath(9). The observations for ultrasonic waves are illustrated in Fig. 2, together with the newly calculated phase relations. The phenomenon for the stationary ultrasonic wave (Fig. 2(b)) can be obtained as a time average from the case of the progressive ultrasonic wave (Fig. 2(a)). (To obtain the image of the progressive ultrasonic wave, it is necessary to use an intermittent light source (the high frequency stroboscope) of the same frequency as the ultrasonic wave).

The observations and the theoretical calculations up to the present time, however, were concerning exclusively with the intensity relations or rather on the periodicity of the image, but not with the phase relations of the wave-surfaces, although Nagendra Nath and the present author have assumed the existence of a pure phase-lattice (corrugated wave surfaces of light) in the plane of emergence of light from the sound field. This assumption was borrowed from the theory of Raman and Nagendra Nath(10) on the diffraction of light by ultrasonic waves, and is in accordance with the fact that the ultrasonic wave is not visible in the plane of emergence of light from it(11)(6).

The experimental investigation of the phase lattice is, naturally, not easy so long as we use the light-wave. So the present author has used the ultrasonic wave and have made some observations concerning the periodicity, and especially the phase modulation of the wave-surfaces in the Fresnel's diffraction by a grating. The present paper treats this problem briefly from both theoretical and experimental viewpoints.

§2. THEORETICAL CONSIDERATIONS.

1. *Ultrasonic grating.* In Table I is repr duced the calculated result for the expressio of the light wave of primary intensity unit received on a screen, after it has pass through the progressive ultrasonic wa These results are obtained by simple transfo mations of the previously obtained expre sions(8). The rise and fall of the phase-latti is illustrated in Fig. 2, together with the pr viously obtained results concerning the perioc change of the intensity-lattice. These figur are only schematical, and we will not tou here the problem of the intensity distributi accompanying a fine-structure, because it w fully treated before(8)(12). We can find in t planes of vanishing of the image, the co rugated wave-surfaces of the same form, those assumed in the plane of the emergen from the ultrasonic wave. The phenomen for the stationary ultrasonic wave is, as abo mentioned, given by a time-average of t phenomenon for the progressive wave, a the vanishing of the image at the distan Δ $\Delta=\Lambda^2/2\lambda$ occurs merely as the time-averag

2. *Diffraction by an intensity-lattice.* N we shall consider the case of the optical the ultrasonic wave diffracted by a suitab amplitude-grating. We take an intensity-latt of a lattice constant a, of which the ha width $a/2$ is transparent and another h opaque to the waves. (More general cases not difficult to treat, but we restrict oursel to this special case because the present expe ment was performed under this condition.)

Now the diffracted light of each order the Fourier component of the light-intens distribution in the plane of the grating, that the emergent waves from such a grati

Table I.

distance	expression of the light wave	nature of the wave
0, 4Δ, ...	$\cos(\omega t-v\sin Kx)$	phase-lattice
2Δ, 5Δ, ...	$\sqrt{2}\cos(v\sin Kx-\pi/4)\cos\omega t$	amplitude-lattice
2Δ, 6Δ, ...	$\cos(\omega t+v\sin Kx)$	phase-lattice
3Δ, 7Δ, ...	$\sqrt{2}\cos(v\sin Kx+\pi/4)\cos\omega t$	amplitude-lattice

Table I. Expressions of the light-wave ϕ behind an ultrasonic wave grating. (Abbreviations: $k=2\pi/\lambda$, $K=2\pi/\Lambda$, $\Delta=\Lambda^2/2\lambda$, $v=2\pi\cdot\delta n\cdot L/\lambda$; Notations: L=Length of the path of the light in the ultrasonic wave, λ light wavelength in air, Λ=ultrasonic wavelength, δn=amplitude of the periodic change of the refractive index of the medium produced by the ultrasonic wave.) (Cf. Fig. 2(a)).

in the case of normal incidence, are given by

$$a=\frac{1}{2}\cos(\omega t-ky)+\frac{1}{\pi}\Big[\cos(\omega t-k_1y-Kx)$$
$$+\cos(\omega t-k_1y+Kx)$$
$$-\frac{1}{3}\cos(\omega t-k_3y-3Kx)$$
$$-\frac{1}{3}\cos(\omega t-k_3y+3Kx)\pm\cdots\cdots\Big], \qquad (2\bullet1$$

where

$$k=2\pi/\lambda, \quad k_n=\sqrt{k^2-(nK)^2}=k\sqrt{1-(n\lambda/a)^2}$$

and where y is taken in the direction of propagation of the incident light, and x in the direction perpendicular to the lines of the grating, the origin of the coordinate being taken as in Fig. 3. By omitting the common constant of the phase ky, we have, by putting $k_n=k-n^2\pi\lambda/a$, in the case $\lambda/a<<1$,

$$a=\frac{1}{2}\cos\omega t+\frac{1}{\pi}\left[\cos\left(\omega t+\pi\frac{\lambda}{a^2}y-Kx\right)\right.$$
$$\left.+\cos\left(\omega t+\pi\frac{\lambda}{a^2}y+Kx\right)\mp\cdots\cdots\right].$$

From this expression we can easily obtain Table II for the expressions of the light wave, in several characteristic distances behind the grating. This result is illustrated schematically in Fig. 3. The phase corrugation in the planes of vanishing of the image is abrupt and its amplitude amounts to 45°, which corresponds to the corrugation of the wave-surface of $\lambda/4$. The periodic distance is given by (1•1).

If the condition $\lambda/a<<1$ is no longer satisfied, as is the case in the present experiment, both the expressions (1•1) and (2•1) must be modified. The priodic distance should satisfy simultaneously the following conditions

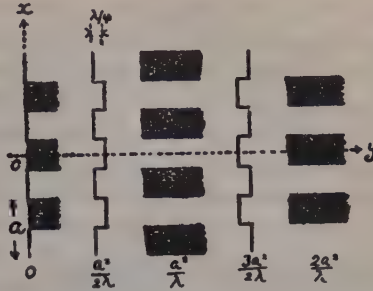

Fig. 3. Periodical exchange between the amplitude-lattice and the phase-lattice behind an diffraction grating of the intensity-lattice type.

$$d\,1-\cos\theta_n=m\lambda,$$
$$(n=1,2,3,\cdots\cdots,\ m=\text{arbitrary integer})$$

which, combined with the expression for the angles of diffraction $\sin\theta_n=n\lambda/a$, can be expressed also in the following form

$$d=\frac{2a^2}{\lambda}\left\{1-\frac{1}{4}\left(\frac{n\lambda}{a}\right)^2\right\}, \quad (n=1,2,\cdots\cdots).$$

But it is of course impossible to satisfy them simultaneously unless $\lambda/a<<1$. We may take, nevertheless, the distance

$$d=\frac{2a^2}{\lambda}\left(1-\frac{1}{4}\frac{\lambda^2}{a^2}\right), \qquad (2\bullet2)$$

as the nearly periodical distance of the phenomenon, because the higher diffraction orders are not present in this case. The angle of diffraction being restricted in the range $\theta_n\leqq\pi/2$, the distance (2•2) becomes practically the exact period in many cases, when $\lambda\sim a$. This is also the case in the present experiment, where $\lambda=a/2$, and where we have only the 0 and ±1-st orders as the diffracted waves. The second orders are not only of grazing emergence, but their intensities

Table II.

distance	expressions of the wave	nature of the wave
0, 4Δ, ……	$\alpha_0\cos\omega t$	amplitude-lattice
Δ, 5Δ, ……	$\frac{1}{\sqrt{2}}\cos(\omega t+\beta)$, $\begin{cases}\beta=\pi/4 \text{ for } \lvert x\rvert<a/4\\ \beta=-\pi/4 \text{ for } a/4<\lvert x\rvert<a/2\end{cases}$	phase-lattice
2Δ, 6Δ, ……	$(1-\alpha_0)\cos\omega t$	amplitude-lattice
3Δ, 7Δ, ……	$\frac{1}{\sqrt{2}}\cos(\omega t-\beta)$, $\begin{cases}\beta=\pi/4 \text{ for } \lvert x\rvert<a/4\\ \beta=-\pi/4 \text{ for } a/4<\lvert x\rvert<a/2\end{cases}$	phase-lattice

Table II. Expressions of the light wave α behind an grating. (Abbreviations: $K=2\pi/a$, $4\Delta=2a^2/\lambda$, $\alpha_0=\frac{1}{2}+\frac{2}{\pi}\left[\cos Kx-\frac{1}{3}\cos(3Kx)+\frac{1}{5}\cos(5Kx)\mp\cdots\cdots\right]$; Notations: a=lattice constant, λ=optical or the ultrasonic wave-length.)

are zero from the beginning. (The vanishing of even orders is the result of the equal width of the lines and gaps of the grating.)

As to the form of the phase-lattice, the exact calculation is impossible, unless the intensity distribution among the orders of the diffracted waves is known. But we can perform an approximate calculation by assuming the amplitudes of the 0 and the ± 1-st orders to be the same as in (2·1), and omitting the higher orders. Thus we obtain the intensity, and the phase relations as represented in Fig. 4. The wave form in this case is not rectangularly corrugated, but is approximately harmonically corrugated in the planes of the phase-lattice. At the same time, the amplitude-lattice is not completely lost in the phase-lattice positions, the change of the amplitude ranging from 1 to 1.6 in relative magnitudes. The positions corresponding to the crests and the bottoms of the valleys are more intense than on the slopes. The amplitude of the phase-change in this case is 52°.

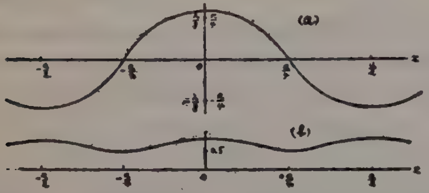

Fig. 4. Approximate result for the form and amplitude of the wave-surface at the phase-lattice positions.
(a) phase distribution (wave-form).
(b) amplitude distribution.

§3. METHODS AND THE RESULTS OF THE EXPERIMENT AND DISCUSSIONS.

The experimental arrangement for producing the images of the wave-surfaces is shown schematically in Fig. 5. *P* is a pin-hole, through which the monochromatic intermitten light emerges. We used an ultrasonic stroboscope of the stationary wave type, as wa first used by Becker, Hanle and Maercks(13) The two quartz plates, *Q* and *Q′* were connected to a common valve-oscillator, and consequently the frequency of illumination wa twice that of the ultrasonic wave. The wave surfaces produced in this manner are consequently half wavelength apart. *T* is a tan containing the liquid, in which the progressiv ultrasonic wave is produced by the oscillatin quartz crystal *Q*, and *G* is the diffractio grating, composed of parallel steel bars (1 mr in diameter) in equal intervals (gap 1 mm lattice constant 2 mm), whose directions bein parallel to the plane of the figure. *L* is collimator lense to produce the parallel bear of light, and *Ph* a photographic plate place at the first position of maximum visibility o the progressive ultrasonic wave. *A*, *A′* ar the sound absorbers to prevent the formatio of stationary waves.

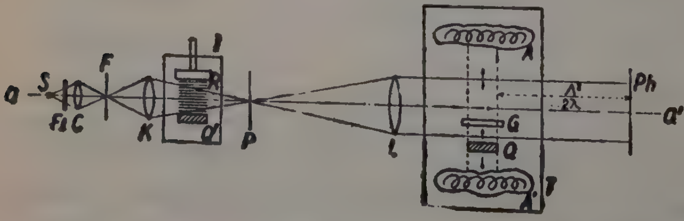

Fig. 5. Apparatus for obtaining the image of the wave-surfaces.

In order to obtain the image of the amplitude field of the ultrasonic wave we used th arrangement shown schematically in Fig.

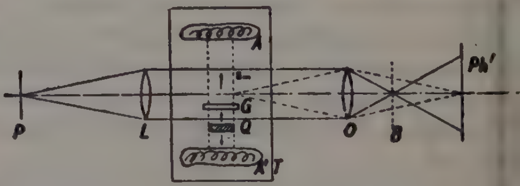

Fig. 6. Apparatus for obtaining the image of the amplitude distribution of the wave-field.

(method of the striae). We obtain this arrang ment from that of the previous figure, simp by disconnecting the quartz *Q′* of the strob scope from the oscillator, and by inserting lense *O* and a light-barrier *B* behind the tan In our arrangement, *B* was placed in the foc plane of the objective lense *O* order to cut off the undiffract light (optical image of the pi hole), so that only the diffract light can arrive on the phot graphic plate *Ph′*, on which focussed the plane of emergen (Em) of the light from the soun field. Thus, the image represen the abilities for diffracting lig f the ultrasonic field (integrated in the direc- ion of the incident light). And the brightness f the image corresponds to the amplitude- istribution of the ultrasonic wave so long as he amplitude does not exceed a certain limit $\leqq 2.4$). This arrangement corresponds to he one originally used by Hiedemann and Hoesch(14) and by Baer(15).

Fig. 7 represents some typical photographs obtained in these manners, where the left column (a) shows the wave-surfaces and the right column (b) the amplitude-fields. The rows (1), (2) and (3) correspond to the angles of incidences of 0° (normal incidence), 10 and

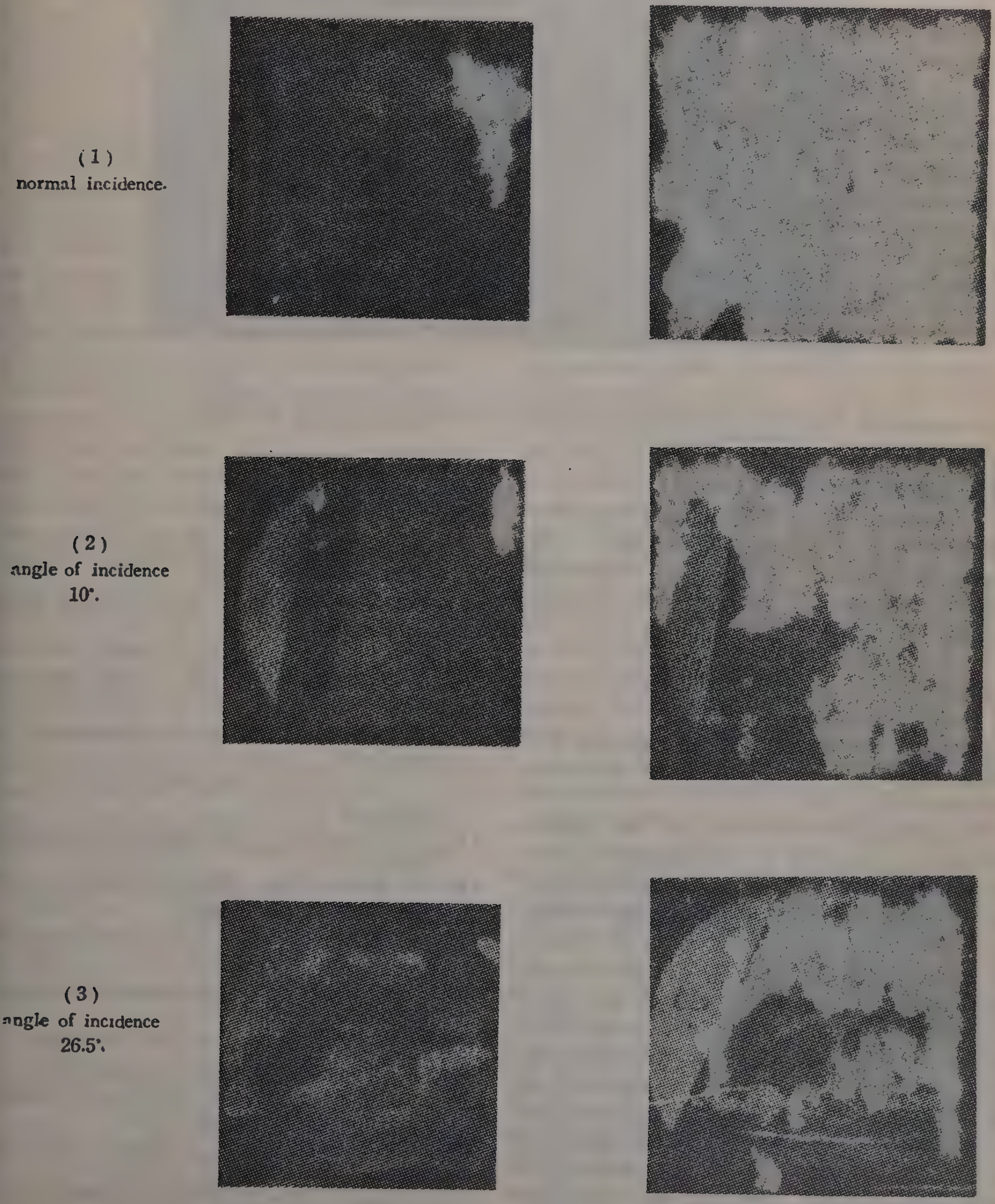

(a) Wave-surfaces. (b) Amplitude-field.

Fig. 7. Fresnel's difiraction phenomenon by grating. (Talbot's phenomenon).

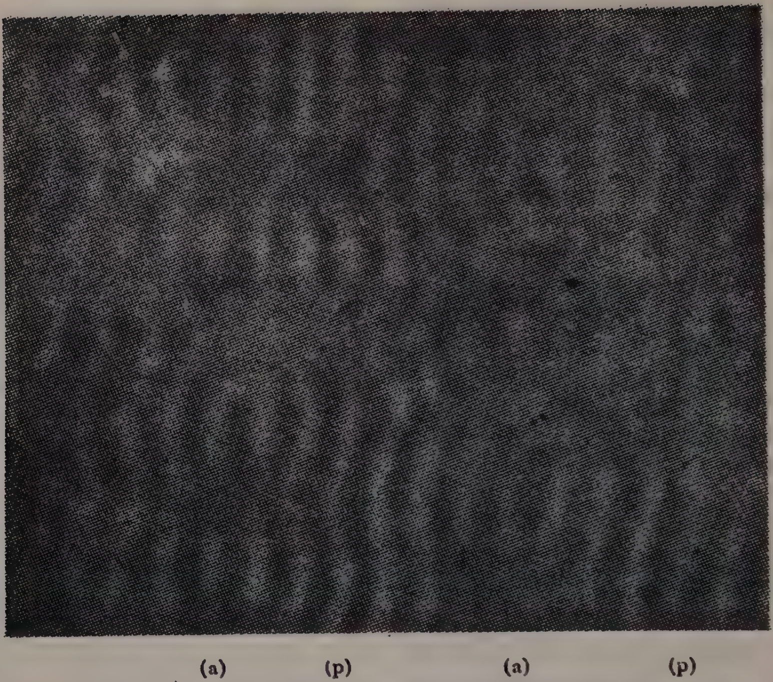

Fig. 8. Enlarged photograph showing the corrugated wave-surfaces (p phase lattice, a-amplitude lattice).

26·5° respectively.

On comparing these photographs with the calculated results of Fig. 4, we find a fair agreement among them. The observed periodic distance in case of the normal incidence is

$$d_{\mathrm{obs.}}=7.3\ \mathrm{mm},$$

and nearly coincides with the value

$$d_{\mathrm{cal.}}=7.5\ \mathrm{mm},$$

calculated from equation (2·2), assuming the lattice constant $a=2$ mm, and the ultrasonic wavelength $\lambda=1$ mm.

The amount (2×amplitude) of the phase-corrugation observed in the planes of the phase-lattice is nearly a quarter wave-length, as is seen on the enlarged photograph of Fig. 8. Whether the amplitude is 45° or 52° cannot be concluded from experiment. The corrugated form of the wave-surfaces are more resembling the curve of Fig. 3, as is to be expected. Moreover, there is some tendency that, the intensity along the wave-surface at the phase-lattice positions is not uniform, and corresponds qualitatively well to the calculated one in Fig. 4 (b). Thus on the whole, the experimental result confirms, the periodical rise and fall of the amplitude and the phase-lattices and the exchange between them very well.

References.

(1) O. Nomoto: Kwagaku (Science, Japanese), **1**
(1943), 440.
(2) F. Talbot: Phil. Mag. Dec. 1836 (Cited in Rayleigh's paper).
(3) Lord Rayleigh: Phil. Mag. **11** (1881), 196.
(4) A. Winkelmann: Ann. Phys. u. Chem. **27** (1908), 905.
(5) E. Hiedemann and E. Schreuer: Zeits. Phys. **10**
(1937), 463.
(6) O. Nomoto: Proc. Phys.-Math. Soc. Japan, **1**
(1936), 402.
(7) S. Parthasarathy: Proc. Indian Acad. Sci. (A), **4**
(1936), 555.
(8) O. Nomoto: Proc. Phys.-Math. Soc. Japan, **1**
(1937), 337, **21** (1939), 495.
(9) N. S. Nagendra Nath: Proc. Indian. Acad. Sci. (A), **4** (1936), 262.
(10) C. V. Raman and N. S. Nagendra Nath, ibid. **2**
(1935), 406.
(11) R. Baer: Helv. Phys. Acta, **9** (1936), 265.
(12) O. Nomoto: J. Phys. Soc. Japan, **2** (1947), 1.
(13) H. E. R. Becker, W. Hanle and O. Maercks: Phys. Zeits. **37** (1936), 414.
(14) E. Hiedemann and K. H. Hoesch: Zeits. Phys. **104** (1937), 197.
(15) R. Baer: Helv. Phys. Acta, **9** (1936), 617, **1**
(1937), 311.

Statistical Theory of Linear Polymers. I. Intramolecular Statistics.

By Ryogo KUBO.

Physical Department, Faculty of Science, Tokyo Imperial University.

(Received July 28, 1946.)

INTRODUCTION.

The molecular statistical theories of rubber- ke substances have been developed by many orkers since W. Kuhn's pioneer work apeared in 1936(1). In our country a considerble progress has been achieved by some orkers(2), but most of their works have not et been published because of the war. The resent paper and the ones which are shortly follow are to be offered to the descriptions the results I have gained in these years.

The statistical theory of linear polymers is vided into two distinct regions; first, the tramolecular statistics or the theory of a ngle giant molecule, and second, the interolecular statistics or the statistics of the ystem composed of a number of macroolecules interacting each other in a very mplicated manner. The latter must be built pon the basis of the former. So I want to scuss here only the first problem which will ter be developed to theories of elastic and tical properties of vulcanized and raw bber.

The mathmatical means used here is the ethod of generating functions well known the probability theory. This leads us to eigenvalue problem, the eigenvalue of hich determines the free energy and the genfunction gives the distribution function cessary for treating the problem of double fraction.

§ 1. PARTITION FUNCTION OF A CHAIN MOLECULE.

As is well known, the intramolecular motion a long chain molecule consists of the ange in bond distances and valence angles, tortional vibrations or rotations of the eleton, and the vibrations of the side chain groups. Various modes of vibration of the skeleton are coupled together, and form bands in wide regions of frequency. But rigorous treatments are almost impossible in the cases of complicated forms of the chain caused by the freedoms of internal motion.

Here we take rather the Einstein model, each submolecule vibrating in the force field determined by the mean distribution of the surrounding ones, because the vibrational waves cannot propagate along the whole molecule on account of the irregularities of its form. Vibrations of atomic distances and bond angles are quantized at ordinary temperatures, but the tortional vibration can be treated classically, the potential barrier being relatively low.

We are mainly interested in the partition function as a function of parameters specifying the forms of the macromolecule or the relative probabilities of the forms it can assume. So the tortional motion is the most essential, and other degrees of freedom including all the kinetic terms can be separated as mere factors at least approximately.

We take several submolecules as our element of the chain, which is enough to allow us to assume that only the correlation of two neighboring elements is to be taken into account. We specify the configuration of each element by a set of variables q, so its skeletal length in the configuration q is represented by a vector $\boldsymbol{a}_q$. Thus in essentials we neglect the finite volume of the constituent submolecules, the effect of which is analogous to the case of van der Waals correction in imperfect gases, and it may be neglected in the first approximation. As the number of the elements n is large, the apparent extent is proportional to $n^{3/2}$, their real volume being proportional to n. The partition function corresponding to the configuration in which the radius vector (or the length of the chain) $\boldsymbol{r}$ connecting the two ends of the chain falls within the elementary volume $d\boldsymbol{r}$ near $\boldsymbol{r}$ has the form

$$Z_n(\boldsymbol{r})d\boldsymbol{r}=\int\int\cdots\int\exp(-E/kT)dq_1dq_2\cdots dq_n, \quad (1)$$

where the integration is to be taken over all configurations satisfying the condition

$$\boldsymbol{r}\leqq\sum_i \boldsymbol{a}(q_i)\leqq\boldsymbol{r}+d\boldsymbol{r}.$$

In Eq. (1) E is the energy of the configuration $q_1, q_2, \cdots\cdots, q_n$. This is the sum of the interaction energy terms between two neighboring elements. This enable us to introduce the van der Waal's correction to a certain degree.

The partition functions (or the relative probability) $Z'_n(\boldsymbol{r}, q)$ of the configuration in which the length vector is $\boldsymbol{r}$ and the end element has the configuration q satisfy the recurrence formula

$$Z'_n(\boldsymbol{r}, q)=\int\exp\left\{-\frac{\varepsilon(q, q')}{kT}\right\}$$
$$\times Z'_{n-1}(\boldsymbol{r}-\boldsymbol{a}(q), q')dq', \quad (2)$$

where ε is the interaction between neighbors. We put

$$\exp\left(-\frac{\varepsilon}{kT}\right)=K(q, q'), \quad (3)$$

and name this correlation function. It can be seen at once that

$$Z_n(\boldsymbol{r})=\int Z'_n(\boldsymbol{r}, q)dq. \quad (4)$$

We introduce the Laplace transformation

$$Q'_n(\boldsymbol{s}, q)=\int Z'_n(\boldsymbol{r}, q)\exp(\boldsymbol{s}\boldsymbol{r})d\boldsymbol{r}. \quad (5)$$

And Eq. (2) is transformed into

$$Q'_n(\boldsymbol{s}, q)=\{\exp(\boldsymbol{s}\boldsymbol{a})\}\int K(q, q')Q'_{n-1}(\boldsymbol{s}, q')dq'. \quad (6)$$

The solution Q'_n must be the linear combination of terms $\lambda^n\Psi$, determined by the eigenvalue problem,

$$\lambda(\boldsymbol{s})\Psi(\boldsymbol{s}, q)=\{\exp(\boldsymbol{s}\boldsymbol{a})\}\int K(q, q')\Psi(\boldsymbol{s}, q')dq'. \quad (7)$$

Since n is large, the prominent term is that of the largest λ, while the others can be omitted asymptotically. $Q_n(\boldsymbol{s})$ or the Laplace transformation of $Z_n(\boldsymbol{r})$ is obtained from

$$Q_n(\boldsymbol{s})=\int Q'_n(\boldsymbol{s}, q)dq, \quad (8)$$

and Z_n itself from

$$Z_n(\boldsymbol{r})=\left(\frac{1}{2\pi i}\right)^3\int\int\int Q_n(\boldsymbol{s})\exp(-\boldsymbol{s}\boldsymbol{r})d\boldsymbol{s}, \quad (9)$$

where the integration is to be taken along th path from $\boldsymbol{s}^*-i\infty$ to $\boldsymbol{s}^*+i\infty$. Put

$$Q'_n(\boldsymbol{s}, q)=\lambda^n(\boldsymbol{s})\Psi(\boldsymbol{s}, q)$$
$$=\Psi(\boldsymbol{s}, q)\exp(n\mu(\boldsymbol{s})). \quad (10)$$

We can evaluate (9) by the method of steepes descent to be

$$Z_n(\boldsymbol{r})=\frac{sc(s)}{((2\pi)^{3/2}r\,n\mu''(s))^{1/2}}$$
$$\times\exp\{n\mu(s)-sr\}, \quad (11)$$

s being determined as a function of r from

$$n\frac{d\mu}{ds}=r, \quad (12)$$

where s and r are the magnitudes of vector $\boldsymbol{s}$ and $\boldsymbol{r}$ respectively and both vectors ar parallel to each other. The coefficient c i a normalizing factor related to Ψ. Helmholt free energy F is given by

$$F=-kT\log Z_n(r)$$
$$=kT(sr-n\mu(s))$$
$$+\text{terms of lower order of } n. \quad (1$$

The tensional force X applied to the ends o the chain is

$$X=\frac{\partial F}{\partial r}=kTs. \quad (14$$

The physical meaning of s first introduced a a mathematical convention is now clear; it i proportional to the force. So the logarithn of eigenvalue λ gives nothing but the Gibb free energy, namely

$$G=-nkT\mu\left(\frac{X}{kT}\right). \quad (15)$$

Thus we know that the free energy is propor tional to n, that is the number of element so that it is also proportional to the numbe of all the consitituent submolecules, and th chemical potential per one submolecule i proved to be some fraction of that of a element derived above.

Similarly we can easily get

$$Z'_n(r, q)=\frac{s\Psi(s, q)}{((2\pi)^{3/2}r\,n\mu'')^{1/2}}\exp(n\mu-sr), \quad (16)$$

which shows that Ψ is the distribution fun tion of end element when the length is r. I can also be proved without difficulty that th orientation probability of constituent element is given by

$$\Psi=[\Psi(s, q)]^2\exp(-\boldsymbol{s}\boldsymbol{a})$$
$$\Big/\int[\Psi(s, q)]^2\exp(-\boldsymbol{s}\boldsymbol{a})dq. \quad (17)$$

§ 2. MEAN VALUES OF POWERS OF THE LENGTH. EXPANSION FORMULAE.

When n is sufficiently large, $\tilde{Z}_n(r)$ is spherically symmetrical, for the asymptotic distribution of r does not depend upon the orientation of the first few elements. This is a case of the generalized Markoff's theorem. So λ involves only the magnitude of vector s. Expanding λ, μ and $Q_n(s)$ as power series of s, the following formulae may be obtained.

$$\lambda=\lambda_0+\frac{1}{3!}\lambda_2 s^2+\frac{1}{5!}\lambda_4 s^4+\cdots\cdots, \tag{18}$$

$$\mu=\mu_0+\frac{1}{3!}\mu_2 s^2+\frac{1}{5!}\mu_4 s^4+\cdots\cdots, \tag{19}$$

$$\mu_0=\log\lambda_0,\quad \mu_2=\lambda_2/\lambda_0,$$

$$\mu_4=(\lambda_4/\lambda_0)-\frac{5}{3}(\lambda_2/\lambda_0)^2\cdots\cdots, \tag{20}$$

$$\left.\begin{aligned}&\overline{r^2}=n\mu_2,\quad \overline{r^4}=\frac{5}{3}n^2\mu_2^2+n\mu_4\\&\overline{r^6}=\frac{35}{9}n^3\mu_2^3+7n^2\mu_2\mu_4+n\mu_6\end{aligned}\right\} \tag{21}$$

$$\frac{r}{n}=\xi=\frac{1}{3}\mu_2 s+\frac{4}{5!}\mu_4 s^3+\frac{6}{7!}\mu_6 s^5+\cdots, \tag{22}$$

$$\begin{aligned}s=&\frac{3}{\mu_2}\xi-\frac{27}{10}\frac{\mu_4}{\mu_2^4}\xi^3\\&+\frac{729}{100}\left(\frac{\mu_4^2}{\mu_2^7}-\frac{5}{42}\frac{\mu_6}{\mu_2^6}\right)\xi^5+\cdots\cdots,\end{aligned} \tag{23}$$

$$F=nkT\left[\frac{3}{2}\frac{\xi^2}{\mu_2}-\frac{27}{40}\frac{\mu_4}{\mu_2^4}\xi^4+\cdots\cdots\right] \tag{24}$$

§ 3. CHAIN WITHOUT CORRELATION.

It is instructive to consider the case where K is constant and equal to $1/4\pi$. Then the solution of (7) is

$$\lambda=\frac{\sinh as}{as},\qquad \Psi=\frac{1}{\lambda}\exp as\cos\theta, \tag{25}$$

where θ is the angle between the length vector r and the elementary vector a, and a is the magnitude of a. It can be easily seen that λ_0, λ_2, λ_4, …… are equal to 1, a^2, a^4, …… respectively. The equation (12) takes the form using the Langevin function L.

$$\frac{r}{na}=L(as),\qquad L(x)=\coth x-\frac{1}{x}. \tag{26}$$

§ 4. SOLUTION FOR SMALL s.

In this section we discuss the relatively simple case where our elements can be represented by mathematical vectors with equal length a and with correlations only between two neighbors. Though it does not correspond exactly to the tortional motion of the chain but rather the variation of bond angles, we can take a few skeletal units together as our element and apply the theory introducing some proper interactions between them. By this model the free rotation with constant bond angles can be treated rigorously, while the hindered internal rotation approximately. Another method of rigorous treatment will be given in another article.

In this case the correlation function K in Eq (13) involves only two variables, that is, the vectors a and a'. Denoting the angle $\angle as$ by θ, we expand the eigenfucntion Ψ as follows,

$$\begin{aligned}\Psi=&\Psi_0+\Psi_1(s)P_1(\cos\theta)\\&+\Psi_2(s)P_2(\cos\theta)+\cdots\cdots,\end{aligned} \tag{27}$$

where Ψ_l is a power series of s beginning with s^l. The correlation function is assumed to be

$$K(a,a')=K(\cos\gamma), \tag{28}$$

where γ is the angle between the two vectors a and a'. Define D_{kl} by the expansion coefficients of

$$\begin{aligned}&P_k(\cos\theta)\exp(as\cos\theta)\\&=\sum_l D_{kl}(as)P_l(\cos\theta).\end{aligned} \tag{29}$$

Then by the theorem of spherical harmonics, (7) becomes

$$\lambda\Psi_l=\sum_k D_{kl}c_k\Psi_k. \tag{30}$$

The c_k is the mean value of $P_k(\cos\gamma)$, namely

$$c_k=\iint K(\cos\gamma)P_k(\cos\gamma)\,d\omega. \tag{31}$$

Correlation function K may be normalized so that c_0 and λ_0 are equal to 1. When $s=0$, the largest eigenvalue λ is 1 and it must increase continuously with s. Using power series expansion of D_{kl}, we can determine λ_2, λ_4 ……, and Ψ_1, Ψ_2, …… step by step. The results are

$$\lambda_2=\frac{1+c_1}{1-c_1}a^2, \tag{32}$$

$$\begin{aligned}\lambda_4=&\left\{1+\frac{4}{3}\frac{c_1(1-8c_1-3c_1^2)}{(1-c_1)^3}\right.\\&\left.+\frac{8}{9}\frac{(1+c_1)(3-c_1)}{(1-c_1)^2}\frac{c_2}{1-c_2}\right\}a^4,\end{aligned} \tag{33}$$

$$\Psi_1=\frac{as}{1-c_1}\Psi_0+\cdots\cdots,$$

$$\Psi_2=\frac{a^2s^2(1+c_1)}{3(1-c_2)(1-c_1)}\Psi_0+\cdots\cdots. \tag{34}$$

Other formulae are omitted here on account of limited space. For the chain rotating freely with constant bond angle α,

$$c_1=\cos\alpha,\quad c_2=\frac{1}{2}(3\cos^2\alpha-1). \tag{35}$$

The function Ψ_1 and Ψ_2 are essential in the theory of double refraction.

§5. SOLUTION FOR LARGE s.

The asymptotic property of the chain as s tends to infinity can be known also from (7). Without going into details, we shall remark only the results. Equation (12) takes asymptotically the form

$$r/r_\infty=1-(1/a^*s). \tag{36}$$

Here r_∞ is the maximum length and a^* is of the same order of magnitude as a. It must be determined by the nature of the correlation. The free energy is given by

$$F=-(nkT\rho_\infty/a^*)\log(\rho_\infty-\rho),$$
$$\rho_\infty=r_\infty/na. \tag{37}$$

§6. CONCLUDING REMARKS.

In the next step we must consider the nature of the internal rotation more closely. We might take as a better model the case where the bond angles are all equal to the tetrahedral angle and the skeleton coordinates on a diamond lattice. The correlation between three or four elements is now taken into account. Their planar forms is most stable, and the other forms are of higher energy. Detailed discussion of this problem will be given in another paper. Here we only remark an approximate results

$$\mu_2=\frac{4}{3}a^2\exp(U/kT), \tag{38}$$

$$\Psi_1=\frac{1}{\sqrt{3}}as\Psi_0\exp(U/kT), \tag{39}$$

$$\Psi_2=\frac{8}{81}a^2s^2\Psi_0\exp(2U/kT),$$

where a is the distance of the skeletal bond. These are only valid for U/kT far larger than 1.

There remains more details to be discussed concerning the intramolecular statistics; for instance, the van der Waals corrections, orientation probabilities of constituent dipoles if any, the extent of the chain and so on. The mathematical method used here is fairly powerful and can be applied to other problems, especially to the theory of Brownian motion.

The author wishes to thank Prof. Ochiai and Prof. Kotani for their continual interest given to this work.

References.

(1) Kuhn: Kolloid-Z. **76** (1936), 258; Naturwiss. **24** (1936), 346; etc.
See also Guth and Mark: Mh. Chem. **65** (1934), 93, Z. Elektrochem. **43** (1937), 353, Guth and James: Ind. Eng. Chem. **33** (1941), 624, Horst-Mueller: Kolloid-Z **95** (1941), 138.

(2) T. Sakai: Nippon Sugakubutsurigakukaishi **17** (1943), 226; R. Kubo: ibid **17** (1943), 273. Since then many works have been presented in the meetings of Physico-Mathematical Society of Japan and Physical Society of Japan by the author and Prof T. Sakai and his coworkers.

Statistical Theory of Linear Polymers. II. Elasticity of Vulcanized Rubber.(1)

By Ryogo KUBO.

Physical Department, Faculty of Science, Tokyo Imperial University.

(Received December 2, 1946.)

INTRODUCTION.

Recent progress in the theory of rubber-like lasticity is rather remarkable. Since the vorks of W. Kuhn(2) much has been done, nd now it forms an important branch of tatistical thermodynamics. Kuhn's theory vas the first that succeeded in finding a relaion between the Young's modulus and moleular constants such as the molecular weight. lis result is

$$\varepsilon_0 = 7dRT/M, \qquad (1)$$

here ε_0=initial value of Young's modulus, =density, R=gas constant, T=absolute temerature, M=Molecular weight of a *single iant molecule.* He found that M was preicted to be 30,000 in rough agreement with xperimental results.

In spite of its apparent success, his theory an not stand severe criticism from the view oints of statistical mechanics. Since the acro-Brownian motion of a large molecule inhibited in rubber state, its weight M canot appear in thermodynamical equations. oreover, according to him most molecules ith curled form do not contribute to the ntropy changes caused by elastic deformaons, and the elastic stress is produced by e contribution of relatively few "fluctuang molecules." Is this "fluctuation" effect ssential to the rubber elasticity? We must y "no" from general concepts of thermoynamics. These difficulties have been pointed t by several workers(3)(4)(5). Among them kai(5) has criticized these points most early. It is not hard to see the origin of ese difficulties. It lies in an internal conflict the theory(6).

The first step of construction of the theory to grasp clearly the correspondence of the acroscopic variables, e. g. strains, to the olecular variables. When this is done, it depends mainly on a mathematical procedure to derive thermodynamical functions as functions of macroscopic variables. This requires us some clear model visualizing the states of molecules.

§ 1. NET-WORK STRUCTURE.

A great number of macromolecules is contained in a block of rubber, which interact each other in a very complicated way. In addition to repulsive and attractive forces between submolecules which construct macromolecules, lateral junctures between macromolecules must exist owing to vulcanization and entanglement characteristic to long chain molecules. Under these interactions it shows the peculiar rubber elasticity in a proper temperature region. Macromolecules must be held each other considerably tight, since they form an amorphous *solid.* On the other hand the structure should be so loose that submolecules can wander over distances far larger than in ordinary solids.

This is revealed in the fact that deformations can be very large, and that the Poisson's ratio is close to 1/2. Young's modulus ε, Poisson's ratio σ, and compressibility κ are connected by

$$\varepsilon_0 = \kappa(1-2\sigma)/3. \qquad (2)$$

In rubber-like substances ε_0 is far smaller than, while κ is of the same order of magnitude as, those of ordinary solids. Thus σ must be approximately equal to 1/2. In a sense rubber is like liquids, but its structure must be so firm as to forbid its parts to flow.

This characteristic property is visualized most clearly by the net work model (Fig. 1). Chain molecules form a three dimensional net, its lateral junctures being chemical or secondary due to van der Waals attraction. The parts of chain molecules lying between the junctures are wandering among their

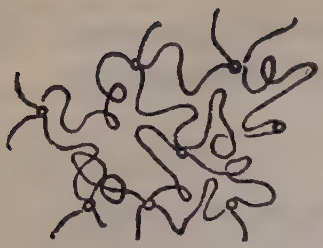

Fig. 1. The net-work model.

various configurations by thermal agitation. The deformation of the whole block causes changes in this thermal motion and also in secondary junctures. Changes in the latter requires some activation energy and relaxation phenomena may naturally be expected. This is essential in raw rubber. If vulcanized, junctures are almost of chemical nature and quite rigid, so that their changes can be neglected.

The compressibility of rubber indicates that the cohesive forces are of the same nature as ordinary solids. They are primarily due to attraction and repulsion between hydrogen atoms. Primary bonds are not affected by any change in the ranges of temperature and deformation of our interest. Therefore, we can put them out of our consideration. Then the cohesive energy will be approximately that of a virtual liquid consisting of elementary submolecules. It may be supposed to be somewhat of the form shown in Fig. 2. as a function of the volume v per element of the chain. The structure of the net is determined by the relative values of cohesion, thermal energy of chains, and binding energies of secondary junctures. As will be shown later, the latter two are far smaller than the first; that is the reason why the Poisson's ratio lies very near to 1/2.

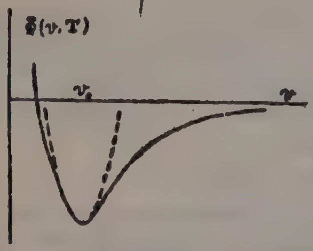

Fig. 2. The cohesive energy.

This paper treats only the case of vulcanized rubber. It exhibits the characteristics almost similar to ideal rubber. The theory of raw rubber will be given in a later paper.

§2. GEOMETRICAL CONSIDERATION ABOUT THE NET STRUCTURE.

Let the total number of the junctures and that of the elements be b and N respectively. Furthermore, we assume that each chain connecting neighboring two junctures contains n elements on the average. If γ chains start from one juncture, the total number of the chains is $\gamma b/2$, so we get

$$N=\frac{1}{2}\gamma bn. \tag{3}$$

Let the length of a chain (or distance between two neighboring junctures) be $na\rho_0$ in unstrained state, where a is the length of an element of the chain, and ρ_0 is a measure of its curling. Then the total volume V can be represented as

$$V=\delta(na\rho_0)^3b, \tag{4}$$

where δ is a constant determined by the structure of the net. The volume per element v is given by

$$v=\tau n^2a^3\rho_0^3,\quad \tau=2\delta/\gamma. \tag{5}$$

It $\gamma=4$ and the four chains make tetrahedral angles, δ would be 1.540 and $\tau=0.76$; if $\gamma=6$ and the six chains are orthogonal $\delta=0.33$. As mentioned above, effects of the deformation and temperature change on specific volume v can safely be neglected, so we put

$$v=\tau n^2a^3\rho_0^3=v_0, \tag{6}$$

where v_0 corresponds to the minimum of the cohesive energy.

Then we have

$$\rho_0=cn^{-2/3},\quad c=v_0/\tau a^3. \tag{7}$$

ρ_0 may be named the ***index of curling*** of the chain, for it shows how the chain is curled up. It is related to n or the density of lateral junctures which is defined by

$$b/N=2/\gamma n. \tag{8}$$

§3. ELEMENTARY THEORY.

In undeformed state chains are orientated in various directions. For the sake of simplicity we first assume that each one-third of the chains lie in x-, y- and z-direction. The macroscopical parameters of a deformation A, B and C will be defined as the ratio of actual lengths to original ones in each direc tion. Then for not too large deformation the partition function of a x-chain will be of Gaussian form(7)

$$Z_x = C\exp\left(-\frac{3}{2}\frac{nA^2\rho_0^2a^2}{\lambda_2}\right), \tag{9}$$

and similar formulae will be given for y- and z-chains. The free energy of the system is

$$F = \frac{1}{3}\frac{b\gamma}{2}kT(\log Z_x + \log Z_y + \log Z_z)$$

$$= \frac{NkT}{2\lambda_2}a^2\rho_0^2(A^2+B^2+C^2) + \text{const.} \tag{10}$$

The volume change can be neglected, so we have

$$ABC = 1. \tag{11}$$

The free energy F_1 per unit volume is written as

$$F_1 = \frac{dRTa^2}{2m\lambda_2}\rho_0^2(A^2+B^2+C^2) + \text{const.}, \tag{12}$$

where d=density, m=molecular weight of an element of the chain.

If the deformation is simply uniaxial in x-direction

$$B = C = 1/\sqrt{A}. \tag{13}$$

The tensional stress X_0 per unit area of original cross section is given by

$$X_0 = \frac{\partial F_1}{\partial A} = \frac{dRTa^2}{m\lambda_2}\rho_0^2\left(A - \frac{1}{A^2}\right). \tag{14}$$

Per unit area of actual cross section the stress is

$$X = AX_0 = \frac{dRTa^2}{m\lambda_2}\rho_0^2\left(A^2 - \frac{1}{A}\right). \tag{15}$$

The initial value ε_0 of Young's modulus is

$$\varepsilon_0 = \frac{3dRTa^2}{m\lambda_2}\rho_0^2. \tag{16}$$

λ_2 is given by Eq. (32), I, which is a function of temperature determined by the nature of internal rotation of the chain. For free rotation with bond angle α, it will be

$$\lambda_2 = \frac{1-\cos\alpha}{1+\cos\alpha}a^2. \tag{17}$$

In the presence of hindering potential, it might be expressed as (cf. Eq. (38), I)

$$a^2/\lambda_2 = \beta_0\exp(-U/kT). \tag{18}$$

Putting $\lambda_2/a^2 = 1$, $T = 300°\mathrm{K}$, $d = 1\,\mathrm{gr/cm^3}$, (16) will be

$$\varepsilon_0 = \frac{75600}{m}\rho_0^2. \tag{19}$$

When the maximum elongation is 700%, ρ_0 will be near 1/8 as Sakai pointed out. And n is estimated to be about 16 from Eq. (7) (with $\rho_0 = 1/10$, $n \sim 30$). If we put $m = 68$ (molecular weight of an isoprene monomer), ε_0 is 17 kg/cm² in agreement with the observed value. Naturally we can expect here agreements only in the order of magnitude, because we have not definite information regarding to what part of the molecule our element corresponds in actual cases. More refined discussion will be given in a later paper.

The expression (16) involves m but not M; this is in accordance with general concept of thermodynamics(5). It must be noticed that it also involves ρ_0^2 which characterizes the structure of the net. From (7) and (8) we have

$$\varepsilon_0 \propto (b/N)^{4/3}, \tag{20}$$

which shows that ε_0 increases with the density of junctures.

When the deformation is large and $A\rho_0$ is nearly 1, the elementary theory breaks down and we must consider in further detail.

§ 4. REORIENTATION OF CHAINS BY DEFORMATION.

If the rubber is isotropic in unstrained state, the orientation of the chains must be isotropic. What change will be observed by macroscopic deformation of the whole block? This question is geometrical and must be solved before a statistical-thermodynamical treatment. In the theories of crystals the corresponding questions is almost clear. In our case, however, its solution is somewhat ambiguous.

A macroscopical deformation is defined by the linear transformation

$$x = Ax,\quad y = By,\quad z = Cz. \tag{21}$$

Direction cosines of the chain, which were (ξ, η, ζ) before the deformation, will become proportional to $(A\xi, B\eta, C\zeta)$. Let the original length be r_0, then its length will be

$$r = r_0(A^2\xi^2 + B^2\eta^2 + C^2\zeta^2)^{1/2}. \tag{22}$$

Hence the index of curling of the chain is given by

$$\rho = \rho_0(A^2\xi^2 + B^2\eta^2 + C^2\zeta^2)^{1/2}, \tag{23}$$

where ρ_0 is its value in unstrained state. Since the substance is originally isotropic, (ξ, η, ζ) must be distributed uniformly on an unit sphere. All quantities must be averaged on it.

§5. GENERAL THEORY OF SMALL DEFORMATION.

The free energy of a chain with the index of curling ρ is given by (Eq. (13), I)(7)

$$f=nkTg(\rho)=nkT(as\rho-\mu(s)), \tag{24}$$

$$\frac{d\mu(s)}{ds}=a\rho. \tag{25}$$

The elastic free energy of chains will be given by the mean of (24). Per unit volume it will be

$$F_1=\frac{dRT}{m}\overline{g(\rho)}. \tag{26}$$

Put

$$A=1+\alpha,\ B=1+\beta,\ C=1+\gamma, \tag{27}$$

and assume that α, β and γ are far smaller than 1. Then we get

$$\begin{aligned}\rho/\rho_0&=1+\alpha\xi^2+\beta\eta^2+\gamma\zeta^2\\&+\frac{1}{2}[\alpha^2(\xi^2-\xi^4)+\beta^2(\eta^2-\eta^4)+\gamma^2(\zeta^2-\zeta^4)\\&-2(\beta\gamma\eta^2\zeta^2+\gamma\alpha\zeta^2\xi^2+\alpha\beta\xi^2\eta^2)].\end{aligned} \tag{28}$$

Strictly speaking, elastic energy change caused by the change of the volume must be added to (28). It may be expressed as

$$(v-v_1)^2/2\kappa v_1. \tag{29}$$

Putting

$$v_1=\tau n^3a^3\rho_1^3, \tag{30}$$

we get for volume v_0 in unstrained state

$$v_0=v_1\left(1-\frac{\kappa kT}{3v_1}\rho_1 g'(\rho_1)\right). \tag{31}$$

The ratio

$$\kappa kT/v_0=\kappa dRT/m$$

is only about 10^{-3} at room temperature. So we can entirely neglect the volume change.

By elementary calculations we can derive for the free energy

$$\begin{aligned}F_1=\frac{dRT}{m}g(\rho_0)+\frac{1}{2}\frac{dRT}{m}\Big[\Big\{\frac{1}{5}as_0\rho_0+\frac{2}{15}a\rho_0^2\\ \times\left(\frac{ds}{d\rho}\right)_0\Big\}(\alpha^2+\beta^2+\gamma^2)+\Big\{a\rho_0^2\left(\frac{ds}{d\rho}\right)_0\\ -as\,\rho_0+\frac{15m}{\kappa dRT}\Big\}(\alpha+\beta+\gamma)^2\Big],\end{aligned} \tag{32}$$

and for the rigidity

$$G=\frac{dRT}{5m}\left\{as\,\rho_0+\frac{2}{3}a\rho_0^2\left(\frac{ds}{d\rho}\right)_0\right\}. \tag{33}$$

When ρ_0 is small G is reduced to

$$G=\frac{dRT}{m}\frac{a^2\rho_0^2}{\lambda_2}, \tag{34}$$

in agreement with (16) ($G=\varepsilon_0/3$). If ρ_0 is clos to its maximum value ρ_∞, we have (§5, I)

$$G=\frac{dRT}{15m}\frac{\rho\,\rho_\infty(3\rho_\infty-\rho_0)}{c'(\rho_\infty-\rho_0)^2}. \tag{35}$$

The behavior of G as the function of ρ and b/N is given in Fig. 3 for chains withou correlation (§3, I).

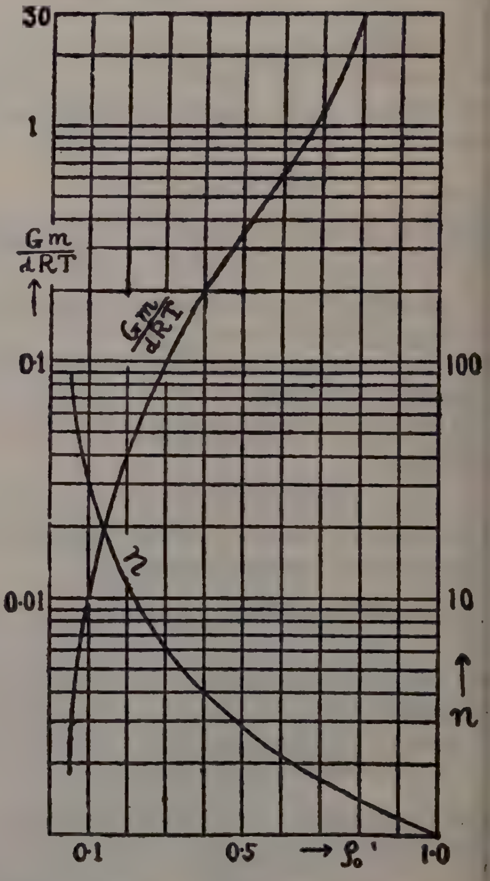

Fig. 3. Rigidity and the average number of elements in a chain as functions of the initial index of curling. For chains without correlation on the assumption $c=1$ in Eq. (7).

§6. LARGE DEFORMATION.

When ρ is not too large we can expan $g(\rho)$ in Eq. (26),

$$g=g_2\rho^2+g_4\rho^4+\cdots\cdots. \tag{36}$$

The expansion coefficients are given by

$$g_2=\frac{3}{2}\frac{a^2}{\lambda_2},\quad g_4=\frac{9}{8}\left(1-\frac{3}{5}\frac{\lambda_4}{\lambda_2^2}\right)\frac{a^4}{\lambda_2^2},$$

$$g_6=\frac{9}{4}\left(1-\frac{27}{20}\frac{\lambda_4}{\lambda_2^2}-\frac{9}{140}\frac{\lambda_6}{\lambda_2^3}+\frac{27}{50}\frac{\lambda_4^2}{\lambda_2^4}\right)\frac{a^6}{\lambda_2^3}, \tag{37}$$

where λ's are given in § 4, I. The free energy F_1 per unit volume can easily be shown to be

$$F_1=\frac{dRT}{m}\Big[\frac{g_2}{3}[\rho_0^2](A^2+B^2+C^2)+\frac{g_4}{5}[\rho_0^4]$$
$$\times\Big\{A^4+B^4+C^4+\frac{2}{3}(B^2C^2+C^2A^2+A^2B^2)\Big\}+\cdots\Big], \tag{38}$$

where $[\cdot]$ means the average values over the initial distribution of the index of curling.

In uniaxial elongation, X_0 is given by

$$X_0=\frac{dRT}{m}\Big[\frac{2}{3}g_2[\rho_0^2]\Big(A-\frac{1}{A^2}\Big)$$
$$+\frac{4}{5}g_4[\rho_0^4]\Big(A^3+\frac{1}{3}-\frac{4}{3A^3}\Big)+\cdots\cdots\Big], \tag{39}$$

and for the stress X referred to the actual cross section we have

$$X=AX_0. \tag{40}$$

For large A we make use of the asymptotic formula (37), I

$$F_1=\frac{dRT}{m}\frac{\rho_\infty}{a^*}\overline{\log(\rho_\infty-\rho)}.$$

Taking the average and differentiating with A we get

$$X_0\sim\frac{dRT}{m}\frac{a\rho_\infty^2}{a^*\rho_0}\frac{1}{A^2}\log\frac{A_1}{A_1-A},$$
$$A_1=\rho_\infty/\rho_0. \tag{41}$$

Similarly for compression it may be shown that

$$X_0\sim-\frac{\pi}{2}\frac{dRT}{m}\frac{\rho_\infty A}{\rho_0\sqrt{A-A_2}},$$
$$A_2=(\rho_0/\rho_\infty)^2. \tag{42}$$

§ 7. DISCUSSIONS.

We wish to add some remarks. The theory presented here concerns the ideal rubber, the definition of which is not unique. We make following assumptions; 1. Elastic deformation is reversible and plastic deformations are small. 2. Thermal equilibrium can be established during our observation. 3. Changes in internal energies are small. 4. Crystallization caused by the deformation is a secondary phenomenon and plays no essential role in producing elastic forces. These conditions are approximately satisfied by suitably vulcanized rubber. The sulfur bridges impose restrictions upon thermal motion of chains. They are almost sufficient to fullfil these conditions.

Thus our theory must be compared with experiments on that kind of rubber. Our theoretical formula (16) gives quite reasonable order of magnitude. Qualitatively (20) is also in agreement with the experience though we do not know how much sulfur is actually combined into bridges. It might be worth while to note that (16) shows that ε_0 of a sample with large maximum elongation ρ_∞/ρ_0 is small and vice versa(5)(8). The equation of state given in (14) seems to be quite general and is not confined to special models. Kuhn's theory leads us to it, too. It was derived by Guth and James(9) by the reasoning similar to ours. It can very closely reproduce the experimental results of Meyer and Ferri(10) up to 400 % elongation. (Fig. 4. For larger deformation the stress strain curve is affected by partial crystallization. If we neglect this effect, it might be expressed by Eq. (39). Fig. 5 gives a theoretical curve for chains without correlation. The stress X_0 shows the so-called S-shape. When referred to the actual cross section, the stress X does not show this peculiar form. This is in accordance with experience. The S-shape of X is usually observed only for raw rubber. We will give some explanations in a later paper.

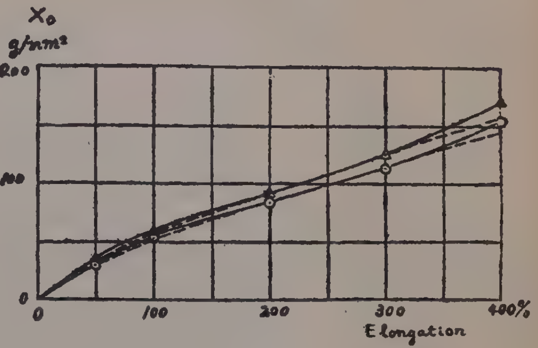

Fig. 4. The stress strain curve for vulcanized rubber.——experimental, ……theoretical curve.

If we could expect the index of curling of the chains to have the same value for all the chains in unstrained state, the average operation [ ] in Eq. (38) might be unneccesary. For not too large values of ρ_0, we have reasons to expect the distribution of ρ_0 is approximately given by

$$\exp(-\rho_0/\rho_1)d\rho_0/\rho_1. \tag{43}$$

Then $[\rho_0^2]$ will be $2\rho_1^2$.

Strictly speaking, the free energies of chains are not given by (9) or (24) in solid state. The

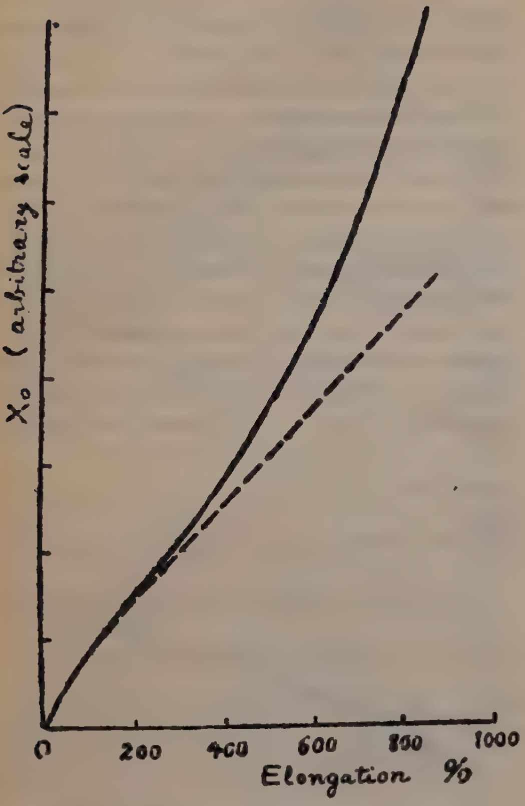

Fig. 5. Theoretical stress-strain curve, Eq. (39) for chains without correlation. $\rho_0=0.1$. ——calculated from (39)……first term of the expansion only.

chains can move in regions far more restricted than in free states considered in the paper I. However, we need only to know the relative changes of probabilities, therefore our assumption (9) or (24) may be expected to be right at least in the first approximation. More refined theories are left in future. but we can expect the essential points not to be affected.

The thermal motions of junctures were not considered explicitly. Their contribution to the change of elastic free energy seems to be small, because thermally agitating forces acting on them are random.

Part III of our studies deals with the elastic double refraction.

In conclusion the author wishes to express his deep appreciation to Dr. S. Oka, Prof. T. Sakai, Prof. K. Ochiai and Prof. M. Kotani for their valuable discussions and interest given to this work.

References.

(1) A part of this work was read in the meeting of Physico-Mathematical Society of Japan in 1943, and the other parts in 1945 and 1946.
(2) W. Kuhn: Kolloid-Z. **76** (1936), 258.
(3) Dostal: Mh. Chem. **71** (1938), 144, 399, 346.
(4) Pelzer: Mh. Chem. **71** (1938), 444.
(5) T. Sakai: Subutsukaishi **17** (1946), 226.
(6) R. Kubo: Kagaku **15** (1945), 43, **16** (1946), 7.
(7) R. Kubo: J. Phys. Soc. Japan, in this issue.
(8) Hatschek: J. Soc. Chem. Ind. **40** (1921), 251T.
(9) Guth and James: Ind. Chem **33** (1941), 624.
(10) Meyer and Ferri: Helv. chim. Acta. **18** (1935), 570.

Dissociation and Ionization of n-Hexane, Cyclohexane and Benzene by Electron Impacts, II.

By Toyozo KAMBARA.

Hitachi Central Research Laboratory, Hitachi Ltd.

(Recived December 26, 1946.)

(1) Investigation on the Cyclohexane C_6H_{12}.

Cyclohexane is a hydrocarbon of naphthene series and its chemical structure is ring shaped. Dissociation products of cyclohexane by electron impacts have already been investigated by Hustrulid, Kusch and Tate⁽¹⁾.

(A) Relative probability of the formation of ions in cyclohexane by electron impacts.

The ions observed as dissociation products of cyclohexane by single electron impact and the relative abundance of formed ions at the electron energies of 30 and 50 eV are tabulated in Table I and II respectively.

Fig. 1 shows the progress of dissociation of cyclohexane as the energy of bombarding electron increases. The typical mass spectrum of the ions of C_6 groups is shown in Fig. 2.

Table I. Nature and relative abundance of ions formed in cyclohexane by electrons with 30 volts energy.

Ion	$n=1$	$n=2$	$n=3$	$n=4$	$n=5$	$n=6$
C_n^+						
C_nH^+						
$C_nH_2^+$		0.17	0.08			
$C_nH_3^+$	0.26	0.69	0.48			
$C_nH_4^+$		3.79	0.44			
$C_nH_5^+$		0.90	9.61	0.36		
$C_nH_6^+$		0.28	6.80	1.78		
$C_nH_7^+$			3.23	9.25	0.50	
$C_nH_8^+$				27.96	1.05	
$C_nH_9^+$				2.71	7.30	
$C_nH_{10}^+$				0.44	0.88	
$C_nH_{11}^+$					0.25	0.87
$C_nH_{12}^+$						19.93
	0.26	5.83	20.64	42.50	9.98	20.80

Table II. Nature and relative abundance of ions formed in cyclohexane by electrons with 50 volts energy.

Ion	$n=1$	$n=2$	$n=3$	$n=4$	$n=5$	$n=6$
C_n^+			0.02			
C_nH^+		0.10	0.31	0.03		
$C_nH_2^+$	0.28	0.53	0.53	0.13		
$C_nH_3^+$	0.85	7.38	7.41	0.49	0.07	
$C_nH_4^+$	0.10	4.42	1.87	0.31	0.03	
$C_nH_5^+$		3.76	15.79	1.20	0.20	0.22
$C_nH_6^+$		0.16	6.08	1.66	0.12	0.28
$C_nH_7^+$			2.89	6.46	0.85	0.20
$C_nH_8^+$				15.57	0.62	0.07
$C_nH_9^+$				1.40	3.92	0.22
$C_nH_{10}^+$					0.48	0.39
$C_nH_{11}^+$					0.14	1.51
$C_nH_{12}^+$						10.95
	1.23	16.35	34.90	27.24	6.43	13.84

As previously mentioned, the ions of C_6 group among the dissociation products of n-hexane almost disappear even if the electron energy is 30 eV, on the other hand ions of C_6 group in cyclohexane considerably appear even at the energy of 50 eV. Consequently, cyclohexane must be more stable than n-hexane under the electron impacts. Moreover, from its molecular structure it seems to be reasonable that in cyclohexane the ion $C_2H_4^+$, $C_3H_6^+$, or $C_4H_8^+$ is more abundant than the others in each group.

(B) Appearance potentials of the formed ions in cyclohexane.

The appearance potentials of the formed ions in cyclohexane was determined by the

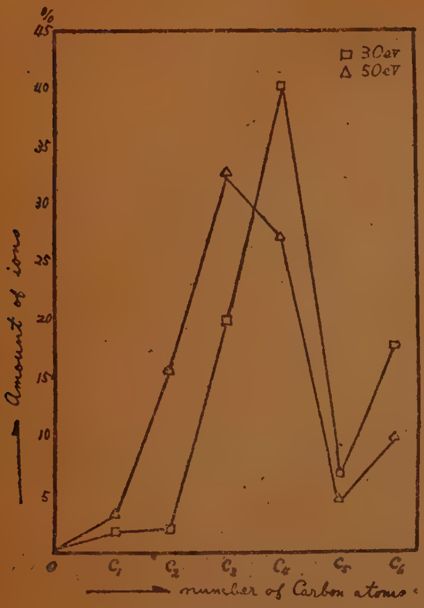

Fig. 1. The progress of dissociation of cyclohexane by electrons with 30 and 50 volts energy.

Table III. Appearance potentials of formed ions in cyclohexane.

Ion	Author	Tate
$C_6H_{12}^+$	10.3±0.2 eV	11.0±0.2 eV
$C_5H_9^+$	11.3±0.3	
$C_4H_8^+$	11.3±0.2	11.7±0.3
$C_4H_7^+$	12.8	
$C_3H_7^+$	13.5	
$C_3H_6^+$	12.9±0.2	
$C_3H_5^+$	14.8±0.2	13.5±0.3
$C_2H_5^+$	18.0	
$C_2H_4^+$	17.7	

same method as in n-hexane, and these values are shown in Table III.

In this Table appearance potential of the ion C_6H_{12} is about 1 eV lower than the value of ions $C_5H_9^+$, $C_4H_8^+$, etc. About this point cyclohexane is differnt from n-hexane, for it is necessary to break two C–C bonds if the latter ions appear.

A discussion will now be given for some particular cases. The heat of formation of cyclohexane is 1.65 eV calculated from the heat of combustion, and the dissociation energy of this molecule is 60.6 eV.

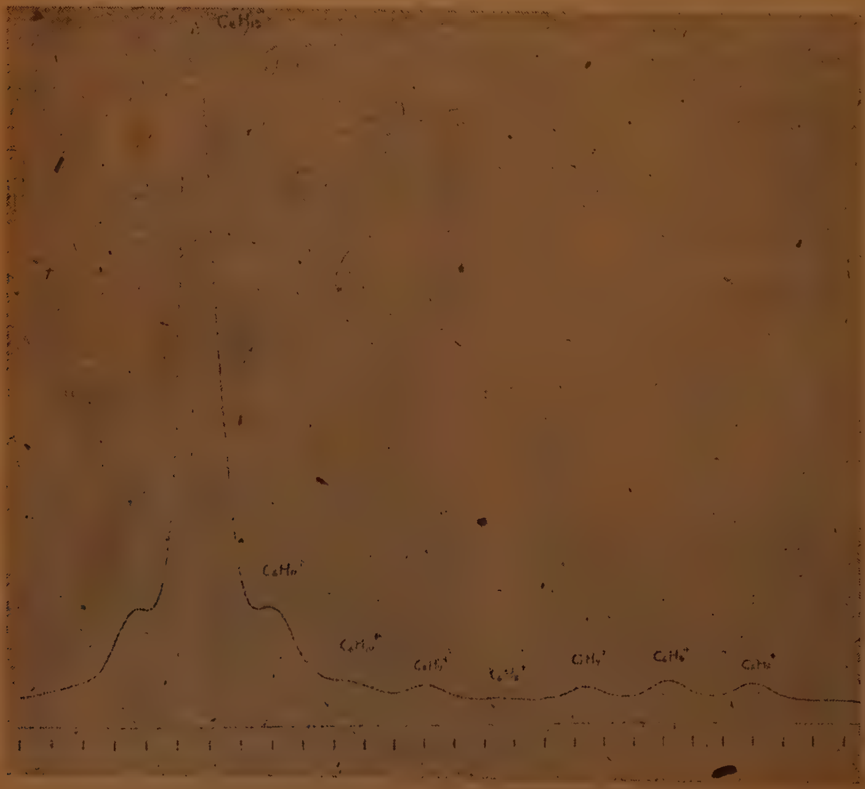

Fig. 2. Mass spectrum of ions of C_6 group in cyclohexane.

Table IV. Energies of dissociation of cyclohexane into its various constituents and interpretaion of the appearance potential.

	Configuration	energy	Appearance potential	Ionization potential
a	C_6H_{12}	0 eV	eV	$I(C_6H_{12}^+)=10.3$ eV
b	$C_5H_9+CH_3$	3.8	$A(C_5H_9^+)=11.3$	$I(C_5H_9^+)\lesssim 7.5$
c	$C_4H_8+C_2H_4$	1.6	$A(C_4H_8^+)=11.3$	$I(C_4H_8^+)\lesssim 9.7$
d	$C_3H_6+C_3H_6$	1.6	$A(C_3H_6^+)=12.9$	$I(C_3H_6^+)\lesssim 11.3$
e	$C_3H_6+C_2H_4+H_2$	3.4		
f	$C_3H_5+C_3H_6+H$	4.6	$A(C_3H_5^+)=14.8$	$I(C_3H_5^+)\lesssim 10.2$
g	$C_3H_5+C_3H_4+H_2+H$	6.4		$I(C_3H_5^+)\lesssim 8.4$
h	$6C+12H$	60.6		

The energies of the possible states in some particular ions are shown in Table IV.

In this case it is assumed that the dissociated products are in normal states.

1. $C_5H_9^+$.

The simplest way to produce this ion in cyclohexane is $C_6H_{12}\longrightarrow C_5H_9^+ + CH_3 + e$, but it should seem rather surprising that this process can happen as a result of single electron impact.

Ionization potential of ion $C_5H_9^+$ in this process is $I(C_5H_9^+)\leq 7.5$ eV, but this value is unreliable, as the state *b* is uncertain.

2. $C_4H_8^+$.

Energetically the most probable process to produce this ion is $C_6H_{12}\longrightarrow C_4H_8^+ + C_2H_4 + e$, and the value of $I(C_4H_8)\leq 9.6$ eV is almost equal to the value of this ion formed in n-hexane.

3. $C_3H_6^+$.

The most probable process to produce this ion from cyclohexane is $C_6H_{12}\longrightarrow C_3H_6^+ + C_3H_6 + e$, then the value of $I(C_3H_6^+)$ is less than 11.3 eV, and in this case the dissociated products have the excess energy of 1.3 eV if the ionization potential of this ion is the same value as in propylene, namely $I(C_3H_6^+)=10.0\pm 0.2$ eV measured by Delfosse and Bleakney⁽³⁾. On the same assumption in the process *e* the appearance potential of this ion is $A(C_3H_6)\geq 13.4$ eV.

4. $C_3H_5^+$.

The simplest way to produce this ion is $C_6H_{12}\longrightarrow C_3H_5^+ + C_3H_6 + H + e$, and in this process the upper limit of $I(C_3H_5^+)$ is 10.2 eV, but in the process *g* this value is 8.4 eV.

It seems to be reasonable that the appearance of $C_2H_5^+$ and $C_2H_4^+$ needs the breaking of three C–C bonds of carbon ring of cyclohexane because the appearance potentials of these ions are very high compared with above ions.

(2) Investigation on the Benzene C_6H_6.

Benzene molecule has the well-known ring-shaped structure and is very stable owing to the resonance effect between Kekulè and Dewar structures.

The dissociation products of benzene by

Table V. Nature and relative abundance of ions formed in benzene by electrons with 30 volts energy.

Ion	*n*=1	*n*=2	*n*=3	*n*=4	*n*=5	*n*=6
C_n^+						
C_nH^+				0.17		
$C_nH_2^+$		0.23		0.87		
$C_nH_3^+$		1.22	5.51	3.59	0.81	0.81
$C_nH_4^+$				8.17		6.55
$C_nH_5^+$						14.14
$C_nH_6^+$						57.94
		1.45	5.51	12.80	0.81	79.44

Table VI. Nature and relative abundance of ions formed in benzene by electrons with 50 volts energy.

Ion	*n*=1	*n*=2	*n*=3	*n*=4	*n*=5	*n*=6
C_n^+		0.03	0.13	0.29		0.13
C_nH^+		1.29	0.45	1.23	0.13	0.52
$C_nH_2^+$	0.13	1.88	1.39	8.29	0.36	1.81
$C_nH_3^+$	0.23	2.53	7.06	11.46	1.55	1.62
$C_nH_4^+$		0.13		8.13		4.15
$C_nH_5^+$						9.07
$C_nH_6^+$						36.01
	0.36	5.86	9.03	29.40	2.04	53.31

electron impacts have already been studied in detail by Hustrulid, Kusch and Tate⁽¹⁾.

(A) Relative probability of formation of ions in benzene by electron impact.

The ions observed as dissociation products of benzene by single electron impact and the relative abundance of formed ions at an electron energy of 30, 50 and 100 eV are tabulated in Table V, VI and VII respectively.

Because of the stability of benzene-ring structure the percentage of C_6 group in the dissociation products is still maintained at about 50 percent even if the energy of impinging electron is 100 eV. About this point benzene

Table VII. Nature and relative abundance of ions formed in benzene by electrons with 100 volts energy.

Ion	$n=1$	$n=2$	$n=3$	$n=4$	$n=5$	$n=6$
C_n^+	0.23	0.46	0.47	0.46	0.22	0.11
C_nH^+	0.19	2.40	2.61	2.24	0.74	0.74
$C_nH_2^+$	0.38	2.16	3.11	9.66	0.81	1.85
$C_nH_3^+$	0.78	1.85	6.80	10.54	3.59	1.17
$C_nH_4^+$	0.14	0.53		8.12		2.94
$C_nH_5^+$						7.43
$C_nH_6^+$						27.26
	1.72	7.40	12.99	31.02	5.36	41.50

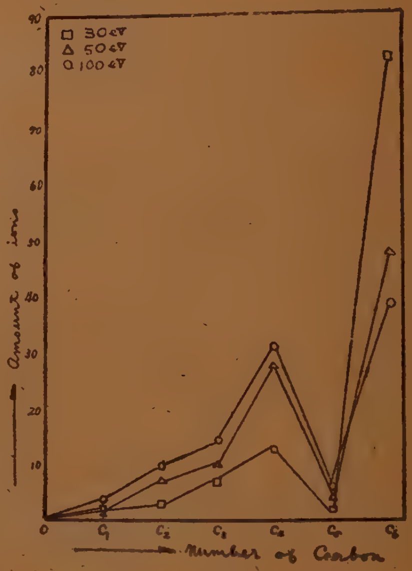

Fig. 3. The progress of dissociation of benzene by electrons with 30, 50 and 100 volts energy.

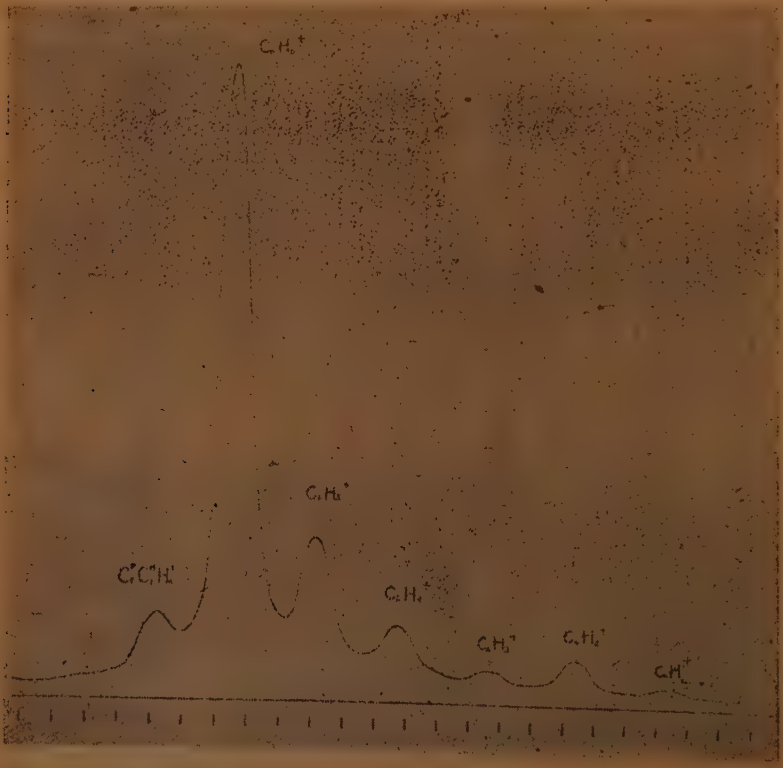

Fig. 4. Mass spectrum of ions of C_6 group in benzene.

is remarkably different from n-hexane and cyclohexane.

Fig. 3 shows the progress of dissociation of benzene as the energy of bombarding electron increases.

The typical mass spectrum of the ions of C_6 groups is shown in Fig. 4.

(B) Appearance potentials of the formed ions in benzene.

Appearance potentials of the particular ions among the dissociation products of benzene were measured by the same method as in n-hexane or cyclohexane and these measured values are shown in Table VIII.

Table VIII. Appearance potentials of formed ions in benzene.

Ion	Author (eV)	Tate (eV)
$C_6H_6^+$	9.2±0.1	9.8±0.1
$C_5H_3^+$	16.2	16.8±0.3
$C_4H_4^+$	15.9±0.1	15.5±0.3
$C_4H_3^+$	18.1±0.3	18.5±0.3
$C_4H_2^+$	18.3	18.3±0.5
$C_3H_3^+$	17.0±0.3	16.1±0.3
$C_2H_3^+$	20.2	21.1±1.0
$C_2H_2^+$	18.7	17.9±1.0

The values of appearance potential of ions containing five or less carbon atoms are much higher than the value of $A(C_6H_6^+)=9.2$ eV, namely $A(C_5H_3^+)=16.2$ eV, $A(C_4H_4^+)=15.9$ eV, etc. From this result the structures of ions $C_6H_5^+$, $C_6H_4^+$, etc. seems to maintain ring-shaped structures.

(3) Relation between the Hardness of Decomposition and the Antiknocking Tendency of Hydrocarbons.

The above mentioned results of the dissociation of n-hexane, cyclohexane and benzene by the electron impacts are closely connected with the antiknocking tendency of these vapors, for the latter property obviously depends upon the hardness of decomposition of the molecules.

Rice(2) explains the knocking phenomena as follows:

The explosions of hydrocarbons are of the chain type. In these reaction, at first the thermal decomposition occurs and there are produced the free radicals by which the reaction chains branch off, and then the oxidation processes takes place.

Thompson and Hinshelwood show that the rate of oxidation of ethylene is proportional to the third power of the ethylene concentration.

The thermal decomposition of the hydrocarbons will increase the concentration and rapidly accelerate the oxidation reaction to the explosion.

However, it is in question which bond in hydrocarbon, C–C bond or C–H bond, will first be broken in the thermal decomposition, but energetically it seems to be reasonable that the C–C bond may first be broken and the parent molecule may decompose into the smaller molecules and radicals.

The amount of products by thermal decomposition depends upon the stability of hydrocarbon molecule.

Now it will be assumed that the following equation f shows the instability of hydrocarbons,

$$f=\frac{\sum\limits_{n=0}^{a}\frac{a}{n}C_n}{\sum\limits_{n=0}^{a}C_n},$$

where a shows the number of carbon atoms in the original molecule, and C_n shows the amount of ions containing n carbon atoms.

Namely the value f is assumed to be nearly equal to the number of moles of product per mole decomposed.

Relation between f and the octane value of several hydrocarbons which were investigated here by massspectrograph is shown in Table IX.

Table IX. Relation between instability of hydrocarbon and its octane value.

Hydrocarbon	f 30 eV	f 50 eV	Octane value
n-hexane	1.93	2.00	25
cyclohexane	1.57	1.89	77
benzene	1.15	1.38	100
propane(3)		1.38, 1.36	100
butane(4)		1.55	92
ethane(5)		1.09	104

As the value of f, becomes smaller, the antiknocking tendency increases.

The author wishes to express his grateful appreciation to Dr. Baba, Dr. Toriyama and Dr. Hamada for their kind advices and encouragements.

References:

(1) Kusch, Hustrulid and Tate: Phys. Rev. **52** (1937), 843.
(2) F. O. Rice: Industrial and Engineering Chemist
26 (1934), 259.
(3) J. Delfosse & W. Bleakney: Phys. Rev. **56** (1939
256.
(4) Stewart & Olson: J. Am. Chem. Soc. **53** (1936
1236.
(5) J. A. Hipple: Phys. Rev. **53** (1938), 530.

On the Formulas for the Relative Multiplet Strengths in *LS* Coupling.

By Ayao AMEMIYA.

Department of Dynamics, 1st Faculty of Engineering, Tokyo University.

(Received June 20, 1946.)

§1. Introduction.

The formulas for the relative multiplet strengths in *LS* coupling have been known for a number of years. These have been derived by Kronig(1), Ornstein(2), Dirac(3), Condon and Ufford(4), Ufford and Millers(5), Shortley(6), and Yamanouchi(7). All of these but the last one have been dealt with as the extension of the Kronig's and in an actual calculation of these quantities we owe to the sum rule. Goldberg has calculated a very complete set of tables of the relative multiplet strengths. As these methods must depend on the sum rule, it is not easy to obtain the general formulas. But treating them group-theoretically, we will be able to get them in some cases. In the following we will analyse this problem.

In the *LS* coupling the electron configurations between which transitions can occur are of two cases, that is;

i) $\alpha+l_1 \rightleftarrows \alpha+l_2$,

ii) $\alpha \rightleftarrows \beta+l$.

i) α is an electron configuration in which no jumping electron involves and no electron is equivalent to any in l_1 or l_2. From the selection rule we must have $l_2=l_1\pm1$. Or, without loss of generality we may assum

$$l_2=l_1+1=l+1, \qquad l_1=l.$$

For example, in $d^3p\to d^3d$, $\alpha=d^3$, $l_1=p$ and $l_2=$ Or, in $d^2ps\to d^2pp'$, $\alpha=d^2p$, $l_1=s$ and $l_2=p'$,

ii) α is an electron configuration whic involves a jumping electron, on the other han β does not. l is a jumping electron. F example, in d^4-d^3p, $\alpha=d^4$, $\beta=d^3$ and $l=$ Also in $d^2p^2-d^2pd'$, $\alpha=d^2p^2$ $\beta=d^2p$ and $l=d$

In this paper we are concerned only wi the case (i).

§2. Method of Calculation.

It is easy to calculate the transition pr bability of the electrodipole radiation. A cording to the above papers it is given the formulas:

$$S(L,S\to L',S)=(2S+1)\sum_{M,M'}\left|\boldsymbol{p}_{S,\,L,\,M}^{\;L',\,M'}\right|^2,$$

or owing to the spherical symmetry of t atom the squared component of $\boldsymbol{p}$ has t same value for any direction.

So we have

$$S(L,S\to L',S)=3(2S+1)\sum_{M,M'}\left|(p_z)_{S,\,L,\,M}^{\;L',\,M'}\right|^2.$$

Since the z-component of the electric m ment p_z has the non-trivial values for $M'=$ only, they are given as follows:

$$(p_z)_{S,L+1,M}^{L,\ M}=C_{S,L}^{L+1}\sqrt{(L+M+1)(L-M+1)},$$

$$(p_z)_{S,L,M}^{L,\ M}=C_{S,L}^{L,}M,$$

$$(p_z)_{S,L,\ M}^{L-1,M}=C_{S,L}^{L-1}\sqrt{(L+M)(L-M)},$$

so that

$$S(L,S\to L+1,S)$$
$$=(2S+1)(L+1)(2L+1)(2L+3)\alpha_{S,L}^{L+1},$$

$$S(L,S\to L,S)=(2S+1)L(L+1)(2L+1)\alpha_{S,L}^{L},$$

$$S(L,S\to L-1,S)=(2S+1)L(4L^2-1)\alpha_{S,L}^{L-1},$$

where $\alpha_{S,L}^{L'}=\dfrac{(C_{S,L}^{L'})^2}{F^2}$.

The next step is that of obtaining $(p_z)_{S,L,\ M}^{L',\ M}$. For this purpose we construct the matrix of (p_z) in the scheme of $X(m_1m_2\cdots\cdots m_n, m)$, $X'(m_1m_2\cdots\cdots m_n, m')$, where X and X' are the sets of $\alpha+l_1$ and $\alpha+l_2$ respectively, and $m_1m_2\cdots\cdots m_n$, m and m' signify the orbitals of α, l_1 and l_2. So we have

$$M=\Sigma m_i+m=\Sigma m_i+m',$$
$$\therefore\quad m=m'.$$

Since $p=-e\Sigma z$,

so, if we use the well-known orthogonal sets of normalized product eigenfunctions, the non-vanishing elements of the matrices may be given by

$$(p_z)_X^{X'}=u(E)p_{xx'}(E),$$

where

$$p_{xx'}(E)=-e(m|p_z|m')$$
$$=-e\int_0^\infty r^3u_{l_2}(r)u_{l_1}(r)dr$$
$$\times\int_0^\pi\Theta(l_1m)\Theta(l_2m)\cos\theta\sin\theta d\theta\int^{2\pi}e^{i(m-m')\varphi}d\varphi$$
$$=-e\sqrt{\frac{(l+1)^2-m^2}{(2l+1)(2l+3)}}\int_0^\infty u_{l_2}u_{l_1}r^3dr$$
$$=\sqrt{(l+1)^2-m^2}\,F,$$

and $u(E)$ is a representation of the unit element of the symmetric group S_{n+1}.

The matrix T which is neccesary to the transformation from X scheme to (LS) scheme is that which diagonalize the square of the angular momentum operator $\mathbf{L}^2$, where

$$\mathbf{L}^2=(\sum_{i=1}^{n}l_i+l)^2=\mathbf{L}_i^2+2\mathbf{L}_il+l^2$$

Now, we are able to show that T has the following form

$$T=UV,$$

where, U is the matrix which diagonalizes $\mathbf{L}_i^2$, then we have

$$T^{-1}(\mathbf{L}_i^2)T=U^{-1}(\mathbf{L}_i^2)U,$$

so that $T^{-1}UU^{-1}(\mathbf{L}_i^2)UU^{-1}T=U^{-1}(\mathbf{L}_i^2)U=G.$

$$\therefore\quad GU^{-1}T=U^{-1}TG.$$

put $U^{-1}T=V,$

so we have

$$T=UV.$$

The matrix V which is defined as above is easily obtained, since V diagonalizes the matrix $U^{-1}(2\mathbf{L}_il)U$. Details have been shown in our paper⁽⁹⁾. From those results we may have U of the following form

$$U=\begin{pmatrix}U_l & & & \\ & U_{l-1} & & 0\\ 0 & & \searrow & \\ & & & U_{-l}\end{pmatrix},$$

where U is a matrix which diagonalizes $\mathbf{L}_i^2$, when $\Sigma m_i=-k$ $(k=l,\ l-1,\ \cdots\cdots-l)$.

As is easily seen, (p_z) matrix has the following form;

m \ m'	$-l-1$	$-l$	$-l+1$	$-l+2$
$-l$	0		0	0
$-l+1$	0	0		0
$-l+2$	0	0	0	
$-l+3$	0	0	0	0

Since the necessary permutation is E only, the blank spaces may be diagonal and these elements are

$$\sqrt{(l+1)^2-k^2}\qquad(k=-l,\ -l+1,\ \cdots l).$$

Accordingly

$$(V(\mathrm{I})^{-1}U(\mathrm{I})^{-1}(p_z)U(\mathrm{II})V(\mathrm{II}))_{ij}$$
$$=\sum_{k=-l}^{l}(V(\mathrm{I})^{-1})_{ik}(V(\mathrm{II}))_{kj}\sqrt{(l+1)^2-k^2},$$

where I and II signify the initial and final state respectively.

§3. Results.

In the following we have a table of the multiplet strengths for several values of l_1, where we omit the factor $\dfrac{2S+1}{F^2}$ for simplicity and put $\mathbf{L}_i^2=L_i(L_i+1)$

$l_1=0$ $L_i\geqq 1$

p \ s	L_i+1	L_i	L_i-1
$L=L_i$	$2L+3$	$2L+1$	$2L-1$

$L_i=0$

p \ s	1
0	3

$l_1=1$ $L_i\geqq 2$

d \ p	L_i+2	L_i+1	L_i	L_i-1	L_i-2
$L=L_i+1$	$6(2L+3)$	$3(2L+1)\frac{L-1}{L}$	$(2L-3)\frac{L-1}{L}$	0	0
$L=L_i$	0	$3(2L+3)\frac{L+2}{L+1}$	$\frac{(2L+3)(4L^2-1)}{L(L+1)}$	$3(2L-1)\frac{L-1}{L}$	0
$L=L_i-1$	0	0	$(2L+5)\frac{L+2}{L+1}$	$3(2L+1)\frac{L+2}{L+1}$	$6(2L-1)$

$L_i=1$

d \ p	3	2	1
2	42	15/2	1/2
1	0	45/2	15/2
0	0	0	10

$L_i=0$

d \ p	2
1	30

$l_1=2$ $L_i\geqq 3$

f \ d	L_i+3	L_i+2	L_i+1	L_i	L_i-1	L_i-2	L_i-3
$L=L_i+2$	$15(2L+3)$	$\frac{5(2L+1)(L-2)}{L}$	$\frac{(2L-5)(L-2)}{L}$	0	0	0	0
$L=L_i+1$	0	$\frac{10(L+2)(2L+3)}{L+1}$	$\frac{2(2L+1)(4L^2-9)}{L(L+1)}$	$\frac{3(2L-3)(L-2)}{L}$	0	0	0
$L=L_i$	0	0	$\frac{6(2L+5)(L+2)}{L+1}$	$\frac{9(L+2)(L-1)(2L+1)}{L(L+3)}$	$\frac{6(2L-3)(L-1)}{L}$	0	0
$L=L_i-1$	0	0	0	$\frac{3(2L+5)(L+3)}{L+1}$	$\frac{2(2L+5)(4L^2-1)}{L(L+1)}$	$\frac{10(2L-1)(L-1)}{L}$	0
$L=L_i-2$	0	0	0	0	$\frac{(2L+7)(L+3)}{L+1}$	$\frac{5(2L+1)(L+3)}{L+1}$	$15(2L-1$

$L_i=2$

f \ d	5	4	3	2	1
4	165	45/2	3/2	0	0
3	0	225/2	63/3	3	0
2	0	0	72	30	3
1	0	0	0	42	21
0	0	0	0	0	21

$L_i=1$

f \ d	4	3	2
3	135	35/3	1/3
2	0	280/3	35/3
1	0	0	63

$L_i=0$

f \ d	3
2	105

Remark: Of course, it is possible to show that the values of these tables satisfy the J-file sum rule.

§4. Summary.

In some cases we are able to obtain the general formulas of the mutiplet strengths in terms of L values of parent terms upon which the supermultiplets are based. As described above the strengths in a definite multiplicity do not change their values for the different types of the core. And they depend on L_i and l only. Our result covers about one half of the Goldberg's table, i.e. $p^n s - p^n p$, $p^n p - p^n d$, $p^n d - p^n f$, $d^n s - d^n p$, $d^n p - d^n d$. $d^n ss' - d^n sp$, $d^n sp - d^n sd$.

References.

(1) Z. S. f. Phys. **33** (1925), 261.
(2) ibid. **24** (1924), 41.
(3) Proc. Roy. Soc. **111** (1926), 302.
(4) P. R. **44** (1933), 740.
(5) ibid. **46** (1934), 283.
(6) Proc. Nat. Acad. **20** (1934), 501.
(7) Astrophys. J. **82** (1935), 1.
(8) Proc. Phys.-Math. Jap. **23** (1941), 1063.
(9) Subutu Kaisi (Phys.-Math. Soc. Jap.) **17** (1943), 567.

Approximate Methods regarding Electromagnetic Waves in Hollow Pipes and Cavities.*

By Taro KIHARA.

Physical Institute, Faculty of Science, Tokyo University.

(Received December 2, 1946.)

In the region of centimeter wave, metallic hollow pipes are widely used as transmission apparatus and metallic cavities are used as resonators. Many mathematical investigations regarding electromagnetic waves in hollow pipes and cavities have been made since the year 1936. Some effective methods, however, are not hitherto put to use. In this paper the following problems are treated: (1) the applications of variation principle to proper oscillations of cavities and pipes, (2) the general formulation for radiation field of a dipole in a pipe, (3) quasi-static approximation and its application to iris-diaphragms, (4) applications of W. K. B. method to pipes with non-uniform cross section and problem of tunnel-effect, (5) application of the perturbation method to curving pipes.

Gauss' system of units is used.

I. APPLICATION OF THE VARIATION PRINCIPLE.

§1. The Variation Principle for Electromagnetic Oscillation.

The variation principle, which is widely used in problems of mechanical oscillation and quantum theory, is also applicable to the electromagnetic oscillation in resonant cavities. Here we consider a cavity enclosed completely with perfect conductor. Let $\mathbf{E}$ be a vactor satisfying

$$\operatorname{div}\mathbf{E}=0, \tag{1·1a}$$

within the cavity and

$$[\mathbf{E},\ \mathbf{n}]=0, \tag{1·2a}$$

on the boundary surface. $\mathbf{n}$ is the normal unit vector. Further put

$$J(\mathbf{E})=\iiint \mathbf{E}^2 dxdydz,$$

$$D(\mathbf{E})=\iiint (\operatorname{rot}\mathbf{E})^2 dxdydz. \tag{1·3a}$$

Here the extent of the integration is the whole inner space of the cavity.

Now we assume that $\mathbf{E}$ makes $D(\mathbf{E})$ minimum under the condition $J(\mathbf{E})=1$. Another vector

$$\mathbf{E}_1=\mathbf{E}+\xi\mathbf{a}+\eta\mathbf{b},$$

which differs from $\mathbf{E}$ a little, is taken using $\mathbf{a}$ and $\mathbf{b}$ which meet the same requirement as (1·1a), (1·2a). From the condition of minimum:

$$\frac{\partial D(\mathbf{E}_1)}{\partial\xi}=k^2\frac{\partial J(\mathbf{E}_1)}{\partial\xi},$$

---

* The greater part of this investigation was reported to the "War-Time Research, April 1944—March 1945", though the latter half of the report was not printed.

$$\frac{\partial \dot{D}(\mathbf{E}_1)}{\partial \eta} = k^2 \frac{\partial J(\mathbf{E}_1)}{\partial \eta},$$

at $\xi = \eta = 0$ (k^2=Lagrangian factor), we have

$$\iiint(-\text{rot}\ \boldsymbol{a}\ \text{rot}\ \mathbf{E} + k^2 \boldsymbol{a}\mathbf{E})dxdydz = 0,$$

and the similer relation as to $\boldsymbol{b}$. Using the vector identity

$$\text{rot}\,\boldsymbol{a}\,\text{rot}\,\mathbf{E} = \text{div}[\boldsymbol{a}, \text{rot}\,\mathbf{E}] + \boldsymbol{a}\,\text{rot}\,\text{rot}\,\mathbf{E},$$

and the assumed boundary condition of $\boldsymbol{a}$ and $\boldsymbol{b}$, we obtain

$$\iiint \boldsymbol{a}(-\text{rot}\,\text{rot}\,\mathbf{E} + k^2\mathbf{E})dxdydz = 0,$$

and the similar one for $\boldsymbol{b}$. From these equations we get

$$-\text{rot}\,\text{rot}\,\mathbf{E} + k^2\mathbf{E} = 0,$$

namely $\boldsymbol{E}$ can represent the electric field of a proper oscillation with time variation $\exp(-ikct)$; and the magnetic field $\boldsymbol{H}$ in this oscillation is given by

$$\text{rot}\,\boldsymbol{E}e^{-ikct} = \frac{-1}{c}\frac{\partial}{\partial t}(\boldsymbol{H}e^{-ikct}) = ik\boldsymbol{H}e^{-ikct}. \quad (1\text{・}5\text{a})$$

The above used normalization $J(\mathbf{E})=1$ can be eliminated when we adopt the condition

$$D(\mathbf{E})/J(\mathbf{E}) = \text{minimum};$$

this form also will be used later. The eigenvalues k^2 ceincide with this minimum values, because

$$D(\mathbf{E}) = \iiint(\text{rot}\,\boldsymbol{E})^2 dxdydz$$

$$= -\iiint \mathbf{E}\,\text{rot}\,\text{rot}\,\mathbf{E}dxdydz = k^2 J(\mathbf{E}).$$

In reference to the above-mentioned theorem we can express the dual theorem: Let $\boldsymbol{H}$ be a vector satisfying

$$\text{div}\,\boldsymbol{H} = 0, \quad (1\text{・}1\text{b})$$

within the cavity and

$$\boldsymbol{H}\boldsymbol{n} = 0, \ [\text{rot}\,\boldsymbol{H}, \boldsymbol{n}] = 0, \quad (1\text{・}2\text{b})$$

on the boundary. If we assume that $\boldsymbol{H}$ makes $D(\boldsymbol{H})$ minimum under the condition $J(\boldsymbol{H})=1$, we get

$$-\text{rot}\,\text{rot}\,\boldsymbol{H} + k^2\boldsymbol{H} = 0, \quad (1\text{・}4\text{b})$$

where k^2 equals this minimum value. Namely $\boldsymbol{H}$ can represent the magnetic field of a proper oscillation with time variation $\exp(-ikct)$; the electric field $\boldsymbol{E}$ in this oscillation is given by

$$-ik\mathbf{E} = \text{rot}\,\boldsymbol{H}.$$

Now let two eigenvalues be k_n^2, k_m^2, and the corresponding eigenfunctions be $\mathbf{E}_n$, $\mathbf{E}_m$; viz.

$$-\text{rot}\,\text{rot}\,\mathbf{E}_n + k_n^2\mathbf{E}_n = 0,$$

$$-\text{rot}\,\text{rot}\,\mathbf{E}_m + k_n^2\mathbf{E}_m = 0,$$

Then

$$(k_n^2 - k_m^2)\iiint \mathbf{E}_n\mathbf{E}_m dxdydz$$

$$= \iiint(\boldsymbol{E}_m\,\text{rot}\,\text{rot}\,\boldsymbol{E}_n - \boldsymbol{E}_n\,\text{rot}\,\text{rot}\,\boldsymbol{E}_m)dxdydz$$

$$= \iiint\{\text{div}\,[\text{rot}\,\boldsymbol{E}_n, \boldsymbol{E}_m] - \text{div}\,[\text{rot}\,\boldsymbol{E}_m, \boldsymbol{E}_n]\}$$

$$\times\, dxdydz = 0,$$

indicating the orthogonality of eigenfunction The same relations hold for $\boldsymbol{H}$.

§2. The Fundamental Oscillation in an Ellipsoidal Cavity.

There are two ways of using the above mentioned principle for practical problem The Ritz method, which will be used in th following sections, is popular; but the othe method applied in this section is also powerfu though the idea of minimum is not so clea

Let us investigate the fundamental oscillation in an ellipsoidal cavity, the equation o which is

$$1 - \frac{x^2}{a^2} - \frac{y^2}{b^2} - \frac{z^2}{c^2} = 0, \quad (a \geq b \geq c).$$

The electric and magnetic field of the fundamental oscillation has the following symmetr property:

$$E_x = xz \times \text{ef}, \ E_y = yz \times \text{ef}, \ E_z = \text{ef},$$

$$H_x = y \times \text{ef}, \ \ H_y = x \times \text{ef}, \ \ H_z = xyz \times \text{ef}, \quad (2\text{・}2$$

where ef's denote even functions of x, y, z.

As the first approximation we adopt as the polynomial of the lowest degree whic has the above-mentioned symmetry and sati fies (1・1a), (1・2a);

$$E_c = 2xz/a^2, \qquad E_y = 2yz/b^2,$$

$$E_z = (F-1)\left(1 - \frac{x^2}{a^2} - \frac{y^2}{b^2}\right) - (F-3)\frac{z^2}{c^2}, \quad (2\text{・}3$$

$$F = (a^2+b^2)c^2/a^2b^2 + 3,$$

and we can take $D(\mathbf{E})/J(\mathbf{E})$ as the first ap proximation $[k^2]_1$ of k^2. Using

$$(\text{rot}\,\mathbf{E})_x = -Fy/b^2, \ \ (\text{rot}\,\mathbf{E})_y = Fx/a^2,$$

$$(\text{rot}\,\mathbf{E})_z = 0,$$

we obtain

$$[k^2]_1 = \left(\frac{1}{a^2} + \frac{1}{b^2}\right)\frac{7F}{2F-1}$$

$$= \left(\frac{1}{a^2} + \frac{1}{b^2}\right)\left(\frac{1}{a^2} + \frac{1}{b^2} + \frac{3}{c^2}\right)$$

$$\div\left(\frac{2}{a^2} + \frac{2}{b^2} + \frac{5}{c^2}\right). \quad (2\text{・}4)$$

As the second approximation we adopt th

polynomial of the lowest degree which has the symmetry-property (2·2) and satisfies (1·1b), (1·2b):

$$H_x = -a^2 y\left(D_1 - A_1\frac{x^2}{a^2} - B_1\frac{y^2}{b^2} - C_1\frac{z^2}{c^2}\right),$$
$$H_y = \ b^2 x\left(D_2 - A_2\frac{x^2}{a^2} - B_2\frac{y^2}{b^2} - C_2\frac{z^2}{c^2}\right),$$
$$H_z = \ D_3 xyz. \qquad (2\cdot5)$$

From (1·1b)

$$2A_1 - 2B_2 + D_3 = 0,$$

from the former of (1·2b)

$$D_2 - D_1 = A_2 - A_1 = B_2 - B_1 = C_2 - C_1 - D_3,$$

and from the latter of (1·2b)

$$\begin{aligned} a^2D_1 + b^2D_2 &= a^2A_1 + 3b^2A_2 = 3a^2B_1 + b^2B_2 \\ &= (a^2 + 2a^2b^2/c^2)C_1 + b^2C_2 - b^2D_3 \\ &= a^2C_1 + (b^2 + 2a^2b^2/c^2)C_2 + a^2D_3. \end{aligned}$$

From these conditions the coefficients in (2·5) are determined as follows:

$$\begin{aligned} D_1 &= (3a^2 + b^2)(F-1)\{(a^2 + 5b^2)F - 2b^2\}, \\ A_1 &= (a^2 + b^2)(F-1)\{3(a^2 + b^2)F - 2b^2\}, \\ B_1 &= (a^2 + b^2)(F-1)\{(a^2 + 5b^2)F - 2b^2\}, \\ C_1 &= (3a^2 + b^2)(F-3)\{(a^2 + 5b^2)F - 2b^2\}, \\ D_3 &= -4(a^2 + b^2)(a^2 - b^2)(F-1). \end{aligned} \qquad (2\cdot6)$$

A_2, B_2, C_2, D_2 can be obtained when we interchange a and b in B_1, A_1, C_1, D_1 respectively. The second approximation $[k^2]_2$ is given by $D(\boldsymbol{H})/J(\boldsymbol{H})$. Using

$$(\mathrm{rot}\,\boldsymbol{H})_x = 2Sxz/a^2, \quad (\mathrm{rot}\,\boldsymbol{H})_y = 2Syz/b^2,$$
$$(\mathrm{rot}\,\boldsymbol{H})_y = S\left\{(F-1)\left(1 - \frac{x^2}{a^2} - \frac{y^2}{b^2}\right) - (F-3)\frac{z^2}{c^2}\right\},$$
$$S = (a^2 + b^2)^3\{2(3F-1) - G^2(3F-2)\},$$
$$G = (a^2 - b^2)/(a^2 + b^2), \qquad (2\cdot7)$$

we obtain

$$[k^2]_2 = \left(\frac{1}{a^2} + \frac{1}{b^2}\right) \times \frac{9F(2F-1)\{2(3F-1) - G^2(3F-2)\}}{(3F-1)(11F^2 - 14F + 9) - G^2(16F^3 - 31F^2 + 27F - 9)}, \qquad (2\cdot8)$$

The calculated values of $100[k^2]_1 - [k^2]_2/[k^2]_1$, the greater part of the error in the first approximation, is nearly equal to $3(1 - 0.4G^2)^{-1}$ for $a = 2b \geq 2c$. In the case when $a = b = c$, the error of $[k^2]_2$ is only 0.5%.

If we wish to get the third approximation we may start from the polynomial of the lowest degree which satisfies (1·1a), and $[\boldsymbol{E}, \boldsymbol{n}] = \boldsymbol{n}\,\mathrm{rot}\,\boldsymbol{E} = 0$ on the boundary, though the more accurate calculation is practically almost impossible and unnecessary.

§3. Cylindrical Fields.

For the investigation of electromagnetic field in a pipe or in a cylindrical cavity, it is convenient to express the field components as follows,

$$E_x = \frac{\partial^2 \Phi}{\partial x \partial z} + ik\frac{\partial \Psi}{\partial y}, \quad H_x = \frac{\partial^2 \Psi}{\partial x \partial z} - ik\frac{\partial \Phi}{\partial y},$$
$$E_y = \frac{\partial^2 \Phi}{\partial y \partial z} - ik\frac{\partial \Psi}{\partial x}, \quad H_y = \frac{\partial^2 \Psi}{\partial y \partial z} + ik\frac{\partial \Phi}{\partial x},$$
$$E_z = \frac{\partial^2 \Phi}{\partial z^2} + k^2\Phi, \qquad H_z = \frac{\partial^2 \Psi}{\partial z^2} + k^2\Psi, \qquad (3\cdot1)$$

where z axis is taken to be parallel to the generating lines of the cylinder, and Φ and Ψ are scalar functions satisfying the wave equations

$$\Delta\Phi + k^2\Phi = 0, \quad \Delta\Psi + k^2\Psi = 0.$$

In the case when $\Phi = 0$ identically, the oscillation is called H-type and when $\Psi = 0$, E type. In a cylinder enclosed with perfect conductor H- and E-type can be treated separately.

Now we first consider purely two-dimensional oscillation which is independent of z. On applying the general theorem in §1, we have the following results. Let $\psi(x, y)$ be a function of x and y, the normal derivative of which satisfies

$$\partial\psi/\partial\nu = 0, \qquad (3\cdot2)$$

on the boundary. Further put

$$J(\psi) = \iint \psi^2 dxdy,$$
$$D(\psi) = \iint \left\{\left(\frac{\partial\psi}{\partial x}\right)^2 + \left(\frac{\partial\psi}{\partial y}\right)^2\right\} dxdy, \qquad (3\cdot3)$$

where the extent of the integration covers the cross section. If ψ makes $D(\psi)$ minimum under $J(\psi) = 1$, then

$$\frac{\partial^2\psi}{\partial x^2} + \frac{\partial^2\psi}{\partial y^2} + \bar{k}^2\psi = 0$$

where $\bar{k}^2$ equals this minimum value. Namely ψ represents the Ψ-function of a proper oscillation, and the field is given by (3·6). (k^2 must be replaced by $\bar{k}^2$, Φ and $\partial/\partial z$ is zero.)

Regarding the oscillation of E-type the matter is similar, when we adopt $\varphi(x, y)$ vanishing on the boundary. In this case the problem is just the same as the oscillation of a membrane, while the H-type is the same as the oscillation of water in a tub.

The orthogonality theorem is expressed as follows. Let ψ_n and ψ_m belong to different eigenvalues, then hold

$$\iint \psi_n \psi_m dxdy=0,$$

$$\iint\left(\frac{\partial\psi_n}{\partial x}\frac{\partial\psi_m}{\partial x}+\frac{\partial\psi_n}{\partial y}\frac{\partial\psi_m}{\partial y}\right)dxdy=0. \quad (3\cdot4)$$

Similarly as to Φ-function hold

$$\iint \varphi_n \varphi_m dxdy=0,$$

$$\iint\left(\frac{\partial\varphi_n}{\partial x}\frac{\partial\varphi_m}{\partial x}+\frac{\partial\varphi_n}{\partial y}\frac{\partial\varphi_m}{\partial y}\right)dxdy=0. \quad (3\cdot5)$$

Further the relations

$$\iint\left(\frac{\partial\psi_n}{\partial x}\frac{\partial\varphi_m}{\partial y}-\frac{\partial\psi_n}{\partial y}\frac{\partial\varphi_m}{\partial x}\right)dxdy=0, \quad (3\cdot6)$$

exist between ψ and φ.

When the field in the cylindrical cavity varies with z as cosh$z$ or sinh$z$ (or exp$\pm ihz$), we can easily obtain the results, using $\bar{k}^2$, ψ or φ in the purely two dimensional case:

$$k^2=\bar{k}^2+h^2,$$

$$\Psi=\psi(x, y)e^{\pm ihz}, \quad \text{for H-type},$$

$$\Phi=\varphi(x, y)e^{\pm ihz}, \quad \text{for E-type}.$$

These formulas represent also the functions of proper waves in hollow pipes, the propagation constant h being determined by

$$h^2=k^2-\bar{k}^2,$$

with given k. $\lambda_c=2\pi/k$ is so-called cut-off wave length.

§4. Elliptic Pipes.

Electromagnetic waves in elliptic hollow pipes were investigated by Chu⁽²⁾ using Mathieu functions. Since this problem offers a most typical example for application of the variation principle mentioned above, let us treat it again. It is sufficient, as already stated, to consider purely two-dimensional oscillations being independent of z. Let the form of pipes be

$$1-\frac{x^2}{a^2}-\frac{y^2}{b^2}=0, \quad (a\geqq b). \quad (4\cdot1)$$

(i) The fundamental mode of oscillation is called eH$_1$-type, the lines of electric force are shown in Fig. 1. This mode has the symmetry-property

$$H_z=x\times\text{ef}, \quad E_x=xy\times\text{ef}, \quad E_y=\text{ef}, \quad (4\cdot2)$$

where ef's denote even functions of x and y. Taking

$$E_x=2xy, \quad E_y=(2a^2+b^2)(1-x^2/a^2)-y^2, \quad (4\cdot3)$$

which satisfies (1•1a) and (1•2a), we have as the first approximation

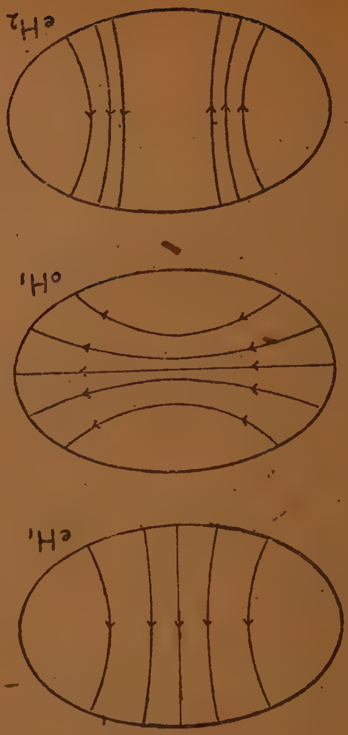

Fig. 1.

$$[k^2]_1=\iint\left(\frac{\partial E_y}{\partial x}-\frac{\partial E_x}{\partial y}\right)^2 dxdy\Big/\iint(E_x^2+E_y^2)dxd$$

$$=\frac{6}{a^2}\frac{3a^2+b^2}{5a^2+2b^2}. \quad (4\cdot4)$$

As to the second approximation we may star from

$$\psi(x, y)=\frac{x}{a}\left(1-\frac{x^2}{3a^2}-\frac{y^2}{2a^2+b^2}\right), \quad (4\cdot5)$$

which satisfies (3•7). Using

$$J(\psi)=\frac{\pi}{6}\frac{ab}{24}\frac{101a^4+80a^2b^2+17b^4}{(2a^2+b^2)^2},$$

$$D(\psi)=\frac{\pi}{6}\frac{b}{a}\frac{(5a^2+2b^2)(3a^2+b^2)}{(2a^2+b^2)^2}, \quad (4\cdot6)$$

we have

$$[\bar{k}^2]_2=\frac{D(\psi)}{J(\psi)}$$

$$=\frac{24}{a^2}\frac{(5a^2+2b^2)(3a^2+b^2)}{101a^4+80a^2b^2+17b^4}$$

$$=[\bar{k}^2]_1\left(1-\frac{a^4+b^4}{101a^4+80a^2b^2+17b^4}\right). \quad (4\cdot7)$$

When $a=b$, the error of $[\bar{k}^2]_2$ is only 0.1%.

(ii) When the axial ratio b/a is not t small, the first heigher mode is oH$_1$-type (c. Fig. 1) having the symmetry-property

$$H_z=y\times\text{ef}, \quad E_x=\text{ef}, \quad E_y=xy\times\text{ef}. \quad (4\cdot$$

It is readily seen that the value $\bar{k}^2$ of th mode can be obtained merely by exchanging a and b in the formulas (4•4) or (4•6).

(iii) When the axial ratio b/a is small, the first heigher mode is eH$_2$-type. The symmetry-property of this type is

$$E_x = y \times \text{ef}, \qquad E_y = x \times \text{ef}. \qquad (4\cdot 9)$$

The polynomial of the lowest degree which satisfies div $\boldsymbol{E}=0$, the boundary condition and this symmetry-property is

$$\begin{aligned} E_x &= y\{A(1-y^2/b^2)+B(x^2+y^2-b^2)\}, \\ E_y &= x\{A(1-x^2/a^2)+B(a^2-x^2-y^2)\}. \end{aligned} \qquad (4\cdot 10)$$

Taking

$$\begin{aligned} \frac{\partial D(\boldsymbol{E})}{\partial A} - \bar{k}^2 \frac{\partial J(\boldsymbol{E})}{\partial A} &= 0, \\ \frac{\partial D(\boldsymbol{E})}{\partial B} - \bar{k}^2 \frac{\partial J(\boldsymbol{E})}{\partial B} &= 0, \end{aligned} \qquad (4\cdot 11)$$

we have the following linear homogeneous equations for A and B

$$\begin{aligned} &(9-15K)A+(a^2-b^2)(6-15K)B=0, \\ &(a^2-b^2)(6-15K)A \\ &\quad +\{(6a^4-4a^2b^2+6b^4)-(15a^4-22a^2b^2+15b^4)K\}B \\ &\qquad =0, \end{aligned} \qquad (4\cdot 12)$$

where

$$K = \bar{k}^2(a^2+b^2)/32. \qquad (4\cdot 13)$$

Since the derterminant composed of these coefficients must vanish, we obtain the equation for K:

$$\begin{aligned} &40a^2b^2K^2-(15a^4+34a^2b^2+15b^4)K \\ &\qquad +6(a^2+b^2)^2=0, \end{aligned} \qquad (4\cdot 14)$$

whose *smaller* root K_1 determines the approximate eigenvalue

$$[\bar{k}^2]_1 = 32K_1/(a^2+b^2). \qquad (4\cdot 15)$$

In the case when $a=b$, the error of this first approximation is 3%.

§5. Semi-coaxial Cavities.*

As the third example let us treat the semi-coaxial cavities, the axially symmetric cavities as shown in Fig. 2. This was investigated by Hansen(3) and recently by Mayer(4). In this section our object is to obtain a simple approximate formula without any complicated numerical calculation. For the fundamental mode of oscillation E_φ, the azimuthal component of $\boldsymbol{E}$, is identically zero, and $\boldsymbol{H}$ has only this component H_φ. The lines of force of electric field are such as shown in Fig. 3 (i). These lines indicate also the lines of equal rH_φ.

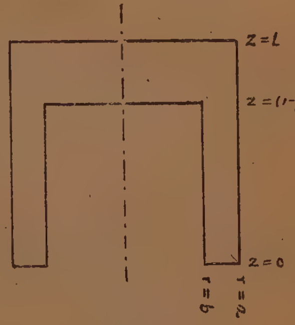

Fig. 2.

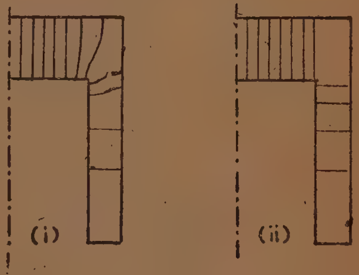

Fig. 3.

Now put H_φ approximately in the form

$$H_\varphi = \begin{cases} Ar/b & r<b, \ (1-g)l<z<l, \\ Ab/r & b<r<a, \ (1-g)l<z<l, \\ A\dfrac{b}{r}+B\dfrac{b}{r}\left\{1-\dfrac{z^2}{l^2(1-g)^2}\right\}, & b<r<a, \ 0<z<(1-g)l. \end{cases} \qquad (5\cdot 1)$$

Then

$$\begin{aligned} (\text{rot}\,\boldsymbol{H})_z &= \begin{cases} 2A/b, & r<b, \ (1-g)l<z<l, \\ 0, & \text{other parts} \end{cases} \\ (\text{rot}\,\boldsymbol{H})_r &= \begin{cases} B\dfrac{b}{r}\,\dfrac{2z}{l^2(1-g)^2}, & b<r<a, \ 0<z<(1-g)l, \\ 0, & \text{other parts,} \end{cases} \end{aligned} \qquad (5\cdot 2)$$

---

* §5 was added on July 24, 1947.

which indicates an uniform electric field in the gap and a simplified radial electric field in the coaxial part. The lines of electric force in this approximation is shown in Fig. 3 (ii). Taking

$$\frac{\partial D(\boldsymbol{H})}{\partial A}-k^2\frac{\partial J(\boldsymbol{H})}{\partial A}=0,$$

$$\frac{\partial D(\boldsymbol{H})}{\partial B}-k^2\frac{\partial J(\boldsymbol{H})}{\partial B}=0, \tag{5·3}$$

we have

$$\left\{2g-k^2b^2\left(\frac{g}{4}+\ln\frac{a}{b}\right)\right\}A$$

$$-k^2b^2\frac{2(1-g)}{3}\ln\frac{a}{b}B=0,$$

$$-k^2b^2\frac{2(1-g)}{3}\ln\frac{a}{b}A$$

$$+\left\{\frac{b^2}{l^2}\frac{4}{3(1-g)}-k^2b^2\frac{8(1-g)}{15}\right\}\ln\frac{a}{b}B=0. \tag{5·4}$$

Eliminating A and B, we obtain the equation for k^2

$$\left\{2g-k^2b^2\left(\frac{g}{4}+\ln\frac{a}{b}\right)\right\}\left\{1-\frac{2}{5}k^2l^2(1-g)^2\right\}$$

$$-\frac{1}{3}k^4b^2l^2(1-g)^3\ln\frac{a}{b}=0, \tag{5·5}$$

whose smaller root of k^2 is the required eigenvalue.

The accuracy of this formula is good in the case when g is small; for $g\ll 1$ we have from (5·5)

$$k^2=\frac{2g}{b^2\ln(a/b)}-\left(\frac{b^2}{8}+\frac{l^2}{3}\right)\left(\frac{2g}{b^2\ln(a/b)}\right)^2. \tag{5·6}$$

For large values of g, the error of (5·5) is rather large. For instance we get $ka=2.59$ when $a^2=2b^2$ and $g=1$, its correct value being 2.40. The values of $(ka)^{-1}=\lambda/2\pi a$ in the case when $a^2=2b^2$ are shown in Fig. 4 as a function of g and l^2/a^2.

References.

(1) W. Ritz, J. reine u. angew. Math. **135** (1908), 1.

(2) L. J. Chu, J. appl. Phys. **9** (1938), 583.

(3) W. W. Hansen, J. appl. Phys. **10** (1939), 1.

(4) E. Mayer, J. appl. Phys. **17** (1946), 1046.

I am publishing the details of my investigation in book form (in Japanese). Therefore, considering the poor capacity of the Journal, I give up the printing of the remaining part of this long paper.

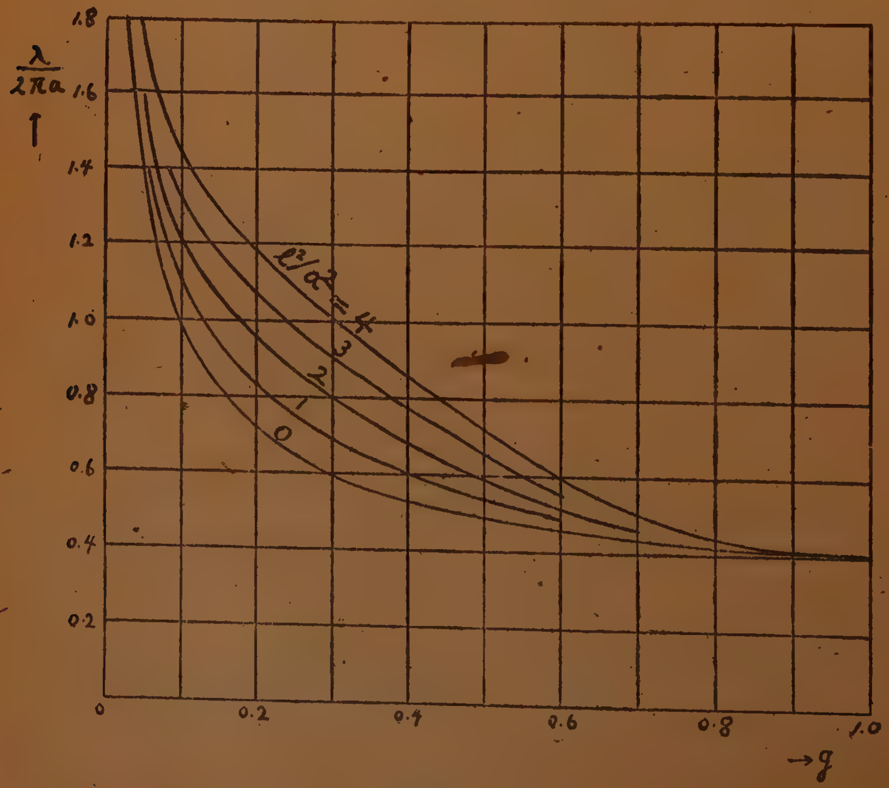

Fig. 4.

The Figures on the Surface of Metal Electrodes Produced by the Breakdown in High Vacuum.

By Kazuzi HASHIMOTO.

Hitachi Central Research Laboratory.

(Received March 6, 1947.)

1. Introduction.

Various authors(1) have reported the breakdown voltage in the uniform electric field as a function of electrode distance and the degree of evacuation. But if we use the non-uniform electric field, e.g. a needle and a plate, what change will occur in the relation between breakdown voltage and electrode polarity or what figures will be produced on the surface of the plate electrode? These problems above mentioned are not always made clear even at present.

We have investigated on the polarity effect and on the figures on the electrode metal surface produced by impulsive breakdown under the pressure of about 10^{-5} mm Hg. or less.

2. Apparatus and Technique.

The needle and plate electrodes are arranged in pyrex glass vacuum cylinder as shown in Fig. 1. In order to be easily opened or closed, the brass screw case A is set in the brass cover B which is cemented to the pyrex glass cylinder, sealing the vacuum chamber C with apiezon grease or compound. The positive or negative voltage is applied to the needle electrode against the plate electrode which is connected to the earth. By this apparatus (Fig. 1) we can investigate the polarity effect or the relation between the breakdown voltage and the electrode distance. After an impulsive voltage is applied between needle and plate electrodes, various figures are produced on the surface of the plate according to the polarity of the needle and the degree of evacuation. Especially, if the thin silver film is evaporated on the brass plate, or the thin copper film on the iron or silver plate, these figures are obtained on the condition of very fine contrast according to the difference of colour between the thin film and the base metal. These thin metal films on the electrode plate are obtained by the evaporation method in another vacuum chamber.

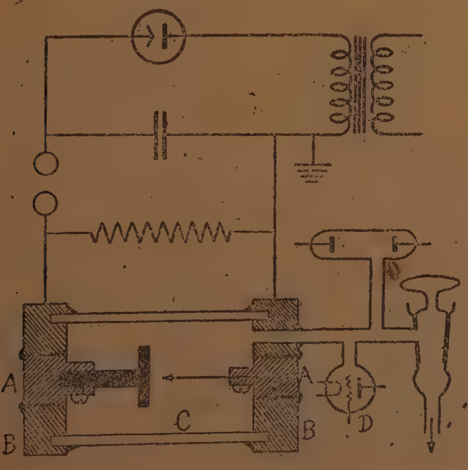

Fig. 1. Diagram of apparatus.
B : Brass cover. A : Screw case.
D : Ionization gauge.

3. Results.

The relation between the breakdown voltage and the electrode, distance or the electrode polarity is shown in Fig. 2. In these experiments we used nickel needle and plate as the electrodes. As is well known, the value of the breakdown voltage is not reproducible even at the constant electrode distance and constant pressure, so that these data are protted using the mean value obtained from several tests concerning the various distances. Another metal electrode, for example, molybdenum needle and brass plate were used, but these data are nearly equal to Fig. 2. above mentioned. From these experiments we can find that when the needle is negative, the value of the breakdown voltage is much lower than that of the positive needle. Bennett(2) once showed the relation between the break-

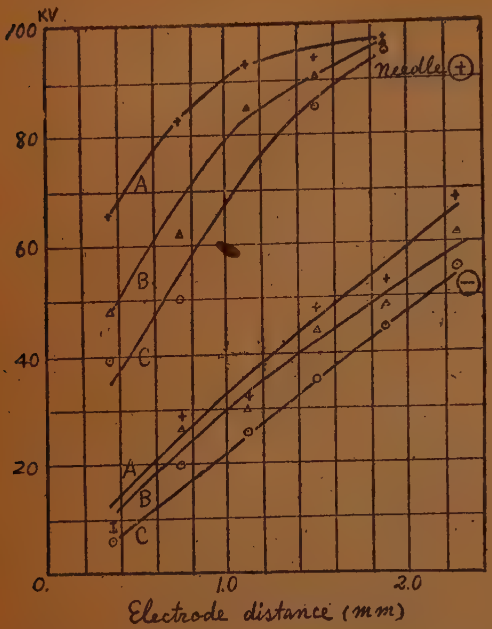

Fig. 2. The breakdown voltage versus electrode separation and electrode polarity. (nickel plate and nickel needle.)

Curve C: The lowest value of breakdown.
A: Upper limit value.
B: Mean value.

down voltage and the character of the electrode, and concluded that the breakdown phenomena in the high vacuum was rather caused by the character of the positive plate than that of the cathode.

But our experimental facts denote the opposite conclusion.

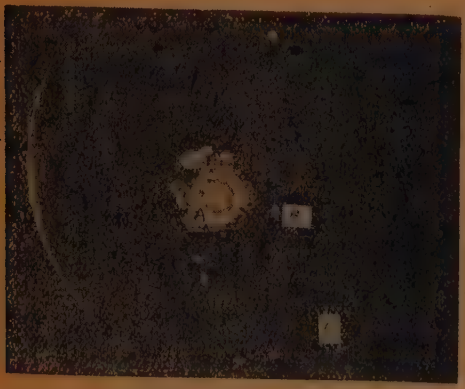

Fig. 3. Negative figures on the thin silver film evaporated on the brass plate.
Impulse voltage 35 kV.
Electrode distance 0.7 mm.
Tungsten needle ⊖
Pressure 5×10^{-6} mm Hg.
Magnification 4X.

Next, we examined what figures will appear on the plate electrode by one breakdown, and found out very beautiful figures, especially when the thin silver film was evaporated on the brass plate. Fig. 3. and Fig. 4. show the examples of the typical negative figures (tungsten needle) on the silver brass plate in the pressure of 5×10^{-6} mmHg or 7×10^{-5} mmHg. Fig. 5., Fig. 6., and Fig. 7. are the magnified figures of parts of Fig. 3 or Fig. 4. In the present experiment two typical figures have

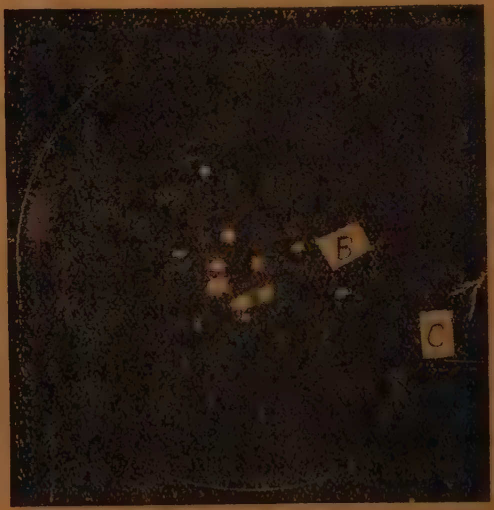

Fig. 4. Negative figures.
Pressure 7×10^{-5} mm Hg.
Other conditions are the same as in Fig. 3.
Impulse voltage 30 kV.
Magnification 2X.

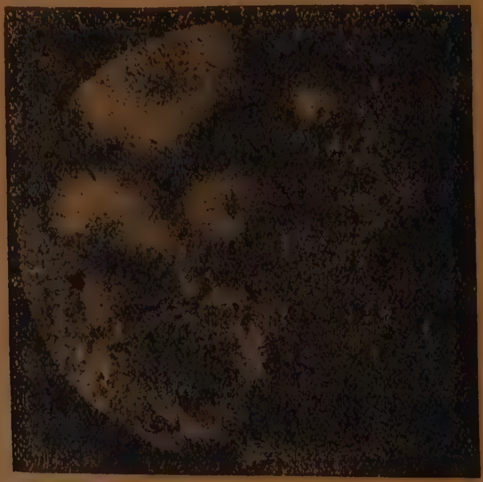

Fig. 5. The magnified photograph of A part in Fig. 3.
Magnification 80X.

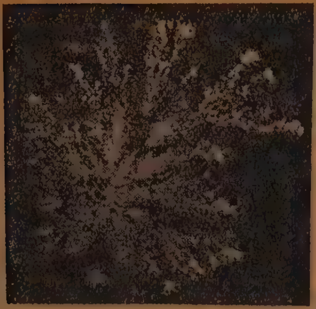

Fig. 6. Magnified photograph of B part in Fig. 3 or Fig. 4. Magnification 130X.

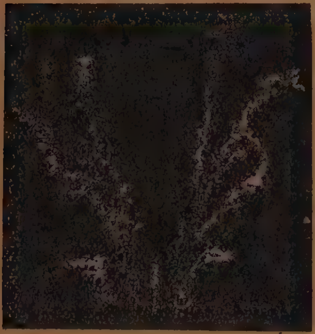

Fig. 7. Magnified photograph of C pact in Fig. 4. or Fig. 3. Magnification 130X.

been found on the positive plate surface. One is an assemblage of fine stripes (Fig. 5.) around the melted center which is produced directly below the needle electrode. The other is a bush-clover type which is produced apart from the melted center (Fig. 6. and Fig. 7.) and Fig. 7 somewhat resembles the photograph of Wilson's cloud chamber when the X-ray beam penetrates it. Moreover, the figure such as Fig. 7. is found on the edge of the positive plate. (see Fig. 3C or Fig. 4C.) On the contrary, when the needle electrode is positive, many beautiful flower type figures are produced on the negative plate surface by one breakdown. Every flowertype figure has a center coloured by the brass base metal and many flower leaves arouned it by the thin silver film. These typical figures are shown in Fig. 8. and Fig. 9.. Fig. 10., and Fig. 11. show two parts of Fig. 8. These breakdown figures, Fig. 3. Fig. 4. Fig. 8 and Fig. 9. somewhat depend upon the pressure of the vacuum chamber. Generally the negative figures are very delicate and are fine stripes and bush-clover type or their assemblage, but on the contrary positive figures are the flower-type. However, these figures do not always appear

Fig. 8. Positive figures on the thin silver film evaporated on the brass plate.
Impulse voltage. 50 kV.
Electrode distance. 0.7 mm.
Pressur 4.5×10^{-6} mmHg.
Tungsten needle ⊕.
Magnification 4X.

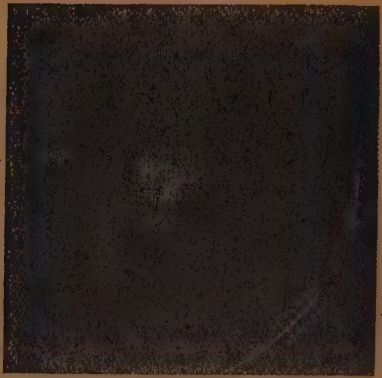

Fig. 9. Positive figures.
Pressure 6×10^{-5} mmHg.
Other conditions are the same as in Fig. 8.
Magnification 2X.

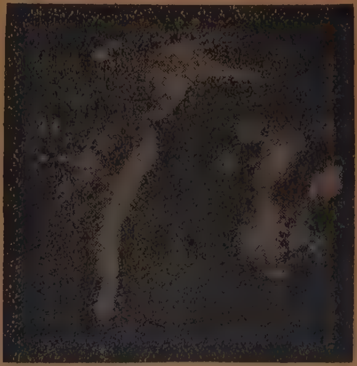

Fig. 10. The magnified photograph of A part in Fig. 8.
Magnification 80.

in the same type, and sometimes there appears the assemblage of the figures above mentioned. These typical figures are shown in Fig. 12, Fig. 13 and Fig. 14. They are produced on the thin copper film evaporated on the iron plate by one breakdown on the condition of positive needle electrode, namely each branch in Fig. 13 and Fig. 14 is the assemblage of the flower type figures.

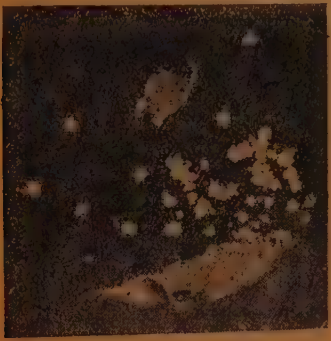

Fig. 11. The magnified photograph of B part in Fig. 8. Magnification 80.

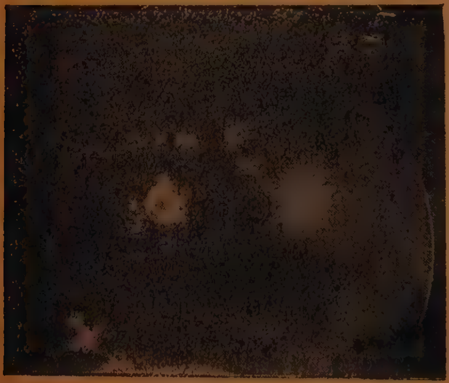

Fig. 12. Positive figures producedon the capper film evaporated on the iron plate. Magnification 2X.

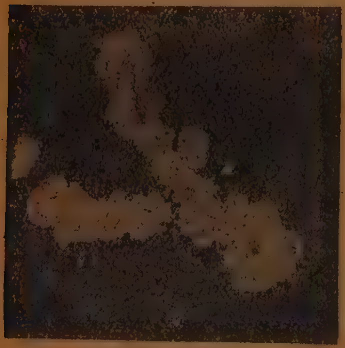

Fig. 13. The magnified photograph of a part in Fig. 12. Magnification 130X.

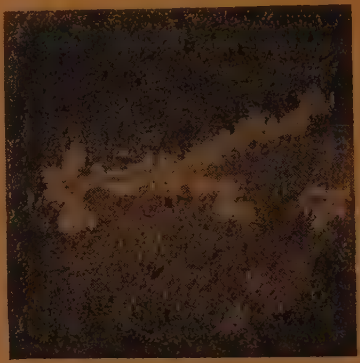

Fig. 14. The magnified photograph of a part in Fig. 12. Magnification 130X.

4. Discussion and Conclusion.

The experiments on the relation between the breakdown voltage and the electrode separation or the electrode polarity have been performed in the vacuum chamber and the value of breakdown voltage has been found to be lower at a negative needle than at a positive one (Fig. 2). These experimental facts will be made clear from the point of view of socalled field emission.

The breakdown phenomenon in the high vacuum will be caused by the electrons which are extracted from cold metal surface purely by the application of sufficiently high field at the surface. These electrons will bombard and melt the metal surface, or ionize various gas molecules which are absorbed or adhered to the electrode metal.

These breakdown phenomena do not always appear in the same manners even on the similar conditions, and the cause will be due somewhat to the emission center destroyed by the ion bombardment, or to the impurity or gas molecules that are adhered to the electrode metal surface.

After one breakdown, the investigations on the figures of the electrode metal surface have been carried out and we found the very beautiful evidence of breakdown on the electrode plate which varies with regard to the needle electrode polarity or to the pressure of the vacuum chamber.

At present the cause of these curious figures is not clear, but, in the author's opinion concerning the negative figure, it is attributable to the field emission center of the nagative needle pole from which many electrons are extracted straight to the pole surface and bombard the metal surface of the positive plate separately, or ionize and burst the gas molecules existed on the surface of the metal.

Besides these causes above mentioned, the figures will be produced by the electric resistance between the surface and base metal for the copious supply of the electric current by the condenser discharge.

On the contrary the positive figure will be produced by the melting phenomenon of the extreme point of the needle metal by the copious electron bombardment. In these cases the molten metal and metal ion will be smashed on the negative plate surface. The flower-type figure that seems to be smashed by some melted matter may be caused by these phenomena.

The author takes pleasure in acknowledging the advice and criticism of Dr. Y, Toriyama. throughout this work.

References.

(1) H. w. Anderson: R. S. I. **6** (1935), 309.
(2) W. Bennett.: Phy. Rev. **37** (1931), 582.

On Sparking Potentials.

By Tatuo KOBAYASI.

Institute of Science and Technology, Tokyo Imperial University.

(Received March, 29, 1947.)

The writer has published three reports on the mechanisms of electric sparks⁽¹⁾⁽²⁾⁽³⁾. In the last report, he discussed the method of calculation of sparking potentials. The first half of this paper is the furthering of the same calculations, the latter part including the results of measurements of sparking potentials in low pressures down to 300 mmHg and the similar calculations applied to that case.

1. Calculation of Sparking Potentials.

The calculation of the electric field ϕ at any point x in the gap (x is measured from the surface of one of the poles), when unit electric potential is applied between two spherical poles symmetrically to the earth (± 0.5 to each pole), was explained in the last report. If ϕ is multiplied by the sparking potential, the field strength F at sparking at that point is obtained. Let the square root of the mean-square-value of ϕ between $x=0$ and $x=X$ be denoted by x_X. Then,

$x_X=\sqrt{\frac{1}{X}\int_0^X \phi^2 dx}$. The integral must be performed by numerical or graphical method. The root-mean-square F between 0 and X at sparking is obtained by multiplying x_X by the sparking potential. Let this value be denoted by $\boldsymbol{F_X}$.

The curve showing the variations of $\boldsymbol{F_X}$ with X in the cases of different pole diameters (5, 10 and 25 cm) and various gap lengths are shown in Fig. 1. All such curves converge to the neighbourhood of a point A about 1 cm from the pole surface. Hence, we come to the conclusion that a spark passes when the root-mean-square of electric field in the range about 1 cm from the pole surface rises to about 30 kV/cm, if the poles are not too small and the gap is wider than 2 cm.

The curves of the same nature for smaller poles (1 and 2 cm) are shown in Fig. 2. The curves in these cases do not converge at any point. Hence, these cases must be considered in a different way. The black curve in the same figure gives the relation between the (mean) field at sparking and the gap-length in the case when the poles are parallel flat plates (or very large spheres; because the gap-lengths considered are small). (In this case, the mean field is equal to the root-mean-square-field.) The curve shows that the electric field necessary to produce a spark increases rapidly with the diminution of the gap.

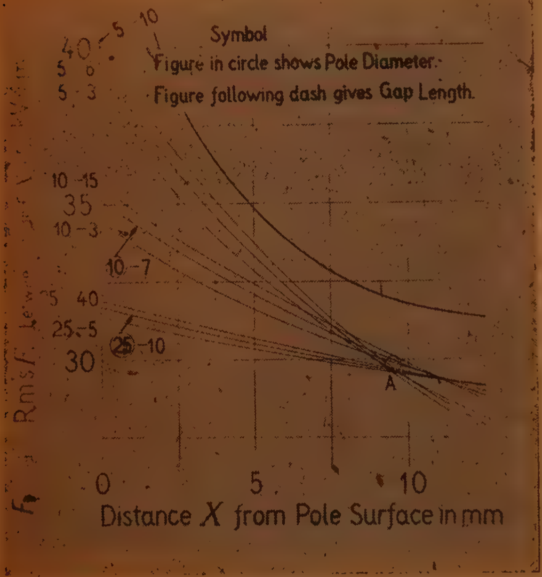

Fig. 1.

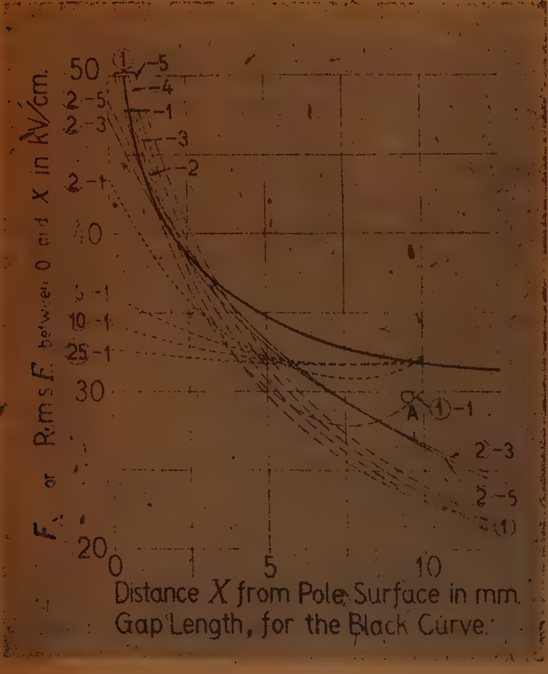

Fig. 2.

In the figure we see all the curves of $\boldsymbol{F_x}$ touch the black curve. This fact explains that, if the poles are small, $\boldsymbol{F_x}$ in a smaller range in front of the pole surface rises to a value to start a spark, before $\boldsymbol{F_x}$ in the 1 cm range reaches 30 kV/cm. The curves for 1 cm poles cut the black curve slightly. This comes most likely from the cause that, if the poles are so small and the gap is wide, the field directly before the pole becomes very great, consequently some kind of discharge must take place in such a layer, (We often observe a thin layer of glow covering the pole surface.) so that the actual $\boldsymbol{F_x}$ may be smaller than the calculated value.

The condition of Fig. 1 is attained when the diameter of the poles comes up to about 3 cm. (According to the writer's experience, the fluctuation of the sparking potential of each measurement is greater when it is influenced by the condition of Fig. 2. Therefore, it may be said that the poles larger than 3 cm in diameter are better fitted for the purpose of high tension measurement.) Hence, there are three different cases in calculating the sparking potentials:— 1. when the pole diameter is smaller than 3 cm; 2. when the gap is narrower than 2 cm; 3. when the poles are larger than 3 cm, the gap being wider than 2 cm.

In the case 1—when the poles are smaller than 3 cm—the x_x versus X curve must be obtained. Then, the factor to be multiplied in order to raise the curve unitil it touches the black curve in Fig. 2 gives the sparking potential.

In the case 2—when the gap is narrower than 2 cm—the root-mean-square of $\boldsymbol{F}$ at sparking in the whole range of the gap is equal to the F in the case of parallel flat poles with the same gap length. In Fig. 2, we see that the right hand ends of all the $\boldsymbol{F_x}$ curves for 1 cm gap (except that of 1 cm poles, which belongs to the case 1) very nearly come on the black curve. Therefore, the sparking potential in this case can be computed by calculating x of the whole gap first, and dividing by it the value of the sparking field between parallel flat poles as given by the black curve in Fig. 2 at the same gap length.

The case 3—when the pole diameter is greater than 3 cm and the gap wider than 2 cm is most important. In order to perform accurate calculation of sparkieg potentials in this case, the exact position of the converging point A in Fig. 1 must be determined. For this purpose, the neighbourhood of A is enlarged in Fig. 3. The $\boldsymbol{F}_X$ curves are drawn by using all the available values of sparking potentials given in Landolt-Boernstein's Physikalisch-chmische Tabellen. (Sparking potentials for 5 cm poles up to 10 cm gap length, for 10 cm poles up to 17 cm gap length, for 25 cm poles up to 40 cm gap length are given.) Of those curves, the one for 25 cm poles 8 cm gap (dotted curve) is evidently too low. If this is eliminated, the point of least confusion is at $X=9.65$ mm. If two more lowest curves are eliminated, the converging point comes to 9.5 mm. Let us take this distance as the abscissa of the point A. (Small change in taking this distance does not affect the results of the final calculatian appreciably.)

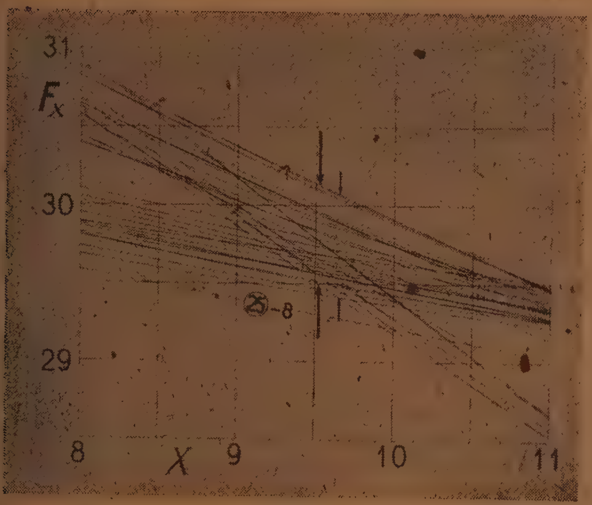

Fig. 3.

The reason why a spark starts from the break down in this 9.5 mm is difficult to explain. But that long sparks always have straight parts at their positive ends or at both their ends (See Photos 4 and 5 in the last Report.) must have a direct connection with this fact.

The values of x_X at $X=9.5$ mm (This be denoted by $x_{.95}$.) are shown in Table I. If $x_{.95}$ is multiplied by the sparking potential, the root-mean-square F between 0 and 9.5 mm at sparking (This be denoted by $\boldsymbol{F}_{.95}$.) is obtained. The values of $\boldsymbol{F}_{.95}$ for 5 cm poles are shown below.

Gap	S.P.	$\boldsymbol{F}_{.95}$	Gap	S.P.	$\boldsymbol{F}_{.95}$
3	80.7	29.66	7	131	29.61
4	97.7	29.58	8	139	29.79
5	111	29.50	9	145	29.80
6	122	29.55	10	150	29.79

The mean value of $\boldsymbol{F}_{.95}$ is 26.66±.03 kV/cm. (The probable error of each value is ±.09.

Table I. Values of $x_{.95}$

Gap in cm	Diameter of Pole Spheres in cm. 3	5	10	25
3	0.3916	0.3675	0.3502	0.3400
4	.3369	.3028	.2763	.2606
5	.3066	.2658	.2330	.2133
6	.2876	.2422	.2048	.1819
7	.2747	.2260	.1849	.1596
8	.2654	.2143	.1703	.1429
9	.2584	.2055	.1592	.1300
10	.2530	.1986	.1505	.11975
11	.2487	.1930	.1435	.11138
12	.2452	.1885	.1377	.10444
13	.2423	.1848	.1328	.09859
14	.2398	.1816	.1267	.09361
15	.2377	.1789	.1251	.08934
20		.1700	.11327	.07455
25		.1649	.10658	.06594
30		.1616	.10232	.06036

Gap in cm	Diameter of Pole Spheres in cm. 10	25	50	100
3	0.3502	0.3400	0.3367	0.3350
5	.2330	.2133	.2067	.2033
10	.1505	.11975	.10980	.10489
15	.1251	.08934	.07775	.07216
20	.11327	.07455	.06186	.05583
30	.10232	.06036	.04620	.03956
40	.09726	.05366	.03857	.03148
50	.09439	.04983	.03413	.02668
60	.09255	.04739	.03125	.02352
100		.04283	.02581	.01738
150		.04077	.02333	.01449
200			.02219	.01314
300			.02112	.011881
400				.011297
500				.010966
600				.010753

The mean value of $\boldsymbol{F}_{.95}$ obtained by using all the values of sparking potentials given in Landolt's Tables for three different pole diameters (5, 10 and 25 cm) is 29.75±.03 kV/cm. Hence, a spark passes when $\boldsymbol{F}_{.95}$ reaches 29.75, the probable error being very small.

Therefore, the sparking potential is calculated by the following:

$$\mathrm{S.P.}=29.75 \div \chi_{.95}.$$

The residuals of $\boldsymbol{F}_{.95}$, calculated from the observed sparking potentials, from the mean value are irregularly distributed. Therefore, the calculated sparking potentials may be qualified to be the more probable values. Some of the calculated values are shown in Table II. The measured values given in Landolt's Tables are added for the purpose of comparison. This method of calculation can possibly be extended to the cases of larger poles and wider gaps, in which we have not reliable measured results. Such calculated values are shown in Table III.

Table II. S. P. in kV, Calc. and Obs.

Gap in cm	Diameter of pole spheres in cm. 5 Calc.	5 Obs.	10 Calc.	10 Obs.	25 Calc.	25 Obs.
3	81.0	80.9	85.0	85.4	87.5	87.3
4	98.3	97.7	107.7	108	114.2	113.5
5	112.0	111	127.7	128	139.5	138
6	122.9	122	145.3	146	163.6	162
8	138.9	139	174.8	176	208.3	205×
10	149.8	150	197.7	199	248.5	247
15	166.3		237.9	241×	333.1	331
20	175.1		262.7		399	398
30	184.2		290.9		493	492
40			306		555	555

Table III. S. P. in kV, Calculated

Gap in cm	Diameter of Pole Spheres in cm. 5	10	25	50	100
3	81.0	85.0	87.5	88.4	88.8
5	112.0	127.7	139.5	144.0	146.4
10	149.8	197.7	248.5	271	284
15	166.3	237.9	333	383	412
20	175.1	262.7	399	481	533
30	184.2	291	493	644	752
40		306	555	771	945
50		315	597	872	1115
60		322	628	952	1265
100			695	1153	1712
150			730	1276	2050
200				1341	2260
300				1409	2500
400					2630
500					2710
600					2770

2. Brushing Discharge.

It is generally stated that, if the gap length is increased to seven times the diameter of the pole spheres, brushing discharge begins to occur and sparks pass no more. But the transition gap-length is not definite. There is a range of gap-length in which both brushes and sparks are produced alternately. The writer observed that the gap-length of about 13 cm was the center of the range of transition from spark to brush, when the diameter of the poles was 2 cm, and the brushing potential in this case was 96.8 kV. This brushing potential coincides well with the sparking potential calculated as the type of Fig. 2.

The writer discussed the formation of spark tracks in the previous paper (Report II) and delivered the following opinion, giving experimental demonstrations. If the sparking potential is attained, a volume charge is created in the gap by the transit of a preliminary discharge. Then, very faint paths of mono-pole sparks, zigzag and dendritic if the gap is wide, extend from one of the poles, according to the sign of the volume charge. If one of the numerous branches of the mono-pole sparks reaches the oposite pole, whole the charge stored in the condenser discharges through that branch, giving luminosity to the path and consequently masking the other faint mono-pole spark tracks.

These mono-pole sparks are of exactly the same nature as brushes. Therefore, we may conclude that the brushing discharges start under the same condition as the sparks, but since the electric field in the central part of the gap is too weak (or the density of the volume change in the central part is too small to allow the development of the mono-pol spark tracks, they end in brushes. The elec tric field at the center of the gap in the above mentioned case (pole diameter 2 cm, gap length 13 cm) is 1845 volts/cm. If we assume this value as the lowest field through which the brush tracks can traverse, we can calculate the transition gap-length for any pole diameter, and the brushing potential at that gap-length. For 5 cm poles, they are 27.7 cm and 183 kV; for 10 cm poles, 51.2 cm and 316 kV.

If we assume that the above-mentioned methods of calculation of sparking potentials (9.5 mm law) are applicable to the calculation of the brushing potential in the case when a single spherical pole is hanging in a space, we can find the brushing potential (potential relative to the earth when the sphere emits brushes), dividing 29.75 by twice $x_{.95}$ at infinite gap.

Pole dia.	$x_{.95} \times 2$	Brushing potential
2 cm	(contact)	50 kV
5 〃	0.2947	101 〃
10 〃	.1689	176 〃

3. Measurement of Sparking Potentials under Low Pressure.

The writer carried out a series of measurements of sparking potentials in reduced air pressure in a cylindrical tunk of about 1 m. both in diameter and in length. The gap-length could be measured from the outside of the tunk with the accuracy of 1/100 mm.

The potentials applied to the poles were measured by two high tension voltmeters of parallel-plates-with-a flap-window type. (The deflection is observed by reflection of light. The measurable range is altered by changing the distance of the plates.) Each voltmeter was set in a large box covered with thin metal plates, and one of the poles was connected to it, in order to shut off stray fields. The calibration of them was made in the following way:—— The distances of the parallel plates of the two voltmeters were adjusted as the measurable range to cover 5 kV, and they were connected in parallel, one pole (box side) being earthed. Voltages up to 5,000 volts were applied to them from a high tension battery, the voltages being measured by means of a high resistance and well calibrated multi-cellular voltmeter, thus the calibration curves were obtained. Then, the two were connected in series (One of the cover box was insulated from the earth by placing it on big insulators.) and the third voltmeter of the same type was connected in parallel with them. The measurable range of the third was adjusted to 10 kV and voltages up to 10,000 volts were applied to them from a high tension source (A. C. rectified by kenotrons) the voltages being measured by the sum of the readings of the first two voltmeters, thus third voltmeter was calibrated. Then, the first two were connected in parallel, the range being changed to 10 kV, and calibrated up to 10,000 volts by the aid of the third. By repeating this procedure, the voltmeters were calibrated up to 100 kV and above as occasion demands. The accuracy of each measurement of the voltage was better than 1/1000.

The sparking potentials were measured in dry air at 20°C. at the pressures of 600, 500, 400 and 300 mmHg. Care was taken to make the potentials (+ and −) applied to both the poles very nearly equal; they were measured

Table IV. S. P. under Low Pressure in kV.

Gap	Pressure 600 mm			Pressure 500 mm		
	Pole Dia. in cm			Pole Dia. in cm		
in cm	3	5	10	3	5	10
1	26.3	26.5	26.6	22.7	22.8	22.9
2	47.4	47.9	48.2	39.3	41.0	41.1
3	60.9	65.7	69.0	50.8	56.3	58.6
4	70.6	79.4	87.4	58.8	68.0	74.6
5	77.6	89.6	103.8	64.2	76.8	88.3
6	82.7	98.4	118.1	67.9	83.8	100.7
7	86.5	105.4	130.7	70.9	89.8	111.0
8	89.6	111.3	142.0	73.9	94.7	120.1
	Pressure 400 mm			Pressure 300 mm		
Gap	Pole Dia. in cm			Pole Dia. in cm		
in cm	3	5	10	3	5	10
1	19.2	19.2	19.1	15.6	15.6	15.5
2	33.4	33.9	34.1	26.5	26.8	27.0
3	42.9	46.5	48.4	33.7	36.5	38.2
4	49.7	56.2	61.3	39.1	44.3	48.4
5	54.3	63.8	72.7	42.8	50.5	57.4
6	57.5	69.8	82.6	45.4	55.2	65.2
7	60.1	74.6	91.1	47.5	59.1	71.7
8	62.9	78.9	98.3	49.7	62.8	77.5

independently, the sum being the potential applied to the electrodes. The potentials were raised very gradually until a spark passed. The results are shown in Table IV.

4. Calculation of Sparking Potentials at Low Pressure.

If F_X versus X curves are drawn by using the sparking potentials at one definite pressure for different pole diameters and gap lengths given in Table IV, it is seen that all the curves converge to the neighbeurhood of a definite point, in the same way as in Fig. 1. The distance of the converging point from the pole surface is slightly less than 1 cm in any case of the pressure. (The ordinate of A only differs according to the pressure.) Therefore, if 9.5 mm is taken as this distance, the values of $x_{.95}$ given in Table I can be used for the purpose of calculating the sparking potentials at any pressure. Hence, $F_{.95}$ at sparking at the four different pressures were calculated and the following were obtained as the mean values. (20°C)

Pressure	$F_{.95}$
600 mm	24.05±.04 kV/cm
500 〃	20.49±.03 〃
400 〃	16.92±.02 〃
300 〃	13.36±.01 〃

The relation between $F_{.95}$ and the pressure p can be expressed by the following experimental formula:

$$F_{.95}=29.75-0.03565(760-p).$$

Therefore, the sparking potential for any pole diameter and gap length at any ai pressure can be calculated from $F_{.95}$ given b the above formula and $x_{.95}$ given in Table I.

References.

(1) Proc. Phys.-Math. Soc. Japan, **12** (1930), 9, 240

(2) Ditto, **13** (1931), 11, 310.

(3) Ditto, **14** (1932), 8, 418.

On the Oxidation of the Thin Single Crystal Film of Copper.

By **Shunji SHIRAI.**

Daini Kotogakko, Sendai.

(Received March 31, 1947.)

In the present investigation we are mainly concerned with the orientation of the oxide crystal with respect to the mother copper crystal when the latter was oxidized. The copper crystal in the form of a thin single crystal film about 40 mμ in thickness was made on the cleavage surface of natrium chloride crystal maintained at a temperature about 300°C by the evaporation method and the film was detached from the substrate by dissolving it in water. The structure of the film was examined by means of the transmission method of cathode-ray diffraction.

The thin single crystal film of copper was completely oxidized by heating in air in an electric furnace for 10 minutes at a temperature higher than 220°C and when the heating temperature was between 220°C and 280°C, the resultant film was composed of cuprous oxide crystals in the following orientations:—(1) at random oriantation, (2) $(001)_{Cu_2O} \parallel (001)_{Cu}$ and $[100]_{Cu_2O} \parallel [100]_{Cu}$ and (3) $(111)_{Cu_2O} \parallel (001)_{Cu}$ and $[\bar{1}10]_{Cu_2O} \parallel [110]_{Cu}$ or $[\bar{1}10]_{Cu}$ (Fig. 1). The proportion of occurrence of any orientation in a film varied from specimen to specimen. The copper film also became a cuprous oxide film by floating it for several hours or longer on the water surface, but, in this case, it contained, in addition to the oxide crystals in the three orientations mentioned above, those having the following orientations —— (4) $(332)_{Cu_2O} \parallel (001)_{Cu}$ and $[\bar{1}10]_{Cu_2O} \parallel [110]_{Cu}$ or $[\bar{1}10]_{Cu}$ and the orientations of the crystals were more perfect than those in the former case (Fig. 2).

When the copper film or cuprous oxide film obtained as described above was heated at 280°C or higher for 10 minutes in air, it became a cupric oxide film (Table I). In many cases the cupric oxide crystals in the film had no orientation (Fig. 3). In some caces, we obtained a film, in which the orientation of some of the minute cupric oxide crystals was completely at random, but a certain number of them had the following orientations: —— a plane of $\{100\}_{CuO} \parallel (001)_{Cu}$ and an edge of the monoclinic parallelepiped of cupric oxide was parallel to an edge of the cube of copper crystal (Fig. 4). The film mainly composed of cuprous oxide crystals in the orientation of the type (2) had a tendency to change to the cupric oxide film of this sort. In other cases, we obtained the cupric oxide film in which a certain number of the cupric oxide crystals were in the following orientations:—a plane of $\{111\}_{CuO} \parallel (001)_{Cu}$ and a face diagonal of the monoclinic parallelepiped of cupric oxide $\parallel [110]_{Cu}$ or $[\bar{1}10]_{Cu}$; and a plane of $\{110\}_{CuO} \parallel (001)_{Cu}$ and an edge of the monoclinic parallelepiped of cupric oxide $\parallel [100]_{Cu}$ or $[010]_{Cu}$, or a face diagonal of the monoclinic parallelepiped of of cupric oxide $\parallel [110]_{Cu}$ or $[110]_{Cu}$, ——the film of this structure being obtained from the cuprous oxide film mainly composed of cuprous oxide crystals in the orientations of the types (3) and (4) (Fig. 5).

A few further experiments were carried out with the object to examine how the orientations of copper oxide crystals were influenced by the changes brought out in the exprimental conditions. (a) The copper single crystal film prepared as described above, contained, though very few in number, a certain number of cuprous oxide crystals. Perhaps they might be produced during the procedure of detaching the film from the substrate sodium chloride crystal by dissolving it in water. When this copper film was annealed for about half an hour at a temperature about 350°C in a hydrogen atmosphere of a low pressure, it became a relatively perfect single crystal film containing copper crystals only. Whether we used the former film or the latter as the specimen, no differences were observed in the orientations of copper oxide crystals in the

Table I.

No.	*hkl*	*d*	*d'*	*I'*	*I*	*I''*
1	110	2.737	2.75	*m*	1	13.4
2	002	2.519	2.52	*S*	9	20.9
3	$\bar{1}11$	2.511				68.3
4	111	2.312	2.31	*S*	10	100.0
5	200	2.295				14.3
6	$\bar{1}12$	1.952	1.95	*w*	¾	3.8
7	$\bar{2}02$	1.855	1.86	*m*	6	28.0
8	112	1.769				2.6
9	020	1.705	1.71	*w*	3	6.7
10	021	1.615			¼	1.6
11	202	1.572	1.58	*m*	5	13.9
12	$\bar{1}13$	1.499	1.50	*S*	6	16.7
13	022	1.412	1.40	*S*	7	13.2
14	$\bar{3}11$	1.400				12.3
15	310	1.396				0.9
16	113	1.373	1.37	*m*	7	5.5
17	220	1.369				11.5
18	221	1.355				0.7
19	312	1.307	1.30	*m*	3	0.7
20	311	1.296				4.2
21	221	1.289				0.6
22	004	1.260	1.27	*m*	5	5.1
23	$\bar{2}22$	1.255				3.4
24	023	1.197				0.4
25	$\bar{2}04$	1.190	1.18	*w*	1	0.8
26	$\bar{1}14$	1.190				0.4
27	$\bar{3}13$	1.163	1.16	*w*	2	2.5
28	222	1.156				2.3
29	312	1.150				0.4
30	400	1.147				3.3
31	223	1.116			½	0.3
32	$\bar{4}02$	1.116				0.6
33	114	1.104				0.3
34	130	1.103				0.0
35	131	1.087	1.09	*w*	1	5.0
36	131	1.069			½	1.0
37	204	1.035			½	0.4
38	$\bar{1}32$	1.026				0.0
39	$\bar{3}14$	1.014	1.01	*w*		0.2
40	223	1.013			½	0.2
41	024	1.013				1.2
42	313	1.002			½	2.5
43	132	0.996				0.0
44	402	0.985	0.98	*w*	2	0.3
45	$\bar{1}15$	0.977				1.1
46	$\bar{2}24$	0.976				2.3
47	$\bar{4}21$	0.960			½	0.1
48	420	0.952				0.9
49	133	0.939	0.93	*w*	1	0.5
50	$\bar{4}22$	0.934				1.8
51	$\bar{4}04$	0.928			½	1.1
52	115	0.917				1.6
53	331	0.914				0.5
54	421	0.913				0.1
55	330	0.912				0.0
56	133	0.906			½	2.0
57	$\bar{5}11$	0.898				0.7
58	510	0.886	0.88	*w*	2	0.1
59	$\bar{3}32$	0.886				0.0
60	224	0.885				1.4
61	331	0.883				1.8
62	$\bar{3}15$	0.882				1.3
63	$\bar{4}23$	0.881				0.1
64	512	0.881				0.1
65	025	0.868				0.1
66	422	0.853	0.85	*w*		1.1
67	040	0.853				0.3
68	$\bar{2}25$	0.852				0.1
69	511	0.850				1.1

d : spacing of planes of CuO crystal calculated from the results by X-ray analysis by G. Tunnel, E. Posnjak and C. J. Ksanda. Z. Kristallogr. **90** (1935), 120. Monoclic system $a=4.653\text{Å}$, $b=3.410\text{Å}$, $c=5.108\text{Å}$ and $\beta=99°39'$, Cu.

d' : spacing of planes of CuO obtained from cathode-ray diffraction photograph.

I : Intensities of D. S.-rings estimated in three degrees of intensities—strong, medium and weak, from the cathode-ray diffraction photograph.

I' : Relative intensities of X-ray D. S. rings of CuO (Mo Kα) by G. Tunnel and others.

I'' : Relative intensities of cathode ray D. S. rings of CuO calculated from pE^2/θ^2. p: number of sets of planes which have the same spacing; E: cathode ray structure amplitude of CuO (In this calculation Cu and O in CuO were regarded as neutral atoms, as the X-ray atomic structure factor of Cu++ could not be utilized); 2θ: angle of diffraction.

films. (b) No differences were also observed, whether the copper film was oxidized by heating for a definite time at a definite temperature or by heating to a desired temperature from the room temperature in a time interval of about an hour. (c) When the copper film prepared on the cleavage surface of sodium chloride was oxidized without being detached from the substrate, we obtained a cuprous oxide film, in which the orientations of cuprous oxide crystals were not so perfect as those in the cuprous oxide film oxidized after being detached from the substrate as described above (Fig. 6), and a cupric oxide film in which oxide-crystals were orientated at random. (d) When the copper film was oxidized by floating on the water surface, we used the city water or the distilled water which was at the room temperature or maintained at an elevated temperature, but we observed no differences in the structure of the cuprous oxide film by changing these conditions. (e) When the thin single crystal film of copper was thinner than that used in the present experiment, the structure of the cuprous oxide film bore a resemblance close to that reported by L. Brück⁽¹⁾.

The three rings substance CuO reported by C. A. Murison⁽²⁾ and S. Miyake⁽³⁾ was not observed in the present experiment. The thinness of the copper film used as the specimen might be a cause of absence of such a compound.

The author is indebted to the Department of Education for the Scientific Research Expenditure.

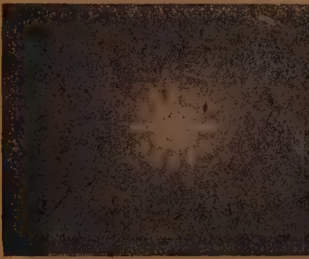

Fig. 1.
Heated in air at 220°C for 10 min. ($^2/_3\times$)

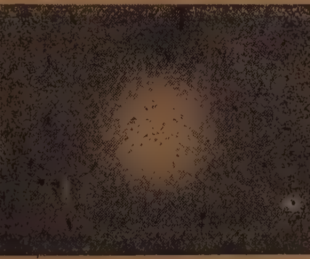

Fig. 2.
Floated on water at room temperature for 20 hr. and 20 min. ($^2/_3\times$)

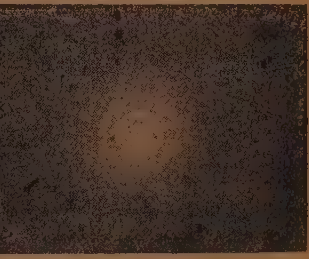

Fig. 3.
Heated in air at 522°C for 10 min. ($^2/_3\times$)

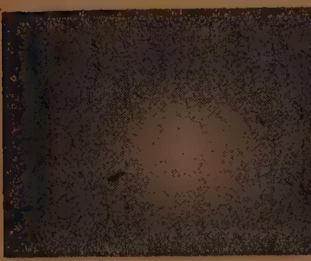

Fig. 4.
Heated in air at 422°C for 10 min. ($^2/_3\times$)

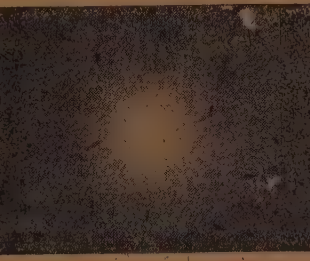

Fig. 5.
Heated in air at 319°C for 10 min. ($^2/_3\times$)

Fig. 6.
Cu film on NaCl crystal heated in air at 186°C for 10 min. ($^2/_3\times$)

References.

(1) L. Brück: Ann. d. Phys. **26** (1936), 233.
(2) C. A. Murison: Phil. Mag. **17** (1936), 96.
(3) S. Miyake: Sci. Pap. Inst. Phys. Chem. Res. Tokyo. **29** (1936), 167.

Statistical Theory of Linear Polymers III. Double Refraction.

By Ryogo KUBO.

Physical Department, Faculty of Science, Tokyo Imperial University.

(Received April 23, 1937.)

Introduction.

If the tensor of polarizability of the sub-molecule of the large molecule is anisotropic, the tensor of refractivity will be anisotropic when the orientation of elements is not isotropic. Unstrained rubber is optically isotropic. When deformed, it shows double refraction, because the orientation of isoprenes comes to be parallel to some preferred directions. If the deformation is large, it may be accompanied by partial crystallization which will give additional anisotropy to the refractivity of the whole system. In this paper we put this crystallization effect out of our consideration. Our theory is concerned only with the re-orientation effect.

A mathematical theory of double refraction was given by F. Horst-Mueller⁽¹⁾ in 1941. In my opinion his basic assumption seems hard to be agreed with. Our theoretical results are somewhat different from his.

§1. Orientation of Elements in a Chain.

We have shown in our papers I and II that the statistical properties of a chain consisting of vectors are determined by the eigenvalue problem

$$\lambda\psi(s,\mathbf{a})=\exp(s\mathbf{a})\int K(\mathbf{a},\mathbf{a}')\psi(\mathbf{a}')d\mathbf{a}', \qquad (1)$$

where K denotes the correlation probability of two neighboring vectors. It can be expanded into a series of the characteristic functions as follows:

$$K(\mathbf{a},\mathbf{a}')=\sum_{\nu}\lambda_\nu\psi_\nu(s,\mathbf{a})\psi_\nu(s,\mathbf{a}')\exp\{-s\mathbf{a}-s\mathbf{a}'\}. \qquad (2)$$

The probability of a configuration of vectors $(\mathbf{a}_1\mathbf{a}_2\cdots\cdots\mathbf{a}_n)$ is given by the product

$$K(\mathbf{a}_1\mathbf{a}_2)K(\mathbf{a}_2\mathbf{a}_3)\cdots\cdots K(\mathbf{a}_{n-1},\ \mathbf{a}_n). \qquad (3)$$

We ask for the orientation probability of a constituent vector when the length of the chain is specified. Multiplying (3) by $\exp\{s\sum\mathbf{a}\}$ and integrating for all $\mathbf{a}_i$'s except one $\mathbf{a}$ we get the orientation probability

$$f=\frac{\exp(-s\mathbf{a})\psi^2(s,\mathbf{a})}{\int\exp(-s\mathbf{a})\psi^2(s,\mathbf{a})d\mathbf{a}}, \qquad (4)$$
$$\frac{d\log\lambda}{ds}=\frac{r}{na}=\rho,$$

provided that the total number n of elements is large. The parameter s in the first equation of (4) is a function of the length r or the parameter ρ defined by the second equation of (4) (c.f. Eqs. (16) and (12), I). ψ in Eq. (4) means the eigenfunction corresponding to the largest eigen-value. The representation of elements by mathematical vectors is not adequate in the case when some hinderance exists for the internal rotation of the chain molecule (for instance long paraffine-like molecule). If the correlation between three or four neighboring skeletal units is to be taken into account, we can represent our new element by a planer figure made up of two neighboring units. Its orientation must be specified by a set of Eulerian angles (θ',ϕ',x'). Then the eigenvalue problem will be of the form

$$\lambda\psi(s;\theta',\phi',x')=\exp(sa\cos\theta')$$
$$\iiint K(\theta',\phi,x';\theta'',\phi'',x'')$$
$$\times\psi(s;\theta'',\phi'',x'')d\cos\theta''d\phi''dx''. \qquad (5)$$

If we make the assumption that ψ corresponding to the largest λ does not depend upon x', (5) is replaced by

$$\lambda\psi(s;\theta',\phi')=\exp(sa\cos\theta')$$
$$\iint K(\theta\phi';\theta''\phi'')\psi(s,\theta'',\phi'')d\cos\theta''dx'', \qquad (6)$$

where

$$K=\frac{1}{2\pi}\iint K(\theta',\phi',x',\theta'',\phi'',x'')dx'dx''. \qquad (7)$$

This is of the same form as the eigenvalue problem (1), the solution of which was discussed in detail in our paper I. We need only calculate the mean values c_1, c_2, …… using the modified correlation function K. As was shown in I, the eigenfunction can be developed as

$$\psi=\frac{1}{4\pi}[1+\psi_1(s)P_1(\cos\theta')+\psi_2(s)P_2(\cos\theta')+\cdots\cdots]. \qquad (8)$$

Inserting (8) in (4) we get

$$f=\frac{1}{4\pi}\Big[1+(2\psi_1-as)P_1(\cos\theta')+\left(\frac{1}{3}a^2s^2+\frac{2}{3}\psi_1^2+2\psi_2-\frac{4}{3}as\psi_1P_2(\cos\theta')+\cdots\cdots\right]\qquad (9)$$

where powers of s higher than s^2 are omitted. In terms of ρ Eq. (9) takes the form

$$f=\frac{1}{4\pi}[1+3\rho P_1(\cos\theta')+D_2\rho^2P_2(\cos\theta')+\cdots\cdots], \qquad (10)$$

where

$$D_2=3\left(\frac{1-c_1}{1+c_1}\right)^2\left[1-\frac{4}{1-c_1}+\frac{2}{(1-c_1)^2}+\frac{2(1+c_1)}{(1-c_1)(1-c_2)}\right]. \qquad (11)$$

In deriving these formulae we have made use of equations given in § 3, I. The expression (10) is valid only when ρ is small.

More generally f may be expressed as

$$f=\frac{1}{4\pi}[1+f_1(\rho)P_1(\cos\theta')+f_2(\rho)P_2(\cos\theta')+\cdots\cdots]. \qquad (12)$$

General expressions for f_i's can not easily be obtained when s is large (with ρ near to its maximum value ρ_∞). For a chain without correlation (§ 3, I), we get

$$f=\frac{1}{4\pi}\frac{as}{\sinh as}\exp\{as\cos\theta'\}=\frac{1}{4\pi}\left[1+3\rho P_1(\cos\theta')+5\left(1-\frac{3\rho}{as}\right)P_2(\cos\theta')+\cdots\cdots\right] \qquad (13)$$

$$L(as)=\coth as-\frac{1}{as}=\rho.$$

Naturally (10) and (13) coincide with each other for small ρ if we put both c_1 and c_2 equal to zero in (11). When the positive and negative directions of the chain are not prescribed, the terms with odd order vanish out from f when averaged over two opposite directions.

§ 2. Orientation Probability as a Function of Deformation.

Here we assume the network model of long chain molecules given in the preceding paper II[(2)]. Notations are the same as there. The index of curling ρ of a chain (e.g. the part of a long chain molecule lying between two neighboring junctures) is given by

$$\rho^2=\rho_0^2(A^2\xi^2+B^2\eta^2+C^2\zeta^2), \qquad (14)$$

when the principal values of the deformation are A, B and C (see II). Direction cosines of the chain after the deformation are assumed to be

$$x=\frac{A\xi}{(A^2\xi^2+B^2\eta^2+C^2\xi^2)}\text{ etc.} \qquad (15)$$

In Eqs. (14) and (15), (ξ, η, ζ) are the direction cosines of the chain before the deformation. We put

$$x=\cos\Theta,\quad y=\sin\Theta\cos\Phi,\quad z=\sin\Theta\sin\Phi \qquad (16)$$
$$\xi=\cos\Theta_0,\quad \eta=\sin\Theta_0\cos\Phi_0,\quad \zeta=\sin\Theta_0\sin\Phi_0.$$

In untrained state the distribution of (ξ, η, ζ) on an unit sphere is assumed uniform; after the deformation, (x, y, z) will distribute on this sphere non-uniformly. Its density function w is given by the equation

$$d\cos\Theta_0 d\Phi_0=w\,d\cos\Theta d\Phi. \qquad (17)$$

Solving Eq. (15) after (ξ, η, ζ), we have

$$\xi=\frac{x}{A}\frac{1}{\left(\frac{x^2}{A^2}+\frac{y^2}{B^2}+\frac{z^2}{C^2}\right)^{1/2}}\text{ etc.} \qquad (18)$$

and from (14),

$$\rho^2=\rho_0^2\Big/\left(\frac{x^2}{A^2}+\frac{y^2}{B^2}+\frac{z^2}{C^2}\right). \qquad (19)$$

By elementary calculations we get

$$w=\frac{\partial(\xi,\Phi_0)}{\partial(x,\Phi)}=\left(\frac{x^2}{A^2}+\frac{y^2}{B^2}+\frac{z^2}{C^2}\right)^{-3/2} \qquad (20)$$

Both ρ and w are functions of Θ and Φ by Eq. (16).

The orientation probability of elements belonging to a chain was given in § 1 as a function of the angle θ' between the axis of the chain (x, y, z) and of an element. As a function of angles referred to the axes of deformation, the distribution function $F(\theta, \phi)$ for all elements belonging to various chains will be obtained by averaging $f(\theta')$ over all possible orientations (x, y, z) of the axes of chains with the weight function w. The relation of various angles will be easily seen in

Fig. 1.

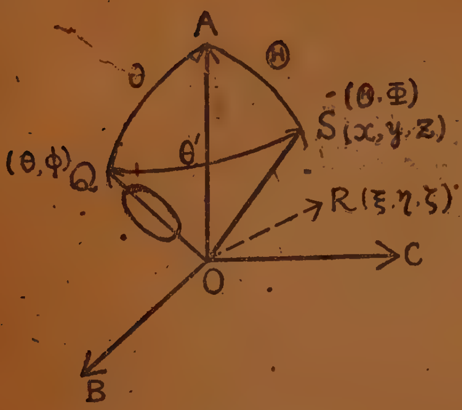

Fig. 1.

$\overrightarrow{OR}$: original direction of a chain.
$\overrightarrow{OS}$: its direction after the deformation.
$\overrightarrow{OQ}$: direction of an element.

Inserting (19) in (12), we get $f_l(\rho)$ as functions of Θ and Φ. Thus we can expand the functions wf_l into a series of spherical harmonics, namely

$$wf_l(\rho)=\Sigma f_{lj}Y_j(\Theta,\Phi). \qquad (21)$$

with

$$\cos\vartheta=\cos\Theta\cos\theta+\sin\Theta\sin\theta\cos(\Phi-\phi). \quad (22)$$

the averaged function will be found to be

$$F(\theta,\phi)=[f]_{Av}=\frac{1}{4\pi}\sum_l\frac{f_{ll}}{2l+1}Y_l(\theta,\phi). \quad (23)$$

where (θ, ϕ) specifies the direction of the element referred to the axes of deformation. Terms with odd l disappear from (23).

As we are interested in mean values of tensors, we need only the term with $l=2$. We can write it as

$$F_2=F_{20}P_2(\cos\theta)+F_{22}P_2^2(\cos\theta)\cos2\phi, \quad (24)$$

for F must be symmetrical to the transformation $\phi\rightarrow-\phi$. The coefficient F_{20} is calculated by

$$F_{20}=\frac{1}{(4\pi)^2}\iint f_2(\rho)wP_2(\cos\Theta)d\cos\Theta d\Phi. \quad (25)$$

For small ρ_0 we can expand f_2 as

$$f_2(\rho)=D_2\rho^2+D_4\rho^4+\cdots\cdots \qquad (26)$$

and after some elementary integrations we arrive at

$$F_{20}=\frac{1}{4\pi}\Big[\frac{D_2}{3}\rho_0^2\Big(A^2-\frac{B^2+C^2}{2}\Big)$$
$$+\frac{D_4}{5}\rho_0^4\Big\{A^4-\frac{B^4+C^4}{2}$$
$$+\frac{1}{6}(A^2B^2+A^2C^2-2B^2C^2)\Big\}+\cdots\cdots\Big], \quad (27)$$

where we have made use of the condition for the constant volume: $ABC=1$.

When the deformation is small, we put

$$A=1+l,\quad B=1+m,\quad C=1+n,$$
$$l,\ m,\ n<<1. \qquad (28)$$

Then the functions ρ and w can be approximated by

$$\rho=\rho_0(1+lx^2+my^2+nz^2)$$
$$w=1+3(lx^2+my^2+nz^2),$$

and F_{20} by

$$F_{20}=\frac{1}{4\pi}\frac{2}{15}(3f_2(\rho_0)+\rho_0f_2'(\rho))$$
$$\times\Big(l-\frac{m+n}{2}\Big). \qquad (29)$$

For the chains without correlation we get from (13)

$$F_{20}=\frac{1}{4\pi}\cdot2\Big[1-\frac{4}{a}\frac{\rho_0}{s_0}+\frac{\rho_0^2}{as_0^2}\frac{ds_0}{d\rho_0}\Big]$$
$$\times\Big(l-\frac{m+n}{2}\Big). \qquad (30)$$

3. The Tensor of Refractivity.

The coordinate system fixed to an element shall be called as (1, 2, 3), the axis 1 of which is its skeletal direction. Let the components of the polarizability tensor be (α_{11}, $\alpha_{22}\cdots\cdots\alpha_{12}\cdots\cdots$). When the axis 1 has the direction (θ, ϕ) and rotated orientations of 2 and 3 about 1 are all equally probable, the components of polarizability referred to the axes of the deformation will be

$$\alpha^0_{XX}=\bar{\bar{\alpha}}+\frac{2}{3}\Delta\alpha P_2(\cos\theta)$$

$$\alpha^0_{YY}=\bar{\bar{\alpha}}-\frac{1}{3}\Delta\alpha P_2(\cos\theta)$$
$$+\frac{1}{6}\Delta\alpha P_2^2(\cos\theta)\cos2\phi$$

$$\alpha^0_{ZZ}=\bar{\bar{\alpha}}-\frac{1}{3}\Delta\alpha P_2(\cos\theta)$$
$$-\frac{1}{6}\Delta\alpha P_2^2(\cos\theta)\cos2\phi \qquad (31)$$

$$\alpha^0_{YZ}=\frac{1}{6}\Delta\alpha P_2^2(\cos\theta)\sin2\phi$$

$$\alpha^0_{ZX}=\frac{1}{3}\Delta\alpha P_2'(\cos\theta)\sin\phi$$

$$\alpha^0_{XY}=\frac{1}{3}\Delta\alpha P_2'(\cos\theta)\cos\phi$$

where

$$\bar{\bar{\alpha}}=\frac{1}{3}(\alpha_{11}+\alpha_{22}+\alpha_{33}),\quad \Delta\alpha=\alpha_{11}-\frac{\alpha_{22}+\alpha_{33}}{2} \qquad (32)$$

multiplying a^0 by F_2 and integrating over all directions of (θ, ϕ), we get the averaged polarizability; for example,

$$[a_{XX}]=\overline{\overline{a}}+\frac{8\pi}{15}\Delta a F_{20}. \tag{33}$$

It can be seen at once that $[a_{YZ}]=[a_{ZX}]=[a_{XY}]=0$. Principal values of refractivity tensor are given by

$$\frac{n_X^2-1}{n_X^2+2}=\frac{4\pi}{3}N[a_{XX}] \qquad \text{etc.} \tag{34}$$

where N denotes the total number of elements in unit volume. Refractivity n_0 in unstrained state is defined by

$$\frac{n_0^2-1}{n_0^2+2}=\frac{4\pi}{3}N\overline{\overline{a}}. \tag{35}$$

Hence we get

$$\frac{n_X^2-1}{n_X^2+2}-\frac{n_0^2-1}{n_0^2+2}=\frac{8\pi}{45}N\Delta a\cdot 4\pi F_{20}, \tag{36}$$

which allows us to calculate n_X as a function of A, B and C.

If $|n_X-n_0|<<n_0$, the formula

$$n_X-n_0=\frac{(n_0^2+2)^2}{6n_0}\frac{8\pi}{45}N\Delta a\cdot 4\pi F_{20} \tag{37}$$

may be used. Inserting the formula

$$N=\frac{dN_L}{m},$$

and Eq. (27), we get

$$n_X-n_0=\frac{4\pi}{405}D_2\frac{dN_L\rho_0^2}{m}\frac{(n_0^2+2)^2}{n_0}\Delta a \times\left(A^2-\frac{B^2+C^2}{2}\right)+\cdots\cdots. \tag{38}$$

Similar formulae for n_Y and n_Z can be easily derived. For uniaxial elongation $(B=C=1/\sqrt{A})$, it will be shown at once that

$$\Delta n=n_{\parallel}-n_{\perp}=\frac{2\pi}{135}D_2\frac{dN\rho_0^2}{m}\frac{(n_0^2+2)^2}{n_0} \times\Delta a\left(A^2-\frac{1}{A}\right). \tag{39}$$

In the paper II we have shown that the stress X referred to the actual cross section is given by

$$X=\frac{dRT\rho_0^2}{m}\frac{1-c_1}{1+c_1}\left(A^2-\frac{1}{A}\right) \tag{40}$$

for not too large elongation A. Thus we get

$$\frac{\Delta n}{X}=\frac{2\pi}{135}\frac{1+c_1}{1-c_1}D_2\frac{(n_0^2+2)^2}{n_0 kT}\Delta a. \tag{41}$$

§4. Discussions.

In Fig. 2 we show the experimental result by Thiessen and Wittstadt(4). The double refraction as the function of elongation shows some hysteresis loop for elongation larger than 400% or so, which is a symptom of partial crystallization.

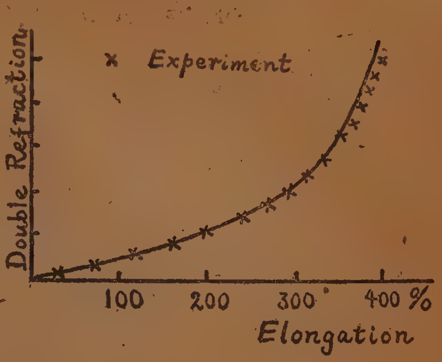

Fig. 2.

Double refraction of vulcanized rubber.
× : experiment, —— : theoretical curve.

The relation

$$\Delta n\propto A^2-\frac{1}{A}, \tag{42}$$

seems to fit well to the actual behavior at least up to 400% elongation. In this range Δn depends little on the temperature (from 20°C to 60°C), which is to be expected from (38) if the effects of hinderance for rotation is small (with D_2 nearly independent of the temperature).

It must be emphasized that the proportionality $\Delta n\propto X$ holds in a wider region than that of Hooke's law. F. Horst.-Mueller has derived a similar formula as Eq. (41), assuming, however, that Δn and X are both proportional to the elengation. In this region the proportionality is rather self-evident. Our result says much more than his. Moreover, the coefficient is different from that he has given. For brevity we write (41) as

$$\frac{\Delta n}{X}\doteq\Gamma\frac{(n_0^2+2)^2}{n_0 kT}\Delta a \tag{43}$$

where Γ can be evaluated from Eq. (11). Its values are:

i. for chains without correlation, $D_2=3$

$$\Gamma\doteq\frac{2\pi}{45}=0.0444\pi. \tag{44}$$

ii. for chains freely rotating with the bond angle equal to 109

$$\Gamma\doteq\frac{\pi}{18}=0.0556\pi. \tag{45}$$

iii. for long paraffine-like chains $(kT<<U$, U=hindering potential)

$$\Gamma=\frac{526\pi}{9009}=0.0584\pi \qquad (46)$$

iv. for long paraffine-like chains $(KT<U)$,

$$\Gamma=\frac{17\pi}{405}e^{U/kT}=0.0420\pi\, e^{U/kT}. \qquad (47)$$

Horst-Mueller gave the result

$$\Gamma=\frac{16}{9}\pi \qquad (48)$$

and from experimental results for $\Delta n/X$ he calculated Δa which are given in the Table. The unit of Δa is 10^{-6}. They are far smaller than $(\Delta a)_{\mathrm{Kerr}}$ obtained from Kerr-effect for liquids of monomers. Though polarizabilities of monomers in polymerized state might be expected to be smaller than that of free monomer molecules, we believe that this coefficient Γ is too large. From our results (44), (45), and (46), $(\Delta a)_{\mathrm{cal.}}$ are about 40 times larger then those given by Horst-Mueller. If we require that $(\Delta a)_{\mathrm{cal}}=(\Delta a)_{\mathrm{Kerr}}$, we get for $\exp(U/kT)$ from (47). Numerical values are given in the table.

Table I.

	Polystyrol	Polyvinyl-chrolide	Polyisoprene
1. $(\Delta\alpha)_{Kerr}$	-50	1~5	20
2. $(\Delta\alpha)_{H}$	$-3.5\sim-2.5$	0.45	0.87
3. $(\Delta\alpha)_{K}$	$-140\sim-100$	18	35
4. $(\Delta\alpha)_{K}$	$-110\sim-80$	14	28
5. $(\Delta\alpha)_{K}$	$-105\sim-75$	10	26
$e^{U/kT}$	3.2~2.3	20~4.1	1.98

3, 4, and 5 are calculated by Eqs. (44), (45) and (46) respectively.

The case i, ii, and iii give nearly the same values for the double refraction. From the table it seems that our coefficients Γ in (44), (45), (46) are somewhat too small, while the hindering potential U obtained from Eq. (47) are surely of reasonable order of magnitude. Certainly our theory is not so rigorous that we can get any detailed picture about the hinderance of the internal rotation. However, it might be interesting to notice the effect of hinderance upon the double refraction.

The double refraction for a given deformation will be larger if the index of curling is larger $(\rho_0\to\rho_\infty)$ because of the strong internal tension of the chains. For example, we can easily verify this in the case of chains without correlation. When the deformation is small uniaxial elongation, from Eqs. (30) and (37) we get

$$\Delta n=\frac{2\pi}{15}\frac{dN_c}{m}\frac{(n_0^2+2)^2}{n_0}\Delta a \times\left[1-\frac{4\rho_0}{as_0}+\frac{\rho_0^2}{as_0^2}\frac{ds_0}{d\rho_0}\right]l, \qquad (49)$$

where the function in the bracket reduces to ρ_0^2 for small ρ_0, and for $\rho_0\to 1$ it approaches to 2; we can see it by the asymptotic formula,

$$\rho_0=L(as_0)=1-\frac{1}{as_0}. \qquad (50)$$

In Eq. (33) II, we gave the rigidity

$$G=\frac{dRT}{5m}\left(as_0\rho_0+\frac{2}{3}a\rho_0^3\left(\frac{ds}{d\rho}\right)_0\right). \qquad (51)$$

Thus we have a general expression for Γ in the case of chains without correlation

$$\Gamma=\frac{2\pi}{9}\,\frac{1-\dfrac{4\rho_0}{as}+\dfrac{\rho_0^2}{as_0^2}\dfrac{ds_0}{d\rho_0}}{as_0\rho_0+\dfrac{2}{3}a\rho_0^3\dfrac{ds_0}{d\rho_0}}. \qquad (52)$$

The behavior of Γ is illustrated in Fig. 3. For a given stress the double refraction becomes smaller as ρ_0 increases.

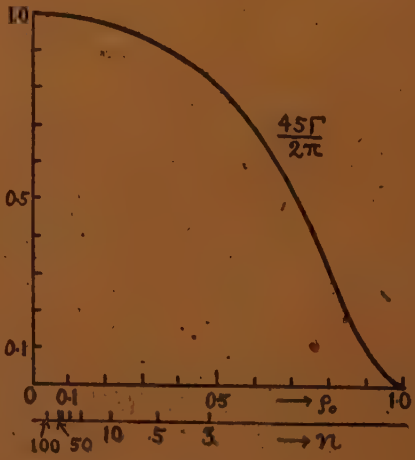

Fig. 3.

Eq. (52) as the function of ρ_0 and n, or the number of units involved in a chain. It is assumed here that $c=1$ in Eq. (7), II (c.f. Fig. 3. II).

Conclusion.

Thus I believe I could give a more satisfactory theory than anyone ever given, based on the network model which are now widely accepted. The approximative nature of our theory exist firstly in the correlation function in Eq. (5), which must take more complicated interactions into account, and secondly the neglection of the repulsive effect of elements in a chain and in different chains, which is the so-called van der Waals correction corresponding to the theory of actual gases. Though not able today to predict how these effect on Γ, we might expect our Γ is right order of magnitude. In the next paper we will discuss the effect of hinderance for internal rotation.

In conclusion the writer wishes to express his thanks to Prof. Ochiai for his interest given to this work.

References.

(1) Horst-Mueller: Kolloid-Z. **95** (1941), 138.

(2) R. Kubo: J. phys. Soc. Japan, **2** (1947), 47.

(3) R. Kubo: J. phys. Soc. Japan, **2** (1947), 51.

(4) Thiessen and Wittstadt: Z. physikal, Chem, B. **41** (1938), 33.

SHORT NOTES.

Further Confirmation of the Angular Correlation of the Successive γ-rays.

By Yuzuru WATASE and Seinosuke OZAKI.

Neuclear Physics Laboratory of
Osaka Imperial University.

(Received June 25, 1947.)

The angular correlation of the successive γ-rays emitted from the daughter element of ^{65}Zn and its variation with the resolving time of the coincidence circuit was studied. The circuit was almost similar to that used by Watase, and its resolving time was varied by changing the resistance of the mixer stage. With the various resolving time, coincidence rate was counted alternatively at 90° and 180° of the angle subtended by the two counters to a γ-ray source. The results were as follows:

resolving time	2.7 ± 0.2	6.2 ± 0.3	10.4 ± 0.5	$14.0\pm0.1\times10^{-7}$ min
$N_{\gamma\gamma}(90°)$	0.75 ± 0.04	0.93 ± 0.04	1.04 ± 0.05	1.06 ± 0.05
$\frac{N_{\gamma\gamma}(180°)}{N_{\gamma\gamma}(90°)}$	0.52 ± 0.15	0.63 ± 0.09		0.71 ± 0.12

This shows that the angular correlation is very prominent in the present case. Therefore, we may conclude that the successive γ-rays have large angular momenta respectively and spin changes between the concerning levels are very large.

From the variation of the coincidence rate with the resolving time, the life-time of the intermediate level can be calculated. In the present case, at least two modes of the successive γ-ray emission which have the intermediate level of the very short life time one and long life time as long as 7×10^{-6} min. are thought to exist. 70% of the disintegation belongs to the latter and 30% to the former. As Hamilton discussed, only the successive γ-rays emitted through the shorter life levels can contribute to the angular correlation. This agrees well with the variation of $N_{\gamma\gamma}(180°)/N_{\gamma\gamma}(90°)$ with the resolving time.

A little detailed description was already given on the Japanese edition of this proceedings.

On the Specific Heat and Thermal Expansion of Barium Titanate.

By Syozo SAWADA, Gen SIRANE
and Hirosi SUGAWARA.

The Second Faculty of Engineering,
Tokyo University.

(Received July 21, 1947.)

We are observing the specific heat and thermal expansion of barium titanate between room temperature and 200°C.

Main results obtained untill now will be reported briefly in the following. The mixtures of $BaCO_3$ and TiO_2 of molecular ratio 1:1 were pressed into circular disks and these were sintered by the gas-furnace. The matures are considerably porous.

The specific heat of powdered samples in a cylindrical vessel of copper was measured by Sykes'method. For the fear of reduction and some other reasons we performed observations in the air, but the samples were thoroughly preheated for the removal of moisture. An apparatus to measure the specific heat in vacuum is now being constructed. An example of observed values of the specific heat is shown in Fig. 1. An anomaly of the λ-type is observed at 108°C. The degree of sinter of samples and other conditions vary the position of the peak between 106 ~ 110°C and displace the curve slightly. Latent heat was not observed. For the sample illustrated in Fig. 1, the peak of the dielectric constant was observed at 111°C. Also for other samples, the position

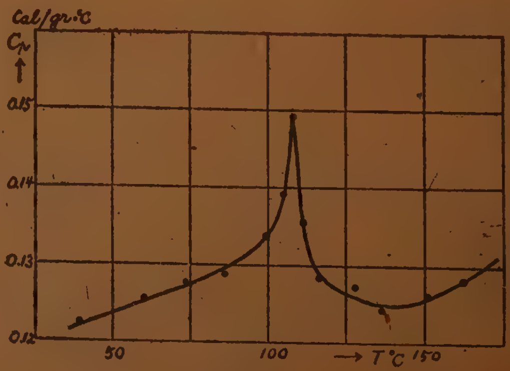

Fig. 1.

of the peak of dielectric constant is always observed at a few degrees above that of the specific heat. As far as we know at present, Vul and Goldman(1) observed an abrupt change of the specific heat at 125°C. Miyake and Ueda(2) expected an anomaly of the λ-type of specific heat in the neighbourhood of the transition point as a result of their differential thermal analysis. Hippel(3), on the other hand, did not observed any anomaly in the cooling curve for a sample composed of 75% $BaTio_3$ and 25% $SrTiO_3$.

The thermal expansion was observed by a thermal dilatometer of a new type, in which the dilatation of samples is magnified by two rods of quartz possessing a small mirror at one end of them respectively. This apparatus allows us to measure the dilatation such as $\Delta l/l \doteqdot 10^{-6}$. Measurements were performed in the air. An example of observed values of the thermal expansion is shown in Fig. 2. A contraction is observed in the range of 10°C near the transition point. For the sample illustrated in Fig. 2, the thermal expansion coefficient shows a negative peak at 110°C. As in the case of specific heat, the position of the peak and the form of the curve varies slightly for different samples. The same curve was obtained for both heating and cooling. The peak of specific heat of the sample of Fig. 2 is also at 110°C. It seems to be probable that the position of the peak of specific heat coincides with that of thermal expansion coefficient and that the peak of dielectric constant is observed at minimal volume. The contraction of volume and the increase of dielectric constant may be in an intricate relation. For a sample of the Tosiba Comp. Ltd. which contains 98% $BaTiO_3$ (excess Ba) and 2% $Al_2O_3+Fe_2O_3$ in weight the dielectric constant showed a maximum at 85°C and the thermal expansion coefficient a minimum at 80°C, but contraction was not observed. Though the broadening of the transition point caused by the addition of impurities and the excess of Ba may extinguish the contraction, the judgement can be given only by further researches. Our observed value of thermal expansion coefficient agrees well with the value(2) calculated from the temperature dependence of lattice constants determined by the X-ray investigation. Though Ueda(4) observed the cubic expansion coefficient using liquid paraffin, the absolute value has not yet been obtained. Hippel(3) observed the thermal expansion coefficient between 80—90 and 1200°C. His values do not agree with ours and moreover he observed neither expansion nor contraction in the neighbourhood of the transition point. We think, however, it would be difficult (with the precision of his apparatus), to observe the contraction as small as we observed even if it indeed existed.

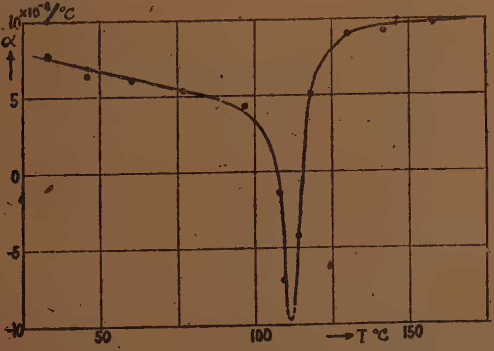

Fig. 2.

Details of this research will be published shortly.

References.

(1) B. M. Vul and I. M. Goldman: C. R. U. S. S. R. **49** (1945), 177.

(2) S. Miyake and R. Ueda: J. Phys. Soc. Jap., **1** (1946), 32.

(3) A. von Hippel: Ind. and Eng. Chem. **38** (1946), 1097.

(4) R. Ueda: Lecture at the Annual Meeting in 1947 of The Physical Society of Japan.

The Relaxation Effect of the Cuprous Oxide Rectifier after the Application of Strong Field.

By Akio KOBAYASHI.

Research Laboratory, Tokyo Shibaura Electric Co.

(Received August 11, 1947.)

When a strong field above 50 volts was applied in the hard flow direction to a cuprous oxide rectifier immersed in an oil bath, the current which was of 20 to 50 mA at the beginning increased steeply and reached some hundred mA after 1 or 2 minutes. After switching off, currents at d. c. 0,2 volt, which were about two times larger than the initial value, decreased with time and approached asymptotically to the initial value. Fig. 1 shows those currents measured instantaneously versus time curves, being the upper line for easy current flow, the lower for hard current flow.

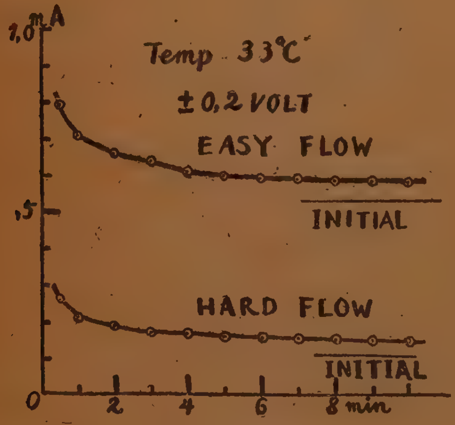

Fig. 1.

The current is empirically given by the following formula

$$j=j_0+ae^{-t/\tau}$$

where τ is the relaxation time varying with temperatures and is given by

$$\tau=Ae^{-Q/kT}$$

as shown in Fig. 2. Q and τ have the values 0.05 eV and 2 minutes at room temperature respectively.

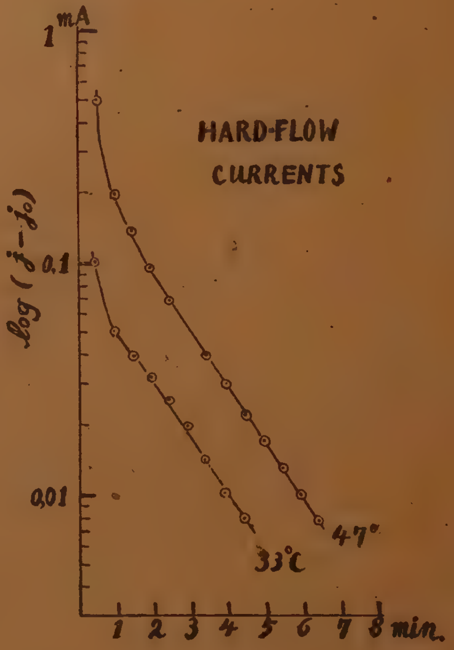

Fig. 2.

The effect can be explained by electrolysis of the blocking layer under strong fields and the variation of the space charge of trapping and impurity centers by ionization by collisions(1)(2).

References.

(1) A. V. Joffe and A. F. Joffe, Journ. of Phys. 2, (1940), 283.

(2) B. Davydov and I, Schmushkevitch, Journ. of Phys. 3, (1940), 359.

On Phase Transformation of $BaTiO_3$.

By Shizuo MIYAKE and Ryuzo UEDA

Kobayasi Institute of Physical Research, Kokubunji-machi, Tokyo.

(Read October 22, 1946; Received April 22, 1947)

1. Introduction.

In 1944, T. Ogawa(1) discovered a remarkable lielectric property of barium titanate ($BaTiO_3$)*. ts dielelctric constant ε is abnormally high, a 2000, at room temperature, and moreover it s found that there is a conspicuous peak in it t about 110° C, wherein the value of ε attanins o about 8000 or higher. Such a behavior reembles very much the so-called ferro-electricity f Rochelle salt and pottasium phosphate(KH_2 PO_4). It is natural to suppose that the peak f ε is related with some kind of phase transitin. But in contrast with the latter two subsances, which involve hydrogen atoms conributing to their dielectric anomaly, barium itanate does not contain any such light ions. he explanation of the $BaTiO_3$ seems to be an nteresting problem in the theory of solid.

The present authors, who are fortunately ffered the sample from Ogawa, performed X-ray and calorimetric studies. The sample we could obtain is of the form of the porcelain, which Ogawa prepared by heating a compressed mixture of $BaCO_3$ and TiO_2 in the molecular proportion of about 50:50 in a gas furnace at about 1380°C.

2. X-ray Study

Utilizing a simple high temprature X-ray camera, the change in the lattice with temperature variation is investigated. In order to detect the minute change, the back-reflection camera (R=50. 20±0. 08mm) is mainly applied. The CuK_α radiation is used. A thin alminum foil is placed in front of the photographic film to eliminate the fog due to the secondary X-rays from Ti-atoms. The Debye photgaaphs are

---

* Last autumn (1946) we could know the independent discovery of the similar phenomenon by B.M. Vul.(2)

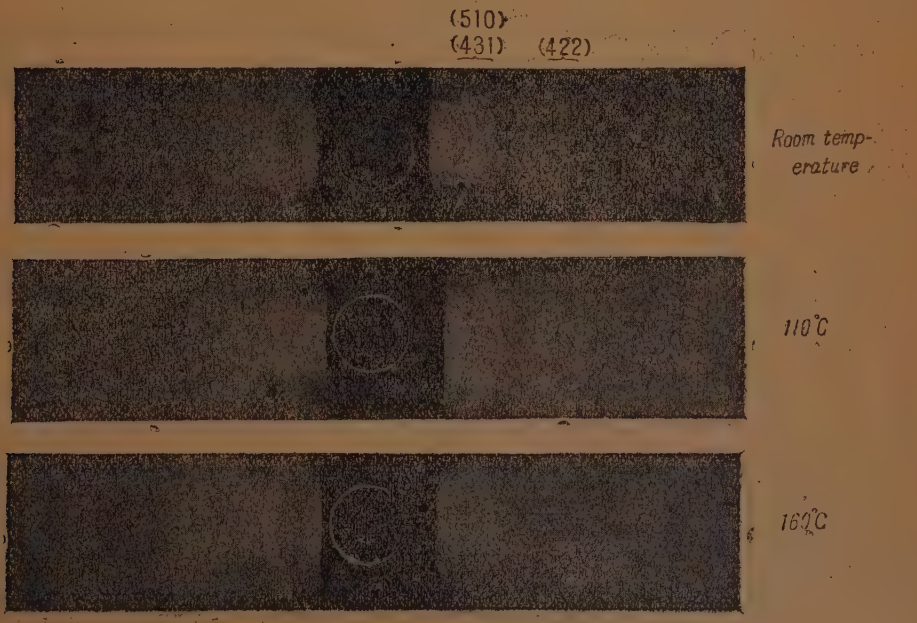

Fig. 1. Debye back-reflection photographs of $BaTiO_3$ ($CuK\alpha$)

taken on the powdered specimen in a temperature range from the room temperature up to about 200°C.

According to Goldschmidt(3) BaTiO$_3$ is known to belong to a cubic structure of the perowskite type, the lattice constant being $a=3.97$ A. But it becomes clear now that the substance can not be regarded as rigorously cubic at lower temperatures, whereas above about 110° it is in fact cubic. At room temperatures the Debye lines corresponding to the cubic structure are not in general singlets but multiplets. (Fig. 1). The split of lines can be most clear at angles of larger deflection, namely for the (510)(431)-line and the (422)-line, on account of the high resolution. The (510)(431)-line is composed of five and (422)-line of three lines, both including the lines due to K_{α_2}. Other lines also show certain fine structures, though the details are not clear because of their poor separation.

The magnitude of the line split decreases gradually when the temperature is raised. and at temperatures a little lower than 110° the lines begin to show a structure that being composed of a main line and a diffuse band (pl a line due to K_{α_2}). Above 110°, the split di appears entirely and the photograph shows perfect cubic character. From the above obs vation,it is evident that a lattice transformati takes place at abeut 110°C.

The lattice form at lower temperature next to be determined. Though the determ nation of the lattice form from the sole kno ledge of Debye photograph is in general difficu but since in the present case it is appar that the deformation of the lattice from t cubic form is only slight, the following pro dure can be applied with success. When lattice deforms from cubic into other latti forms, the Debye lines are anticipated to sp into the multiplets as indicated in Table On comparing the Table with the observ multiplicity for the (510)(431)-and the (422 lines, the only possible case is the deformati into the tetragonal structure. The possibili of the deformation into other lattice forms n included in the Table is out of question.

Table I. Line multiplicity which results when a cubic lattice deforms into other lattices.

	hkl	hhl	hhh	hko	hho	hoo
Tetragonal	3	2	1	3	2	2
Orthorhombic	6	3	1	6	3	3
Rhombohedral	4	3	2	2	2	1
Monoclinic	12	6	2	8	3	3
$\beta \doteqdot 90°$, $a=c$	6	4	2	4	2	2
$\beta \doteqdot 90°$, $a=b=c$	2	2	2	2	1	1

The spacing d of the tetragonal lattice expressed by the formula,

$$d=\frac{a}{\sqrt{h^2+k^2+\left(\frac{c}{a}\right)^2 l^2}}$$

We assume $c=a\cdot(1+\delta)$, where δ is a small quantity, then the deviation Δd of the spacing d from the cubic value is expressed by

$$\Delta d=d\frac{l^2}{h^2+k^2+l^2}\cdot\delta$$

Comparing this with the experimetally observed separation of lines, we can assign the tetragonal indices to every line. In the Table II the values of $l^2/(h^2+k^2+l^2)$ for the (510)(431)-line are indicated. The relative magnitudes of the observedseparation of the lines are in accordance with the present tetragonal assumption. The

Table II.

No. of lines	Tetragonal index	$\frac{l^2}{h^2+k^2+l^2}$
1	(510)	$\frac{0}{26}$
2	(501)	$\frac{1}{26}$
3	(431)	$\frac{1}{26}$
4	(413)	$\frac{9}{26}$
5	(134)	$\frac{16}{26}$
6	(105)	$\frac{25}{26}$

nes No. 1, 2, 3 merge into a single line, so at the multiplet should appear like a quartet, s the actual case is, when a line due to K_{α_2} neglected. For the doublet of (422)-line, milarly we can assign the tetragonal indices 22) and (224) raspectively.

From the line indices thus assigned the lattice nstant a and δ (or c) can be computed. In able III these values corresponding to various

able III. Lattice constants and lattice volumes.

emp. °C	a (Å)	δ_1	δ_2	$C=a$ $(1+\delta_1)$ (Å)	Volume (Å^3)
10	3.982	0.0091	0.0067	4.017	63.69
20	3.983	0.0089	4.0074	4.018	63.70
50	3.984	0.0082	0.0059	4.015	63.73
70	3.986	0.0075	0.0059	4.014	63.78
100	3.988	0.0066	0.0047	4.012	63.80
120	3.996				63.90
170	3.999				63.93
220	4.000				64.00
350	4.006				64.26

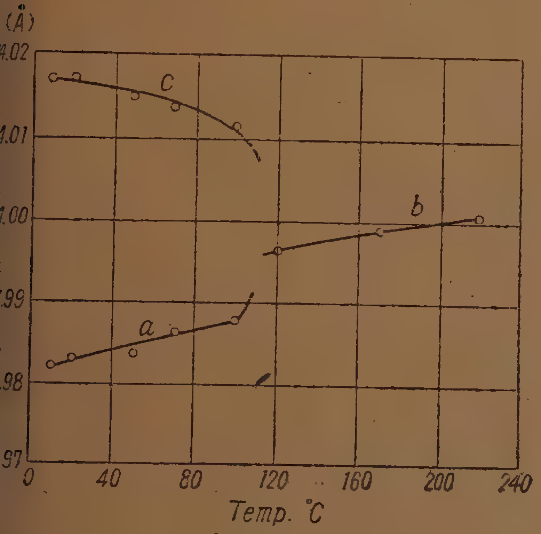

Fig. 2. Change of lattice constants.

peratures are shown, wherein δ_1 is the value δ computed on (510) (431)-lines, and δ_2, on 2)-lines. In the last column the volume of unit cell $V=a^2\cdot c$ is represented. In Figs. and 4 they are graphically reproduced. e discrepancy between δ_1 and δ_2 is somewhat large to be ascribed to the experimental or, though the general trend of the both ves is the same. The error may probably e from the disturbance of K_{α_2}.

he variation of the lattice constants is likely

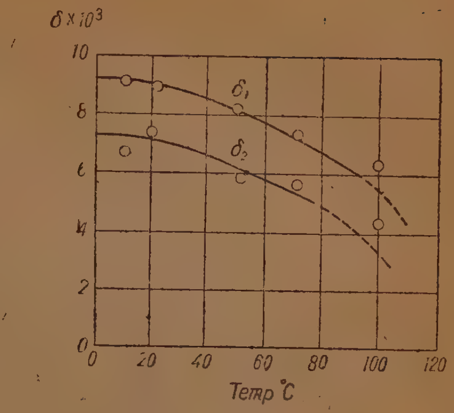

Fig. 3. Change of δ.

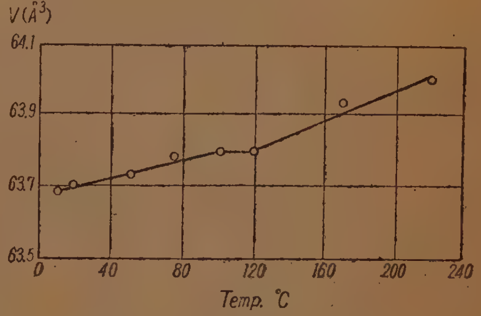

Fig. 4. Change of lattice volume.

to start from far below the transformation point T_c (ca 110°C), but the variation near T_c seems especially rapid. Whether or not the change of the tetragonal structure into the cubic one at T_c is continuous is not clear, because in a temperature range 100°~110°, the multiplet takes a diffuse appearance as mentioned before. (See Fig. 1)

On the other hand, the volume of the unit cell V has surely no discontinuity at the trasition point, although there is probably a discontinuity in the expansion coefficent.

The volume expasion coefficent α of this substance in the cubic-region is given by

$\alpha=3\cdot2\times10^{-5}/°C$ in the cubic region,
$\alpha=1\cdot9\times10^{-5}/°C$ in the tetragonal region.

The intensity of lines. Whether the transformation now encountered involves displacements of some ions in the lattice or not is the next question. At a glance the difference in the intensity distribution of Debye lines can not be observed between the two forms of this crystal, except the splitting of lines.

More quantitative intensity measurements are performed for the multiplet of (510)(431)-

lines No. 1, 2, 3 merge into a single line, so line. The line intensities measured with the microphotometer are compared with those which are expected when the ion arrangement of the perowskite type as below is assumed.

$$\mathrm{Ba}: 000, \quad \mathrm{Ti}: \tfrac{1}{2}\tfrac{1}{2}\tfrac{1}{2},$$

$$\mathrm{O}: \tfrac{1}{2}\tfrac{1}{2}0,\ \tfrac{1}{2}0\tfrac{1}{2},\ 0\tfrac{1}{2}\tfrac{1}{2}.$$

For the (510) (431)-line the structure factor F becomes

$$F = f_{Ba} + f_{Ti} - f_O$$

The line intensity is calculated according to the formula,

$$I \propto F^2 \cdot P \cdot \frac{1+\cos^2 2\theta}{\sin^2\theta \cos\theta}$$

where p is the number of the multiplicitiy of the Debye line and θ, the Bragg angle. The result is shown in Table IV, in which the

Table IV Claculated and observed intensities.

planes	sin θ	p	I colc.	I obs.
(510)	0.9853	8	34	34
(501) (431)	0.9850	24		
(413)	0.9823	16	16	21
(134)	0.9799	16	15	21
(105)	0.9723	8	6	8

scale of the intensity is so adjusted that the observed intensity (I_{obs}) and the calculated intensity (I_{calc}) coincide for the line No. 1. We can see I_{obs} and I_{calc} fairly agree to each other. So far as this result is concerned, accordingly, the evidence can not be found for the occurence of ion displacments upon the lattice transformation. Though the displacements less than few per cent of the lattice constant can not be excluded, the change of the ion con figuration will hardly be very large.

3. Thermal Analysis.

Through the X-ray study it becomes clear that $BaTiO_3$ makes a phase transformation of some kind at about 110°C. A simple thermal measuremet is next carried out to determine the transition temperature more precisely and to know if this transition accompanies the latent heat or other thermal anomaly. The so-called differential calorimetric method is adopted. The calorimeter, as shown diagrammatically in Fig. 5, consists of a duralmin cylindrical block, in which two holes are bor to be filled with the $BaTiO_3$ and the cont substance of similar quantity respectively. the latter substance is used a mixture of Ti and $BaCO_3$ in the molecular ratio 50:50. T temperature difference of these two is measu by differential thermojunctions (constantan-A constantan), connected to a galvanometer o sensitivity $4 \cdot 10^{-7}$ volt/div. The deflection one division on the lamp scale correspo to the temperature difference of about $4 \cdot 10^{-}$ The calorimeter is placed in an electric f nace and heated gradually with the speed the temperature rise about 1° to 1·5°/m The temperature of the calorimeter is measu by another thermojunction inserted within central hole of it. In Fig. 6 an example the heating curve thus obtained is sho In this curve a knick appears at about 11 which is considered to correspond to the tra tion temperature. Also a slight hump is served at a temperature range below it. But evidence for the existance of the latent h can not be detected. The anomaly in the cu therefore, may be due to the anomaly

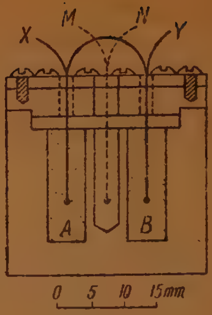

Fig. 5.

A : Sample.
B : Control Substance.
XY : Differential thermojunction.
MN : Thermojunction.

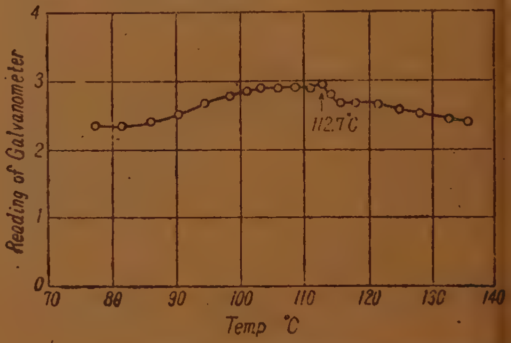

Fig. 6. Reading of differential calorimeter.

me kind in the specific heat, such that in the
-called λ-transition*. Averaging the results
several experiments, the transition tem-
rature T_c of the present sample is deter-
ined to be

$$T_c=112{\cdot}6°\pm0.5°\mathrm{C}.$$

In the cooling experiment is also found the
ick due to the transition at the temperature
e same as above within the experimental
ror.

Vul and Goldman(4) reported that the peak
the dielectric constant occurs at 125°C.
ccording to Coursey and Brand(5) this tem-
rature is 120°C. These values are somewhat
gher than ours, 120°C. This discrepancy
ems to be caused by the difference of the
emical composition of the samples. In our
mple is included impurities of few per cent
r the reason of the ceramic technique, and
ey may be responsible for the lowering of
e transition temperature.

4. Remark.

By the analaogy of the dielectric anomaly
the Rochelle salt crystal and $BaTiO_3$, it is
ry natural to suppose that the crystal of
e latter substance below the trasition tempe-
ture likewise possesses the spontaneous elect-
polarization. In other words, $BaTiO_3$ may be pyroelectric in the low temperature form. According to the crystallophysical consideration, the polarization should take place in the direction of the *c*-axis, since the lattice form is now known to be tetragonal. The experimental result shows that large displacments of ions is not likely to take place in the transition. To explain the polarization, therefore, the electronic origin is more plausible than the ionic origin. In the direction of *c*-axis there are arrays of ……O-Ti-O-Ti……and it is most probable that the peculiar nature of these bonds is the determinant factor in the phenomena, though the more extended consideration is difficult in the present stage. More ample experimental evidences are highly desired in order to establish the detailed theory.

In conclusion the authors wish to express their sincere thanks to Mr. T. Ogawa who kindly gave them the sample of $BaTiO_3$. A part of the present study owed the research grant delivered from the Ministry of Education.

References

(1) T.Ogawa: Unpublished yet.
(2) B.M. Vul: Nature, 196 (1945) 480.
(3) V.W.Goldschmid: Cited in Strukturberichte 1 (1931), 333.
(4) B.M.Vul and I.M.Goldman: C.R. U.S.S.R. 46 (1945), 139. (Cited in Chem. Abs. 40 (1946), 4575)
(5) P.R.Coursey, and K.G.Brand: Nature 157 (1946) 297.

This supposition is recently confirmed by the specific heat measurement due to Mr. S. Sawada (unpublished yet) and also by our similar preliminary measurement.

Effect of External Stress on X-ray Intensity Reflected from Rochelle Salt Crystal.

By Shizuo MIYAKE.

Kobayashi Institute of Physical Research, Kokubunji, Tokyo.

(Read July, 1943, Received May 3, 1947.)

§ 1. Introduction.

In the previous two papers(1)(2) the present author reported the change in reflected X-ray intensity from Rochelle salt crystal due to the effect of temperature variation and of electric field. It was shown there that the experimental results are fully explained when Rochelle salt below the Curie point, about 24°C, is assumed to possess a domain structure composed of many small regions which are spontaneously polarized in either of the two alternative c-directions, the polarizations of the neighboring domains being of opposite senses to each other. Since a single domain is considered to be a tetragonal crystal, and the crystal as a whole, on the other hand, is considered to be orthorhombic, the inhomogeneous distribution of strain is produced internally in the crystal as a consequence of the domain structure: It is well known that, in general, the reflected intensity of X-rays is very sensitive to the lattice deformation through the so-called extinction effect,(3)(4) so that the domain structure will possess an important influence upon the X-ray reflection. In the previous papers it was shown that the variation of the relected X-ray intensity from Rochelle salt with temperature change and application of electric field can be thoroughly understood by relating it to the corresponding changes of the domain structure.

If the assumption as made above is valid, then it is expected that the reflected intensity may also suffer a large effect by external stress, since the latter is considered to possess a large influence upon the domain structure. The following experiment deals with this problem.

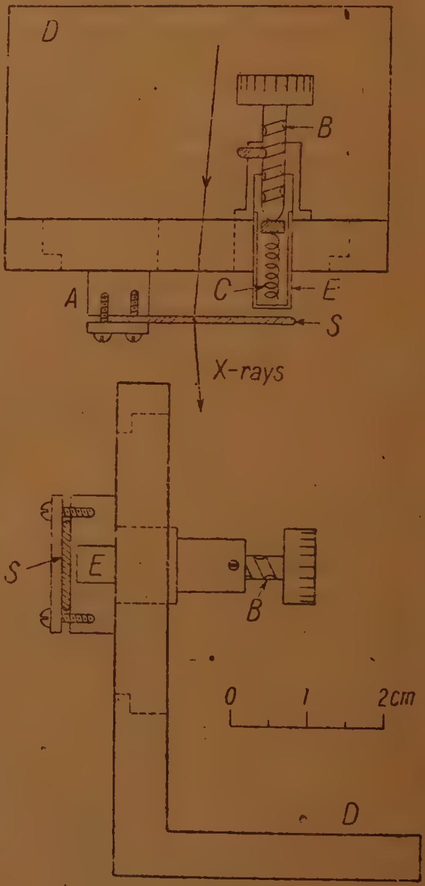

Fig. 1. Sample holder.

§ 2. Experimental Procedure.

The crystal holder used for the present purpose is shown in Fig. 1. The sample of the crystal S, a rectangular thin plate, is clampe at one end of it, and on the other end th force is applied with a metal rod E of diam ter 5 mm, which is pressed by a spring C an an advancing screw B. The force can be adjusted by the rotation of the screw, whos advance being 2 mm per one rotation. On a count of the mechanical fragileness of Rochel salt, however, special precautions must be pai on clamping and applying the stress. To avoi the breaking of the sample, therefore, thi ubber sheets are applied at the contact suraces of the crystal and metal parts at *A* and E. These circumstances necessarily make the nechanical condition of the crystal very obcure. In later paragraphs, the division numer of rotation of the screw is indicated, in rder to give a measure of the magnitude f stress applied on the sample, where the umber 10 (180°-rotation of the screw) being orresponding to the force of about 50 gr. veight. But it is meaningless to speak of the bsolute value of the force, because the mehanical condition of samples is not rigid. he division number of rotation, therefore, hould be understood merely as the value oughly proportinal to the applied stress.

The measurement of the reflected X-ray is erformed by using a double crystal X-ray pectrometer (d.c.s.), as well as by an ordinary ingle crystal spectrometer (s.c.s.). We can now the integrated intensity of reflection by stimating the area of the rocking curve obained by d.c.s., or simply by the value of peak ntensity of the curve obtained by s.c.s. The etail concerning the state of the lattice deforation are inferred from the form of the rockng curve obtained by d.c.s.

The samples of the Rochelle salt crystal are ll rectangular plates with the longer sides of bout 25 mm and the shorter sides of about 0mm and the thickness about 1.0mm. The bservation is performed on the following four amples which are cut from large single crystals f about 400 gr:

No. 1. The face of the plate ⊥ *c*-axis, the longer side ∥ *b*-axis.

No. 2. The face of the plate ⊥ *c*-axis, the longer side ∥ *a*-axis.

No. 3. The face of the plate ⊥ *b*-axis, the longer side ∥ *c*-axis.

No. 4. The face of the plate ⊥ *b*-axis, the longer side ∥ *a*-axis.

he clamping is always made at the shorter de as shown in Fig. 2.

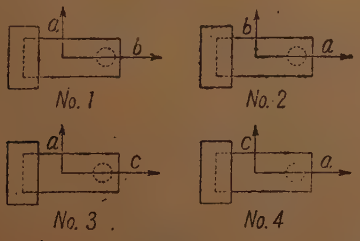

Fig. 2

All measurements are performed on the intensity of reflection of the rays transmitted through the crystal. They are kept at room temperatures which were in general below the Curie point. Mo-Kα-line is used.

§ 3. Experimental Results.

Three examples of the result obtained on the sample No. 1 are shown in Figs. 3, where the ordinates indicate the integrated intensity in arbitrary scale, and the abscissae the division

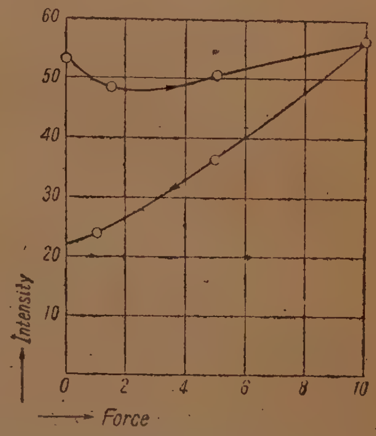

Fig. 3 a. (080)-reflection from the sample No. 1. Measured with d.c.s. 20.2°C.

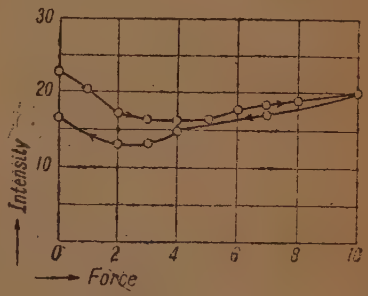

Fig. 3 b. (080)-reflection from the sample No. 1. Measured with s.c.s. 20.2°C.

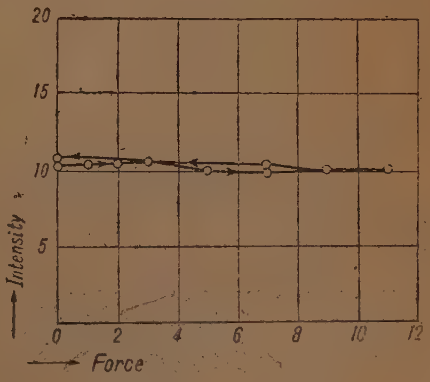

Fig. 3 c. (200)-reflection from the sample No. 1. Measured with s.c.s. 19.0°C.

number of rotation of the screw that is propotional to the exerted force. Similar results for the samples No. 2, No. 3 and No. 4 are shown in Figs. 4, Figs. 5 and Fig. 6 respectively.

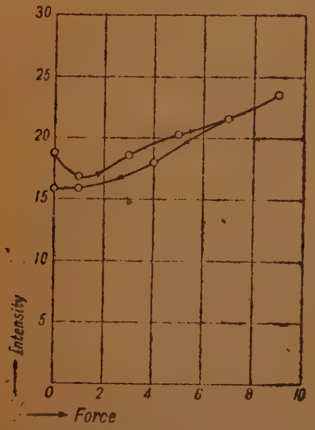

Fig. 4 a. (080)-reflection from the sample No. 2. Measured with a.c.s. 19.5°C.

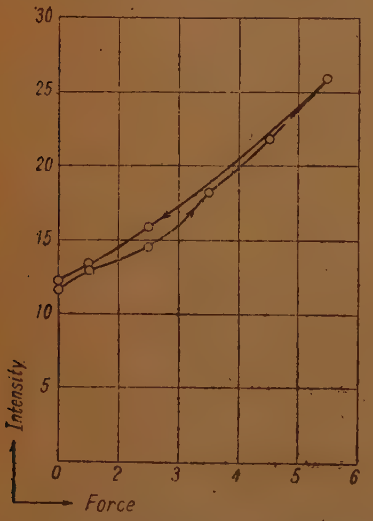

Fig. 4 b. (200)-reflection from the sample No. 2. Measured with s.c.s.. 20.8°C.

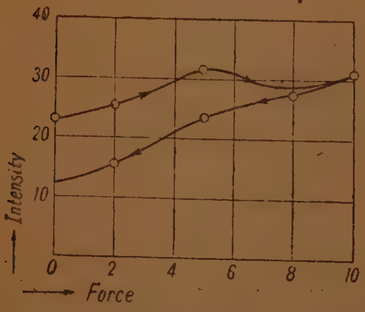

Fig. 5 a. (001)-reflection from the sample No. 3. Measured with d.c.s.. 18.3°C.

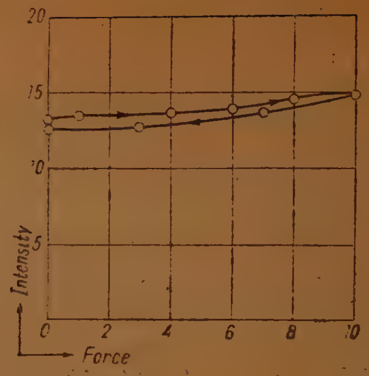

Fig. 5 b. (200)-reflection from the sample No. 3. Measured with s.c.s. 20.8°C.

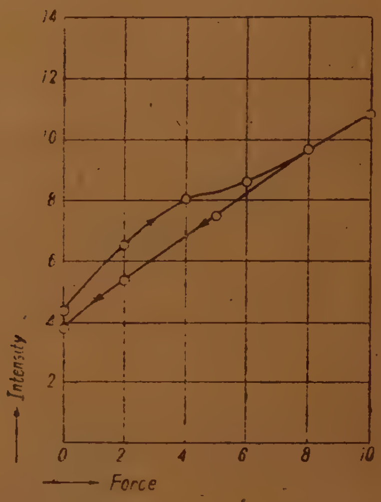

Fig. 6. (200) reflection from the sample No. 4. Measured with d.c.s.. 23.0°C.

DISCUSSION

§ 4. Domain Structure and External Stress.

As mentioned before,(1)(2) the fact that Rochelle salt crystal in a single domai tetragonal, implies that a finite deforma y_{zo} is spontaneously produced with respect the rhombic axes, even when no external f is applied. The sign of y_{zo} is alternati positive or negative for different domains, that an inhomogeneous distribution of st results.

According to the crystallophysical consid tion, the deformation y_z is related to the e tric field E_z and the stress component Y the following manner.(5)

$$y_z = d_{14}E_x + s_{44}Y_z\,.$$

Experimental results show that s_{44} is large r small value of Y_z and y_z shows a satura- n for large stress, when the temperature is the ferro-electric region. This fact means at the domains with spontaneous deforma- ns $-|y_{zo}|$ (or $+|y_{zo}|$) are very easy to trans- rm to the ones of $+|y_{zo}|$ (or $-|y_{zo}|$) by the plication of a small positive (or negative) ess. When the stress is sufficiently large, e whole crystal may therefore become a rge single domain, so that the inhomogeneous ain due to the domain structure will disap- ar in this case.

§ 5. X-ray Intensity and External Force.

t is well known that, in general, the extinc- n effect for the X-ray reflection from crystals exceedingly influenced by the distribution the inhomogeneous strain in the lattice. the case of the present experiment it is nsidered that there are two sources for the tice deformation, the one is that provoked ectly by the force externally applied, and other that being due to the domains. hen the force is exerted on the crystal, then inhomogeneous deformation of the former gin is naturally increased, so that the extinc- n effect is lessend, accordingly the reflected ensity should increase. On the contrary, shown in the above section, the lattice de- rmation due to the latter origin would in s case tend to disappear, and X-ray intensity y decrease. The intensity variation actually served will be the result of the combination these two effects.

The curve I in Fig. 7 indicates schematically intensity variation with the external stress ected when the lattice plane is nearly per- t, not being distorted by the existence of the domain structure. If the lattice plane is the one distorted by the domain structure, then the X-ray intensity may take a larger value already at the beginning (the point B), and the intensity variation with the applied stress may follow the curve II, whereby it is assumed that the domain structure is kept unchanged in the process so that the strain produced by the external stress is simply superposed on the strain due to the domains. Actually, the intensity variation may be represented by intermediate curves (the curves III in Fig. 7), since the domain structure is supposed to disappear gradually by the external stress.

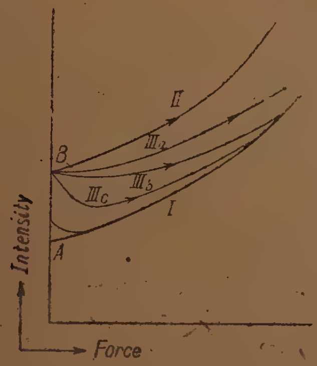

Fig. 7.

§ 6. Intensity Variation.

In the present experiment, the stress externally produced in the crystal will be of the following manner:

For the sample No. 1, only Y_z may be predominant as compared with other components, and similarly for No. 2, Z_x, for No. 3, Y_z and for No. 4 X_y are the prevailing stresses.

As fully dicussed in the previous papers, the distortion of the net plane by the domains is supposed to be most pronounced for (0K0) and (00*l*), whereas (*h*00)-plane is supposed to be approximately independent of this structure. In fact, (200)-reflection is showing the normal behavior such as expected from the curve I in Fig. 7 against the applied stress, as seen in Fig. 3*c* and 4*b* etc. The difference between Fig. 3*c* and Fig. 4*b* is understood as being due to the manner of the produced stress as above mentioned. These curves are all reversible for increasing and decreasing stress.

On the other hand the curves obtained on (080) and (001)-reflections have very peculiar characters. (Fig's. 3*a*, 3*b*, 4*a*, 5*a*). First, in the curve for increasing stress, there appears a minimum, except Fig. 5*a*. Such a behavior is explained by considering that the intensity of these reflections follows some of the intermediate curves III in Fig. 7. If stress is sufficiently large, the intensity may finally come to move completely along the curve I.

Second, the intensity curve is irreversible against the decreasing stress, so that always a hysteresis loop is resulted in. This is explained as being due to a relaxation of the reestablishment of the domain structure after removing the applied stress. On account of this relaxation the intensity for decreasing stress should nearly follow the curve I in Fig. 7, and in general the intensity at zero stress (the point A) will take a much smaller value than the initial intensity (the point B). This is exactly corresponding to the experimental results as seen in the figures.

§ 7. Form of Rocking Curve.

Just like intensity, the line-form of the reflected X-rays depends on two kinds of the lattice distortion, the one due to the domains and the other due to the strain produced directly by the external stress. In the present experiment it is observed that the width of the line is always broadend by the external stress, although the case in which the width becomes narroweris not impossible. If the applied stress is removed from the sample, however, the strain produced by the external force will then disappear, but since the reestablishment of the domain structure seems not to begin at once, s that the crystal may be regarded as of fairl perfect lattice in this short period. This ca be actually confirmed as shown in Fig. 8, i which the rocking curves of (080)-reflectio obtained for the crystal sample No. 1 befor applying and shortly after removing the stres are compared. It is seen that the line become considerably steeper for the latter case as expected.

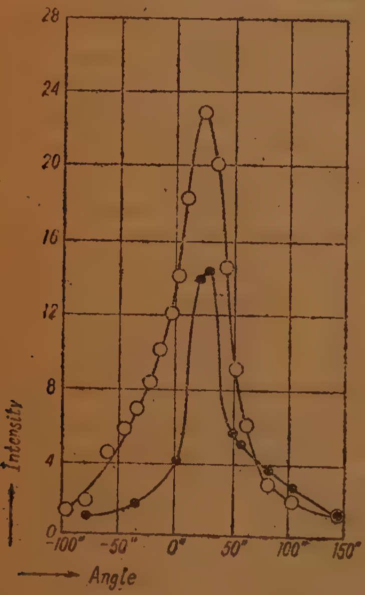

Fig. 8. Rocking curve of (080)-reflection from the sample No. 1. Measured with d.c.s. 20.2°C. —○—: Before applying stress. —●—: After removing stress.

The reestablishment of the domains seem to take place in about one hour after the removal of the stress, which can be known b the recovery of intensity and line width t the initial values.

§ 8. Conclusion.

From the above description we are convinced that the assumption of domains in the Rochelle salt crystal is valid. Three experiments, the previous two and the present one, can be fully explained through this assumption without any contradiction. The above results, however, do not tell us the more detailed knowledge of domains, such as their size as well as their shape. This may be the question which is to be researched in future.

I wish to express my sincerest thanks to Professor S. Nishikawa for his good advices. A part of this work is indebted to the research grant from the Ministry of Education.

References

(1) S. Miyake: Proc. Phys.-Math. Soc. Japan, 23 (1941), 377.
(2) S. Miyake: Proc. Phys.-Math. Soc. Japan, 23 (1941), 810.
(3) Y. Sakisaka and I. Sumoto: Proc. Phys.-Math. Soc. Japan, 13 (1931), 211.
(4) E. Fukushima: Bull. of I.P.C.R. (Tokyo) (in Japanese), 14 (1935), 1105, 1199; 15 (1936), 1.
(5) H. Mueller, Phys. Rev. 57 (1940), 829; 58 (1940), 565, 805.

The Optical Theory of the Spectral Sensitivity of Caesium-Oxide Photocathode

By Yoshihiro SAYAMA.

Electronic Engineering Research Lab., Tokyo Shibaura Electric Co., Ltd.

(Received May 11, 1947.)

Abstract

Silver which is dispersed as small particles in the intermediate layer of Cs_2O photocathode, has the characteristic optical constants of a thin film, and hence has an absorption band in visible range. On the other hand, the spectral sensitivity of the cathode shows a remarkable maximum in visible range. We assume that the selective maximum is due to the volume photoelectric effect corresponding to the foregoing absorption band of silver thin film. We have calculated the light absorption in the surface layer of a silver thin film lying on a glass plate and obtained the spectral sensitivity which is in qualitative agreement with the experimental one.

1. Introduction.

t is well known that the spectral sensitivity Cs_2O photocathode has a remarkable maxi- m between 6000 and 8000 Å, and its thresh- l lies at about 12000 Å. Such a selective ximum of the spectral sensitivity is also served for all metal surfaces covered with ali metal films. Ives⁽¹⁾ interpreted success- lly this selective effect of thin films of alkali etal, calculating the electric vector of light the surface, and assuming that the number photoelectrons was proportional to the ab- ption of light in the surface layer of the thode.

n this article the author will attempt to w that the selective effect of Cs_2O photo- hode can also be interpreted by such an tical factor.

2. Structure of Cs_2O Photocathode.

ves⁽²⁾ investigated the spectral sensitivity of O photocathode by the above method of soning and concluded that the selective ect in the mentioned photocathode could t be interpreted by the optical factor. He ployed a simplified model for the structure Cs_2O photocathode, that is, a platinum base metal covered with an intermediate layer of quartz, whose surface is covered with a thin photosensitive film of caesium. Such a model, however, is far from the real situation in the Cs_2O photocathode. Therefore, we will start with the discussion of the structure of Cs_2O photocathode.

Cs_2O photocathode is usually prepared by the following method. A silver oxide film of about fifty molecular layers is prepared on the surface of a thick silver film by the discharge in oxygen gas. The caesium vapour is introduced onto the surface of the oxide layer. Then the silver oxide is reduced and the fine silver particles are dispersed in the layer of the caesium oxide. This cathode can be further sensitised by the deposition of a small quantity of silver upon it.⁽³⁾ The spectral sensitivity of the cathode thus prepared is shown in Fig. 1.⁽⁴⁾ (curve 1). In this type of cathode, the boundary plane between the base of silver metal and the Cs_2O layer is not smooth enough due to the oxidation and the reduction, so it is not adequate to proceed our calculation for such photocathode.

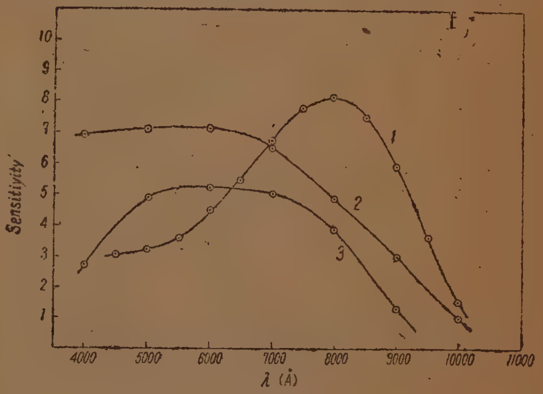

Fig. 1. Spectral Sensitivity of Cs_2O Photocathodes of Varions Types.
Curve 1. [Ag]-Cs_2O, Ag, Cs-Ag
Curve 2. [Glass]-Ag, Cs_2O, Cs-Ag
Curve 3. [Quartz]-Cs_2O, Cs-Ag

Another type of Cs$_2$O photocathode is a semitransparent one, which is prepared by the following method. The silver film of a few mμ thickness is deposited on the surface of a glass plate, and then it is thoroughly oxidised. The subsequent procedure is the same as for the first type of cathode. In this case Cs$_2$O layer is produced directly on the glass surface and the layer contains the silver particles. The spectral sensitivity of this type is shown in Fig. 1.(5) (curve 2). We shall try to calculate the optical factor for the latter type of photocathode, as the structure of this type is simpler than the former. However, there is no essential difference in the mechanism of the electron emission between these two types of cathodes.

According to Asao(6) Cs$_2$O layer which contains no silver particles shows no significant absorption in the visible spectral range. On the other hand, the silver film evaporated on the layer for the purpose of the sensitization shows a transmission and reflexion characteristic to the thin film of silver and not to the thick one. The spectral sensitivity of the mentioned cathode is represented by curve 3. (Fig. 1). According to Miyazawa's exhaustive study(7) of the semitransparent Cs$_2$O cathode, the reduced silver particles in the Cs$_2$O layer are found to play photoelectrically or optically a similar role to the silver film deposited for sensitization. Thus we are inclined to take up the following simplified model for this photocathode: On the glass surface lies a silver thin film of about 100 Å thickness which has not the optical constants of bulk state but for thin film-state, and whose photoelectric threshold wavelength lies at about 12000 Å due to the very thin covering film of Cs$_2$O. The optical behavior of Cs$_2$O: (Fig. 2) is entirely neglected.

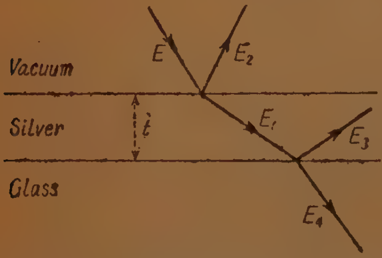

Fig. 2. Simplified Model of Semitransparent Cs$_2$O Photocathode.

3. Calculation of the Spectral Sensitivity

When the incident light whose electric vect E lies perpendicular to the incident plane i pinges upon the silver film (fig. 2), the co plex amplitude of the reflected beam E_2 given by the formula.(8)

$$\frac{E_2}{E}=\frac{(k-k_1)(k_1+k_4)X^2+(k+k_1)(k_1-k_4)}{(k+k_1)(k_1+k_4)X^2+(k-k_1)(k_1-k_4)}, \tag{1}$$

where k's and X are

$$k=(N+iK)c$$

and $X=\exp\left\{\frac{-2\pi i}{\lambda_0}(N+iK)t\right\}$ respectivel

$(N+iK)$ is the optical constant of each me um, c is the direction cosine of the directi of each beam with respect to z-axis which taken perpendicular to the boundary pla toward the vacuum side, t is the thickness the silver film, λ_0 the wave length in vacu and the suffixes specify the quantities c cerning the medium in which these beams passing as shown in Fig. 2. The amplitu of the electric vector in the surface layer the silver film is given by an algebraic s $(E+E_2)$ of the amplitudes of the incident a the reflected beams. Therefore from equati (1), we have

$$\frac{E+E_2}{E}=2\frac{k(k_1+k_4)X^2+k(k_1-k_4)}{(k+k_1)(k_1+k_4)X^2+(k-k_1)(k_1-k_4} \tag{2}$$

Now we shall consider only the case normal incidence, and if we express the optic constant of silver film by $N+iK$ and put for that of glass, we obtain

$$c=c_1=c_4=-1,$$

$$k=-1,\ k_1=-(N+iK)\ \text{and}\ k_4=-1.5.$$

Then the equation (2) becomes

$$\frac{E+E_2}{E}=2\frac{e^a(N+1.5+iK)(\cos b}{e^a(N+1+iK)(N+1.5+iK)}$$

$$\frac{-i\sin b)+N-1.5+iK}{(\cos b-i\sin b)+(1-N-iK)(N-1.5+iK)} \tag{3}$$

where

$$a=\frac{4\pi t}{\lambda_0}K,\quad b=\frac{4\pi t}{\lambda_0}N.$$

If we assume that the volume photoelect effect is predominant in the spectral ran under consideration, the intensity of the pho electrons is proportional to the light energy absorbed per uuit time by the unit area of the surface layer (thickness t') of silver film and is given by

$$f(\nu)\frac{c_0}{\lambda_0}NK|E+E_2|^2t' \qquad (4)$$

where the proportional constant $f(\nu)$ is a function of the frequency of incident radiation and means a probability of emission of an electron which has absorbed a quantum $h\nu$, c_0 is the light velocity in vacuum and t' the mean depth where photoelectrons are produced. Since the incident energy per unit time and unit area is given by

$$\frac{c_0}{4\pi}|E|^2,$$

the spectral sensitivity is given by

$$\frac{\frac{c_0}{\lambda_0}NK|E+E_2|^2t'f(\nu)}{\frac{c_0}{4\pi}|E|^2h\nu} \qquad (5)$$

At present we have no information on the explicit form of the function $f(\nu)$. When we assume that the probability of absorption of light is independent of the initial value of the electronic wave number, then it follows that

$$f(\nu)\propto(\nu-\nu_c)^2,$$

where ν_c is the threshold frequency. Finally the spectral sensitivity S is given by

$$S=NK(\nu-\nu_c)^2\left|\frac{E+E_2}{E}\right|^2, \qquad (6)$$

where we have omitted the various factors ndependent of frequency of radiation. The ast factor of (6) is given by the equation (3).

4. Comparison with Experiment.

It is well known that silver has abnormal ptical constants in the state of a thin film, amely, the strikingly large index of refrac-ion. We put Goos-Murmann's values(9) of N nd K into (3) and (6). The results are shown n fig. 3 and 4 respectively, in which the thres-old frequency was put to be

$$\nu_c=2{,}43\times10^{14}\,\text{sec}-1(\lambda_c=12340\,\text{A}).$$

n these figures, d means the thickness in Goos' easurement of the optical constants and t he value substituted into (3) and (6). Both alues do not always coincide with each other ince the grain size of silver particles in the hotocathode may change owing to the pro-esses of oxidation, reduction and heat treatment. For N and K of bulk silver we use Minor's.(10) Fig. 3 shows that if the characteristic optical constants of thin film (d≲120 Å) are used, there appears the selective maximum of spectral sensitivity between about 5000 Å and 6000 Å, being rather shorter as compared with the experimental value (Fig. 1). Taking into consideration the bold simplification adopted here the calculated spectral sensitivity may be taken to be in qualitative agreement with the experimental one. Since the values of $|E+E_2|^2/|E|^2$ show no preferable enhanacement in the selective maximum for thin film (Fig. 2), the selective maximum of the calculated spectral sensitivity is mainly due to the factor NK in (3), namely, the amount of incident light. The spectral sensitivity corresponding to the optical constants of thicker film (Fig. 3 curve 4.5) shows no pronounced maximum in conformity with experimental observation.

5. Discussion.

The optical and photoelectrical properties of the semitransparent Cs_2O photocathode are primarily determined by the silver thin film consisting of the reduced silver particles and the sensitising silver particles, whose surfaces are covered with thin Cs_2O layer and consequently have low work function of nearly 1 electron volt. The photoelectrons originate from these silver particles and the process may be considered to be the volume photoelectric effect.

In texts(11) the light-absorption by metal in visible spectral range has been treated usually as the classical forced oscillation of free electrons. This, however, is insufficient for the theoretical treatment of the volume photoelectric effect in the mentioned spectral range. Muto(12) carried out the quantum mechanical calculation of this process, which was not yet compared with any experiment.

The serious weakness of Ives' and also the author's investigations seems to lie in the classical method of the treatment of the phenomena. It is highly desirable that the quantum-mechnical treatments of this process are developped in future.

6. Appendix.

Accoading to Hirai(13), the higher sensitivity of the semitransparent Cs_2O photocathode is obtained when the incident light is thrown

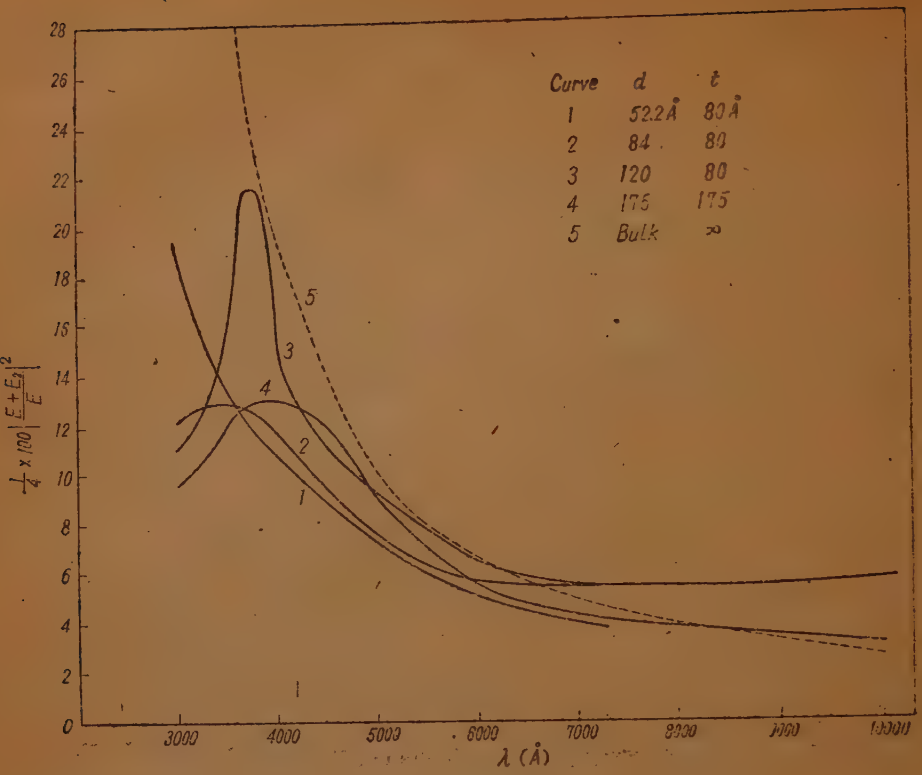

Fig. 3. Light Energy in the Surface Layer of Silver Film.

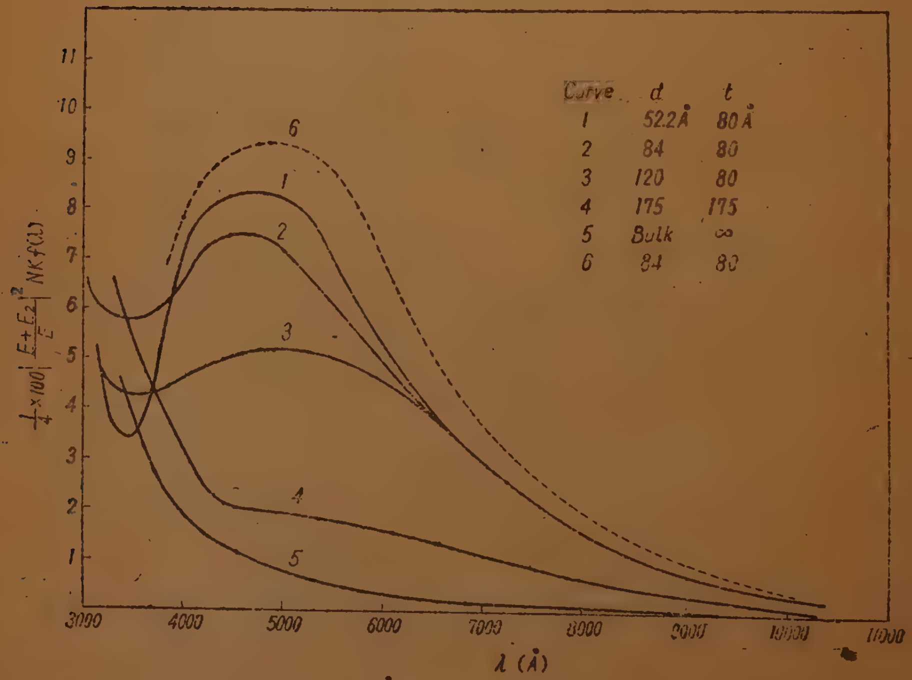

Fig. 4. Spectral Sensitivy (Calculated)

rom the base side, (upwards incident in Fig.) in comparison with that under the light- llumination from the vacuum side (down- vards incident in Fig. 2). His results are hown in Fig. 5. This phenomenon is also

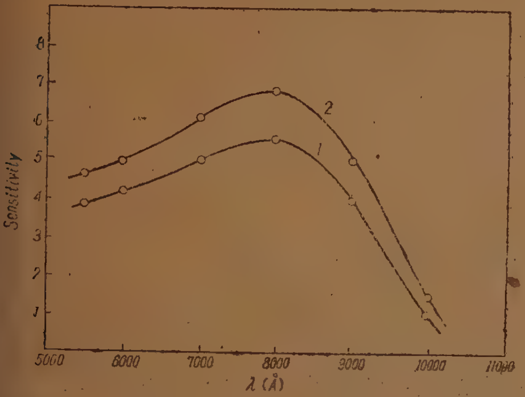

Fig. 5. Spectral Sensitivity of Semitransparent Cs_2O Photocathode (Observed)
Curve 1 "Vacuum Side Incidence"
Curve 2 "Glass Side Incidence"

bserved for the other thin film$^{(14)}$ and can be asily deduced from the optical factor as ollows.

Now the case of "base-side-incidence" is hown schematically in Fig. 6. If we consider

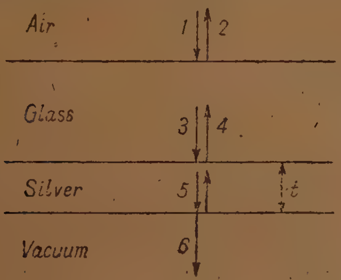

Fig. 6. Schematic Diagram of the Case of "Glass Side Incidence"

he case of normal incidence, the amplitude f E-vector in the surface layer of silver is qual to the amplitude of the beam 6 and is iven by$^{(15)}$

$$\frac{E_6}{E_3}=\frac{4k_3k_5X}{(k_3+k_5)(k_5+k_6)X^2+(k_3-k_5)(k_5-k_3)}, \tag{7}$$

where E_3 is the amplitude of beam 3 (incident beam in glass), X and k's have the same meanings as in (1) and we shall neglect the back side reflexion of beam 4 on the glass-air boundary plane. The amplitude E_3 is given by

$$E_3=\frac{2}{N_0+1}E_1 \tag{8}$$

where N_0 is the index of refraction of glass and E_1 the amplitude of the iucident beam. Substituting into eq. (6) E_6/E_1 obtained from (7) and (8) in place of $(E+E_2)/E$, we obtain the spectral sensitivity for the case of "glass side incidence". The calculated curve for $d=$ 84 A, $t=80$ A is described in Fig. 4 (curve 6) in order to show the difference compared with the sensitivity of the case of "vacuum side incidence" (curve 2.)

References

(1) H. E. Ives: Phys. Rev. **38** (1931), 1209.
H. E. Ives: H. B. Briggs, Phys. Rev. **38** (1931), 1477. **40** 802 (1932), J. O. S. A. **26** (1936), 247. **28** (1938), 330.
(2) H. E. Ives: A. R. Olpin, J. O. S. A. **24** (1934), 198.
(3) S. Asso: Proc. Phys. Math. Soc. Jap. **22** (1940), 448.
(4) Y. Sayama: Toshiba Kenkyu Jiho **19** p. 26 (in Japanese)
(5) H. Miyazawa:
(6) S. Asso: l. c.
(7) H. Miyazawa: l. c.
(8) T. C. Fry: J. O. S. A. **22** (1932), 307.
(9) F. Goos: Z. S. Phys. **100** (1936), 95.
H. Murmann: Z. S. Phys. **101** (1936), 643.
(10) Minor: Ann. Phys. **10** (1903), 581.
(11) for examrle. H. Fröhlich: Elektronen Theorie der Metalle
(12) T. Muto: Sci. Pap. Inst. Phys. Chem. Reser. **27** (1935), 179.
(13) S. Hirai: Mazda Kenkyu Jiho **16** p. 397 (in Japan)
(14) P. Gorlich: Z. S. Phys. **101** (1936), 335.
A. L. Hughes, L. A. Du Bridge: Photoelectric Phenomena (1932) p. 122
(15) T. C. Fry: l. c.

Crystallite Theory of Liquid.

I. On the Specific Heat.

By Akiya OOKAWA.

Kobayashi Institute of Physical Research, Kokubunji, Tokyo.

(Read and received May 11, 1947)

1. Introduction

A general survey on the physical properties of gas, liquid and solid suggests that liquid has an intermediate state between gas and solid. The X-ray diffraction pattern of liquid, for example, indicates that it has an internal structure clearer than in gas but not so regular as in solid. The specific heat also suggests that the thermal agitation of the constituent elements of liquid is nearly vibrational at low temperature, but almost non-vibrational at high temperature.

The liquid state, being describable monistically with the gas state by the use of the van der Waals' equation of state, has been considered to be akin to the gas state rather than to the solid state. The statistical mechanics applied by Mayer and others[1] to the condensed system is an excellent approach on this line, which gives explanations for many characteristic properties of liquid at elevated temperture. In this theory, the existence of many aggregates consisting of a few constituent elements, the so called *clusters*, is assumed, and the straightforward calculation becomes extraordinarily difficult when the system contains aggregates that consist of more than several elements.

The fact that solid deforms rigidly and liquid flows visocously on the application of a shearing force is accepted as the criterion between the two, and it may be not without reason to compare the melting point of solids with the temperature at which the modulus of rigidity vanishes.[2] But it is to be emphasized that the rigidity and the fluidity are not exclusive properties to each other. Whether the rigidity or the fluidity predominates in a material under given experimental condition is only determined by the experimental period relative to the so-called relaxation time characteristic of the
material, that was shown first phenomen
cally by Maxwell.[3]. With the acceler
accumulation of available informations
on the internal structure of material anc
the rate process of reaction in the last de
the investigation of the problem from
molecular standpoint is now possible.
plastic deformation of the metallic solid,
example, is now being treated with the
ception of the *dislocation*[4]. On the similar
Bragg[5] recently suggested that the boun
layer between two crystallites with diffe
orientations behaves like a dislocation, and
the total system takes the dynamical *f*
structure.

Among the theoretical treatments of li
based on the assumption of its solid-like inte
structure, we can cite the following two ;
the hole theory[6] that assumes some transl
nal vacant sites in the otherwise perfect cry
and second, the order-disorder theory[7]
goes in close analogy to the succes
consideration of the phase transition of al
Both these theories presume the long r
order of the lattice site that can be occu
by the element, while the analysis of the X
diffraction pattern of liquid reveals only
short range order of sites occupied by
elements.

The specific heat is one of the macrosc
properties that reflect fairly truly the m
of thermal motion of the constituent elem
in different states of aggregation, and it
for long provided important knowledges
investigation of gas and solid. The spe
heat of liquid, at low temperatures, has a
aproximate to that of solid, that is $3R$ for
tems consisting of monoatomic molecules,
decreases gradually with the rising of te
ature. In connection with the Rayleigh
tering, Brillouin[8] gave a remark concer

is problem that, of the two modes of thermal astic waves in the solid state, the longitudinal ne will subsist also in the liquid state, but the ansverse one will degenerate into whirl sysm, the degree of degeneracy being increased rogressively with the elevation of the temperure. According to this argument, the specific eat of the *ideal liquid* should decrease from R to $2R$ with increasing temperature. He sugested9) that the deviations of the calculated alue of the specific heat from the observed ne can be related partly to the non-sinusoidal ature of the longitudinal waves, and partly o the possible existence of ultra-microscopic olid clusters. Bernal10) attempted to explain he excess of the specific heat over $3R$ at low emperatures as being due to the cofigurational pecific heat, which is caused by the change of he average configurational energy of liquid.

2. A Molecular Model of Liquid at Low Temperature.

Based on these introductory considerations, a new molecular model of liquid at low temperature is proposed, assuming a solid-like nternal structure. Among the conceivable three types of the lattice defect in the perfect crystal, the point-like, the line-like, and the plane-like ones, the last one may be chosen as the most essential, in the light of the uncertain existence of the long range order in the liquid state. Thus, the proposed structure is akin to the foam structure proposed by Bragg5) in the case of work-hardened metallic solid. The statical feature of the model can be described as follows; a mosaic composed of many fragments which are in contact with each other on well-defined interfaces, each having a perfect crystalline pattern throughout its own domain.

The thermally agitated element at the transition layer changes its allegiance from the orientation prevailing on one side to that prevailing on the other side. When the crystallites are sufficiently large, the change of allegiance of each element surrounding any one crystallite will take place independently of each other, which is consequently accompanied by the elastic waves in the crystallite. On the contrary, when the crystallites are sufficiently small, the changing allegiance of the elements will be somewhat cooperative with each other, which may result in some translational motion of the crystallite. In other words the non-vibrational mode of the crystallite shall be accompanied by the changing allegiance of the elements at the interface, namely the displacement of the interfaces themselves.

The system of a given configuration, as above introduced, may obviously possess an execss energy over that of a perfect crystalline system, on account of the elements at the crystallite interfaces necessarily having some misfit between the neighbouring elements. This excess configurational energy may be roughly proportional to the total area of the momentary interfaces. The interfaces behave, in this respect, like films with surface tensions, and the crystllites are likened to bubbles in a foam seperated by the films from each other.

Suppose some displacement process of the interfaces, by which an existing crystallite is annihilated and another new crystallite is recreated successively. The minimum activation energy of the excited state for such a process being assumed to be sympathetic with the size of the crystallite, the process will be rare for a system of large crystallites (e.g. for work-hardened metallic solid), but may be frequent for a sytem with sufficiently small crystallites, and in the latter case the thermal displacement of the boundary layers will be nearly free. It is now assumed that the state of liquid is corresponding to such a fine configuration.

In short, the above proposed molecular model of liquid at low temperature is of the follwing features:

a) A structure of a mosaic of fine fragments meeting on well-defined interfaces, each having a perfect crystalline pattern throughout its own domain;
b) Existence of an excess configurational energy, due to the misfit of the elements at the interfaces;
c) Dynamic rather than static equilibrium, accompanied by some degenerate translational degrees of freedom for each crystallite.

3. Approximate Treatment of the Proposed Model.

Take a system consisting of N elements. Assuming n spherical crystallites each consisting of α^3 elements in the closest packed state with the relation

$$n\alpha^3=N, \qquad (1)$$

the excess configurational energy of the configuration over that of a perfect crystalline system is $n\alpha^2\varepsilon$, ε being the misfit energy per one element at the boundary layer.

In fact the crystallites of a momentary configuration are not always of the same size, so that the above formulation may not be true. If each crystallite, however, is sufficiently small, the real configuration may be well approximated by the avearge configuration as considered here.

Each crystallite has some translational degrees of freedom, which may be assumed to be truly translational in a smoothed potential as given by $n\alpha^2\varepsilon$. The partial translational partition function f_t^3 per one crystallite will be represented by

$$f_t^3 = \frac{(2\pi mkT)^{3/2}}{h^3}\,\beta(\alpha a)^3\,, \qquad (2)$$

where T, k, and h are the absolute temperature, the Boltzmann's constant and the Planck's constant respectively. m is in strict the effective mass of the momentary crystallite, but may be approximated by the mean value $\alpha^3 m_o$, m_o denoting the mass of one elemant. $\beta(\alpha a)^3$ is the accessible volume of the center of the gravity of a crystallite, which is determined by the mean life time of the crystallite in successive recreation and annihilation, and which is assumed proportional to the volume of the crystallite itself.

The remaining $3N-3n$ degrees of freedom of the system are to be taken to have vibrational character as in the normal sollid. If they are all of sinusoidal nature, and if the temperature is sufficiently high relaive to their characteristic temperature, the partial partition function f_v per one vibrational degree of freedom will be approximated by $kT/h\nu$, ν being the characteristic frequency.

Then the total partition function of the sytem is given by

$$\Xi = \sum_{\alpha} \exp\left(-\frac{n\alpha^2\varepsilon}{kT}\right)$$

$$\left[\frac{(2\pi\alpha^3 m_c kT)^{3/2}}{h^3}\,\beta(\alpha a)^3\right]^n \left[\frac{kT}{h\nu}\right]^{3N-3n}, \qquad (3)$$

where the summation is to be taken over all different configurations of different sizes of the crystallites. The energy term due to the volume difference of the configurations is negligible at low external pressure as is usually the case.

The number of crystallites n is related to its mean size α by the equation (1), so th the replacement of n by α gives

$$\Xi = \left[\frac{kT}{h\nu}\right]^{3N} \sum_{\alpha} \left[\xi(\alpha)\right]^N, \qquad (4$$

with the following abbreviations:

$$(\alpha) = \alpha^{-\frac{15}{2}\alpha^{-3}}\, e^{-\frac{1}{\alpha}\frac{\varepsilon}{Tk}} \left(\frac{\theta'}{T}\right)^{\frac{3}{2}\alpha^{-3}} \qquad (5$$

$$\theta' \doteq \beta^{\frac{2}{3}} \left(\frac{h\nu}{k}\right)^2 \frac{2\pi m_o k a^2}{h^2}\,. \qquad (6$$

Differentiation of $\log\xi$ by α at a consta temperature gives

$$\frac{\partial \log\xi}{\partial\alpha} = \alpha^{-4}\left(\alpha^2\frac{\varepsilon}{kT} - \frac{45}{2}\log\alpha\right.$$

$$\left. + \frac{15}{2} - \frac{9}{2}\log\frac{\theta'}{T}\right)$$

and

$$\frac{\partial^2 \log\xi}{\partial\alpha^2} = -4\alpha^{-1}\frac{\partial \log\xi}{\partial\alpha}$$

$$+ 2\alpha^{-5}\left(\alpha^2\frac{\varepsilon}{kT} - \frac{45}{4}\right).$$

$\log\xi$ has therefore a maximum in a configu tion such that the mean crystallite size is giv by

$$\frac{45}{4}\log\alpha_*^2 = \frac{15}{2} + \frac{9}{2}\log\frac{T}{\theta'} + \frac{\varepsilon}{kT}\alpha_*^2\,, \qquad (7$$

where

$$(\varepsilon/kT)\alpha_*^2 < 45/4. \qquad (8$$

Aproximating the partition function Ξ large N by the maximum term $\log\xi(\alpha$ corresponding to the most probable configu tion, it follows that

$$\Xi \doteq \left(\frac{kT}{h\nu}\right)^{3N} \left(\frac{5}{2}\alpha_*^{-3} + \frac{2}{3}\frac{\varepsilon}{kT}\alpha_*^{-1}\right)^N. \qquad ($$

The free energy of the system, F, or free energy per one element, f, are given $f = F/N = -kT\log\Xi/N$

$$\doteq -3kT\log\frac{kT}{h\nu} + kT\alpha^{-3}\left(\frac{2}{3}\frac{\varepsilon}{kT}\alpha^2 - \frac{5}{2}\right). \qquad (10$$

For the sake of brevity, α_* will be repla α in the following.

The most probable configuration at e temperature is determined by equation (Differentiating (7) by T,

$$\frac{d\alpha}{dT} = \frac{\alpha}{2T}\left(\frac{\varepsilon}{kT}\alpha^2 - \frac{9}{2}\right) \Big/ \left(\frac{\varepsilon}{kT}\alpha^2 - \frac{45}{4}\right).$$

Now the internal energy e and the specific eat c are deduced by the thermodynamical lations, $e=-T^2\partial(f/T)/\partial T$ and $c=\partial e/\partial T$. aking accout of the temperature dependence α, it follows

$$e=3kT-\frac{3}{2}kT\alpha^{-3}+\varepsilon\alpha^{-1} \tag{12}$$

d

$$c=3k-\frac{3}{2}k\alpha^{-3}$$
$$+\frac{1}{2}k\alpha^{-3}\left(\frac{\alpha^2\varepsilon}{kT}-\frac{9}{2}\right)^2\Big/\left(\frac{45}{4}-\frac{\alpha^2\varepsilon}{kT}\right). \tag{13}$$

is to be noted that c has the form

$$c=c_0+c_-+c_+$$

ne partial specific heats c_0, c_-, and c_+ may conveniently called the perfect ystalline, the kinematic deficit, and e configurational one, respectively.

4. Discussion.

In order to discuss the results of the oposed model of liquid quantitaely with reference to the experiental data, much more detailed ecifications of the model concerning accessible volume and the misfit ergy, as well as the more rigorous eatment of the model are necessary. t the following rather qualitative scussion may be not without interest. The equation (7) has two values α at moderate temperature, one rresponding to a stable configuran α_1 ($\alpha_1^2\varepsilon/kT<45/4$ and maximum ξ) and the other corresponding to a labile configuration α_2 ($\alpha_2^2\varepsilon/kT>45/4$ and mininum ξ). If the system is to transform itself from the stable configuration α_1 to the perfect crystalline state by a uniform increment of α, it must necessarily pass through the labile state α_2, which may be regarded to give one cause of possible supercooling in freezing phenomena.

On lowering the temperature, the stable value α_1 increases and the labile value α_2 decreases. Finally the two values coinside at a definite temperature T_c ($\alpha^2\varepsilon/kT_c=45/4$), below which the equation (7) has no solution and ξ is monotonously increasing with α. As T tends to T_c, the configurational specific heat tends to infinity, as is to be seen from the equation (13).

Table I

Temperature Dependence of the Crystallite Size and the Specific Heat

K	α^3	kinematic deficit sp. heat (in k)	configurational sp. heat (in k)	resultant sp. heat (in k)
	16.85	−0.0890	+0.7000	+3.6110
	13.75	.1091	.1414	3.0327
	12.34	.1215	.0470	2.9255
	11.70	.1282	.0185	2.8903
	11.33	.1324	.0021	2.8697
	11.30	.1327	.0000	2.8673
	11.36	.1321	.0019	2.8698
	11.53	.1301	.0049	2.8748
	11.73	.1278	.0082	2.8804
	11.97	.1253	.0088	2.8835

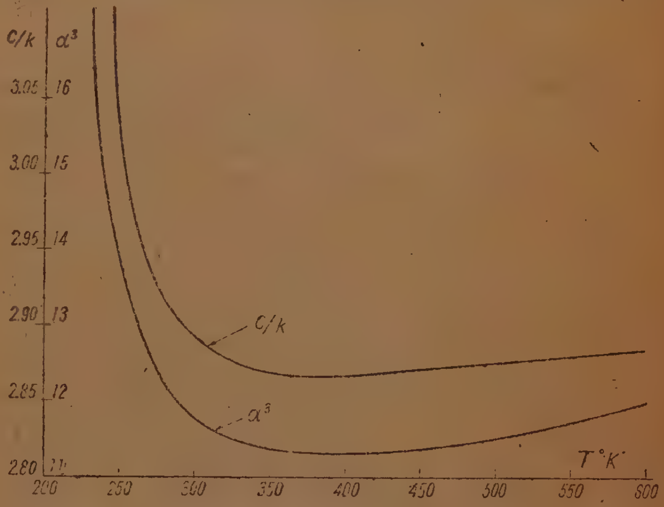

Fig. 1. Temperature Dependence of the Crystallite Size and the Specific Heat.

The crystallite size of the stable configuration decreases with increasing temperature in the range $45/4>\alpha^2\varepsilon/kT>9/2$. But the configuration is stationary in the neighbourhood of $T'=2\alpha^2\varepsilon/9k$, at which the system has the smallest crystallite configuration. It is easy to see that the specific heat shows flat minimum at this temperature, and its deviation from $3k$ being entirely due to the kinematic deficit specific heat.

For the mere interest of illustration, a numerical result is shown in Fig. 1 (in reference to Table I). It was assumed $\varepsilon/k=350°$, $\theta'=100°$, which is equivalent to $h\nu/k\sim100°$, $m_c=200\times1.660\times10^{-24}$, $a\sim10^{-8}$ and $\beta\sim10^{-3}$.

In order to make a more quantitative discussion with respect to the specific heat, it is indispensable, as was stated above, to specify the model in more detail and rigour. At the same time, however, it will be equally worth while to apply this model to the explanation of the transformation phenomena between liquid and solid and the viscous behaviour of liquid, the result of which will be reported successively.

5. Summary.

Following the introductory conisderations, a solid-like molecular model of the liquid state was proposed. A mosaic system composed of fine fragments was assumed, which are in contact with each other on well-defined interfaces characterized by the existence of an excess misfit energy and some translational degrees of freedom for each crystallite. An approximate treatment of the model shows that the crystallite size of the stable configuration decreases with temperature at moderate temperature, and that the specific heat consists of three parts, the perfect crystalline, the kinematic deficit, and the configuratioal ones.

In conclusion the author wishes to expre his sincere thanks to Dr. S. Oka and Dr. Miyake for their continuous encourageme and useful discussion throughout this study

References.

1) J. E. Mayer: J. Chem. Phys. **5** (1937) 67;
——, P. G. Ackermann: ibid. **5** (1937) 74;
——, F. H. Harrison: ibid. **6** (1938) 87, 101.
2) M. Bron: J. Chem. Phys. **7** (1939) 591.
3) J. C. Maxwell: Phil. Mag. **35** (1868) 134.
4) G. I. Taylor: Proc. Roy Soc. **145** (1934) 362,
405.
5) W. L. Bragg: Proc. Phys. Soc. **52** (1940) 54,
Nature **149** (1942) 511.
6) H. Eyring: J. Chem. Phys. **4** (1936) 284;
J. Hirschfelder, J. Phys. Chem. **41** (1937) 249.
7) J. E. Lennard-Jones, A. F. Devonshire: Proc.
Soc. **162** (1937) 53; **165** (1938) 1.
8) L. Brillouin: J. physique (7) **7** (1936) 153.
9) L. Brillouin: Trans. Faraday Soc. **34** (1937)
10) J. D. Bernal: Trans. Faraday Soc. **34** (1937)

The Influence of Temperature and Humidity on the no Load Voltage Sensitivity of Rochelle Salt.

By Heiji KAWAI.

Kobayasi Institute of Physical Research, Kokubunji Tokyo, Japan.

(Received June 11, 1947.)

1. Introduction

Rochelle salt is well known for its conspicuous piezolectric effect and its anomalous dielectric properties, and is widely applied for various purposes. The application of the Rochelle salt, however, is very much limited n making use of the voltage produced by the force applied to the crystal. Nevertheless he direct experimental investigation about he voltage sensitivity with infinite load impedance is hitherto quite lacking.

The relation between the pressure applied o the Rochelle salt and the voltage produced by it is represented by the formula

$$V=\frac{-\frac{ib}{2a}d_{14}\omega ZF}{1+\frac{ibc}{4\pi a}\varepsilon_a\omega Z}$$

$$=\frac{-\frac{2\pi}{c}\frac{d_{14}}{\varepsilon_a}FZ}{Z+1/i\omega C_f}\quad\cdots\cdots(1)$$

he notation must be referred to the author's revious paper⁽¹⁾.

From 1 it is known that V is equal to the oltage drop across Z in the diagram of Fig. when the alternating voltage

$$V_0=-\frac{2\pi}{c}\frac{d_{14}}{\varepsilon_a}F\quad\cdots\cdots(2)$$

s applied. Consequently, the voltage produced on the sample when the impedance Z is infinite is equal to the voltage V_0 which must be applied to the circuit shown in Fig. 1, in order to produce the same vol- ge across Z as in the case of the real rcuit.

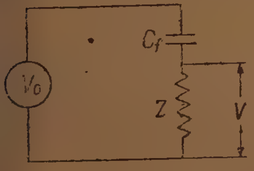

Fig. 1.

Using the a-plate, generally

$$Y_\varepsilon=f(a,b,c)F,$$

so that V_0 produced on the a-plate by F is generally represented by the following equation.

$$V_0=g(a,b,c)\frac{d_{14}}{\varepsilon_f}F,$$

where ε_f is the dielectric constant of the freely deformable crystal. Thus the voltage on Rochelle salt produced by F is proportional to d_{14}/ε_f.

The writer's previous investigation shows that both ε_a and d_{14} have anomalous properties with regard to their temperature and humidity variation, and that the variations have very similar characteristics. Therefore, it is expected that d_{14}/ε_a does not vary considerably with temperature and humidity. H. Mueller⁽²⁾ reported the value of d_{14}/ε_a above the Curie point which is almost independent of temperature. In this experiment it was studied whether the voltage sensivity of the Rochelle salt, i. e. d_{14}/ε_a, has such an anomaly in temperature and humidity dependence as ε_a and d_{14}

2. Experimental Method

The sample of the rectangular plate was cut from the single crystal of Rochelle salt of 300 gm. in weight, its sides being at 45° to the b- and c-axes, 3.98 cm and 2.00 cm long respectively, and its thickness 0.498 cm along the a-axis((4) of Fig. 2).

Thin foils of silver were used as electrodes. The method of sticking the electrode is as described in the former paper.

On the two sides facing each other (2.00 cm in length), were attached the bases of bakelite ((2) of Fig. 2) and outside of them the copper wires ((3) of Fig. 2, diameter: 0.5 mm) were attached with the alcohol solution of shellac. These wires were placed in the magne-

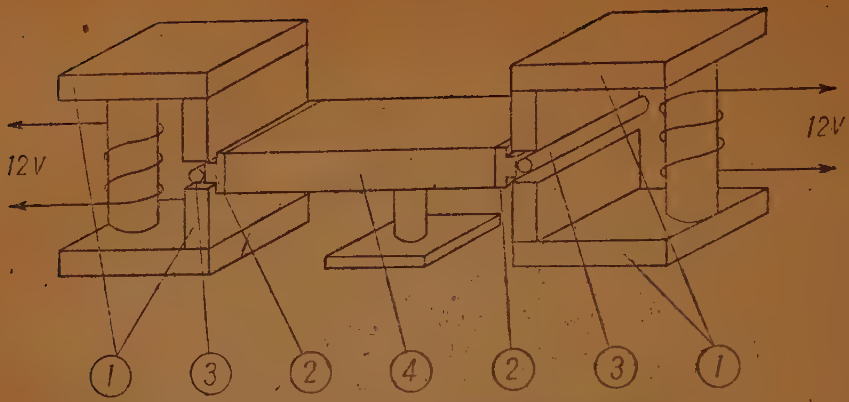

Fig. 2. The outline of experimental apparatus.

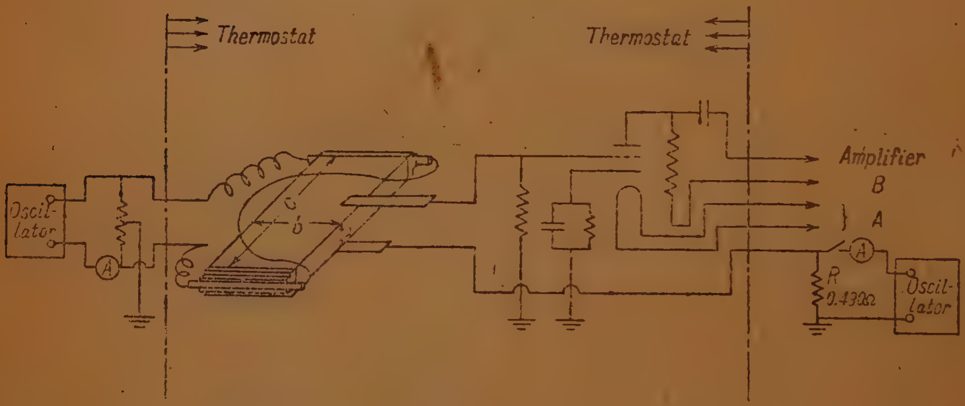

Fig. 3. Circuit diagram.

tic field (2.00cm long). Through these copper wires the alternating current was made to flow, and the sample was subjected to the alternating force of 200～2000 Hertz, the voltage between electrodes being measured. The outline of this experimental apparatus is shown in Fig. 2. This apparatus and head amplifier were put entirely in the case of glass, which was kept in constant humidity with sulphuric acid of proper concentration, and was put in the thermostat.

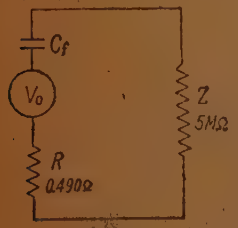

Fig. 4.

The circuit as shown in Fig. 3 was used. Considering the equation (1), the circuit shown in Fig. 3. is equivalent to that of Fig 4, so that whether V_0 be produced by the piezoelectric effect of the crystal or in any other ways, the voltage drop across the impedance Z is identical. Consequently, the voltage V_0 produced on the sample by applying the force was determined by comparing the
put voltage produced by pressing the sar
with that produced by giving suitable vol
to the resistance R (manganin wire
0.490 ohm) in Fig. 3. In the experiment,
voltage produced on the sample lay alv
between 0.2 and 0.3 mV. The magnetic
which causes the alternating force
measured to be 1.66×10^3 and 1.54×10^3
magnetic flux density when 400 mA d.c. flo
through the exciting coil, and 1.60×10^3,
mean value of them, was used in the ca
lation.

3. Experimental Results

All the measurements were done after
crystal having been kept at constant tem
ature for more than 24 hours, and someti
once more after further 24 hours to
whether that value changes or not. Sulph
acid of constant concentration was usec
keep humidity constant.

In Fig. 5. the results of the experin
are shown. The ordinate represents d_{14}/ε_a

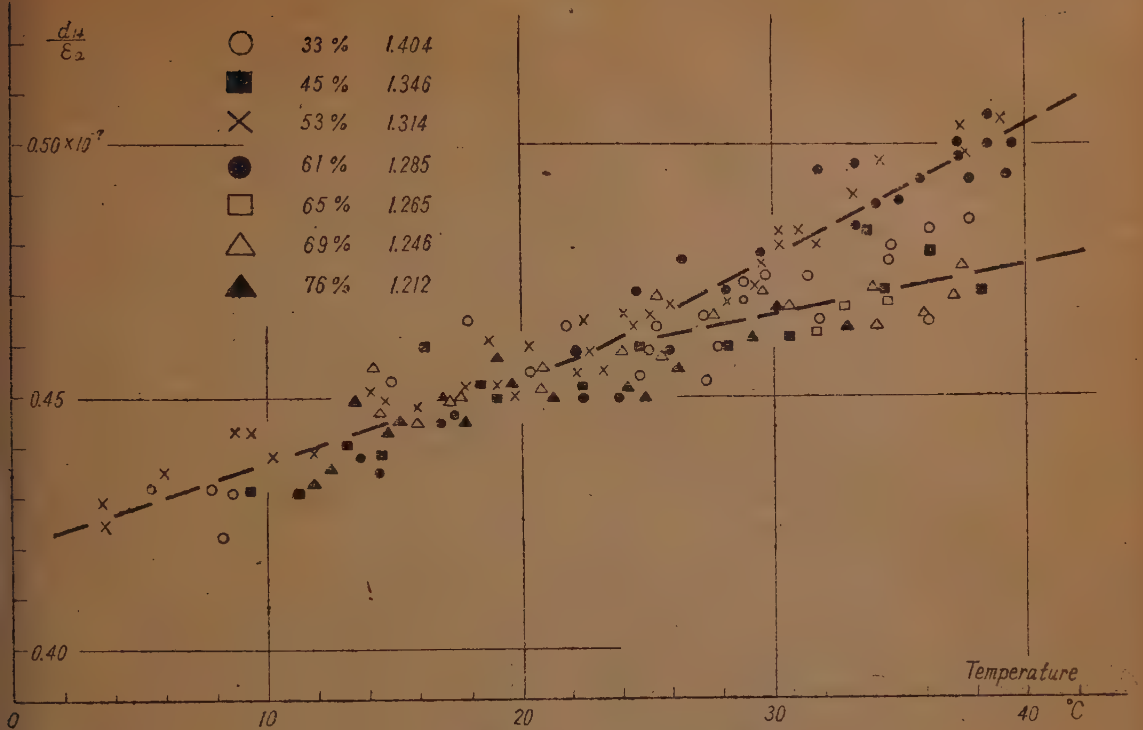

Fig. 5. d_{14}/ε_a, temperature and humidity.

e abscissa the temperature, and figures show e approximate relative humidity and the ensity of sulphuric acid used at 20°C. The esults shows that d_{14}/ε_a has not such an iomaly to the temperature as ε_a and d_{14} have, it has a tendency to increase linearly as the emperature rises. It has not a large anoma- at the Curie point, 23°C., but it seems to ave a knick point there. In the measure- ent of ε_a and d_{14}, it was known that ε_a and 4 have quasi-stable values for some time fter the temperature changes passing the urie point⁽¹⁾, but this phenomenon was not oserved in the measurement of d_4/ε_a. Also, $_4/\varepsilon_a$ does not vary sensibly with humidity, it it was known that in 54 % and 61 % imidity it clearly has larger values than other humidity. To make it sure, the easurement in 53 % humidity was again re- ated after all the measuremnnts in other imidity finished, and quite the same values before were obtained. d_{14}/ε_a has approxi- ately a linear relation to the temperature, and it seems to have a knick-point at the Curie point. And in 61 % and 53 % humidity, it has clearly different linear relation with the case corresponding to other humidity value. Below the Curie point, too, it seems to vary a little with humidity, but it is not certain, for the differences are not much larger than experimental errors. The fact that d_{14}/ε_a has no anomally but has a temperature coefficient of ordinary magnitude, and does not vary sensibly with temperature and humidity, indicates that ε_a and d_{14} vary with temperature and humidity in the same manner, and that voltage sensitivity of Rochelle salt with infinite load impedence does not vary sensibly with temperature and humidity. It seems noteworthy, however, that d_{14}/ε_a has a slight anomaly at about 65 % humidity quite the same as in the case of ε_a⁽¹⁾.

References

(1) H. Kawai: J. Phys. Soc. Jap. 2 (1947).
(2) H. Mueller: Phys. Rev., 57 (1940), 829.

The Rotation Spectrum of Water Vapor. I.

By Toyokiti NOSAWA,

Department of Dynamics, First Faculty of Engineering, University of Tokyo,

and

Tosiyuki TOYODA.

Institute of Applied Mathematics, Second Faculty of Eng., University of Tokyo.

(Read December 22, 1946; Received June 18, 1947.)

1. INTRODUCTION

The rotation spectrum of the water vapor, as an example of the non-linear triatomic XY_2-type of molecule, has been studied by many investigators.3)4)11)12)15)17) The first elaborate analysis of the vibration rotation bands of H_2O we owe to Mecke and his collaborators,11) who analyzed the 12 absorption bands in the solar spectrum and found the effective moments of inertia of H_2O molecule in each vibrational state. The most successful interpretation of the pure rotation band of water vapor in the far infrared, however, has been made by Randall, Dennison, Ginsburg and Weber,17) who measured the rotational lines with high dispersion spectrometer, identified 160 lines, and determined 155 rotational levels of the molecule with great precision (this work will hereafter be used as a constant source of reference under the abbreviation R. D. G. W.). The theoretical calculations of the energy levels were thereby carried by choosing the slightly modified values of the moments of inertia found by Mecke,11) merely for the convenience of the numerical work. The work R. D. G. W. has been followed by the investigation made by Fuson, Randall and Dennison,19) who studied the rotational structure of the heavy water vapor molecule.

Analyses of the positions of the centers of the fundamental and overtone bands of water vapor have, after Mecke, been made by Bonner13) and, more satisfactorily, by Darling and Dennison20). The latter (, which will hereafter often be referred to as D. D.,) treated the problem of the vibration rotation spectrum of H_2O by means of the theory of se rigid polyatomic molecule developed by son and Howard.16) They recognized a sonance interaction between certain of overtone bands, calculated the effec moments of inertia in each 16 vibratic bands by considering the interaction betw vibration and rotation, and supplemented analysis made by Mecke11) by taking acco of the rotational stretching.

On the theoretical side, the theory of asymmetrical rotator with the parameter asymmetry of finite magnitude has ear been established by Kramers and Ittma and has later been brought into the m convenient form for calculation by m authors: Wang,6) (Klein,7) Casimir,8)9)) D nison1) and Nielsen.10) But their treatme were based on the rigid model and co hardly explain the centrifugal effect and coupling interaction of the angular mome of vibration and rotation. Wilson and Howar have treated these problems by developing theory of semi-rigid asymmetric top mole and shown that the applicability of the W equation for the rigid rotator with the *effec* moments of inertia is to be limited in case when no accidental degeneracy occ and centrifugal stretching terms are sn enough to be neglected. As an applica of this theory to the molecule of XY_2-t has appeared the work of Shaffer, Nie and Thomas18); and Darling and Dennisc have, as above mentioned, also applied theory to the case of water vapor mole and obtained the satisfactory results.

Among these investigations, however,

equate numerical calculation of the rota-
nal stretching effect of water vapor mole-
le has been found, except for the lowest
v levels in D. D.. Nor have the intensities
the rotational lines yet been rigorously
mputed as an asymmetrical rotator.

The writers had been occupied, during the
st war-time, in the theoretical calculations
ncerning these quantities. Some of the
sults obtained will be reported in this and
llowing papers. The calculations were
rried out in the following manner.

In the first step, the energy levels of the
re rotation band up to J=13 were computed
om the Wang's *H*-matrix[6] regarding the
olecule as an asymmetrical rigid rotator,
hich was assumed to have slightly different
lues of the moments of inertia from those
ed by R. D. G. W.. We computed the eigen-
ctors of the *H*-matrix as well as its eigen-
lues, the former of which were used in the
xt step of approximation, that is, the evalua-
on of the centrifugal stretching effect of the
tating molecule. The relative intensities of
e rotational lines were also calculated by
ing as a better approximation these asym-
etrical rotator amplitudes.

The second step of our calculation was, as
as already stated, to evaluate the centrifugal
retching effect of the molecule, being regarded
w as a semi-rigid rotator. The potential
ergy constants used were those found by
D., from which the stretched shape of the
olecule in every rotating state was to be
termined. In the course of this computation
e need to know the derivatives $d\lambda/d\kappa$ of
ch eigenvalue λ with respect to the para-
eter of asymmetry κ. A simple lemma allows
s to evaluate exactly the values of these
$\lambda/d\kappa$ by using the eigenvectors of the *H*-
atrix. The agreement of the resulted levels
ith the observed ones was found to be re-
arkably good, and it was thus proved that
e most part of the differences between the
bserved levels and those calculated by R. D.
W. are explained almost satisfactorily by
e stretching effect even in our approxima-
on of the first order.

The last step is, of course, to obtain with
eater precision the true moments of inertia
the molecule. One of the writers (T.N.)
w intends to be concerned with this problem.

2. CALCULATION OF ENERGY LEVELS BASED ON THE RIGID MODEL.

The present work started from the investigation R.D.G.W.[17] They have computed the rotational energy levels of the non-vibrating rigid molecule up to and including $J=11$, whereby the algebraic equations obtained by Nielsen[10] from the Wang secular determinant were employed. We, however, had rather preferred a different course of work from theirs and used the Wang's *H*-matrix directly.

As is well known,[6] *H*-matrix of the asymmetrical rotator is independent of the magnetic quantum number, diagonal in J, and consequently factors into finite matrices H's, each being of the order $2J+1$. Further reductions of H are possible due to the symmetry properties. In the first place, as is easily shown by the Laplace development, the Wang secular determinant det. $(H-\lambda)$ can be expressed as a product of two smaller determinants; that is,

$$\text{det.}\,(H-\lambda)=\text{det.}\,(H_e-\lambda)\cdot\text{det.}\,(H_0-\lambda)\,; \quad (2.1)$$

where H_e is a matrix of the order J or $J+1$, and H_0 of the order $J+1$ or J, respectively, depending upon whether J is even or odd. For brevity, let us take a simpler case of $J=6$. Then the explicit forms of H_e and H_0 are as follows:

$$H_e=\begin{Vmatrix} 6^2 & e_5 & \cdot & \cdot & \cdot & \cdot & \cdot \\ e_5 & 4^2 & e_3 & \cdot & \cdot & \cdot & \cdot \\ \cdot & e_3 & 2^2 & e_1 & \cdot & \cdot & \cdot \\ \cdot & \cdot & e_1 & 0^2 & e_1 & \cdot & \cdot \\ \cdot & \cdot & \cdot & e_1 & 2^2 & e_3 & \cdot \\ \cdot & \cdot & \cdot & \cdot & e_3 & 4^2 & e_5 \\ \cdot & \cdot & \cdot & \cdot & \cdot & e_5 & 6^2 \end{Vmatrix},$$

$$H_0=\begin{Vmatrix} 5^2 & e_4 & \cdot & \cdot & \cdot & \cdot \\ e_4 & 3^2 & e_2 & \cdot & \cdot & \cdot \\ \cdot & e_2 & 1^2 & e_0 & \cdot & \cdot \\ \cdot & \cdot & e_0 & 1^2 & e_2 & \cdot \\ \cdot & \cdot & \cdot & e_2 & 3^2 & e_4 \\ \cdot & \cdot & \cdot & \cdot & e_4 & 5^2 \end{Vmatrix}, \quad\cdots\cdots\cdots\ (2.2)$$

where

$$e_\sigma=\kappa\cdot f(6,\sigma);\ f(J,\sigma)$$
$$=-\frac{1}{2}[(J-\sigma)(J+1-\sigma)(J+\sigma)(J+1+\sigma)]^{\frac{1}{2}}, \quad (2.3)$$

and κ is the parameter of asymmetry. When we write the eigenvectors of H_e and H_0 as $(a_6, a_4, a_2, a_0, a_{-2}, a_{-4}, a_{-6})$ and $(a_5, a_3, a_1, a_{-1}, a_{-3}, a_{-5})$, resp., the characteristic equations will take the forms

$$\begin{Vmatrix} d_6 & e_5 & \cdot & \cdot & \cdot & \cdot & \cdot \\ e_5 & d_4 & e_3 & \cdot & \cdot & \cdot & \cdot \\ \cdot & e_3 & d_2 & e_1 & \cdot & \cdot & \cdot \\ \cdot & \cdot & e_1 & d_0 & e_1 & \cdot & \cdot \\ \cdot & \cdot & \cdot & e_1 & d_2 & e_3 & \cdot \\ \cdot & \cdot & \cdot & \cdot & e_3 & d_4 & e_5 \\ \cdot & \cdot & \cdot & \cdot & \cdot & e_5 & d_6 \end{Vmatrix} \cdot \begin{Vmatrix} a_6 \\ a_4 \\ a_2 \\ a_0 \\ a_{-2} \\ a_{-4} \\ a_{-6} \end{Vmatrix} = 0,$$

$$\begin{Vmatrix} d_5 & e_4 & \cdot & \cdot & \cdot & \cdot \\ e_4 & d_3 & e_2 & \cdot & \cdot & \cdot \\ \cdot & e_2 & d_1 & e_0 & \cdot & \cdot \\ \cdot & \cdot & e_0 & d_1 & e_2 & \cdot \\ \cdot & \cdot & \cdot & e_2 & d_3 & e_4 \\ \cdot & \cdot & \cdot & \cdot & e_4 & d_5 \end{Vmatrix} \cdot \begin{Vmatrix} a_5 \\ a_3 \\ a_1 \\ a_{-1} \\ a_{-3} \\ a_{-5} \end{Vmatrix} = 0, \qquad \cdots\cdots\cdots(2.4)$$

which may be transformed into

$$\begin{Vmatrix} d_6 & e_5 & \cdot & \cdot & \cdot & \cdot & \cdot \\ e_5 & d_4 & e_3 & \cdot & \cdot & \cdot & \cdot \\ \cdot & e_3 & d_2 & e_1 & \cdot & \cdot & \cdot \\ \cdot & \cdot & e_1 & \frac{1}{2}d_0 & \cdot & \cdot & \cdot \\ \cdot & \cdot & \cdot & \cdot & d_2 & e_3 & \cdot \\ \cdot & \cdot & \cdot & \cdot & e_3 & d_4 & e_5 \\ \cdot & \cdot & \cdot & \cdot & \cdot & e_5 & d_6 \end{Vmatrix} \cdot \begin{Vmatrix} b_6 \\ b_4 \\ b_2 \\ b_0 \\ b_{-2} \\ b_{-4} \\ b_{-6} \end{Vmatrix} = 0,$$

$$\begin{Vmatrix} d_5 & e_4 & \cdot & \cdot & \cdot & \cdot \\ e_4 & d_3 & e_2 & \cdot & \cdot & \cdot \\ \cdot & e_2 & d_1+e_0 & \cdot & \cdot & \cdot \\ \cdot & \cdot & \cdot & d_1-e_0 & e_2 & \cdot \\ \cdot & \cdot & \cdot & e_2 & d_3 & e_4 \\ \cdot & \cdot & \cdot & \cdot & e_4 & d_5 \end{Vmatrix} \cdot \begin{Vmatrix} b_5 \\ b_3 \\ b_1 \\ b_{-1} \\ b_{-3} \\ b_{-5} \end{Vmatrix} = 0, \qquad (2.5)$$

where

$$d_\sigma = \sigma^2 - \lambda,$$

and

$$\begin{Vmatrix} b_6 \\ b_4 \\ b_2 \\ b_0 \\ b_{-2} \\ b_{-4} \\ b_{-6} \end{Vmatrix} = \frac{1}{2} \begin{Vmatrix} 1 & \cdot & \cdot & \cdot & \cdot & \cdot & 1 \\ \cdot & 1 & \cdot & \cdot & \cdot & 1 & \cdot \\ \cdot & \cdot & 1 & \cdot & 1 & \cdot & \cdot \\ \cdot & \cdot & \cdot & 2 & \cdot & \cdot & \cdot \\ \cdot & \cdot & 1 & \cdot & -1 & \cdot & \cdot \\ \cdot & 1 & \cdot & \cdot & \cdot & -1 & \cdot \\ 1 & \cdot & \cdot & \cdot & \cdot & \cdot & -1 \end{Vmatrix} \cdot \begin{Vmatrix} a_6 \\ a_4 \\ a_2 \\ a_0 \\ a_{-2} \\ a_{-4} \\ a_{-6} \end{Vmatrix},$$

$$\begin{Vmatrix} b_5 \\ b_3 \\ b_1 \\ b_{-1} \\ b_{-3} \\ b_{-5} \end{Vmatrix} = \frac{1}{2} \begin{Vmatrix} 1 & \cdot & \cdot & \cdot & \cdot & 1 \\ \cdot & 1 & \cdot & \cdot & 1 & \cdot \\ \cdot & \cdot & 1 & 1 & \cdot & \cdot \\ \cdot & \cdot & 1 & -1 & \cdot & \cdot \\ \cdot & 1 & \cdot & \cdot & -1 & \cdot \\ 1 & \cdot & \cdot & \cdot & \cdot & -1 \end{Vmatrix} \cdot \begin{Vmatrix} a_5 \\ a_3 \\ a_1 \\ a_{-1} \\ a_{-3} \\ a_{-5} \end{Vmatrix} \qquad (2.6)$$

The reduction of H is thus completed and the rotational states of any J group factor into four symmetry classes denoted by the symbols e^+, e^-, o^+, and o^-, of which the characteristic equations are given as follows, respectively:

$$e^+: \begin{Vmatrix} d_6 & e_5 & \cdot & \cdot \\ e_5 & d_4 & e_3 & \cdot \\ \cdot & e_3 & d_2 & e_1 \\ \cdot & \cdot & e_1 & \frac{1}{2}d_0 \end{Vmatrix} \cdot \begin{Vmatrix} x_6 \\ x_4 \\ x_2 \\ x_0 \end{Vmatrix} = 0 \quad ,$$

$$e^-: \begin{Vmatrix} d_6 & e_5 & \cdot \\ e_5 & d_4 & e_3 \\ \cdot & e_3 & d_2 \end{Vmatrix} \cdot \begin{Vmatrix} x_{-6} \\ x_{-4} \\ x_{-2} \end{Vmatrix} = 0 \quad ,$$

$$o^+: \begin{Vmatrix} d_5 & e_4 & \cdot \\ e_4 & d_3 & e_2 \\ \cdot & e_2 & d_1+e_0 \end{Vmatrix} \cdot \begin{Vmatrix} x_5 \\ x_3 \\ x_1 \end{Vmatrix} = 0 \quad ;$$

$$o^-: \begin{Vmatrix} d_5 & e_4 & \cdot \\ e_4 & d_3 & e_2 \\ \cdot & e_2 & d_1-e_0 \end{Vmatrix} \cdot \begin{Vmatrix} x_{-5} \\ x_{-3} \\ x_{-1} \end{Vmatrix} = 0 \quad , \qquad \cdots\cdots(2.7)$$

where we write x_σ for $b_\sigma/\sqrt{2}$ for the sake
simplicity of the normalization. Since t
vectors (a_σ)'s are to be considered as t
amplitudes of the asymmetrical rotator, the
have naturally to be normalized as

$$e^+: \; a_6^2+a_4^2+a_2^2+a_0^2+a_{-2}^2+a_{-4}^2+a_{-6}^2=1,$$

$$e^-: \; a_6^2+a_4^2+a_2^2+a_{-2}^2+a_{-4}^2+a_{-6}^2=1,$$

$$o^+: \; a_5^2+a_3^2+a_1^2+a_{-1}^2+a_{-3}^2+a_{-5}^2=1,$$

$$o^-: \; a_5^2+a_3^2+a_1^2+a_{-1}^2+a_{-3}^2+a_{-5}^2=1, \qquad \cdots\cdots(2.8)$$

from which follows that the normalizatio
of the vectors (b_σ)'s are to be

$$e^+: \; 2b_6^2+2b_4^2+2b_2^2+b_0^2=1,$$

$$e^-: \; 2b_{-6}^2+2b_{-4}^2+2b_{-2}^2=1,$$

$$o^+: \; 2b_5^2+2b_3^2+2b_1^2=1,$$

$$o^-: \; 2b_{-5}^2+2b_{-3}^2+2b_{-1}^2=1, \qquad \cdots\cdots\cdots\cdots\cdots\cdots\cdots(2.9)$$

and therefrom those of (x_σ)'s are

$$e^+: \; x_6^2+x_4^2+x_2^2+\tfrac{1}{2}x_0^2=1,$$

$$e^-: \; x_{-6}^2+x_{-4}^2+x_{-2}^2=1,$$

$$o^+: \; x_5^2+x_3^2+x_1^2=1,$$

$$o^-: \; x_{-5}^2+x_{-3}^2+x_{-1}^2=1. \qquad \cdots\cdots\cdots\cdots\cdots\cdots\cdots(2.10)$$

These formulae show that some care nee
to be taken in normalizing the vectors belon
ing to the class e^+. It is fortunate for ou
computation that the reduced H-matrices ha
the forms (2.7), which are finite forms of t
so-called Jacobi matrix. Thus, when an eige
value λ is known for given κ, we can readil
specify the orientation of the eigenvect
(x_σ)'s as the ratio of the components x_σ et
by a kind of recurrence formula. This mig
not so easily be attained if we took the cour
of work developed by Shaffer, Nielsen an
Thomas.[17]

The numerical results of our computati

pear in Table II, where the eigenvalues λ rresponding to each energy level J_τ up to =13 and the values of the normalized eigen- ctors (x_σ)'s belonging to these eigenvalues e listed.

The energy values obtained to the present proximation (i.e. based on the rigid model) ill be given in the Table of the succeeding per (part III).

For the values of the effective moments of ertia I_{xx}, I_{yy} and I_{zz} (cf. the notations in e next paper II), we chose the intermittent lues between the observed ones and the lculated ones by D.D., as are listed in the iddle row of the following Table Ia:

Table Ia

	I_{xx}	I_{yy}	I_{zz}
Observed values	1.007	1.929	3.013
Adopted by us	1.007	1.930	3.014
Calc. by D. D.	1.007	1.932	3.016

(In units of 10^{-40} g cm²),

here the values in the first row and those the last one are taken from the Table III the paper D.D.. From these follow the lues of $h/8\pi^2cI_{\alpha\alpha}$ and of the parameter of ymmetry κ:

Table Ib.

	$h/8\pi^2cI_{xx}$	$h/8\pi^2cI_{yy}$	$h/8\pi^2cI_{zz}$	κ
pted y us	27.790913	14.507750	9.288234	-0.1640146
by D.G.W.	27.805500	14.499724	9.279276	-0.164
nd by lecke	27.806	14.497	9.282	

ere the values adopted by R.D.G.W. and se found by Mecke are also listed for comparison and we have thereby taken $h/8\pi^2c$ to be 2.798545×10^{-39} g cm.

The writers wish here to express their sincere thanks to Prof. T. Yamanouchi, Prof. T. Inui, and Assist. Prof. A. Amemiya for their kind advices and encouragement. They are also indebted for being assisted in the numerical work to Miss T. Tuda, T. Ueda, T. Matui, S. Ôi and Mr. S. Iida.

References.

1) D.M. Dennison: Rev. Mod. Phys. 3 (1931) 280.
2) D.M. Dennison: Rev. Mod. Phys. 12 (1940) 175.
3) W.W. Sleator: Astrophys. J. 48 (1918) 125.
4) W.W. Sleator and E.R. Phelps: Astrophys. J. 62 (1925) 28.
5) H.A. Kramers and G.P. Ittman: Zeits. f. Phys. 53 (1929) 553. Ibid. 58 (1929) 217.
6) S.C. Wang: Phys. Rev. 34 (1929) 243.
7) O. Klein: Zeits. f. Phys. 58 (1929) 730.
8) H.B.G. Casimir: Zeits. f. Phys. 59 (1930) 623.
9) H.B.G. Casimir: Dissertation (Leyden, 1931).
10) H.H. Nielsen: Phys. Rev. 38 (1931) 1432.
11) R. Mecke, W. Baumann, and K. Freudenberg: Zeits. f. Phys. 81 (1933) 313, 445, 465.
12) N. Wright and H.M. Randall: Phys. Rev. 44 (1933) 391.
13) L.G. Bonner: Phys. Rev. 46 (1935) 458.
14) C. Eckart: Phys. Rev. 47 (1935) 552.
15) R.B. Barnes, W.S. Benedict and C.M. Lewis: Phys. Rev. 47 (1935) 918.
16) E.B. Wilson and J.B. Howard: J. Chem. Phys. 4 (1936) 261, 313, 526.
17) H.M. Randall, D.M. Dennison, N. Ginsburg and L.R. Weber: Phys. Rev. 52 (1937) 160.
18) W.H. Shaffer, H.H. Nielsen and L.H. Thomas: 56 (1939) 895.
19) N. Fuson, H.M. Randall and D.M. Dennison: Phys. Rev. 56 (1939) 982.
20) B.T. Darling and D.M. Dennison: Phys. Rev. 57 (1940) 128.

Table II.

$J=0.$ $e^+: 0_0$ $x_0=1$

$J=1.$ $0^+: 1_1$ $x_1=1$ $0^-: 1_0$ $x_{-1}=1$ $e^+: 1_{-1}$ $x_0=1$

2.

e^+	2_2	2_{-2}
λ	4.07914	-0.07914
x_2	0.99044	0.13795
x_0	0.19509	-1.40068

$e^-: 2_1$ $x_{-2}=1$ $0^+: 2_0$ $x_1=1$ $0^-: 2_{-1}$ $x_{-1}=1$

$J=3.$

0^+	3_3	3_{-1}
λ	9.05705	1.92704
x_3	0.99599	0.08945
x_1	0.08945	−0.99599

0^-	3_2	3_{-2}
λ	9.04469	−0.02878
x_{-3}	0.99753	0.07019
x_{-1}	0.07018	−0.99765

e^+	3_1	3_{-3}
λ	4.36940	−0.36940
x_2	0.92486	0.20139
x_0	0.38030	−0.97951

e^-: 3_0
$x_{-2}=1$

$J=4.$

e^+	4_4	4_0	4_{-4}
λ	16.0640	4.91685	−0.98088
x_4	0.99724	0.07129	0.02080
x_2	0.07358	−0.91044	−0.40705
x_0	0.01425	−0.57623	1.29130

e^-	4_3	4_{-1}
λ	16.0624	3.9378
x_{-4}	0.99743	0.07176
x_{-2}	0.07176	−0.99740

0^+	4_2	4_{-2}
λ	9.2562	2.3840
x_3	0.98119	0.19307
x_1	0.19307	−0.98119

0^-	4_1	4_{-3}
λ	9.1727	−0.8128
x_{-3}	0.99131	0.13151
x_{-1}	0.13152	−0.99132

$J=5.$

0^+	5_5	5_1	5_{-3}
λ	25.0763	9.6511	2.7328
x_5	0.99758	0.06764	0.01599
x_3	0.06917	−0.94363	−0.32371
x_1	0.00678	−0.32402	0.94602

0^-	5_4	5_0	5_{-4}
λ	25.0761	9.3411	−1.8775
x_{-5}	0.99760	0.06878	0.00788
x_{-3}	0.06901	−0.97885	−0.19257
x_{-1}	0.00553	−0.19267	0.98125

e^+	5_3	5_{-1}	5_{-5}
λ	16.2514	5.70007	−1.9515
x_4	0.98885	0.14112	0.04762
x_2	0.14585	−0.85276	−0.50152
x_0	0.04267	−0.71117	1.22164

e^-	5_2	5_{-2}
λ	16.2374	3.7626
x_{-4}	0.99044	0.13795
x_{-2}	0.13796	−0.99044

$J=6.$

e^+	6_6	6_2	6_{-2}	6_{-6}
λ	36.0894	16.5576	6.6288	−3.2758
x_6	0.99774	0.06633	0.01039	0.00267
x_4	0.06695	−0.96790	−0.22896	−0.07927
x_2	0.00573	−0.23304	−0.79102	0.56564
x_0	0.00107	−0.09460	−0.80220	−1.16084

e^-	6_5	6_1	6_{-3}
λ	36.0894	16.4905	3.4201
x_{-6}	0.99774	0.06676	0.00860
x_{-4}	0.06693	−0.97750	−0.21035
x_{-2}	0.00563	−0.21091	0.97763

0^+	6_4	6_0	6_{-4}
λ	25.2806	10.3399	2.8238
x_5	0.99105	0.12608	0.04384
x_3	0.13202	−0.87731	−0.46142
x_1	0.01973	−0.46308	0.88610

0^-	6_3	6_{-1}	6_{-5}
λ	25.2786	9.5225	−3.2454
x_{-5}	0.99126	0.13061	0.01859
x_{-3}	0.13115	−0.95952	−0.24926
x_{-1}	0.01472	−0.24952	0.96826

J=7.

0^+	7_7	7_3	7_{-1}	7_{-5}
λ	49.1027	25.5755	11.3622	2.5520
x_7	0.99784	0.06519	0.00789	0.00284
x_5	0.06550	-0.97597	-0.18991	-0.08435
x_3	0.00540	-0.20333	0.78974	0.57875
x_1	0.00053	-0.04336	0.58326	-0.81114

0^-	7_6	7_2	7_{-2}	7_{-6}
λ	49.1027	25.5638	9.6712	-4.9301
x_{-7}	0.99784	0.06524	0.00793	0.00099
x_{-5}	0.06550	-0.97717	-0.19946	-0.03269
x_{-3}	0.00539	-0.20008	0.93294	0.29936
x_{-1}	0.00043	-0.02925	0.29973	-0.95358

e^+	7_5	7_1	7_{-3}	7_{-7}
λ	36.3172	17.0544	7.5703	-4.9420
x_6	0.99198	0.12266	0.02976	0.00690
x_4	0.12542	-0.92620	-0.33722	-0.11261
x_2	0.01546	-0.33391	0.71962	0.60861
x_0	0.00384	-0.17659	0.85735	-1.11073

e^-	7_4	7_0	7_{-4}
λ	36.3170	16.8253	2.8577
x_{-6}	0.99201	0.12436	0.02155
x_{-4}	0.12533	-0.95041	-0.28462
x_{-2}	0.01492	-0.28502	0.95840

J=8.

e^+	8_8	8_4	8_0	8_{-4}	8_{-8}
λ	64.1161	36.6254	17.8404	8.3607	-6.9426
x_8	0.99791	0.06427	0.00706	0.00206	0.00033
x_6	0.06447	-0.97915	-0.18131	-0.06372	-0.00130
x_4	0.00518	-0.18991	0.85580	0.45859	0.14562
x_2	0.00045	-0.03185	0.43986	-0.63153	-0.63771
x_0	0.00008	-0.01013	0.28708	-0.87952	-1.06953

e^-	8_7	8_3	8_{-1}	8_{-5}
λ	64.1161	36.6236	17.2280	2.0323
x_{-8}	0.99791	-0.06427	0.00720	0.00117
x_{-6}	0.06448	-0.97932	-0.18751	-0.04023
x_{-4}	0.00518	-0.18949	0.91509	0.35598
x_{-2}	0.00044	-0.02998	0.35700	-0.93363

0^+	8_6	8_2	8_{-2}	8_{-6}
λ	49.3556	25.9969	12.6625	1.8895
x_7	0.99252	0.11998	0.02101	0.00818
x_5	0.12126	-0.94813	-0.26232	-0.13243
x_3	0.01402	-0.28259	0.69317	0.66293
x_1	0.00184	-0.08250	0.67103	-0.73683

0^-	8_5	8_1	8_{-3}	8_{-7}
λ	49.3556	25.9486	9.7294	-6.9382
x_{-7}	0.99252	0.12034	0.02027	0.00257
x_{-6}	0.12125	-0.95294	-0.27344	-0.04933
x_{-3}	0.01396	-0.27382	0.89869	0.34232
x_{-1}	0.00143	-0.04947	0.34231	-0.93829

=9.

0^+	9_9	9_5	9_1	9_{-3}	9_{-7}
λ	81.1295	49.6840	26.6012	14.1147	0.8512
x_9	0.99796	0.06354	0.00663	0.00133	0.00042
x_7	0.06370	-0.98078	-0.17778	-0.04383	-0.01675
x_5	0.00504	-0.18171	0.90175	0.34681	0.18309
x_3	0.00043	-0.02789	0.36740	-0.59114	-0.71754
x_1	0.00004	-0.00476	0.14217	-0.72688	0.67187

0^-	9_8	9_4	9_0	9_{-4}	9_{-8}
λ	81.1295	49.6837	26.4436	9.6350	−9.2725
x_{-9}	0.99796	0.06355	0.00667	0.00111	0.00011
x_{-7}	0.06370	−0.98030	−0.17948	−0.03909	−0.00511
x_{-5}	0.00504	−0.18168	0.91679	0.34914	0.06760
x_{-3}	0.00043	−0.02766	0.34876	−0.85689	−0.37860
x_{-1}	0.00003	−0.00348	0.07491	−0.37724	0.92307

e^+	9_7	9_3	9_{-1}	9_{-5}	9_{-9}
λ	64.3948	37.0359	19.0030	8.8405	−9.2742
x_8	0.99289	0.11754	0.01767	0.00679	0.00094
x_6	0.11831	−0.95660	−0.23999	−0.11302	−0.02086
x_4	0.01320	−0.25974	0.75650	0.57332	0.17711
x_2	0.00149	−0.05717	0.53438	−0.52788	−0.65766
x_0	0.00034	−0.02252	0.41040	−0.87158	1.03507

e^-	9_6	9_2	9_{-2}	9_{-6}
λ	64.3948	37.0274	17.6641	0.9138
x_{-8}	0.99289	0.11760	0.01826	0.00336
x_{-6}	0.11831	−0.95745	−0.25533	−0.06405
x_{-4}	0.01319	−0.25839	0.86951	0.42073
x_{-2}	0.00145	−0.05193	0.42241	−0.90492

$J=10.$ e^+	10_{10}	10_6	10_2	10_{-2}	10_{-6}	10_{-10}
λ	100.143	64.7456	37.5789	20.5532	8.9142	−11.9349
x_{10}	0.99799	0.06298	0.00630	0.00097	0.00039	0.00004
x_8	0.06310	−0.98203	−0.17382	−0.03425	−0.01560	−0.00198
x_6	0.00493	−0.17600	0.92134	0.29897	0.17271	0.03018
x_4	0.00041	−0.02575	0.33320	−0.63921	−0.66113	−0.20647
x_2	0.00004	−0.00366	0.09406	−0.60283	0.42068	0.67132
x_0	0.00001	−0.00101	0.04475	−0.52432	0.84365	−1.00550

e^-	10_9	10_5	10_1	10_{-3}	10_{-7}
λ	100.143	64.7456	37.5463	18.0815	−0.5164
x_{-10}	0.99799	0.06298	0.00630	0.00098	0.00016
x_{-8}	0.06310	−0.98203	−0.17416	−0.03533	−0.00708
x_{-6}	0.00493	−0.17600	0.92426	0.32605	0.09183
x_{-4}	0.00041	−0.02572	0.32977	−0.81437	−0.47686
x_{-2}	0.00004	−0.00351	0.08138	−0.47880	0.87413

0^+	10_8	10_4	10_0	10_{-4}	10_{-8}
λ	81.4343	50.1041	27.4733	15.5516	−0.5425
x_9	0.99315	0.11555	0.01638	0.00457	0.00130
x_7	0.11611	−0.96099	−0.23607	−0.08051	−0.02856
x_5	0.01263	−0.24638	0.83010	0.44242	0.23309
x_3	0.00136	−0.04838	0.45197	−0.47953	−0.75062
x_1	0.00017	−0.01049	0.22508	−0.75353	0.61759

0^-	10_7	10_3	10_{-1}	10_{-5}	10_{-9}
λ	81.4343	50.1027	27.0463	9.3352	−11.9343
x_{-9}	0.99315	0.11555	0.01666	0.00335	0.02034
x_{-7}	0.11611	−0.96118	−0.24196	−0.06470	−0.00863
x_{-5}	0.01263	−0.24619	0.86798	0.42230	0.08670
x_{-3}	0.00134	−0.04763	0.42064	−0.80839	−0.40902
x_{-1}	0.00013	−0.00711	0.10425	−0.40493	0.90836

$J=11.$

0^+	11_{11}	11_7	11_3	11_{-1}	11_{-5}	11_{-9}
λ	121.156	81.8089	50.6360	28.7160	16.7860	−2.2784
x_{11}	0.99803	0.06252	0.00603	0.00083	0.00028	0.00006
x_9	0.06258	−0.98286	−0.17023	−0.03085	−0.01152	−0.00288
x_7	0.00485	−0.17171	0.93069	0.29089	0.13344	0.04330
x_5	0.00040	−0.02429	0.31377	−0.72922	−0.53897	−0.28056
x_3	0.00003	−0.00324	0.07689	−0.52544	0.35538	0.76923
x_1	0.00000	−0.00049	0.02079	−0.32649	0.75185	−0.57245

0^-	11_{10}	11_6	11_2	11_{-2}	11_{-6}	11_{-10}
λ	121.156	81.8089	50.6302	27.7355	8.7680	−14.9240
x_{-11}	0.99802	0.06252	0.00603	0.00085	0.00016	0.00001
x_{-9}	0.06262	−0.98285	−0.17029	−0.03191	−0.00740	−0.00076
x_{-7}	0.00485	−0.17171	0.93119	0.30650	0.09650	0.01310
x_{-5}	0.00040	−0.02429	0.31322	−0.80679	−0.48891	−0.10604
x_{-3}	0.00003	−0.00323	0.07481	−0.48551	0.75497	0.43448
x_{-1}	0.00000	−0.00038	0.01299	−0.13567	0.42618	−0.89432

e^+	11_9	11_5	11_1	11_{-3}	11_{-7}	11_{-11}
λ	100.474	65.1822	38.2988	22.4021	8.5671	−14.9242
x_{10}	0.99336	0.11395	0.01547	0.00314	0.00130	0.00013
x_8	0.11439	−0.96373	−0.23187	−0.05627	−0.02895	−0.00350
x_6	0.01221	−0.23715	0.86924	0.36158	0.23581	0.04066
x_4	0.00128	−0.04384	0.40739	−0.51508	−0.71573	−0.23353
x_2	0.00014	−0.00767	0.14530	−0.64131	0.32257	0.68081
x_0	0.00003	−0.00253	0.08151	−0.61507	0.80898	−0.98011

e^-	11_8	11_4	11_0	11_{-4}	11_{-8}
λ	100.474	65.1820	38.1952	18.4166	−2.2679
x_{-10}	0.99336	0.11395	0.01554	0.00299	0.00050
x_{-8}	0.11439	−0.96375	−0.23327	−0.05934	−0.01249
x_{-6}	0.01221	−0.23718	0.87810	0.39701	0.12175
x_{-4}	0.00128	−0.04374	0.40042	−0.75053	−0.52187
x_{-2}	0.00013	−0.00720	0.11808	−0.52496	0.83960

$J=12.$

e^+	12_{12}	12_8	12_4	12_0	12_{-4}	12_{-8}	12_{-12}
λ	144.170	100.873	65.7200	39.2634	24.3913	7.8240	−18.2418
x_{12}	0.99805	0.06214	0.00582	0.00076	0.00018	0.00006	0.00000
x_{10}	0.06223	−0.98348	−0.16725	−0.02907	−0.00778	−0.00309	−0.00029
x_8	0.00478	−0.16838	0.93634	0.28880	0.09627	0.04669	0.00556
x_6	0.00039	−0.02322	0.30057	−0.79562	−0.43005	−0.29741	−0.05199
x_4	0.00003	−0.00299	0.06842	−0.47743	0.38653	0.74251	0.25816
x_2	0.00000	−0.00038	0.01452	−0.21285	0.65216	−0.23880	−0.68713
x_0	0.00000	−0.00010	0.00562	−0.13781	0.67971	−0.77590	0.95757

e^-	12_{11}	12_7	12_3	12_{-1}	12_{-5}	12_{-9}
λ	144.170	100.873	65.7191	38.9800	18.6000	−4.3452
x_{-12}	0.99805	0.06214	0.00582	0.00076	0.00015	0.00002
x_{-10}	0.06228	−0.98349	−0.16726	−0.02941	−0.00680	−0.00116
x_{-8}	0.00478	−0.16838	0.93642	0.29352	0.09055	0.01983
x_{-6}	0.00039	−0.02322	0.30049	−0.81822	−0.46476	−0.15394
x_{-4}	0.00003	−0.00299	0.06810	−0.46654	0.67929	0.56237
x_{-2}	0.00000	−0.00037	0.01330	−0.16075	0.56065	−0.81219

0^+	12_{10}	12_6	12_2	12_{-2}	12_{-6}	12_{-10}
λ	121.5380	82.2417	51.3047	30.4026	17.6553	−4.3494
x_{11}	0.99322	0.11510	0.01506	0.00259	0.00106	0.00020
x_9	0.11556	−0.96538	−0.22701	−0.05070	−0.02376	−0.00536
x_7	0.01214	−0.23036	0.88762	0.33969	0.19963	0.06077
x_5	0.00125	−0.04088	0.38173	−0.60398	−0.61848	−0.32577
x_3	0.00013	−0.00661	0.11479	−0.57525	0.22485	0.78106
x_1	0.00002	−0.00120	0.03841	−0.43167	0.72561	−0.53659

0^-	12_9	12_5	12_1	12_{-3}	12_{-7}	12_{-11}
λ	121.538	82.2417	51.2835	28.4698	7.9155	−18.2418
x_{-11}	0.99323	0.11519	0.01508	0.00267	0.00056	0.00005
x_{-9}	0.11556	−0.96538	−0.22728	−0.05335	−0.01373	−0.00140
x_{-7}	0.01214	−0.23036	0.88932	0.37124	0.13315	0.01845
x_{-5}	0.00125	−0.04087	0.38043	−0.73465	−0.54610	−0.12517
x_{-3}	0.00013	−0.00655	0.10964	−0.54006	0.69892	0.45583
x_{-1}	0.00001	−0.00087	0.02166	−0.16718	0.44201	−0.88103

= 13.

o^+	13_{13}	13_9	13_5	13_1	13_{-3}	13_{-7}	13_{-11}
λ	169.183	121.938	82.8156	52.1480	32.5145	18.0775	−6.7520
x_{13}	0.99807	0.06182	0.00565	0.00070	0.00013	0.00005	0.00001
x_{11}	0.06190	−0.98398	−0.16480	−0.02755	−0.00583	−0.00272	−0.00046
x_9	0.00473	−0.16570	0.94029	0.28385	0.07726	0.04191	0.00881
x_7	0.00038	−0.02239	0.29075	−0.82922	−0.38398	−0.27124	−0.07972
x_5	0.00003	−0.00281	0.06302	−0.44728	0.46679	0.66729	0.36441
x_3	0.00000	−0.00034	0.01214	−0.16334	0.59527	−0.10100	−0.78014
x_1	0.00000	−0.00005	0.00265	−0.06582	0.52376	−0.68497	0.50214

o^-	13_{12}	13_8	13_4	13_0	13_{-4}	13_{-8}	13_{-12}
λ	169.183	121.938	82.8155	52.0820	29.1912	6.7522	−21.8877
x_{-13}	0.99807	0.06182	0.00565	0.00070	0.00013	0.00002	0.00000
x_{-11}	0.06190	−0.98393	−0.16479	−0.02762	−0.00594	−0.00132	−0.00011
x_{-9}	0.00473	−0.16570	0.94030	0.28490	0.08167	0.02261	0.00231
x_{-7}	0.00038	−0.02239	0.29074	−0.83425	−0.43414	−0.17295	−0.02458
x_{-5}	0.00003	−0.00281	0.06298	−0.44485	0.65296	0.59255	0.14378
x_{-3}	0.00000	−0.00034	0.01197	−0.15191	0.58271	−0.64248	−0.47376
x_{-1}	0.00000	−0.00004	0.00181	−0.03359	0.19727	−0.45353	0.86849

e^+	13_{11}	13_7	13_3	13_{-1}	13_{-5}	13_{-9}	13_{-13}
λ	144.554	101.351	66.3774	40.5681	26.3253	6.7123	−21.8877
x_{12}	0.99365	0.11158	0.01410	0.00226	0.00070	0.00222	0.00002
x_{10}	0.11189	−0.96718	−0.22244	−0.04743	−0.01667	−0.00605	−0.00055
x_8	0.01162	−0.22490	0.89815	0.34036	0.14846	0.06832	0.00815
x_6	0.00118	−0.03866	0.36452	−0.69630	−0.50088	−0.35473	−0.06389
x_4	0.00012	−0.00598	0.10030	−0.53524	0.25092	0.74952	0.28048
x_2	0.00001	−0.00091	0.02553	−0.29535	0.63704	−0.16894	−0.69120
x_0	0.00000	−0.00027	0.01142	−0.21613	0.71836	−0.74717	0.93747

e^-	13_{10}	13_6	13_2	13_{-2}	13_{-6}	13_{-10}
λ	144.554	101.351	66.3754	39.8919	18.5802	−6.7504
x_{-12}	0.99365	0.11158	0.01410	0.00230	0.00051	0.00006
x_{-10}	0.11189	−0.96718	−0.22248	−0.04867	−0.01304	−0.00224
x_{-8}	0.01162	−0.22490	0.89845	0.35324	0.12839	0.02888
x_{-6}	0.00118	−0.03866	0.36431	−0.74501	−0.52554	−0.18592
x_{-4}	0.00012	−0.00597	0.09943	−0.52429	0.60273	0.59321
x_{-2}	0.00001	−0.00087	0.02261	−0.20721	0.58640	−0.78275

The Rotation Spectrum of Water Vapor. II

By Toyokiti NOZAWA.

Department of Dynamics, First Faculty of Engineering, Tokyo University.

(Read December 22, 1946; Received June 18, 1947)

3. Evaluation of $d\lambda/d\kappa$.

It will prove necessary for the rotational stretching, which is to be treated in the section 5 of this paper, that we know the value of $d\lambda/d\kappa$ for each eigenvalue λ. A method is, therefore, shown here to compute it by using the eigenvector. Let H be a symmetric matrix, of which the elements vary with a paramater κ. The eigenvalues λ's and the eigenvectors x's of H depend then also upon κ, and they satisfy the characteristic equation

$$Hx=\lambda x \tag{3.1}$$

where x is to be regarded as a column matrix. We shall write M^T for the transposed of a matrix M, and M' for the matrix which is obtained by differentiating all elements of M with respect to the parameter κ. Assuming that the eigenvector x is normalized, i.e. $x^Tx=1$,

$$\lambda=x^THx \tag{3.2}$$

from which follow

$$\begin{aligned}\lambda' &= x^{T\prime}Hx+x^TH'x+x^THx'\\ &=\lambda x^{T\prime}x+x^TH'x+\lambda x^Tx'\\ &=x^TH'x+\lambda(x^Tx)'\\ &=x^TH'x,\end{aligned}$$

and

$$\begin{aligned}\lambda'' &= x^{T\prime}H'x+x^TH''x+x^TH'x'\\ &=x^TH''x+2\,x^TH'x'.\end{aligned}$$

We thus have a simple but useful

Lemma: The derivative λ' of each eigenvalue λ, of a symmetric matrix H, with respect to the parameter κ is given by

$$\lambda'=x^TH'x \tag{3.3}$$

where x is a normalized eigenvector belonging to λ.

And the second derivative λ'' is given by

$$\lambda''=x^TH''x+2\,x^TH'x'. \tag{3.4}$$

When we take the case $J=6$, as before, the explicit forms of H, H', and λ', for each group e^+, e^-, o^+, and o^-, are given as follows (cf. the formulae (2.3,)(2.7), and (2.10) in the preceding section 2.):

$$e^+:\quad H=\begin{Vmatrix}6^2 & e_5 & \cdot & \cdot\\ e_5 & 4^2 & e_3 & \cdot\\ \cdot & e_3 & 2^2 & e_1\\ \cdot & \cdot & e_1 & \cdot\end{Vmatrix},\qquad H'=\begin{Vmatrix}\cdot & f_5 & \cdot & \cdot\\ f_5 & \cdot & f_3 & \cdot\\ \cdot & f_3 & \cdot & f_1\\ \cdot & \cdot & f_1 & \cdot\end{Vmatrix}$$

$$\lambda'=2(x_6f_5x_4+x_4f_3x_2+x_2f_1x_0) \tag{3.5}$$

$$e^-:\quad H=\begin{Vmatrix}6^2 & e_5 & \cdot\\ e_5 & 4^2 & e_3\\ \cdot & e_3 & 2^2\end{Vmatrix},\qquad H'=\begin{Vmatrix}\cdot & f_5 & \cdot\\ f_5 & \cdot & f_3\\ \cdot & f_3 & \cdot\end{Vmatrix}$$

$$\lambda'=2(x_{-6}f_5x_{-4}+x_{-4}f_3x_{-2}) \tag{3.6}$$

$$o^+:\quad H=\begin{Vmatrix}5^2 & e_4 & \cdot\\ e_4 & 3^2 & e_2\\ \cdot & e_2 & 1^2+e_0\end{Vmatrix},\qquad H'=\begin{Vmatrix}\cdot & f_4 & \cdot\\ f_4 & \cdot & f_2\\ \cdot & f_2 & f_0\end{Vmatrix}$$

$$\lambda'=2(x_5f_4x_3+x_3f_2x_1)+x_1^2f_0 \tag{3.7}$$

$$o^-:\quad H=\begin{Vmatrix}5^2 & e_4 & \cdot\\ e_4 & 3^2 & e_2\\ \cdot & e_2 & 1^2-e_0\end{Vmatrix},\qquad H'=\begin{Vmatrix}\cdot & f_4 & \cdot\\ f_4 & \cdot & f_2\\ \cdot & f_2 & -f_0\end{Vmatrix}$$

$$\lambda'=2(x_{-5}f_4x_{-3}+x_{-3}f_2x_{-1})+x_{-1}^2f_0 \tag{3.8}$$

where

$$f_\sigma=f(6,\sigma)=-\frac{1}{2}[(6-\sigma)(7-\sigma)(6+\sigma)(7+\sigma)]$$

And H'' is found to vanish for every symmetr group.

The numerical values of $d\lambda/d\kappa$ for each J computed according to this lemma, will b listed in the second column of Table III.

Table III

J_τ	λ'	$-\Delta E$	$-\delta W$
6_6	-0.5491	27.17	28.46
6_5	-0.5488	27.17	28.46
6_4	-1.7340	11.94	12.83
6_3	-1.7042	11.95	12.83
6_2	-3.6367	4.25	5.05
6_1	-2.8574	4.33	4.92
6_0	-8.5391	3.08	2.29
6_{-1}	-2.2792	1.46	1.80
6_{-2}	-15.9512	1.21	2.08
6_{-3}	3.3937	0.82	1.30
6_{-4}	-0.2269	0.93	1.50
6_{-5}	14.4828	1.00	0.51
6_{-6}	14.1952	1.02	0.54

J_τ	λ'	$-\Delta E$	$-\delta W$
7_7	−0.6305	50.57	52.05
7_6	−0.6305	50.57	52.05
7_5	−1.9503	25.31	27.20
7_4	−1.9457	25.31	27.20
7_3	−3.5975	10.95	12.80
7_2	−3.4224	10.99	12.80
7_1	−7.1365	3.97	5.75
7_0	−4.5430	4.18	5.68
7_{-1}	−13.7311	1.88	4.00
7_{-2}	−2.2892	1.88	3.06
7_{-3}	−11.1192	1.78	3.76
7_{-4}	6.4910	1.46	1.76
7_{-5}	3.9592	1.58	2.03
7_{-6}	20.3419	1.84	0.82
7_{-7}	20.2063	1.85	0.84
8_8	−0.7126	86.57	86.75
8_7	−0.7127	86.58	86.75
8_6	−2.1846	47.61	50.12
8_5	−2.1837	47.61	50.12
8_4	−3.8574	23.54	27.07
8_3	−3.8250	23.54	27.07
8_2	−6.3785	10.18	13.57
8_1	−5.6684	10.30	13.59
8_0	−12.6868	4.12	7.89
8_{-1}	−6.2548	4.44	7.13
8_{-2}	−18.7369	2.99	4.65
8_{-3}	−1.3842	2.69	4.52
8_{-4}	−9.9196	2.86	5.89
8_{-5}	10.7923	2.45	2.56
8_{-6}	9.2993	2.55	3.00
8_{-7}	27.2371	1.58	1.32
8_{-8}	27.1366	1.58	1.32
9_9	−0.7950	139.04	134.90
9_8	−0.7950	139.04	134.90
9_7	−2.4242	82.15	84.29
9_6	−2.4241	82.15	84.29
9_5	−4.2046	44.74	49.64
9_4	−4.2007	44.74	49.64
9_3	−6.4386	22.02	27.57
9_2	−6.2854	22.06	27.57
9_1	−10.6240	9.79	15.66
9_0	−8.3800	10.09	15.47
9_{-1}	−20.1529	5.04	11.65
9_{-2}	−7.5770	5.28	10.21
9_{-3}	−22.3768	4.68	11.40
9_{-4}	0.7759	3.98	6.79
9_{-5}	−6.1089	4.26	8.48
9_{-6}	16.2867	3.89	3.89
9_{-7}	15.5036	3.97	4.20
9_{-8}	35.1494	4.97	2.06
9_{-9}	35.1243	4.97	2.06
10_{10}	−0.8775	212.38	198.44
10_9	−0.8775	212.38	198.44
10_8	2.6669	132.75	131.51
10_7	2.6669	132.75	131.51
10_6	−4.5812	77.80	83.25
10_5	−4.5810	77.80	83.25
10_4	−6.8064	42.13	50.25
10_3	−6.7785	42.14	50.25
10_2	−9.9684	20.92	29.79
10_1	−9.3937	21.06	29.75
10_0	−17.0871	10.03	18.87
10_{-1}	−11.3329	10.58	18.56
10_{-2}	−28.2579	9.71	20.53
10_{-3}	−4.5243	6.95	13.75
10_{-4}	−23.4784	6.92	16.70
10_{-5}	4.2061	5.82	9.67
10_{-6}	−0.3771	6.11	11.22
10_{-7}	22.9187	5.91	5.57
10_{-8}	22.5387	5.96	5.73
10_{-9}	44.0718	7.55	3.00
10_{-10}	44.0494	7.55	3.00
11_{11}	−0.9595	311.50	279.19
11_{10}	−0.9602	311.50	279.19
11_9	−2.9111	203.74	193.68
11_8	−2.9111	203.74	193.68
11_7	−4.9682	126.52	130.06
11_6	−4.9688	126.51	130.06
11_5	−7.2726	73.74	83.77
11_4	−7.2670	73.74	83.77
11_3	−10.1400	40.00	52.51
11_2	−10.0178	40.05	52.47
11_1	−21.8942	18.72	33.80
11_0	−13.1362	20.80	33.26
11_{-1}	−26.2406	11.35	25.74
11_{-2}	−14.1358	11.98	26.65
11_{-3}	−35.3011	10.11	27.39
11_{-4}	−7.2505	9.11	22.39
11_{-5}	−21.1521	9.64	25.36
11_{-6}	9.0842	8.31	14.26
11_{-7}	6.4059	8.55	14.64
11_{-8}	30.3975	8.69	7.68
11_{-9}	30.4611	8.69	7.80
11_{-10}	53.9959	4.94	4.33
11_{-11}	53.9934	4.94	4.33

4. Displacement Coordinates and Moments of Inertia

In order to define the stretched configuration of the molecule, we need to introduce a set of geometric displacement coordinates. This may most conveniently be done following Darling and Dennison[20].

Let us consider H_2O molecule which rests in the vibrational and rotational normal state. We first take the Cartesian axes whose origin lies at the center of gravity of the system, whose *x*-axis is parallel to the line joining the equilibrium positions of the two H atoms, and

y-,z-axis lie in, perpendicular to the plane of the molecule respectively.

	Masses	Coordinates
O	M	(x_1, y_1)
H(2)	m	(x_2, y_2)
H(3)	m	(x_3, y_3)

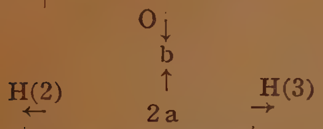

Between the six coordinates of these three atoms, there must exist three relations as follows:

$$Mx_1+m(x_2+x_3)=0$$
$$My_1+m(y_2+y_3)=0$$
$$M(x_1\dot{y}_1-\dot{x}_1y_1)+m(x_2\dot{y}_2-\dot{x}_2y_2)+m(x_3\dot{y}_3-\dot{x}_3y_3)=0 \tag{4.1}$$

The first two of these imply that the origin of the moving system is at the center of gravity of the molecule, and the last one states that there is no angular momentum relative to the moving system. Introducing the displacement coordinates δ_x and δ_y defined by

$$x_1=\delta x_1, \qquad y_1=\frac{2m}{M+2m}b+\delta y_1$$
$$x_2=-a+\delta x_2, \quad y_2=-\frac{M}{M+2m}b+\delta y_2$$
$$x_3=a+\delta x_3, \qquad y_3=-\frac{M}{M+2m}b+\delta y_3, \tag{4.2}$$

the relations (4.1) will become

$$M\delta x_1+m(\delta x_2+\delta x_3)=0$$
$$M\delta y_1+m(\delta y_2+\delta y_3)=0$$
$$a(\delta\dot{y}_3-\delta\dot{y}_2)+\frac{M}{M+2m}b(\delta\dot{x}_2+\delta\dot{x}_3-2\,\delta\dot{x}_1)=0 \tag{4.3}$$

of which the last is obtained by neglecting the terms $\delta x\delta y$ etc. as small quantities of the second order and may also be rewritten as

$$b(\delta x_2+\delta x_3)+a(\delta y_3-\delta y_2)=0 \tag{4.3'}$$

The same equations as these will follow, if we adopt the Eckart's rotating system(14), that is, if we introduce the condition that there is no angular momentum, to the first approximation, relative to the rotating system of coordinates.

So as to get a simpler form of the potential function, it is covenient to use Dennison's displacement coordinates, which are as follows:

$$\xi=\delta x_1-\frac{1}{2}(\delta x_2+\delta x_3)+\frac{b}{2a}(\delta y_3-\delta y_2)$$
$$\eta=\delta y_1-\frac{1}{2}\,\delta y_2+\delta y_3$$
$$\zeta=\delta x_3-\delta x_2 \tag{4.4}$$

The general potential function in terms of these will contain only four constants (since it must be even in the coordinate ξ) and may be assumed to have the form

$$2V=m(\xi)^T(V)(\xi), \tag{4.5}$$
$$(\xi)=\begin{Vmatrix}\xi\\ \eta\\ \zeta\end{Vmatrix}, \qquad (V)=\begin{Vmatrix}\alpha & \cdot & \cdot\\ \cdot & \beta & \delta\\ \cdot & \delta & \gamma\end{Vmatrix} \tag{4.5'}$$

Letting

$$\mu=\frac{2M}{M+2m}, \quad \frac{1}{f}=1+\frac{b^2}{a^2}\frac{\mu}{2}=1+\frac{b^2}{a^2}\frac{M}{M+2m}, \tag{4.6}$$

we find:

$$\delta x_1=\frac{m}{M}(\mu f\xi), \qquad \delta y_1=\frac{m}{M}(\mu\eta)$$
$$2\,\delta x_2=-(\mu f\xi)-\zeta, \qquad 2\,\delta y_2=-(\mu\eta)-\frac{b}{a}(\mu f\xi)$$
$$2\,\delta x_3=-(\mu f\xi)+\zeta, \qquad 2\,\delta y_3=-(\mu\eta)+\frac{b}{a}(\mu f\xi) \tag{4.7}$$

and hence the kinetic energy T, when expressed in terms of ξ, η, and ζ, is given by

$$2T=m(\dot{\xi})^T(T)(\dot{\xi}), \tag{4.8}$$
$$(\dot{\xi})=\begin{Vmatrix}\dot{\xi}\\ \dot{\eta}\\ \dot{\zeta}\end{Vmatrix}, \qquad (T)=\begin{Vmatrix}\mu f & \cdot & \cdot\\ \cdot & \mu & \cdot\\ \cdot & \cdot & \frac{1}{2}\end{Vmatrix} \tag{4.8'}$$

The normal coordinates q_1, q_2, and q_3 may now be introduced by the transformation

$$(\xi)=(\varDelta)(q), \tag{4.9}$$
$$(\varDelta)=\begin{Vmatrix}\delta_{33} & \cdot & \cdot\\ \cdot & \delta_{22} & \delta_{21}\\ \cdot & \delta_{12} & \delta_{11}\end{Vmatrix}, \qquad (q)=\begin{Vmatrix}q_1\\ q_2\\ q_3\end{Vmatrix} \tag{4.9'}$$

by which (T) and (V) should be brought into the forms

$$(\varDelta)^T(T)(\varDelta)=(1) \tag{4.10}$$
$$(\varDelta)^T(V)(\varDelta)=\begin{Vmatrix}\lambda_3 & \cdot & \cdot\\ \cdot & \lambda_2 & \cdot\\ \cdot & \cdot & \lambda_1\end{Vmatrix}. \tag{4.11}$$

The equation (4.10) yields the relations

$$\mu f\cdot\delta_{33}^2=1, \qquad \text{or } \delta_{33}=(\mu f)^{-\frac{1}{2}}$$
$$\mu\delta_{21}^2+\frac{1}{2}\delta_{11}^2=1,$$
$$\mu\delta_{22}^2+\frac{1}{2}\delta_{12}^2=1,$$
$$\mu\delta_{21}\delta_{22}+\frac{1}{2}\delta_{11}\delta_{12}=0. \tag{4.12}$$

from which follow that between the δ_{ij} exist further relations:

$$\delta_{11}^2+\delta_{12}^2=2, \qquad \mu\delta_{21}^2=\frac{1}{2}\delta_{12}^2,$$

$$\delta_{21}^2+\delta_{22}^2=\frac{1}{\mu}, \qquad \mu\delta_{22}^2=\frac{1}{2}\delta_{11}^2,$$

$$\delta_{21}\delta_{11}+\delta_{22}\delta_{12}=0. \tag{4.12'}$$

Although the above four potential constants and accordingly four δ_{ij} can not be determined by the knowledge of three normal frequencies of H_2O, those of D_2O will supply the remaining datum. According to Darling and Dennison their values are given as follows:

$m\alpha=10.672\times10^5$ dynes/cm, $m\gamma=3.1344$
$m\beta=7.1810$ $m\delta=3.1588$
$\delta_{11}=1.14678$ $\delta_{12}=0.82758$
$\delta_{21}=0.43910$ $\delta_{22}=-0.60845$
$\delta_{33}=0.92828$

The normal frequencies are given in terms of the roots $(\lambda_i=4\pi^2 w_i^2 c^2)$ of the secular equation

$$\det.(\lambda T-V)=0 \tag{4.13}$$

which may be expressed as follows:

$$\lambda_1\lambda_2=\frac{2}{\mu}(\beta\gamma-\delta^2)$$

$$\lambda_1+\lambda_2=\frac{\beta}{\mu}+2\gamma$$

$$\lambda_3=\frac{\alpha}{\mu f} \tag{4.14}$$

The equations (4.10) and (4.11) allow us to xpress δ_{ij} in terms of (T), (V), and λ_i as ollows:

$$(\Delta)^T(\lambda T-V)(\Delta)=\begin{Vmatrix}\lambda-\lambda_3 & \cdot & \cdot\\ \cdot & \lambda-\lambda_2 & \cdot\\ \cdot & \cdot & \lambda-\lambda_1\end{Vmatrix} \tag{4.15}$$

ccordingly

$$\lambda_i T-V)((4-i)\text{-th column of }\Delta)=(\Delta)^{TI}\cdot\begin{Vmatrix}0\\0\\0\end{Vmatrix}=0$$

specially for $i=1, 2$

$$\begin{Vmatrix}\lambda_i\mu-\beta & -\delta\\ -\delta & \lambda_i\frac{1}{2}-\gamma\end{Vmatrix}\cdot\begin{Vmatrix}\delta_{2i}\\ \delta_{1i}\end{Vmatrix}=0 \tag{4.16}$$

rom which we get

$$\delta_{1i}=\frac{\delta}{\left[\mu\left(\frac{\lambda_i}{2}-\gamma\right)^2+\frac{1}{2}\delta^2\right]^{1/2}}$$

$$\delta_{2i}=\frac{\frac{\lambda_i}{2}-\gamma}{\left[\mu\left(\frac{\lambda_i}{2}-\gamma\right)^2+\frac{1}{2}\delta^2\right]^{1/2}} \tag{4.17}$$

The moments and products of inertia in the rotating coordinate system defined by Wilson and Howard may now readily be expressed as functions of the displacement coordinates ξ, η, and ζ:

$$I_{xx}=m\left[\mu(b+\eta)^2+\frac{b^2}{2a^2}(\mu f\xi)^2\right],$$

$$I_{yy}=m\left[\frac{1}{2}(2a+\zeta)^2+\mu f^2\xi^2\right],$$

$$I_{zz}=I_{xx}+I_{yy},$$

$$I_{xy}=-m(\mu f\xi)\left(2b+\eta+\frac{b}{2a}\zeta\right),$$

$$I_{yz}=I_{zx}=0 \tag{4.18}$$

The reciprocal angular momenta $\mu_{\alpha\beta}$ which appear in the Hamiltonian function are

$$\mu_{xx}=\frac{I_{yy}}{I_{xx}I_{yy}-I_{xy}^2}, \qquad \mu_{yy}=\frac{I_{xx}}{I_{xx}I_{yy}-I_{xy}^2},$$

$$\mu_{xy}=\frac{-I_{xy}}{I_{xx}I_{yy}-I_{xy}^2}, \qquad \mu_{zz}=\frac{1}{I_{zz}-m\sum Z_k},$$

$$\mu_{yz}=\mu_{zx}=0$$

The Z_k thereof are obtained in the following manner. The only component of the internal angular momenta p_α which does not vanish is p_z and has the value

$$p_z=M\begin{vmatrix}\delta x_1 & \delta y_1\\ \delta\dot{x}_1 & \delta\dot{y}_1\end{vmatrix}+\frac{m}{4}\begin{vmatrix}2\delta x_2 & 2\delta y_2\\ 2\delta\dot{x}_2 & 2\delta\dot{y}_2\end{vmatrix}+\frac{m}{4}\begin{vmatrix}2\delta x_3 & 2\delta y_3\\ 2\delta\dot{x}_3 & 2\delta\dot{y}_3\end{vmatrix},$$

$$=m\cdot\mu f\cdot\begin{vmatrix}\xi & \eta-\frac{b}{2a}\zeta\\ \dot{\xi} & \dot{\eta}-\frac{b}{2a}\dot{\zeta}\end{vmatrix} \tag{4.19}$$

This may be expressed as a function of the normal coordinates; thus

$$p_z=m[(K_1q_3)\dot{q}_1+(K_2q_3)\dot{q}_2+(-K_1q_1-K_2q_2)\dot{q}_3]$$

where

$$K_i=(\mu f)^{\frac{1}{2}}\left(\delta_{2i}-\frac{b}{2a}\delta_{1i}\right) \tag{4.20}$$

It may readily be shown from the relations (4.12′) that $K_1^2+K_2^2=1$. A substitution yields the result that for H_2O, $K_1^2=0.000019$, $K_2^2=0.999981$. The quantity Z_k is the coefficient of $\dot{q}_k$ in the formula for p_z. Thus

$$Z_1=K_1q_3, \quad Z_2=K_2q_3, \quad Z_3=-K_1q_1-K_2q_2,$$

The $\mu_{\alpha\beta}$ may now be expressed as functions of the normal coordinates. We develop them as power series in ξ, η, ζ, and retain no terms beyond the second.

$$m\mu_{xx}=\frac{1}{\mu b^2}\left(1-\frac{2}{b}\eta+\frac{3}{b^2}\eta^2\right)+\frac{3f^2}{2a^2b^2}\xi^2,$$

$$m\mu_{yy}=\frac{1}{2a^2}\left(1-\frac{1}{a}\zeta+\frac{3}{4a^2}\zeta^2\right)+\frac{3\mu f^2}{4a^4}\xi^2,$$

$$m\mu_{zz}=\frac{f}{2a^2}\left[1-\frac{f}{a^2}(\mu b\eta+a\zeta)+\frac{3}{4}\frac{f^2}{a^4}(\mu b\eta+a\zeta)^2\right],$$

$$m\mu_{xy}=\frac{f\xi}{a^2b}\left(1-\frac{3}{2b}\eta-\frac{3}{4a}\zeta\right) \tag{4.21}$$

The last term in the bracket of the expression of $m\mu_{zz}$ may also be written as $\frac{3}{2}\frac{f}{a^2}(K_2q_1-K_1q_2)^2$. It is believed that the results in D. D. contain slight numerical errors: $-\frac{1}{2}$ in the coefficient of q_1q_2 in μ_{33} should be $-\frac{3}{2}$ and $-\frac{3}{4}$ in the coefficient of $\delta_{33}q_3(\delta_{21}q_1+\delta_{22}q_2)$ in μ_{12} should be $-\frac{3}{2}$.

In terms of these $\mu_{\alpha\beta}$, the Hamiltonian of H_2O, when expressed in the Wilson and Howard notation, is written out as follows:

$$\begin{aligned}H=&\frac{1}{2}\sum\mu_{\alpha\alpha}P_\alpha+\frac{1}{2}\mu_{xy}(P_xP_y+P_yP_x)\\&+\frac{1}{2}\mu^{\frac{1}{4}}p_z\mu_{zz}\mu^{-\frac{1}{2}}p_z\mu^{\frac{1}{4}}-\frac{1}{2}(p_z\mu_{zz}+\mu_{zz}p_z)P_z\\&+\frac{1}{2}\sum_{k=1}^{3}\mu^{\frac{1}{4}}p_k\mu^{-\frac{1}{2}}p_k\mu^{\frac{1}{4}}+V\end{aligned} \tag{4.22}$$

As is pointed out in D. D., the quantities in the Hamiltonian, except the first and the last two parts, yield nothing in the first order of approximation, and the terms that contain p_z or μ_{zz} may be neglected; thus

$$H=\frac{1}{2}(\mu_{xx}P_x^2+\mu_{yy}P_y^2+\mu_{zz}P_z^2)+\sum_{k=1}^{3}p_k^2+V(q_1,q_2,q_3) \tag{4.23}$$

We pick up, for the later use, the terms of $\mu_{\alpha\alpha}$ which are linear in ξ, η, and ζ:

$$\begin{aligned}&mb^3\cdot\mu_{xx}:-\frac{2}{\mu}\eta,\\&mb^3\cdot\mu_{yy}:-\frac{1}{2}\left(\frac{b}{a}\right)^3\zeta\\&mb^3\cdot\mu_{zz}:-\frac{f^2}{2}\left(\frac{b}{a}\right)^3\left[\mu\left(\frac{b}{a}\right)\eta+\zeta\right]\\&\left(mb^3\cdot\mu_{xy}:f\left(\frac{b}{a}\right)^2\xi\right)\end{aligned} \tag{4.24}$$

5. Evaluation of the Stretching Effect.

In the first place, an elementary direct derivation of the condition, which specify the centrifugal distortion of the molecule in any rotational state, will be attempted; this might serve to give an essential feature of the problem.

Consider the atom i being in equilibrium relative to a uniformly rotating ($\omega=0$) coordinate system fixed to the molecule. We have then, as the classical condition of balancing of force, the equation

$$+m_i[\omega\times(\omega\times r_i)]=F_i,$$

where F_i may be assumed in our case to be derived from the interatomic potential V. Denoting by δ_iV the variation of V correspondin to δr_i, a virtual displacement δr_i will yiel the equation

$$-m_i(\omega\times r_i)\cdot(\omega\times\delta r_i)+\delta_iV=0,$$

We get therefore

$$-\sum m_i(\omega\times r_i)\cdot(\omega\times\delta r_i)+\delta V=0,$$

from which we would have

$$\delta\left[-\sum\frac{m_i}{2}(\omega\times r_i)^2+V\right]=0$$

under the restriction $\delta\omega=0$.

Since, however, the restriction which mu be imposed in our problem is that the varia tion δP of the total angular momentum shoul vanish and hence

$$\omega\cdot\delta P=\omega\cdot\delta\sum\left[m_i(r_i\times(\omega\times r_i))\right]$$
$$=\delta\left[\sum\frac{m_i}{2}(\omega\times r_i)^2\right]+\sum m_i(\omega\times r_i)\cdot(\omega\times\delta r$$
$$=0,$$

it follows accordingly, as the required cond tion,

$$\delta\left[\frac{m_i}{2}(\omega\times r_i)^2+V\right]=0 \tag{5.1}$$

The first term in the bracket of this equatio forms evidently the pure rotational part o the total energy E and this part will be denote by W in the following discussion.

The so-called stretching effect is, of course, Δ in the *total* energy E caused by the centrifuga distortion, and is made up of a contributio ΔW from the rotational energy and ΔV fro the increased potential energy; $\Delta E=\Delta W+\Delta$ It might generally be found that ΔW is s much negative as to cancel out the incremen ΔV and the resulted ΔE finds itself negative

The present calculation was carried unde the assumption that the molecule is distorte *symmetrically* by the centrifugal force so tha $\xi=0$ in Eq. (4.21). The justification of thi point will be considered later. For the momen we regard E to contain as variables only tw displacement coordinates η and ζ, and accordingly two normal coordinates q_1 and q_2. T and V may then be expanded into the form

$$\begin{aligned}W(q_1,q_2)=&W+q_1W^1+q_2W^2\\&+\frac{1}{2}q_1^2W^{11}+q_1q_2W^{12}+\frac{1}{2}q_2^2W^{22},\end{aligned}$$

$$\begin{aligned}V(q_1,q_2)=&\frac{1}{2}(\lambda_1q_1^2+\lambda_2q_2^2)\\&+(a_1q_1^3+a_2q_2^3+a_3q_1^2q_2+a_4q_1q_2^2)\end{aligned} \tag{5.2}$$

where W^i means $\frac{\partial}{\partial q_i}W(0,0)$ and W^{ij} doe $\frac{\partial^2}{\partial q_i\partial q_j}W(0,0)$.

We are now able to determine the stretching coordinates q_1 and q_2 from the equations

$$W^1+\lambda_1 q_1+[q_1 W^{11}+q_2 W^{12}]$$
$$+[3\,a_1 q_1^2+2\,a_3 q_1 q_2+a_4 q_2^2]=0,$$
$$W^2+\lambda_2 q_2+[q_1 W^{12}+q_2 W^{22}]$$
$$[3\,a_2 q_2^2+a_3 q_1^2+2\,a_4 q_1 q_2]=0 \qquad (5.3)$$

In terms of these q_1 and q_2, $\varDelta E$ can be given as follows:

$$\varDelta E=W(q_1,\ q_2)+V(q_1,\ q_2)-W(0,\ 0)$$
$$=-\frac{1}{2}(\lambda_1 q_1^2+\lambda_2 q_2^2)$$
$$-\frac{1}{2}[q_1^2 W^{11}+2\,q_1 q_2 W^{12}+q_2^2 W^{22}]$$
$$-2[a_1 q_1^3+a_2 q_2^3+a_3 q_1^2 q_2+a_4 q_1 q_2^2] \qquad (5.4)$$

It will make the calculation terribly elaborate to take into account the terms in the above brackets which in general amount merely to small quantities of the second order, so that we neglected them in our approximation. To this order of approximation, the explicit expressions for the stretching coordinates and $\varDelta E$ are readily obtained in the following manner.

The value of the rotational energy $W_{J\tau}$ of a state J_τ is given, according to Wang, by

$$\frac{8\pi^2}{h^2}\cdot W_{J_\tau}=J(J+1)\cdot\mu_+ +\lambda_{J_\tau}(\mu_0-\mu_+), \qquad (5.5)$$

where $\lambda_{J\tau}$ is one of the $2J+1$ roots of the Wang secular determinant and is fully determined by the parameter of asymmetry κ;

$$\lambda_{J_\tau}=f(\kappa), \qquad \kappa=\frac{\mu_-}{\mu_0-\mu_+} \qquad (5.6)$$

We have thereby adopted the abbreviations

$$\mu_+=\frac{1}{2}(\mu_{zz}+\mu_{yy}),$$
$$\mu_0=\mu_{xx},$$
$$\mu_-=\frac{1}{2}(\mu_{zz}-\mu_{yy}) \qquad (5.7)$$

If the differentiation of a quantity ( ) with respect to the normal coordinate q_i is designated by $(\quad)^i$, the following formula is obtained:

$$\frac{8\pi^2}{h^2}W_{J_\tau}^i=J(J+1)\cdot\mu_+^i+\lambda_{J_\tau}\cdot(\mu_0^i-\mu_+^i)$$
$$+\frac{d\lambda_{J_\tau}}{d\kappa}[\mu_-^i-(\mu_0^i-\mu_+^i)\kappa], \qquad (5.8)$$

which will be found convenient to be rewritten as

$$\frac{W_{J_\tau}}{hc}=\frac{h}{8\pi^2 c}$$
$$\cdot\frac{1}{mb^3}\left[J(J+1)\cdot A_i+\lambda_{J_\tau}\cdot B_i+\frac{d\lambda_{J_\tau}}{d\kappa}C_i\right] \qquad (5.9)$$

where

$$A_i=mb^3\cdot\mu_+^i,$$
$$B_i=mb^3\cdot(\mu_0^i-\mu_+^i),$$
$$C_i=mb^3\cdot[\mu_-^i-(\mu_0^i-\mu_+^i)\kappa] \qquad (5.10)$$

and μ_+, μ_0, and μ_- may be obtained from (4.24) and (5.7) as follows:

	$i=1$
$mb^3\cdot\mu_+^i$	$-\frac{1}{4}\left(\frac{b}{a}\right)^3\left[(f^2+1)\delta_{11}+\mu\frac{b}{a}f^2\delta_{21}\right]$
$mb^3\cdot\mu_0^i$	$-\frac{2}{\mu}\delta_{21}$
$mb^3\cdot\mu_-^i$	$-\frac{1}{4}\left(\frac{b}{a}\right)^3\left[(f^2-1)\delta_{11}+\mu\frac{b}{a}f^2\delta_{21}\right]$
	$i=2$
$mb^3\cdot\mu_+^i$	$-\frac{1}{4}\left(\frac{b}{a}\right)^3\left[(f^2+1)\delta_{12}+\mu\frac{b}{a}f^2\delta_{22}\right]$
$mb^3\cdot\mu_0^i$	$-\frac{2}{\mu}\delta_{22}$
$mb^3\cdot\mu_-^i$	$-\frac{1}{4}\left(\frac{b}{a}\right)^3\left[(f^2-1)\delta_{12}+\mu\frac{b}{a}f^2\delta_{22}\right]$ (5.11)

From these, we can find the values of A_i, B_i, and C_i:

	$i=1$	$i=2$
A_i	-0.21942	-0.09551
B_i	-0.27501	0.78064
C_i	0.00159	0.22443
D_i	0.78590×10^{-2}	4.20416×10^{-2}
$\varDelta_i$	-2.02705×10^{-3}	-7.13015×10^{-3}

where the values of other quantities D_i and $\varDelta_i$ are also given, which will shortly be introduced.

The potential function V is known in full account owing to the Darling and Dennison's elaborate analysis;

$$\frac{V}{hc}=\frac{1}{2}(\omega_1\bar{q}_1^2+\omega_2\bar{q}_2^2+\omega_3\bar{q}_3^2)+(\alpha_1\bar{q}_1^3+\alpha_2\bar{q}_2^3$$
$$+\alpha_3\bar{q}_1^2\bar{q}_2+\alpha_4\bar{q}_1\bar{q}_2^2+\alpha_5\bar{q}_1\bar{q}_3^2+\alpha_3\bar{q}_2\bar{q}_3^2)$$
$$+(\beta_1\bar{q}_1^4+\beta_2\bar{q}_2^4+\beta_3\bar{q}_3^4+\beta_4\bar{q}_1^2\bar{q}_2^2$$
$$+\beta_5\bar{q}_1^2\bar{q}_3^2+\beta_6\bar{q}_2^2\bar{q}_3^2) \qquad (5\cdot12)$$

where the $\bar{q}_i$ are the dimensionless coordinates describing the normal vibrations and are related to the normal coordinates q_i by

$$\bar{q}_i=2\pi[mc\,\omega_i/h]^{1/2}\cdot q_i\,;$$

and the values of the potential constants ω, α, and β are as follows:

$\omega_1=3825.32\ \mathrm{cm}^{-1}$,	$\alpha_1=-322$,	$\alpha_4=+216$,
	$\beta_1=+39$,	$\beta_4=-116$.
$\omega_2=1653.91\ \mathrm{cm}^{-1}$,	$\alpha_2=-47$,	$\alpha_5=-909$,
	$\beta_2=+2$,	$\beta_5=+212$.
$\omega_3=3935.59\ \mathrm{cm}^{-1}$,	$\alpha_3=+1$,	$\alpha_6=+160$,
	$\beta_3=+35$,	$\beta_6=-108$.

In our calculation, however, only the quadratic terms of V were retained. Noting that

$$\frac{1}{hc}\frac{\partial V}{\partial q_i}=2\pi[mc\,\omega_i^3/h]^{1/2}\cdot\bar{q}_i\,,$$

we have the explicit expressions for the stretching coordinates $\bar{q}_i$ that specify the centrifugally stretched shape of the molecule:

$$\bar{q}_i=\Delta_i\cdot[J(J+1)A_i+\lambda_{J_\tau}B_i+\lambda_{J_\tau}'C_i] \tag{5·13}$$

where

$$\Delta_i=-\frac{1}{2}\left[\frac{h}{4\pi^2c}\frac{1}{mb^2\omega_i}\right]^{3/2}$$

And the depression of energy due to the stretching is given by

$$\Delta E=-\frac{1}{2}(\omega_1\bar{q}_1^2+\omega_2\bar{q}_2^2)$$
$$=-\sum_{i=1}^{2}D_i\cdot[J(J+1)A_i+\lambda_{J_\tau}B_i+\lambda_{J_\tau}C_i]^2 \tag{5·14}$$

where

$$D_i=\frac{1}{2}\omega_i\Delta_i^2$$

Some of the numerical results appear in Tabl III in the following form. The third colum gives the vlues of $-\Delta E$ as determined fron the above formula (5.14), while the fourt column shows the differences $-\delta W$ betwee the experimental and theoretical energy level as calculated from the rigid rotator formul (5.5). A good agreement of the values in thes two columns indicates that we can procee further to obtain with greater precision th true moments of inertia of the molecule b treating the rotational stretching effect as i the present attempt.

The list of the physical constants used is a follows:

$h=6.624\times10^{-27}$g.cm^2. sec^{-1}. $c=2.99777\times10^{10}$cn

$m=1.6734\times10^{-24}$g. $\frac{m}{M}=\frac{1.00813}{16.00000}$

OH$=0.9580\times10^{-8}$cm. $2\arctan\frac{a}{b}=104°31'$

For assisting the numerical work, the write is grateful to Miss A. Asakawa, T. Mikosib and K. Nakamura.

Anomalies in Electron-Diffraction Debye-Scherrer Ring.

by Goro HONJO

Kobayasi Institute of Physical Research, Kokubunzi, Tokyo, Japan.

(Read. October 22. 1946; Received June 23, 1947)

§ 1 Introduction

It is well known that the effect of the inner potential of the crystal appears in the electron diffraction pattern through the refractive index μ, which is given by the relation

$$\mu=\sqrt{1+\frac{\Phi_0}{E}}$$

where Φ_0 is the mean inner potential of the crystal and E, the potential accelerating the electron beam. If we write

$$\mu=1+\delta$$

the quantity δ, which may be called the "unit increment of the refractive index", can be written as

$$\delta=\frac{\Phi_0}{2E}$$

for fast electrons.

The order of its magnitude being $1^{-3}\sim10^{-4}$ for fast electrons, its effect has been used to be neglected, except for the grazing incidence of the beam to the crystalline surface.

Recently Hillier and Baker,⁽¹⁾ and independently Sturkey and Frenel,⁽²⁾ however, observed anomalous separations in (111)-, (220)- and other rings of electron-diffraction Debye-Scherrer patterns due to MgO and CdO smoke. The latters interpreted these anomalies as an effect of the refraction of electrons at crystalline surfaces of the smoke particles.

To confirm and extend this interpretation, the present author investigated these phenomena in further detail.

§ 2 Experimental Results

Apparatus used was an electron-diffraction camera with the camera length L about 18 cm. The accelerating potential was about 40 K. V. The smoke samples of MgO and Sb_2O_3 were studied. The smoke was prepared by igniting the metal powder in air and was deposited on a fine mesh, which was subjected to electron diffraction.

MgO: The photograph obtained for MgO is represented in Phot. 1 and corresponding spacings of MgO are tabulated in Table I, in which the two spacings assigned to one ring are to show the ring broadening under the condition of $L\fallingdotseq180$ mm and $E\fallingdotseq3.97\times10^{+}$ volts.

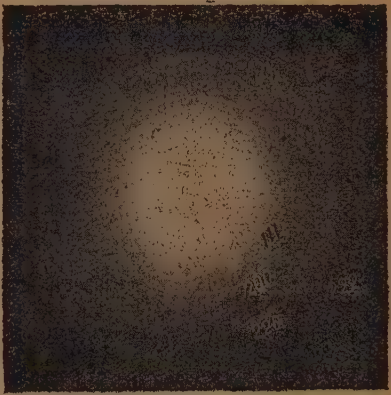

Photo 1. MgO

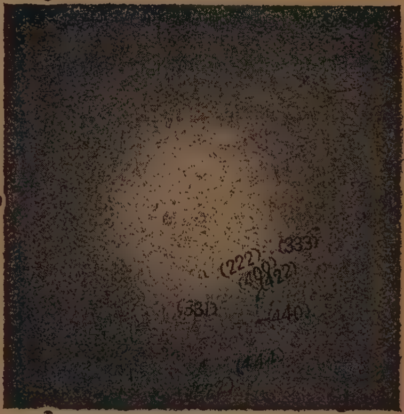

Photo 2. Sb_2O_3

Sb_2O_3: As oxides of Sb, there are known Sb_2O_3, Sb_2O_4 and Sb_2O_5, which are all isomorphous and differing from each other only slightly in their lattice dimensions. Through a precise measurement of the spacings by a simultaneous photograph of Au-pattern as the reference, however, it became certain that the smoke should be Sb_2O_3. The photograph is represented in Phot. 2 and the data of spacings are tabulated in Table II, which are obtained when $L=185$ mm and $E=4.33\times10^4$ volts.

Table I MgO

h k l	d x-ray	d obs.
111	2.426	2.463 2.400
200	2.101	2.101
220	1.486	1.506 1.475
222	1.213	1.221 1.207
400	1.050	1.052

Table II Sb_2O_3

h k l	d x-ray	d obs.
222	3.212	3.198
400	2.783	2.803 2.691
331	2.556	2.541
422	2.274	2.248
333	2.141	2.128
440	1.966	1.980 1.923
444	1.606	1.602

Observing these photographic plates under a comparator microscope, notable fine structures characteristic of each ring were revealed. Superposed on the continuous intensity of the somewhat broadened ring, there appeared spots showing a peculiar distribution.

Each of these spots is considered to come from a certain single particle in the smoke. In Fig. 4 and 5, typical patterns of this fine structure were sketched for MgO and Sb_2O_3, respectively. The numerical figures inscribed in these diagrams, show the distances Δr in mm. between these spots on the photographic plate.

In these observations it was noted that the distributions of the spots and the general broadening of the rings occured on both sides of the normal "Bragg point".

As the former observers did, it seems quite natural to consider that such a deviation of reflection from the Bragg point is caused by the refractions of electrons at crystalline faces bounding crystallites of smoke particles.

The magnitude of the deviations convinces us that the refraction concerned is one corresponding to comparatively larger glancing angle.

§ 3 General Consideration

In Fig. I, XX′ indicates the electron beam. XYZ represents the boundary plane of a crystallite through which the electron beam enters into the body of the crystallite, and X′YZ, another boundary through which the electron beam leaves the crystallite. XOY is the ne plane concerned, and OZ, its normal. OA an OA′ are the normals to XYZ- and X′YZ-plan drawn from O, A and A′ being their feet. The lines ZA and ZA′ meet the net plane at the points B and B′ respectively. Writing XOB= φ, BOB′=Λ, AOB=α and A′OB′=α', then α α' and Λ are angles which are to be deter mined in connection with the habit of the crystallite and the net plane concerned.

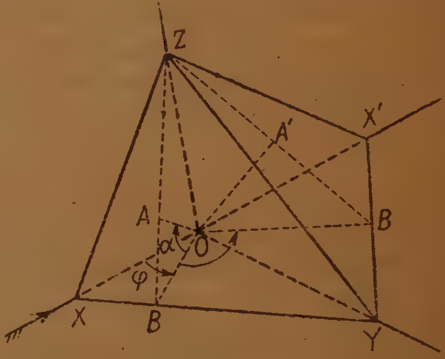

Fig. 1.

Since it is anticipated, as mentioned above that only the refraction corresponding to the larger glancing angle of electron beam against the boundary takes the important parts of the phenomena, the Bragg anale is neglected in our present considerations. The angle C between XX′ and OA, that is the angle of the incidence of the beam against the surface XYZ, can be calculated by the equation

$$\cos C=\cos\alpha\cdot\cos\varphi$$

The angular deviation Δ_A due to the refractio at the entrance surface XYZ can be written as

$$\Delta_A=\delta\tan C$$

and it occurs within the plane XOA. Th corresponding displacement of the spot fro the Bragg point on the photographic plat may be regarded as a vector from the Bragg point with the magnitude $\Delta_A L$ in the directio of the intersection of XOA and the plate where L is the camcra length.

The beam thus entered into the crystallin body should suffer in turn one more refractio at the excit plane X′YZ, which results in a angular deviation

$$\Delta'_A=\delta\tan C'$$

where C' is the angle of emergence of electro

---

* If we denote the angle of refraction by C'', the $C''=C-\Delta_A$. Following the Snell's law, $\sin C=(1+\delta)$ $\sin C''$, and neglecting the higher order term of δ an Δ_A, it follows that $\Delta_A=\delta\tan C$.

from the exit plane. In our present apporximation, this angle can also be calculated by the following relation

$$\cos C' = \cos\alpha' \cos(\varphi + \Lambda).$$

The corresponding displacement of spot from the Bragg point on the photographic plate may be regarded as a vector of the mangnitude $\Delta'_{A}L$ in the direction of the intersection of XOA′ and the plate.

In this way, the resultant of the refraction effect due to the boundary surfaces upon the electron beam of a certain path can be deduced, by calculating the angular deviations Δ_A and Δ_A' at the entrance and the exit surface respectively and adding them vectorially, if the geometrical relations of the boundaries to the net plane and the azimuthal angle are known.

The orientations of crystallites in the powder specimens are at random, so that φ takes arbitrary values. The deviated spot traces a locus for varying φ. In the crystallite of a certain external shape, there are in general several pairs of the entrance and the exit surface, and correspondingly a set of loci can be considered. In Fig. 2 and Fig. 3 such loci are shown for crystallites of the cubic and octahedral habit respectively, in which the angular deviations are represented in the unit of the unit increment δ of the refractive index. In these figures the angle φ are referred to a paticuler one of its boundaries.

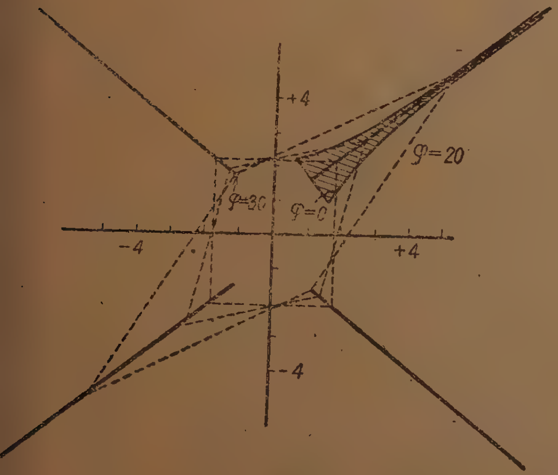

Fig. 2a Cubic habit (111)-reflection.

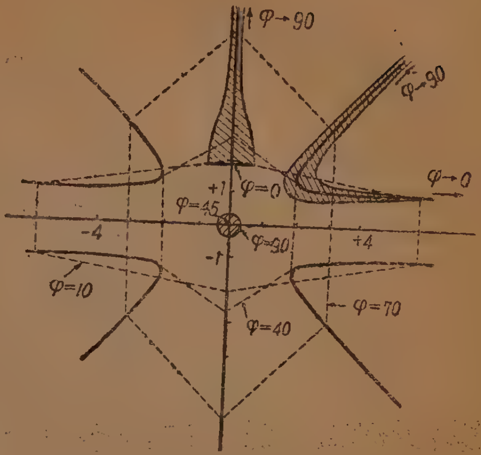

Fig. 2b Cubic habit (110)-reflection.

The origins of these figures correspond to the Bragg point. By the refraction effects, the diffracted beam in general deviates from this point, and separates into a group of several points, each of which lies on one of the loci. In the figures, the points corresponding to the same value of φ are connected with a dotted line.

The intensity of a deviated reflection depends on the effective cross section of the boundary surface against the beam, and the path length of the beam in the crystallite. The former effect can be roughly estimated simply by the geometrical consideration. The width attached to one of equivalent loci in Fig. 2 and Fig. 3 indicates the intensity weight supposed by such

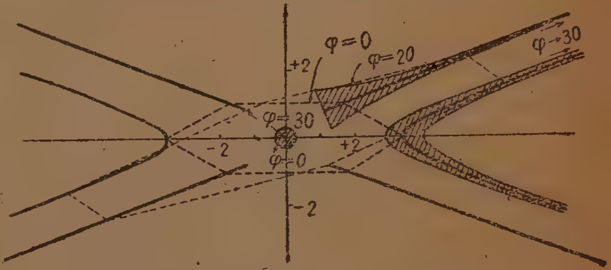

Fig. 3a Octahedral habit (111)-reflection.

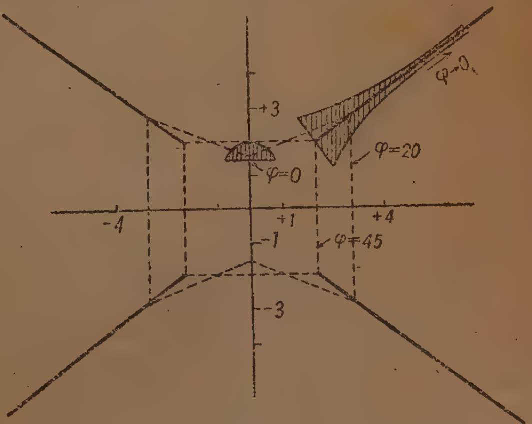

Fig. 3b Octahedral habit (100)-reflection.

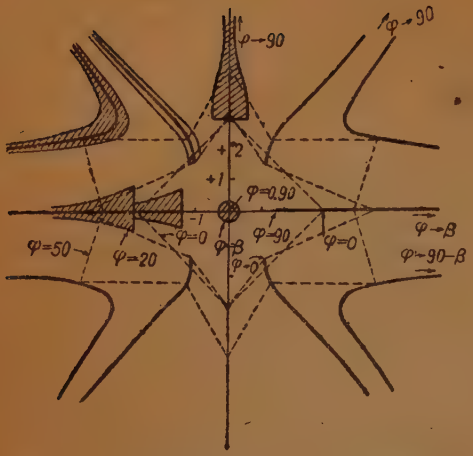

Fig. 3c Octahedral habit (110)-reflection.

consideration.

As to the effect of the path length the matter is more complicated. But it is safe to say, that the absorption of electron may be most pronounced for the beam corresponding to the Bragg point, on account of the longest path length in the crystallite. The other parts of the figures, however, may affected only little by this absorption effect, because for other beams there are always some short paths through edge corners of crystallite.

As to the case in which the glancing angle of the beam to the surface becomes comparable with Bragg angle θ, the following consideration should be mentioned: In this case, the deviation due to the refraction may be larger than that hitherto considered. For suc an incident beam, however, the effective cros section of the surface is so small that th corresponding reflection may be of vanishingl weak intensity.

To understand the whole nature of the refractiton effects of the crystalline surface o electron-diffraction Debye-Scherrer rings, th total probability with which the deviate beams fall on various regions on the loc should be considered. This probability, bein proportinal to the two factors above mentione is, moreover, inversely proportional to $\frac{ds}{d\varphi}$ where ds means the line element on the loci The latter factor is the largest in the regio where the weight factor of cross section i the largest, and decreases gradually from her quite parallel to this factor. Accordingly, th probability density along each locus is roughl similar to that of the weight fator of cros section which is assigned in Fig. 2 and 3, bu may be more exaggerated by the new facto Therefore, with the most parts of their probability, the deviated spots may fall on som restricted regions on the loci, which are i general the positions on each locus neares to the origin. Corresponding to these restricte regions, the Debye-Scherrer rings separate int multiplets, and spots due to single crystallit take frequently the characteristic distributio such as Fig. 4 and 5.

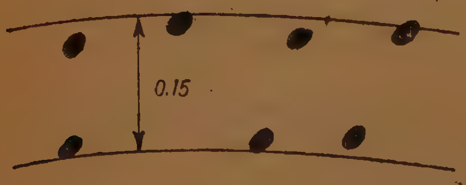

Fig. 4a MgO (111), (222)

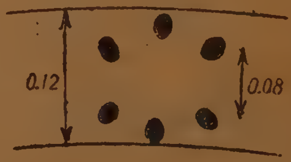

Fig. 4b MgO (220)

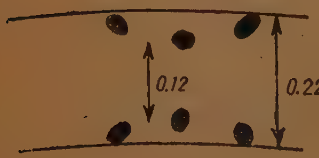

Fig. 5a Sb_2O_3 (400)

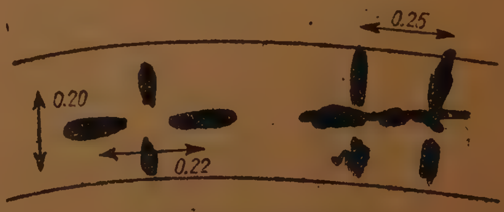

Fig. 5b Sb_2O_3 (440)

§ 4. Comparison with Experiment

Following above consideration, the distances Δr between the spots in Fig. 4 and 5 can be related to the unit increment δ and camera length L by the expression

$$\Delta r = \delta \cdot s \cdot L,$$

where s is a factor which indicates the angular distance between the regions of maximum probability in Fig. 2 and 3, measured by the unit increment δ. The correspondence between Δr in Fig. 4 and 5 and s of Fig. 2 and 3 are tabulated in Table III. From this relation, δ and accordingly the mean inner potential Φ_0 can be calculated.

Table 3.

Substance	Index of Ring	s	$\Delta\gamma$ in mm	Φ_0 in volt
MgO	(111)	$s=5.4$	0.15	12.2
	(222)	$s=5.4$	0.14	11.4
	(220)	$s_1=3.6$	0.08	9.8
	(220)	$s_2=8.0$	0.19	10.5
		Mean		11 volt
Sb_2O_3	(400)	$s_1=3.4$	0.12	16.5
	(400)	$s_2=5.3$	0.22	19.4
	(440)	$s_1=6.7$	0.20	13.9
	(440)	$s_2=7.0$	0.22	14.7
	(440)	$s_3=8.0$	0.25	14.6
			Mean v	16 volt

MgO:—It is sure that particles in MgO smoke possess the cubic form, which is the well-established fact in electron-microscopic works. Assuming this form, the experimental observations on MgO are well understood. The marked sharpness of (200)-ring is explained when we consider the fact that the reflecting net planes are parallel or rectangular to the boundaries of crystallite, so that deviations of beam by the refraction effect always occur in the tangential direction to the Debye-Scherrer ring. The well-defined separation of (111)-and (222)-rings into doublets may also be understood from Fig. 2a. The correspondence between the spots on (220)-ring (Fig. 4b) and Fig. 2b is clear. (In our experiment the Bragg point did not appear on account of absorption effect.) The separation of this ring into a quintet, which was first observed by Hillier and Baker, is explained by this figure.

The value 11 volts obtained for the mean inner potential of MgO agrees well with the value 12 volt of Sturkey and Frenel, and is reasonable when compaired with the value 10 volt predicted from a theoretical consideration.(3)(4)

Sb_2O_3:—One of our chief interests was to examine a supposition that the Sb_2O_3 smoke have the octahedral crystal habit, which came into our mind from the Miyake's work of Sb_2O_3 formed on stibnite.(5) This supposition was verified quite well, as is seen from the correspondence between Phot. 2, Fig. 5 and Fig. 3. Also the agreement of our value 16 volts with that of Miyake's 17 volts for the mean inner potential is satisfactory. It sould be mentioned here that the (222)-ring, which is due to the net plane having the same indices as the crystalline boundary, is considerably well defined, but is not so sharp as that of (200)-ring of MgO. This is because of the fact that in the octahedron the surfaces are not exactly rectangular to each other on the contrary to the case of the cube. These facts are also understood from Fig. 3a.

§ 5. Conclusion

The fine structures in the electron-diffraction Debye-Scherrer ring due to smoke samples was understood very well by attributing a particular crystalline form to the smoke particles and assuming the refraction effect of the surfaces. Using this phenomenon, it is possible to infer the crystalline habit of the powder specimen. And further, when the crystalline habit are known, the mean inner potential of the crystals can be deduced, even if large single crystal with flat surfaces can not be obtained. Although, as is seen from our discussion, its very precise measurement can not be expected on account of the nature of the phenomenon itself.

In conclusion, the author wishes to express his sincere thanks to Dr. S. Miyake for his useful advices and encouragements.

Reference

(1) Hillier and Baker: Phys. Rev. 68 (1945) p. 98

(2) Sturkey and Frenel: Phys. Rev. 68 (1945) p. 56

(3) S. Miyake: Proc. of Physico-Math. Soc. Jap. 22 (1940) p. 666

(4) H. Kawamura and K. Hirano: Proc. of Physico-Math. Soc. Jap. 24 (1942) p. 211

(5) S. Miyake: Sc. Pap. I.P.C.R. Jap. 34 (1938) p. 565

On the Sticking Probability of Fast Neutron in the Nuclear Reactions*

By

Toshinosuke MUTO and Mokitiro NOGAMI.

(Institute of Science and Technology, Tokyo University and Physical Institute, Faculty of Science, Kyusyu University.)

(Received July 1, 1947)

§ 1. Sticking Probability

When our considerations are restricted to nuclear reactions of fast particles, for example, to the case of the collision of fast neutrons with heavy nuclei, we are always allowed to disregard resonance effects and other features due to the properties of individual nuclear states on account of the extremely small distance between the energy levels of the highly excited nuclei, compared with the possible spread of relatively homogeneous beam of incident neutrons. As shown in the theoretical consideration by Bohr and others,(1) therefore, the statistical informations of these nuclear reactions may be obtained by averaging the nuclear cross section over the mentioned quantum states of approximately equal energy and then nuclear reaction may be considered to take place in two well-separated stages; the formation of a compound nucleus from an initial nucleus and an incident particle and the subsequent disintegration of the compound nucleus into a residual nucleus and an ejected particle. These states of affairs enable one to express the effective cross section $\sigma(E_0)$ of nuclear reaction in the following way.(2)

$$\sigma(E_0)=\sigma_f(E_0)\cdot\omega_a(E), \qquad (1)$$

where $\sigma_f(E_0)$ expresses the cross section of the formation of a compound nucleus, E_0 the energy of incident particles, $\omega_a(E)$ the probability of a definite mode of disintegration taking place in the second stage, and E the average energy of quantum states of a compound nucleus concerned in the mentioned nuclear reactions. Furthermore, $\omega_a(E)$ may be expressed by the transition probabilities $\Gamma_a/\hbar$ for the process that the compound nucleus excited to the energy E makes transition into the residual nucleus, an ejected particle a' of a definite kinetic energy.

$$\omega_a(E)=\Gamma_a/\sum_{a'}\Gamma_{a'}, \qquad (2)$$

where the summation extends over all mod
of disintegrations from the compound nucleu
As theoretically shown by the "detailed ba
ance" consideration of Weisskopf,(3) it is po
sible to give an expression for Γ_a as a functio
of the effective cross section $\sigma^{(l)}_{a\alpha}(E_a)$ co
rsponding to the reverse process, i. e., of th
mean cross section $\sigma^{(l)}_{a\alpha}$ for the collision of
neutron of energy E_a with a residual nucle
in a state α producing a compound nucle
with an angular momentum $l\hbar$.

$$\therefore \Gamma_a=$$

$$\sum_{l,\alpha}\Gamma^{(l)}_{a,\alpha}\doteqdot\sum_{l,\alpha}\frac{(2s+1)(2i+1)}{\omega_c(E)}\frac{mE_a}{\hbar^2\pi^2}\sigma^{(l)}_{a,\alpha}(E_a), \qquad (3)$$

where $s\hbar$ and $i\hbar$ denote spin angular moment
of a particle a and a residual nucleus respe
tively, m the mass of an ejected particle a
$\omega_c(E)$ the state density of a compound nucle
corresponding to the energy E, which can
approximately computed for a suitable choi
of nuclear model. Thus, the relative probabili
$\omega_a(E)$ in (1) is able to be calculated theoret
cally through a detailed knowledge of the cro
section of the formation of a compound nucle
$\sigma^{(l)}_{a,\alpha}(E_a)$.

In a similar way of consideration to that
the condensation phenomena of molecules
solids, the cross section of the formation of
compound nucleus can be written as(4)

$$\sigma_f(E)=F(E_0)(E_0)\cdot\xi_a(E), \qquad (4)$$

where $F(E_0)$ is the penetration probability
the incoming particle into the nuclear surfa
which becomes approximately the classical lim

---

* Although the computation of this note was alrea
completed in October, 1943, the publication of t
content has beed delayed owing to the unfovoura
wartime condition.

πR^2 for de Broglie wave length small compared with the nuclear radius R, and $\xi_a(E_0)$ is the so-called sticking probability of the particle. The splitting of $\sigma_f(E)$ into the mentioned two factors can be approximately permitted in an attempt to distinguish between the well-known part of the collision process which takes place outside of the nucleus and the unknown part inside. Since the penetration probability $F(E_0)$ through the field outside the nucleus can be easily computed⁽⁵⁾ by using the wave function of an incident particle over the nuclear surface, we have here as the only unknown factor the sticking probability $\xi_a(E_0)$, a direct calculation of which is impossible on account of our lack of knowledge of the interior of nucleus at the present stage of the nuclear physics. By a qualitative consideration of the nuclear cross section, however, the sticking probability may be supposed to increase from zero to one with the energy of incident particle in a rough agreement with the experimental observation with fast particles.

In view of the inaccurate knowledge about the sticking probability in spite of its importance in the process of nuclear reaction, we have here attempted to evaluate numerically the energy-dependences of the sticking probabilities by making use of the experimental results of (n, n) nuclear reaction, which have been actually observed by Aoki,⁽⁷⁾ using relatively homogeneous beam of D-D neutrons. Although Weisskopf and Ewing⁽⁸⁾ have already tried the empirical determination of the sticking probability by the use of the observed data of (p, n) reactions, their method of evaluation is easily found to involve some disagreeable ambiguities on account of the substitution of the relation $\xi_n(E)\sim 1$ into the theoretical cross section of (p, n) reactions,[+] which unsatisfactory point can easily be removed in our case as follows.

§ 2. Method of Determination of the Energy-Dependences of Sticking Probabilities.

According to the dispersion theory of nuclear reactions,⁽⁹⁾ the total absorption of fast neutron by heavy nuclei, as measured by the decrease in the intensity of a collimated beam of fast neutrons when passing through matter, will be determined by the mean cross section averaged over an energy region large compared with the level spacing, namely,

$$\sigma_t(E_n)=\left\{\frac{\pi}{k^2}\sum_{l=0}^{\infty}(2l+1)P^{(l)}_{(kR)}\right\}\xi_n(E_n)+\sigma_{\text{pot}}(E_n), \tag{5}$$

where the first term represents the cross section of the formation of a compound nucleus initiated by the fast neutron impact, the penetration probability $F_n(E_n)$ in (4) being given an explicit expression in the above equation, the second one the cross section for potential scattering and the mixed terms due to interference of potential scattering and resonance elastic scattering are easily seen to vanish upon averaging over a available energy interval. Further, $\xi_n(E_n)$ denotes the sticking probability of a neutron with energy E_n, $k^2=\frac{2m}{\hbar^2}E_n$ (m=mass of a neutron), and R the nuclear radius, being approximately expressed by the well-known relation $R=r_0\sqrt{A}$, A=mass number). Although the values of r_0 have been determined by several authors⁽¹¹⁾ using various kinds of experimental evidences, Landau-Bohr's value⁽¹²⁾ of $r_0=1.75\times10^{-13}$ cm is used in the present computation since the value seems to be reasonable from the theoretical viewpoint.

$$P^{(l)}{}_{(kR)}=\frac{2}{\pi kR}\left|H^{(1)}_{l+1/2}(kR)\right|^2, \tag{6}$$

where $H^{(1)}_{l+1/2}(x)$ expresses the Hankel's function of the first kind. According to Bethe's discussion about a reasonable convergence of the perturbation expansion, we shall here adopt the repulsive potential model in the computation of $\sigma_{\text{pot}}(E_n)$, which may be written as

$$\sigma_{\text{pot}}(E_n)=\frac{4\pi}{k^2}\sum_{l=0}^{\infty}(2l+1)\left|A_l(k,k';R)\right|^2, \tag{7}$$

$$A(k,k';R)$$
$$=\frac{k'J_{l+1/2}(kR)I'_{l+1/2}(k'R)-kJ'_{l+1/2}(kR)I_{l+1/2}(k'R)}{kI_{l+1/2}(k'R)H^{(1)}_{l+1/2}(kR)-k'I'_{l+1/2}(kR)H^{(1)}_{l+1/2}(k'R)} \tag{7'}$$

where $k'^2=\frac{2m}{\hbar^2}(V_0-E_n)$, V_0=the potential height of model, $J_{l+1/2}(x)$ and $I_{l+1/2}(x)$ express Bessel functions of real and imaginary variables respectively, the same functions with dashes being their derivatives with respect to x. When the experimental values of the absorption cross section are substituted into the left hand side of (5), and further both the penetration probability and the cross section for potential scatter-

---

[+] $\frac{\sigma(\text{obs.})}{\sigma(\text{theory})}=\xi_p$

ing can be evaluated numerically for reasonable values of V_0, using (6) and (7), we are able to determine immediately the sticking probability $\xi_n(E_n)$ in accordance with the equation (5), which procedure shall be adopted in the present computation. The only available experimental data for the total absorption by heavy nuclei of homogeneous neutron beam are due to Aoki(13) who measured the mentioned total absorption of relatively homogeneous D-D neutrons for many elements, their energies ranging from 2.25 Mev to about 3 Mev according to the angle of ejection in the D-D nuclear reaction. The results of computation are described in Figures 1-10 in which the energy dependences of the sticking probabilities $\xi_n(E_n)$ for $V_0=10$ Mev, 15 Mev. 20 Mev, 30 Mev, and 40 Mev have been determined respectively.

§ 3. Discussion of the Results

Since the application of the statistical formula for neutron impacts in (5) is restricted to heavy elements ($A \lesssim 50$) and to bombarding energies larger than 1 Mev, the results for $A<50$ may be considered to be less reliable compared with those for $A>50$. Furthermore, since the isotope separation of various elements has not been attempted in the absorption measurement mentioned above, the results for $\xi_n(E_n)$ are to be understood to represent the average behaviours of $\xi_n(E_n)$ for element except for $^{209}Bi_{83}$, $^{56}Fe_{26}$, $^{32}S_{16}$, $^{31}P_{15}$ and $^{29}Al_{13}$ which are known to have no isotope or one isotope with predominant abundance.

As was expected on the general grounds, the sticking probabilities here computed are clearly seen to increase with neutron energies with the more or less amount of fluctuations characteristic of each element. Moreover, as seen in the figures, the values of $\xi_n(E_n)$ are found to become of the order of 0.20 or less for neutron energy of 2.9 Mev, which appears to be rather small compared with the usually adopted ones(14) of $\xi_n(E_n)$, roughly guessed without direct calculations. The difference
between both values is evidently ascribed t
the larger penetration probability in (5) tha
the classical limit πR^2 even for the neutro
energy of about 3 Mev, the classical value bein
adopted usually without careful examinatio
in many nuclear reactions. In this connec
tion it should be pointed out that the assumptio
of the penetration probability being equal t
πR^2 leads to the sticking probability of $\xi_n >$
for E=2.9 Mev and $^{120}Sn_{82}$, which result is quit
disagreeable on the theoretical viewpoint. Sinc
the results obtained above are valid only fo
the high speed neutron energies of 2 Mev c
more, it is highly desirable for the genera
discussion of the nuclear reactions to get a
information about ξ_n for the intermediate an
lower neutron energies in which the availabl
experimental observations are now lacking.

Refereces.

1) Bohr and Kalckar: K. Dans. Vid. Sel. **24** (1937) 1
Landau: Phys. ZS. Sowj. U. **11** (1937), 556.
Konopinski and Bethe: Phys. Rev. **54** (1938), 13
Bethe: Rev. Mod. Phys. **9** (1937), 69.

2) Bohr and Kalckar: loc. cit.
Frenkel: Phys. ZS. Sowj. U. **9** (1936), 533.
Weisskopf: Phys. Rev. **52** (1937), 295.
Weisskopt and Ewing: Phys. Rev. **57** (1939), 47
3) Weisskopt: loc. cit.
4) Bethe: loc. cit.
5) Kapur and Peierls: Proc. Roy. Soc. A **166** (1938
277.
Weisskopf and Ewing: loc. cit.
6) Bethe: loc. cit.
7) Aoki: Proc. Phys. Math. Soc. Japan, **21** (1939
232.
8) Weisskopt and Ewing: loc. cit.
9) Bethe: loc. cit. Weissyopf and Ewing: loc. ci
10) Kapur and Peierls: loc. cit. Weisskopf and Ewin
loc. cit.
11) Bethe: loc. cit. Phys. Rev. **54** (1938) 436.
Barkas: Phys. Rev. **55** (1939) 691.
Wigner: Phys. Rev. **56** (1939) 519.
Landau: Kalckar: loc. cit.
12) Landau: loc. cit.
13) Aoki: loc. cit.
14) Bethe: loc. cit.

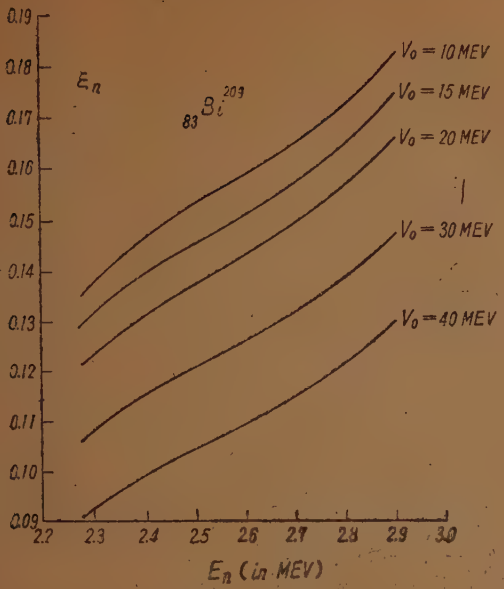

Fig. 1

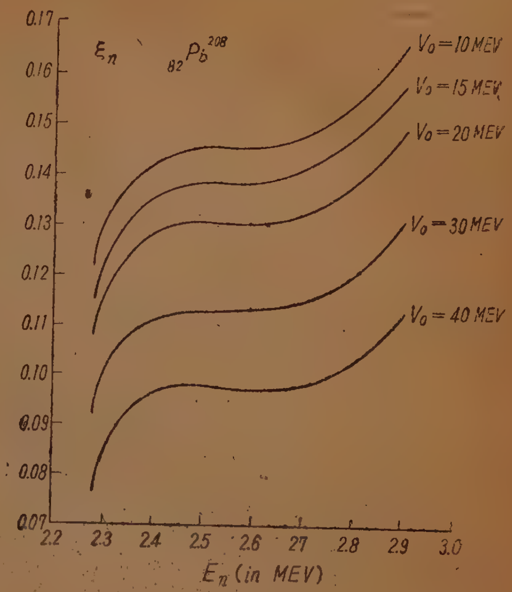

Fig. 2

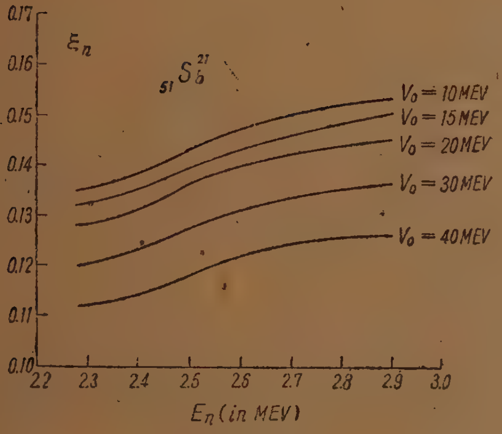

Fig. 3

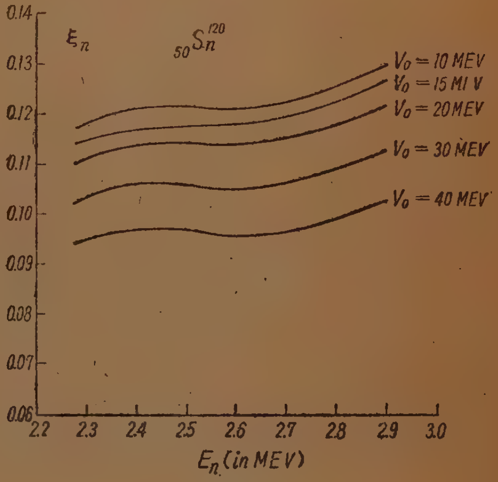

Fig. 4

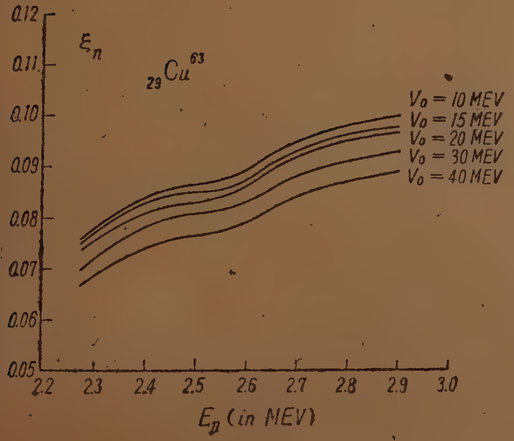

Fig. 5

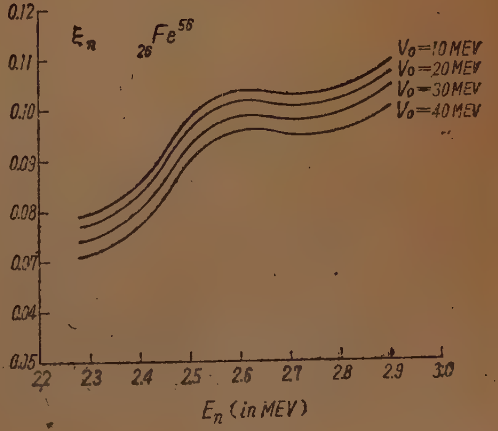

Fig. 6

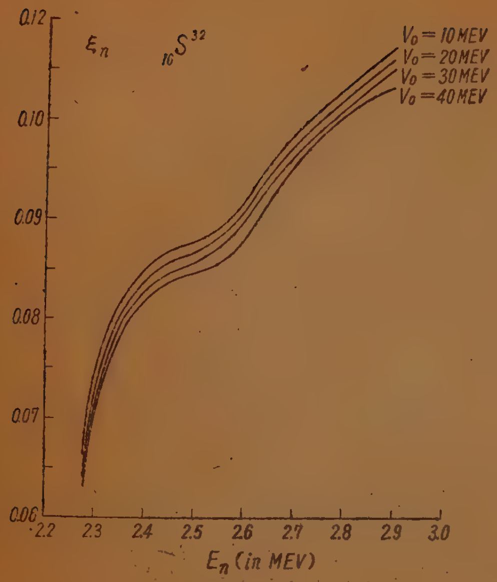

Fig. 7

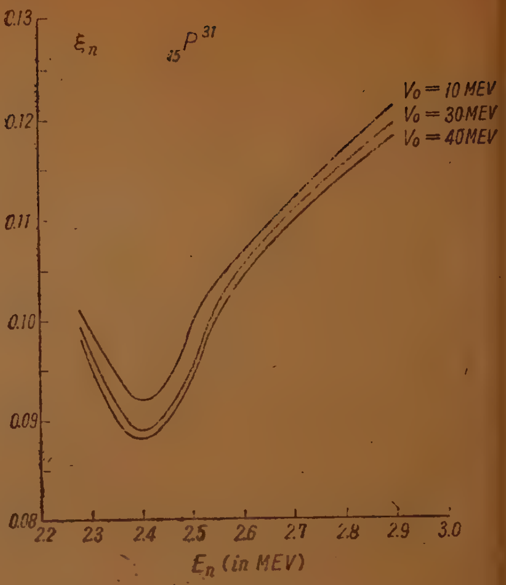

Fig. 8

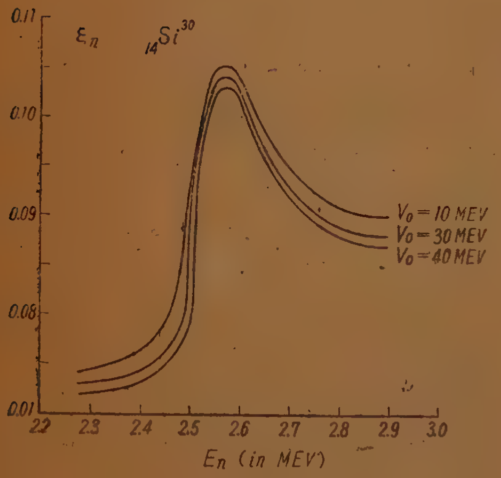

Fig. 9

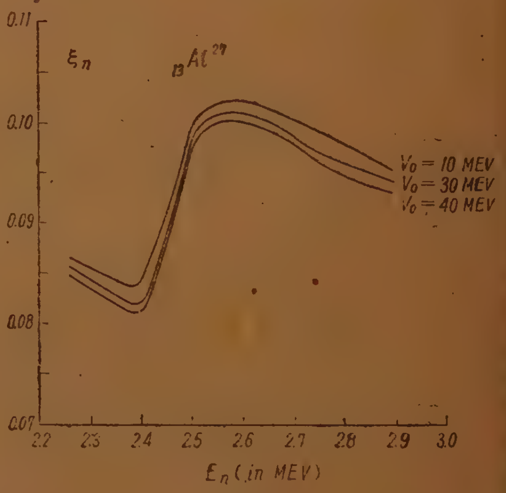

Fig. 10

The Graphical Calculation of Solar Radiation at the Earth's Surface.

Part I.

By Isao OSIDA

Department of Dynamics, Faculty of Engineering, Nagoya University.

(Read April 28, 1946. Received May 12, 1947.)

1. Introduction and Summary.

The solar radiation arriving at the earth's surface is preeminently important quantity in meteorology, the amount of which causes the distinction between the tropical, the temperate and the frigid zones. Its variation with latitude and with season has been calculated by a French meteorologist Angot, in 1883, and more extensively by Milankowitch in 1920. The numerical calculations seem to be considerably laborious chiefly owing to the fact that the sun's zenith distance Z varies with as much as three variable; i.e. the latitude ϕ, the solar declination δ and its hour angle t.

In this paper, it is shown that the whole procedure of the calculation can be carried out graphically in a simple manner. As an example, the variation of the amount of the solar radiation at $\phi=35°N$, the mean latitude of Japan, is obtained after this plan.

2. The Graphical Construction of the Solar Zenith Distance Z.

If we dealt with a fixed point on the earth, .e. with constant latitude, it would be advantageous to use the nomograph proposed n the *Popular Astronomy* published in January 1935. But in general, especially in climatological problems, it is necessary to proceed with the calculation from place to place; so that we must take the trouble to prepare so much omographs. In such a case, the following method can be conveniently applied.

The sun's zenith distance Z is given by

$$\cos Z \doteq \cos\delta\cos\phi\cos t+\sin\delta\sin\phi \qquad (2.1)$$

n which δ is the solar declination, ϕ the atitude of the place in question and t the our angle. We draw three straight lines OB, OC and OE, making angles ϕ, $\phi+\delta$ and $\phi+90°$ with a fundamental line OX (Fig. I). Then me take such points L and Q on OC that $\overline{OL}=1$ (the unit length) and $\overline{OQ}=\cos t$, and draw the four perpendiculars: LM from L to OE, MN from M to OX, QR from Q to OB and RS from R to OX.

It follows that

$$\begin{aligned}\overline{NS}&=\overline{ON}+OS\\&=\overline{OM}\cos(90°-\phi)+\overline{OR}\cos\phi\\&=\overline{OL}\cos(90°-\delta)\cos(90°-\phi)\\&\quad+\overline{OQ}\cos\delta\cos\phi\\&=\sin\delta\sin\phi+\cos t\cos\delta\cos\phi,\end{aligned}$$

according to (I), i.e. the length of NS gives $\cos Z$.

3. The Determination of Solar Radiation.

In the following, let I the amount of the direct solar radiation which falls per unit time and per unit area on a surface pependicular to the sun's beams, S that on a horizontal surface and H the amount of scattered radiation from the sky which falls on a unit horizontal surface per unit time. All the quantities can be expressed as follows in terms of the sun's zenith distance Z and air mass m.

$$I=I_0\,a^m \qquad (3.1)$$

$$Z=I\cos Z=I_0a^m\cos Z \qquad (3.2)$$

$$H=\frac{1}{2}I_0\cos Z\frac{1-a^m}{1-1.4\log_e a} \qquad (3.3)^{1)}$$

in which I_0 represents the intensity of the solar radiation directly outside of the atmosphere and a the opacity of the atmosphere, that is, the fraction of the radiation reaching the earth's surface if the sun is at zenith. Since the air mass m is the function of Z, which is approximately equal to $\sec Z$ and more accurately takes the values tabulated by Bemperad or others (Tab. I), I, S, and H become, after all, functions of Z only. We have already obtained a simple construction for cos Z. In the former section we need only the simple conversion of cos Z to I, S and H, which can be achieved at a single stroke by the use of the functional scales which are graduated in I, S or H against cos Z.

4. The Practicals and Illustrative Example.

Strictly speaking, the opacity a varies largely with wave-length of the radiative rays. Accordingly the formlae (3.1) to (3.3) holds only for each very narrow band of the spectrum a to be treated as a constant; and for the radiation as a whole we must adopt their integral form. To avoid this trouble we prefer some conventionals in the following which seem not to be largely apart from the fact.

As for the value of I to m, we adopt that proposed by Moon[2] taking the solar constant as

$$I_0=1.846 \text{ cal. cm}^{-2}\text{min}^{-1}$$

(Tab. II and Fig. 2). We can compute a for each value of m by the use of the relation

$$a=\frac{1}{m}\log\frac{I}{I_0} \qquad (4.2)$$

which is derived from (3.1), and find that a is not constant but varies with m (Tab. II). Inserting the values of a thus derived and relation m vs. cos Z in table I to (3.2) and (3.3), we can express S and H in terms of cos Z and vice versa (Tab. IV). It is an easy task to make the functional scales used for the direct reading of I, S or H from the length $\overline{NS}$ in the construction of § 2 (Fig. 3).

An an illustrative example we calculate the seasonal variation of the solar radiation for $\phi=35°N$. If we denote the sun's celestial longitude by ⊙, its declinatisn δ is given by

$$\sin\delta=\sin\epsilon\sin\odot \qquad (4.3)$$

where ϵ means the inclination of the ecliptic and equals to 23° 27′. From (4.3), we comput δ for every 30° of ⊙, which we see in Tab. V Then we can pnt in practice the constrction of § 2, as shown in Fig. 4. In this figure, many lines and points are omitted which are unnecessary owing to its symmetrical nature As for the hour angle t we have used the every 15° values, 0°, ±15°, ±30°, ±45°, ±60° ±75°, ±90°, ±105° etc., corresponding to every an hour.

By applying the scales in Fig. 3, we fin the values of I, S, H pr $S+H$ for every ar hour on the 12 dates of the same year. The results are given in Tab. IV and Fig. 5, 6 and 7

Of these quantities, $S+H$ is considered t be most influential upon the climate. The total amount of $S+H$ in a day can be obtained from Fig. 7 by the aid of a planimete (Tab. IV and Fig. 3).

Further application of the planimeter t Fig. 8 gives us the total amount of $S+H$ i every month and in a whole year, which are listed in Tab. VII. We see that 1cm² of a horizontal surface at 35°N receives 1.83×10 gramcalories yearly. This is 0.348 g cal./cm. min. on the average. Of course, the influence of clouds and surface reflections must be take into consideration to discuss climatologica problems, still the above calculations remai as the fundamentals.

In conclusion the author expresses his thank to the Hattori Hoko Kai for the financia support.

Literatures.

1) H. P. Berlage: Zur Theorie der Beugung ein horizontalen Fläche durch Tageslicht, Met. Zeit 45 (1928).

2) P. Moon: Proposed Standard Solar-Radiatio Curves for Engineering Use. Journ. Franklin Ins 230 (1940), 583-618.

Tab. I.

Z	m	Z	m
0°	1.000	72°	3.209
5	1.004	74	3.588
10	1.015	76	4.075
15	1.035	78	4.902
20	1.064	80	5.600
25	1.103	81	6.177
30	1.154	82	6.884
35	1.220	83	7.768
40	1.304	84	8.900
45	1.413	85	10.395
50	1.553	86	12.439
55	1.740	87	15.365
60	1.995	88	19.787
62	2.123	89	26.959
64	2.274	90	(39.7)
66	2.447		
68	2.654		
70	2.904		

Tab. II.

$\cos Z$	I	S	H	$S+H$
0	(0.004)	0	0	0
0.025	(0.040)	0.002	0.018	0.020
0.05	0.114	0.006	0.036	0.042
0.1	0.301	0.030	0.062	0.092
0.15	0.490	0.070	0.081	0.151
0.2	0.620	0.124	0.097	0.221
0.3	0.828	0.245	0.119	0.364
0.4	0.964	0.385	0.135	0.520
0.5	1.063	0.531	0.148	0.679
0.6	1.133	0.678	0.159	0.837
0.7	1.195	0.839	0.168	1.007
0.8	1.250	0.999	0.175	1.174
0.9	1.294	1.161	0.182	1.343
1.0	1.331	1.331	0.189	1.250

The unit of I, S, H and $S+H$ is 1 cal. cm^{-2} min^{-1}.

Tab. III.

m	Z		$\cos Z$	I	a	S	H	$S+H$
0	—		—	1.896	—	—	—	—
1	0°	0′	1	1.331	0.702	1.331	0.189	1.520
1.2	33	36	0.8329	1.266	0.714	1.056	0.177	1.233
1.5	48	24	0.6634	1.175	0.727	0.780	0.165	0.945
2	60	4	0.4990	1.062	0.748	0.530	0.148	0.678
3	70	38	0.3316	0.872	0.772	0.289	0.125	0.414
4	75	43	0.2467	0.730	0.788	0.180	0.108	0.288
5	78	41	0.1962	0.616	0.799	0.121	0.0955	0.217
6	80	40	0.1622	0.527	0.808	0.0855	0.0853	0.171
8	83	14	0.1178	0.380	0.818	0.0448	0.0697	0.114
10	84	46	0.0912	0.279	0.825	0.0254	0.0582	0.084
12	85	49	0.0729	0.207	0.831	0.0151	0.0490	0.064
14	86	36	0.0593	0.155	0.836	0.0092	0.0413	0.050
16	87	3	0.0515	0.118	0.840	0.0061	0.0369	0.043
18	87	40	0.0407	0.090	0.844	0.0037	0.0296	0.033
(39.7)	90	0	0	(0.004)	—	0.0000	0.0000	0.000

Tab. V.

☉				δ
0°	180°		360°	0
30	150	210°	330	±11°28′
60	120	2 0	300	±20 9
30		270		±23 30
+		−		

Tab. IV.

t	cos Z	S	cos Z	H	cos Z	$H+S$	cos Z
(0.0)	(0)	0.0	0.000	0.00	0	0.0	0.0
0.1	0.044	0.1	0.178	0.02	0.028	0.1	0.107
0.2	0.075	0.2	0.264	0.04	0.057	0.2	0.185
0.3	0.099	0.3	0.339	0.06	0.095	0.3	0.256
0.4	0.124	0.4	0.410	0.08	0.148	0.4	0.323
0.5	0.153	0.5	0.478	0.10	0.212	0.5	0.380
0.6	0.190	0.6	0.549	0.12	0.305	0.6	0.450
0.7	0.232	0.7	0.615	0.14	0.433	0.7	0.513
0.8	0.284	0.8	0.675	0.16	0.606	0.8	0.575
0.9	0.350	0.9	0.740	0.18	0.870	0.9	0.638
1.0	0.433	1.0	0.800	0.19	—	1.0	0.696
1.1	0.550	1.1	0.861			1.1	0.756
1.2	0.719	1.2	0.924			1.2	0.813
1.3	0.915	1.3	0.983			1.3	0.872
						1.4	0.935
						1.5	0.989

Tab. VI.

δ / t	$S+H$ cal. cm^{-2}. min^{-1}						
	−23.5°	−20.2°	−11.5°	0°	+11.5°	+20.2°	+23.5°
0	0.70	0.77	0.98	1.20	1.36	1.45	1.47
15	0.66	0.72	0.93	1.15	1.31	1.40	1.43
30	0.54	0.61	0.80	1.01	1.18	1.28	1.30
45	0.36	0.42	0.60	0.80	0.96	1.07	1.10
60	0.14 (72°=0)	0.18 (74°=0)	0.34	0.53	0.69	0.81	0.84
75			0.08 (82°=0)	0.23	0.39	0.52	0.55
90				0.00	0.11 (98°=0)	0.22 (105°=0)	0.26
105							0.03 (107°=0)

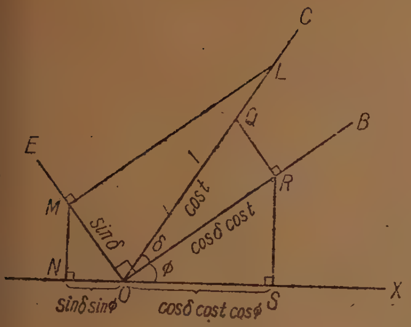

Fig. 1.

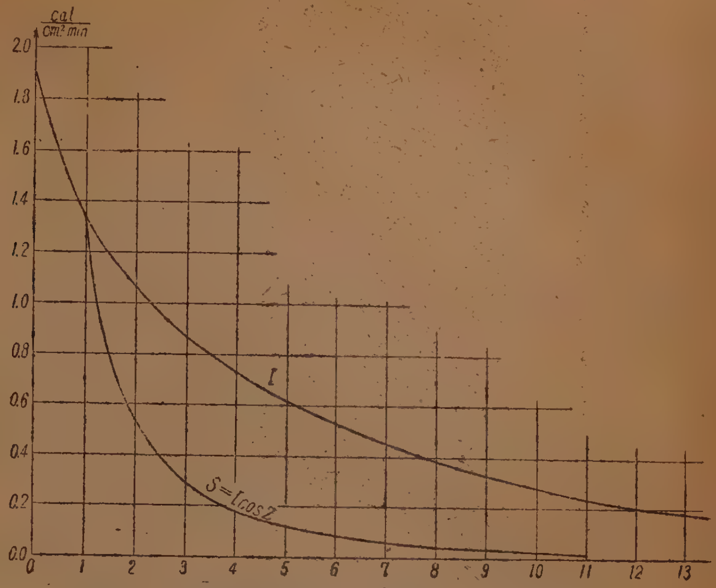

Fig. 2. Calculated Solar irradiation at sea level.
(by P. Moon, J. F. I. 230 (1940), 583–618)

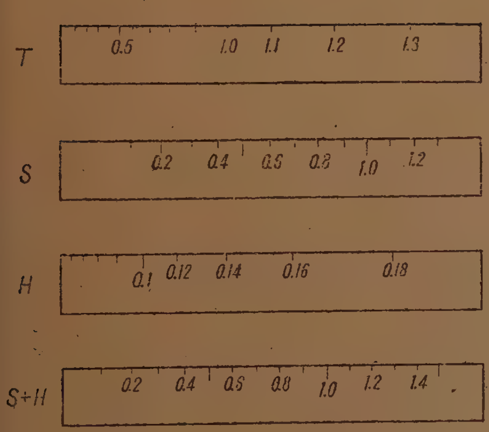

Fig. 3.

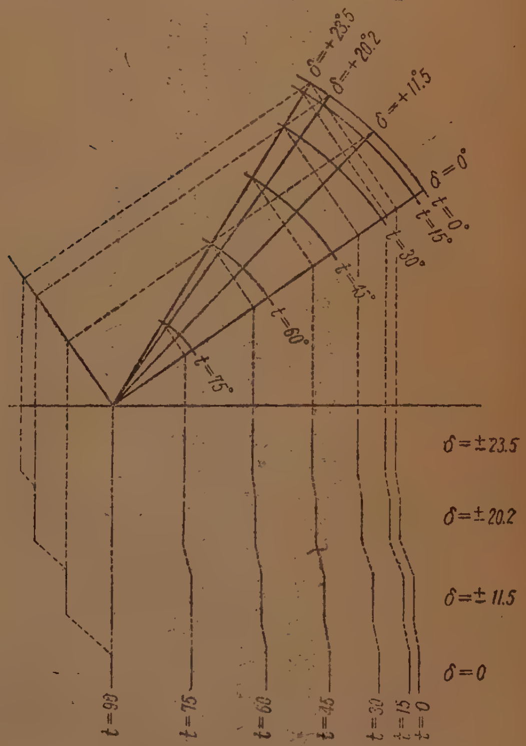

Fig. 4.

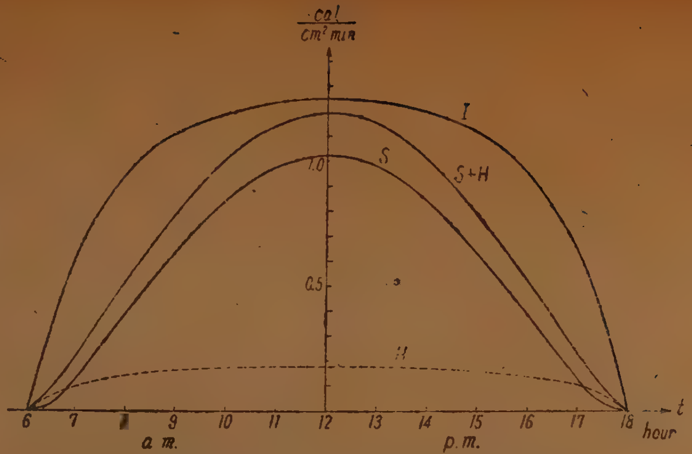

Fig. 5. Daily change of the solar irradiation at the earth's surface. (Lat. 35°N, at the vernal and autumnal equinox.)

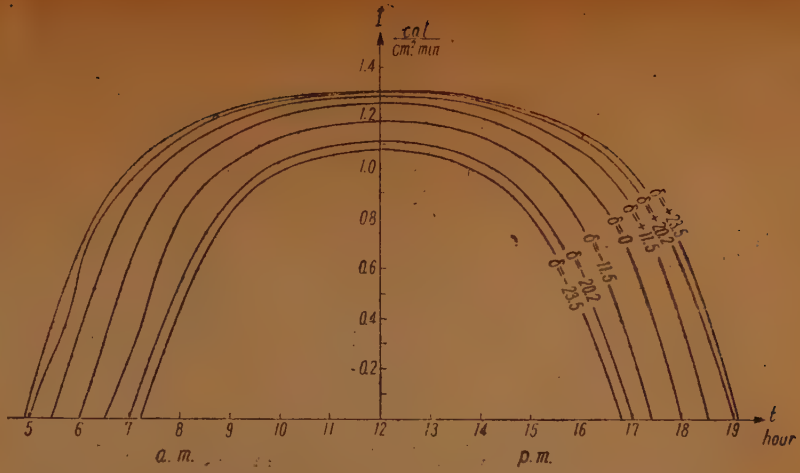

Fig. 6. The direct solar irradiation reaching unit area perpendicular to the sun's beam. (Lat. 35°N)

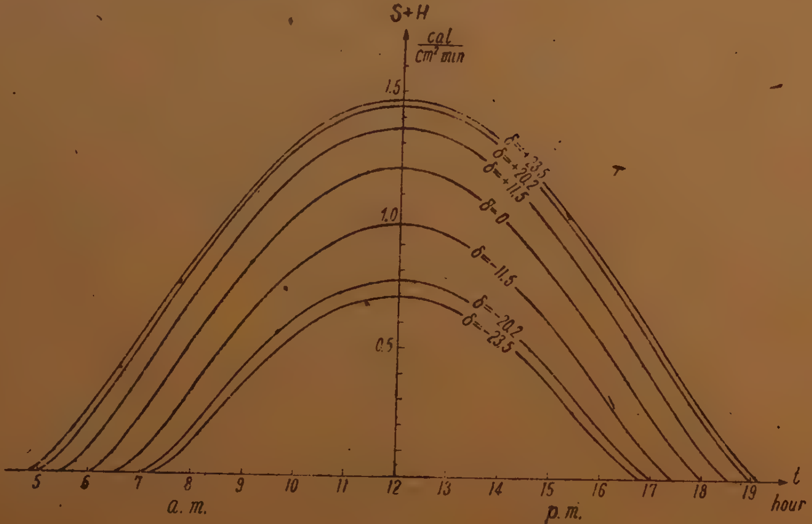

Fig. 7. The total solar irradiation reaching a horizontal unit area at the earth's surface. (Lat. 35°N)

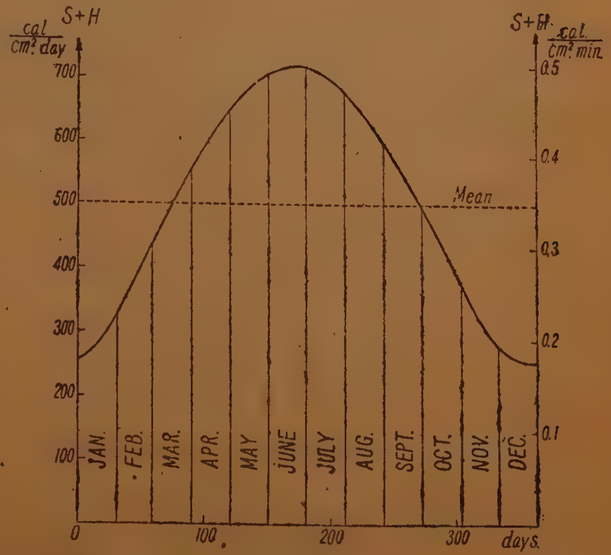

Fig. 8. The annual variation of the daily amount of the solar irradiation reaching horizontal unit

The Graphical Calculation of Solar Radiation at the Earth's Surface, Part II.

By Isao OSIDA

Department of Dynamics, Faculty of Engineering, Nagoya University.

(Read December 14, 1946. Received May 12, 1947)

Abstract:—The amount of solar radiation reaching unit area of the earth's surface in one day and in one year is calculated for every 15 degree of the latitude by the graphical method roported in the previous paper. The result is shown in Fig. 1 and Table I, II and III.

In the previous paper, a simple graphical method calculating the amount of solar radiation reaching the horizontal unit area of any part of the earth's surface in any time was reported and was applied to the place of 35°N of the latitude as an illustrative example.

In this paper, the same procedure is applied to every 15 degree of the latitude from the North to the South pole i.e. 90°N, 75°N, 60°N, 45°N, 30°N, 15°N, the Equator, 15°S, 30°S, 45°S, 60°S, 75°S, and 90°S. The variation of the insolation in a day are shown in Fig. 1 for the Northern hemisphere. The variation of the distance of the earth from the sun is not taken into account in those figures. The variation of the insolation in a year, taking the change of the sun's distance into consideration, is tabulated in Table I, II and III: the former gives the direct insolation and the latter two includes that coming from the sky owing to the scattering. The unit is 1 gram-calorie per square centimeter throughout.

The author expresses his thanks to the Hattori Hoko Kai for the financial support.

Table I.

Calculated direct insolation reaching the earth

Sun's longitude	Date (approx)	Sun's latitude	Sun's distance	Latitude												
				90N	75N	60N	45N	30N	15N	Equat.	15 S	30 S	45 S	60 S	75 S	90 S
300°	Jan. 19	−20.2	0.984	—	—	21	130	269	405	522	605	621	605	535	449	392
330	Feb. 17	−11.5	0.988	—	5	86	223	352	451	545	590	557	497	389	255	175
0	Mar. 21	0	0.996	0	74	213	347	455	536	556	536	455	347	213	74	0
30	Apr. 23	11.5	1.005	169	247	377	481	538	571	528	436	340	216	83	5	—
60	May 24	20.2	1.013	371	424	505	571	586	572	493	383	254	123	19	—	—
90	June 22	23.5	1.016	528	521	562	600	601	572	473	357	222	95	7	—	—
120	July 23	20.2	1.016	367	421	501	566	582	568	489	380	252	122	19	—	—
150	Aug. 22	11.5	1.011	167	244	372	474	532	564	520	431	335	213	81	5	—
180	Sep. 24	0	1.003	0	73	200	342	449	530	548	530	449	342	200	73	0
210	Oct. 27	−11.5	0.994	—	5	85	221	347	446	538	584	550	491	385	252	173
240	Nov. 25	−20.2	0.987	—	—	20	129	267	403	518	602	616	601	531	446	389
270	Dec. 23	−23.5	0.984	—	—	7	99	233	381	505	610	642	639	600	556	564

Table II.

Calculated total insolation reaching the earth

Sun's longitude	Date (approx)	Sun's latitude	Sun's distance	Latitude												
				90N	75N	60N	45N	30N	15N	Equat.	15 S	30 S	45 S	60 S	75 S	90 S
300°	Jan. 19	−20.2	0.984	—	—	43	189	348	497	634	718	749	729	660	616	640
330	Feb. 17	−11.5	0.988	—	11	134	297	445	545	661	699	676	608	490	366	322
0	Mar. 21	0	0.996	0	132	293	446	562	634	670	634	562	446	293	132	0
30	Apr. 23	11.5	1.005	312	354	473	588	655	675	639	526	430	287	130	11	—

60	May 24	20.2	1.013	665	583	623	689	707	678	599	469	329	178	41	—	—
90	June 22	23.5	1.016	720	687	697	725	725	679	579	439	288	143	20	—	—
120	July 23	20.2	1.016	600	578	619	684	703	673	595	465	327	177	41	—	—
150	Aug. 22	11.5	1.011	307	349	467	580	645	667	631	520	425	284	128	11	—
180	Sep. 24	0	1.003	0	130	290	441	555	625	662	625	555	441	290	130	0
210	Oct. 27	−11.5	0.994	—	11	132	294	440	559	654	690	668	601	484	362	318
240	Nov. 25	−20.2	0.987	—	—	43	187	346	493	630	715	745	725	655	613	636
270	Dec. 23	−23.5	0.984	—	—	22	152	307	468	616	725	774	774	744	734	770

Table III.

Yearly amount in cal cm^{-2}

Lat	S	S+H	H
+90°	48700	79300	30600
+75	60900	87500	26600
+60	90600	118400	27800
+45	128500	162000	33500
+30	159500	197500	38000
+15	183500	217900	34400
0	190300	230800	40500
−15	183300	218900	35600
−30	159900	196700	36800
−45	128200	160500	32300
−60	90500	117600	27100
−75	61800	86800	25000
−90	49400	78300	28900
Mean	182000 $=0.346 \dfrac{\text{g cal}}{\text{min. cm}^2}$	147200 $=0.280 \dfrac{\text{g cal}}{\text{min. cm}^2}$	34800 $=0.066 \dfrac{\text{g cal}}{\text{min. cm}^2}$

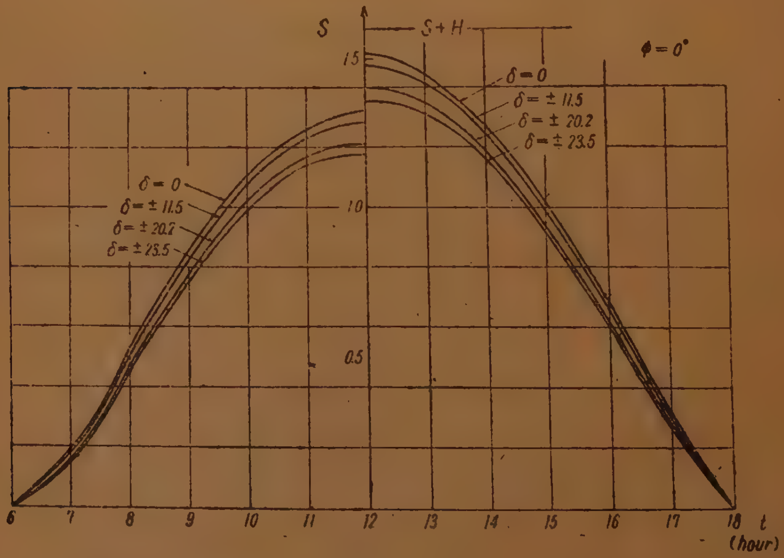

Fig. 1. a.

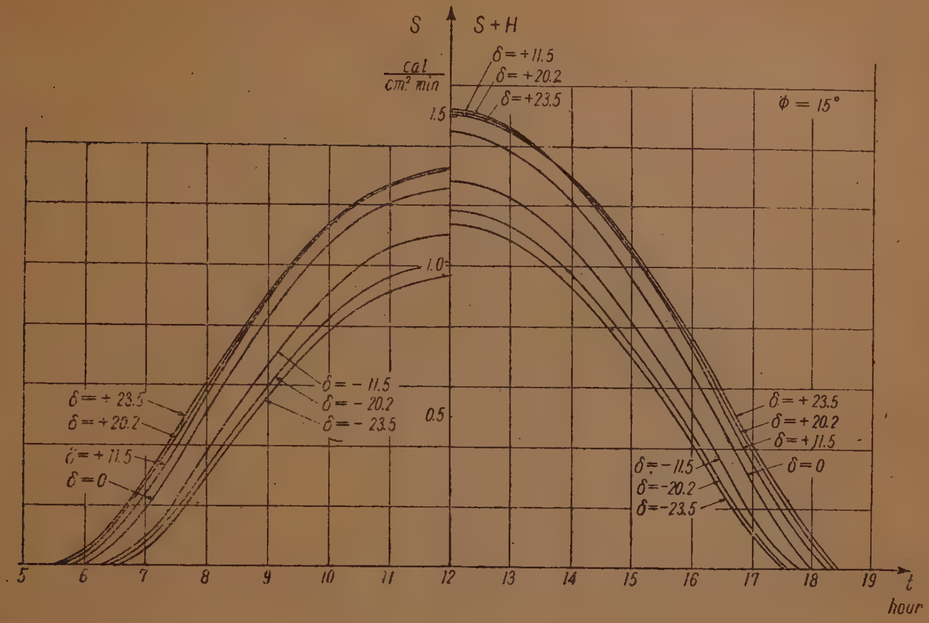
S
S + H
cal/cm² min
1.5
1.0
0.5
Φ = 15°
δ = +11.5
δ = +20.2
δ = +23.5
δ = + 23.5
δ = +20.2
δ = + 11.5
δ = 0
δ = − 11.5
δ = − 20.2
δ = − 23.5
δ = + 23.5
δ = + 20.2
δ = + 11.5
δ = 0
δ = −11.5
δ = −20.2
δ = −23.5
5
6
7
8
9
10
11
12
13
14
15
16
17
18
19
t
hour

Fig 1. b.

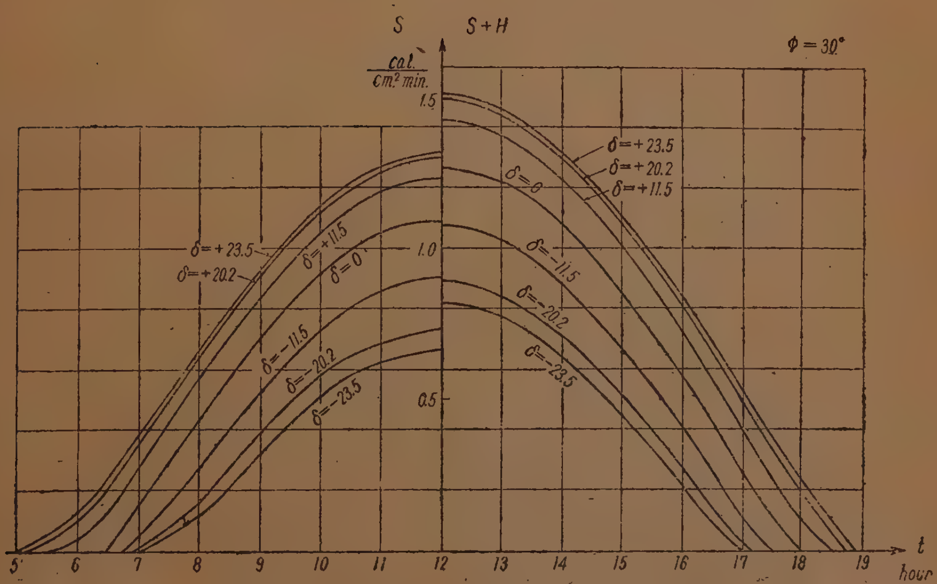
S
S + H
cal./cm² min.
1.5
1.0
0.5
Φ = 30°
δ = + 23.5
δ = + 20.2
δ = + 11.5
δ = 0
δ = + 23.5
δ = + 20.2
δ = + 11.5
δ = 0
δ = −11.5
δ = −20.2
δ = −23.5
δ = −11.5
δ = −20.2
δ = −23.5
5
6
7
8
9
10
11
12
13
14
15
16
17
18
19
t
hour

Fig. 1. c.

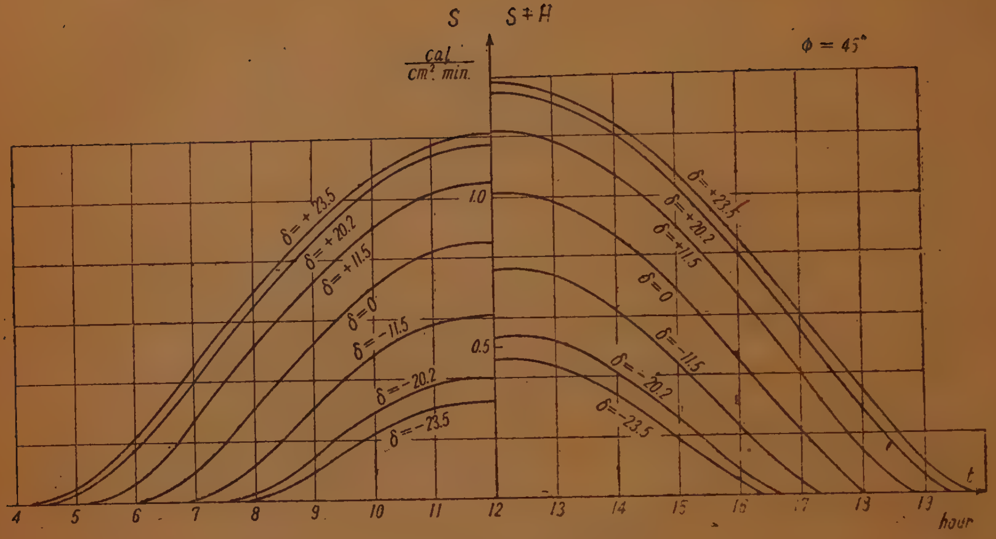
S
S+H
cal / cm² min.
φ = 45°
δ=+23.5
δ=+20.2
δ=+11.5
δ=0
δ=−11.5
δ=−20.2
δ=−23.5
1.0
0.5
t
hour
4
5
6
7
8
9
10
11
12
13
14
15
16
17
18
19

Fig. 1. d.

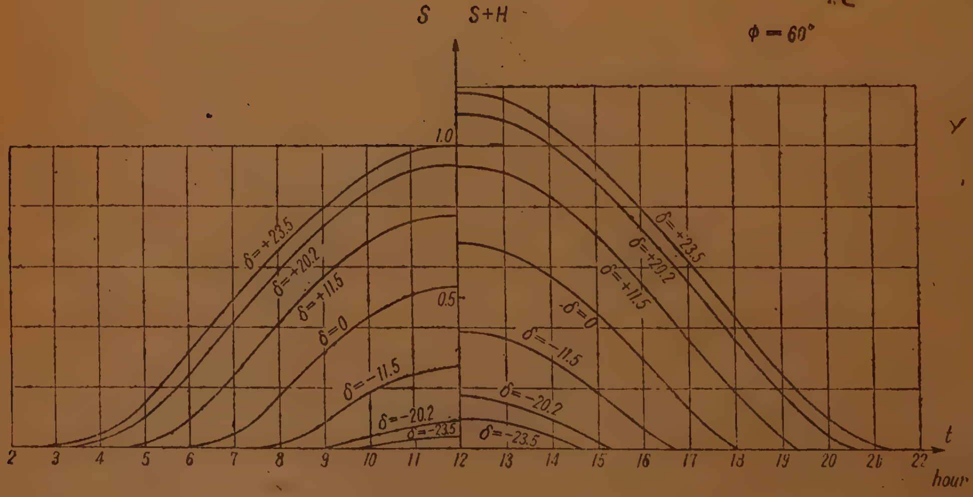
S
S+H
φ = 60°
δ=+23.5
δ=+20.2
δ=+11.5
δ=0
δ=−11.5
δ=−20.2
δ=−23.5
1.0
0.5
t
hour
2
3
4
5
6
7
8
9
10
11
12
13
14
15
16
17
18
19
20
21
22

Fig. 1. e.

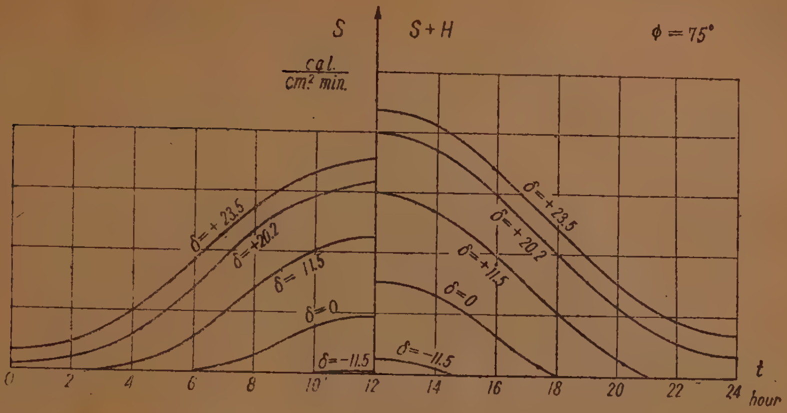
S
S+H
$\phi = 75°$
$\frac{cal.}{cm^2 min.}$
$\delta = +23.5$
$\delta = +20.2$
$\delta = 11.5$
$\delta = 0$
$\delta = -11.5$
$\delta = +23.5$
$\delta = +20.2$
$\delta = +11.5$
$\delta = 0$
$\delta = -11.5$
0
2
4
6
8
10
12
14
16
18
20
22
24
t
hour

Fig. 1. f.

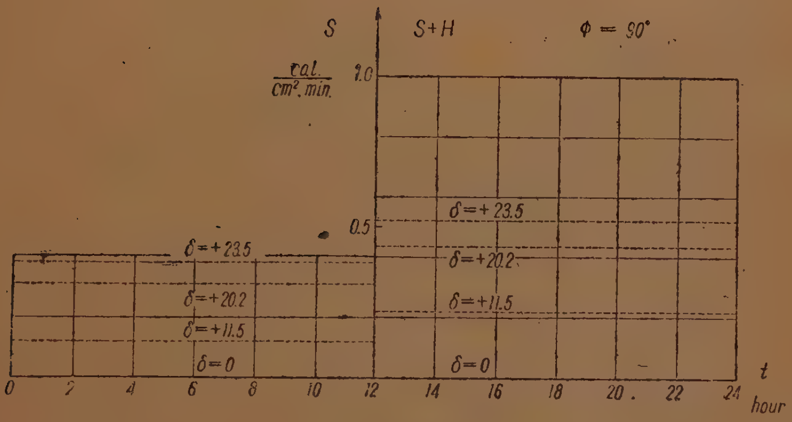
S
S+H
$\phi = 90°$
$\frac{cal.}{cm^2 min.}$
1.0
0.5
$\delta = +23.5$
$\delta = +20.2$
$\delta = +11.5$
$\delta = 0$
$\delta = +23.5$
$\delta = +20.2$
$\delta = +11.5$
$\delta = 0$
0
2
4
6
8
10
12
14
16
18
20
22
24
t
hour

Fig. 1. g.

日本物理學會歐字報告
第2巻　第5號
(昭和22年10~11月號)

昭和23年5月10日印刷
昭和23年5月15日發行
定價1部 80圓 (郵税を含まない)

編輯兼發行者　清水武雄
東京都板橋區志村清水町 375 番地
印刷者　石井完一
印刷所　帝都第一印刷株式會社
東京都新宿區山吹町 305 番地
配給元　日本出版配給株式會社
東京都千代田區神田淡路町 2 丁目 9 番地

日本出版協會會員番號 B 114032
發行所　日本物理學會
東京都文京區本富士町1 東京大學理學部内
振替口座 東京 167544 番
電話小石 (85) 693 番(内線 720 番)

賣捌所　株式會社 アカデメイア プレス
東京都目黒區平町 111 番地
東京都港區芝高輪南町 17 (ツバメ館ビル)
電話大崎 (49) 5050・5154 番

Agent.　AKADEMEIA PRESS Co., Ltd.
No. 111 Tairamachi Meguro-ku Tokyo, Japan.
No. 17 Shiba Takanawa Minamicho Minatoku, Tokyo, Japan.
Tel. (49)—5050・5154.

Étude d'une Théorie Statistique de la Turbulence Homogène

Par Hitosi IOI

(Reçu Octobre 9, 1944)

Le présent travail a pour but d'établir une théorie statistique de la turbulence homogène. Mises à part quelques problèmes d'un type tout à fait particulier dite la turbulence isotropique, on peut dire que seules les problèmes de la turbulence homogène ont fait l'objet d'une étude approfondie grâce surtout aux travaux remarquables de M. Th. de Kármán(1) à ce sujet.

Cependant reste-il encore quelques problèmes très importants et non résolus c'est à dire rechercher les lois auxquelles suivent l'intensité de turbulence ainsi que la longueur de mélange etc. C'est ce que l'auteur veut présenter dans ce travail.

Remarquons ici le mot l'homogénéité de la turbulence. Bien entendu, cela correspond d'après M.M. Slutsky,(2) Khintchine,(3) Dedebant, Wehrlé(4)1 (4)2 et Kampé de Fériet(5)1 (5)2 à cette condition: Les lois statistiques du mouvement sont independantes de l'instant choisi comme origine du temps; pourtant on entend ici en nous référant aux définitions de Th. de Kármán c'est à dire à la condition que le coefficient de corrélation entre les deux composantes des vitesses correspondantes à deux points choisis d'une manière arbitraire demeure invariant partout dans ce champ. Par conséquent ce domaine est plus général que celui mécaniquement homogène donné par M. M. O. Reynolds(6) et Th. de Kármán(1). Or en ce qui concerne la loi de décroissance de l'intensité de turbulence qui règné sur le domaine isotropique, M.M. G. I. Taylor(7), Th. de Kármán(1) et Millionshtchikov(8 l'ont déjà réduits chacun aux points de départs bien differents. Cependant celle qui règne sur le champ statistiquement homogène, cela n'est pas encore découverte. Le but de ce mémoire ce n'est rien d'autre que la reduction de cette loi ainsi que la longueur de mélange attachée à celle-là. La seule hypothèse donnée par l'auteur c'est que règne dans presque toutes les domaines de la turbulence homogène la loi de logarithme généralisée.

Partons de deux équations fondamentaux suivantes(1)

$$-\frac{d}{dx_2}\left[\overline{u_2'\left(\frac{p}{\rho}+\frac{q^2}{2}\right)}\right]+\frac{\tau}{\rho}\,\frac{dU}{dx_2}$$

$$=\nu\sum_i\sum_\varkappa\overline{\left(\frac{\partial u_i'}{\partial x_\varkappa}\right)^2}\quad\cdots\cdots(1)$$

$$-\frac{d}{dx_2}\overline{\left(u_2'\frac{w'^2}{2}\right)}=\nu\sum_i\sum_\varkappa\overline{\left(\frac{\partial w_i'}{\partial x_\varkappa}\right)^2}\quad\cdots\cdots(2)$$

En négligeant d'abord le premier terme à cause de la turbulence statistiquement homogène,

$$\frac{\tau}{\rho}\,\frac{dU}{dx_2}=\nu\sum_i\sum_\varkappa\overline{\left(\frac{\partial u_i'}{\partial x_\varkappa}\right)^2}\quad\cdots\cdots(1)'$$

Puisque le coefficient de corrélation entre les deux composantes des vitesses à deux points arbitrairement choisis est par définition invariant dans le domaine,

$$\frac{\tau}{\rho}=\kappa_1\cdot\overline{q^2}\quad\cdots\cdots\cdots\cdots\cdots\cdots(3)$$

D'autre part, à la suite de l'analyse de dimension (donnée par exemple par Th. de Kármán)

$$\sum_i\sum_\varkappa\overline{\left(\frac{\partial u_i'}{\partial x_\varkappa}\right)^2}=\kappa_2\cdot\frac{\overline{q^2}}{\lambda^2}\quad\cdots\cdots(4)$$

Avant d'aborder avec ces données l'équation (1)′ on fait à cause de la simplicité les substitutions suivantes:

$$I\equiv\frac{\overline{q^2}}{U^2_{\max}},\quad \frac{x_2}{r}\equiv\eta,\quad \frac{U}{U_{\max}}\equiv U^*,$$
$$\frac{\lambda^2}{\nu}\,\frac{U_{\max}}{r}\equiv Z$$

où signifient:

r: rayon du tube..

η: distance normale de la surface exprimée comme non dimension.

$U_{\max}$: vitesse du fluide au centre du tube lorsqu'on en se rende compte le mouvement du fluide.

U^*: vitesse locale du fluide exprimée comme non dimension.

λ: dimension du tourbillon.

ν: viscosité cinétique du fluide (de l'air).

I: carré de l'intensité de turbulence.

u_i': composante des vitesses turbulentes.

x_1: distance le long de l'écoulement moyen.

Et maintenant, en utilisant les formules (3) et (4), on tire de l'équation (1)′

$$\left.\begin{array}{l}\kappa_1\dfrac{dU^*}{d\eta}=\dfrac{\kappa_2}{Z(\eta)}\quad\text{ou bien}\\[2ex] U^*=\displaystyle\int\frac{dU^*}{d\eta}d\eta=U_0^*+\frac{\kappa_2}{\kappa}\int_{\eta_1}^{\eta_2}\frac{d\eta}{Z(\eta)}\end{array}\right\}\quad(1)''$$

Or, on revient à l'hypothèse fondamentale exprimée d'une manière suivante:

$$U^*=\beta(R_e)+\alpha(R_e)\log\eta\cdots\cdots\cdots(5)$$

En comparant (5) avec la première relation de (1)″, on obtient la suivante:

$$Z(\eta)\sim\eta\quad\text{ou}\quad Z(\eta)=\left(\frac{\kappa_2}{\kappa_1}\,\frac{1}{\alpha}\right)\eta\quad\cdots\cdot(6)$$

Nous allons réduire la relations (5).

Puisque la loi de logarithme est représentée d'une manière suivante:

$$\frac{U}{\sqrt{\tau_0/\rho}}=A\log\frac{x_2v^*}{\nu}+B\cdots\cdots(5)_1\cdots\cdot\text{à la}$$

bibliothèque (9) où A et B ce sont des constantes dont les valeurs numériques seront données à la fin.

D'autre part la vitesse de frottement v^* a pour l'expression la suivante

$$v^*=\sqrt{\frac{\tau_0}{\rho}}=\gamma\cdot U_{\max}\cdot R_e^{-\frac{1}{4}}\cdots\cdot(5)_2\cdots\cdot(10)$$

ou γ est constante.

En faisant dans $(5)_1$ la dernière expression $(5)_2$, on a

$$\frac{U}{U_{\max}}\equiv U^*$$
$$=\gamma\cdot R_e^{-\frac{1}{4}}\left\{A\log\left[\frac{x_2}{r}\gamma\cdot\frac{rU_{\max}}{\nu}R_e^{-\frac{1}{4}}\right]+B\right\}$$
$$=\gamma\cdot R_e^{-\frac{1}{4}}\left(A\log\eta+A\log R_e^{\frac{3}{4}}+D\right),$$

ou $\quad D\equiv B+A\log\gamma$

c.a.d. $\quad U^*=\alpha(R_e)\log\eta+\beta(R_e)\quad\cdots\cdot(5)$

où

$$\begin{cases}\alpha(R_e)=A\gamma\,R_e^{-\frac{1}{4}}\\ \beta(R_e)=\gamma R_e^{-\frac{1}{4}}(A\log R_e^{\frac{3}{4}}+B+A\log\gamma)\end{cases}$$

Revenons maintenant à l'équation (2).

D'une façon analogue à celle donnée par Kármán, soit données ici les quatres relations suivantes:

$$\left.\begin{array}{l}\overline{u_2'\dfrac{w'^2}{2}}=-lu_2'\dfrac{d}{dx_2}\left(\dfrac{\overline{w'^2}}{2}\right)\\[2ex] \overline{w'^2}=\text{const}\dfrac{\overline{q^2}}{\lambda^2}\\[2ex] \displaystyle\sum_i\sum_\kappa\overline{\left(\frac{\partial w_i'}{\partial x_\kappa}\right)}=\kappa_3\frac{\overline{w'^2}}{\lambda^2}\\[2ex] lu_2'=\kappa_4\dfrac{\lambda^2}{\nu}\cdot\overline{q^2}\end{array}\right\}\cdots\cdots(7)$$

signifiant que

w_i': la composante des vortices aléatoires, $(\sum_i w_i'^2=w'^2)$.

l: longueur analogue à celle de mélange donnée par L. Prandtl (ou G. I. Taylor).

Nous nous arrêterons ici sur la dernière relation: Par suite de l'analyse de dimension pour l'équation (2), on a immédiatement

$$\overline{\frac{q\lambda^2}{\nu L}\sim1}\quad\text{ou}\quad\frac{L}{\lambda}=\frac{q\lambda}{\nu},$$

$$\text{puisque } w_i' \text{ et } w'\sim\frac{q}{\lambda}$$

si l'on pose $\quad\dfrac{l}{\lambda}=f\left(\dfrac{u_2'\lambda}{\nu}\right)$, ou $f\left(\dfrac{u_2'\lambda}{\nu}\right)$ c'est une certaine fonction du nombre de Reynolds pour la turbulence $\frac{u_2'\lambda}{\nu}$;

(ou $u_2' \equiv \sqrt{\overline{u_2'^2}}$) à la condition $l \sim L$ au cas d'un nombre de Reynolds très grand,

on a $$\frac{l}{\lambda} = \mathrm{const}\frac{u_2'\lambda}{\nu}, \quad \text{puisque} \quad u_2' \sim q$$

ou bien $$l = \mathrm{const}\frac{u_2'\lambda^2}{\nu} \quad \therefore \quad \text{C.Q.F.D.}$$

Les relations susmentionnées (7), en les faisant dans (2), on a

$$\frac{d}{dx_2}\left\{\overline{q^2}\cdot\lambda^2\cdot\frac{d\left(\frac{\overline{q^2}}{\lambda^2}\right)}{dx_2}\right\} = c\frac{\overline{q^2}}{\left(\frac{\lambda^2}{\nu}\right)^2},$$

$$\left(\text{où} \quad c = 2\frac{\kappa_3}{\kappa_4}\right) \cdots\cdots\cdots\cdots (2)'$$

ou bien à la formule de non dimension,

$$I\left(\frac{Z'}{Z}\right)' + 2I'\left(\frac{Z'}{Z}\right) - \left(I'' + \frac{I'^2}{I}\right) = \frac{-c}{Z^2} \cdots\cdots\cdots\cdots (2)''$$

Si nous nous reportons à (6), nous obtenons de (2)″

$$I\left(\frac{1}{\eta}\right)' + 2I'\left(\frac{1}{\eta}\right) - \left(I'' + \frac{I'^2}{I}\right) = -\frac{c'}{\eta} \cdots\cdots\cdots\cdots (8)$$

et si nous posons $I \equiv y, \quad \eta \equiv x$

nous avons

$$x^2(yy'' - y'^2) - 2xyy' + y^2 = c'y \quad \cdots\cdots (9)$$

en substituant, ensuite $y^2 = z$, on a

$$x^2z'' - 2xz' + 2z = 2c'\sqrt{z} \quad \cdots\cdots (10)$$

et enfin selon $z = x \cdot u$

on est arrivé à la formule suivante:

$$\frac{d^2u}{dx^2} = 2c'u^{\frac{1}{2}}x^{-\frac{5}{2}} \equiv f(x, u) \cdots\cdots (11)$$

Nous allons expliquer comment on détermine le nombre c':

(I) la première formule

$$c' = \frac{c}{\left(\frac{\kappa_2}{\kappa_1}\frac{1}{\alpha}\right)^2} = \frac{2\frac{\kappa_3}{\kappa_4}}{\left(\frac{\kappa_2}{\kappa_1}\frac{1}{\alpha}\right)^2}$$

$$= \frac{\kappa^2}{\kappa_1}\cdot\alpha^2, \quad \text{puisque} \quad \kappa^2 = 2\frac{\kappa_1^3\kappa_3}{\kappa_2^2\kappa_4}$$

puisque α est égale à $A\cdot\gamma\cdot R_e^{-\frac{1}{4}}$; on a

$$c' = \frac{\kappa^2}{\kappa_1}\alpha^2 = \frac{(A\gamma\kappa)^2}{\kappa_1}R_e^{-\frac{1}{2}} \cdots\cdots\cdots (\mathrm{I})$$

où A, γ, κ ce sont des constants

$$\begin{cases} A = 5.93 \cdots\cdots \text{à la bibliothèque} \cdots\cdots (9) \\ \gamma = 0.576 \cdots \quad ,, \quad \cdots\cdots (10) \\ \kappa = 0.38 \cdots\cdots \quad ,, \quad (1),\ (10) \end{cases}$$

(II) la seconde formule

$$(1)'' \qquad \frac{dU^*}{d\eta} = \frac{\kappa_2}{\kappa_1}\frac{1}{Z(\eta)}$$

$$(6) \qquad Z(\eta) = \left(\frac{\kappa_2}{\kappa_1}\frac{1}{\alpha}\right)\eta$$

si l'on élimine entre ces deux équations, on a sans difficultés $$\alpha = \eta\frac{dU^*}{d\eta}$$

par conséquent, en nous référant à la première formule (1), on arrive à la seconde

$$c' = \frac{\kappa^2}{\kappa_1}\left(\eta\frac{dU^*}{d\eta}\right)^2 \cdots\cdots\cdots (\mathrm{II})$$

lorsqu'on trouve dans l'exposé de l'expérience le nombre de Reynolds, on emploie la première, tandis qu'au cas de l'expression de la vitesse U^* seulement, par exemple, pour le résultat de l'expériences de M.F.L. Wattendorf,(12) il est nécessaire de s'appuyer sur la seconde.

Or, l'équation (11), c'est là l'équation différentielle ordinaire du second ordre non linéaire, on peut là résoudre, soit par la méthode d'approximation successive établie par E. Picard,(13) soit par celle du calcul numérique donnée par Runge et Koenig,(14) pas à pas, en partant de la condition initiale ou finale soit à $\underset{(\eta)}{x} = 0.1$, soit à $\underset{(\eta)}{x} = 0.6$.

En définitif, nous arrivons à la coincidence presque parfaite de la valeur de l'intégrale vis-à-vis des résultats expérimentaux obtenus par M.F.L. Wattendorf.(12)

⊙ Conférence à l'Assemblée de la Société physico-mathématique du Japon, qui a en lieu le 18, Juillet,

1943, à Sendai.

⊙ Discours à l'Assemblée mensuelle de la Société physico-mathématique du Japon qui a eu lieu le 15. Janvier, 1944, à Tokyo-To.

* ⊙ Conférence à l'Assemblée de la Société aéronautique du Nippon qui a eu lieu le 17, avril, 1944 à Tokyo-To.

Bibliographie

(1) Th. de Kármán: Jour. Aéro. Sci. Vol. 4, No. 4, 1937.

(2) Eugène Slutsky: Comptes Rendus, Paris. Vol. 187.

(3) A. Khintchine: Math. Annal. Bd. 109.

(4)$_1$ G. Dedebant et P. Wehrle: C.R. Vol. 208, 1937/2.

(4)$_2$ G. Dedebant et P. Wehrle: ibid; Vol. 208, 1939/4.

(5)$_1$ J. Kampé de Fériet: C.R. Vol. 208, 1939 3.

(13) E. Picard: Traité d'analyse, Tome III, Chap. VII.

(14) C. Runge und Koenig: ,, Numerisches Rechnen,'' (Berlin, 1924, S. 311-316).

(5)$_2$ J. Kampé de Fériet: Ann. Soc. Sci. Bruxelles, 1939.

(6) O. Reynolds: Phil. Trans. Roy. Soc., 1894; Scientific papers Vol. 2.

(7) G. I. Taylor: Proc. Roy. Soc. A. 151 1935.

(8) Millionshtchikov: C.R. Acad Sci. U.R.S.S. 22 (1937.).

(9) F. Schult-Grunow: Lufo, Bd. 17, 1940.

(10) H. Blasiun: Zts. Math, Phy. Bd. 56.

(11) Th. de Kármán: Proc. III Inter. Cogr. Appl. Mech. Vol. 1, Stockholm, 1930.

(1a) F. L. Wattendorf: Jour. Aero. Sci. Vol. 3 No. 6, 1938.

A General Theory of Ultra-short Wave Circuits I.

By Sin-itiro TOMONAGA

Institute of Physics, Tokyo Bunrika-Daigaku.

(Received August 19, 1946)

Introduction.

In recent years, since ultra-short radio waves found their applications in wider field, study of new kinds of circuit elements, such as wave guides, cavity resonators, or electromagnetic horns has become more and more important. Combinations of such circuit elements are now widely used in many parts of apparatus. Therefore, we are compelled to investigate the properties of these complicated combined systems.

Suppose, for instance, a circuit as shown in Fig. 1, consisting of several wave guides or concentric cables* as openings. As indicated in the picture, cavity resonators of any forms may also be attached to the circuit. One of the main tasks of the circuit theory is to find the amplitudes and the phases of the waves propagating into and out of the openings.

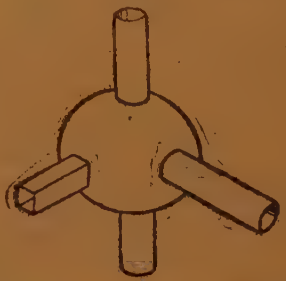

Fig. 1. System of wave guides and a cavity resonator.

To treat such problems one has to solve the

---

* The openings may be also Lecher wiresso provided that the leakage of waves at the connection of the wires and the resonators can be neglected.

Maxwell equations under the boundary conditions corresponding to the given forms of the wave guides and the resonators and also to the given loads and driving conditions at the openings. Since, however, one thus meets with very complicated boundary-value problems, it is in majority of cases impossible to find the explicit solution of the problem.

In spite of these circumstances it is still possible to give a general point of view which enables us to deal with the complicated circuit systems. There exist, as will be shown below, some general relations between the amplitudes and the phases of the various waves at the various openings. These relations, which can be obtained without solving the Maxwell equations explicitly, give so many informations about the circuit that the general consideration alone often suffices to find the properties of the circuit.

Even when this is not the case, further experimental determination of a few characteristic constants is usually sufficient for many purposes. As a mathematical tool for such a general consideration I propose in this paper to introduce a concept which seems to me as useful as the concept of impedance in the ordinary circuit theory. I shall call this new concept "characteristic matrix." I think that it will be also possible to set up a general circuit theory on the basis of this new term, and that it is especially desirable in the region of ultra-shortwaves, because there the new circuit elements are widely used and the application of the concept of impedance is, I think, too artificial. The final decision, however, whether or not the new concept is here preferable to impedance should of course be given not only by a theoretical physicist but also by general electro-engineers.

In terms of this new concept the general relations which exist between the amplitudes and the phases of the various waves are expressed in terms of the characteristic matrix which is symmetric and unitary. Although this expression seems rather newish, its physical contents are not new. As we shall see later, the symmetry of the characteristic matrix is nothing but the mathematical expression of the well known reciprocity relation between various waves. The unitary character, on the other hand, means that the energies transported by the incoming and the outgoing waves must be balanced with each other.

The notion accompanied by the characteristic matrix is not so strange to physicists. In their consideration about the quantum mechanical collision problem Breit(1) has already introduced the idea "scattering matrix." The purpose of the present paper is to notice the usefulness of this idea in the electromagnetic phenomena.

§ 1. General remarks

Let us suppose that the electromagnetic field in the circuit of Fig. 1 depends on time in the form $e^{-i\omega t}$. The frequency* ω may be either real or complex. Then the Maxwell equations for the electric field $\boldsymbol{E}$ and for the magnetic field $\boldsymbol{H}$ have the form:

$$\begin{cases}\text{curl } \boldsymbol{E} = i\omega\mu\boldsymbol{H} \\ \text{curl } \boldsymbol{H} = -i\omega\varepsilon\boldsymbol{E}\,, \end{cases} \qquad (1,1)$$

where μ and ε mean respectively the magnetic permeability and the dielectric constant of the medium.

We introduce in every wave guide the coordinate axes, the z-axis being directed outwards parallel to the axis of the wave guide, while x- and y-axes lie in its cross section. The origin of the coordinates is taken at some suitably chosen standard position on the axis of the wave guide. We label the wave guides by the suffix N. Thus the coordinates x_N, y_N and z_N are referred to the N-th wave guide.

---

* We use, for simplicity, the word "frequency" in place of "angular frequency."

In the N-th wave guide a complete set of special solutions of (1, 1) satisfying the boundary condition at the wall of this wave guide is known.(2) These special solutions have the form:

$$\begin{cases} E_l^+ = F_l^+(x,y)e^{+ik_lz} \\ H_l^+ = G_l^+(x,y)e^{+ik_lz} \end{cases} \qquad (1,2)$$

or

$$\begin{cases} E_l^- = F_l^- e^{-ik_lz} \\ H_l^- = G_l^- e^{-ik_lz} \end{cases} \qquad (1,3)$$

If k_l is real, it is assumed to be positive (see below), so the solutions of the form (1, 2) represent waves propagating outwards through the openings, and the solutions of the form (1, 3) represent inwards propagating waves. The suffix l specifies the mode of the wave and the wave with a specified value of l has the wave length

$$\lambda_l = \frac{2\pi}{k_l}.$$

The waves in the wave guide can be further classified into so-called E- and H-waves. For the E-wave $\boldsymbol{F}$ and $\boldsymbol{G}$ in (1, 2) or (1, 3) have the form

$$\begin{cases} F^{\pm}_{l,x} = \pm i\sqrt{\dfrac{2k_l}{\varepsilon}}\,\dfrac{\partial U_l}{\partial x}, \\ F^{\pm}_{l,y} = \pm i\sqrt{\dfrac{2k_l}{\varepsilon}}\,\dfrac{\partial U_l}{\partial y}, \\ F^{\pm}_{l,z} = \sqrt{\dfrac{2}{\varepsilon k_l}}(-k_l^2+\omega^2\mu\varepsilon)U_l, \\ G^{\pm}_{l,x} = -i\omega\sqrt{\dfrac{2\varepsilon}{k_l}}\,\dfrac{\partial U_l}{\partial y} \\ G^{\pm}_{l,y} = i\omega\sqrt{\dfrac{2\varepsilon}{k_l}}\,\dfrac{\partial U_l}{\partial x} \\ G^{\pm}_{l,z} = 0, \end{cases} \qquad (1,4)$$

and for the H wave we have

$$\begin{cases} F^{\pm}_{l,x} = i\omega\sqrt{\dfrac{2\mu}{k_l}}\,\dfrac{\partial U_l}{\partial y}, \\ F^{\pm}_{l,y} = -i\omega\sqrt{\dfrac{2\mu}{k_l}}\,\dfrac{\partial U_l}{\partial x}, \\ F^{\pm}_{l,z} = 0, \\ G^{\pm}_{l,x} = \pm i\sqrt{\dfrac{2k_l}{\mu}}\,\dfrac{\partial U_l}{\partial x} \\ G^{\pm}_{l,y} = \pm i\sqrt{\dfrac{2k_l}{\mu}}\,\dfrac{\partial U_l}{\partial y} \\ G^{\pm}_{l,z} = \sqrt{\dfrac{2}{\mu k_l}}(-k_l^2+\omega^2\mu\varepsilon)U_l, \end{cases} \qquad (1,5)$$

where $U_l(x,y)$, a function of x and y, is the l-th eigen-function of the equation

$$\frac{\partial^2 U_l}{\partial x^2}+\frac{\partial^2 U_l}{\partial y^2}+\kappa_l^2 U_l=0, \qquad (1,6)$$

κ_l^2 being the corresponding eigenvalue. The boundary condition for U_l is, for the E-waves

$$U_l(x,y)_{\text{boundary}}=0, \qquad (1,7)$$

and for the H-wave

$$\left(\frac{\partial U_l(x,y)}{\partial n}\right)_{\text{boundary}}=0, \qquad (1,8)$$

where n denotes the normal to the boundary contour of the cross section of the wave guide.

The eigenvalue κ_l^2 is connected with the wave number k_l in (1, 2) and (1, 3) by means of

$$k_l=\sqrt{\omega^2\mu\varepsilon-\kappa_l^2}. \qquad (1,9)$$

As to the sign of the square root we make the following convention: when k_l is real, the positive square root should be taken. In the case of complex k_l, its imaginary part should be positive. The field in the wave guide does not then have a sinusoidal form. In this case the field is cut off by the wave guide.

We assume further that U_l is normalised by

$$\int_\Sigma\left\{\left(\frac{\partial U_l}{\partial x}\right)^2+\left(\frac{\partial U_l}{\partial y}\right)^2\right\}dxdy=1, \qquad (1,10)$$

the integral being taken over the area of the cross section Σ of the wave guide. To see the physical meaning of this normalisation we calculate the energy transported by the wave (k_l being assumed to be real). According to Poynting's theorem the energy flow per unit time through the wave guide is

$$S=\frac{1}{4}\int_\Sigma\{[\boldsymbol{E}\times\overset{*}{\boldsymbol{H}}]_z+[\overset{*}{\boldsymbol{E}}\times\boldsymbol{H}]_z\}dxdy, \qquad (1,11)$$

(the symbol * means the conjugate complex number.) If we substitute for $\boldsymbol{E}$ and $\boldsymbol{H}$ in this equation by their values (1, 2) or (1, 3) and use (1, 4) or (1, 5), then we obtain

$$S=\omega\int_{\Sigma}\left\{\left(\frac{\partial U_l}{\partial x}\right)^2+\left(\frac{\partial U_l}{\partial y}\right)^2\right\}dxdy. \quad (11,12)$$

In this way we see that the normalisation (1, 10) means that the energy transported in one period* of oscillation is unity.

As there are two kinds of waves, E- and H-waves, we need one more suffix to specify the elementary wave (1, 2) or (1, 3), but we avoid this complication by making the convention that we use even l for E-waves and odd l for H-waves.

Since the complete set of special solutions is thus known in each wave guide, any electromagnetic field with the frequency ω can be, in the N-th wave guide, expressed in the form:

$$\left\{\begin{aligned}\boldsymbol{E}(x_N,y_N,z_N)&=\sum_l\{q_{N,l}\boldsymbol{F}^-(x_N,y_N)e^{-ik_{N,l}z_N}\\&\qquad+p_{N,l}\boldsymbol{F}^+(x_N,y_N)e^{+ik_{N,l}z_N}\\\boldsymbol{H}(x_N,y_N,z_N)&=\sum_l\{q_{N,l}\boldsymbol{G}^-(x_N,y_N)e^{-ik_{N,l}z_N}\\&\qquad+p_{N,l}\boldsymbol{G}^+(x_N,y_N)e^{+ik_{N,l}z_N}\ .\end{aligned}\right. \quad (1, 13)$$

In order to determine the (complex) amplitudes $p_{N,l}$ and $q_{N,l}$ ($N=1,\ 2,\ 3\ldots;\ l=1,\ 2,\ 3,\ldots$) so that the solution may satisfiy the boundary condition at the wall of the cavity, we need precise prescriptions about the form of the circuit system (forms of the cavities and art of connections of wave guides and so on). These amplitudes depend also on the load conditions and the method of excitation at the openings, which impose various boundary conditions on $\boldsymbol{E}$ and $\boldsymbol{H}$ at the openings. However, among these manifold problems corresponding each to a set of possible boundary conditions at the openings, there exist several simplest and most fundamental ones, the knowledge of which is already sufficient for obtaining the solutions for any other problems.

As such simplest problems we consider the followings. Suppose that from one opening (say the N-th opening) a wave of a simple mode (say of the l-th mode) of unit amplitude is coming in (the unit amplitude means here that unit energy is transported in one period), and that no waves of other modes are propagating into this opening. Further, no incoming waves at all exist in the remaining other openings. Then what waves will propagate out of each opening?**

The reason why we call this problem fundamental is that if we can once answer this problem for all values of N and l, then the problem with more complicated conditions at the openings can be solved algebraically without returning to the Maxwell equations in each case anew. Examples will be given below.

§ 2. Introduction of characteristic matrix

In the preceding section we have considered the following fundamental problem: From the N-th opening the wave of the l-th mode of unit amplitude is coming in, and no further incoming waves exist in this wave guide. No waves at all are coming into from the remaining openings. Then what will be the waves going out of each opening? We suppose now this problem to be solved, and let the amplitude of the l'-th wave going out of the N'-th opening be denoted by

---

* We use, for simplicity, the word "period" for the reciprocal of ω, whereas the true period is given by $T=2\pi/\omega$.

** It is always supposed that the reflections of waves at the outer ends of the wave guides are prevented by some suitable devices.

$$a^{N,l}_{N',l'} \cdot \qquad (2,1)$$

Here the upper suffixes N and l are introduced to indicate that this amplitude is due to the incoming wave of the l-th mode through the N-th opening.

By this definition of $a^{N,l}_{N',l'}$ the electric and the magnetic fields in the N'-th wave guide are given by

$$\left\{\begin{aligned} &\boldsymbol{E}^{N,l}(x_N',y_N',z_N') \\ &=\sum_{l'}\{\delta^N_{N'}\delta^l_{l'}\boldsymbol{F}^-(x_N',y_N')e^{-ik_{N',l'}z_{N'}} \\ &+a^{N,l}_{N',l'}\boldsymbol{F}^+(x_N',y_N')e^{+ik_{N',l'}z_{N'}}\} \\ &\boldsymbol{H}^{N,l}(x_N',y_N',z_N') \\ &=\sum_{l'}\{\delta^N_{N'}\delta^l_{l'}\boldsymbol{G}^-(x_N',y_N')e^{-ik_{N',l'}z_{N'}} \\ &+a^{N,l}_{N',l'}\boldsymbol{G}^+(x_N'y_N')e^{+ik_{N',l'}z_{N'}}\}\,. \end{aligned}\right. \qquad (2,2)$$

The upper suffixes N and l of these $\boldsymbol{E}$ and $\boldsymbol{H}$ are introduced to emphasise that these fields are due to the incoming wave of the l-th mode from the N-th opening. δ^a_b in (2, 2) is the well-known Kronecker symbol having the property

$$\delta^a_b=\begin{cases}1 & \text{for } a=b \\ 0 & \text{for } a\neq b.\end{cases} \qquad (2,3)$$

To obtain $a^{N,l}_{N',l'}$ explicitly we must solve the Maxwell equations for the prescribed circuit system under the above stated boundary conditions at the openings. But if it is once done and $a^{N,l}_{N',l'}$ is known for all values of N, l and N',l', we can obtain, as mentioned in the preceding section, the solution for any load and excitation condition by means of algebraic operations alone without solving the Maxwell equations for each problem.

As an example we shall determine the amplitudes of the waves going out of the openings, when the amplitudes of the waves coming into the circuit through every opening are given. Let $q_{N,l}$ be the given amplitude* of the l-th wave which comes in from the N-th opening, and $p_{N,l}$ be the unknown amplitude of the l-th wave going out of the N-th opening. Then the fields $\boldsymbol{E}$ and $\boldsymbol{H}$ which satisfy the Maxell equations and the boundary conditions must have in the N'-th wave guide the from

$$\left\{\begin{aligned} &\boldsymbol{E}(x_N',y_N',z_N') \\ &=\sum_{l'}\{q_{N',l'}\boldsymbol{F}^-(x_N',y_N')e^{-ik_{N',l'}z'} \\ &+p_{N'l'}\boldsymbol{F}^+(x_N'y,_N')e^{+ik_{N',l'}z'}\} \\ &\boldsymbol{H}(x_N',y_N',z_N') \\ &=\sum_{l'}\{q_{N',l'}\boldsymbol{G}^-(x_N',y_N')e^{-ik_{N',l'}z'} \\ &+p_{N',l'}\boldsymbol{G}^+(x_N',y_N')e^{+ik_{N',l'}z'}\}\,. \end{aligned}\right. \qquad (2,4)$$

On the other hand, on multiplying (2, 2) by $q_{N,l}$ and summing over all N and l, we obtain

$$\left\{\begin{aligned} &\sum_N\sum_l q_{N,l}\boldsymbol{E}^{N,l}(x_N',y_N',z_N') \\ &=\sum_{l'}\{q_{N',l'}\boldsymbol{F}^-(x_N',y_N')e^{-ik_{N',l'}z'} \\ &+\sum_N\sum_l a^{N,l}_{N',l'}q_{N,l}\boldsymbol{F}^+(x_N',y_N')e^{+ik_{N',l'}z'}\} \\ &\sum_N\sum_l q_{N,l}\boldsymbol{H}^{N,l}(x_N',y_N',z_N') \\ &=\sum_{l'}\{q_{N',l'}\boldsymbol{G}^-(x_N',y_N')e^{-ik_{N',l'}z'} \\ &+\sum_N\sum_l a^{N,l}_{N',l'}q_{N,l}\boldsymbol{G}^+(x_N',y_N')e^{+ik_{N',l'}z'}\}\,. \end{aligned}\right. \qquad (2,5)$$

Since for each value of N and l (2, 2) satisfies the Maxwell equations and the boundary condition at the wall of the circuit, (of the resonators as well as of the wave guides), which are both linear in the field quantities, (2, 5) also satisfies the Maxwell equations and the boundary conditions at the wall. Since, further, the amplitudes of the incoming waves contained in (2, 5) are $q_{N,l}$, (2, 5) must be identically equal to (2, 4). In this way, by identifying the amplitudes of the incoming waves in (2, 4) and

---

* Since the amplitude is complex, it contains also the information about the phase of the oscillation.

(2, 5) we obtain the unknown amplitudes $p_{N,l}$ in terms of the known amplitudes algebraically:

$$p_{N,l}=\sum_{N'}\sum_{l'}a_{N,l}^{N',l'}q_{N',l'}. \qquad (2,6)$$

This relation is often very useful in the following considerations.

Since the solution of the problem under any given load and excitation conditions is calculated by means of $a^{N,l}_{N',l'}$, as illustrated in the example given above, all characteristics of the given circuit are involved in the assembly of quantities $a^{N,l}_{N',l'}$. This assembly of quantities arranged in the form of a matrix

$$A=||a^{N,l}_{N',l'}||, \qquad (2,7)$$

the upper suffixes referring to the column and the lower to the row, may be thus called "characteristic matrix."

To calculate the characteristic matrix of a given circuit, we must, of course, solve the Maxwell equations explicitly. This requires in majority of cases the solution of a very complicated mathematical problem, which forces us to give up to find the explicit solution. As we shall show in the next section, however, the characteristic matix is nevertheless a very useful concept for treating the complicated circuit system owing to the considerably many intrinsic relations existing between its matrix elements $a^{N,l}_{N',l'}$. This situation is analogous to that, although the explicit calculation of the impedance is often very difficult, this does never prevent us from useing of this concept as the foundation of the general circuit theory.

From the fundamental relation (2, 6) we see that the characteristic matrix could also be introduced as the transformation matrix which expresses the amplitudes of the outgoing waves in terms of the amplitudes of the incoming waves. That these amplitudes can be obtained from one another by a linear transformation is obvious because of the linearity of the Maxwell equations as well as the boundary conditions at the walls and the openings.

Also in the ordinary circuit theory the corresponding transformation matrix have been used. In this case the usefulness of such matrix is based upon the linearity of the fundamental equations of the electromagnetic phenomena. In the case of a four terminal system, for instance, the impedance matrix is used

$$\begin{pmatrix} Z_{11}, & Z_{12} \\ Z_{21}, & Z_{22} \end{pmatrix}. \qquad (2,8)$$

which can be regarded as defining the transformation from the currents I_1 and I_2 at the terminals 1 and 2 into the voltages V_1 and V_2 at the same terminals:

$$\begin{pmatrix} V_1 \\ V_2 \end{pmatrix}=\begin{pmatrix} Z_{11}, Z_{12} \\ Z_{21}, Z_{22} \end{pmatrix}\begin{pmatrix} I_1 \\ I_2 \end{pmatrix}. \qquad (2,9)$$

But in the ordinary circuit theory such transformations are always defined referring to current and voltage. Since in such circuit elements, as wave guides and cavity resonators, current and voltage cannot be defined in the sence of ordinary circuit theory, it is impossible to introduce the transformation matrix in such a way. However, also in these new circuit elements the amplitudes of the incoming and the outgoing waves have well-defined meanings, so our concept of characteristic matrix can be used also in these new circuit systems.

In the special case of a system with only one opening in which only one mode of wave is possible (for instance, when the opening is a sufficiently narrow wave guide, or a concentric cable, or eventually Lecher wires) the characteristic matrix has only one row and one column so that it reduces into an ordinary (complex) number. In such a case it can be defined from (2, 6) simply as the ratio:

$$\frac{p}{q}=\frac{\text{amplitude of the outgoing wave at the opening}}{\text{amplitude of the incoming wave at the opening}}. \qquad (2,10)$$

This definition of the characteristic matrix may be compared with the ordinary definition of the impedance as the ratio:

$$\frac{V}{I}=\frac{\text{voltage at the terminal}}{\text{current at the terminal}}. \qquad (2,11)$$

Both of these ratios are characteristics of the circuit under consideration owing to the linearity of the fundamental equations, and the former ratio could equally be used as the latter in developing the general theory of alternating-current circuits. The reason why this has not been done lies in the fact that the latter ratio is more preferable in the study of low-cycle alternating-current circuits, since one has here nothing to do with propagating waves. However, in the study of ultrashort-wave-circuits one is forced to use the former because one meets here with circuit elements in which voltage and current can not be properly defined.

§ 3. General properties of the characteristic matrix.

To obtain the above mentioned intrinsic relations existing between various matrix elements, we use the following two theorems. Let $\boldsymbol{E}$ and $\boldsymbol{H}$ satisfy the Maxwell equations

$$\begin{cases}\text{curl}\,\boldsymbol{E}=i\omega\mu\boldsymbol{H}\\ \text{curl}\,\boldsymbol{H}=-i\omega\varepsilon\boldsymbol{E},\end{cases} \qquad (3,1)$$

and let $\boldsymbol{E}'$ and $\boldsymbol{H}'$ satisfy

$$\begin{cases}\text{curl}\,\boldsymbol{E}'=i\omega'\mu\boldsymbol{H}'\\ \text{curl}\,\boldsymbol{H}'=-i\omega'\varepsilon\boldsymbol{E}'.\end{cases} \qquad (3,2)$$

The frequency ω and ω' may be either real or complex. Also the case $\omega=\omega'$ is not excluded. Then we have the following two relations which can be proved easily by means of Green's theorem:

1 st relation

$$\int_{\Sigma}\{[\boldsymbol{E}\times\boldsymbol{H}']_n-[\boldsymbol{E}'\times\boldsymbol{H}]_n\}d\Sigma$$
$$=i(\omega-\omega')\int\{\mu(\boldsymbol{H}\cdot\boldsymbol{H}')$$
$$-\varepsilon(\boldsymbol{E}\cdot\boldsymbol{E}')\}dV \qquad (3,3)$$

2-nd relation

$$\int_{\Sigma}\{[\boldsymbol{E}\times\overset{*}{\boldsymbol{H}}{}']_n+[\overset{*}{\boldsymbol{E}}{}'\times\boldsymbol{H}]_n\}d\Sigma$$
$$=i(\omega-\omega')\int_{V}\{\mu(\overset{*}{\boldsymbol{H}}\cdot\boldsymbol{H}')$$
$$+\varepsilon(\boldsymbol{E}\cdot\overset{*}{\boldsymbol{E}}{}')\}dV. \qquad (3,4)$$

Here the integral on the left-hand side is taken over a closed surface Σ, n being the outward normal to this surface, and the integral on the right-hand side is taken in the volume V enclosed by Σ.

We now apply the first theorem taking for $\boldsymbol{E}$ and $\boldsymbol{H}$ those due to the l-th incoming wave through the N-th opening, i.e. $\boldsymbol{E}^{N,l}$ and $\boldsymbol{H}^{N,l}$ of (2, 2). For $\boldsymbol{E}'$ and $\boldsymbol{H}'$ we use the fields due to the l'-th incoming wave through the N'-th opening, i.e. $\boldsymbol{E}^{N',l'}$ and $\boldsymbol{H}^{N',l'}$. We assume further $\omega=\omega'$. We take as Σ a closed surface consisting of the inner wall of the circuit and planes crossing the wave guides at the openings. Since on the inner wall of the circuit we have

$$[\boldsymbol{E}\times\boldsymbol{H}']_n=[\boldsymbol{E}'\times\boldsymbol{H}]_n=0, \qquad (3,5)$$

we need only to take the surface-integral over the cross section at each opening and add them.* Using (3, 2) and (3, 3) and putting $\omega=\omega'$, we obtain

$$\sum_{N''}\sum_{l''}\sum_{l'''}\int_{\Sigma}\{[(\delta^{l}_{l''}\delta^{N}_{N''}\boldsymbol{F}_{l''}e^{-ik''_{l''}z''}$$
$$+a^{N,l}_{N'',l''}\boldsymbol{F}_{l''}e^{+ik''_{l''}z''})$$
$$\times(\delta^{l'}_{l'''}\delta^{N'}_{N''}\boldsymbol{G}_{l'''}e^{-ik''_{l'''}z''}$$

---

* We assume throughout this paper that the wall of the circuit is a perfect conductor.

$$
\begin{aligned}
&+a^{N',l'}_{N'',l'''}\boldsymbol{G}^{+}_{l'''}e^{+ik''_{l'''}z''})]_{z''}\\
&-[(\delta^{l'}_{l'''}\delta^{N'}_{N''}\boldsymbol{F}^{-}_{l'''}e^{-ik''_{l'''}z''}\\
&+a^{N',l'}_{N'',l'''}\boldsymbol{F}^{+}_{l'''}e^{+ik''_{l'''}z''})\\
&\times(\delta^{l}_{l''}\delta^{N}_{N''}\boldsymbol{G}^{-}_{l''}e^{-ik''_{l''}z''}\\
&+a^{N,l}_{N'',l''}\boldsymbol{G}^{+}_{l''}e^{+ik''_{l''}z''})]_{z''}\}dx''dy''\\
&=0. \qquad (3, 6)
\end{aligned}
$$

Here we have written, for simplicity, x'',y'' z'' and k'' instead of $x_{N''},y_{N''},z_{N''}$ and $k_{N''}$. The arguments in $\boldsymbol{F}$ and $\boldsymbol{G}$ are x'' and y''.

If we substitute for $\boldsymbol{F}$ and $\boldsymbol{G}$ in (3, 6) those of (1, 4) and (1, 5), and use the orthogonal property of U_l, we see that, on integrating over x'' and y'' the terms on the left hand side for which l'' is not equal to l''' vanish. Further we obtain for terms with $l''=l''$

$$
\begin{cases}
\int[\boldsymbol{F}^{+}_{l''}\times\boldsymbol{G}^{+}_{l''}]_{z''}dx''dy''=-2\omega\\
\int[\boldsymbol{F}^{+}_{l''}\times\boldsymbol{G}^{-}_{l''}]_{z''}dx''dy''=-(-1)^{l}2\omega\\
\int[\boldsymbol{F}^{-}_{l''}\times\boldsymbol{G}^{+}_{l''}]_{z''}dx''dy''=(-1)^{l}2\omega\\
\int[\boldsymbol{F}^{-}_{l''}\times\boldsymbol{G}^{-}_{l''}]_{z''}dx''dy''=2\omega.
\end{cases}
\qquad (3, 7)
$$

By using these relation and noting that U's are normalised according to (1, 10), the relation (3, 6) is reduced to the very simple form:

$$2\omega\{a^{N,l}_{N',l'}-a^{N',l'}_{N,l}\}=0. \qquad (3, 8)$$

This last relation gives, as ω is not zero, a set of relations between matrix elements:

$$
\begin{aligned}
&a^{N,l}_{N',l'}=a^{N',l'}_{N,l},\ (N,N'=1,2,3,\cdots,\\
&l,l'=1,2,3\cdots\cdots). \qquad (3, 9)
\end{aligned}
$$

The set of relations (3, 9) leads us to the conclusion that the characteristic matrix is symmetric.

These symmetry relations mean in words that the amplitude of the l'-th wave going out of the N'-th opening when the l-th wave of unit amplitude and no further waves are coming in through the N-th opening is equal to the amplitude of the l-th wave going out of the N-th opening when the l'-th wave of unit amplitude and no further waves are coming in through the N'-th opening. This theorem is well known under the name of reciprocity relation. Our relations (3, 9) are thus the mathematical expression for this reciprocity theorem in terms of the characteristic matrix. The relation (3, 9) holds for either real or complex freqnency.

We apply now the second theorem (3, 4) using $\boldsymbol{E}^{N,l}$ and $\boldsymbol{H}^{N,l}$ for $\boldsymbol{E}$ and $\boldsymbol{H}$, and $\boldsymbol{E}^{N',l'}$ and $\boldsymbol{H}^{N',l'}$ for $\boldsymbol{E}'$ and $\boldsymbol{H}'$. We assume also here $\omega=\omega'$, but ω must be real in this case. After several calculations we get

$$
\begin{aligned}
&\delta^{l}_{l'}\delta^{N}_{N'}\left(\frac{\sqrt{k_{N,l}}}{\sqrt{\overset{*}{k}_{N,l}}}+\frac{\sqrt{\overset{*}{k}_{N,l}}}{\sqrt{k_{N,l}}}\right)e^{-i(\overset{*}{k}_{N,l}-k_{N,l})z}\\
&-a^{N,l}_{N',l'}\left(\frac{\sqrt{k_{N',l'}}}{\sqrt{\overset{*}{k}_{N',l'}}}-\frac{\sqrt{\overset{*}{k}_{N',l'}}}{\sqrt{k_{N',l'}}}\right)\\
&\times e^{-i(k_{N',l'}+\overset{*}{k}_{N',l'})z}\\
&+\overset{*}{a}{}^{N',l'}_{N,l}\left(\frac{\sqrt{k_{N,l}}}{\sqrt{\overset{*}{k}_{N,l}}}-\frac{\sqrt{\overset{*}{k}_{N,l}}}{\sqrt{k_{N,l}}}\right)e^{-i(k_{N,l}+\overset{*}{k}_{N,l})z}\\
&-\sum_{N''}\sum_{l''}\overset{*}{a}{}^{N''l''}_{N',l'}a^{N,l}_{N'',l''}\left(\frac{\sqrt{k_{N'',l''}}}{\sqrt{\overset{*}{k}_{N'',l''}}}+\frac{\sqrt{\overset{*}{k}_{N'',l''}}}{\sqrt{k_{N'',l''}}}\right)\\
&\times e^{i(k^{N''}_{l''}-k^{N''}_{l''})z}=0. \qquad (3, 10)
\end{aligned}
$$

We shall here classify the waves of various modes into those for which k_l is real and those for which k_l is imaginary. To emphasize that k_l is imaginary and thus the mode represents a damped wave, we affix a bar on l, such as $\bar{l}$. On the other hand, we consider k_l with unbarred l always to be real. Then the relation (3, 10) is splitted into several relatons as follows:

$$\delta^{l}_{l'}\delta^{N}_{N'}-\sum_{N''}\sum_{l''}\overset{*}{a}{}^{N'',l''}_{N',l'}a^{N,l}_{N'',l''}=0 \qquad (3, 11)$$

and

$$\begin{cases} -ia^{N,l}_{N',\bar{l}'}-\sum\limits_{N''}\sum\limits_{l''}\overset{*}{a}{}^{N'',l''}_{N',\bar{l}'}\,a^{N,l}_{N'',l''}=0 \\ ia^{N,\bar{l}}_{N',l'}-\sum\limits_{N''}\sum\limits_{l''}\overset{*}{a}{}^{N'',l''}_{N',l'}\,a^{N,l}_{N'',l''}=0 \\ -ia^{N',\bar{l}'}_{N,\bar{l}}+i\overset{*}{a}{}^{N',\bar{l}'}_{N,\bar{l}}-\sum\limits_{N''}\sum\limits_{l''}\overset{*}{a}{}^{N'',l''}_{N',\bar{l}'}\,a^{N,\bar{l}}_{N'',l''}. \end{cases} \tag{3, 12}$$

If the wave guides are long enough, so that the waves with imaginary k_l which are eventually generated in the circuit are perfectly damped at the openings, we may consider all a's with barred l to vanish. We need, as a consequence, only to consider the a's without bars, so that also the characteristic matrix can be thought as containing only a's with unbarred l. Then only the first relation, (3, 11), has a significance, which in mathematical words says that the characteristic matrix is unitary.

In the case of $N=N', l=l'$, (3, 11) is

$$\sum_{N''}\sum_{l''}a^{N'',l''}_{N,l}\,\overset{*}{a}{}^{N,l}_{N'',l''}=1. \tag{3, 13}$$

That this relation physically means the conservation of energy is obvious. Since the energy transported by the wave with the amplitude a is $\overset{*}{a}a$, the left-hand side of (3, 13) gives the sum of the energies transported by the various outgoing waves when a wave of unit amplitude is coming in, while the unity standing on the right hand side means the energy transported by this incoming wave of unit amplitude. The relation (1, 13) expresses thus the balance of these incoming and outgoing energies.

The remaining relations of (3, 11):

$$\sum_{N''}\sum_{l''}\overset{*}{a}{}^{N'',l''}_{N',l'}\,a^{N,l}_{N'',l''}=0 \tag{3, 14}$$

for which $N'=N$ and $l'=l$ are not simultaneously satisfied cannot be interpreted so directly. However, just by these relations, together with (3, 13), the energy balance between incoming and outgoing waves is guaranteed also for more general cases. Namely, multipling side by side the equation (2, 6), which exists generally between the amplitudes of the incoming and the outgoing waves, by its conjugate complex equation, and taking the summation over all values of N and l, we obtain

$$\sum_N\sum_l\overset{*}{p}_{N,l}p_{N,l}$$

$$=\sum_{N'}\sum_{l'}\sum_{N''}\sum_{l''}\sum_N\sum_l\overset{*}{a}{}^{N'',l''}_{N,l}\,a^{N',l'}_{N,l}\,\overset{*}{q}_{N'',l''}q_{N',l'}. \tag{3, 15}$$

If we use here the unitary relation (3, 11) noting the symmetry property (3, 9), we obtain

$$\sum_N\sum_l\overset{*}{p}_{N,l}p_{N,l}=\sum_N\sum_l\overset{*}{q}_{N,l}q_{N,l}, \tag{3, 16}$$

which means that the energies transported by the incoming waves and the outgoing waves are equal to one another.

As stated above, our relations (the symmetry and the unitary relations) are often very useful to give insight of the properties of a given circuit system without carrying out the detailed calculation. Considerably many information about the circuit can be thus obtained by a general consideration alone. Such examples will be given in § 5 of this paper and in § 9 of the second paper.

§ 4. Some Simple examples

We shall now give some simple examples showing how we can solve the problem with more complicated conditions at the openings by means of algebraical operations alone when the characteristic matrix of the circuit is known.

Let us suppose, for instance, a circuit with two openings. What waves must propagate into and out of the second opening when the waves of given amplitudes are propagating into and out of the first opening?

Let q_l be the known amplitude of the l-th incoming wave in the first wave guide, and let p_l the amplitude of the l-th outgoing wave ($l=1,2,3\cdots\cdots$) in the same wave guide. Further, let y_l denote the unknown amplitude of the l-th incoming wave and x_l the unknown amplitude of the l-th outgoing wave in the second wave guide. Then, according to the fundamental relation (2, 6) we have

$$\begin{cases} p_l=\sum\limits_{l'} a^{1,l'}_{1,l}\, q_{l'}+\sum\limits_{l'} a^{2,l'}_{1,l}\, y_{l'} \\ x_l=\sum\limits_{l'} a^{1,l'}_{2,l}\, q_{l'}+\sum\limits_{l'} a^{2,l'}_{2,l}\, y_{l'}. \end{cases} \tag{4, 1}$$

When the characteristic matrix $a^{N',l'}_{N,l}$ is known, we can obtain the answer by solving this simultaneous algebraic equations for the unknowns x_l and y_l.

Next we shall give another example. We suppose a circuit with three openings 0, 1 and 2 as shown in Fig. 2(A). We insert a piston P in the zero-th wave guide, (see Fig. 2(B)). This piston is supposed to reflect back each wave without changing its mode. The amplitudes of the waves transmitted to the opening 2 and those reflected to the opening 1 are required as a function of the position of the piston when the wave of the first mode, say, of unit amplitude is incident through the first opening.

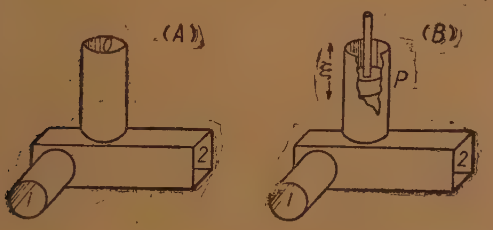

Fig. 2. Circuits with and without a piston.

If the characteristic matrix A of the three-opening circuit of Fig. 2(A) is known, we can solve this problem in the following way: The amplitude of the l-th wave directly reflected back to the first opening is $a^{1,1}_{1,l}$ by the definition of the characteristic matrix. However, waves will be partly transmitted into the zero-th wave guide and reach the piston, which will reflect them backward. Let now ξ denote the displacement of the piston from the standard position, and the l'-th wave which has thus arrived at the piston has there the amplitude $a^{1,1}_{0,l'}e^{ik_{l'}\xi}$ (by the definition of the characteristic matrix this wave has the amplitude $a^{1,1}_{0,l'}$ at the standard point 0). The waves which are in this way once reflected by the piston can now be regarded as the secondary waves propagating into the zero-th opening. They will partly transmitted into the first opening and partly reflected back again to the piston. Since the amplitude of the l'-th wave contained in the secondary waves is at the standard point $a^{1,1}_{0,l'}e^{2ik_{l'}\xi}$, the amplitude of the l-th outgoing wave at the first opening which is due to these secondary waves is $\sum\limits_{l'} a^{0,l'}_{1,l}\, a^{1,1}_{0,l'}e^{2ik_{l'}\xi}$, and the amplitude of the l th wave which comes back towards the piston is $\sum\limits_{l'} a^{0,l'}_{0,l}\, a^{1,1}_{0,l'}e^{2ik_0\xi}$ (at the standard point). This latter wave will be reflected again by the piston and can be regarded as the tertiary wave propagating into the zero-th opening. The tertiary waves which are in this way reflected twice by the piston will contribute to the amplitude of the l'-th outgoing wave at the first opening; this contribution is $\sum\limits_{l''}\sum\limits_{l'''} a^{0,l'''}_{1,l}\, e^{2ik_{l'''}\xi}\, a^{0,l''}_{0,l'''}e^{2ik_{l''}\xi}\, a^{1,1}_{0,l''}$. By adding the amplitudes of the directly reflected wave and those due to the secondary, the tertiary,···· waves, we obtain finally the amplitude of the l'-th wave reflected to the first opening:

$$\begin{aligned} x_{1,l'}&=a^{1,1}_{1,l'}+\sum_{l''} a^{0,l''}_{1,l'}\, e^{2ik_{l''}\xi}\, a^{1,1}_{0,l''} \\ &\quad+\sum_{l'''}\sum_{l''} a^{0,l'''}_{1,l'}\, e^{2ik_{l'''}\xi}\, a^{0,l''}_{0,l'''}e^{2ik_{l''}\xi}\, a^{1,1}_{0,l''} \\ &\quad+\cdots\cdots \end{aligned} \tag{4, 2}$$

The amplitude of the l'-th wave transmitted to the second opening can also be obtained in a similar way:

$$x_{2,l'}=a^{1,0}_{2,l'}+\sum_{l''} a^{0,l''}_{2,l'}\, e^{2ik_{l''}\xi}\, a^{1,1}_{0,l''}$$

$$+\sum_{l'''}\sum_{l''} a^{0,l'''}_{2,l'} e^{2ik_{l'''}\xi} a^{0,l''}_{0,l'''} e^{2ik_{l''}\xi} a^{1,1}_{0,l''}$$
$$+\cdots\cdots \qquad (4,3)$$

It is often convenient for such treatments to introduce the symbolism of the matrix algebra. If we denote by the partial matrix of A obtained by picking up the matrix elements referring to the N-th and N'-th opening, $A_N^{N'}$,

$$A_N^{N'}=\begin{bmatrix} a^{N',1}_{N,1} & a^{N',2}_{N,1} & a^{N',3}_{N,1} & \cdots\cdots \\ a^{N',1}_{N,2} & a^{N',2}_{N,2} & a^{N',3}_{N,2} & \cdots\cdots \\ a^{N',1}_{N,3} & a^{N',2}_{N,3} & a^{N',3}_{N,3} & \cdots\cdots \\ \cdots\cdots & \cdots\cdots & \cdots\cdots & \cdots\cdots \end{bmatrix} \qquad (4,4)$$

Then, for instance, (2, 6) can be written as

$$P_N=\sum_{N'} A_N^{N'} Q_{N'} \quad (N=1,2,3,\cdots\cdots), \qquad (4,5)$$

where P_N is the one-column matrix (or vector) whose matrix elements represent the amplitudes of the outgoing waves in the N-th wave guide:

$$P_N=\begin{bmatrix} p_{N,1} \\ p_{N,2} \\ p_{N,3} \\ \cdots \end{bmatrix}, \qquad (4,6)$$

and Q_N is the one-column matrix whose matrix elements are the amplitudes of the incoming waves in the N-th wave guide:

$$Q_N=\begin{bmatrix} q_{N,1} \\ q_{N,2} \\ q_{N,3} \\ \cdots \end{bmatrix}. \qquad (4,7)$$

Using this symbolism the equation (4, 1) can now be written as

$$\begin{cases} P=A_1^1 Q+A_1^2 Y \\ X=A_2^1 Q+A_2^2 Y, \end{cases} \qquad (4,8)$$

the formal solution of which is readily written down:

$$\begin{cases} Y=(A_1^2)^{-1}(P-A_1^1 Q)=(A_1^2)^{-1}P \\ \qquad -(A_1^2)^{-1}A_1^1 Q \\ X=A_2^1 Q+A_2^2(A_1^2)^{-1}(P-A_1^1 Q) \\ \qquad =A_2^2(A_1^2)^{-1}P \\ \qquad +\{A_2^1-A_2^2(A_1^2)^{-1}A_1^1\}Q. \end{cases} \qquad (4,9)$$

By introducting the matrix symbolism the infinite series of (4, 2) and (4, 3) can also be expressed in a closed form. At first the series is written in the form

$$\begin{cases} X_1=\{A_1^1+A_1^0 D(\xi)A_0^1 \\ \qquad +A_1^0 D(\xi)A_0^0 D(\xi)A_0^1+\cdots\cdots\}I_1 \\ \qquad =[A_1^1+A_1^0 D(\xi)\{1+A_0^0 D(\xi) \\ \qquad +A_0^0 D(\xi)A_0^0 D(\xi)+\cdots\}A_0^1]I_1 \\ X_2=\{A_2^1+A_2^0 D(\xi)A_0^1 \\ \qquad +A_2^0 D(\xi)A_0^0 D(\xi)A_0^1+\cdots\}I_1 \\ \qquad =[A_2^1+A_2^0 D(\xi)\{1+A_0^0 D(\xi) \\ \qquad +A_0^0 D(\xi)A_0^0 D(\xi) \\ \qquad +\cdots\}A_0^1]I_1 \end{cases} \qquad (4,10)$$

where I_1 means the following one column matrix:

$$I_1=\begin{bmatrix} 1 \\ 0 \\ 0 \\ \vdots \\ \vdots \end{bmatrix}, \qquad (4,11)$$

and $D(\xi)$ is the diagonal matrix

$$D(\xi)=\begin{bmatrix} e^{2ik_1\xi} & & & \\ & e^{2ik_2\xi} & & \\ & & e^{2ik_3\xi} & \\ & & & \ddots \end{bmatrix}. \qquad (4,12)$$

Then, it is noticed that the series in (4,10) is a geometrical series with 1 as the first term and $A_0^0 D(\xi)$ as the common ratio. We obtain thus

$$\begin{cases} X_1=[A_1^1+A_1^0 D(\xi)\{1 \\ \qquad -A_0^0 D(\xi)\}^{-1}A_0^1]I_1 \\ X_2=[A_2^1+A_2^0 D(\xi)\{1 \\ \qquad -A_0^0 D(\xi)\}^{-1}A_0^1]I_1. \end{cases} \qquad (4,13)$$

By generalising the above consideration we can easily obtain the characteristic matrix for the two-opening circuit of Fig. 2(B) in terms of the characteristic matrix of the three-opening circuit of Fig. 2(A). Let this unknown matrix of the two-opening circuit be denoted by B. Then the matrix B is found to be

$$\left\{\begin{aligned} B^1_1&=A^1_1+A^0_1D(\xi)\{1\\ &\qquad -A^0_0D(\xi)\}^{-1}A^1_0\\ B^1_2&=A^1_2+A^0_2D(\xi)\{1\\ &\qquad -A^0_0D(\xi)\}^{-1}A^1_0\\ B^2_2&=A^2_2+A^0_2D(\xi)\{1\\ &\qquad -A^0_0D(\xi)\}^{-1}A^2_0\\ B^2_1&=A^2_1+A^0_1D(\xi)\{1\\ &\qquad -A^0_0D(\xi)\}^{-1}A^2_0\,. \end{aligned}\right. \tag{4, 14}$$

The result (4, 14) can also be obtained directly from the fundamental relation (4, 5) in the following way, if it is noted that, owing to the existence of the piston at the position ξ, which reflects the waves backward, the amplitudes of the incoming waves in the zero-th guide must be related to those of the outgoing waves in the same wave guide by

$$Q_0=D(\xi)P_0\,. \tag{4, 15}$$

For our three-opening circuit the relation (4, 5) is

$$\left\{\begin{aligned} P_0&=A^0_0Q_0+A^1_0Q_1+A^2_0Q_2\\ P_1&=A^0_1Q_0+A^1_1Q_1+A^2_1Q_2\\ P_2&=A^0_2Q_0+A^1_2Q_1+A^2_2Q_2\,. \end{aligned}\right. \tag{4, 16}$$

If we eliminate P_0 and Q_0 from (4, 16) and (4, 15), we obtain the relation between P_1, P_2 and Q_1, Q_2:

$$\left\{\begin{aligned} P_1=&[A^1_1+A^0_1D(\xi)\{1\\ &\qquad -A^0_0D(\xi)\}^{-1}A^1_0]Q_1\\ &+[A^2_1+A^0_1D(\xi)\{1\\ &\qquad -A^0_0D(\xi)\}^{-1}A^2_0]Q_2\\ P_2=&[A^1_2+A^0_2D(\xi)\{1\\ &\qquad -A^0_0D(\xi)\}^{-1}A^1_0]Q_1\\ &+[A^2_2+A^0_2D(\xi)\{1\\ &\qquad -A^0_0D(\xi)\}^{-1}A^2_0]Q_2 \end{aligned}\right. \tag{4, 17}$$

which means that the characteristic matrix of the two-opening circuit with the piston at ξ is given really by (4, 14).

§ 5. Application to symmetrical traps.*

As a simple example of our theory we discuss the properties of a symmetrical trap. Suppose that a side-tube is attached to the wave guide AB (see Fig. 3). The wave guide and the side-tube may have any form, but the combined system must have a symmetry with respect to A and B. So the circuit may also have a form as indicated in (B′) in the figure. A piston is then inserted in the side tube. We shall further assume that the wave guides are long and narrow enough so that we need not consider the waves of higher modes. We shall call such a system "symmetrical trap."

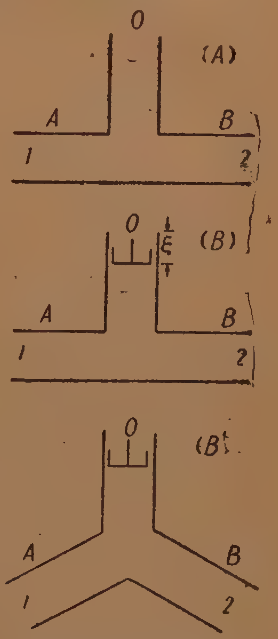

Fig. 3. Symmetrical trap.

To obtain the properties of the symmetrical trap we consider first the three-opening system (A), drawing the piston out of the side-tube. We label the openings by 0, 1 and 2 as shown in the figure. The characteristic matrix has then 3×3=9 matrix elements. The number of the independent parameters which are needed to characterise the circuit is, however, much less owing to the symmetry and the unitary character of the matrix. Moreover, they are still reduced in our case by the above mentioned symmetrical structure of the circuit. We have, namely, besides the relations

---

* This paragraph is partly due to Miyazima.

$$a_0^1=a_1^0,\quad a_0^2=a_2^0,\quad a_2^1=a_1^2 \qquad (5,1)$$

which express the symmetry character of the matrix, further relations

$$a_1^1=a_2^2,\quad a_0^1=a_0^2, \qquad (5,2)$$

which follow from the symmetrical structure of the circuit. We write here the partial matrices by small letters, because they are ordinary numbers in our case where only one mode exists in each wave guide.

In this way the characteristic matrix can be written in the form

$$A=\begin{pmatrix} a_0^0 & a_1^0 & a_1^0 \\ a_1^0 & a_1^1 & a_2^1 \\ a_1^0 & a_2^1 & a_1^1 \end{pmatrix}, \qquad (5,3)$$

where the unitary condition imposes the further conditions on four quantities a_0^0, a_1^1, a_1^0 and a_2^1:

$$\begin{cases} |a_0^0|^2+2|a_1^0|^2=1 \\ |a_1^0|^2+|a_1^1|_2+|a_2^1|^2=1 \\ a_0^0\overset{*}{a}_1^0+a_1^0\overset{*}{a}_1^1+a_1^0\overset{*}{a}_2^1=0 \\ a^0\overset{*}{a}_1^0+a_1^1\overset{*}{a}_2^1+a_2^1\overset{*}{a}_1^1=0\,. \end{cases} \qquad (5,4)$$

Since a's are complex, (5, 3) contains eight real parameters, which are not independent but are related to each other by (5, 4). It is desirable to reduce the number of the parameters expressing the matrix A so that it contains only independent parameters.

For this purpose we put

$$\begin{cases} a_0^0=|a_0^0|e^{i\theta_0^0}, \quad a_1^1=|a_1^1|e^{i\theta_1^1} \\ a_1^0=|a_1^0|e^{i\theta_1^0} \\ a_2^1=|a_2^1|e^{i\theta_2^1}\,. \end{cases} \qquad (5,5)$$

Then the fourth relation of (5, 4) can be written in the form

$$|a_1^0|^2+2|a_1^1|\,|a_2^4|\cos(\theta_1^1-\theta_2^1) = 0. \qquad (5,4')$$

If we use here the second relation, we have

$$|a_1^1|^2+|a_2^1|^2-2|a_1^1|\,|a_2^1|\cos(\theta_1^1-\theta_2^1) = 1. \qquad (5,4'')$$

On the other hand, the third relation of (5, 4) gives

$$|a_1^1|e^{i\theta_1^1}+|a_2^1|e^{i\theta_0^1} = -|a_0^0|e^{i(\theta_1^0-\theta_0^0)}. \qquad (5,4''')$$

If we now represent a_1^1 and a_2^1 as vectors on the Gauss plane and let them be $\overrightarrow{\mathrm{OA}}$ and $\overrightarrow{\mathrm{OB}}$ respectively, see Fig. 4. Then (5, 4'') means that their sum $\overrightarrow{\mathrm{OC}}$ represents $-|a_0^0|e^{i(\theta_1^0-\theta_0^0)}$. The relation (5, 4'') shows further that the length of $\overrightarrow{\mathrm{BA}}$ is unity.

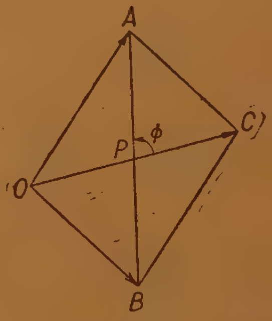

Fig. 4. Vector diagram for a_1^1, a_2^1 and $|a_0^0|e^{i(2\theta_1^0-\theta_0^0)}$

Putting now

$$\angle \mathrm{CPA}=\varphi. \qquad (5,6)$$

P being the center of the parallelogram OACB, and noting

$$\begin{cases} \overrightarrow{\mathrm{OA}}=\overrightarrow{\mathrm{OP}}+\overrightarrow{\mathrm{PA}} \\ \overrightarrow{\mathrm{OB}}=\overrightarrow{\mathrm{OP}}-\overrightarrow{\mathrm{PA}}, \end{cases} \qquad (3,7)$$

we obtain

$$\begin{cases} a_1^1=\dfrac{1}{2}[e^{i\varphi}-|a_0^0|]e^{i(2\theta_1^0-\theta_0^0)} \\ a_2^1=\dfrac{1}{2}[e^{i\varphi}+|a_0^0|]e^{i(2\theta_1^0-\theta_0^0)}\,. \end{cases} \qquad (5,8)$$

By these two relations together with the relation

$$a_1^0=\sqrt{\frac{1-|a_0^0|}{2}}\;e^{i\theta_1^0}, \qquad (5,9)$$

which is obtained directly from the first relation of (5, 4), we can exprese four a's in terms of the four independent real parameters

$|a_0^0|$, θ_0^0, θ_1^0 and φ: thus

$$\begin{cases} a_0^0=|a_0^0|e^{i\theta_0^0} \\ a_1^1=\dfrac{1}{2}(e^{i\varphi}-|a_0^0|)e^{i(2\theta_1^0-\theta_0^0)} \\ a_1^0=\sqrt{\dfrac{1-|a_0^0|}{2}}\; e^{i\theta_1^0} \\ a_2^1=-\dfrac{1}{2}(e^{i\varphi}+|a_0^0|)e^{i(2\theta_1^0-\theta_0^0)} \end{cases} \quad . \qquad (5,19)$$

It can be easily verified that these a's satisfy the unitary condition (5, 4).

We now insert the piston in the side-tube, and let ξ denote its distance from the standard position. To obtain the characteristic matrix B for the two-opening circuit (B) we eliminate p_0 and q_0 from

$$\begin{cases} p_0=a_0^0q_0+a_1^0q_1+a_1^0q_2 \\ p_1=a_1^0q_0+a_1^1q_1+a_2^1q_2 \\ p_2=a_1^0q_0+a_2^1q_1+a_1^1q_2 \end{cases} \qquad (5,11)$$

and

$$q_0=e^{2ik\xi}p_0 \,; \qquad (5,12)$$

were p's and q's have the obvious meanings.

We have then

$$\begin{aligned} p_1=&\left\{a_1^1+\frac{(a_1^0)^2e^{2ik\xi}}{1-a_0^0e^{2ik\xi}}\right\}q_1 \\ &+\left\{a_2^1+\frac{(a_1^0)^2e^{2ik\xi}}{1-a_0^0e^{2ik\xi}}\right\}q_2 \\ p_2=&\left\{a_2^1+\frac{(a_1^0)^2e^{2ik\xi}}{1-a_0^0e^{2ik\xi}}\right\}q_1 \\ &+\left\{a_1^1+\frac{(a_1^0)^2e^{2ik\xi}}{1-a_0^0e^{2ik\xi}}\right\}q_2 \,, \end{aligned} \qquad (5,13)$$

which means that the characteristic matrix B or (B) is given by

$$B=\begin{pmatrix} b_1^1 & b_2^1 \\ b_2^1 & b_1^1 \end{pmatrix}$$

$$\begin{pmatrix} a_1^1+\dfrac{(a_1^0)^2e^{2ik\xi}}{1-a_0^0e^{2ik\xi}} & a_2^1+\dfrac{(a_1^0)^2e^{2ik\xi}}{1-a_0^0e^{2ik\xi}} \\ a_2^1+\dfrac{(a_1^0)^2e^{2ik\xi}}{1-a_0^0e^{2ik\xi}} & a_1^1+\dfrac{(a_1^0)e^{2ik\xi}}{1-a_0^0e^{2ik\xi}} \end{pmatrix} \qquad (5,14)$$

By introducing (5, 10), this gives

$$\begin{cases} b_1^1=\dfrac{1}{2}e^{i(2\theta_1^0-\theta_0^0)} \\ \times\dfrac{(e^{i\varphi}-|a_0^0|)-(1-|a_0^0|e^{i\varphi})e^{i(\theta_0^0+2k\xi)}}{1-|a_0^0|e^{i(\theta^0_0+2k\xi)}} \\ b_2^1=-\dfrac{1}{2}e^{i(2\theta_1^0-\theta_0^0)} \\ \times\dfrac{(e^{i\varphi}+|a_0^0|)+(1+|a_0^0|e^{i\varphi})e^{i(\theta_0^0+2k\xi)}}{1-|a_0^0|e^{i(\theta_0^0+2k\xi)}} . \end{cases} \qquad (5,15)$$

Now, the first conclusion drawn from these formulae is that by suitably adjusting the piston the trap can be made so that it reflects the wave perfectly or transmits it without reflection. Thus one can make the numerator of either b_1^1 or b_2^1 vanish by adjusting ξ suitablly. This is possible because of the identity

$$|e^{i\varphi}\pm|a_0^0||=|1\pm|a_0^0|e^{i\varphi}|. \qquad (5,16)$$

The second conclusion drown from (5, 15) is that the symmetrical trap can be used as a matching device. Since this problem was treated by Miyazima,(3) we shall not enter into this. We are not contented with the result that the essential properties of our symmetrical trap is already characterized if we give two parameters $|a_0^0|$ and φ, since the other parameters θ_1^0 and θ_0^0 can be adjusted at will by displacing the standard points. Thus, essentially, only two sort of experiments suffice to determine the character of our symmetrical trap.

(To be continued).

References.

(1) G. Breit: Phys. Rev. **58** (1940), 1068.
(2) Lord Rayleigh: Phil. Mag., **43** (1897), 125.
(3) T. Miyazima: Sc. Pap. I.P.C.R., **42** (1947), Phys. 121.

On the Elimination of the Auxiliary Condition in the Quantum Electrodynamics. I.

By Satio HAYAKAWA,
Central
Meteorological Observatory.

Yonezi MIYAMOTO
Physical Institute,
Tokyo University.

and

Sin-itiro TOMONAGA
Physical Institute,
Tokyo Bunrika Daigaku.

(Received December 2, 1946)

§ 1. Introduction

Since the discovery of the quantum mechanics various attempts have been made to build up the quantum-mechanical description of the interaction between electrons and electromagnetic field. Among such theories the so-called many-time theory of Dirac is the most satisfactory one from the standpoint of the theory of relativity. This many-time theory was first put forward by Dirac and then comyleted by Dirac, Fock and Podolsky$^{(1)}$ in a perfectly relativistic form free from any undesirable feature of other formalisms of the quantum electrodynamics, in which the time variable t plays a role quite distinguished from the space variables x, y, and z. But in the elimination of the so-called auxiliary condition, which was carried out by Fock,$^{(2)}$ an undesirable element has been again introduced into the theory by separating the longitudinal and the transverse components of the field, since this distinction of the field components has the definite meaning only referring to some specified Lorentz frame.

The aim of the present paper is to show how one has to do if in this elimination the relativistic form of the theory should be maintained. As we shall show in the following paragraphs this is possible through the relativistic generalization of the idea of transverse and longitudinal components of the field. For the sake of easier understanding we shall begin with a brief outline of the method developed by Fock.

Let the components of the fundamental tensor be $g_{\mu\nu}$, which have the values

$$g_{00}=-1, \quad g_{11}=g_{22}=g_{33}=1$$
$$g_{\mu\nu}=0 \text{ for } \mu\neq\nu. \tag{1.1}$$

We use thick letters to denote four-vectors. Thus the position of the world point with the coordinates $(ct;\ x,y,z)$ is denoted by $\boldsymbol{x}$. The space component of a four-vector is denoted by a letter affixed with an arrow, such as $\vec{x}=(x,y,z)$. The symbols such as Grad, Div. etc. mean the differential operators in the four-dimensional world. On the other hand, the symbols grad div, curl etc. mean the corresponding operators in the three-dimensional space.

We first consider the case of no charge. The Lagrange function for the electromagnetic field is given by

$$L=-\frac{1}{4}(\text{Curl } \boldsymbol{A})^2$$
$$-\frac{1}{2}(\text{Div } \boldsymbol{A})^2 \tag{1.2}$$

where $\boldsymbol{A}$ is the four-potential of the field having the components $(A_0 A_1 A_2 A_3)$. By applying the well-known procedure we obtain the canonical equations for the potential A_0, A_1, A_2 and A_3 and their canonically conjugate variables $P_0 P_1 P_2$ and

P_3. These equations of motion yield then

$$\Box \mathbf{A}=0 \quad \text{and} \quad \Box \mathbf{P}=0. \tag{1.3}$$

But the Maxwell equations are first obtained when we put

$$\mathrm{Div}\, \mathbf{A}=0. \tag{1.4}$$

in the canonical equations. The auxiliary condition (1.4) is satisfied for all values of t if it is initially satisfied with the condition $\frac{\partial}{\partial t}\mathrm{Div}\mathbf{A}=0$. The equation (1.4) is usually called Lorentz condition.

Since the potential $\mathbf{A}$ satisfies the d'Alembert equation (1.3), it can be represented by a superposition of plane waves:

$$\mathbf{A}(x)=\frac{1}{(2\pi)^{3/2}}\int\{\mathbf{A}(\vec{k})e^{i(kx)}$$

$$+\mathbf{A}^{+}(\vec{k})e^{-i(kx)}\}\frac{d\vec{k}}{k} \tag{1.5}$$

where k is the (four-dimentional) propagation vector of the plane wave. Since the waves propagate with the light velocity, we have

$$k_0=|\vec{k}|\equiv k. \tag{1.6}$$

The amplitudes $\mathbf{A}(\vec{k})$ and $\mathbf{A}^{+}(\vec{k})$, which are conjugate complex with each other, are now used to discribe the field.* As noticed by Fock, these Fourier amplitudes are transformed as four vectors, and this justifies our way of denoting them by thick letters.

The commutation relations between these amplitudes are then found, which are

$$\begin{cases} [A^{+}_{\mu}(\vec{k}),\ A_{\nu}(\vec{k}')] \\ \qquad =-\dfrac{hck}{2}g_{\mu\nu}\delta(\vec{k}-\vec{k}') \\ \qquad \text{all other commutors}=0. \end{cases} \tag{1.7}$$

Since $k\delta(\vec{k}-\vec{k}')$ is an invariant and since $\mathbf{A}(\vec{k})$ and $\mathbf{A}^{+}(\vec{k})$ are four-vectors, the commutation relations (1.7) have invariant forms with respect to Lorentz transformations. The relations (1.7) show that $A_{\mu}(\vec{k})$ and $A_{\mu}^{+}(\vec{k})$ are a set of canonically conjugate variables.

Now, it is convenient to introduce the representation in which $A_0(\vec{k})$ and $A^{+}(\vec{k})$ are diagonal. Although this manner of introducing the representation is unsatisfactory from the standpoint of the relativity theory because the space and time components of A are unsymmetrically treated, this is an easier way of eliminating the auxiliary condition. In this representation the Ψ vector representing the state is represented by a functional of the argument functions $A_0(k)$ and $\vec{A_j^{+}}(k)$, $j=1,2$ and 3; the operators $A_0(k)$ and $A_j^{+}(\vec{k})$ being simply the multiplication of this functional by $A_0(k)$ and $A_j^{+}(k)$ respectively. The operators $A_0^{+}(k)$ and $A_j(\vec{k})$, on the other hand, are respectively $\frac{hck}{2}$ times the functional differentiation $\frac{\delta}{\delta A_0(\vec{k})}$ and $\frac{\delta}{\delta A_j^{+}(k)}$ of Ψ:

$$\begin{cases} A_0(\vec{k})\rightarrow A_0(\vec{k})\times\ , \\ A_0^{+}(\vec{k})\rightarrow \dfrac{hck}{2}\dfrac{\delta}{\delta A_0(\vec{k})} \\ A_j^{+}(\vec{k})\rightarrow A_j^{+}(\vec{k})\times\ , \\ A_j(k)\rightarrow \dfrac{hck}{2}\dfrac{\delta}{\delta A_j^{+}(\vec{k})} \end{cases} \tag{1.8}$$

In terms of the Fourier amplitudes the Lorentz condition (1.4) is expressed by

$$\begin{cases} (\mathbf{k},\mathbf{A}(\vec{k}))=0 \\ (\mathbf{k}\,\overset{+}{\mathbf{A}}(\vec{k}))=0. \end{cases} \tag{1.9}$$

But, as is well known, these conditions cannot be regarded as conditions imposed on the operators $\mathbf{A}(k)$ and $\mathbf{A}^{+}(k)$ because (1.9) are not then compatible with the commutation relations (1.7). Thus we should use

---

* The amplitudes $A(\vec{k})$ and $\overset{+}{A}(\vec{k})$ here are k times larger than those of Fock.

$$\begin{cases} (k, A(\vec{k}))\,\Psi = 0 \\ (k, \vec{A}^{+}(\vec{k}))\,\Psi = 0 \end{cases} \qquad (1,\ 9')$$

in place of (1. 9), regarding the Lorentz condition as a condition imposed upon Ψ. That the conditions in (1. 9′) are compatible with each other can be proved easily.

We proceed now to the case where the field is interacting with electrons. In the presence of electrons, the Schrödinger functional Ψ is no longer constant but changes with time, or more correctly, changes with the times each belonging to one electron. The dependence of Ψ on the time belonging to the s-th electron is determined by means of the fundamental equation of the many-time theory:

$$\left\{\left(\alpha^{(s)}, \frac{h}{i}\mathrm{Grad}^{(s)} - \frac{e_s}{c}A(x^{(s)})\right) + mc\beta^{(s)}\right\}\Psi = 0$$
$$s = 1, 2, 3 \cdots n \qquad (1.\ 10)$$

where $\vec{\alpha}$ and β are the Dirac matrices and $\alpha_0 = 1$. The superscript (s) means that the quantity belongs to the s-th electron, thus $x^{(s)}$ denotes the position of the s-th electron in the world and e_s its charge. The total number of the existing electrons must be constant in this theory and is denoted by n. It is the characteristic of the many-time theory that the potential $A(x)$ in (1. 10) satisfies the d'Alembert equation (1. 3) notwithstanding the presence of the electrons.

In the presence of the electrons we must modify the Lorentz condition (1. 9′) because they are not compatible with (1. 10). The modified conditions are

$$\begin{cases} \left\{(k, A(\vec{k})) + \frac{f}{2}\right\}\Psi = 0 \\ \left\{(k, A^{+}(\vec{k})) + \frac{f^*}{2}\right\}\Psi = 0 \end{cases} \qquad (1.\ 11)$$

where f is defined by

$$f = \frac{1}{(2\pi)^{2/3}} \sum_{s=1}^{n} e_s e^{-i(k, x^{(s)})}$$

and f^* is its conjugatex complex quantity. The conditions (1. 11) restrict the Ψ vector, so that not all Ψ's satisfying (1. 10) represent the actual states of the system. Thus, only those portions of the Ψ-space in which the conditions (1. 11) are satisfied has a physical significance, the other portion being superfluous. It is, therefore, desirable to eliminate this superfluous element from the theory, and to construct it in such a form that the conditions (1. 11) are satisfied from the begining.

For this purpose one first distinguishes the longitudinal and the transverse components of the field. One introduces $\Theta(\vec{k})$, $\vec{B}(\vec{k})$ $\Theta^{+}(\vec{k})$ and $B^{+}(k)$ defined by

$$\begin{cases} \Theta(\vec{k}) = \dfrac{(\vec{k}, \vec{A}(\vec{k}))}{k} \\ \Theta^{+}(\vec{k}) = \dfrac{(\vec{k}\vec{A}^{+}(\vec{k}))}{k} \\ \vec{B}(\vec{k}) = \vec{A}(\vec{k}) - \vec{k}\,\dfrac{(\vec{k}\vec{A}(\vec{k}))}{k^2}, \\ \vec{B}^{+}(\vec{k}) = \vec{A}^{+}(\vec{k}) - \vec{k}\,\dfrac{(\vec{k}\vec{A}^{+}(\vec{k}))}{k^2} \end{cases} \qquad (1.\ 12)$$

and uses them in place of $A_j(\vec{k})$ and $A_j^{+}(\vec{k})$, $j = 1, 2, 3$, to describe the field. Since one has then $(\vec{B}(\vec{k}), \vec{k}) = 0$, the vector $\vec{B}(\vec{k})$ is perpendicular to k. Since, moreover, $\vec{B}(\vec{k}) + \vec{k}/k \cdot \Theta(\vec{k}) = \vec{A}(\vec{k})$, the separation of $\vec{A}$ into $\vec{B}$ and Θ corresponds just to separating $\vec{A}$ into transverse and longitudinal components.

In terms of $\Theta, \vec{B}$ and $\Theta^{+}, \vec{B}^{+}$ the conditions (1. 11) are

$$\begin{cases} \left\{k\Theta(\vec{k}) - kA_0(\vec{k}) + \frac{f}{2}\right\}\Psi = 0 \\ \left\{k\Theta^{+}(k) - kA_0^{+}(k) + \frac{f^*}{2}\right\}\Psi = 0. \end{cases} \qquad (1.\ 11')$$

If we use the representation in which $\Theta^+(\vec{k})$ and $A_0(k)$ are diagonal, (1.11′) are

$$\begin{cases} \dfrac{\delta\Psi}{\delta\Theta^+}=\left(\dfrac{2}{hck}-\dfrac{f}{hck^2}\right)\Psi \\ \dfrac{\delta\Psi}{\delta A_0(\vec{k})}=\left(\dfrac{2}{hck}+\dfrac{f^*}{hck^2}\right)\Psi. \end{cases} \quad (1.11'')$$

The conditions (1.11″) result in that Ψ must have the form

$$\Psi=e^x\,\Omega \quad (1.13)$$

with

$$x=\frac{2}{hc}\int\Theta^+(\vec{k})A_0(\vec{k})\frac{d\vec{k}}{k} +\frac{1}{hc}\int\{A_0(\vec{k})f^*-\Theta^+(\vec{k})f\}\frac{d\vec{k}}{k^2}, \quad (1.14)$$

where Ω is a functional depending, besides on the coordinates of the electrons, only on the transverse components of the field. Ω can be therefore regarded as a functional of two independent components of $B^+(k)$, which will be denoted by $B^+(k)$ and $C^+(k)$. Since Ψ of the form of (1.13) satisfies (1.11″) identically, the manifold of the functional Ω corresponds just to the portion of the Ψ space to which one can attribute physical meanings.

As has been shown by Fock, one obtains the equation which must be satisfied by Ω by substituting (1.13) into (1.10) and multiplying $e^{-\chi}$ from the left. This equation contains, besides the coordinates of the electrons, only operators operating upon B^+ and C^+. Since Ψ, constructed according to (1.13) satisfies the condition (1.11) automatically, we need for Ω no more the auxiliary condition, and consequently the theory contains no superfluous element more. As is well known, there appears then in the equation for Ω the static coulomb interaction between electrons separately from the magnetic interaction and from the effect of retardation, which appear as indirect effects caused by the emission and the re-absorption of the virtual transverse photons by the electrons.

Although in this way the undesirable complication of the theory, first to solve the equations which contain the superfluous solutions and then select the significant solutions by imposing the condition (1.11), is removed, this way is by no means satisfactory from the standpoint of the relativity theory, because the separation of the field into longitudinal and transverse parts by means of (1.12) is a nonrelativistic procedure. The result obtained has, as the consequence, quite a non-relativitic form, in which the Coulumb interaction on one hand and the magnetic interaction and the effect of retardation on the other hand appear in a quite different manner in the theory.

§ 2. Relastivistic Generalization ot the Longitudinal and the Transverse Components of the Field.

The method of Fock described in § 1 is, as we have often mentioned, rather unsatisfactory from the standpoint of the relativity theory. This is because the quantities Θ, Θ^+, B and B^+ introduced through (1.12) have no simple transformation properties in the Lorentz transformation. It is more convenient to use some other linear conbinations of A's and A^+'s having simple transformation properties. It would be most satisfactory when we could use some eight invariant combinations of A's and A^+'s as coordinates and momenta describing the field. For this purpose we put

$$\begin{cases} K^+=-(\Theta-A_0)k \\ L^+=(\Theta^+-A_0{}^+)k \end{cases} \quad (2.1)$$

and regard the quantities K^+ and L^+ as first two momenta discribing the field whose canonically conjugate coordinates are denoted by

K and L respectively.* K^+ and L^+ are invariants obviously because they are the scalar products

$$\begin{cases} K^+ = -(\boldsymbol{k},\boldsymbol{A}) \\ L^+ = (\boldsymbol{k},\boldsymbol{A}^+). \end{cases} \tag{2. 2}$$

The convenience of using these quantities is suggested by the fact that just these linear combinations appear in the auxiliary conditions (1. 9).

Now the canonically conjugate sets of variables, K and K^+ on one hand, and L and L^+ on the other hand, must satisfy the commutation relations

$$\begin{cases} [K(\vec{k}),K^+(\vec{k}')] = [L(\vec{k}),L^+(\vec{k}')] \\ \quad = \dfrac{hck}{2}\delta(\vec{k}-\vec{k}') \\ \text{other commutators} = 0. \end{cases} \tag{2. 3}$$

As we require that K and L should be invariant linear combinations of $A's$ and $A^+{}'s$, they must be of the form;

$$\begin{cases} K = (\boldsymbol{l},\boldsymbol{A}^+) \\ L = (\boldsymbol{l},\boldsymbol{A}) \end{cases} \tag{2. 4}$$

where $\boldsymbol{l}$ is a four-vector. The commutation relations (2. 3) can be then satisfied if $\boldsymbol{l}$ has the properties:

$$\begin{cases} (\boldsymbol{l},\boldsymbol{l}) = 0 \\ (\boldsymbol{l},\boldsymbol{k}) = 1. \end{cases} \tag{2. 5}$$

In this way we obtain two sets of invariant coordinates and momenta. The remaining two coordinates and momenta can be obtained also by introducing two vectors $\boldsymbol{r}$ and $\boldsymbol{s}$ having the properties:

$$\begin{cases} (\boldsymbol{l},\boldsymbol{r}) = 0, \quad (\boldsymbol{k},\boldsymbol{r}) = 0, \quad (\boldsymbol{r},\boldsymbol{r}) = 1 \\ (\boldsymbol{l},\boldsymbol{s}) = 0, \quad (\boldsymbol{k},\boldsymbol{s}) = 0, \quad (\boldsymbol{s},\boldsymbol{s}) = 1. \end{cases} \tag{2. 6}$$

Then it can be shown that the quantities

$$\begin{cases} R = (\boldsymbol{r},\boldsymbol{A}) \\ S = (\boldsymbol{s},\boldsymbol{A}) \end{cases} \tag{2. 7}$$

can be used as coordinates, and the quantities

$$\begin{cases} R^+ = (\boldsymbol{r},\boldsymbol{A}^+) \\ S^+ = (\boldsymbol{s},\boldsymbol{A}^+) \end{cases} \tag{2. 8}$$

can be used as the corresponding momenta. In fact, it can be immediately shown that the commutation relations

$$\begin{cases} [R(\vec{k}),R^+(\vec{k}')] = [S(\vec{k}),S(\vec{k}')] \\ \quad = \dfrac{hck}{2}\delta(\vec{k}-\vec{k}') \\ \text{other commutators} = 0 \end{cases} \tag{2. 9}$$

are satisfied. We obtain in this way four sets of coordinates and momenta as tabulated below.

Cordinates	Momenta
$K = (\boldsymbol{l},\boldsymbol{A}^+)$	$K^+ = -(\boldsymbol{k},\boldsymbol{A})$
$L = (\boldsymbol{l},\boldsymbol{A})$	$L^+ = (\boldsymbol{k},\boldsymbol{A}^+)$
$R = (\boldsymbol{r},\boldsymbol{A})$	$R^+ = (\boldsymbol{r},\boldsymbol{A}^+)$
$S = (\boldsymbol{s},\boldsymbol{A})$	$S^+ = (\boldsymbol{s},\boldsymbol{A}^+)$

Tab. 1. Four sets of invariant cordinates and momenta.

In terms of these coordinates and momenta the amplitudes $\boldsymbol{A}(\vec{k})$ and $\boldsymbol{A}^+(\vec{k})$ are expressed by

$$\begin{cases} \boldsymbol{A}(\vec{k}) = L(\vec{k})\boldsymbol{k} - K^+(\vec{k})\boldsymbol{l} \\ \qquad + R(\vec{k})\boldsymbol{r} + S(\vec{k})\boldsymbol{s} \\ \boldsymbol{A}^+(\vec{k}) = K(\vec{k})\boldsymbol{k} + L^+(\vec{k})\boldsymbol{l} \\ \qquad + R^+(\vec{k})\boldsymbol{r} + S^+(\vec{k})\boldsymbol{s}. \end{cases} \tag{2. 10}$$

It is to be noticed that the vectors $\boldsymbol{l}$, $\boldsymbol{r}$ and $\boldsymbol{s}$ are arbitrary except for the conditions (2.5) and (2.6), so that we have infinitely many ways of choosing invariant coordinates and momenta, any of which may be considered as describing a possible set of the generalized longitudinal and transverse components of the field. We consider namely, that the components of the field described by any K,L,K^+ and L^+ defined by a specified $\boldsymbol{l}$ represent equally a set of generalised longitudinal waves, and the components dercribed by R, S, R^+, and S^+ represent a set of generalised transerse waves. Since there are infinitely many ways of specifying $\boldsymbol{l}$, we have no unique definition of the generalized longitudinal waves, but this arbitrariness is unavoidable when we will define the longitudinal waves without referring to any Lorentz frame. That the transverse components R and S can not be defined uniquely is, on the other hand, a quite familiar fact. Also in the ordinary definition of the transverse wave, one has many degrees of freedom, since one can choose any two mutually perpendicular directions prependicular to the direction of propagation as those of polarization of the wave under consideration.

---

* In (1.5) the symbol + has been introduced to denote the conjugate complex quantity, but we shall use hereafter this symbol to denote the canonically conjugate momenta.

We shall next show that the ordinary definition of the longitudinal and the transverse components is contained in ours as a special case. Take the following special choice of $\boldsymbol{l}$, $\boldsymbol{r}$ and $\boldsymbol{s}$

$$\begin{cases} \boldsymbol{l}=\left(-\dfrac{k}{2k^2},\ \dfrac{\vec{k}}{2k^2}\right) \\ \boldsymbol{r}=(0,\vec{\eta}_1) \\ \boldsymbol{s}=(0,\vec{\eta}_2), \end{cases} \tag{2.11}$$

$\overleftarrow{\eta_1}$ and $\overleftarrow{\eta_2}$ being two unit vectors perpendicular to each other and to $\vec{k}$. That these $\boldsymbol{l}, \boldsymbol{r}$ and $\boldsymbol{s}$ satisfy (2. 5) and (2. 6) can be immediately shown. We have then

$$K=\frac{(\vec{k}\vec{A})}{2k^2}+\frac{kA_0}{2k^2}$$

$$L=\frac{(\vec{k}\vec{A}^+)}{2k^2}+\frac{kA_0{}^+}{2k^2} \tag{2.12}$$

which, on account of the Lorentz condition (1. 9), are reduceed to

$$K=\frac{(\vec{k}\vec{A})}{k^2} \quad \text{and} \quad L=\frac{(\vec{k}\vec{A})}{k^2},$$

which, after being multiplied by k, are just eqnivalent to Θ and Θ^+ introduced in (1. 12). It is also obvious that R, S, R^+ and S^+ correspond to B, C, B^+ and C^+ respectively.

We shall now proceed to see the physical meaning of the generalized longitudinal and transverse waves with some specified values of $\boldsymbol{l}, \boldsymbol{r}$ and $\boldsymbol{s}$. For this purpose we transform the coordinate system from the (ct, x, y, z) -system to the new one having the orthogonal vectors $-\dfrac{k}{2k'}+k'\boldsymbol{l}, \boldsymbol{r}, \boldsymbol{s}$, and $\dfrac{k}{2k'}+k'\boldsymbol{l}$ as the ct$'$-x'-, y'- and z'- axis respectively. Thereby the constant k' may be chosen arbitrarily. We shall call this dashed system "Γ-system." The matrix representing this Lorentz transformation is given by

$$\Lambda=\begin{array}{c|cccc} & \text{ct}' & x' & y' & z' \\ \hline \text{ct} & -\dfrac{k'}{2k}+k'l_0 & -\dfrac{k_x}{2k'}+k'l_x & -\dfrac{k_y}{2k'}+k'l_y & -\dfrac{k_z}{2k'}+k'l_z \\ x & r_0 & r_x & r_y & r_z \\ y & S_0 & S_x & S_y & S_z \\ z & \dfrac{k}{2k'}+k'l_0 & \dfrac{k_x}{2k'}+k'l_x & \dfrac{k_y}{2k'}+k'l_y & \dfrac{k_z}{2k'}+k'l_z \end{array} . \tag{2.13}$$

In this Γ-system the vectors $\boldsymbol{k}, \boldsymbol{l}\, \boldsymbol{r}$ and $\boldsymbol{s}$ have the components:

$$\boldsymbol{k}=(k'\ 0,\ 0,\ k')$$

$$\boldsymbol{l}=\left(-\frac{1}{2k'},\ 0,\ 0,\ \frac{1}{2k'}\right)$$

$$\boldsymbol{r}=(0,\ 1,\ 0,\ 0)$$

$$\boldsymbol{s}=(0,\ 0,\ 1,\ 0). \tag{2.14}$$

As is obvious from (2. 13), the Γ-system is moving with the four-velocity $\boldsymbol{v}$:

$$\mathbf{v}=-\frac{\mathbf{k}}{2k'}+k'\mathbf{l} \qquad (2.15)$$

relative to the (ct, $x,y,z,$) -system. The velocity $\overrightarrow{cu}$ of the Γ system in the ordinary sense is then given by

$$\overrightarrow{cu}=\frac{-\overrightarrow{k}/2k'+k'\overrightarrow{l}}{-k/2k'+k'l}, \qquad (2.15')$$

which is related with $\mathbf{v}$ by means of

$$\mathbf{v}=\left(\frac{1}{\sqrt{1-u^2}},\ \frac{\overrightarrow{u}}{\sqrt{1-u^2}}\right). \qquad (2.15'')$$

From (2.15) we obtain immediatery

$$\mathbf{l}=\frac{\mathbf{k}+2\mathbf{v}(\mathbf{k},\mathbf{v})}{2(\mathbf{k},\mathbf{v})^2}, \qquad (2.16)$$

or separating the time and the space components

$$\begin{cases} l_0=\dfrac{k(1-u^2)-2\{k-(\overrightarrow{k}\overrightarrow{u})\}}{2\{k-(\overrightarrow{k}\overrightarrow{u})\}^2} \\ l=\dfrac{\overrightarrow{k}(1-u^2)-2\overrightarrow{u}\{k-(\overrightarrow{k}\overrightarrow{u})\}}{2\{k-(\overrightarrow{k}\overrightarrow{u})\}^2}. \end{cases} \qquad (2.16')$$

Further, if one multiplies (2.15) by $\mathbf{k}$ and uses (2.5), one obtains

$$k'=(\mathbf{k},\mathbf{v})$$

$$=\frac{k-(\overrightarrow{k}\overrightarrow{u})}{\sqrt{1-u^2}} \qquad (2.17)$$

From this last relation, or directly from (2.14), it is seen that k' is the frequency of the wave observed in the Γ -system. Further, from (2.15) and (2.16) we have relations

$$(\mathbf{r},\mathbf{v})=(\mathbf{s},\mathbf{v})=0 \qquad (2.18)$$

It is now obvious from (2.14) that in this Γ -system the propagation vector has a non-vanishing component only in the z' -direction. This means that the Γ -system is a system whose z' -axis is taken in the direction of propagation of the wave. Further, the vector $\mathbf{l}$ has, in this system, the standard form of (2.11). This means that the generalized longitudinal wave with the specified $\mathbf{l}$ is nothing but the longitudinal wave in the ordinary sense in this Γ -system. The sets of coordinates and momenta K,K^+ and L,L^+ describe thus the longitudinal waves in this Γ -system. That the sets of coodinates and momenta R,R^+ and S, S^+ describe the ordinary transverse waves in the Γ -system is also obvious by the fact that the vectors $\mathbf{r}$ and $\mathbf{s}$ have their non-vanishing components only in the x'- and the y'- direction respectively.

Since $\mathbf{l}$ may be chosen arbitrarily except for the condition (2.5), $\mathbf{l}$ may be different for the different Fourier component of the field. Thus the Γ-system can be different for the different Fourier component. Accordingly, the velocity u may be an arbitrary function of the propagation vector $\mathbf{k}$. However, since such a general choice of the Γ-system seems to be of little use, we consider that velocity of the Γ -system is independent of $\mathbf{k}$.

It is to be noticed that, althogh our generalized transverse waves differ in general coordinate systems from the transverse waves in the ordinary sense, our generalized transverse waves are still transverse in the sense that the components of the electric and the magnetic vectors represented by our generalized transverse wave are perpendicular to the direction of propagation of the wave. This can be seen by calculating the curl of $\{R\mathbf{r}+S\mathbf{s}\}e^{i(\mathbf{k},\mathbf{x})}+\{R^+\mathbf{r}+S^+\mathbf{s}\}e^{-i(\mathbf{k},\mathbf{x})}$:

$$\overrightarrow{E}_{tr}(\overrightarrow{k})=i\{R(\overrightarrow{rk}-r_0\overrightarrow{k})$$

$$+S(\overrightarrow{sk}-s_0\overrightarrow{k})\}e^{i(\mathbf{k},\mathbf{x})}+\text{conj.},$$

$$\overrightarrow{H}_{tr}(\overrightarrow{k})=i\{R[\overrightarrow{r},\overrightarrow{k}]$$

$$+S[\overrightarrow{s},\overrightarrow{k}]\}e^{i(\mathbf{k},\mathbf{x})}+\text{conj.}$$

Putting here

$$\overrightarrow{\eta}_r=\overrightarrow{rk}-r_0\overrightarrow{k}$$

$$\overrightarrow{\eta}=\overrightarrow{sk}-s_0\overrightarrow{k}, \qquad (2.19)$$

it can be immediataly verified that, on account of $(r,r)=(s,s)=0$ and $(k,k)=0$, $\vec{\eta}_r$ and $\vec{\eta}_s$, the three-dimensional polarization vectors, are in fact perpendicular to $\vec{k}$ as well as to each other.

§ 3. Elimination of the Auxiliary Condition

We shall now proceed to the elimination of the auxiliary condition. It is convenient to introduce the representation in which the coordinates K, L, R, and S are diagonal. The arguments of the Schrödinger functional are then these K, L, R, and S. The Lorentz condition (11. 1) has in this representation the form

$$\left\{\begin{aligned}&\left(\frac{hck}{2}\frac{\delta}{\delta K}+\frac{f}{2}\right)\Psi=0\\&\left(-\frac{hck}{2}\frac{\delta}{\delta L}+\frac{f^*}{2}\right)\Psi=0.\end{aligned}\right. \tag{3. 1}$$

The solution of these equations is given by

$$\Psi=e^{\varkappa}\,\Omega, \tag{3. 2}$$

where

$$\varkappa=-\frac{1}{hc}\int fk\frac{d\vec{k}}{k}+\frac{1}{hc}\int \overset{*}{f}L\frac{d\vec{k}}{k}, \tag{3. 3}$$

and $\varkappa$ contains no longer K and L. It is to be noticed that this $\varkappa$ is an invariant whereas $\varkappa$ in (1. 14) was not.

Now, since the operation $h/i\ \mathrm{Grad}^{(s)}-\frac{\varepsilon_s}{c}A(x^{(s)})$ in (1. 10) commutes with the auxiliary condition in (1. 11), $(h/i\ \mathrm{Grad}^{(s)}-\frac{\varepsilon_s}{c}A(x^{(s)}))\Psi$ also satisfies the Lorentz condition. This results in that $(h/i\ \mathrm{Grad}^{(s)}-\frac{\varepsilon_s}{c}A(x^{(s)}))\Psi$ has the form: $e^{\varkappa}(h/i\ \mathrm{Grad}^{(s)}-\frac{\varepsilon_s}{c}A'(x^{(s)}))\Omega$, where $A'(x^{(s)})$ contains no longer K, L, K^+ and L^+. Thus Ω satisfies the equations

$$\left\{\left(\alpha^{(s)},\ h/i\ \mathrm{Grad}^{(s)}-\frac{\varepsilon_s}{c}A'(x^{(s)})\right)+m^{(s)}c\beta^{(s)}\right\}\Omega=0,$$
$$s=1,2,3,\cdots n \tag{3. 4}$$

in which the longitudinal components of the field are eliminated.

Our task is now to find $A'(x)^{(s)}$. The calculation for this problem is as follows:

First we notice that

$$\frac{h}{i}\mathrm{Grad}^{(s)}\Psi=\frac{h}{i}\mathrm{Grad}^{(s)}e^{\varkappa}\,\Omega$$
$$=e^{\varkappa}\left\{\frac{h}{i}\mathrm{Grad}^{(s)}+\frac{\varepsilon_s}{c}\left(\frac{1}{2\pi}\right)^{3/2}\int(Ke^{-(k,x^{(s)})}+Le^{i(k,x^{(s)})})k\frac{d\vec{k}}{k}\right. \tag{3. 5}$$

Since we have, on account of (1. 5) and (2. 10),

$$A(x)=\frac{1}{(2\pi)^{3/2}}\int\left\{(Lk-K^+l)e^{i(k,x)}+(Kk+L^+l)e^{-i(k,x)}\right\}\frac{d\vec{k}}{k}+B(x), \tag{3. 6}$$

where $\boldsymbol{B}(\boldsymbol{x})$ is defined by

$$\boldsymbol{B}(\boldsymbol{x})=\frac{1}{(2\pi)^{3/2}}\int\left\{(Rr+Ss)e^{i(k,x)}+(R^{+}r+S^{+}s)e^{-i(k,x)}\right\}\frac{\overrightarrow{dk}}{k}, \tag{3.7}$$

we obtain

$$-\frac{\varepsilon_s}{c}A(x)^{(s)}\Psi=e^{x}\left[-\frac{\varepsilon_s}{c}\frac{1}{(2\pi)^{3/2}}\int(Ke^{-i(k,x^{(s)})}+Le^{i(k,x^{(s)})})k\frac{\overrightarrow{dk}}{k}-\frac{\varepsilon_s}{c}\boldsymbol{B}(x^{(s)})\right.$$

$$\left.+\frac{\varepsilon_s}{c}\frac{1}{(2\pi)^{3/2}}\int\frac{1}{2}(fe^{i(k,x^{(s)})}+f^{*}e^{-i(k,x^{(s)})})\boldsymbol{l}\frac{dk}{k}\right]\Omega. \tag{3.8}$$

If we add (3.5) to (3.8), the first term in (3.8) cancels the second one in (3.5), so that we obtain

$$\left(\frac{h}{i}\mathrm{Grad}^{(s)}-\frac{\varepsilon_s}{c}A(x^{(s)})\right)\Psi=e^{x}\left(\frac{h}{i}\mathrm{Grad}^{(s)}-\frac{\varepsilon_s}{c}\boldsymbol{B}(x^{(s)})\right.$$

$$\left.-\frac{\varepsilon_s}{c}\boldsymbol{G}(x^{(s)})\right)\Omega, \tag{3.9}$$

where $\boldsymbol{G}(x^{(s)})$ is the operator containing only the coordinates of the electrons and no field quantites. It is given by

$$\boldsymbol{G}(x^{(s)})=\sum_{w}\varepsilon_w\boldsymbol{L}(x^{(s)}-x^{(w)})$$

$$\text{with}\quad \boldsymbol{L}(x)=\frac{1}{16\pi^{3}}\int(e^{i(k,x)}+e^{-i(k,x)})\boldsymbol{l}\frac{dk}{k}. \tag{3.10}$$

The function $\boldsymbol{L}(x)$ satisfies the equation

$$\mathrm{Div}\ \boldsymbol{L}(x)=D(x), \tag{3.11}$$

whereas $\boldsymbol{B}(x)$ in (3.9) satisfies

$$\mathrm{Div}\ \boldsymbol{B}(x)=0. \tag{3.12}$$

It is obvious that the potential $\boldsymbol{B}$ represents the generalized transverse component of the field. On multiplying the equation (3.9) by e^{-x} from the left. we obtain the equations for Ω

$$\left\{\left(\alpha^{(s)},\frac{h}{i}\mathrm{Grad}^{(s)}-\frac{\varepsilon_s}{c}\boldsymbol{B}(x^{(s)})-\frac{\varepsilon_s}{c}\boldsymbol{G}(x^{(s)})\right)+mc\beta^{(s)}\right\}\Omega=0. \tag{3.13}$$

These are the required equations for Ω, in which the longitudinal components of the field are eliminated, but, on the other hand, it contains the term $\boldsymbol{G}(x^{(s)})$, which represents the effect of other electrons on the s-th electoron. This term coutains only the coordinates of the electrons, so that in (3.13) some part of the interaction between electrens appears as if it were an action at a distance. In the ordinary theory this action has the form of the static coulomb interaction. It is expected that $\boldsymbol{G}(x)$ in our theory will have the form of the Liénard-Wiechert potential obtained by means of the Lorentz transformation from the coulomb potential in the Γ-system (provided that the velocity of the Γ-system is independent of $\boldsymbol{k}$). This can be shown by the direct calculation as follows:

Substituting $\boldsymbol{l}$ of (2.16′) into (3.10), we obtain

$$\boldsymbol{G}(x^{(s)})=-\sum_{w}\varepsilon_w\boldsymbol{L}(x^{(s)}-x^{(w)})=-\sum_{w}\varepsilon_w\{\boldsymbol{L}_1(x^{(s)}-x^{(w)})+\boldsymbol{L}_2(x^{(s)}-x^{(w)})\} \tag{3.14}$$

with

$$L_1(x)=\frac{1}{16\pi^3}\int\frac{1-u^2}{2\{k-(\vec{k}\vec{u})\}^2}k\{e^{i(ckt-(\vec{k}\vec{x}))}+e^{-i(ckt-(\vec{k}\vec{x}))}\}\frac{d\vec{k}}{k}$$

$$L_2(x)=-\frac{1}{16\pi^3}v\sqrt{1-u^2}\int\frac{1}{k-(\vec{k}\vec{u})}\left\{e^{i(ckt-(\vec{k}\vec{x}))}+e^{-i(ckt-(\vec{k}\vec{x}))}\right\}\frac{d\vec{k}}{k}. \tag{3.15}$$

Then putting

$$\left\{\begin{aligned} L_1(x)&=\frac{1}{i}\,\frac{1}{16\pi^3}\mathrm{Grad}\ I_1\\ L_2(x)&=-\frac{1}{16\pi^3}vI_2, \end{aligned}\right. \tag{3.15$'$}$$

we have

$$\left\{\begin{aligned} I_1&=-\int\frac{1-u^2}{2\{k-(\vec{k}\vec{u})\}^2}\left\{e^{i(ckt-(\vec{k}\vec{x})}-e^{-i(ckt-(\vec{k}\vec{x}))}\right\}\frac{d\vec{k}}{k}\\ I_2&=\int\frac{1}{\{k-(\vec{k}\vec{u})\}/\sqrt{1-u^2}}\left\{e^{i(ckt-(\vec{k}\vec{x}))}+e^{-i(ckt-(\vec{k}\vec{x}))}\right\}\frac{d\vec{k}}{k}. \end{aligned}\right. \tag{3.15$''$}$$

Now we calculate I_2. In doing this we carry out the Lorentz transformation

$$k_x'=\frac{k_x-uk}{\sqrt{1-u^2}},\ k_y'=k_y,\ k_z'=k_z,\ k'=\frac{k-(\vec{k}\vec{u})}{\sqrt{1-u^2}}, \tag{3.16}$$

first supposing that the x-axis has been taken in the direction of $\vec{u}$. On account of the fact that $d\vec{k}/k$ is an invariant, we have then

$$I_2=\int\left\{e^{i(ck't'-(\vec{k}\vec{x}))}+e^{-i(ck't'-(\vec{k}'\vec{x}'))}\right\}\frac{d\vec{k}'}{k'^2} \tag{3.17}$$

where x' and t' are defined by

$$x'=\frac{x-uct}{\sqrt{1-u^2}},\ y'=y,\ z'=z,\ ct'=\frac{ct-ux}{\sqrt{1-u^2}}. \tag{3.16$'$}$$

To calculate (3. 17) we introduce the polar coorinates (k',θ,φ) of $\vec{k}'$. Then we have

$$I_2=\int_0^{2\pi}d\varphi\int_0^{\infty}dk'\int_0^{\pi}\sin\vartheta d\vartheta\ 2\cos(c'k'-k'r'\cos\theta)$$

in which r' denotes $|\vec{x}'|$. Carrying out the integration with regard to φ and k', this reduces to

$$\begin{aligned} I_2&=4\pi^2\int_0^{\pi}\sin\theta\,d\theta\,\delta(ct'-r'\cos\theta)\\ &=\begin{cases}0 & \text{for } |ct'|>r'\\ 4\pi^2/r' & \text{for } r'>|ct'|.\end{cases} \end{aligned} \tag{3.18}$$

We obtain thus

$$L_2(x)=\frac{1}{16\pi^3}\begin{cases}-v\dfrac{4\pi^2\sqrt{1-u^2}}{\sqrt{(x-uct)^2+(1-u^2)(y^2+z^2)}} & \text{for } r>c|t|\\ 0 & \text{for } r>c|t|.\end{cases} \tag{3.19}$$

Next we calculate I_1. On carrying out the Lorentz transformation (3. 16) and (3. 16′), and introducing the polar coordinates of $\vec{k}'$, we obtain.

$$I_1=\frac{1}{i}\int_0^{2\pi}d\varphi\int_0^{\infty}dk'\int_0^{\pi}\sin\theta d\theta\frac{\sin k'(ct-r\cos\theta)}{k'}$$

$$=\frac{\pi^2}{i}\int_0^\pi \sin\theta\, d\theta\, \mathrm{sign}(ct'-r'\cos\theta)$$

$$=\frac{\pi^2}{i}\int_{-1}^{+1} d\xi\, \mathrm{sign}\,(ct'-r'\xi),$$

which yields

$$\begin{cases} \dfrac{2\pi^2}{i} & \text{for } ct'>r' \\ \dfrac{2\pi^2 ct'}{ir'} & \text{for } r'>c|t'| \\ -\dfrac{2\pi^2}{i} & \text{for } -r'>ct'. \end{cases} \tag{3.20}$$

We obtain thus

$$L_1(x)=\frac{1}{16\pi^3}\begin{cases} -2\pi^2\,\mathrm{Grad}\dfrac{ct-ux}{\sqrt{(x-uct)^2+(1-u^2)(y^2+z^2)}} & \text{for } r>c|t| \\ 0 & \text{for } r<c|t|. \end{cases} \tag{3.21}$$

Substituting L_1 and L_2 obtained in this way into (3.14), we find that the required potential $G(x^{(s)})$ is

$$\begin{cases} G(x^{\infty})=\sum\limits_w \dfrac{\varepsilon_w}{8\pi}\mathrm{Grad}^{(s)}\dfrac{c(t^{(s)}-t^{(w)})-u(x^{(s)}-x^{(w)})}{r^{(sw)}}+\sum\limits_w \dfrac{\varepsilon_w}{4\pi}\,v\,\dfrac{\sqrt{1-u^2}}{r^{(sw)}}. \\ \text{with} \quad r^{(sw)}=\sqrt{\{(x^{(s)})-cu(t^{(s)}-t^{(w)})\}^2+(1-u^2)\{(y^{(s)}-y^{(w)})^2+(z^{(s)}-z^{(w)})^2\}} \end{cases} \tag{3.22}$$

where the summation $\sum\limits_w$ is taken over all particles lying in space-like distances from the particle s.

When the x-axis does not coincide with the direction of $\vec{u}$, the potential $G(x)$ with its space and time components being separated, is given by

$$\begin{cases} G_0(\vec{x},t)=\dfrac{1}{8\pi}\left[\dfrac{1}{r'}-\dfrac{\{ct-(\vec{x}\vec{u})\}\{(\vec{x},\vec{u}_0)-uct\}u}{r'^3}\right] \\ \vec{G}(\vec{x},t)=\dfrac{1}{8\pi}\left[\dfrac{\vec{u}}{r'}-\dfrac{\{ct-(\vec{x},\vec{u})\}[\{(\vec{x},\vec{u}_0)-uct\}\vec{u}_0+(1-u^2)\{\vec{x}-(\vec{x},\vec{u}_0)\vec{u}_0\}]}{r'^3}\right] \\ \text{with} \quad r'=\sqrt{\{(\vec{x},\vec{u}_0)-uct\}^2+(1-u^2)\{\vec{x}-(\vec{x},\vec{u}_0)\vec{u}_0\}^2} \end{cases} \tag{3.23}$$

provided that the point $(t,\vec{x})$ lies in the space-like region with respect to the origin, $\vec{u}_0$ being the unit vector in the direction of $\vec{u}$. If the point $(t,\vec{x})$ lies in the time-like region, G_0 and $\vec{G}$ vanish identically.

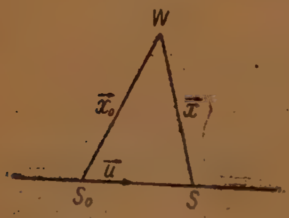

Fig. 1. W: virtual electron.
S: electron moving with velocity $\vec{u}$.
S_0: retarded point.
$\dfrac{\overline{S_0S}}{\overline{WS_0}}=u,$

In order to see the physical meaning of G, we imagine a virtual electron S moving with the velocity $\vec{u}$ and a virtual electron W which is at rest. For the sake of simplicity we assume that the x-axis is in the direction of $\vec{u}$. Let the retarded point of S be S_0, and let $\vec{x}_0$ denote the vector $\overrightarrow{WS_0}$ (see Fig. 1.). On account of $uWS_0=SS_0$, we obtain

$$\vec{x}^2=\vec{x}_0^2+u^2x_0^2-2(\vec{x}_0,\vec{u})\,|x_0|$$

$$u^2(y^2+z^2)=[\vec{u},\vec{x}]^2=[\vec{u},\vec{x}_0]^2=u^2\vec{x}_0^2-(\vec{u},\vec{x}_0)^2,$$

Adding these two equations, we obtain

$$\sqrt{\vec{x}^2-u^2(y^2+z^2)}=|x_0|-(u,x_0). \tag{3.24}$$

We introduce next the null-vector $\boldsymbol{x}_0=(|x_0|,\ x_0,y_0,z_0)$. Then $\boldsymbol{x}_0$ is the vector which connects the point W to the point S_0, the point at which the world line of S crosses the light cone whose vertex is at W (see Fig. 2). Then from (3.24) we have

$$\sqrt{x^2+(1-u^2)(y^2+z^2)}$$
$$=-\sqrt{1-u^2}\,(\boldsymbol{v},\boldsymbol{x}_0). \tag{3.25}$$

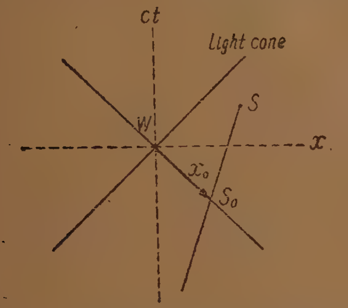

Fig. 2. S_0S: world line of election S.

If we use the relation (3.25), (3.22) can be written in the form:

$$\boldsymbol{G}(x^{(s)})=\sum_w\frac{\varepsilon_w}{8_w}\mathrm{Grad}^{(s)}\frac{(\boldsymbol{v},\boldsymbol{x}^{(s)}-\boldsymbol{x}^{(w)})}{(\boldsymbol{v},\boldsymbol{x}_0{}^{(sw)})}$$
$$+\sum_w\frac{-\varepsilon_w}{4\pi}\frac{\boldsymbol{v}}{(\boldsymbol{v},\boldsymbol{x}_0{}^{(sw)})}. \tag{3.26}$$

The physical meaning of each term in the second summation of (3.26) is well known.(3) It is the Liénard-Wiechert potential caused by the virtual electron W observed by an observer on the moving electron S. The first summation has no such direct meaning, but since this term has the form of a four-dimensional gradient, it can be brought to zero by a suitable gauge transformation. It is also obvious that our result (3.23) can be obtained by the Lorentz transformation from the result of Fock, in which G_0, and G have the forms

$$\begin{cases} G_0=\dfrac{1}{8\pi}\,\dfrac{1}{r} \\[2ex] \vec{G}=\dfrac{-1}{8\pi}\,\dfrac{ct}{r^3}\vec{x} \end{cases} \tag{III, 44 of Fock}$$

The remaining part of the paper will appear in a later issue of this journal.

References.

(1) P. A. M. Dirac: V. Fock and B. Podolsky: Phys. ZS. USSR., 2(1932) 468.
(2) V. Fock: ibid. 6 (1934) 425. P. A. M. Dirac: Ann. Inst. Poincaré 9 (1939) 13.
(3) R. Becker: Theorie der Elektrizität, Bd. II (1933). 63 and 317.

On the Entropy of the Supraconductor.

Hirosi ITIMURA

Physical Institute, Faculty of Science, Tokyo University.

(Received January, 20, 1947)

1. Introduction

Supraconductivity which appears in some metals and alloys at extremely low temperatures is considered from the beginning to have its origin in the properties of the group of conduction electrons in metals. Many authors(1) proposed various models for this group of electrons, some of which are very interesting and suggestive, but it is considered none of them are very satisfactory. In this short treatment we calculate statistically the entropy and the specific heat of supraconducting electron gas in the absence of magnetic fields with a very simple model which is extracted from these models.

Conduction electrons in the normal state of metals behave as the degenerate Fermi gas. By this so-called Sommerfeld's model we can explain very well the low temperature properties of electrons in the metals. For the appearance of the supraconduction, however, this is quite imcompetent. It would be necessary to consider some intense interaction between electrons and ion lattices and to give up to use the one electron approximation. But if we would imagine something like the electron liquid after Welker,(2) we could not treat it exactly. So we here consider very simply as follows without entering in the details.

2. Model and Calculations

In metals which become supraconducting, there are N conduction electrons per unit volume and they form the degenerate Fermi gas in the normal state. On lowering the temperature they begin to condense on account of some interaction and supraconductivity appears.

At some temprature the condensed part consists of p groups of electrons per unit volume, each cantains γ electrons. On each electrons in the condensed phase there operates the attraction potential φ';

$$\varphi'=\varphi s(1-\nu s)\,; \quad s=\frac{p}{p_M},\ \nu<1,$$

where φ and ν are some constants, p_M is the value of p at the absolute zero. The above assumption means that the attracting force becomes stronger with increasing number of condensed electrons at first, then it becomes weaker in the final stage.

The assembly of states of the above considered system of electrons can be assumed to form the canonical ensemble of Gibbs, and following the principle of statistical mechanics we can calculate the thermodynamical properties of such a system. We take Ψ as the free energy of the whole system, so we have

$$e^{-\Psi/kT}=\left(\sum_{p=0}^{p_M}\frac{p_M\,!}{p\,!(p_M-p)\,!}\exp -(\delta-\varphi s(1-\nu s))\gamma p/kT(f(T))p\right)$$
$$\times\left(\sum_{N_1,N_2,N_3}\prod_{\lambda}\frac{\varDelta_\lambda\,!}{N_\lambda\,!(\varDelta_\lambda-N_\lambda)!}\exp -\varepsilon_\lambda N_\lambda/kT\right) \qquad (1)$$

and

$$\sum N_\lambda+\gamma p=N, \qquad (2)$$

where we count the number of states disregarding the individuality of each electron, but regarding that of condensed group of γ

electrons as a whole. The second bracket of the equation (1) is the partition function of Fermi particles, and $\varDelta_\lambda$ is the number of levels of energy ε_λ. The ground level of condensed phase is above that of Fermi gas by δ. $f(T)$ is the partion function of the internal degrees of fredom and the translational motion as a whole of a group of γ particles. We take approximately $f(T)=1$. This implies that in condensed states the interactions are so strong that statistically there exists only one wave function of the group as a whole and its internal degrees of freedom do not enter in the problem. Its translational motion is quantised by the periodic nature of the ionic lattice and distances of its levels are large compared with the thermal energy of Fermi gas at low temperature, so we can consider it to be in its lowest level apporoximately.

Under the condition of the equation (2), the first variation of $\varPsi$ with respect to variations δp, δN_λ should be zero. From this we obtain the temperature dependence of p and N_λ.

Treating as usual, we obtain apporoximately;

$$\varPsi=kT[\{\log p_M!-\log(p_M-p)! \\ -(\delta-\varphi s(1-\nu s))\gamma p_M s/kT\} \\ +\sum_\lambda\{\log\varDelta_\lambda!-\log N_\lambda!-\log\varDelta_\lambda-N_\lambda)! \\ -\varepsilon_\lambda N_\lambda/kT\}]\mathrm{Max},$$

and using Stirling's formula,

$$\delta\varPsi=-kT[-\delta p\{\log p-\log(p_M-p) \\ +\gamma(\delta-(2s\varphi-3\nu\varphi s^2))\} \\ -\sum_\lambda\delta N_\lambda\{\log N_\lambda-\log(\varDelta_\lambda-N_\lambda) \\ \varepsilon_\lambda/kT\}]=0 \qquad (3)$$

and

$$\sum\delta N_\lambda+\gamma\delta p=0. \qquad (4)$$

From these equations;

$$p=p_M/\exp[\gamma\alpha+\gamma(\delta-2\varphi s-3\nu\varphi s^2))/kT] \\ +1 \qquad (5)$$

$$N_\lambda=\varDelta_\lambda/\exp[\alpha+\varepsilon_\lambda/kT]+1 \qquad (6)$$

where $\alpha=-\zeta/kT$. ζ is the thermodynamical potential per electron. By the equation

$$\sum_\lambda N_\lambda+\gamma p=N \qquad (2')$$

the value of ζ at one temperature is determined and from it thermal properties of the system are deduced. As usual

$$\sum_\lambda N_\lambda=\frac{2}{3}N\left(\frac{kT}{\mu^0}\right)^{\frac{3}{2}}\int_0^\infty x^{\frac{1}{2}}/e^{(x-\zeta)/kT} \\ +1dx,$$

where

$$\mu_0=\frac{h^2}{8m}\left(\frac{3}{\pi}N\right)^{\frac{2}{3}}$$

and m is the mass of the electron.

We assume that the condition $\zeta\gg kT$ is always valid for the temperature under consideration, namely γp_M is very small compared with N. Expanding the integral, we get from (2)

$$N\left(\frac{\zeta}{\mu_0}\right)^{\frac{3}{2}}\left(1+\frac{\pi^2}{8}\frac{k^2T^2}{\mu_0^{\,2}}\right) \\ +\gamma p=N. \qquad (7)$$

From this

$$\zeta=\mu_0-\frac{\pi^2}{12}\frac{k^2T^2}{\mu_0}-\frac{2}{3}\mu_0\frac{\gamma p_M}{N}s \qquad (8)$$

$$s=1\Big/\exp\left[-\frac{\gamma}{kT}(\zeta-\delta+(2\varphi s-3\nu\varphi s^2))\right] \\ +1 \\ =1\Big/\exp\left[-\frac{1}{kT}\left\{\gamma\left(\mu_0-\delta-\frac{\pi^2}{12}\frac{k^2T^2}{\mu_0}\right)\right.\right. \\ \left.\left.+\gamma\left((\varphi-\frac{2}{3}\mu_0\frac{\gamma p_M}{N}\right)S-3\nu\varphi S^2\right)\right\}\right] \\ +1. \qquad (9)$$

The first term of (8) is the thermodynamical potential of the ordinary Fermi gas. Rearranging (9)

$$2\tan h^{-1}(1-2s) \\ =-\gamma(\mu_0-\delta)/kT+\gamma\frac{\pi^2}{12}\frac{k^2T^2}{\mu_0} \\ +\frac{\gamma}{kT}\left\{\left(2\varphi-\frac{2}{3}\mu_0\frac{\gamma p_M}{N}\right)s-3\gamma\nu\varphi s^2\right\} \qquad (10)$$

From (10) or (9) the temperature dependence of s is determined, so we put it into (8). For the entropy S and specific heat Cp we obtain

$$S=-\left(\frac{\partial\zeta}{\partial T}\right)_p=\frac{\pi^2}{6}\frac{k^2T}{\mu_0}+\frac{2}{3}\mu_0\frac{\gamma p_M}{N}\frac{\partial s}{\partial T} \tag{11}$$

$$Cp=-T\left(\frac{\partial^2\zeta}{\partial T^2}\right)_p=\frac{\pi^2}{2}\frac{k^2T}{\mu_0}+\frac{2}{3}\mu_0\frac{\gamma p_M}{N}T\frac{\partial^2 s}{\partial T^2} \tag{12}$$

The first terms of these equations are that of Fermi gas.

3. Comparison with experiments

By the thermodynamical theory of Gorter⁽³⁾ and Casimir⁽⁴⁾ which is in good agreement with experiments, we can determine experimentally the electronic entropy of supraconductors, measuring the magnetic threshold value. In Fig. 1 the full line shows experimental values on mercury after Daunt and Mendelssohn.⁽⁵⁾ From our formulae we calculated the dotted lines taking various constants as follows,

$\gamma=6563.6$ $\gamma p_M=193\times10^{16}$

$\delta=\mu_0-9.96\times10^{-20}$ erg/electron

$\varphi=11.9\times10^{-20}$,, $\nu=0.43$

($\mu_0=0.883\times10^{-12}$ erg and $N=8.44\times10^{22}$ from the specific heat in the normal state.)

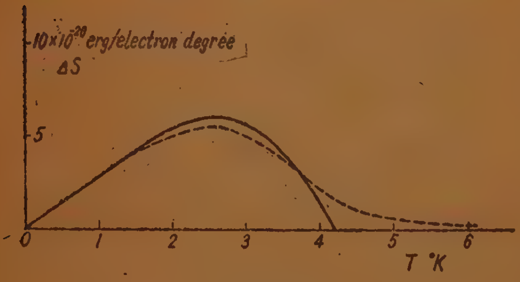

Fig. 1. (a)

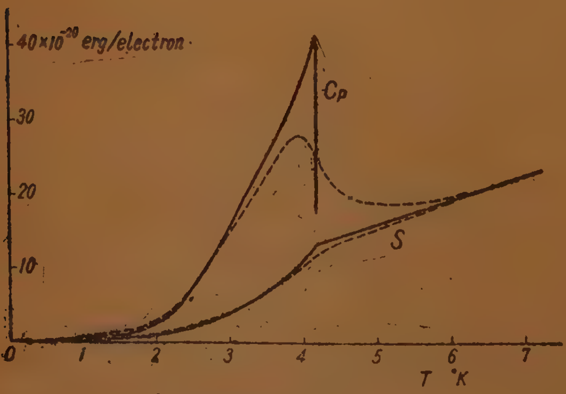

Fig. 1. (b)

In Fig. 2 the $s-T$ curve with these constants is shown. Although our theory cannot explain the sharp knick in the curves, theoretical curves express the general feature of the experimental ones.

From the avove value of γ, we can imagine the domain of cubes of ten atomic distances, assuming 2 conduction electrons per atom. γp_M is very small compared with N and does not contradict with the former assumption. φ and δ are of the order of Bohr magneton, this can be interpreted as the magnetic interaction⁽³⁾ energy between electrons (not spin-spin) which is neglected in the present election theory of metals. And also this fact will be convenient to consider the mechanism of condensation.

5. Conclusion

As indicated above, our simple model can at least qualitatively explain the experimental entropy curves for zero magnetic fields. Detailed treatment of the mechanism of condensation is

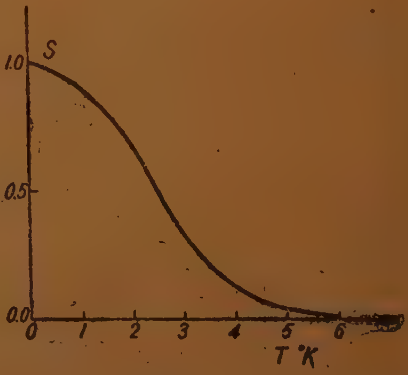

Fig. 2.

the matter of the future, but it will not be unreasonable to consider that magnetic interactions play important parts in this problem. Finally the author expresses his hearty thanks to his instructor Prof. Takuzo Sakai for his very kind guidance and encouragements, and also to his friends Mr. Ryoiti Kikuti and Mr. Akira Isihara for their valuable discussions.

Literatures.

(1) R. de Kronig: Zs. f. Physis. **78** (193) 744, J. C. Slater; Phys. Rev. **51** (1937), 195, 52 (1937) 214, H. Welker: Zs. f. Phys. **111** (19).

(2) H. Welker: Zs. f. Phys. **111** (19).

(3) Z. Gorter: Arch. Mus. Teyler, **7** (1933) 378.

(4) Gorter and Casimir: Physica, **1** (1934) 306.

(5) J. G. Daunt and K. Mendelssohn: Proc. Roy. Soc. **160** (1937) 127.

Theory of the External Photoelectric Effect in Semiconductor. Part I. BaO–, SrO–, and Cu_2O–Semiconductors Behaviours of the Photosensitivity near Threshold.

By Toshinosuke MUTO and Jiro YAMASHITA

Institute of Science and Technology, Tokyo University.

(Received July, 1, 1947)

The external photoelectric effect in semiconductors has drawn much attention in connection with the elucidation of the atomic processes in the oxide cathodes which have been extensively available, as thermionic emitter of high efficiency, in the field of electronics. Although many investigators(1) have studied experimentally the thermionic properties and the electrical conductivity of the oxide cathodes together with the theoretical discussion of their results by the aid of Wilson's theory of semiconductors, not a detailed information concerning the photoelectric characteristics is as yet available both experimentally and theoretically. In view of the mentioned situation, therefore, it is highly desirable to work out theoretically the external photoelectric effect in semiconductors in order to make clear the rather different characteristics of the photosensitivity of semiconductors compared with those of pure metals.

In order to establish theoretically the method of determination of photoelectric work function from the photosensitivity curve, we have worked in detail the photosensitivity near the threshold for the photoelectrons originating from the impurity atoms involved (excess alkaline earth atoms for BaO and SrO, and excess oxygen atoms for Cu_2O), the result of which are

$$P=en(N_F,T)\Phi\frac{1}{(h\nu)^2}\left(\sqrt{h\nu-\Delta E}-\sqrt{-E_0^s}\right)\left(1+C\sqrt{h\nu-\Delta E}\right), \quad (1)$$

$$\Phi=\frac{e^2(m^*)^{3/2}A}{\sqrt{2}\,\pi m^2h^2nc},$$

e = electronic charge, m^* = effective mass of conduction electron, c = light velocity, m = true mass of an electron, n = index of refraction of the crystal, $h\nu$ = incident light quantum, h = Planck's constant divided by 2π, A = quantity related with the transition matrix element, ΔE=energy difference between the bottom of conduction band and the impurity level.

E^s_0=energy of the bottom of conduction band. C=ratio of the matrix elements $<$ 1.

$n(N_F,T)$ expresses the average number[(2)] of electrons within the impurity atoms at temperature T and is approximately equal to N_F. total number of impurity atoms involved, except for the extremely high temperature range.

The detailed behaviours of (1) are described graphically in Fig. 1, corresponding to the appropriate values of $C=0.1$ and 0.01, the quantitative estimation of C being difficult at present owing to the lack of an accurate knowledge of the eigenfunctions of crystal electrons. In the mentioned numerical evaluations of the photosensitivity, the observed values of $E^s_0=-0.3$ ev. $\Delta E=1.33$ ev. (BaO) and $\Delta E=2.28$ ev (SrO) have been substituted in (1) in accordance with Nishibori and his coworkers' experiment.[(3)] As seen in the figure, the photosensitivity near the threshold is found to be represented by the nearly straight line with respect to the incident light quantum, which result may be considered to permit us to determine the threshold value (work function) of the photoelectric effect in semiconductors by the aid of the linear extrapolation method. From (1), it follows, for the mentioned threshold value,

$$h\nu_m=-E^s_0+\Delta E. \qquad (2)$$

Since $n(N_F,T)$ is nearly independent of T except for the extremely high temperature, the mentioned photosensitivity in (1) will have less sensitive behaviours for the temperature of the crystal.

Photosensitivity due to a small number of conduction electrons will be computed in a similar way to the former case. A careful examination, however, shows that the concerned matrix elements of photoelectrons are extremely small compared with that of the former due to the impurity atoms involved, on account of which the mentioned photocurrent plays a role in the extremely long wave length region where the former contribution approaches zero. A simple calculation shows that the temperature behaviours of the photosensitivity

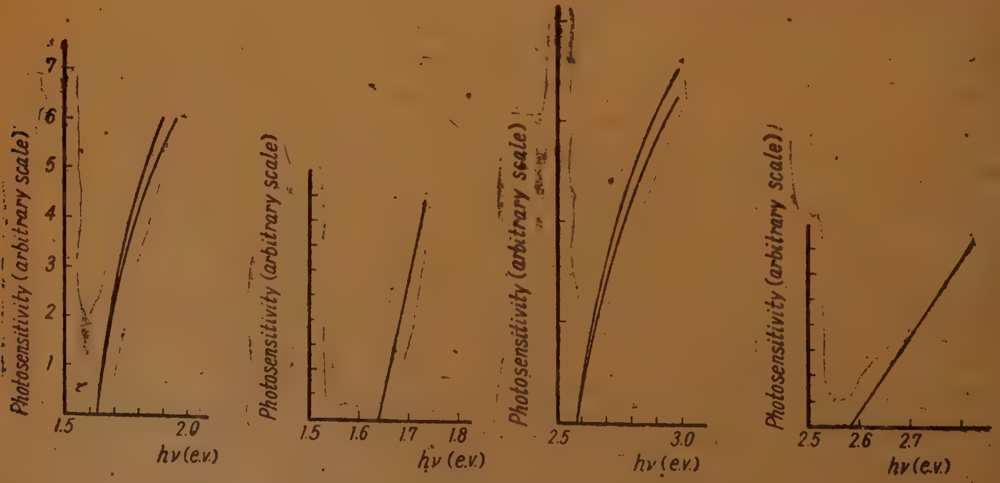

Fig. 1.
Pho'osenstivity near Threshold.

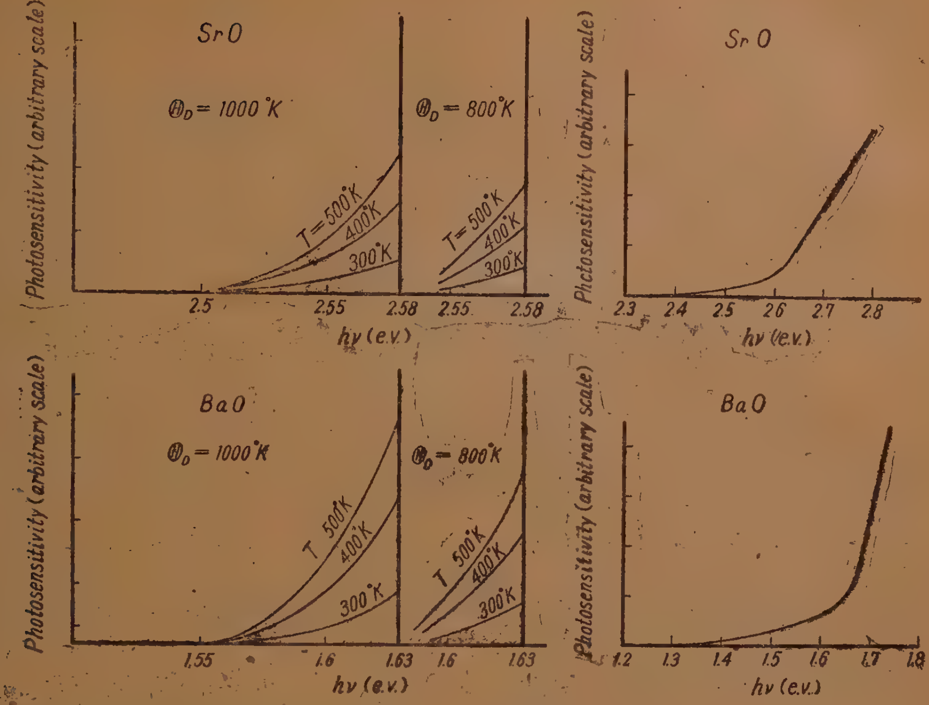

Fig. 2.

Photosensitivity of the Mixed Photoelectric Effect.

Total Photosensitivity near Threshold.

due to the conduction electrons becomes

$$P = \text{constant}\cdot T^{9/4}e^{-\Delta E/kT}, \qquad (3)$$

in sharp contrast to (1).

As clearly seen in the experimental observation, the tail part of the photosensitivity makes its appearance in the long wave length side of the threshold, the characteristics of which is to show a remarkable increase with temperature. A careful consideration of the mentioned tail part shows that the "mixed" photoelectric effect due to the simultaneous absorption of both an incident light quantum and a heat quantum of lattice vibrations is responsible for the tail part of the photosensitivity of semiconductors, which combined process shall be dealt with theoretically on a quite similar line to the case(4) of the secondary absorption of light in metals. Making use of the formula for the transition probability due to the mentioned double absorption process, worked out by one(4) of the authors, it follows, after some process of computations,

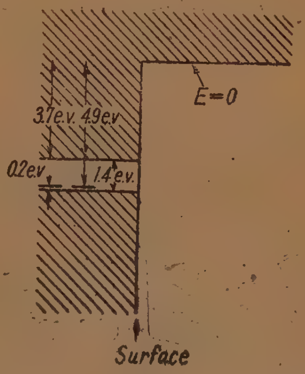

Fig. 3.

Energy Band Structure of C_2O-Semiconductor.

$$P=en(N_F,T)\Phi_1\frac{4\pi}{h^3}\left(\frac{1}{u_1{}^5}+\frac{2}{u_2{}^5}\right)\frac{kT^{7/2}}{(h\nu)^2}$$

$$\int_{(h\nu_m-h\nu)/kT}^{\Theta/T}\frac{\xi}{e^\xi-1}\left\{\sqrt{\frac{h\nu-\Delta E}{kT}+\xi}-\sqrt{\frac{-E_0}{kT}}\right\}$$

$$\times(1+C_1\sqrt{h\nu-\Delta E+\xi hT})d\xi,$$

$$\Phi=\frac{\sqrt{2}\,e^2\hbar^2a^3(m^*)^{3/2}}{4\pi^3m^4Mcn}K^2A_1\,.$$

u_1,u_2 = propagation velocities of logitudinal and transverse elastic waves respectively, Θ ≐ Debye temperature of the crystal, K = quantity connected with transition matrix element accompanied by heat quantum absorption, A_1 = that accompanied by optical transitions.

It should be mentioned that P in (4) shows a remarkable temperature dependency in contradistinction to P in (1), and, furthermore, it plays an important role only in the tail part, being of a higher order of smallness compared with P in (1). The results of the numerical evaluation of (4) are represented graphically in Fig. 2 together with possible forms of total photosensitivity (1)+(4).

All the theoretical results of the photosensitivity near threshold are found to be in satisfactory agreements with Nishibori and his coworkers' experiments⁽⁵⁾ of activated BaO and SrO, though the origin of the much smaller photocurrent in the extremely long wave length side of the threshold appears to be still unclarified.

By the linear extrapolation method established above, we have estimated the photoelectric work function of Cu_2O semiconductors to be $h\nu=4.9$ ev from Wasser's experimental result, which value has been made use of to obtain the energy band structure of Cu_2O together with the experimental result of the electrical conductivity and the Hall effect due to Juse and Kurchatov,⁽⁷⁾ and Engelhard.⁽⁸⁾ (Fig. 3)

A full account of this short note shall be published in the journal when the unfavourable condition of paper-shortage will be eliminated in future.

---

* Read in the first annual meeting of the Physical Society of Japan held on 2nd, May, 1946.

References.

(1) Blewett: J. Appl. Phys. **10** (1939) 831. Sayama: Subutsu Kaishi, **17** (194-) 203.

(2) Wilson: Proc. Roy. Soc. **A133** (1932) 458; **A143** (1932) 277.

(3) Nishibori, Kawamura and Hirano: Proc. Phys. Math. Soc. Japan, **23** (1941) 37.

(4) Muto: Sci. Pap. I.P.C.R. **27** (1935) 179.

(5) Nishibori and his coworkers: loc. cit.

(6) Wasser: ZS. USRR. **6** (1934) 350.

(7) Juse and Kurtchatow: ibid. 2 (1933) 353.

(8) Engelhard: Ann. d. Phys. **17** (1933) 501.

Theory of the External Photoelectric Effect in Semiconductors.
Part I. BaO–, SrO– and Cu_2O–Semiconductors Total Photosensitivity.

By Toshinosuke MUTO

Institute of Sience and Technology, Tokyo Imperial University.

(Received July 1, 1947)

In order to obtain the influence on the photosensitivity of the electronic states within the impurity atoms, the accurate knowledge of the eigenfunction of electrons trapped within the

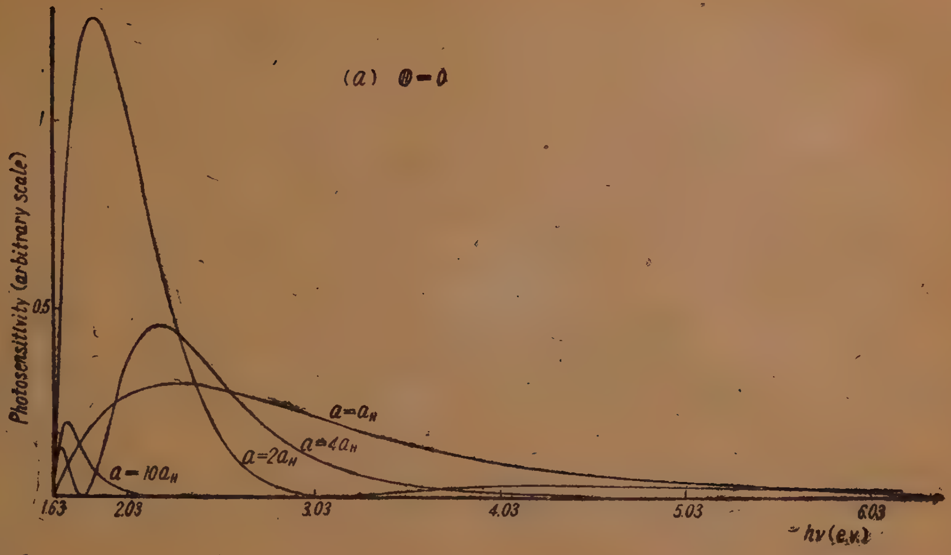

Fig. 1. (a)
Photosensitivity (a_H= Bohr's radius)

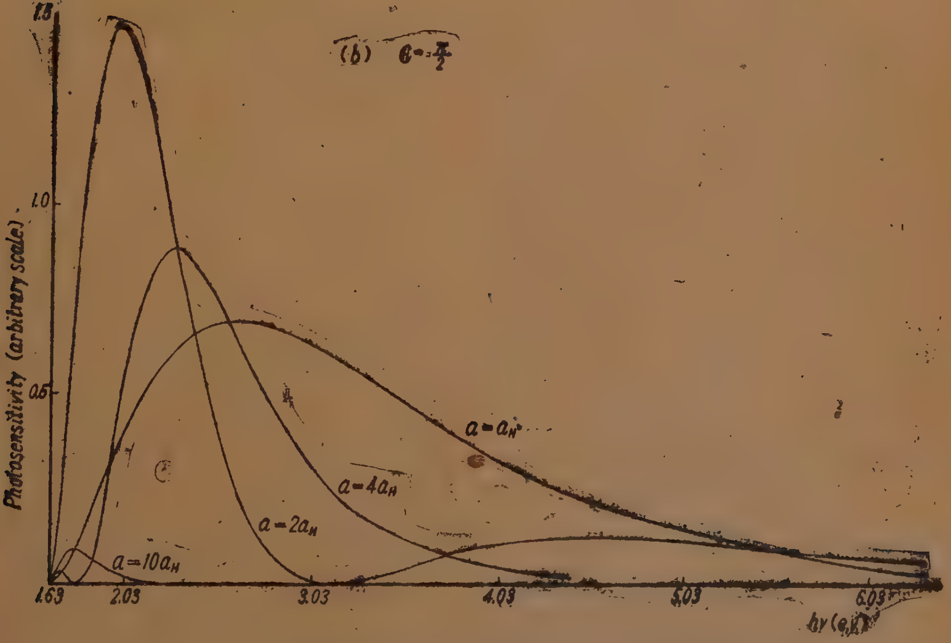

Fig. 1. (b)
Photosensitivity (a_H= Bohr's radius)

impurity atoms is essentially required. In view of the unfortunate situation of the exact information of electronic eigenfunction being now lacking in the mentioned oxide-cathode, however, we shall tentatively assume for the eigenfunction of trapped electrons to be of an *s* eigenfunction of atomic type, taking into account the valence electrons of Ba and Sr atoms to be 6*s*- and 5*s*-electrons respectively, and shall compute the possible influence on the photosensitivity of electronic state within the impurity atoms.

According to Slater's method⁽¹⁾ of shielding constant, we are able to construct the explicit form of trapped electron's eigenfunction as follows.

$$\frac{1}{3}\sqrt{\frac{2}{5\pi}\left(\frac{Z^*}{a_0}\right)^7}\, r^3 e^{-\frac{z^*}{a_0}r}, \qquad (1)$$

where Z^* means the effective nuclear charge for the mentioned valence electrons, a_0 the parameter responsible for the linear extension of the mentioned electronic orbit. As seen from the simple consideration of the potential filed of ions surounding the mentioned impurity atoms, a_0 becomes larger as the influence on valence electron of the surrounding ions, thus a_0 giving some measure of the binding (single or group binding) of electron attached near the impurity atoms.

Evaluating the transition matrix elements concerned in the phenomena by the use of (1), we obtain, for the photosensitivity,

$$P = en(N_F, T)\,\Phi_1\left(\frac{Z^*}{a_0}\right)^7 \frac{k_r^3}{(h\nu)^2}\,\frac{\left\{5\left(\frac{Z^*}{a_0}\right)^4 - 10\left(\frac{Z^*}{a_0}\right)^2 k_r^2 + k_r^4\right\}^2}{\left\{\left(\frac{Z^*}{a_0}\right)^2 + k_r^2\right\}^{10}}$$
$$\times\left\{\frac{2\pi}{3}\cos^2\Theta\left[1-\left(\frac{-E^s_0}{h\nu-\varDelta E}\right)^{3/2}\right]\right.$$
$$+\pi\sin^2\Theta\left[\left(1-\frac{-E^s_0}{h\nu-\varDelta E}\right)^{1/2}\right.$$
$$\left.\left.-\frac{1}{3}\left(1-\left(\frac{-E^s_0}{h\nu-\varDelta E}\right)^{3/2}\right)\right]\right\}, \qquad (2)$$

$$\Phi_1 = \frac{(32)^2\pi}{5}\cdot\frac{u_0 e^2 h m^*}{G^3 c n m},$$

$$k_r = \sqrt{\frac{2m^*}{h^2}(h\nu - \varDelta E)}\,,$$

$u_0 = \overline{u}$, G^3 = No. of atoms involved.

where Θ denotes the inclination of the polarization vector of an incident radiation with respect to the boundary surface of the crystal.

As seen in (2), P not only has sharp threshold value in the relatively long wave length side but also approaches zero in the short wave length region,, being $P\alpha(h\nu)^{-13/2}$. Furthermore, P tends to zero for extremely large or small values of a_0 ($P\alpha a_0^{-7}$ or a^5_0). The general behaviours of (1) shall be represented graphically in the accompanying figure corresponding to some of the assigned values of a_0, which results will be found clearly to be in satisfactory accord with experimental observations of Huxford.⁽²⁾ Now it should be stressed that a predominant maximum of the photosensitivity makes its apperance for the relatively small or large values of a_0 while for the intermediate ones there appear two maxima of comparable magnitudes in spite of the assumption of a single electronic state involved. These states of affairs should be taken into consideration for the careful analysis of the observed photosensitivity in semiconductors.

A full account of this short note shall be published in the journal when the unfavorable condition of paper-shortage will be eliminated in future.

References

(1) Slater: Phys. Rev. **36** (1930) 57.
(2) Huxford: ibid. **38** (1931) 379.

Theory of the External Photoelectric Effect in Semiconductors.

Part II. Coloured Alkali Halides.

By Toshinosuke MUTO

Institute of Science and Technology, Tokyo Imperial University.

(Received July 1, 1947)

As clearly pointed out experimentally by Asmus,(1) the external photoelectric effect in coloured alkali halides under the illumination of visible light appears to show the remarkable different variation with time of the photocurrent in comparison with that of the ordinary one treated in Part I,(2) although the detailed observation of the photosensitivty of the former is still lacking unfortunately. According to Asmus,(3) the mentioned photocurrent observed with the visible light is known experimentally to make its appearance only for the coloured alkali halides but not for the colourless ones, and, further, its time variations associated with or without the change of colours of illuminating light are found to be taken place in a quite similar way to that of the phosphorescence in crystalphosphors. Taking into account the detailed behaviours of photocurrent, Asmus(4) has suggested reasonably the following mechanisms to be taken place during the photoemission.

On account of the incident light quantum being absorbed within the F-centers involved, the F*-centers may be produced afresh in the crystal from which centers the photoelectrons are considered to originate under visible light illumination since the incident light quantum in the visible region is not sufficient for the trapped electrons within the F-centers to go away from the crystal according to Tartakowsky's(5) energy diagram of alkali halide. Thus, the relatively long life-time of F-*centers is essentially responsible for the time-effect of the mentioned photocurrent similarly to Lenard-centers in the crystalphosphors. From the observed variation with time of the photocurrent just after the interruption of the incident radiation, Asmus(6) has estimated for the life time of F*-centers to be of 10^5-10^6 sec at room temperatures. Through the extensive experimental studies of alkali halides with or without F-centers mainly due to Pohl(7) and his school in Göttingen, the physical properties of the mentioned crystals may be considered to be brought into much light recently and, furthermore, the electronic structures of alkali halides have been worked out theoretically(8) by many investigators, from the modern view of the solid state, in a close connection with the light absorption and the photocurrent produced within the mentioned crystals.

In view of the now available informations of alkali halides mentioned above, the following process of electronic transitions may be reasonably supposed to be realized in the photoelectric emission during the visible light illumination of the coloured alkali halides. The visible light is absorbed in the F-centers of alkali halides on account of which the trapped electrons at E^S_F are able to jump up into the lower part of the conduction band of the crystal directly or indirectly through the intermediate states E^P_F of the F-centers. According to the theory of the temperature-dependency of the photoconduction by Mott, however, the thermal agitation of the lattice may be considered to remove the excited electrons within F-centers before it has time to fall back into the normal state. The released electrons in the conduction band give rise to the photoconduction observed by Gudden and Pohl, and then they may in some way be trapped at another F-centers or at the surface levels on the internal but minute cracks of the crystal, F*-centers being thus produced within the crystal. Furthermore, the trapped electrons within the metastable $E^S{}_F{}^*$ level are able to be ejected outside by the visible light absorption owing to the relatively higher energy states in F*-centers, thus giving rise to the external photocurrent. The mentioned photocurrent, therefore, may be considered to be realized through four kinds of transition processes of electrons originating from F-centers, two of which are due to the optical transitions and the others to thermal ones, as schematically represented by the arrows in the accompanying figure, The rather complex transition processes mentioned above are found to be quite similar to those of the phosphorescence in crystalphosphors which has been worked out theoretically by the author.(9) The close correlation among the phosphorescence, the internal photoconduction and the external photocurrent, therefore, may be expected theoretically to exist in the coloured alkali halides, which fact appears to be actually observed experimentally by Gudden and Pohl,(10) and Asmus.(11)

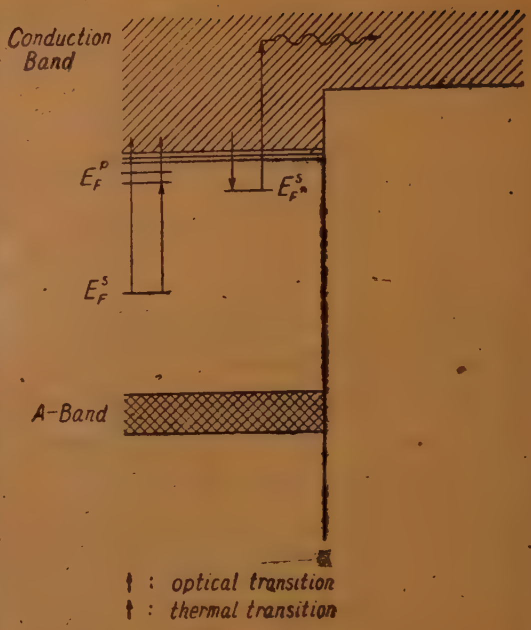

Fig. 1.

In order to obtain the photocurrent in accordance with the mentioned modes of transition processes of trapped electrons during the visible light illnmination, we may proceed to carry out the quantum mechanical manipulations in a quite similar way to the case of the phosphorescence in crystalphosphor worked by the auther,(12) and, then, we obtain, after a rather tedious process of calculations,

$$J=en_F(T)\cdot 4\pi\frac{\pi L(\nu_P^k)}{h}\,\frac{\Gamma^A}{\Gamma^B{}_{\rho\cdot1}-\Gamma^A}\cdot\sum_i\frac{\pi L^{(i)}(\nu_{S*}^k)}{h}\Gamma^{C(i)}_{\rho\beta\cdot1}$$
$$\times\left\{\frac{e^{-4\pi\Gamma^{C(i)}_{\rho\beta\cdot1}t}-e^{-4\pi\Gamma^{A}t}}{(\Gamma^A-\Gamma^{C(i)}_{\rho\beta\cdot1})(\Gamma^C_{\rho\alpha\cdot1}-\Gamma^A)}+\frac{e^{-4\pi\Gamma^{C(i)}_{\rho\beta\cdot1}t}-e^{-4\pi\Gamma^{B}_{\rho\cdot1}t}}{(\Gamma^B_{\rho\cdot1}-\Gamma^{C(i)}_{\beta\cdot1})(\Gamma^B_{\rho\cdot1}-\Gamma^C_{\rho\alpha\cdot1})}\right.$$
$$\left.+\frac{\Gamma^B_{\rho\alpha\cdot0}-\Gamma^A}{(\Gamma^C_{\rho\alpha\cdot0}-\Gamma^A)(\Gamma^C_{\rho\alpha\cdot0}-\Gamma^B_{\rho\cdot0})}\cdot\frac{e^{-4\pi\Gamma^{C(i)}_{\rho\beta\cdot0}t}-e^{-4\pi\Gamma^{C}_{\rho\alpha\cdot0}t}}{\Gamma^C_{\rho\alpha\cdot0}-\Gamma^{C(i)}_{\rho\beta\cdot0}}\right\}, \tag{1}$$

where

$$L(\nu)=\frac{e^4}{4\pi^2a^3M}\cdot\frac{1}{\nu}\,\frac{1}{e^{h\nu/kT}-1}\left|\int\psi^*_{\vec{k}}(\vec{r})e^{-i(\vec{q}\vec{r})}\psi^P_F(\vec{r})\,d\tau\right|^2, \tag{2}$$

$$L^{(i)}(\nu)\doteq\frac{e^4}{4\pi^2a^3M}\cdot\frac{1}{\nu}\cdot\frac{1}{e^{h\nu/kT}-1}\left|\int\psi_F^{(i)*}(\vec{r})e^{i(\vec{q}\vec{r})}\psi_{\vec{k}}(\vec{r})d\tau\right|^2, \tag{3}$$

$$\Gamma^{A}(\nu_S^P)=\frac{e^2}{2h^2m^2(\nu_S^P)^2}D(\nu_S^P)\frac{1}{3}\left|\int\psi_F^{P*}(\vec{r})\,\frac{t}{i}\,\mathrm{grad}\,\psi_F^S d\tau\right|^2, \tag{4}$$

$$\Gamma^{B}_{p\cdot0}(\nu)=\Gamma^{A}(\nu_S^P)+\frac{\pi}{h}L(\nu_P^k) \tag{5}$$

$$\Gamma^{C}_{p\,i\cdot0}(\nu_{S*}^k)=\sum_i\frac{\pi}{h}L^{(i)}(\nu_{S*}^k)\ ,$$

$$\Gamma^{C(i)}_{p\beta\cdot0}(\nu_{S_*}^{k'})=\frac{\pi}{h}\left(\frac{e}{2mc}\right)^2\frac{N}{4\pi^2m\nu_S^k}u_0\frac{\sqrt{2}\,(m^*)^{3/2}}{h}\sqrt{h\nu-\Delta E}$$
$$\times\int_0^{\theta_1}\sin\theta d\theta\int_0^{2\pi}d\varphi\,|\vec{M}_{F*}^{rk'}|^2\ , \tag{6}$$

$$\vec{M}_{F*}^{nk'}=G^{-3/2}\int u^*_{n\vec{k}}(\vec{r})(\vec{e}_A\,\mathrm{grad}\,u_F(\vec{r}))\,e^{-i\vec{k}\vec{r}}\,dk.$$

i designates each of the F-centres.

$n_F(T)$ = number of trapped electrons within F-centers at temperatuae T, e = electronic charge, a = lattice constant, N = number of incident photons, M = reduced mass of ion pairs, $D(\nu)$ = energy density of incident light, m = electronic mass, $\nu^P{}_S=(E^P{}_F-E^S{}_F)/h$ etc.

All the other notations described above have the same meanings as in Part I. The integrals in (6) are entirely equivalent to those in the photoelectric transition probability worked in Part I, giving the photoelectric threshold as usual., The damping constants in (2)-(6) can not be evaluated without a detailed knowledge of the eigenfunctions of crystal electrons in the conduction band and also in the F-and F*-centers of coloured alkali halides.

In general, the mentioned photocurrent may be expected, from (1), to exhibit the rather complicated behaviours with respect to incident photo quantum $h\nu$ and the crystal temperature T. Furthermore, the mentioned photocurrent increases with time at first rapidly with the light illumination and then decreases, after passing through a maximum, rapidly or gradually according to the temperature, the colour of incident light and the energy band structure of the crystal. All the experimental results of Asmus,(13) therefore, may be satisfactorily understood, though qualitatively, by the aid of the theoretical formula (1). In Asmus' experiment, however, the accurately monochromatic light has not been used, and the photosensitivity and its temperature-effect have not been observed so that the thorough discussion of the phenomena under consideration seems to be rather premature at present. We, therefore, shall postpone the detailed theoretical discussion of the interesting phenomena through the evaluation of (2)-(6) until the reliable experimental informations will be accumulated in the near future.

A full account of the short note shall be published in the journal when the unfavourable situations of paper-shortage will be eliminated in future.

---

* Read in the first annual meeting of the Physical Society of Japan held on 2nd, May, 1936.

References.

(1) Asmus: Ann. d. Phys. **26** (1936) 723.
(2) Muto & Yamashita; Rikoken-hokoku (1947) (in pres).
(3) Asmus: loc. cit. (4) Asmus: loc. cit.
(5) Tartakowsky: ZS. f. Phys. **90** (1934) 504.
(6) Asmus: loc. cit.
(7) Phol: Proc. Phys. Soc. **49** (extra), (1937) 16.
(8) Mott & Gurney: Electronic Processes in Ionic Crystals (1940).
(9) Muto: Sci. Pap. I.B.C.R. **28** (1933) 171; 31 (1937) 150.
(10) Gudden & Pohl: ZS. f. Phys. **31** (1925) 651.
(11) Asmus: loc. cit. (12) Muto: loc. cit.
(13) Asmus: loc. cit.

On the Resistance Experienced by a Body Which Moves along the Plane Surface of an Elastic Solid

By Hirosi HAYASI

(Received February 9, 1944)

I. Introduction.

In the former propers(1) the wrighter has treated the problem of deformation of the earth's surface when a disturbance travels on it with a uniform velocity on the assumption that the disturbance exerts only pressure which is uniformly distributed over a circular area of the surface. In the present paper the writer will calculate the resistance which is experienced by the disturbing body due to the dissipation of energy.

II. Calculations.

The work done per unit time through a surface S is given by the formula

$$\Pi = \iint_S \left(X_\nu \frac{\partial}{\partial t} \mathfrak{R} D_x + Y_\nu \frac{\partial}{\partial t} \mathfrak{R} D_y + Z_\nu \frac{\partial}{\partial t} \mathfrak{R} D_z \right) dS,$$

where the integration is extended over the whole surface under consideration. The resistance experienced by the body is defined by

$$R = \Pi / v.$$

In the present case

$$S : \begin{cases} z = 0 \\ x^2 + y^2 \leqq a^2 \end{cases} \quad \text{at} \quad t = 0,$$

and

$$\left. \begin{aligned} X_\nu &= Y_\nu = 0 \\ Z_\nu &= Z_z = P/\pi a^2 \end{aligned} \right\} \quad \text{on} \quad S.$$

$$\therefore \quad \Pi = \frac{P}{\pi a^2} \iint\limits_{x^2+y^2 \leqq a^2} \left[\frac{\partial}{\partial t} \mathfrak{R} D_z \right]_{\substack{z=0 \\ t=0}} dx dy$$

$$= \frac{P}{\pi a^2} \mathfrak{R} \iint\limits_{x^2+y^2 \leqq a^2} \left[\frac{\partial}{\partial t} D_z \right]_{\substack{z=0 \\ t=0}} dx dy.$$

Now

$$\left[\frac{\partial}{\partial t} D_z \right]_{\substack{z=0 \\ t=0}} = \frac{-ivP}{2\pi^2 \mu a} \int_0^\infty J_1(sa)$$

$$\times \begin{cases} \int_{-\pi}^{\pi} \cos\phi f(\phi)^{irs\cos(\phi-\theta)} d\phi & 0 < v < c \\ \int_{-\pi}^{\pi} \cos(\theta+\Psi) f(\theta+\Psi) e^{irs\cos\Psi} d\Psi & c < v. \end{cases}$$

$$\therefore \quad \Pi = \frac{vP^2}{2\pi^3 \mu a^3} \mathfrak{R} \cdot -i \int_0^a r dr \int_{-\pi}^{\pi} d\theta \int_0^\infty J_1(sa) ds$$

$$\times \begin{cases} \int_{-\pi}^{\pi} \cos\phi f(\phi) e^{irs\cos(\phi-\theta)} d\phi & 0 < v < c \\ \int_{-\pi}^{\pi} \cos(\theta+\Psi) f(\theta+\Psi) e^{irs\cos\Psi} d\Psi & c < v. \end{cases}$$

(i) $0 < v < c$.

$$\Pi = \frac{vP^2}{2\pi^3 \mu a^3} \mathfrak{J} \int_0^\infty J_1(sa) ds \int_{-\pi}^{\pi} \cos\phi f(\phi) d\phi$$

$$\times \int_0^a r dr \int_{-\pi}^{\pi} e^{irs\cos(\phi-\theta)} d\theta .$$

$$= \frac{vP^2}{\pi^2 \mu a^3} \mathfrak{J} \int_0^\infty J_1(sa) ds \int_{-\pi}^{\pi} \cos\phi f(\phi) d\phi$$

$$\times \int_0^a J_0(rs) r dr$$

$$= \frac{vP^2}{\pi^2 \mu a^2} \mathfrak{J} \int_0^\infty \frac{\{J_1(sa)\}^2}{s} ds \int_{-\pi}^{\pi} \cos\phi f(\phi) d\phi = 0.$$

$$\therefore \quad R = 0.$$

(ii) $c < v$.

$$\int_{-\pi}^{\pi} \cos(\theta+\Psi) f(\theta+\Psi) e^{irs\cos\Psi} d\Psi$$

$$= I \int_{-\pi}^{\pi} \cos(\theta+\Psi) f(\theta+\Psi) e^{irs\cos\Psi} d\Psi$$

$$-\pi i R(\beta_1) - \pi i R(\beta_2) + \pi i R(\beta_2) + \pi i R(\beta_1)$$

$$= P \int_{-\pi}^{\pi} \cos\phi f(\phi) e^{irs\cos(\phi-\theta)} d\phi - \pi i R(\beta_1) \ldots\ldots$$

$$\therefore \int_0^a r dr \int_{-\pi}^{\pi} d\theta \int_0^\infty J_1(sa) ds P \int d\Psi$$

$$= \int_0^\infty J_1(sa) ds P \int_{-\pi}^{\pi} \cos\phi f(\phi) d\phi$$

$$\times \int_0^a r dr \int_{-\pi}^{\pi} e^{irs\cos(\phi-\theta)} d\theta$$

$$= 2\pi a\int_0 \frac{\{J_1(sa)\}^2}{s}\,dsP\int_{-\pi}^{\pi}\cos\phi f(\phi)d\phi$$

$c < v \leqq b.$

$$P\int\cos\phi\, f(\phi)d\phi = 0.$$

$$-\pi i R(\beta_1)\ldots.$$

$$= \pi i\cos\phi_0 Rf(\phi_0)\{e^{-i\omega s\cos(\phi_0-\theta)}+e^{i\omega s\cos(\phi_0+\theta)}$$
$$+e^{i\omega s\cos(\phi_0-\theta)}+e^{-i\omega s\cos(\phi_0+\theta)}\}.$$

$$\Pi = \frac{vP^2}{2\pi^2\mu a^3}\cos\phi_0 Rf(\phi_0)$$
$$\times\int_0^\infty J_1(sa)ds\int_0^a rdr\int_{-\pi}^{\pi}[e^{-i\omega s\cos(\phi_0-\theta)}+\ldots\ldots]d\theta$$
$$= \frac{4vP^2}{\pi\mu a^3}\cos\phi_0 Rf(\phi_0)\int_0^\infty J_1(sa)ds\int_0^a J_0(rs)rdr$$
$$= \frac{4vP^2}{\pi\mu a^2}\cos\phi_0 Rf(\phi_0)\int_0 \frac{\{J_1(sa)\}^2}{s}ds$$
$$= \frac{2vP^2}{\pi\mu a^2}\frac{\tau_0\sqrt{1-\nu\tau_0}}{\left(\frac{\partial\varsigma}{\partial\tau}\right)_{\tau=\tau_0}\cdot -2\varepsilon\sqrt{1-\frac{\tau_0}{\varepsilon}}}.$$

$$\therefore\quad R = \frac{P^2}{\pi\mu a^2}\cdot\frac{\sqrt{1-\nu\tau_0}}{-(\partial\varsigma/\partial\tau)_{\tau=\tau_0}}\cdot\frac{c^2/v^2}{\sqrt{1-c^2/v^2}}.$$

$b < v \leqq a.$

$$a_1'' = \Im P\int_{-\pi}^{\pi}\cos\phi f(\phi)d\phi.$$

The evaluation of this integral was already given in the previous paper²⁾.

$$\Pi = \frac{vP^2}{2\pi^2\mu a^3}a_1''+\frac{vP^2}{\pi\mu a^2}$$
$$\times\frac{\sqrt{1-\nu\tau_0}}{-(\partial\varsigma/\partial\tau)_{\tau=\tau_0}}\cdot\frac{c^2/v^2}{\sqrt{1-c^2/v^2}},$$

$$R = \frac{P^2}{2\pi^2\mu a^2}a_1''+\frac{P^2}{\pi\mu a^2}$$
$$\times\frac{\sqrt{1-\nu\tau_0}}{-(\partial\varsigma/\partial\tau)_{\tau=\tau_0}}\cdot\frac{c^2/v^2}{\sqrt{1-c^2/v^2}}.$$

$a < v.$

$$a_1''' = \Im P\int_{-\pi}^{\pi}\cos\phi f(\phi)d\phi.$$

$$\Pi = \frac{vP^2}{2\pi^2\mu a^2}a_1'''+\frac{vP^2}{\pi\mu a^2}$$
$$\times\frac{\sqrt{1-\nu\tau_0}}{-(\partial\varsigma/\partial\tau)_{\tau=\tau_0}}\cdot\frac{c^2/v^2}{\sqrt{1-c^2/v^2}},$$

$$R = \frac{P^2}{2\pi^2\mu a^2}a_1'''+\frac{P^2}{\pi\mu a^2}$$
$$\times\frac{\sqrt{1-\nu\tau_0}}{-(\partial\varsigma/\partial\tau)_{\tau=\tau_0}}\cdot\frac{c^2/v^2}{\sqrt{1-c^2/v^2}}.$$

The remaining problem is to calculate a_1'''. The integral or the integrals

$$a'''_{2m-1} = \Im P\int_{-\pi}^{\pi}f(\phi)\cos(2m-1)\phi d\phi$$
$$= 2\left\{\Im\int_{-\phi_2}^{\phi_2}+\Im P\int_{\phi_2}^{\pi-\phi_2}\right\}f(\phi)\cos(2m-1)\phi d\phi$$

appeared already in the preceding paper³⁾ The second integral in the last expression can be evaluated in the same way as in the article V or VII in the former paper.

$$\Im P\int_{\phi_2}^{\pi-\phi_2}f(\phi)\cos(2m-1)\phi d\phi$$
$$= \sum_{n=0}^{\infty}\frac{F_2^{(n)}(0)}{n!}$$
$$\times\Im P\int_{\phi_2}^{\pi-\phi_2}\frac{(\sqrt{1-\varepsilon\cos^2\phi})^n}{\varepsilon\cos^2\phi-\tau_0}\cos(2m-1)\phi d\phi$$

n : even integer

$$\Im P\int_{\phi}^{\pi-\phi_2}\frac{(\sqrt{1-\varepsilon\cos^2\phi})^n}{\varepsilon\cos^2\phi-\tau_0}\cos(2m-1)\phi d\phi = 0.$$

n : odd integer

$$\Im P\int_{\phi_2}^{\pi-\phi_2}\frac{(\sqrt{1-\varepsilon\cos^2\phi})^n}{\varepsilon\cos^2\phi-\tau_0}\cos(2m-1)\phi d\phi$$
$$= \sum_{k=0}^{\leq m-1}\sum_{j=0}^{k}\frac{(2m-1)!\,k!\,(-1)^{k+j}}{2k!\,(2m-2k-1)!\,j!\,(k-j)!}$$
$$\times\Im P\int_{\phi_2}^{\pi-\phi_2}\frac{(\sqrt{1-\varepsilon\cos^2\phi})^n}{\varepsilon\cos^2\phi-\tau_0}\cos^{2m+2j-2k-1}\phi d\phi.$$

Put $\sqrt{\nu\varepsilon}\cos\phi = \cos\Psi$,

$$\Im P\int_{\phi_2}^{\pi-\phi_2}\frac{(\sqrt{1-\varepsilon\cos^2\phi})^n}{\varepsilon\cos^2\phi-\tau_0}\cos^{2m+2j-2k-1}\phi d\phi$$
$$= \frac{1}{(\nu\varepsilon)^{m+j-k}}\Im P\int_0^{\pi}\frac{(\sqrt{1-\cos^2\Psi/\nu})^n}{\cos^2\Psi/\nu-\tau_0}$$
$$\times\frac{\cos^{2m+2j-2k-1}\Psi}{\sqrt{1-\cos^2\Psi/\nu\varepsilon}}\sqrt{1-\cos^2\Psi}\,d\Psi$$
$$= \sum_{s=0}^{\infty}\sum_{t=0}^{\infty}(-1)^{s+t}\binom{\frac{1}{2}}{s}\binom{-\frac{1}{2}}{t}\frac{1}{(\nu\varepsilon)^{t+m+j-k}}$$
$$\times\Im P\int_0^{\pi}\frac{(\sqrt{1-\cos^2\Psi/\nu})^n}{\cos^2\Psi/\nu-\tau_0}\cos^{2m+2j+2s+2t-2k-1}\Psi d\Psi.$$

$$\Im P\int_0^{\pi}\{\ ''\ \}d\Psi$$
$$= \frac{1}{2}\Im P\smile\int_{-\pi}^{\pi}\smile d\Psi = \frac{1}{2}\left\{\Im\smile\int_{-\pi}^{\pi}\smile d\Psi-\pi i\Sigma R\right\},$$

$$\Sigma R = \frac{-2\nu(\sqrt{1-\tau_0})^n}{\sqrt{1-\nu\tau_0}}(\nu\tau_0)^{m+j+s+t-k-1},$$

Put $e^{-i\Psi}=z$,

$$\Im \upsilon\!\int\!\upsilon\, d\Psi = \Im \int \frac{4\nu z^{2}}{(z^{2}+1)^{2}-4\nu\tau_{0}z^{2}}$$

$$\times \frac{(\sqrt{4\nu z^{2}-(z^{2}+1)^{2}})^{n}}{2^{n}\nu^{n/2}z^{n}}\cdot\frac{(z^{2}+1)^{2m+2j+2t+2s-2k-1}}{(2z)^{2m+2j+2t+2s-2k-1}}\cdot\frac{dz}{iz}$$

$$=\Im \frac{-i}{2^{n+2m+2j+2s+2t-2k-3}\nu^{n/2-1}}$$

$$\times \sum_{j,k=0}^{\leq\frac{n}{2}-1}\sum_{\alpha=0}^{2m+2j+2s+2t-2k-1}\frac{\left(\frac{n-1}{2}\right)!}{j!\,k!\left(\frac{n-1}{2}-j-k\right)!}$$

$$\frac{(2m+2j+2s+2t-2k-1)!}{\alpha!(2m+2j+2s+2t-2k-1-\alpha)!}$$

$$(4\nu-2)^{j}(-1)^{\frac{n-1}{2}-j}$$

$$\times\int z^{2j+4k+2-n-2m-2j-2s-2t+2k+1+2\alpha}\frac{dz}{iz},$$

$$\int\left\{\;''\;\right\}\frac{dz}{iz}=2\pi\delta,$$

$$\delta=\begin{cases}1 & 2j+4k+3+2k+2\alpha = n+2m+2j+2s+2t\\ 0 & \quad ,, \qquad \neq \qquad ,,\end{cases}$$

Next we can see $1/\varsigma(\tau,\nu)$ is regular in the region $|\tau-\varepsilon|<\varepsilon-1/\nu$ on the upper sheet, and $\sqrt{1-\nu\tau}$ is also regular in the region $|\tau-\varepsilon|<\varepsilon-1/\nu$. Hence $F(\tau)$ is regular for the suitable branch in the same region in which the interval $(-\phi_2,\phi_2)$ in the ϕ-plane corresponds. So we may put

$$F(\tau)=\sum_{n=0}^{\infty}\frac{F^{(n)}(\varepsilon)}{n!}(\tau-\varepsilon)^{n},$$

where $F^{(n)}(\varepsilon)$ are purely imaginary.

$$\Im\int_{-\phi_2}^{\phi_2}f(\phi)\cos(2m-1)\phi\, d\phi$$

$$=\sum_{n=0}^{\infty}\frac{F^{(n)}(\varepsilon)}{n!\,i}\varepsilon^{n}(-1)^{n}\int_{-\phi_2}^{\phi_2}\sin^{2n}\phi\cos(2m-1)\phi\, d\phi$$

$$=\sum_{n=0}^{\infty}\sum_{k=0}^{\leq m-1}\frac{F^{(n)}(\varepsilon)}{n!\,i}\varepsilon^{n}(-1)^{n}\frac{(2m-1)!\,(-1)^{k}}{2k!\,(2m-2k-1)!}$$

$$\times\int_{-\phi_2}^{\phi_2}\sin^{2n+2k}\phi\cos^{2m-2k-1}\phi\, d\phi$$

$$=\sum_{n=0}^{\infty}\sum_{k=0}^{\leq m-1}\sum_{j=0}^{n-k-1}\frac{F^{(n)}(\varepsilon)}{n!\,i}\varepsilon^{n}(-1)^{n}\frac{(2m-1)!\,(-1)^{k+j}}{2k!\,(2m-2k-1)!}$$

$$\times\frac{(m-k-1)!}{j!\,(m-k-j-1)!}\int_{-\phi_2}^{\phi_2}\sin^{2n+2k+2j}\phi\, d\sin\phi$$

$$=2\sum_{n=0}^{\infty}\sum_{k=0}^{\leq m-1}\sum_{j=0}^{m-k-1}\frac{F^{(n)}(\varepsilon)}{n!\,i}\varepsilon^{n}(-1)^{n}$$

$$\times\frac{(2m-1)!\,(-1)^{k+j}(m-k-1)!}{2k!\,(2m-2k-1)!\,j!\,(m-k-j-1)!}$$

$$\times\frac{(1-1/\nu\varepsilon)^{n+k+j+\frac{1}{2}}}{2n+2k+2j+1}.$$

Finally the writer expresses his thanks to Dr. T. SAKAI for the kindness of suggesting him the problem.

References.

(1) H. Hayasi: Proc. Phys.-Math. Soc. Japan, **24** (1942), 533; **24** (1942), 800; **24** (1942), 915; **25** (1943), 47; **25** (1943), 198; **25** (1943), 391; **25** (1943), 468; **25** (1943), 648.

(2) H. Hayasi: Proc. Phys.-Math. Soc. Japan, **25** (1943), 203.

(3) H. Hayasi: Proc. Phys-Math. Soc. Japan, **25** (1943), 470, 472, 477.

On the Elimination of the Auxiliary Condition in the Quantum Electrodynamics II.*

By Satio HAYAKAWA, Yonezi MIYAMOTO and Sin-itiro TOMONAGA.

Central Meteorological Observatory

Physical Department, Faculty of Science, University of Tokyo

Physical Institute, Tokyo Bunrika Daigaku

(Received December 2, 1946)

§4. Applications.

1. *Self-energy of an electron.*

Our method is now applied to the calculation of the self-energy of an electron. It is an advantageous feature of our method that, by taking v equal to the four-velocity of the electron itself, the classical (contracted coulomb+magnetic) and the quantum (fluctuation) self-energies appear separately, so that we can give a clearer interpretation of the result than by the method usually adopted.(4)

From (1.10) and (3.9) we find the Schrödinger equation for one electron:

$$\left[\left(\gamma, \frac{h}{i}\,\text{Grad} \;\; \frac{\varepsilon}{c}B - \frac{\varepsilon^2}{c}L\right) + mc\right]\Omega = 0 \qquad (4.1)$$

where γ means the four-vector

$$\gamma = (\beta\vec{\alpha},\ \beta). \qquad (4.2)$$

We solve this equation in a power series of ε, putting

$$\Omega = \chi_0 + \varepsilon\chi_1 + \varepsilon^2\chi_2 + \ldots. \qquad (4.3)$$

The equations for χ_0, χ_1, χ_2, ... are then

$$\left[\left(\gamma, \frac{h}{i}\,\text{Grad}\right) + mc\right]\chi_0 = 0 \qquad (4.4)$$

$$\left[\left(\gamma, \frac{h}{i}\,\text{Grad}\right) + mc\right]\chi_1 = \frac{1}{c}(\gamma, B)\,\chi_0 \qquad (4.5)$$

$$\left[\left(\gamma, \frac{h}{i}\,\text{Grad}\right) + mc\right]\chi_2 = \frac{1}{c}(\gamma, B)\chi_1 + \frac{1}{c}(\gamma, L)\chi_0\,. \qquad (4.6)$$

We now put the zero-th approximation

$$\chi_0 = u_0\, e^{\frac{i}{h}(p_0,\, x)}\,. \qquad (4.7)$$

As mentioned above, it is supposed that the definitions of B and L in (4.1) are referred to the four-velocity v which is equal to the velocity of the electron itself. We have thus to put

$$v = \frac{p_0}{mc} \qquad (4.8)$$

in (2.15″).

The equation (4.5) for the first correction yields now

$$\chi_1 = \frac{1}{(2\pi)^{3/2}}\,\frac{1}{c}\,\frac{1}{\left(\gamma, \frac{h}{i}\,\text{Grad}\right) + mc}$$

$$\times \int \{R^{+}(\gamma, r) + S^{+}(\gamma, s)\}\, e^{-i(k,\,x)}\,\frac{d\vec{k}}{k}\,\chi_0 \qquad (4.9)$$

In the integrand on the right-hand side of this expression the terms containing the operators R and S are omitted, since there exist no photons in the state represented by χ_0, so that these operators give rise to the vanishing results when applied to χ_0. The right-hand side of (4.9) can be further expressed in the form

$$-\frac{1}{(2\pi)^{3/2}}\,\frac{1}{c}\int \frac{(\gamma, p_0 - hk) - mc}{(p_0 - hk)^2 + m^2c^2}$$

$$\{R^{+}(\gamma, r) + S^{+}(\gamma, s)\}\, e^{-i(k,\,x)}\,\frac{d\vec{k}}{k}\,\chi_0,$$

which, on account of $(p, k) = 0$ and $(p_0, P_0) = -m^2c^2$, yields

$$\chi_1 = \frac{1}{(2\pi)^{3/2}}\,\frac{1}{c}\int \frac{(\gamma, p_0 - hk) - mc}{2(p_0, hk)}$$

$$\times \{R^{+}(\gamma, r) + S^{+}(\gamma, S)\}\, e^{-i(k,\,x)}\,\frac{d\vec{k}}{k}\,\chi_0\,. \qquad (4.10)$$

We bring this χ_1 into the equation (4.6) for the second correction. We multiply thus (4.10) with $\frac{1}{c}(\gamma, B)$ from the left, noticing $R(\vec{k}')R^{+}(\vec{k})\chi_0 = S(\vec{k}')S^{+}(\vec{k})\chi_0 = \frac{kck}{2}\delta(k-k)\chi_0$, then we get

---

* Continuation of the paper in the same volume, p. 172.

$$\frac{1}{c}(\gamma, B)\chi_1 = \frac{1}{32\pi^3}\frac{h}{c}\int\sum_{\iota=r,s}(\gamma,\iota)\{)\gamma, \boldsymbol{p}_0-h\boldsymbol{k})-mc\}$$

$$\times(\gamma,\iota)\frac{1}{(\boldsymbol{p}_0, h\boldsymbol{k})}\frac{d\vec{k}}{k}\chi_0. \tag{4.11}$$

(We have omitted the terms of the type $R^{+}R^{+}\chi_0$, since we are interested only in that part of χ_2, which corresponds to the state with no photons) We notice now, that the vectors $\boldsymbol{r}$ and $\boldsymbol{s}$ are orthogonal to the vector $\boldsymbol{v}$ on account of (2.18), so that they are orthogonal to $\boldsymbol{p}_0$. Further they are orthogonal to $\boldsymbol{k}$. These facts result in that $(\gamma, \boldsymbol{s})$ and $(\gamma, \boldsymbol{s})$ are anticommutable with $(\gamma, \boldsymbol{p}_0-h\boldsymbol{k})$, so that we obtain

$$\frac{1}{c}(\gamma, B)\chi_1 = -\frac{1}{16\pi^3}\frac{h}{c}\int\frac{(\gamma, \boldsymbol{k})}{(\boldsymbol{p}_0, \boldsymbol{k})}\frac{d\vec{k}}{k}\chi_0; \tag{4.12}$$

we have used $\{(\gamma, \boldsymbol{p}_0)+mc\}\chi_0 = 0$ in deriving (41.2) from (4.11).

$$\left\{\left(\gamma, \frac{h}{i}\,\mathrm{Grad}\right)+mc\right\}\chi_2$$

$$= \left\{-\frac{1}{16\pi^3}\frac{h}{c}\int\frac{(\gamma, \boldsymbol{k})}{(\boldsymbol{p}_0, \boldsymbol{k})}\frac{d\vec{k}}{k}+\frac{1}{c}(\gamma, L)\right\}\chi_0. \tag{4.13}$$

On multiplying with $-\left\{\left(\gamma, \frac{d}{i}\,\mathrm{Grad}\right)-mc\right\}$ from the left, this

$$\left\{\left(\frac{h}{i}\,\mathrm{Grad}\right)^2+m^2c^2\right\}\chi_2 = \{(\gamma, \boldsymbol{p}_0)-mc\}$$

$$\times\left\{\frac{1}{16\pi^3}\frac{h}{c}\int\frac{(\gamma, \boldsymbol{k})}{(\boldsymbol{p}_0, \boldsymbol{k})}\frac{d\vec{k}}{d}-\frac{1}{c}(\gamma, L)\right\}\chi_0. \tag{4.14}$$

The right-hand side of (4.14) is now to be calculated: First we have

$$\frac{1}{16\pi^3}\frac{h}{c}\int\{(\gamma, \boldsymbol{p}_0)-mc\}(\gamma, \boldsymbol{k})\frac{1}{(\boldsymbol{P}_0, \boldsymbol{k})}\frac{d\vec{k}}{k}\chi_0$$

$$= -\frac{1}{8\pi^3}\frac{h}{c}\int\frac{d\vec{k}}{k}\chi_0 \tag{4.15}$$

On account of the formula $\{(\gamma, \boldsymbol{p}_0)-mc\}(\gamma, \boldsymbol{k})\chi_0 = -2(\boldsymbol{p}_0, \boldsymbol{k})\chi_0$, which is valid for any vector $\boldsymbol{k}$. Using (3-10) and (2.16) we obtain next

$$\{(\gamma, \boldsymbol{p}_0)-mc\}\frac{1}{c}(\gamma, L)\chi_0$$

$$= -\frac{1}{16\pi^3}\frac{1}{c}\int\{(\gamma, \boldsymbol{p}_0)-mc\}\left(\gamma, \frac{\boldsymbol{k}+2\boldsymbol{v}(\boldsymbol{k}, \boldsymbol{v})}{(\boldsymbol{k}, \boldsymbol{v})^2}\right)\frac{d\vec{k}}{k}\chi_0,$$

and the application of the above formula gives

$$= -\frac{m}{8\pi^3}\int\frac{1}{(\boldsymbol{k}, \boldsymbol{v})}\frac{d\vec{k}}{k}\chi_0 \tag{4.16}$$

The expression (4.16) contains $\boldsymbol{v}$, but this dependence on $\boldsymbol{v}$ is merely apparent. We can make sure of this by noticing that the integral on the right-hand side of (4.16) is invariant because $(\boldsymbol{k}, \boldsymbol{v})$ and $d\vec{k}/k$ are both invariant. The integral may, therefore, be evaluated referring to the coordinate system in which $\boldsymbol{v}$ has the component (1, 0, 0, 0), thus giving rise to

$$\{(\gamma, \boldsymbol{p}_0)-mc\}\frac{1}{c}(\gamma, L)\chi_0 = \frac{m}{8\pi^3}\int\frac{d\vec{k}}{k^2}\chi_0. \tag{4.17}$$

The iterated equation (4.14) becomes then

$$\left\{\left(\frac{h}{i}\,\mathrm{Grad}\right)^2+m^2c^2\right\}\chi_2$$

$$= \frac{\varepsilon^2}{8\pi^3}\left\{-m\int\frac{d\vec{k}}{k^2}-\frac{h}{c}\int\frac{d\vec{k}}{k}\right\}\chi_0. \tag{4.18}$$

As we can easily verify, the iterated equation of the same form is obtained if we start from the equation

$$\left[\left(\gamma, \frac{h}{i}\,\mathrm{Grad}\right)+mc+\frac{1}{16\pi^3}\frac{\varepsilon^2}{c}\right.$$

$$\left.\left\{\int\frac{d\vec{k}}{k^2}+\frac{h}{mc}\int\frac{d\vec{k}}{k}\right\}\right]\Omega = 0 \tag{4.19}$$

and solve this equation by putting

$$\Omega = \chi_0+\varepsilon^2\chi_2+\dots. \tag{4.20}$$

This fact means that the interaction of the electron with its self-field causes, in our approximation, the apparent increase of its mass by the amount

$$\Delta m = \frac{1}{16\pi^3}\frac{\varepsilon^2}{c^2}\left\{\int\frac{d\vec{k}}{k^2}+\frac{h}{mc}\int\frac{d\vec{k}}{k}\right\}. \tag{4.21}$$

The first term on the right-hand side of this expression represents the classical electromagnetic mass of a point electron while the second term the quantum effect due to the fluctuation of the transverse photon wave.

Since in this way the effect of the interaction between the electron and its self-field can be introduced as the apparent change of the mass, the self-energy ΔE of an electron has the correct dependence on its velocity:

$$\Delta E = \frac{c^2 \Delta m}{\sqrt{1-u'^2}}\,, \tag{4.22}$$

if we define u' by means of

$$\vec{u}' = \frac{\vec{p}_0}{(m+\Delta m)c} \tag{4.23}$$

It is to be noticed, that, if one calculated the integrals $\int \frac{d\vec{k}}{k}$ in (4,15) and $\int \frac{1}{(\boldsymbol{k}, \boldsymbol{v})} \frac{d\vec{k}}{k}$ in (4.16) straightforward by introducing the polar coordinates of $\vec{k}$ (the direction of $\vec{u}$ being taken as the polar axis), one would obtain

$$\left\{\begin{aligned} \int \frac{d\vec{k}}{k} &= 4\pi \int k dk \\ \int \frac{1}{(\boldsymbol{k}, \boldsymbol{v})} \frac{d\vec{k}}{k} &= 2\pi \frac{\sqrt{1-u^2}}{u} \log \frac{1-u}{1+u} \int dk\,. \end{aligned}\right. \tag{4.24}$$

The second integral of (4.24) depends on the velocity of the electron in disagreement with our statement above. The result (4.24) does not then give the correct dependence of the self-energy on the velocity, but gives rise to

$$\Delta E = \frac{1}{4\pi^2} \frac{\varepsilon^2 h}{mc} \sqrt{1-u^2}$$

$$\int k dk + \frac{1}{8\pi^3} e^2 \frac{1-u^2}{u} \log \frac{1-u}{1+u} \int dk \tag{4.25}$$

as has been already found by Waller. But this way of the calculation, in which one uses the polar coordinates of $\vec{k}$, presupposes that the spherical symmetry of the $\vec{k}$-space; which, owing to the Lorentz contraction, is not valid when the electron is moving. One could obtain also other velocity dependence of these integrals if one evaluates the integrals by using other integration variables. Properly speaking, we can attribute no velocity dependence to the integrals in (4.24) because they have no convergent values at all.* In such a situation our method provides us the way of obtaining the significant velocity dependence of these integrals in such a way that the requiriment of the relativity theory is fulfilled, and hence the way of subtracting these diverging quantity in a relativistically invariant manner from our theory. In fact, Dirac(2) has shown, by means of his λ-limiting process, that the first term in Δm of (4.21) can be subtracted without destroying the relativistic invariance of the theory.

2. *Radiation field of the electron.*

When we take $\boldsymbol{v}$ equal to the four-velocity of the electron itself, our generalized longitudinal field $\varepsilon \boldsymbol{L}(x)$ can be interpreted as the self-field attached to the electron in the approximation in which the quantum fluctuation is neglected. In fact, if we replace γ in (4.1) by $\boldsymbol{v}$, which corresponds, according to Bloch and Nordsieck,(5) to the neglect of the quantum fluctuation, we obtain

$$\left[\left(\boldsymbol{v}, \frac{h}{i} \mathrm{Grad} - \frac{\varepsilon}{c} \boldsymbol{L}\right) + mc\right] \Omega = 0\,, \tag{4.1'}$$

because $\boldsymbol{v}$ and $\boldsymbol{B}$ are orthogonal to each other according to (2.18). The fact that the term containing $\boldsymbol{B}$ disappears in (4.1′) means that our longitudinal field alone is already sufficient to represent the self-field around the electron.

According to Bloch and Nordsieck the Bremsstrahlung emitted by the electron in a sudden change of its velocity is nothing but the liberation of the field which has become surplus at the instance of the collision owing to the difference of the self-field before and after collision. This problem will be now treated by our method.

Let the velocity of the electron before collision $\boldsymbol{v}$ the velocity after collision $\boldsymbol{v}'$. We introduce two schemes of separating the field into longitudinal and transverse parts, one referring to $\boldsymbol{v}$ and the other to $\boldsymbol{v}'$. We define thus, besides K, L, R, S and their conjugates K^+, L^+, R^+, S^+ defined by means of (Table I), dashed quantities K', L', R', S' and their conjugates K'^+, L'^+, R'^+, S'^+ using dashed vectors $\boldsymbol{l}', \boldsymbol{r}'$ and $\boldsymbol{s}'$ which refer to the velocity $\boldsymbol{v}'$; especially $\boldsymbol{l}'$ is defined by

$$\boldsymbol{l}' = \frac{\boldsymbol{k} + 2\boldsymbol{v}'(\boldsymbol{k}, \boldsymbol{v}')}{2(\boldsymbol{k}, \boldsymbol{v}')^2} \tag{4.26}$$

As one can easily verify, there exist, then, between undashed and dashed quantities the following relations:

---

* We can give any desired velocity dependence $f(u)$ to the diverging integral of the form $\int_0^\infty dx$ by transforming the integration variable to y defined by $x = f(u)y$. We obtaine namely $\int_0^\infty dx = f(u)\int_0^\infty dy$. The right-hand side having the apparent velocity dependence $f(u)$.

$$\begin{cases} K' = K+(l', lL^+ + rR^+ + sS^+) \\ L' = L-(l', lK^+ - rR - sS) \\ R' = (r', -lK^+ + rR + sS) \\ S' = (s', -lK^+ + rR + sS) \end{cases} \tag{4.27}$$

and

$$\begin{cases} K'^+ = K^+ \\ L'^+ = L^+ \\ R'^+ = (r', lL^+ + rR^+ + sS^+) \\ S'^+ = (s', lL^+ + rR^+ + sS^+). \end{cases} \tag{4.28}$$

According to our above ascertainment, that part of the field which is not bound to the electron after collision is described by the quantities R', S' and their conjugates R'^+ and S'^+, so that the operators representing the number of free photons after the collision is

$$\begin{cases} N_r' = \dfrac{2}{hck} R'^+ R' \\ N_s' = \dfrac{2}{hck} S'^+ S' . \end{cases} \tag{4.29}$$

The number of photons liberated with the propagation vector k lying in the region $d\vec{k}$ is then given by

$$N d\vec{k} = \frac{2}{hck}(R'^+R' + S'^+S')d\vec{k} ,$$

which, on account of (4.27) and (4.28), gives rise

$$\begin{aligned} = \frac{2}{hck}\Big[&-\{(r', l)^2+(s', l)^2\}K^+L^+ \\ &-\{(r', l)(r', r\overline{R^+K^+}+s\overline{S^+K^+}) \\ &\quad +(s', l)(s', r\overline{R^+K^+}+s\overline{S^+K^+})\} \\ &\quad +\overline{(r', rR^+ + sS^+)(r', rR + sS)} \\ &\quad +\overline{(s', rR^+ + sS^+)(s', rR + sS)}\Big] d\vec{k}. \end{aligned} \tag{4.30}$$

Since there are no free photons before the collision we have to put in (4.30) $\overline{R^+R} = \overline{S^+S} = 0$. Further, the mean values of the cross terms, such as $\overline{R^+K^+}$ and $\overline{S^+K^+}$, vanish. The term $\overline{K^+L^+}$, on the other hand, has to be substituded by $-|f|^2/4$ on accont of the auxiliary conditions (3.1). In this way wo obtain

$$\begin{aligned} N' d\vec{k} &= \frac{1}{2hck}\{(r', l)^2+(s', l)^2\}|f|^2 d\vec{k} \\ &= \frac{\varepsilon^2}{16\pi^3 hck}\{(r', l)^2+(s', l)^2\} d\vec{k} , \end{aligned}$$

which, introducing (2.16) and noticing $(r', k) = (s', k) = 0$, reduces into

$$N' = \frac{\varepsilon^2}{16\pi^3 hck}\left\{\left(\frac{(r', v)}{(k, v)}\right)^2 + \left(\frac{(s', v)}{(k, v)}\right)^2\right\} \tag{4.31}$$

The fobmula (4.31) can be brought into the more familiar form. First we observe that

$$\begin{cases} \dfrac{(r', v)}{(k, v)} = \dfrac{(r', v)}{(k, v)} - \dfrac{(r', v')}{(k, v')} \\ \dfrac{(s', v)}{(k, v)} = \dfrac{(s', v)}{(k, v)} - \dfrac{(s', v')}{(k, v')} \end{cases} \tag{4.32}$$

because of (2.18). Then we express r' and s' in (4.32) in terms of the three dimensional polarization vector η_r and η_s according to (2.19):

$$\begin{cases} \vec{r}' = \dfrac{1}{k}(\vec{\eta}_r' + r'\vec{k}) \\ \vec{s}' = \dfrac{1}{k}(\vec{\eta}_s' + s'\vec{k}) . \end{cases} \tag{4.33}$$

This results in

$$\begin{cases} \dfrac{(r', v)}{(k, v)} - \dfrac{(r', v')}{(k, v')} = \dfrac{1}{k}\left\{\dfrac{(\vec{\eta}_r, \vec{u})}{(\vec{k}, \vec{u})-k} - \dfrac{(\vec{\eta}_r, \vec{u}')}{(\vec{k}, \vec{u}')-k}\right\} \\ \dfrac{(s', v)}{(k, v)} - \dfrac{(s', v')}{(k, v)} = \dfrac{1}{k}\left\{\dfrac{(\vec{\eta}_s', \vec{u})}{(\vec{k}, \vec{u})-k} - \dfrac{(\vec{\eta}_s', \vec{u}')}{(\vec{k}, \vec{u}')-k}\right\}, \end{cases} \tag{4.34}$$

which give rise to

$$N' = \frac{\varepsilon^2}{16\pi^3 hck^2}\sum_{t=r,s}\left\{\frac{(\vec{\eta}_t', \vec{u})}{k-(\vec{k}, \vec{u})} - \frac{(\vec{\eta}_t', \vec{u}')}{k-(\vec{k}, \vec{u}')}\right\}^2,$$

or carrying out the summation over t,

$$\begin{aligned} N' &= \frac{\varepsilon^2}{16\pi^3 hck^3} \\ &\times\left\{\left(\frac{\vec{u}}{1-u_l} - \frac{\vec{u}'}{1-u_l'}\right)^2 - \left(\frac{u_e}{1-u_l} - \frac{u_e'}{1-u_l'}\right)\right. \\ &= \frac{\varepsilon^2}{16\pi^3 hck^3} \\ &\times\left\{\left(\frac{\vec{u}}{1-u_l} - \frac{\vec{u}'}{1-u_l'}\right)^2 - \left(\frac{1}{1-u_l} - \frac{1}{1-u_l'}\right)^2\right\}, \end{aligned} \tag{4.35}$$

where u_l, u_l' are the component of $\vec{u}$, $\vec{u}'$ along $\vec{k}$. One sees that our result (4.35) does really agree with the results of Bloch and Nordsieck and of Nordsieck* ((31) of Bloch and Nordsieck and (2) of Nordsieck).

It is easy to verify that the same result is obtained by means of the above mentioned picture of the phenomena. According to this the field radiated in the collision is the difference between the self-fields before and after the collision. The vector potential of this radiated field is, therefore, given by

---

* Our result differs from Bloch's by the factor 4π. This is due to the difference of the electromagnetic unit used in these two treatments.

$$\boldsymbol{A}_{\mathrm{rad}}(x)=\varepsilon\{L(x)-L'(x)\}$$

$$=\frac{\varepsilon}{16\pi^3}\int(l-l')(e^{i(k,x)}+e^{-i(k,x)})\frac{d\vec{k}}{k}\,. \qquad (4.36)$$

Then, the Fourier amplitudes of the radiated field are

$$\boldsymbol{A}_{\mathrm{rad}}(\vec{k})=\boldsymbol{A}^{+}{}_{\mathrm{rad}}(\vec{k})$$

$$=\frac{\varepsilon}{2}\,\frac{1}{(2\pi)^{3/2}}(l-l')\,. \qquad (4.37)$$

The spectrum of the radiated energy is then given by

$$E_{\mathrm{rad}}(\vec{k})d\vec{k}=2(\vec{A}^{+}{}_{\mathrm{rad}}(\vec{k}),A_{\mathrm{rad}}(\vec{k}))\,d\vec{k}$$

$$=\frac{\varepsilon^2}{16\pi^3}(l-l')^2d\vec{k} \qquad (4{,}38)$$

Using here (2.16) and (4.26), the spectrum becomes

$$Erad=\frac{\varepsilon^2}{16\pi^3}\Big[\frac{k}{2}\Big\{\frac{1}{(k,v)^3}-\frac{1}{(k,v')^2}\Big\}$$

$$+\Big\{\frac{v}{(k,v)}-\frac{v'}{(k,v')}\Big\}\Big]^2=\frac{\varepsilon^2}{16\pi^3}\Big\{\frac{v}{(k,v)}-\frac{v^2}{(k,v')}\Big\}^2,$$

or, expressed in terms of the three-dimensional velocities

$$=\frac{\varepsilon^2}{16\pi^3}\,\frac{1}{k^2}\Big\{\Big(\frac{\vec{u}}{1-u_l}-\frac{\vec{u}'}{1-u_l'}\Big)^2$$

$$-\Big(\frac{1}{1-u_l}-\frac{1}{1-u_l'}\Big)^2\Big\}\,. \qquad (4.39)$$

This gives, after divided by *chk*, by the energy of the single photon, the mean number of the emitted photons which agrees with (4.35).

We shall now notice that the consideration of Weizsäcker and Williams⁽⁶⁾ who have dealt with the Bremsstrahlung of high speed electron on colliding with an atom can be accounted for also from the stand-point of the above mentioned picture. Following these authors we observe the phenomena in the coordinate system in which the electron is at rest before the collision. Let the velocity of the nucleus observed in this system be $c\vec{V}$. We first calculate the velocity gain of the electron in the collision. If p denote the collision parameter of the nucleus with respect to the electron, the transverse componeht of the electric field acting on the electron is

$$E(t)=\frac{1}{4\pi}\,\frac{\varepsilon Z\xi p}{(p^2+\xi^2c^2V^2t^2)^{3/2}}\,, \qquad (4.40)$$

where εZ is the charge of the nucleus, ξ is defined by $\xi=1/\sqrt{1-V^2}$. The velocity of the electron after the collision is then given by

$$cu'=\frac{\varepsilon}{m}\int_{-\infty}^{+\infty}E(t)dt$$

$$=\frac{1}{4\pi}\,\frac{2\varepsilon^2Z}{mcVp}\,. \qquad (4.41)$$

Since this velocity is perpendicular to the velocity of the nucleus and in the direction connecting the electron and the nucleus at the instant of collision, we have

$$u_l'=u'\sin\theta\cos(\varphi-\varphi_0), \qquad (4.42)$$

θ and φ being the polar angle and the azimuth of of $\vec{k}$, and φ_0 the azimuth of the electron with respect to $\vec{V}$.

We bring now this u' into our formula (4.35), noticing that u, the velocity before the collision, is zero. We notice further that only such collision contributes mainly to the collision cross-section in which the velocity after collision is small compared with the light velocity. Thus we may put $1-u_l'=1$ in (4.35).

$$N(p,\varphi_0\,;\,k,\theta,\varphi)\,dk\sin\theta\,d\theta\,d\varphi$$

$$=\frac{1}{4\pi^2}\,\frac{4\varepsilon^6Z^2}{16\pi^3hc^3}\,\frac{1}{m^2c^2V^2p^2}$$

$$\times\{1-\sin^2\theta\cos^2(\varphi-\varphi_0)\}\frac{dk}{k}\sin\theta\,d\theta\,d\varphi. \qquad (4.43)$$

The total mean number of the emitted photons can be obtained by multiplying (4.43) with $pdpd\varphi_0$, with the probability for that the impact parameter and the azimuth lie in the interval $(p, p+dp\,;\,\varphi_0, \varphi_0+d\varphi_0)$, and then integrating over p and φ_0. Thereby the lower limit of p is $\lambda_c=h/mc$, and the upper limit is $a_0Z^{-1/3}$, the screening radius of the atom.

We obtain thus

$$N(k,\theta,\varphi)\,dk\sin\theta\,d\theta\,d\varphi$$

$$=\frac{1}{64\pi^4}\,\frac{\varepsilon^2Z^2}{hc}\Big(\frac{\varepsilon^2}{mc^2}\Big)^2\frac{1}{V^2}\log\frac{a_0}{\lambda_cZ^{1/3}}$$

$$\times(1+\cos^2\theta)\frac{dk}{k}\sin\theta\,d\theta\,d\varphi \qquad (4.44)$$

Integrated over all direction of $\vec{k}$, this gives

$$N(k)dk = \frac{1}{12\pi^3}\left(\frac{\varepsilon^2}{mc^2}\right)^2 \frac{1}{V^2} \log \frac{a_0}{\lambda_c Z^{1/3}} \frac{dk}{k} \qquad (4.45)$$

This result can be now compared with the result of Weizsäcker:

$$N(k)dk$$
$$= \frac{1}{16\pi^3} \frac{\varepsilon^2 Z}{hc}\left(\frac{\varepsilon^2}{mc^2}\right)^2 \left[\frac{4}{3}(1-\varepsilon)+\varepsilon^2\right] \log \frac{a_0}{\lambda_c Z^{1/3}} \frac{dk}{k} \qquad (4.46$$

(in Weizsäcker's (36) the factor $\frac{1}{16\pi^3}$ does not appear. This is due to the difference of the electromagnetic unit). One sees that, when $V \approx 1$ and $\varepsilon < 1$, ε being the energy of the emitted photon measured in the scale of initial energy of the electron, our result agrees perfectly with Weizsäcer's. Because the difference between 3/4 and 3/4 $(1-\varepsilon)+\varepsilon^2$ is not significant over all values of ε between zero and unity, we can conclude that the main feature of the phenomena under consideration is already accounted for by means of our classical picture. In fact, the appearance of the factor $(1+\cos^2\theta)$ in (4.44) instead of the more complicated one in the treatment of Weizsäcker corresponds to the use of Thomson's formula instead of Klein-Nishina's used by him.

We wish to express our hearty thanks to Mr. Koba who has given various contributions in many parts of this work.

References.

(4) I. Waller: Zs. f. Phys. **62** (1930), 673. See also Dirac loc. cit.

(5) F. Bloch and A. Nordsieck: Phys. Rev. **52**, (1937), 54. A. Nordsieck: ibid, 59.

(6) C. F. Weizsäcker: Zs f. phys. **88** (1934), 612. E. J. Williams: D. kgl. Danske Videsk. Selskab, Math. fis. Medd, **13**, 4, (1935). 1.

On the Chemical Composition of Some Late Type Stars.

By Yoshio FUJITA.

Department of Astronomy, University of Tokyo.

(Received March 13, 1947)

1. Introduction.

The problem of the chemical composition of stellar atmospheres closely related to the knowledge of the relative abundance of elements in stellar atmospheres is very interesting; even in the problem itself, we find many important facts such as special abundance of certain elements, according which stars are classified into carbon stars, oxygen stars, etc. Lately from the standpoint of nuclear physics it is believed that the chemical composition of the stellar atmospheres is related closely to the evolution of stars. In my previous papers(1), it was clarified that the relative abundance of hydrogen, oxygen, nitrogen and carbon differs from star to star, and that taking this point into consideration, the spectral branching of the late type stars can be explained. In the late type stars, as the result of the combination of hydrogen, oxygen, nitrogen and carbon with each other and of these elements with other metallic elements, several molecules can exist in the stellar atmosphere If we know the relative abundance of these molecules, we can find the variable abundance of these elements composing such molecules. However, up to the present, it seems that the abundance of the stellar atmospheres has not been treated sufficiently in detail except R Coronae Borealis studied by Berman.(2) The solar atmosphere has been only the source of this research(3) Now, in this paper, we select some late typestars the spectra of which were measured photometrically, and try to deduce the relative abundance of elements and molecules with the intension of discussing ths problem. As the method of attack, we draw the curve of growth for each star by the sum rule intensity method. By this curve the number of atoms and molecules can be obtained from the measured equivalent widths of each element.

2. Quantum Physical Data.

In the treatment of our problem, the necessary data are multiplets and their relative intensities. We use the relative intensities of multiplet triads for the calibration. The advantage in using supermultiplets lies in the fact that a larger number of lines are connected by a single set of theoretical relations and less weight is lost in the determination of zero points. In Table I are listed the multiplet triads which have been used in such calibration.4)

Table I. Triad Table.

Sc II	$3d^2-3d4p$	$a^3F-z^3D^0$ $a^3F-z^3F^0$		
Ti I	$3d^3(^4F)4s\ 3d^3(^4F)4p$	$a^5F-x^5D^0$ $a^5F-y^5F^0$ $a^5F-y^5G^0$	$3d^3(^4P)4s-3d^3(^4P)4p$	$a^5P-y^5S^0$ $a^5P-y^5P^0$ $a^5P-w^5D^0$
	$3d^3(^2H)4s-3d^3(^2H)4p$	$a^3H-u^3G^0$ $a^3H-x^3H^0$ $a^3H-z^3I^0$		
Ti II	$3d^3-3d^2(^3F)^34p$	$a^2G-z^2F^0$ $a^2G-z^2G^0$		
V I	$3d^34s^2-3d^34s(^5F)4p$	$a^4F-z^4D^0$ $a^4F-z^4F^0$ $a^4F-z^4G^0$	$3d^4(^5D)4s-3d^4(^5D)4p$	$a^6D-z^6P^0$ $a^6D-y^6D^0$ $a^6D-y^6F^0$
V II	$3d^4-3d^3(^4F)4p$	$b^3G-z^3F^0$ $b^3G-z^3G^0$		
Cr I	$3d^44S^2-3d^44S(^6D)4p$	$a^5D-y^5P^0$ $a^5D-z^5D^0$ $a^5D-z^5F^0$		
Mn I	$3d^6(^5D)4s-3d^6(^5D)4p$	$a^4D-y^4P^0$ $a^4D-z^4D^0$ $a^4D-z^4F^0$		
Fe I	$3d^7(^4P)4s-3d^7(^4P)4p$	$a^5P-z^5S^0$ $a^5P-x^5P^0$ $a^5P-w^5D^0$	$3d^7(^4F)4s-3d^7(^4F)4p$	$a^3F-y^3D^0$ $a^3F-y^3F^0$ $a^3F-z^3G^0$
	$3d^7(^2G)4s-3d^7(^2G)4p$	$b^3G-x^3F^0$ $b^3G-y^3G^0$ $b^3G-z^3H^0$		

3. The Curve of Growth.

The stars treated here are those, the spectra of which were measured spectrophotometrically. Some of them were analysed by the equivalent widths, while the others were measured by eye estimation. We reduced these intensities by eye estimation into the equivalent widths, applying Mulders' calibration curve connecting the Rowland intensity to the equivalent widths. The stars selected here are *Z* And,5) α Sco,6) α Boo,7) *R* CBor8) and δ Cep.9) In the first three stars, the eye estimation intensities being known, we reduce them

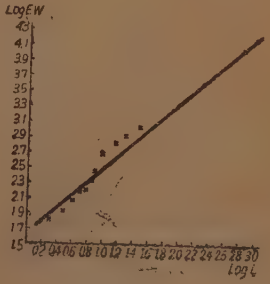

Fig. 1.

to the equivalent widths. Fig. 1 shows the curve connecting the Rowland intensity to the equivalent width. For the construction of the curve of growth, the emission intensity relative to the total intensity of the supermultiplet, expressed in appropriate units, is given by

$$FG\left(\frac{\lambda_0}{\lambda}\right)^4 e^{\frac{-h(\nu_2-\nu_1)}{kT}} = I\infty NFf \qquad (1)$$

or

$$\log F+\log G+4\log\frac{\lambda_0}{\lambda}-\frac{5040}{T}\Delta E = \log I = \log NFf+\text{const}, \qquad (2)$$

where F represents the theoretical intensity of the component line relative to the multiplet and G the multiplet intensity relative to the other comprising the triad. $(\lambda_0/\lambda)^4$ the frequency correction, $h\nu_2$, $h\nu_1$, the excitation potentials of the upper and lower energy-levels respectively, k the Boltzmann constant, and T the absolute temperature. In equation (2), ΔE is the difference in excitation potential between the two states expressed in volts. relative intensities, multiplied by suitable factors necessary for comparing the members of a supermultiplet widely separated in the spectrum, may be used to calculate the observed emission intensities I. A plot of the logarithms of the theoretical intensities $\log I$ against the logarithms of the observed absorption intensities $\log A$, establishes an empirical relation between the two quantities for each atom. In default of information regarding the relative abundance of the elements and the absolute values of the oscillator strengths Ff, the diagrams for each supermultiplet set are displaced horizontally (keeping $\log A$ fixed) with respect to each other in order to obtain the best possible superposition. Finally, by adding the results of isolated multiplet, a general curve connecting the calculated with the observed intensities is established. To fix the zero point on the horizontal scale the relation

$$A = \frac{\pi e^2\lambda_0^2}{mc^2}\times 10^8\times NFf = 1.8\times10^{-13}NFf, \qquad (3)$$

where $\lambda_0 = 4500$ Å, was assumed to hold for faint lines whose profiles are defined solely on Doppler motion. The curves of growth obtained in such a manner are shown in Fig. 2~Fig. 6.

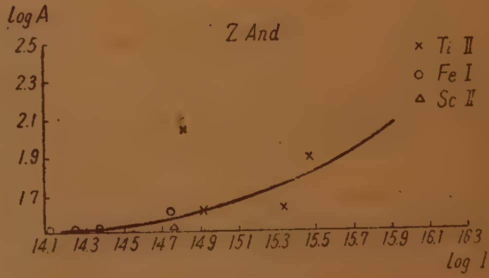

Fig. 2.

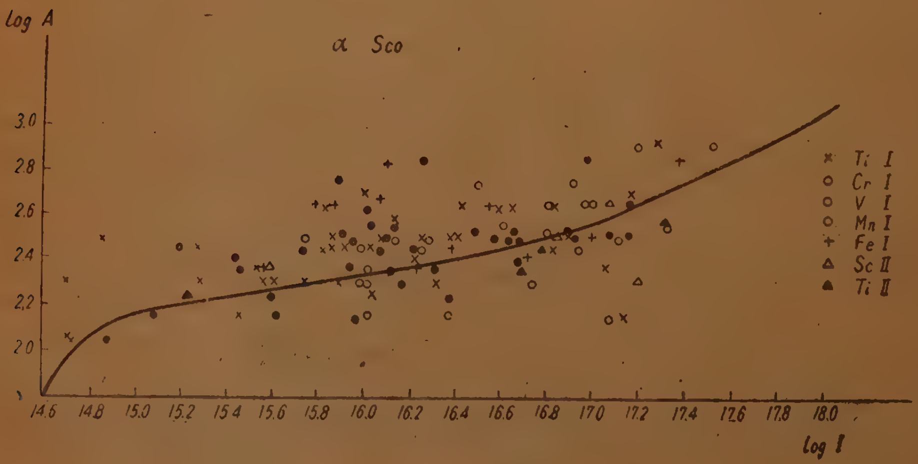

Fig. 3.

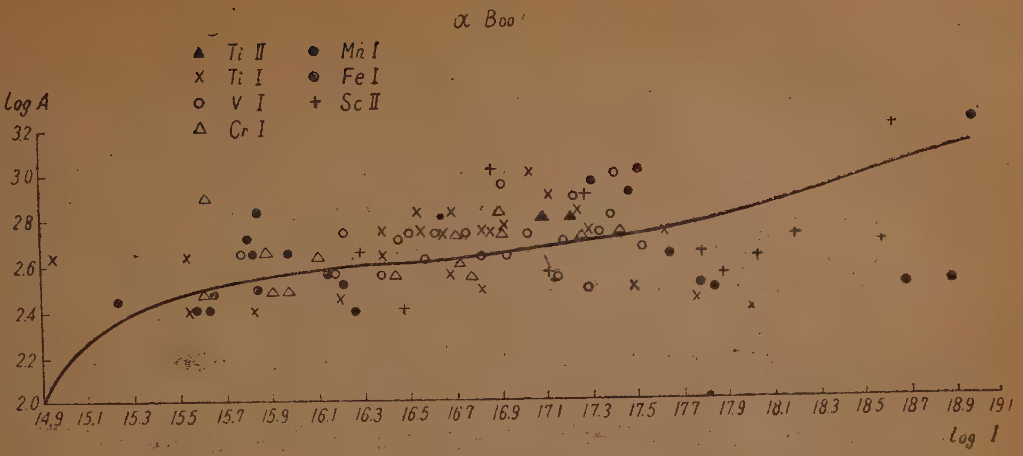

Fig. 4.

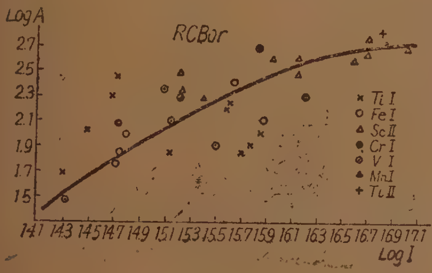

Fig. 5.

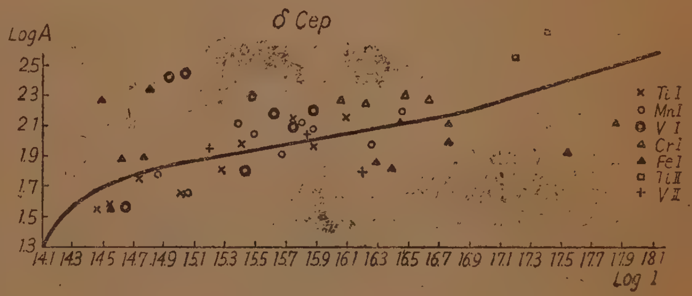

Fig. 6.

4. Number of Atoms.

The construction of the intensity calibration is independent of any theory relating to the formation of stellar absorption lines, with the exception of the aid rendered in locating the zero point on the horizontal axis. The empirical relation between the observed and the theoretical intensities, with the help of the ionization theory, should, to the first approximation, lead to a comparative census of the elements. It must be notisfied that the following assumptions are made: (1) Interlocking and redistribution in frequency when the energy-levels are not sharp may be neglected; (2) collision processes do not play a vital rôle in the formation of the absorption lines, except for their possible effect on the damping constant; (3) the vertical distribution of the neutral and the ionized atoms is the same for a thoroughly mixed isothermal atmosphere; (4) the atmosphere is in thermal equilibrium with a mean electron pressure equal to exactly half the pressure on its base; (5) the atmosphere is situated above an opaque photosphere corresponding to the optical depth $\tau \sim \frac{2}{3}$, such that the observed lines approximate those of the model atmosphere, which is assumed to be transparent to its own radiation, except in these lines. To find the number of neutral atoms N_0 (or ionized atoms N_1) in the normal state, we employ the Boltzmann equation

$$N = N_0 \frac{g}{B} e^{-\frac{E}{vk}} \qquad (4)$$

or

$$\log\frac{NFf}{Ff} - \log\frac{g}{B} = \log N_0 - \frac{5040}{T}E = \log D, \qquad (5)$$

where NFf is the number of atoms actively engaged in the production of the lines, Ff the subdivided oscillator strengths of the component line of the multiplet, g the weight of the state, B the partition function computed for the assumed temperature, E the excitation potential corresponding to the lower state, and $v = 1/11600$, For the lines of a given element, $\log NFf$ corresponding to $\log A$ is read from the calibration curve and after insertion of the factors Ff and g/B $\log D$ is plotted against E, representing the horizontal axis. The intercept yields the number of atoms in the ground state, and the slope the inverse absolute temperature of the reversing layer. The resource for obtaining the absolute values of the f's is to determine them empirically from Russell's[10] investigation for the composition of the solar atmosphere. The oscillator strengths are not known completely except for hydrogen and other some metals. Incidentally, the summation of the f's for strong series is equal to unity, which is mostly contributed by the principal members of the series, although this is not necessarily the case for higher series where Σf may be >1. Adopting the Rowland calibration, one derives the values of $\log f$ by comparing the observed intensities of different multiplets arising from the same lower level with Russell's quantity, $\log M_{\text{comp}}$ which represents the predicted total intensity for all the lines in the spectrum originating from the given level. In a few instances, where $\log M_{\text{comp}}$ is not given in Russell's list, it is possible to determine it in a similar manner from Menzel's[11] work on the solar chromosphere.

5. Number of Molecules.

The number of ionized and neutral atoms may be used to derive the mean electron pressure in the atmosphere from the ionization equation

$$\frac{N_1}{N_0} = \frac{K}{P}, \quad K = 0.267\frac{B_1}{B_0}T^{5/2}e^{-\frac{I}{vT}}. \tag{6}$$

In the form available for computation, equation (6) becomes

$$\log P = 2.74 - \log\frac{N_1}{N_0} + \log\frac{B_1}{B_0} - 0.95\,I. \tag{7}$$

As we can obtain the numerical value of P corresponding to each element in a star by adopting the mean value of P, we may slightly adjust the observed values of N_0 and N_1 so that they correspond to the mean electron pressure. The total pressure p is written as follows:

$$p = \frac{1+\beta}{\beta} \cdot P, \tag{8}$$

where

$$\beta = \sum_{\text{all elements}}^{i} (\varepsilon x_1)_i, \tag{9}$$

where ε is the relative abundance of the element by volume (unit : 1) and x_1 the ionized fraction. Now consider a molecule AB which consists of element A and element B, we take the formula of dissociative equilibrium.

$$K_{AB} = P_A P_B / P_{AB} \tag{10}$$

where

$$\left.\begin{aligned} P_A &= \varepsilon_A \cdot p = \frac{N_A}{\Sigma N}p \\ P_B &= \varepsilon_A \cdot p = \frac{N_B}{\Sigma N}p \\ P_{AB} &= \varepsilon_{AB} \cdot p = \frac{N_{AB}}{\Sigma N}p \end{aligned}\right\}, \tag{11}$$

where ΣN is the total number of particles. Combining (10) with (11) we obtain

$$\log\frac{P_A P_B}{P_{AB}} = \log\frac{N_A}{\Sigma N} \cdot \frac{N_B}{N_{AB}} \cdot p \tag{12}$$

$$\log K = \log N_A + \log N_B$$
$$- \log N_{AB} + \log p - \log \Sigma N. \tag{13}$$

By the formula (13), if the mean total pressure, ΣN, N_A, N_B and the temperature are known, we can calculate N_{AB}. And conversely if the number of molecules, N_{AB} is known, we can also calculate the number of atoms A or B according to the condition that one of them is known. In our materials the existence of molecular lines of some compounds is acknowledged but their intensities can not be measured. Therefore, adopting the rough assumption that the intensities of the molecular lines are nearly comparable with those of the atomic lines which can be measured, we can deduce the abundance of the element A or B which composes a molecule AB.

6. Discussion.

It is shown in the star R CBor that the calculated values of CH and C_2, $\log N_{CH} = 16.09$ and $\log N_{C_2} = 17.43$ are comparable with the value for the element La $\log N_{La} = 16.61$ obtained from the observation, and it confirms the observational fact that CH and C_2 were really observed. It is shown in the star *Z* And that the calculated values of CaH and MgH, $\log N_{CaH} = 6.69$ and $\log N_{MgH} = 9.44$ are lower than the value for the element Sc $\log N_{Sc} = 13.67$ obtained from the observation; this is a proof for the observational fact that MgH and CaH could not be observed practically. In the star α Sco, the calculated values of MgH and CaH $\log N_{MgH} = 12{,}34$, $\log N_{CaH} = 12.63$ are situated lower than the limiting observed value $\log N_{La} = 15.39$; this may give some evidence that the existence of such molecules are doubtful and this is shown practically in the observations. The relative abundance of each molecule which were calculated from the elements and molecules of every star by the method already cited are shown in the following table.

Table II. Relative Abundance of Elements.

Z And

	log *N*
H	24.61
Ni	22.09
Fe	19.69
Mg	19.37
Cr	18·98
Ti	17.48
V	17.41
Ca	15.68
Sc	13.67
CaH	6.69
MgH	9.44

Adopting $\log N_{TiO} = 13.00$, we have $\log N_O = 23.79$.

	Abundance
H	86
O	13
Ni	0.26
Fe	0.0010
Mg	0.0005
Cr	0.0002
Ti	0·00001

α Sco

	log *N*
H	25.30
Mg	23.32
Ca	22.62
Ni	21.84
Fe	21.83
V	20.45
Cr	20.15
Mn	19.21
Al	19.02
Co	18.88
Ti	17.87
Ba	17.76
Sc	17.33
Y	17.30
Zr	16.20
La	15.39
MgH	12·34
CaH	12.63

Adopting $\log N_{TiO} = 15{\cdot}00$, we have $\log N_O = 26.63$.
Adopting $\log N_{ZrO} = 15.00$, we have $\log N_O = 26.91$. } Mean : 26.80
Adopting $\log N_{CH} = 15.00$, we have $\log N_C = 22.75$.
Adopting $\log N_{CN} = 15.00$, we have $\log N_N = 19{\cdot}90$.

	Abundance
O	96
H	3
Mg	0.032
C	0.0086
Ca	0·0075
Ni	0.0009
Fe	0.0004
V	0.00004
Cr	0.00002
N	0.00001

α Boo

log N	
H	27.35
Mg	24.32
Ni	23.20
Ca	23.18
Na	22.89
Ti	22.67
Fe	22.56
Cr	22.45
V	20.81
Mn	20.49
Co	18.89
Sc	17.63
La	17.43
Y	17.10
Ba	16.89
Zr	15.22

Adopting $\log N_{CH} = 15.00$, we have $\log N_C = 22.08$. (Case I)
Adopting $\log N_{C_2} = 15.00$, we have $\log N_C = 25.05$. (Case II)
Adopting $\log N_{CN} = 15.00$ and assuming $\log N_C = 22.08$, we have $\log N_N = 24.43$. (Case I)
Adopting $\log N_{CN} = 15.00$ and assuming $\log N_C = 25.05$, we have $\log N_N = 21.46$. (Case II)

Abundance

Case I		Case II	
H	99	*H*	99
N	0.11	*C*	0.48
Mg	0.092	*Mg*	0.092
Ni	0.0070	*Ni*	0.0070
Ca	0.0067	*Ca*	0.0067
Na	0.0034	*Na*	0.0034

R C Bor

log N	
H	23.69
C	24.19
Mg	22.79
Na	21.60
Fe	22.16
Ca	21.20
Mn	20.86
Ti	19.57
Co	20.61
V	19.35
Ba	19.59
Zn	19.37
Ni	21.18
Cr	20.30
Zr	18.22
Sr	18.15
Y	17.80
La	16.61
CH	16.09
C_2	17.43

Adopting $\log N_{CN} = 16.00$, we have $\log N_N = 21.63$.

Abundance	
C	73
H	22
Mg	2.8
Fe	0.68
N	0.19
Na	0.19
Ca	0.073
Ni	0.068
Mn	0.033
Co	0.018
Cr	0.0091
Ba	0.0017
Ti	0.0016
Zn	0.0010

δ Cep

log N	
H	24.80
Fe	21.15
Cr	20.53
Ni	20.68
Ti	20.17
Ca	21.88
Mn	19.78
Zr	17.47
Y	17.20
V	20.19
Co	17.66
Zn	19.56
La	17.04
Ba	18.27
CaH	14.35

Adopting $\log N_{CH} = 17.00$, we have $\log N_C = 23.20$.
Adopting $\log N_{CN} = 17.00$ and assuming $\log N_C = 23.20$, we have $\log N_N = 23.46$.

Abundance	
H	93
N	4
C	2.3
Ca	0.11
Fe	0.020
Ni	0.0071
Cr	0.0050
V	0.0023
Ti	0.0022
Mn	0.0009

If we take $\log N = 13.00$ as the number showing the observable limit in *Z* And, we have comparatively large abundance of oxygen, and in α Sco, taking the limiting value $\log N = 15.00$, we obtain very large abundance of the same element. We may surely call this an oxygen star. If in these stars, *TiO* and other molecules containing oxygen are observed and their intensities can be measured quantitatively, we shall be able to determine the abundance of oxygen and clarify the uncertainty of these points. Berman has shown the great abundance of carbon in R C Bor which is called a carbon star. Our calculation also shows its special characteristics. It is also remarkable that nitrogen is abundant in δ Cep. When we take the abundance ratio of hydrogen, oxygen, carbon and nitrogen against other metallic elements as a measure of the abundance of elements, it is shown that the stars of lower temperatures have small numerical values with regards to this ratio. This fact is not inconsistent with the result that the relative abundance of hydrogen-like elements to metallic ones is 8000 to 1 as was shown by Strömgren. It may have some meaning on the evolution of stars. It is also confirmed that hydrogen is not always the most abundant element in the stellar atmospheres.

References.

(1) Y. Fujita: Jap. Jour. Astr. and Geophys. **13** (1935), 21; **17** (1939), 17; **18** (1940), 45, 177; **20** (1943), 101; Proc. Phys.-Math. Soc. Japan **20** (1938), 149.

(2) L. Berman: Ap. J. **81** (1935), 369.

(3) H. N. Russell: Ap. J. **70** (1929), 11. B. Strömgren: Festschrift E. Strömgren (1940).

(4) For the calculation of relative multiplet intensity, we used Goldberg's Table (Ap. J. **82** (1935), 1.)

(5) P. Swings and O. Struve: Ap. J. **91** (1940), 546.

(6) D. N. Davis: Ap. J. **86** (1937), 109; **89** (1939), 46.

(7) S. G. Hacker: Contr. Princeton Univ. Obs., No. 16 (1935); Ap. J. **88** (1938), 65.

(8) L. Berman: Ap. J. **81** (1935), 369.

(9) A. Pannekoek and v. Albada; Pub. Astr. Inst. Univ. Amsterdam, No. 6 (1939).

(10) H. N. Russell: Ap. J. **70** (1929), 11.

(11) D. H. Menzel: Publ. Lick. Obs. No. 17 (1931), 278

Short Note

Experimental Studies on the Electric Conduction and Heat Capacity of Cuprous Sulfide Semiconductors.

By Eiji, HIRAHARA.

Hiroshima Municipal Higher Technical School.

(Received August 25, 1947)

The electrical conduction and heat capacity of cuprous sulfide have been observed experimentally by several workers(1) within a rather limited range of temperature. We, therefore, have made a thorough observation of the electrical conduction and heat capacity of the mentioned sulfide in a wider temperature range in order to clarify the characteristic properties of the mentioned semiconductors.

Specimens are prepared through heating at 600°C in a electric furnace, a vacuum Pyrex tube which contains a stoichiometric quantity of sulphur powder and copper metal.

The measurement of ionic conductivity has been performed from room temperature to 600°C by the similar method to C. Tubandt's(2). The results obtained are as follows: below 100°C no ionic current is observed at all, but near 150°C it does appear to a measurable amount and increases exponentially with temperature until 440°C, and then begins to decrease rather suddenly until 500°C where the ionic current almost disappears within the limit of our experimental accuracy. The results are seen clearly in the following table. Moreover, the charge-carriers are experimentally confirmed to be copper-ions only.

Table. Ionic Current per Electronic Current.

Temp (C°)	100°	150°	200°	300°	400°	500°	600°
I_i/I_e %	0	0.032	0.11	0.61	1.27	0.07	0.05

The temperature-dependenay of the total current (ionic and electronic current) was measured from room temperature to 600°C. Theresults were described graphically in Fig. 1. It may be considered approximately to consist of three straight lines with kinks at 120°C and 440° respectively. It should be remarked that at 440°C the total con-

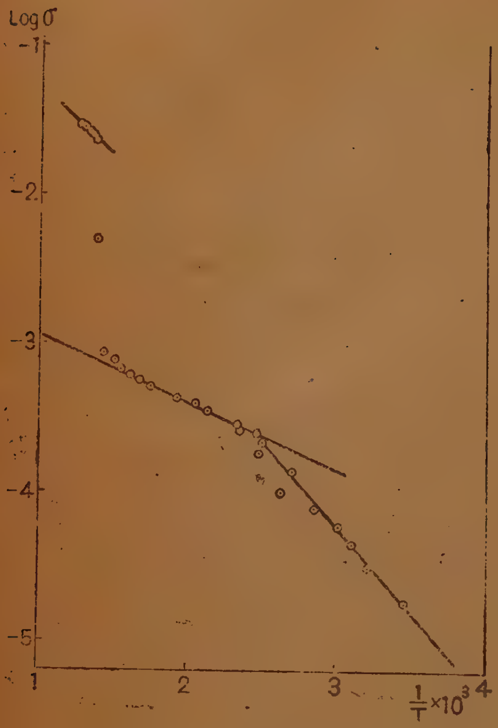

Fig. 1. Total Conductivity.

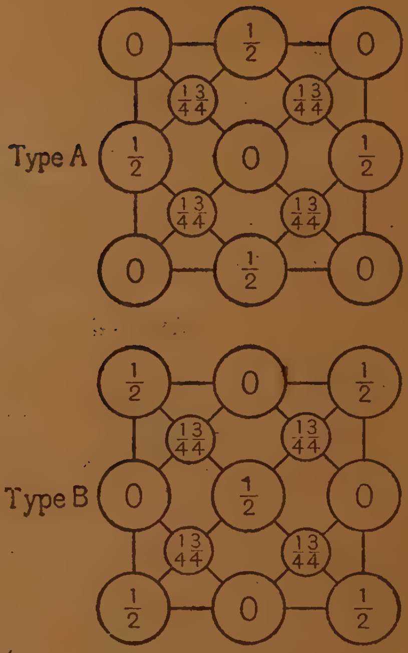

Fig. 3. Crystal Structnre

Numbers within the atomic circles indicate distances of these atoms below the plain of projection (in fraction of the length of the cube edge). Large circles: S-atoms, Small circles: Cu-atoms.

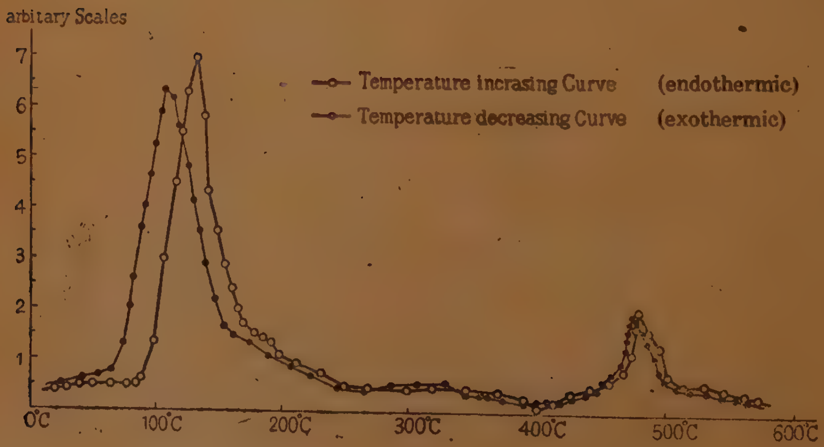

Fig. 2. Anomalous Heat Capacity.

ductivity makes a rather discontinous jump to high value and above 440°C the total current appears to show rather steady and smooth behaviour.

The measurement of the heat capacity was performed from room temperature to 600°C by the differential method with a standard body of copper. The results obtained show two sharp peaks at 150°C and at 480°C respectively.

The above results shall be discussed qualitatively from the viewpoint of modern theory of solid as follows. The physical properties of cuprous sulfide have at least two anomalies at 120°C and at 440°C respectively in view of our observation of electrical conduction and anomalous heat capacity. The anomaly at 120°C may be considered to be due to the change of crystal-structure from rhombic (below 120°C) to cubic (above 120°C) in accordance with P. Rahlfs'(3) crystal-analysis by X-rays. Although no definite interpretation concerning the the anomaly at 440°C is obtained successfully as yet, a plausible one may be shown as follows. Below 440°C the arrangement of sulphur atoms will be disordered among lattice sites (mixture type of Fig. 3, A and B) and become ordered above 440°C (single type of A or B). Since the disordered arrangement of ions makes the change of positions of current-carrier much feasible, as seen from the energetic consideration, the ionic current will easily be observed below 440°C. In the ordered arrangement of ions, however, it will disappear owing to the remarkable decrease of the mobility of the current-carrier in the stable arrangement of ordered ions (above 440°C). On the other hand, the abrupt increase of electronic current may be understood to be ascribed to the considerable increase of the mean free path of electrons in the ordered arrangement of ions above 440°C. The anomalous heat capacity was found to have a large peak at 120°C and a small peak at 440°C, because the former will be associated with the change of crystal-structure and the latter with the change of ordering of sulphur ions among the crystal sites. It should be noted that the appearance of the ordering of sulphur ions within cuprous sulfide above 440°C will be consistent with the well-known fact that the stable equilibrium may be realized within cuprous sulfide at high temperature.

The detaled acconnt of this short note shall be described in "Bussei-Ron Kenkyu", 7, 1947.

The author wishes to express his hearty thanks to Prof. T. Muto, (Tokyo Univ.) for his kind guidance throughout this work and also to Prof. T. Fujiwara (Hiroshima Univ.) and Asst. Prof. T. Okada (Kyushu Univ.) for their experimental supports.

Literature

(1) C. Tubandt, S. Eggert, G. Schibbe: Z. allgem. Chem. **117** (1921), 1. G. Trumplex: Z. phys. Chem. **99** (1921), 9. K. Fischleck, O. Dorner: ibid. **181** (1921), 372. V.A. Kozheurov: Colloid. J. (U. S. S. R.) **5** (1939), 45. W. P. White: J. am. Chem. Soc, **55** (1933) 1047. C. T. Anderson: ibid **54** (1932) 107.

(2) C. Tubandt: op. cit.

(3) P. Rahls: Z. phys. Chem. (B), **31** (1936) 157. See also R. W. G. Wyckoff; The Structure of Crystals. 2nd. Ed. p 230.

Notes on the Condensation of Two-Component Systems.

By Yosio MUTŌ.

Maebashi Medical College, Maebashi, Japan.

(Received September 5, 1947)

Prof. J. E. Mayer has studied the statistical mechanics of condensing systems with two components and deduced the formula[1)]

$$df=\left[\left(\frac{x}{y}-v\right)W-\left(\frac{\chi}{\eta}-v\right)w\right]\frac{dy}{y}$$
$$-\left[\left(\frac{x}{y}-v\right)w-\left(\frac{\chi}{\eta}-v\right)\Omega\right]\frac{d\eta}{\eta}=0 \qquad (1)$$

where

$$f=x\left(\ln y-\frac{1}{y}G_{1,0}\right)+\chi\left(\ln\eta-\frac{1}{\eta}G_{0,1}\right)$$
$$+v(y+\eta-G_{1,0}-G_{0,1}+G_{0,0}) \qquad (2)$$

is the configurational part of the logarithm of the partition function per molecule.

Let D and $\varDelta$ denote the densities of molecules of type a and type α respectively in the liquid phase. Let the densities in the vapor phase be y and η, and we get

$$x=y\,V_g/N+D\,V_l/N$$
$$\chi=\eta\,V_g/N+\varDelta\,V_l/N$$

where V_g and V_l are the volumes of vapor phase and liquid phase respectively. Applying these relations and $v=V_g/N+V_l/N$ we get from (1)

$$\left[\left(\frac{D}{y}-1\right)W-\left(\frac{\varDelta}{\eta}-1\right)w\right]\frac{dy}{y}$$
$$=\left[\left(\frac{D}{y}-1\right)w-\left(\frac{\varDelta}{\eta}-1\right)\Omega\right]\frac{d\eta}{\eta}. \qquad (3)$$

If we neglect the small intermolecular forces in the vapor phase and also y and η against D and $\varDelta$ this formula is the Duhem-Margules' relation. Hence (3) may be regarded as a refinement of it.

---

(1) J. E. Mayer: J. Phys. Chem., **43**, 71 (1939).

CONTENTS

Page

Otohiko Nomoto: On the Fine Structure of the Visibility Curves of the Stationary Ultrasonic Waves. 1

Kenji Kondo: Thermionic Constants of Platinum. 6

Ryoji Uyeda, Shinkiti Ito and Kazuo Kimoto: Investigation of Carbonized Tungsten Surfaces by the Method of Electron-Diffraction. 9

Hiromu Wakesima: Ueber die Rotation des OH Molekuels (III). 12

Shizuo Miyake and Mieko Kubo: Electron-Diffraction. Study on Behaviors of Metals deposited on Crystal Surfaces.

Part I. Metals deposited on Galena. 15

Part II. Diffusion Phenomena of Metal Atoms on Galena 20

Toyozo Kambara: Dissociation and Ionization of n–Hexane, Cyclohexane and Benzene by Electron Impacts, I. 25

Kenji Kondo: On the Relation between Thermionic Constant and Work Fnnction 32

Kenji Kondo: Thermionic Constant of Platinum II, on Face Excess Developed by Etching. 36

Otohiko Nomoto: On the Phenomenon of the Periodical Exchange between the Phase Lattice and the Amplitude Lattice in the Fresnel's Diffraction Phenomenon by Graitings.—Theoretical Consideration and Experiment by the Ultrasonic Wave. 41

Ryogo Kubo: Statistical Theory of Linear Polymers, I. Intramolecular Statistics. 47

Ryogo Kubo: Statistical Theory of Linear Polymers, II. Elasticity of Vulcanized Rubber. 51

Toyozo Kambara: Dissociation and Ionization of n–Hexane, Cyclohexane and Benzene by Electron Impacts, II. 57

Ayao Amemiya: On the Formulas for the Relative Multiplet Strength in LS Coupling. 62

Taro Kihara: Approximate Methods regarding Electro-Magnetic Waves in Hollow Pipe and Cavities. 65

Kazuzi Hashimoto: The Figures on the Surface of Metal Electrodes Produced by the Breakdown High Vacuum. 71

Tatuo Kobayasi: On Sparking Potentials. 75

Shunji Shirai: On the Oxidation of the Thin Single Crystal Film of Copper 81

Ryogo Kubo: Statistial Theory of Linear Polymers, III. Double Refraction 84

Shizuo Miyake and Ryuzo Ueda: On Phase Transformation of $BaTiO_3$. 93

Shizuo Miyake: Effect of External Stress on X-Ray Intensity Reflected from Rschelle Salt Crystal. 98

Yoshihiro Sayama: The Optical Theory of the Spectral Sensitivity of Caesium-Oxide Photocathode. 103

Akiya Ookawa: Crystallite Theory of Liquid, I. On the Specific Heat. 108

Heiji Kawai: The Influence of Temperature and Humidity on the no Load Voltage Sensitivity of Rochelle Salt. 113
Toyokiti Nosawa and Tosiyuki Toyoda: The Rotation Spectrum of Water Vapor, I. ...116
Toyokiti Nosawa: The Rotation Spectrum of Water Vapor, II. 126
Goro Honzyo: Anomalies in Electron-Diffraction Debye-Scherrer Ring. 133
Toshinosuke Muto and Mokitiro Nogami: On the Sticking Probability of fast Neutron in the Nuclear Reactions. 138
Isao Osida: The Graphical Calculation of Solar Radiation at the Earth's Surface,
Part, I. 143
Part, II. 148
Hitosi Ioi: Étude d'une théorie statistique de la turbulence homogène. 155
Sin-itiro Tomonaga: A General Theory of Ultrashort-Wave Circuits. I. 158
Satio Hayakawa, Yonezi Miyamoto and Sin-itiro Tomonaga: On the Elimination of the Auxiliary Condition in the Quantum Electrodynamics, I. 172
Hirosi Itimura: On the Entropy of the Supraconductor. 184
Toshinosuke Muto: Theory of External Photoelectric Effect in Semiconductors.
Part I. BaO–, SrO– and Cu_2O Semiconductors 187
(1) Behaviors of the Photosensitivity near Threshold.
(2) Total Photosensitivity.
Part II. Coloured Alkali Halides. 193
Hirosi Hayasi: On the Resistance Experienced by a Body which Moves along the Plain Surface of an Elastic Solid. 196
Satio Hayakawa, Yonezi, Miyamoto and Sin-itiro Tomonaga: On the Elimination of the Auxilliary Condition in the Quantum Electrodynamics, II. 199
Yosio Fujita: On the Chemical Composition of Some Late Type Stars. 204

SHORT NOTES

Yuzuru Watase and Seinosuke Ozaki: Further Confirmation of the Angular Correlation of the Successive γ-rays. 90
Syozo Sawada, Gen Shirane and Hirosi Sugawara: On the Specific Heat and Thermal Expansion of Barium Titanate. 90
Akio Kobayashi: The Relaxation Effect of the Couprous Oxide Rectifier after the Application of Strong Field. 92
Eiji Hirahara: Experimental Studies on the Electric Conduction and Heat Capacity of Cuprous Sulphide Semiconductors. 211
Yoshio Muto: Notes on the Condensation of Two Component System. 214

Author Index to Volume 2.

Page

Amemiya Ayazo: On the Formulas for the Relative Multiplet strengths in LS Coupling ······ 62

Fujita Yoshio: On the chemical Composition of Some Late Type Stars ······ 204

Hashimoto Kazuzi: The Figures on the Surface of Metal Electrodes Produced by the Breakdown High Vacuum ······ 71

Hayakawa Satio, Miyamoto Yonezi and Tomonaga Sin-itiro: On the Elmination of the Auxiliary Condition in the Quantum Electro-dynamics I. ······ 172

Hayakawa Satio, Miyamoto Yonezi and Tomonaga Sin-itiro: On the Elimination of the Auxiliary Condition in the Quantum Electro-dynamics II. ······ 199

Hayasi Hirosi: On the Resistance Experienced by a Body which Moves along the Plain Surface of an Elastic Solid ······ 196

Hirahara Eiji: Experimental Studies on the Elctric Conduction and Heat Capacity of Cuprous Sulfide Semiconductors ······ 211

Honzyo Goro: Anomalies in Electro-Diffraction Debye-Scherrer Ring ······ 133

Ioi Hitosi: Étude d'une théorie statistique de la turbulence homogêne ······ 155

Itimura Hiroshi: On the Entropy of the Superconductor ······ 184

Ito Shinkiti, Uyeda Ryoji and Kimoto Kazuo: Investigation of Carbonized Tungsten Surfaces by the Method of Electron-Diffraction ······ 9

Kambara Toyozo: Dissociation and Ionization of *n*-Hexane, Cyclohexane and Benzene by Electoron Impacts, I. ······ 25

Kambara Toyozo: Dissociation and Ionization of *n*-Hexane, Cyclohexane and Benzene by Electron Impacts, II. ······ 57

Kawai Heiji: The Influence of Temperature and Humidity on the no Load Voltage Sensitivity of Rochelle Salt ······ 113

Kihara Taro: Approximate Methods regarding Electro-magnetic Waves in Hollow Pipes and Cavities ······ 65

Kimoto Kazuo, Uyeda Ryoji and Ito Shinkiti: Investigation of Carbonized Tungsten Surfaces by the Method of Electron-Diffraction ······ 9

Kobayashi Akio: The Relaxation Effect of the Couprous Oxide Rectifier after the Application of Strong Field ······ 92

Kobayashi Tatuo: On Sparking Potentials ······ 75

Kondo Kenji: Thermionic Constants of Platinum ······ 6

Kondo Kenji: On the Relation between Thermionic Constant and Work Function ······ 32

Kondo Kenji: Thermionic Constant of Platinum, II. On Face Excess Developed by Etching ······ 36

Kubo Ryogo: Statistical Theory of Linear Polymers, I. Intramoleculer Statistics ······ 47

Kubo Ryogo: Statistical Theory of Linear Polymers, II. Elasticity of Valcanized Rubber ······ 51

Kubo Ryogo: Slatistical Theory of Linear Polymers, III. Double Refraction ······ 84

Kubo Mieko and Miyake Shizuo: Electron-Diffraction Study on Behaviors of Metals deposited on Crystal Surfaces
Part I. Metals deposited on Galena ········ 15
Part II. Diffusion Phenomena of Metal Atoms on Galena ········ 20
Miyake Shizuo and Kubo Mieko: Electron-Diffraction Study on Behaviors of Metals deposited on Crystal Surfaces
Part I. Metals deposited on Galena ········ 15
Part II. Diffusion Phenomena of Metal Atoms on Galena ········ 20
Miyake Shizuo and Ueda Ryuzo: On Phase Transformation of $BaTiO_3$ ········ 93
Miyake Shizuo: Effect of External Stress on X-ray Intensity Reflected from Rochell Salt Crystal ········ 98
Miyamoto Yonezi, Hayakawa Satio and Tomonaga Sin-itiro: On the Elimination of the Auxiliary Condition in the Quantum Electrodynamics I. ········184
Miyamoto Yonezi, Tomonaga Sin-itiro and Hayagawa Satio: On the Elimination of the Auxiliary Condition in the Quantum Electrodynamics, II. ········199
Muto Toshinosuke and Nogami Mokitiro: On the Sticking Probability of Fast Neutron in the Nuclear Reactions ········138
Muto Tosinosuke: Theory of External Photoelectric Effect in Semiconductors······
Part I. BaO-, SrO- and Cu_2O Semiconductors ········187
(1) Behaviors of the Photosensitivity near Threschold ········187
(2) Total Photosensitivity ········187
Part II. Coloured Alkali Halides ········193
Muto Yoshio: Notes on the Condensation of Two Component System. ········214
Nogami Mokitiro and Muto Toshinosuke: On the Sticking Probability of Fast Neutron in the Nuclear Reactions. ········138
Nomoto Otohiko: On the Fine Structure of the Visibility Curves of the Stationary Ultrasonic Waves. ········ 1
Nomoto Otohiko: On the Phenomenon of the Periodical Exchange between the Phase Lattice and the Amplitude Lattice in the Frensnel's Diffraction Phenomenon by Graitings—Theoretical Considerations and Experiment by the Ultrasonic Waves ········ 41
Nosawa Toyokiti and Toyoda Toshiyuki: The Rotation Spectrum of Water Vapor, I ········116
Nosawa Toyokiti: The Rotation Spectrum of Water Vapor II. ········126
Ookawa Akiya: Crystallite Theory of Liquid, I. On the Specific Heat. ········108
Osida Isao: The Graphical Calculation of Solar Radiation at the Earth's Surface, Part I. ········143
Osida Isao: The Graphical Calculation of Solar Radiation at the Earth's Surface, Part II. ········148
Ozaki Seinosuke and Watase Yuzuru: Further Confirmation of the Angular Correlation of the Successive γ-rays. ········ 90
Sawada Syozo, Sirane Gen and Sugawara Hirosi: On the Specific Heat and Thermal Expansion of Barium Titanate. ········ 90
Sayama Yoshihiro: The optical Theory of the Spectral Sensitivity of Caesium

Oxide Photocathode. ……103

Shirai Shunji: On the Oxidation of the Thin Single Crystal Film of Copper. …… 81

Sirane Gen, Sawada Syozo and Sugawara Hirosi: On the Specific Heat and Thermal Expansion of Barium Titanate. …… 90

Sugawara Hirosi, Sirane Gen and Sawada Syozo: On the Specific Heat and Thermal Expansion of Barium Titanate. …… 90

Tomonaga Sin-itiro: A General Theory of Ultrashort-Wave Circuits I. ……158

Tomonaga Sin-itiro, Miyamoto Yonezi and Hayakawa Satio: On the Elimination of the Auxiliary Condition in the Quantum Electro-dynamics I. ……184

Tomonaga Sin-itiro, Hayakawa Satio and Miyamoto Yonezi: On the Elimination of the Auxiliary Condition in the Quantum Electrodynamics, II. ……199

Toyoda Toshiyuki and Nosawa Toyokiti: The Rotation Syectrum of Water Vapor, I. ……116

Ueda Ryuzo and Miyake Shizuo: On Phase Transformation of $BaTiO_3$. …… 93

Uyeda Ryoji, Ito Shinkiti, and Kimoto Kazuo: Investigation of Carbonized Tungsten Surfaces by the Method of Electron-Diffraction. …… 9

Wakesima Hiromu: Ueber die Rotation des OH Molekuels (III). …… 12

Watase Yuzuru and Ozaki Seinosuke: Further Confirmation of the Angular Correlation of the Successive γ-rays. …… 90